Tracy I. George
Daniel A. Arber
Editors

Atlas of Bone Marrow Pathology

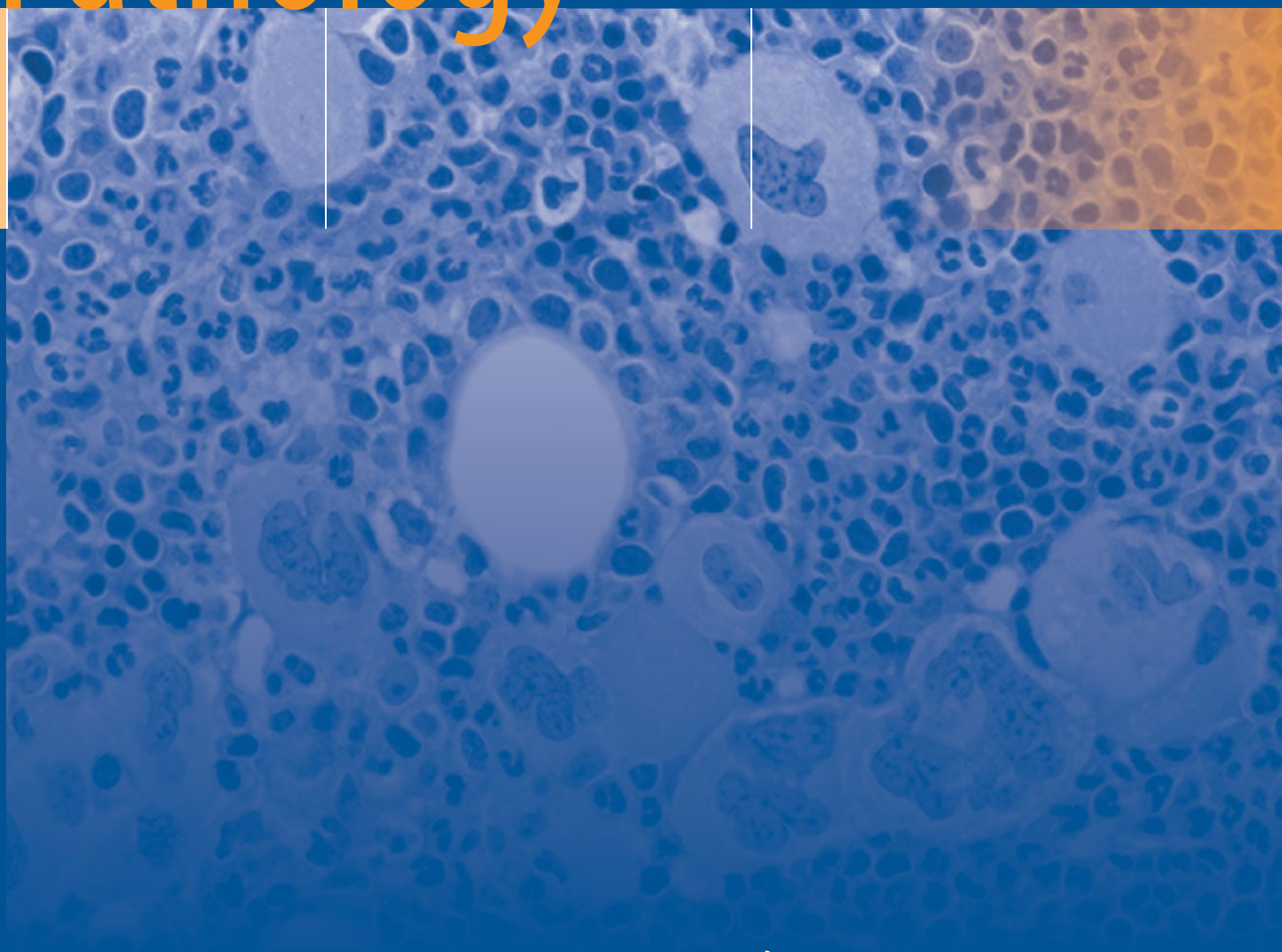

Springer

Atlas of Anatomic Pathology

Series Editor

Liang Cheng
Indianapolis, Indiana
USA

This Atlas series is intended as a "first knowledge base" in the quest for diagnosis of usual and unusual diseases. Each atlas will offer the reader a quick reference guide for diagnosis and classification of a wide spectrum of benign, congenital, inflammatory, nonneoplastic, and neoplastic lesions in various organ systems. Normal and variations of "normal" histology will also be illustrated. Each atlas will focus on visual diagnostic criteria and differential diagnosis. It will be organized to provide quick access to images of lesions in specific organs or sites. Each atlas will adapt the well-known and widely accepted terminology, nomenclature, classification schemes, and staging algorithms. Each volume in this series will be authored by nationally and internationally recognized pathologists. Each volume will follow the same organizational structure. The first Section will include normal histology and normal variations. The second Section will cover congenital defects and malformations. The third Section will cover benign and inflammatory lesions. The fourth Section will cover benign tumors and benign mimickers of cancer. The last Section will cover malignant neoplasms. Special emphasis will be placed on normal histology, gross anatomy, and gross lesion appearances since these are generally lacking or inadequately illustrated in current textbooks. The detailed figure legends will concisely summarize the critical information and visual diagnostic criteria that the pathologist must recognize, understand, and accurately interpret to arrive at a correct diagnosis.This book series is intended chiefly for use by pathologists in training and practicing surgical pathologists in their daily practice. The atlas series will also be a useful resource for medical students, cytotechnologists, pathologist assistants, and other medical professionals with special interest in anatomic pathology. Trainees, students, and readers at all levels of expertise will learn, understand, and gain insights into the complexities of disease processes through this comprehensive resource. Macroscopic and histological images are aesthetically pleasing in many ways. This new series will serve as a virtual pathology museum for the edification of our readers.

More information about this series at http://www.springer.com/series/10144

Tracy I. George • Daniel A. Arber
Editors

Atlas of Bone Marrow Pathology

Springer

Editors
Tracy I. George
Department of Pathology
University of New Mexico School of Medicine
Albuquerque, NM, USA

Daniel A. Arber
Department of Pathology
The University of Chicago
Chicago, IL, USA

Atlas of Anatomic Pathology
ISBN 978-1-4939-7467-2 ISBN 978-1-4939-7469-6 (eBook)
https://doi.org/10.1007/978-1-4939-7469-6

Library of Congress Control Number: 2017962322

Printed on acid-free paper

This Springer imprint is published by Springer Nature
The registered company is Springer Science+Business Media, LLC
The registered company address is: 233 Spring Street, New York, NY 10013, U.S.A.

Thank you, Chris, for your unwavering support and understanding.

Tracy I. George

To Carol, James, and William.

Daniel A. Arber

Series Preface

One Picture Is Worth Ten Thousand Words. (*Frederick Barnard, 1927*)

Remarkable progress has been made in anatomic and surgical pathology during the last 10 years. The ability of surgical pathologists to reach a definite diagnosis is now enhanced by immunohistochemical and molecular techniques. Many new clinically important histopathologic entities and variants have been described using these techniques. Established diagnostic entities are more fully defined for virtually every organ system. The emergence of personalized medicine has also created a paradigm shift in surgical pathology. Both promptness and precision are required of modern pathologists. Newer diagnostic tests in anatomic pathology, however, cannot benefit the patient unless the pathologist recognizes the lesion and requests the necessary special studies. An up-to-date atlas encompassing the full spectrum of benign and malignant lesions, their variants, and evidence-based diagnostic criteria for each organ system is needed. This atlas is not intended as a comprehensive source of detailed clinical information concerning the entities shown. Clinical and therapeutic guidelines are served admirably by a large number of excellent textbooks. This atlas, however, is intended as a "first knowledge base" in the quest for definitive and efficient diagnosis of both usual and unusual diseases.

The *Atlas of Anatomic Pathology* is presented to the reader as a quick reference guide for diagnosis and classification of benign, congenital, inflammatory, nonneoplastic, and neoplastic lesions organized by organ systems. Normal and variations of "normal" histology are illustrated for each organ. The atlas focuses on visual diagnostic criteria and differential diagnosis. The organization is intended to provide quick access to images and confirmatory tests for each specific organ or site. The atlas adopts the well-known and widely accepted terminology, nomenclature, classification schemes, and staging algorithms.

This book series is intended chiefly for use by pathologists in training and practicing surgical pathologists in their daily practice. It is also a useful resource for medical students, cytotechnologists, pathologist assistants, and other medical professionals with special interest in anatomic pathology. We hope that our trainees, students, and readers at all levels of expertise will learn, understand, and gain insight into the pathophysiology of disease processes through this comprehensive resource. Macroscopic and histological images are aesthetically pleasing in many ways. We hope that the new series will serve as a virtual pathology museum for the edification of our readers.

Indianapolis, IN, USA — Liang Cheng

Preface

We developed this atlas in order to provide a practical tool for the practicing pathologist and trainees in the field. Using experts in the field of diagnostic hematopathology, we have crafted individual chapters comprised of numerous high-quality images, useful tables, and diagrams that illustrate areas of diagnostic concern for pathologists, contrasting problem areas and morphologic mimics, as well as discussing the latest classification of neoplasms.

Our intent is not to create exhaustive, lengthy treatises on each disease entity. Instead, this atlas contains helpful hints from seasoned diagnosticians about how they approach an individual patient's biopsy and thus encompasses multiple modalities, from cytomorphology and histopathology to flow cytometry and genetic testing.

Key references are provided to help guide the reader and provide a starting point for further education. Our final result is an atlas of bone marrow pathology that can be used daily, from troubleshooting of difficult cases to recognition of unusual entities.

Please enjoy!

Albuquerque, NM, USA — Tracy I. George
Chicago, IL, USA — Daniel A. Arber

Contents

Contributors

Daniel A. Arber Department of Pathology, The University of Chicago, Chicago, IL, USA

Katherine R. Calvo, MD, PhD Department of Laboratory Medicine, National Institutes of Health Clinical Center, Bethesda, MD, USA

Joanna M. Chaffin, MD Department of Pathology, Medical College of Georgia at Augusta University, Augusta, GA, USA

Yi-Hua Chen, MD Department of Pathology, Northwestern University Feinberg School of Medicine, Chicago, IL, USA

Devon Chabot-Richards, MD Department of Pathology, University of New Mexico Sciences Center, Albuquerque, NM, USA

Juehua Gao, MD, PhD Department of Pathology, Northwestern University Feinberg School of Medicine, Chicago, IL, USA

Tracy I. George Department of Pathology, University of New Mexico School of Medicine, Albuquerque, NM, USA

Sandeep Gurbuxani, MBBS, PhD Department of Pathology, Section of Hematopathology, University of Chicago, Chicago, IL, USA

Matthew T. Howard, MD Division of Hematopathology, Mayo Clinic, Rochester, MN, USA

Rebecca L. King, MD Division of Hematopathology, Mayo Clinic, Rochester, MN, USA

Perikala Vijayananda Kumar, MD Department of Pathology, Shiraz Medical School, Shiraz, Fars, Iran

Jason H. Kurzer, MD, PhD Stanford University School of Medicine, Stanford, CA, USA

Lee J. McGhan, MD Department of Pathology, University of Arizona/Banner University Medical Center, Tucson, AZ, USA

Ahmad Monabati, MD Department of Pathology, Shiraz Medical School, Shiraz, Fars, Iran

Megan Parilla, MD Department of Pathology, University of Chicago Medical Center, Chicago, IL, USA

Maria A. Proytcheva, MD Department of Pathology, University of Arizona/Banner University Medical Center, Tucson, AZ, USA

Kaaren K. Reichard, MD Department of Laboratory Medicine and Pathology, Division of Hematopathology, Mayo Clinic, Rochester, MN, USA

Heesun J. Rogers, MD, PhD Department of Laboratory Medicine, Cleveland Clinic, Cleveland, OH, USA

Aaron Paul Rupp, MD Department of Pathology, University of New Mexico Center, Albuquerque, NM, USA

Natasha Marie Savage, MD Department of Pathology, Medical College of Georgia at Augusta University, Augusta, GA, USA

Kristian T. Schafernak, MD, MPH Department of Pathology and Laboratory Medicine, Phoenix Children's Hospital, Phoenix, AZ, USA

Min Shi, MD, PhD Department of Laboratory Medicine and Pathology, Division of Hematopathology, Mayo Clinic, Rochester, MN, USA

Luke R. Shier, MD Department of Pathology and Laboratory Medicine, University of Ottawa, Ottawa, ON, Canada

Payal Sojitra Department of Pathology, University of New Mexico School of Medicine, Albuquerque, NM, USA

Mohammad Vasef, MD Department of Pathology, University of New Mexico Health Sciences Center, Albuquerque, NM, USA

Girish Venkataraman, MD Department of Pathology, University of Chicago Medical Center, Chicago, IL, USA

Olga K. Weinberg, MD Pathology Department, Boston Children's Hospital, Boston, MA, USA

Carla S. Wilson, MD, PhD Department of Pathology, University of New Mexico Health Sciences Center and Tricore Reference Laboratories, Albuquerque, NM, USA

Qian-Yun Zhang, MD, PhD Department of Pathology, University of New Mexico, Albuquerque, NM, USA

Normal Bone Marrow

1

Heesun J. Rogers

The bone marrow examination is an important diagnostic procedure used for a wide variety of clinical conditions such as the diagnosis of myeloid or lymphoid neoplasms, various reactive conditions or metastatic, non-hematopoietic malignancies. Bone marrow examination is also used for confirmation or monitoring of a remission state, residual or recurrent disease state, or regeneration of bone marrow after various therapies. Bone marrow aspiration and biopsy of adequate quality are considered to represent overall bone marrow function.

A basic understanding of bone marrow structures and the correct identification of cells comprising normal bone marrow are very important in the interpretation of bone marrow pathology. The bone marrow is a well-organized structure confined in cortical bone and traversed by medullary or trabecular bone. The bone marrow has three components: hematopoietic cells, stroma/microenvironment, and medullary bone. Hematopoietic cells are embedded in a connective tissue stroma in intertrabecular spaces of medullary bone. The bone marrow is almost entirely occupied by hematopoietic cells, with the highest cellularity at birth or early infancy. The hematopoietic cells gradually decrease in the bone marrow with aging, and the bone marrow is replaced by adipose cells (fat cells). Hematopoietic cells derived from multipotent stem cells can be further differentiated into several lineage cells: erythrocytes, granulocytes, monocytes, megakaryocytes, and lymphocytes.

Tables 1.1, 1.2, and 1.3 list the characteristic cytologic features of erythroid cells, granulocytic cells, and megakaryocytic cells. These tables illustrate the various stages of maturation from the earliest recognizable immature cells to mature cells in the bone marrow. Erythroid precursor cells (normoblast or erythroblast) develop adjacent to macrophages and are subdivided into pronormoblasts, basophilic normoblasts, polychromatophilic normoblasts, and orthochromic normoblasts. Immature granulocytic cells develop adjacent to trabecular surfaces or arterioles and are further subdivided into blasts, promyelocytes, myelocytes, metamyelocytes, band neutrophils, and segmented neutrophils. Megakaryocytes, the largest hematopoietic cells in bone marrow, can be easily identified adjacent to sinusoids, but megakaryoblasts or immature megakaryocytes are often difficult to recognize in the bone marrow and can be readily identified in conjunction with immunohistochemistry or immunophenotype.

The marrow stroma is composed of fibroblasts, macrophages, adipose cells, osteoblasts, osteoclasts, sinusoids or capillaries, and endothelial cells.

In this chapter, characteristic cytologic and histologic features of various types of hematopoietic cells (particularly a spectrum of maturing hematopoietic cells) and stromal cells observed in normal bone marrow are described with representative pictures (Figs. 1.1, 1.2, 1.3, 1.4, 1.5, 1.6, 1.7, 1.8, 1.9, 1.10, 1.11, 1.12, 1.13, 1.14, 1.15, 1.16, 1.17, 1.18, 1.19, 1.20, 1.21, 1.22, 1.23, 1.24, 1.25, 1.26, 1.27, and 1.28). Bone marrow cells that are morphologically similar and easy to misidentify are illustrated with a comparison of their cytologic features.

H.J. Rogers (✉)
Department of Laboratory Medicine, Cleveland Clinic,
Cleveland, OH, USA
e-mail: rogersj5@ccf.org

T.I. George, D.A. Arber (eds.), *Atlas of Bone Marrow Pathology*, Atlas of Anatomic Pathology,
https://doi.org/10.1007/978-1-4939-7469-6_1

Table 1.1 Maturation of erythroid cells in bone marrow

Cell type	Characteristic morphology	Description
Pronormoblast (proerythroblast)	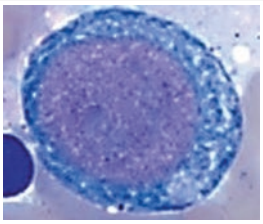	The most immature and largest cells in erythroid lineage (12–24 μm), relatively high nuclear to cytoplasmic (N/C) ratio (7–8:1), round to slightly oval nucleus, finely reticulated chromatin, prominent nucleoli (≥ 1), and agranular basophilic cytoplasm
Basophilic normoblast	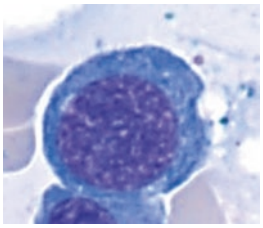	Smaller cells (10–17 μm) than pronormoblast, round nucleus, high N/C ratio (6:1), open to slightly condensed chromatin, distinct parachromatin, rarely visible or absent nucleoli in later stage, and deep basophilic cytoplasm
Polychromatophilic normoblast	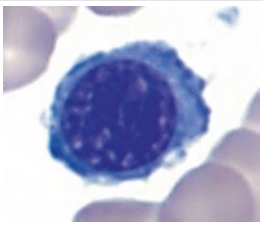	Smaller cells (10–15 μm) and lower N/C ratio (4:1) than basophilic normoblasts, round nucleus with condensed chromatin, often cartwheel appearance, visible perinuclear halo, no nucleoli, and blue-gray to pink-gray cytoplasm
Orthochromic normoblast	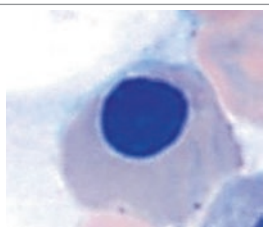	More mature and smaller cells (8–12 μm) than polychromatophilic normoblast, abundant cytoplasm (N/C ratio 1:2) with pink-orange and minimally basophilic color similar to erythrocytes, round nucleus, and densely condensed or pyknotic chromatin
Erythrocyte	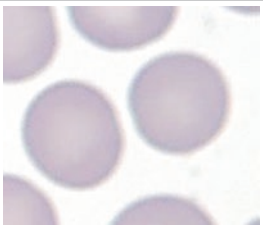	The most mature cells (7–8.5 μm), pink-orange to salmon color, and no nucleus

Table 1.2 Maturation of granulocytic cells in the bone marrow

Cell type	Characteristic morphology	Description
Myeloblast	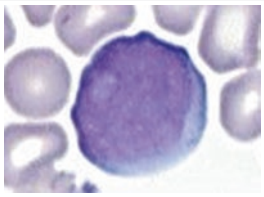	The most immature granulocytic cells (15–20 μm), with high N/C ratio (4–7:1), round to oval nucleus, fine to reticular chromatin with distinct nucleoli (1–5), and moderately basophilic cytoplasm with absent or minimal azurophilic granules
Promyelocyte	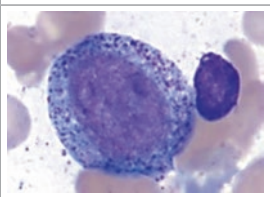	Slightly larger cells (14–24 μm) than myeloblasts, with high N/C ratio (3–5:1), eccentric round to oval nucleus, slightly coarse or finely reticular chromatin, distinct nucleoli (1–3), basophilic cytoplasm with paranuclear hof and prominent azurophilic (primary) granules, which may overlie the nucleus
Myelocyte	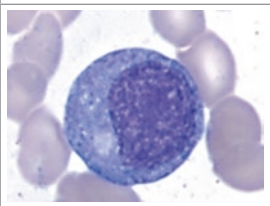	Slightly smaller cells (10–18 μm) than blasts, with more abundant cytoplasm (N/C ratio 1–2:1), eccentric round to oval nucleus, more condensed chromatin, no nucleoli, bluish to pink cytoplasm with paranuclear hof, abundant lilac (secondary) granules, and scattered few azurophilic (primary) granules
Metamyelocyte	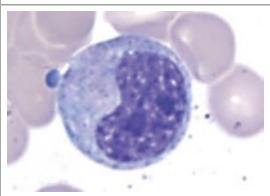	Size similar to or slightly smaller (10–18 μm) than myelocytes, with abundant cytoplasm (N/C ratio 1–1.5:1), indented or kidney-shaped nucleus (indentation less than half the width of the nuclear margin), condensed chromatin, no nucleoli, pinkish cytoplasm with many secondary granules and rare primary granules
Band neutrophil	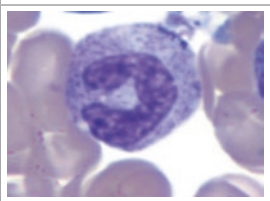	More mature cells (10–18 μm) similar to metamyelocytes, abundant cytoplasm (N/C ratio 1:1.2–1.5), indented or band-like or sausage-like nucleus (indentation more than half the width of the nuclear margin), condensed chromatin, no nucleoli, and pinkish cytoplasm with abundant secondary granules
Segmented neutrophil	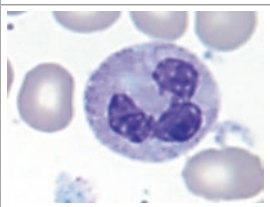	The most mature cells (10–18 μm), with abundant cytoplasm, more condensed nucleus with 3 to 5 distinct lobes connected by thin filaments, and pinkish cytoplasm packed with secondary granules

Table 1.3 Maturation of megakaryocytic cells in the bone marrow

Cell type	Characteristic morphology	Description
Immature megakaryocyte	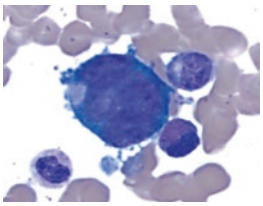	Smaller cell (size > 20 μm) than mature megakaryocytes, with high N/C ratio, one round lobe, horseshoe-shaped or slightly lobulated nucleus, variably clumped chromatin, and deeply basophilic cytoplasm with cytoplasmic blebbing
Mature megakaryocyte	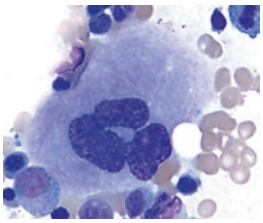	The largest hematopoietic cells (20–160 μm) with variable size and shape, more abundant pink cytoplasm with abundant azurophilic granules, and highly folded and connected nuclei with multilobation (2–16 lobes) on later stage of maturation, clumped chromatin, and no nucleoli
Platelet	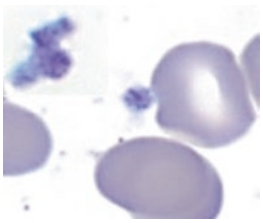	The most mature and smallest (2–4 μm) megakaryocytic cells, with pale to gray-blue cytoplasm, no nucleus, and dispersed purple to red azurophilic granules

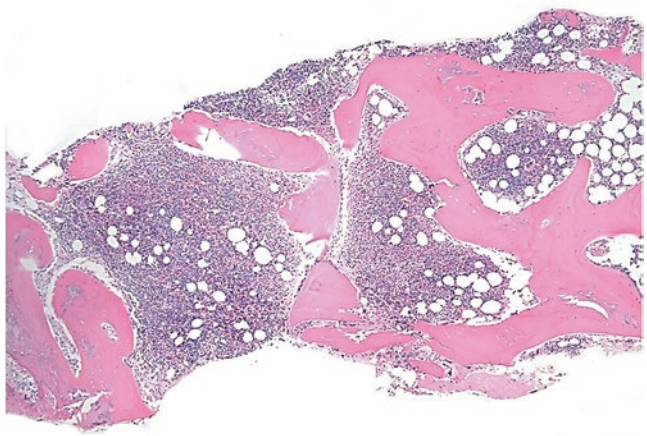

Fig. 1.1 Bone marrow core biopsy from a 4-year-old boy shows a good quality with adequate size, cortical bone, and several intertrabecular spaces with hematopoietic cells and adipose cells. The marrow cellularity is estimated by the percentage of hematopoietic cells in the total volume of marrow space; it declines with age, showing the highest cellularity in an infant or a young child and the lowest in an elderly person. In this slide, the bone marrow space is occupied by approximately 90% cellularity with hematopoietic cells and approximately 10% by adipose cells, which is normal cellularity for the age of 4 years

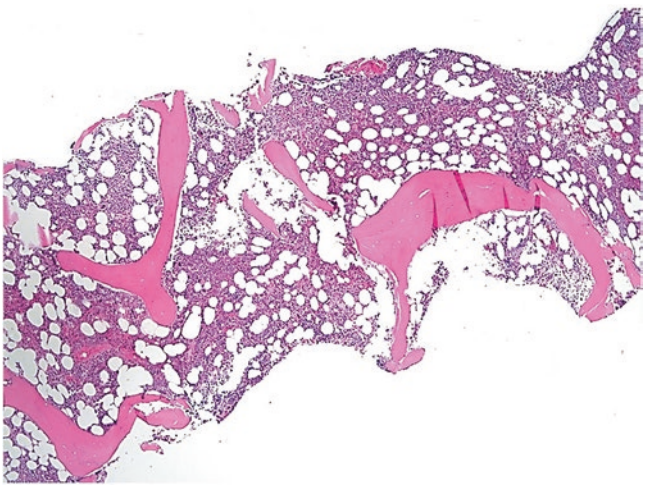

Fig. 1.2 Bone marrow core biopsy from a 42-year-old woman shows that the marrow space is occupied by approximately 50—60% hematopoietic cells with trilineage hematopoiesis and approximately 40—50% adipose cells, which is normal cellularity for the age of 42 years

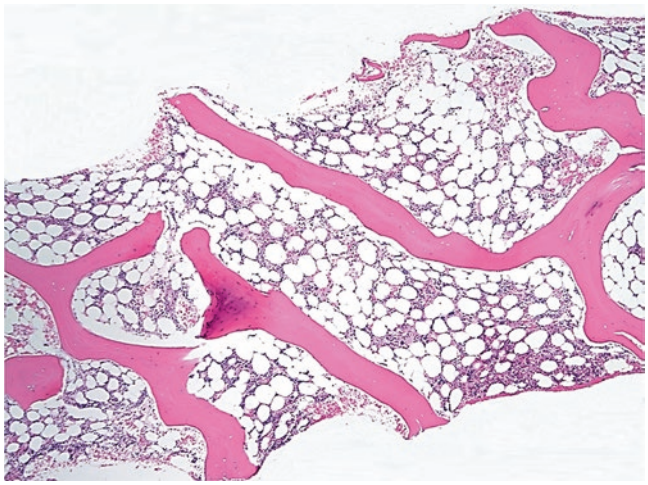

Fig. 1.3 Bone marrow core biopsy from a 78-year-old man shows that the marrow space has significantly reduced hematopoietic cells (approximately 20%), which are replaced by adipose cells (approximately 80%). The cellularity in this figure is normal for the age of 78 years

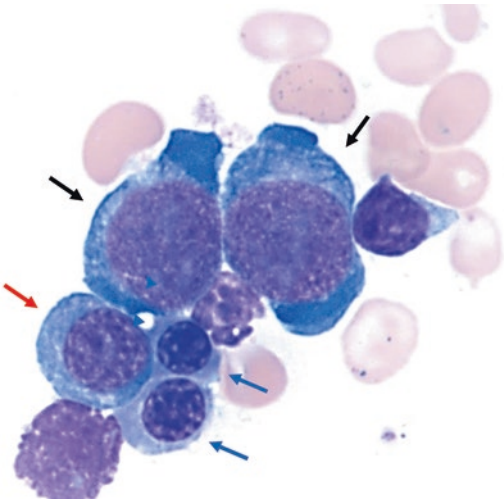

Fig. 1.4 Bone marrow aspirate smear shows various stages of maturation in erythroid precursors. The two largest cells (*black arrow*) are pronormoblasts (or proerythroblasts), the most immature erythroid cells, which are characterized by intensely basophilic cytoplasm, a large nucleus with immature chromatin, and few prominent nucleoli. A basophilic normoblast (*red arrow*), the cell in the next stage of erythroid maturation, is smaller than pronormoblasts but has basophilic cytoplasm owing to abundant RNA, slightly condensed chromatin, and visible nucleoli. Two cells in the bottom (*blue arrow*) are polychromatophilic normoblasts, which can be differentiated from basophilic normoblasts by their smaller size, gray cytoplasmic color related to an accumulation of hemoglobin, significantly condensed chromatin with clumping, and absent nucleoli. A mature lymphocyte is also shown

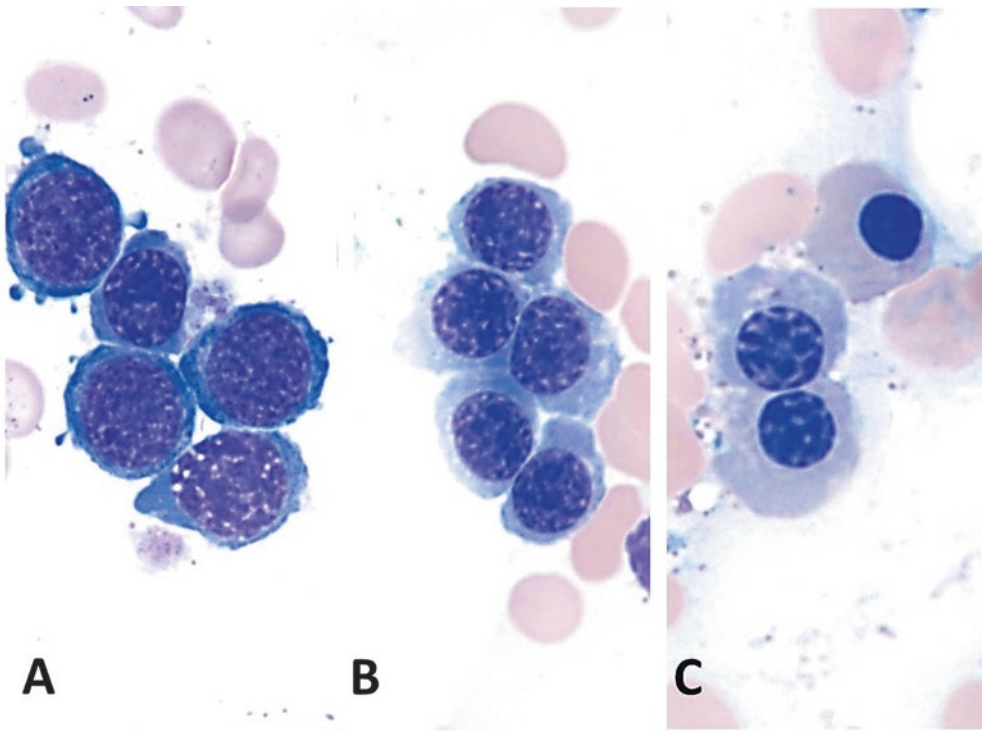

Fig. 1.5 A spectrum of maturing erythroid precursors in bone marrow aspirate smears. (**A**) Basophilic normoblasts. (**B**) Polychromatophilic normoblasts. (**C**) Orthochromic normoblasts. As erythroid precursors mature, a gradual change in cytoplasm from deep blue to gray-blue to pink-orange color, with progressive maturation of nuclear chromatin from less condensed to significantly clumped to very dense and homogeneous chromatin, and a slight reduction in the size of the cells

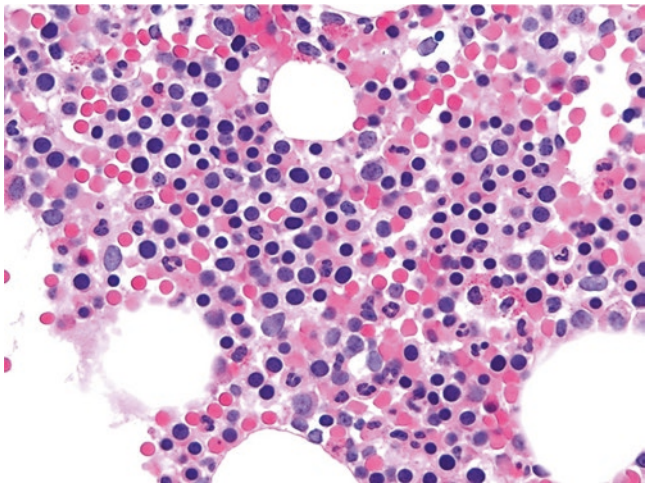

Fig. 1.6 Bone marrow core biopsy shows normal hematopoietic cells with prominent erythroid precursors in the marrow space. Erythroid precursors can be differentiated from other hematopoietic cells by their distinct round nuclear contours and very dense, homogenous nuclear chromatin

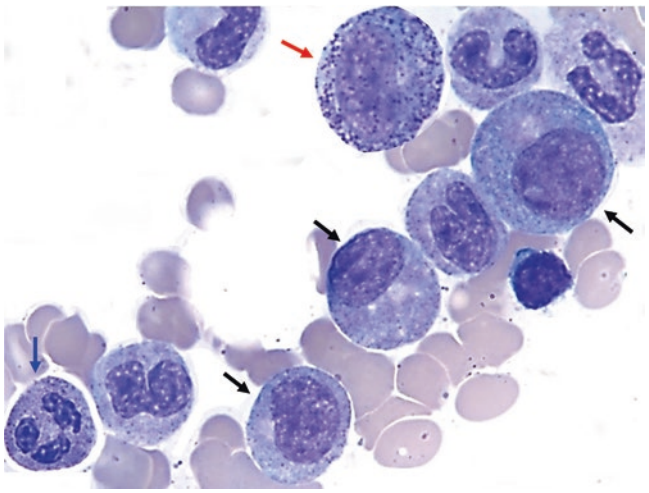

Fig. 1.8 Bone marrow aspirate smear shows various stages of maturing granulocytic cells. One promyelocyte (*red arrow*), three myelocytes (*black arrow*), four band neutrophils (*no arrow*), and one segmented neutrophil (*blue arrow*) are shown. The promyelocyte has basophilic cytoplasm with a paranuclear hof, an eccentric, round to oval nucleus, visible nucleoli, and distinct, prominent, and coarse azurophilic (primary) granules overlying the nucleus and cytoplasm. The myelocytes have a similar or slightly smaller size, a similar eccentric, round to oval nucleus, and a paranuclear hof corresponding to Golgi apparatus, but they have more condensed chromatin and blue to pink cytoplasm with abundant lilac (secondary) granules. Band and segmented neutrophils can be differentiated by the shape of their nucleus and chromatin. The segmented neutrophil has more condensed nuclear chromatin with clumping and nuclear lobes that are connected by thin filaments; the band neutrophils have a band-shaped, sausage-shaped, C-shaped, or U-shaped nucleus

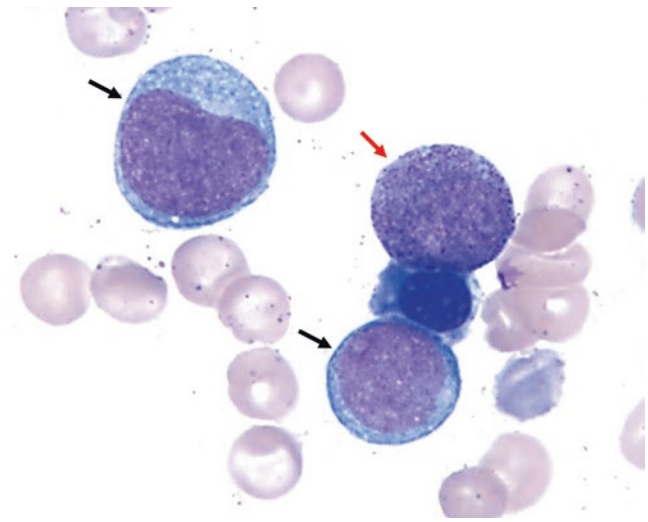

Fig. 1.7 Bone marrow aspirate smear shows two myeloblasts (*black arrow*), one promyelocyte (*red arrow*), and one polychromatophilic normoblast (*no arrow*). Myeloblasts, the most immature granulocytic cells, have an intermediate to large size, a high nuclear to cytoplasmic (N/C) ratio, moderate basophilic cytoplasm, a round nucleus, fine, uniform chromatin, and several nucleoli. Promyelocytes can be similar or slightly larger in size than blasts, with a high N/C ratio, a round nucleus with slightly coarse chromatin and visible nucleoli, and basophilic cytoplasm with a paranuclear hof; however, they have prominent azurophilic granules in the cytoplasm and overlying the nucleus, which often obscure the nucleus border

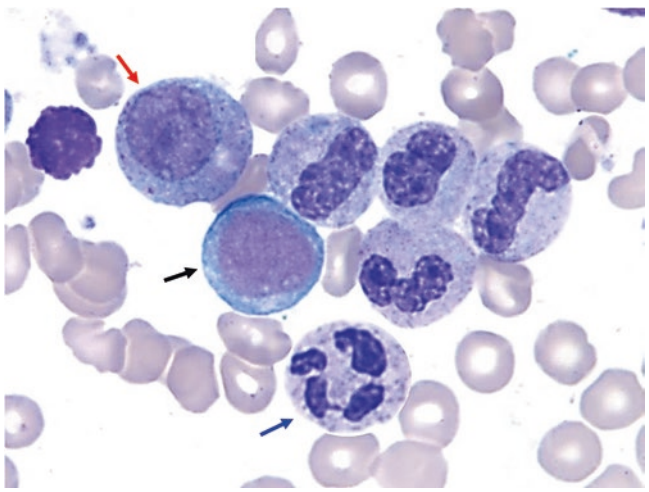

Fig. 1.9 Bone marrow aspirate smear shows a spectrum of maturing granulocytic cells. One myeloblast (*black arrow*), one myelocyte (*red arrow*), four band neutrophils (*no arrow*), and one segmented neutrophil (*blue arrow*) are shown. Band neutrophils often can be difficult to differentiate from segmented neutrophils because their nucleus can be folded or twisted, as shown in this figure. The constricted, thin filaments between nuclear lobes can be seen only in segmented neutrophils

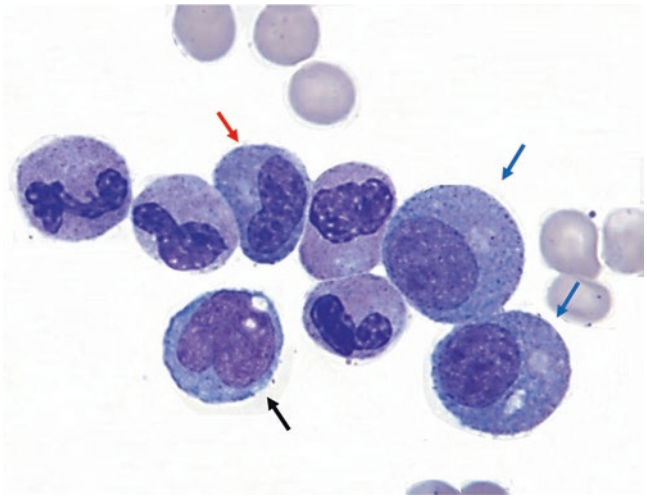

Fig. 1.10 Bone marrow aspirate smear shows various stages of maturing granulocytic cells and one monocyte. Two myelocytes (*blue arrow*), one metamyelocyte (*red arrow*), and four band neutrophils are shown. The metamyelocyte (*red arrow*) can be differentiated from a band neutrophil by its nuclear shape. The nucleus of a metamyelocyte is indented or kidney-shaped and has less indentation (less than half the width of the nucleus) compared with the nucleus of band neutrophils, which has an indentation greater than half of the width of the farthest margin. The monocyte (*black arrow*) is a large cell (10–20 μm) with round to oval shape and abundant gray to gray-blue cytoplasm (N/C ratio 2:1–4:1) with azurophilic granules and/or vacuoles, a round to indented, lobulated, or irregular nucleus, clumped chromatin that is less dense than in neutrophils, and no nucleoli

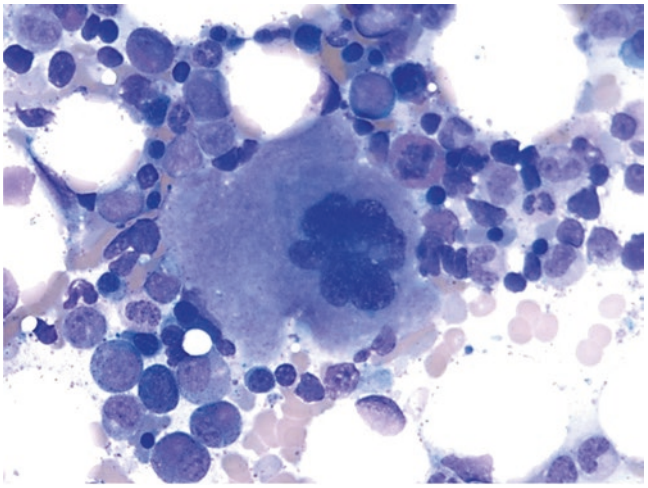

Fig. 1.12 Bone marrow aspirate smear shows a large, mature megakaryocyte, with other hematopoietic cells surrounding the megakaryocyte. As shown here, the megakaryocyte is the largest hematopoietic cell in the marrow and it is pleomorphic; it has abundant pink cytoplasm with numerous azurophilic granules that can produce platelets, and it has clumped nuclei with multiple lobes generated by endomitosis. The multiple nuclear lobes are connected by fine chromatin threads and often are highly folded or overlying other nuclear lobes

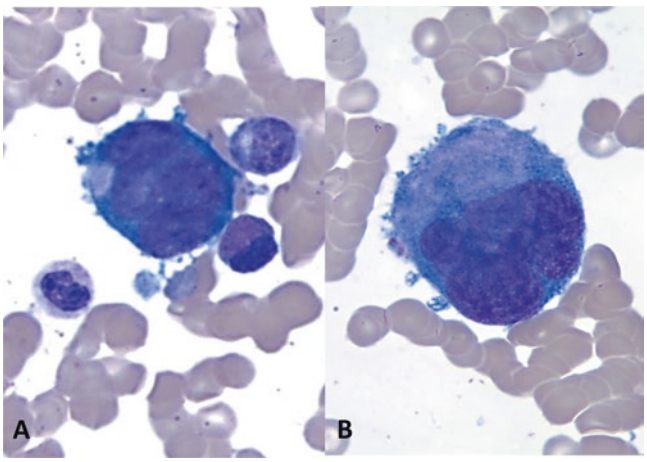

Fig. 1.11 (**A**) and (**B**). Bone marrow aspirate smears show two immature megakaryocytes with larger size than neutrophils, high N/C ratio, deep basophilic cytoplasm, non-lobulated or less-lobulated nucleus, and cytoplasmic blebs. Megakaryocytes in the early, immature stage can have nucleoli. These cells lack cytoplasmic granules, which are seen in mature megakaryocytes

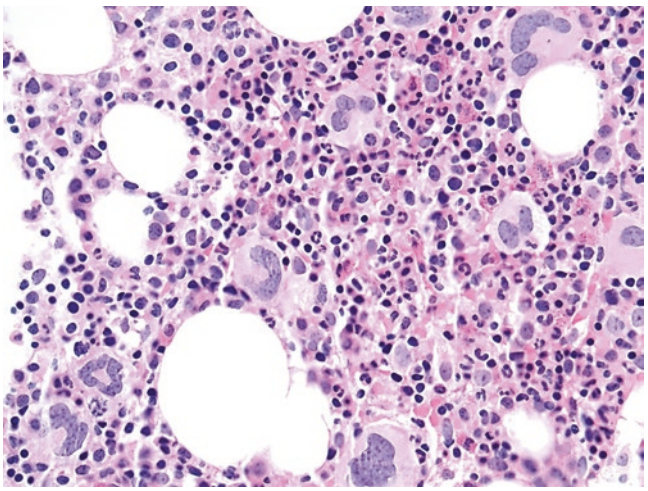

Fig. 1.13 Bone marrow core biopsy shows multiple mature megakaryocytes and other hematopoietic cells. Mature megakaryocytes are very large and pleomorphic, showing variable numbers of nuclear lobes and abundant pink cytoplasm. Megakaryocytes can be readily identified adjacent to sinuses in the marrow

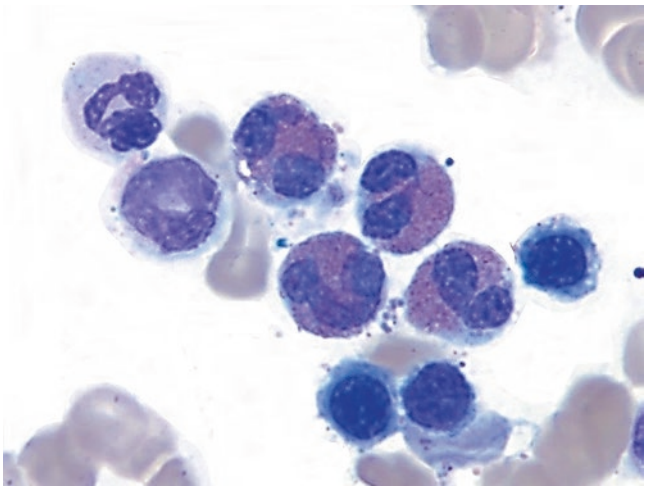

Fig. 1.14 Bone marrow aspirate smear shows four mature eosinophils in the center of the image. Eosinophils (10–17 μm) have abundant cytoplasm with numerous coarse, bright red to orange refractile granules of uniform size, segmented nuclei with two or three lobes connected by thin filaments of chromatin, and coarsely clumped nuclear chromatin

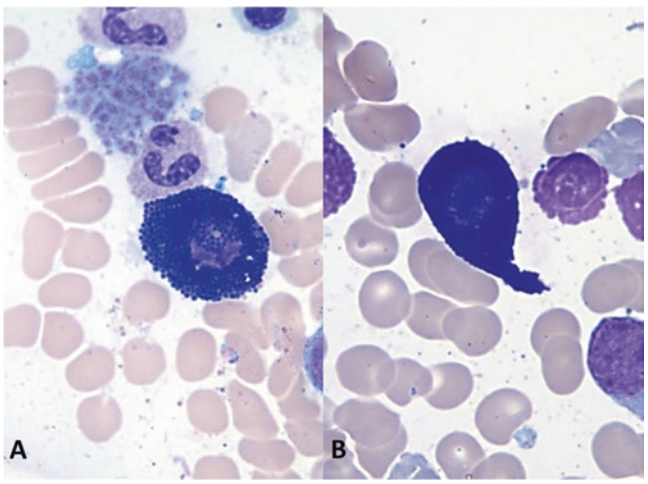

Fig. 1.16 (**A**) and (**B**). Bone marrow aspirate smears illustrate two mast cells. Mast cells (12–30 μm), called *tissue basophils*, are connective tissue cells of hematopoietic origin. Mast cells are round to oval-shaped cells with a single small, round nucleus and abundant cytoplasm packed with numerous coarse, round purple to bluish-dark metachromatic granules overlying and obscuring the border of the nucleus and cytoplasm. Mast cells are approximately twice as large as blood basophils and have more abundant cytoplasm, a round nucleus, and numerous round, uniform basophilic granules obscuring the nucleus and often extending out to the cytoplasm

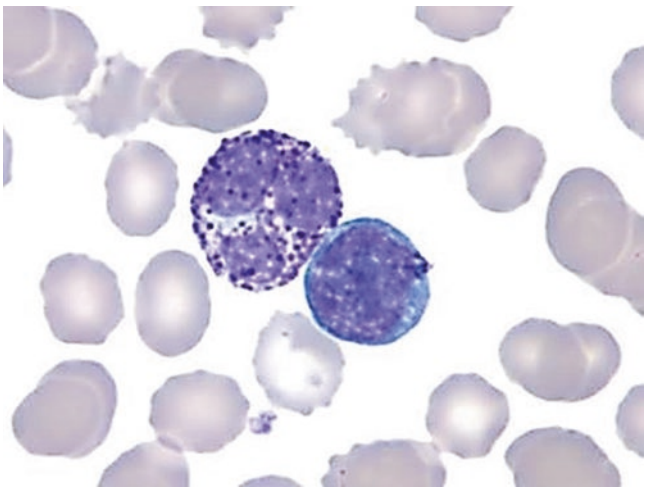

Fig. 1.15 Bone marrow aspirate smear shows a mature basophil (on the left) and a lymphocyte. Basophils (10–15 μm) have abundant cytoplasm with coarse, dense, purple to dark granules, which vary in size and shape, are unevenly distributed in the cytoplasm, overlie the nucleus, and obscure segmented nuclei with two or three lobes. Cells morphologically resembling basophils are segmented neutrophils with toxic granulation or mast cells

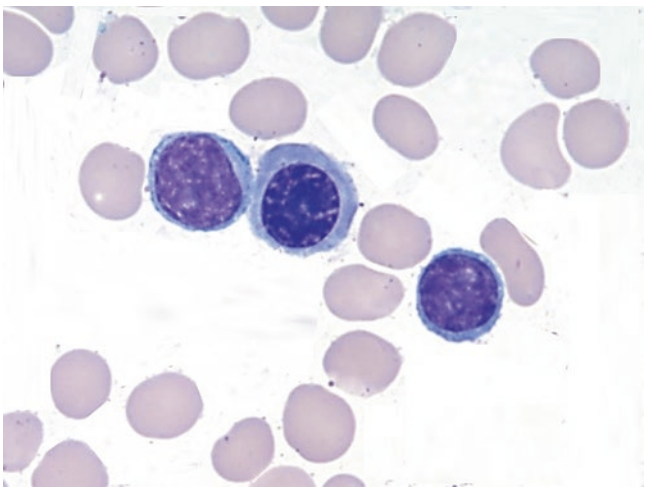

Fig. 1.17 Bone marrow aspirate smear shows two mature lymphocytes, with one polychromatophilic normoblast in the center of the image. Lymphocytes are small cells (7–15 μm) with a single, round, ovoid, or slightly indented nucleus, a scant to moderate amount of cytoplasm (N/C ratio 2:1 to 5:1), pale blue color, and sometimes a perinuclear halo, diffusely dense chromatin, and no visible nucleoli. Some larger lymphocytes may have variable numbers of coarse, azurophilic granules in the cytoplasm

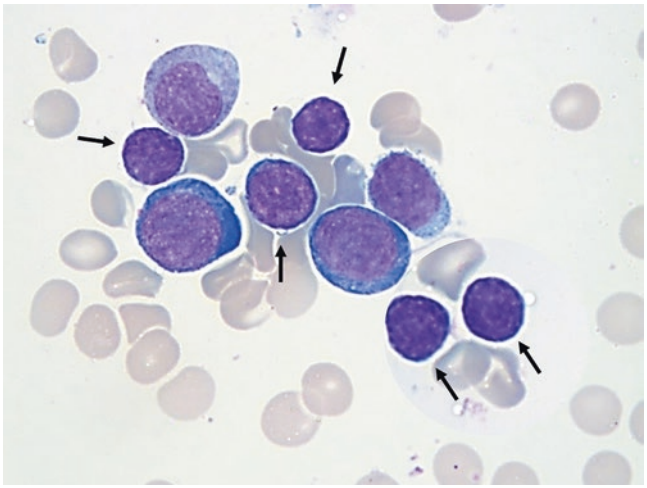

Fig. 1.18 Bone marrow aspirate smear shows five hematogones (*black arrow*) in a young child. Also present are one mature lymphocyte, two basophilic normoblasts, and one myelocyte. Hematogones are small- to intermediate-sized cells with very scant cytoplasm, a round to slightly irregular nucleus, dense homogenous chromatin, and indistinct nucleoli. Hematogones are benign lymphocyte precursors encountered in the bone marrow of an infant or a young child, associated with solid tumors, after aggressive chemotherapy or transplantation, or in an immunosuppressed state. By morphology, hematogones are often difficult to differentiate from lymphoblasts in acute lymphoblastic leukemia. Characteristic immunophenotype as well as certain clinical conditions can help to make a correct identification of hematogones

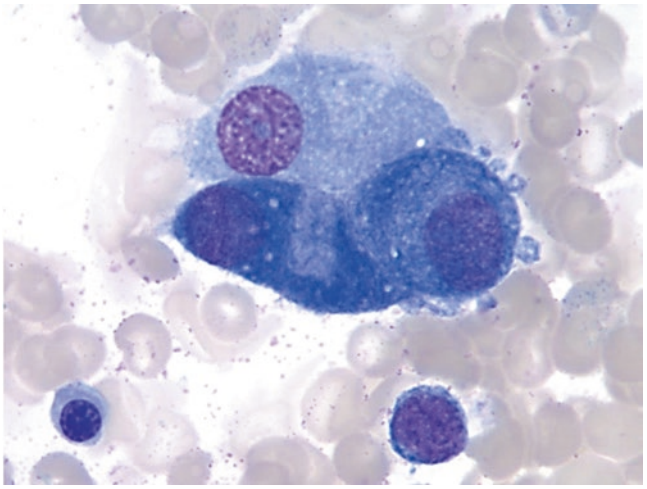

Fig. 1.20 Bone marrow aspirate smear shows a small cluster of osteoblasts. Osteoblasts, bone-forming cells, are large cells (20–50 μm) with an oval, comet, or tadpole shape, abundant deep basophilic cytoplasm with indistinct borders, an eccentrically located or partially extruded, single round to oval nucleus with reticular chromatin, prominent Golgi apparatus, called the *hof*, or pale, staining cytoplasm away from the nucleus, and one or more nucleoli. Osteoblasts can be differentiated from plasma cells by their large size, the prominent hof away from the nucleus, and their often indistinct cytoplasmic borders. Osteoblasts can be seen as small clusters in growing children or adolescents

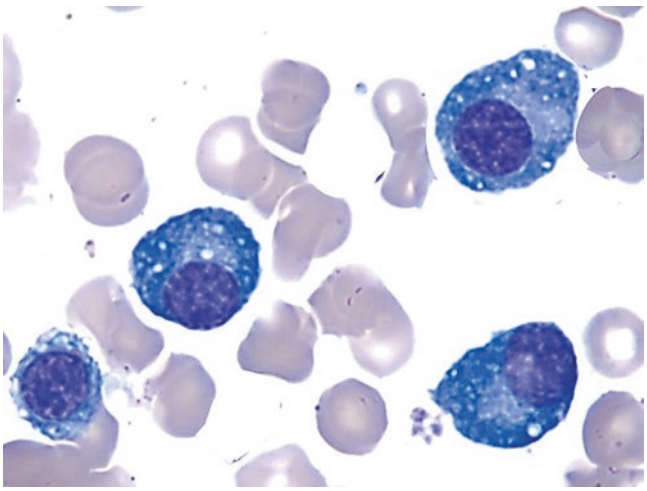

Fig. 1.19 Bone marrow aspirate smear shows three mature plasma cells as well as one polychromatophilic normoblast (left bottom). Plasma cells are medium-sized (8–20 μm), round to oval cells with a moderate amount of deep basophilic cytoplasm, an eccentric, round nucleus, coarse, clumped chromatin, often with a wheel-like pattern, a prominent perinuclear hof, called the Golgi zone, or pale staining in the perinuclear cytoplasm, sometimes with small cytoplasmic vacuoles and no nucleoli

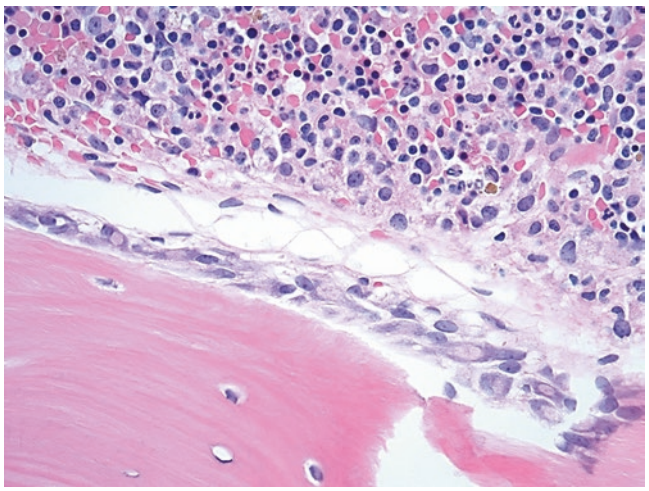

Fig. 1.21 Bone marrow core biopsy section from a child illustrates osteoblasts lining the trabecula, osteocytes within bone lacunae, and hematopoietic cells from immature granulocytic cells near the trabecula to maturing granulocytes and erythroid precursors in the central intramedullary region. Osteoblasts have an eccentric nucleus with distinct Golgi apparatus (hof) away from the nucleus; some show small nucleoli

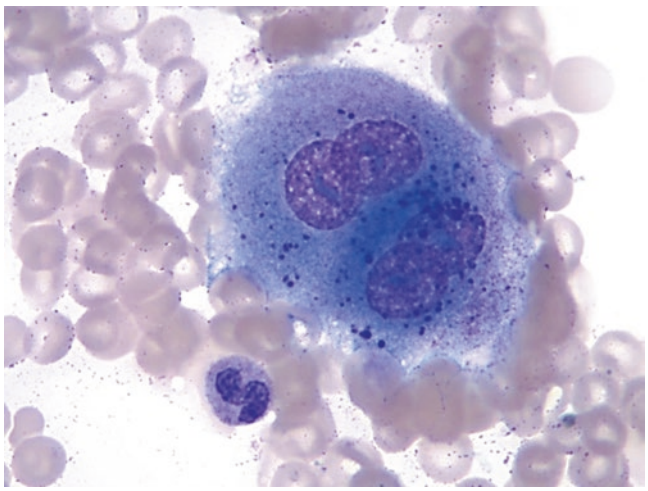

Fig. 1.22 Bone marrow aspirate smear shows an osteoclast and a segmented neutrophil. Osteoclasts, cells involved in the resorption of bone, are very large cells (> 100 μm) with oval to irregular shape, abundant cytoplasm, and coarse granules with variable blue, reddish-purple, or pale pink staining; distinct, multiple nuclei, which are relatively uniformly shaped and widely separated with reticular chromatin, and one or more prominent nucleoli. As multinucleated, giant cells, osteoclasts need to be differentiated from megakaryocytes, metastatic tumor cells, and macrophages. Osteoclasts differ from megakaryocytes by their large size, widely separated nuclei, and coarse cytoplasmic granules with variable staining

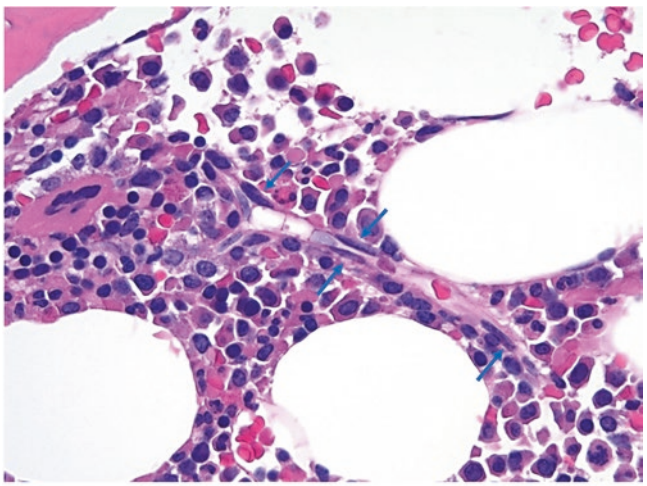

Fig. 1.24 Bone marrow core biopsy section shows endothelial cells lining a sinusoid and trilineage hematopoietic maturation. *Blue arrows* indicate the nucleus of the endothelial cells. Endothelial cells lining sinuses or capillaries are large, elongated cells (20–30 μm) with a moderate amount of pink to light blue cytoplasm, an oval to elongated nucleus with tapering of both ends of the nucleus, dense chromatin, and small, variable nucleoli

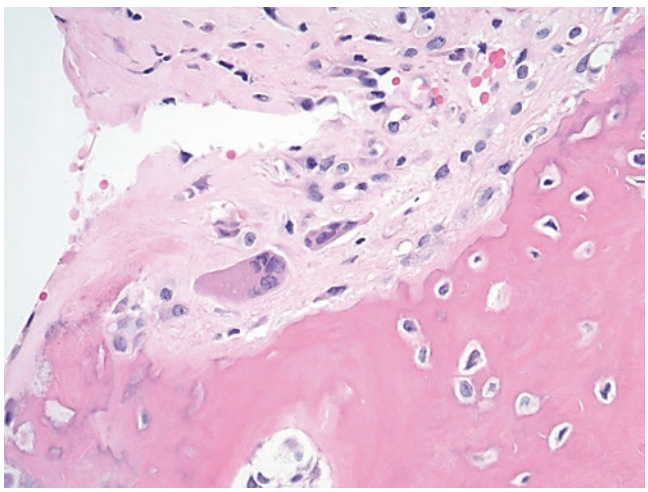

Fig. 1.23 Bone marrow core biopsy section from a child shows two large osteoclasts with multiple separate nuclei and abundant cytoplasm, adjacent to bone trabecula

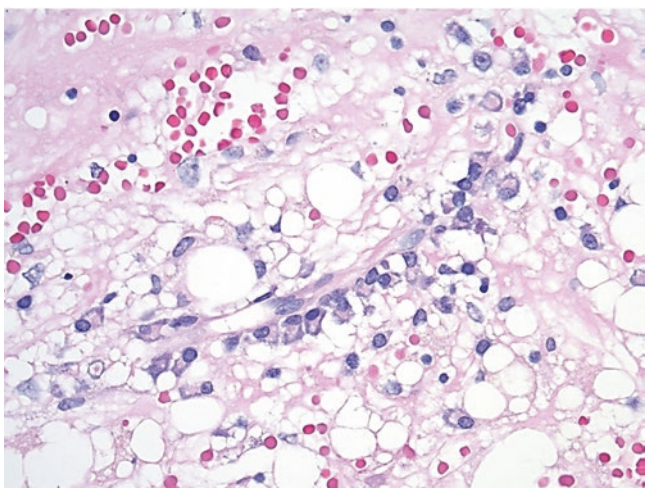

Fig. 1.25 Bone marrow core biopsy section shows marrow stroma composed of sinusoid, endothelial cells, plasma cells (scattered as single cells or in a perivascular location), histiocytes, lymphocytes, and adipose cells in a hypocellular marrow

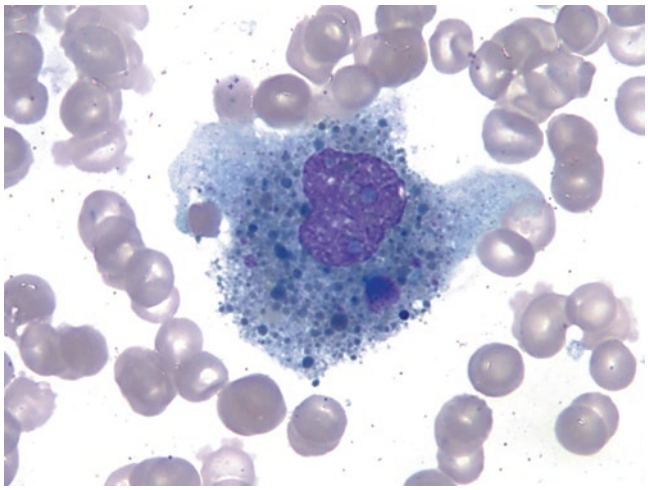

Fig. 1.26 Bone marrow aspirate smear shows a macrophage (or histiocyte). Macrophages involved in phagocytosis are large cells (15–80 μm) with an irregular shape and shaggy margins, abundant blue to pale-pink cytoplasm with large, amorphous debris or phagocytosed materials, often vacuoles, azurophilic granules and pseudopodia, an eccentric nucleus with reticulated chromatin, and one or more small nucleoli

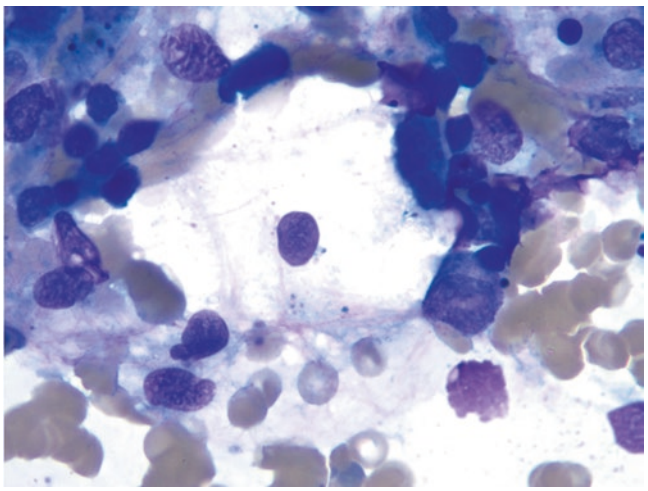

Fig. 1.28 Bone marrow aspirate smear shows a large adipocyte (adipose cell) at the center, surrounded by hematopoietic cells. Adipocytes are very large (25–80 μm), with abundant pale blue to colorless cytoplasm containing numerous large fat vacuoles and delicate eosinophilic fibrils. They often have an eccentric, small, oval to round nucleus, dense chromatin, and small nucleoli

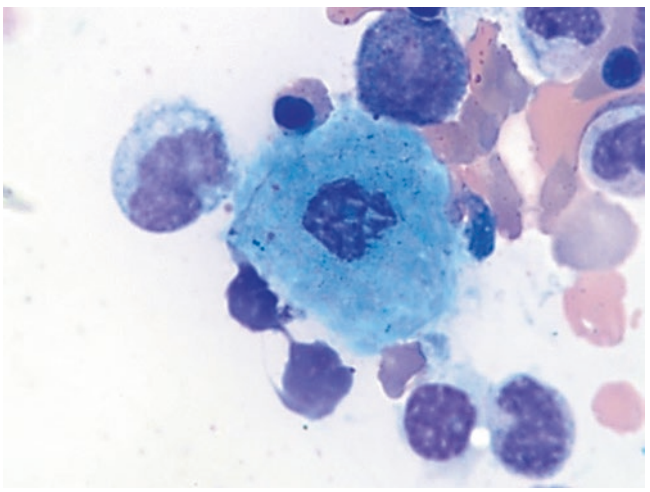

Fig. 1.27 Bone marrow aspirate smear shows a sea-blue histiocyte at the center. This histiocyte (20–60 μm) has abundant cytoplasm with variably blue or blue-green pigments or globules that contain an insoluble lipid pigment called *ceroid*. Small numbers of sea-blue histiocytes can be observed in normal bone marrow

Suggested Reading

1. Bain BJ. The bone marrow aspirate of healthy subjects. Br J Haematol. 1996;94:206–9.
2. Bain BJ. Bone marrow trephine biopsy. J Clin Pathol. 2001;54:737–42.
3. Brown DC, Gatter KC. The bone marrow trephine biopsy: a review of normal histology. Histopathology. 1993;22:411–22.
4. CAP Hematology and Clinical Microscopy Resource Committee. In: Glassy EF, editor. Color atlas of hematology: An illustrated field guide based on proficiency testing. Northfield: College of American Pathologists; 1998. ISBN: 0-930304-66-7.
5. Chasis JA, Mohandas N. Erythroblastic islands: niches for erythropoiesis. Blood. 2008;112:470–8.
6. Deutsch VR, Tomer A. Megakaryocyte development and platelet production. Br J Haematol. 2006;134:453–66.
7. De Wolf-Peeters C. Bone marrow trephine interpretation: diagnostic utility and potential pitfalls. Histopathology. 1991;18:489–93.
8. Foucar K. Hematopoiesis. Morphologic review of blood and bone marrow. In: Foucar K, Reichard K, Czuchlewski D, editors. Bone marrow pathology, vol. 1. 3rd ed. Chicago: Chicago American Society for Clinical Pathology; 2010. p. 3–52.
9. Gulati GL, Ashton JK, Hyun BH. Structure and function of the bone marrow and hematopoiesis. Hematol Oncol Clin North Am. 1988;2:495–511.
10. Hyun BH, Stevenson AJ, Hanau CA. Fundamentals of bone marrow examination. Hematol Oncol Clin North Am. 1994;8:651–63.
11. Jacobsson B, Bernell P, Arvidsson I, Hast R. Classical morphology, esterase cytochemistry, and interphase cytogenetics of peripheral blood and bone marrow smears. J Histochem Cytochem. 1996;44:1303–9.
12. Kaushansky K. Historical review: megakaryopoiesis and thrombopoiesis. Blood. 2008;111:981–6.
13. Riley RS, Hogan TF, Pavot DR, Forysthe R, Massey D, Smith E, et al. A pathologist's perspective on bone marrow aspiration and biopsy: I. Performing a bone marrow examination. J Clin Lab Anal. 2004;18:70–90.
14. Riley RS, Williams D, Ross M, Zhao S, Chesney A, Clark BD, Ben-Ezra JM. Bone marrow aspirate and biopsy: a pathologist's perspective. II. Interpretation of the bone marrow aspirate and biopsy. J Clin Lab Anal. 2009;23:259–307.
15. Rimsza LM, Larson RS, Winter SS, Foucar K, Chong YY, Garner KW, Leith CP. Benign hematogone-rich lymphoid proliferations can be distinguished from B-lineage acute lymphoblastic leukemia by integration of morphology, immunophenotype, adhesion molecule expression, and architectural features. Am J Clin Pathol. 2000;114:66–75.
16. Ryan DH. Examination of the marrow. In: Kaushansky K, Beutler E, Seligsohn U, Lichtman MA, Kipps TJ, Prchal JT, editors. Williams hematology. 8th ed. New York: McGraw-Hill; 2010. p. 25–36.

Reactive Changes

2

Rebecca L. King and Matthew T. Howard

Recognition of bone marrow pathology requires an understanding not only of normal marrow cytology and architecture but also of the myriad ways in which the marrow can change in response to extramedullary insults or stimuli. Reactive marrow changes can be quantitative (hyperplasia or hypoplasia) or qualitative (left-shifted maturation, cytologic atypia), and they can affect one or multiple hematopoietic lineages as well as the lymphoid, histiocytic, or stromal marrow compartments (Figs. 2.1, 2.2, 2.3, 2.4, 2.5, 2.6, 2.7, 2.8, 2.9, 2.10, 2.11, 2.12, 2.13, 2.14, 2.15, 2.16, 2.17, 2.18, 2.19, 2.20, 2.21, 2.22, 2.23, 2.24, 2.25, 2.26, 2.27, 2.28, 2.29, 2.30, 2.31, 2.32, 2.33, 2.34, 2.35, 2.36, 2.37, 2.38, 2.39, 2.40, 2.41, 2.42, 2.43, 2.44, 2.45, 2.46, 2.47, and 2.48).

Causes of reactive bone marrow changes typically originate outside of the marrow itself. The differential diagnosis for many of the changes illustrated includes autoimmune disease (Figs. 2.3, 2.4, 2.5, 2.18, 2.19, and 2.26), nutritional deficiency or excess (Figs. 2.10, 2.11, 2.12, 2.13, 2.14, 2.15, 2.15, 2.16, and 2.17), toxic insults, medications (*see* Chap. 3), and infections (*see* Chap. 5; Fig. 2.22).

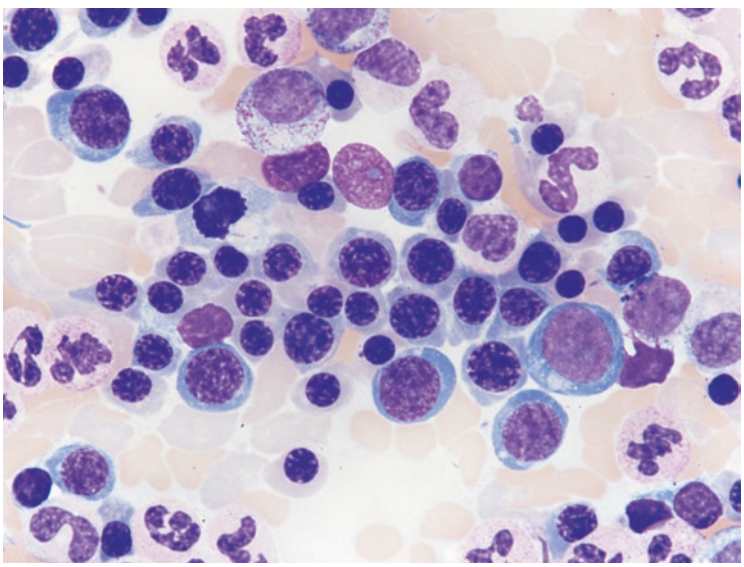

Fig. 2.1 Erythroid hyperplasia can be seen as a normal response to anemias of various causes, particularly those involving peripheral red blood cell (RBC) destruction, sequestration, or bleeding. Increased erythropoietin secretion, from either a normal physiologic response to a hypoxic state or inappropriate secretion by various tumors, may also lead to erythroid hyperplasia. This bone marrow aspirate is from a female patient with metastatic renal cell carcinoma with a hemoglobin of 19.0 g/dL. The serum erythropoietin level was markedly elevated. A bone marrow biopsy was undertaken to exclude a myeloproliferative neoplasm such as polycythemia vera. Aspirate shows an erythroid predominance, but with complete maturation and without cytologic atypia. Molecular studies for *JAK2*, *CALR*, and *MPL* mutations were negative

R.L. King (✉) • M.T. Howard
Division of Hematopathology, Mayo Clinic, Rochester, MN, USA
e-mail: rebecca.king98@gmail.com; howard.matthew@mayo.edu

T.I. George, D.A. Arber (eds.), *Atlas of Bone Marrow Pathology*, Atlas of Anatomic Pathology,
https://doi.org/10.1007/978-1-4939-7469-6_2

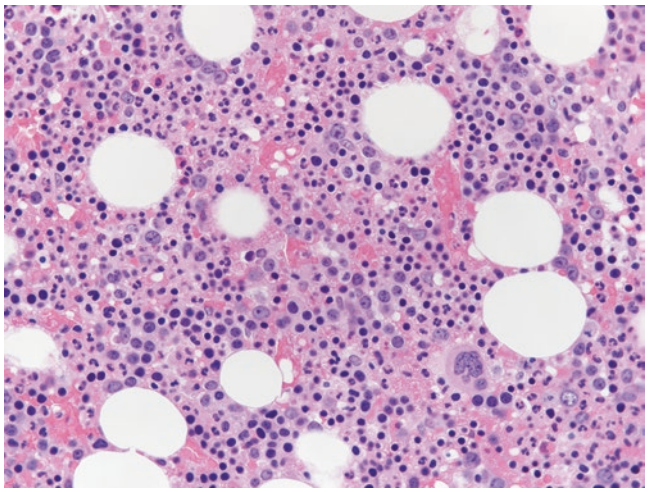

Fig. 2.2 The bone marrow core biopsy specimen from the patient described in Fig. 2.1 shows erythroid hyperplasia with increased numbers of erythroid islands, but with normal and complete maturation

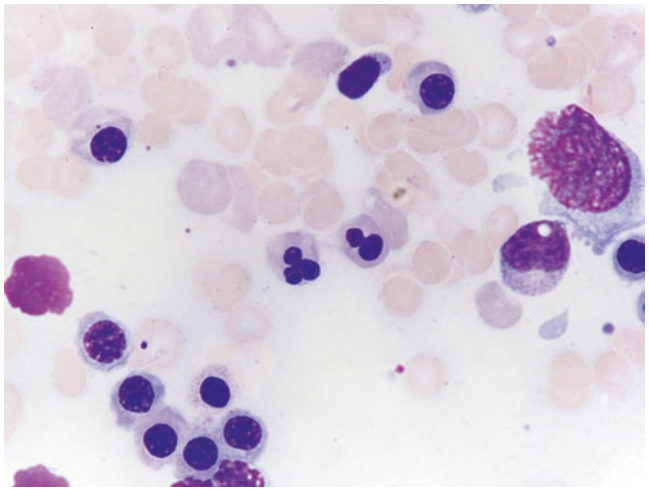

Fig. 2.4 Bone marrow aspirate in a patient with an autoimmune hemolytic anemia. Erythropoiesis may show striking cytologic atypia, akin to that seen in myelodysplasia ("stress dyserythropoiesis"). Shown here are erythroid precursors with nuclear irregularity and budding. Clinical history, as well as morphologic evaluation of the other lineages, is critical to avoid a misdiagnosis of myelodysplastic syndrome in this setting

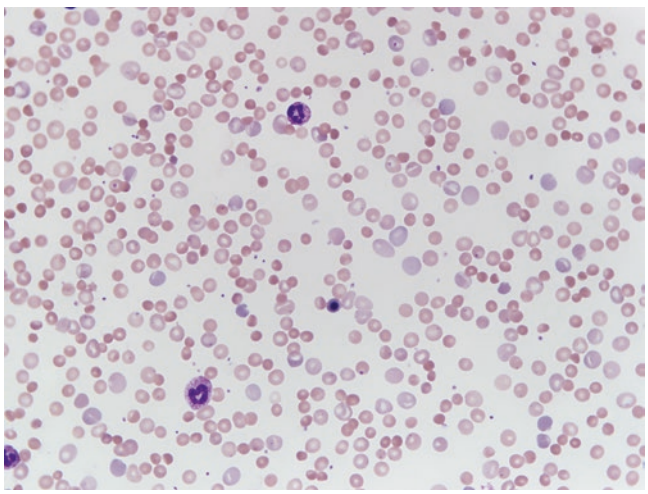

Fig. 2.3 Erythroid hyperplasia can accompany peripheral RBC destruction, as in this patient with an autoimmune hemolytic anemia. Peripheral blood smear showing marked increase in polychromatophilic RBCs, spherocytes, and circulating nucleated RBCs

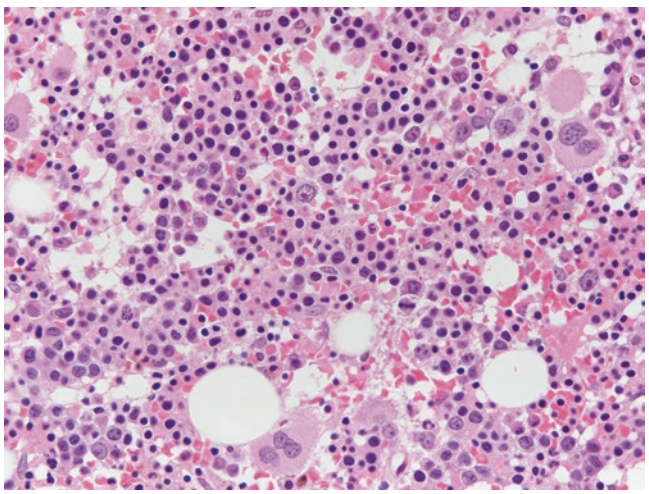

Fig. 2.5 Bone marrow biopsy in a patient with an autoimmune hemolytic anemia shows hypercellularity secondary to erythroid hyperplasia

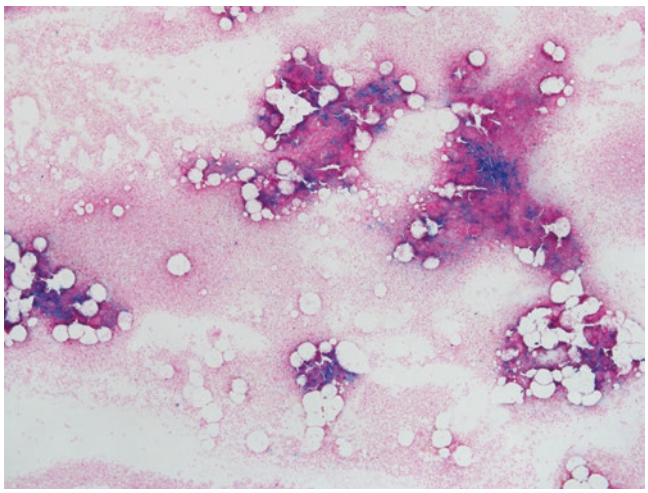

Fig. 2.6 Prussian blue iron stain on a bone marrow aspirate smear from a patient with anemia of chronic disease, showing increased storage iron (*blue*)

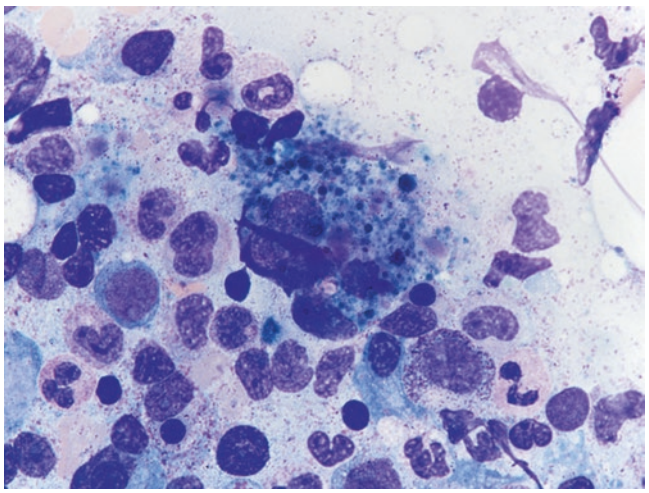

Fig. 2.8 Bone marrow aspirate in a patient with anemia of chronic disease. The macrophage contains chunky hemosiderin granules, which appear blue-black on Wright-Giemsa stain

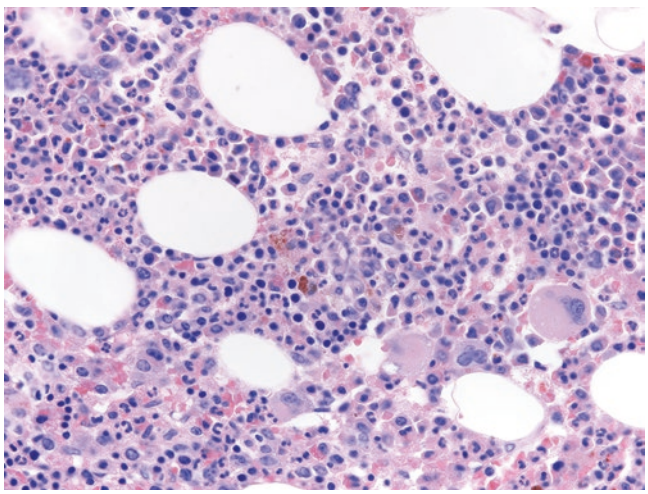

Fig. 2.7 Bone marrow core biopsy in a patient with anemia of chronic disease demonstrates increased hemosiderin-laden macrophages

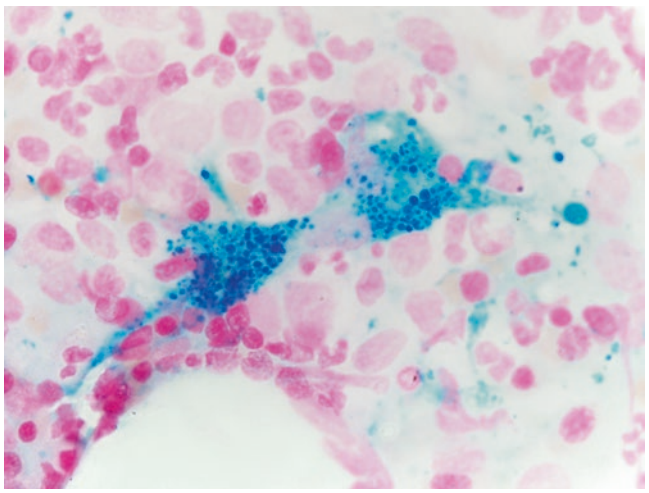

Fig. 2.9 This higher-power image of Prussian blue stain shows iron within a macrophage from the same patient as depicted in Fig. 2.8

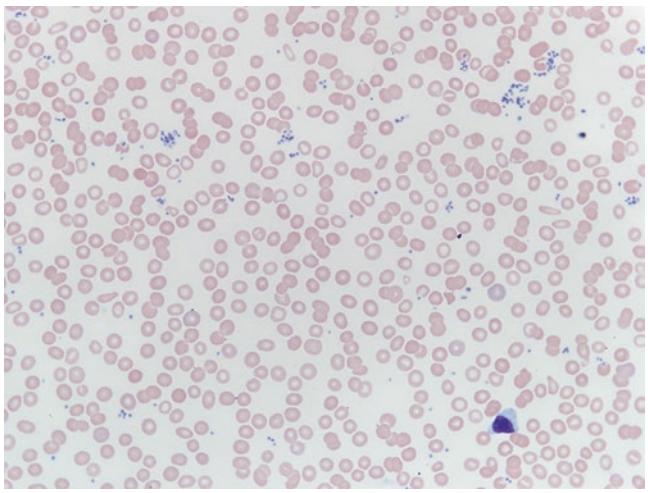

Fig. 2.10 Iron deficiency anemia is common and presents with typical CBC and peripheral smear findings, usually not requiring bone marrow biopsy. Shown here is an example of a peripheral blood smear in a patient with iron deficiency anemia (hemoglobin 9.2 g/dL, MCV 76.0 fL). Reactive thrombocytosis is often seen, along with characteristic elongated elliptocytes ("pencil cells") and hypochromic, microcytic RBCs

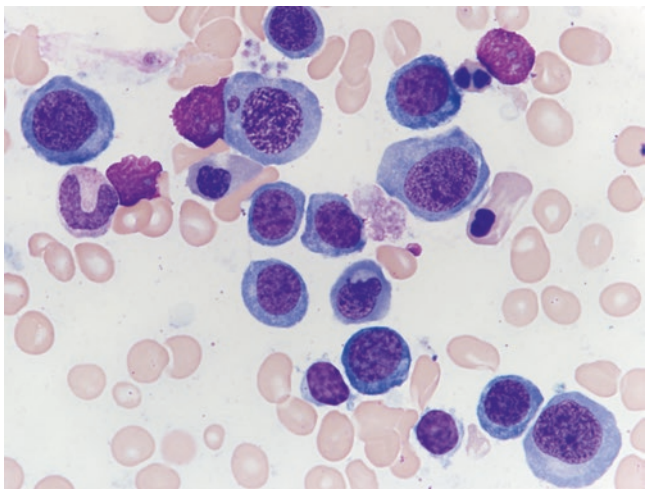

Fig. 2.12 Bone marrow aspirate in a patient with vitamin B12 deficiency and megaloblastic anemia (hemoglobin 7.3 g/dL, MCV 121.6 fL). Note the characteristic megaloblastic erythroid maturation. Erythroid precursors show nuclear-cytoplasmic dyssynchrony and are left shifted. Abnormally large nuclei show abnormal chromatin described as "sievelike," "sausage-like," or "ropey." Occasional nuclear budding and terminal dyserythropoiesis are also seen here and may be mistaken for a myelodysplastic process if the clinical history and other characteristic morphologic features are not appreciated

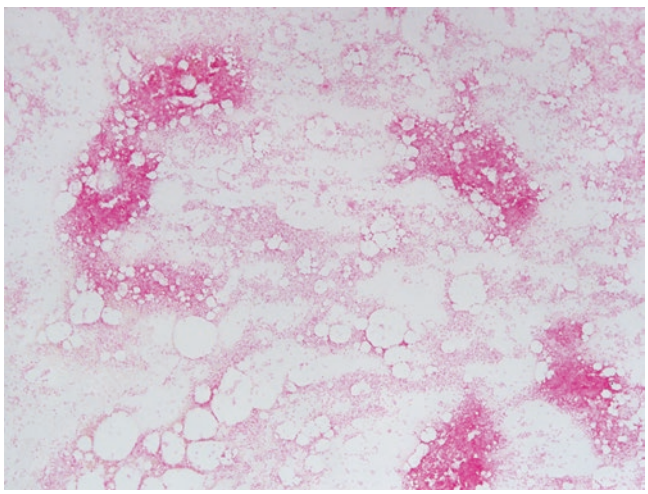

Fig. 2.11 Although bone marrow is not typically required for a diagnosis of iron deficiency anemia, a Prussian blue stain for iron on bone marrow aspirate is still considered the "gold standard" for assessment of iron deficiency [1]. Absence of stainable iron (*blue*) is shown here in a patient with iron deficiency anemia

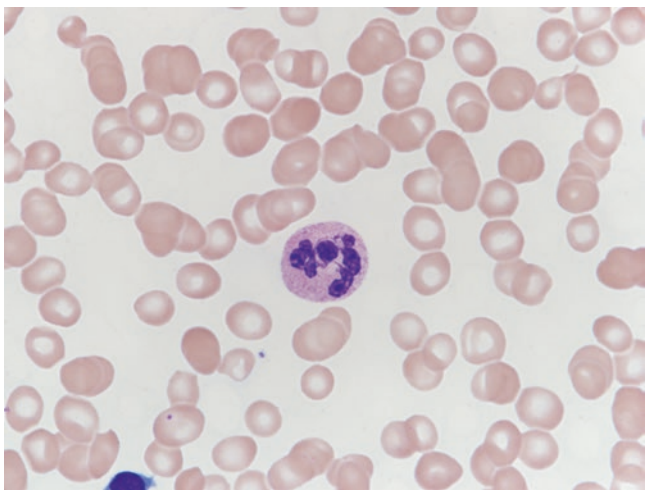

Fig. 2.13 In vitamin B12 deficiency, the granulocytic lineage is also affected, with hypersegmented neutrophils being a characteristic morphologic finding in the peripheral blood and sometimes in the bone marrow

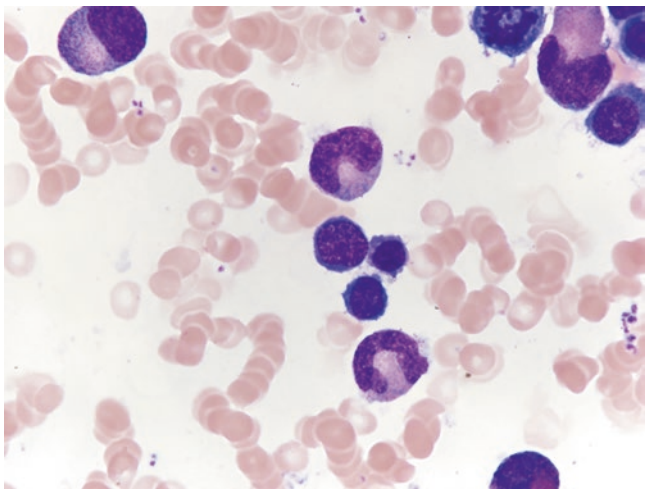

Fig. 2.14 Giant bands ("horseshoe") and metamyelocytes are another common feature of vitamin B12 deficiency

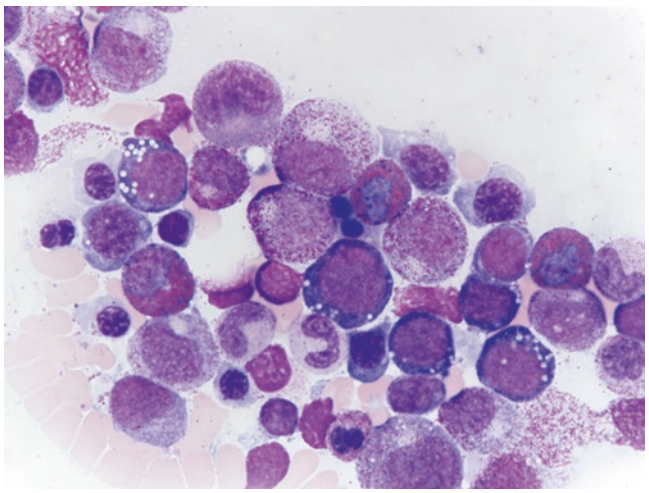

Fig. 2.16 Copper deficiency (often caused by over-ingestion of zinc) can cause cytopenias with peripheral blood and bone marrow features mimicking myelodysplastic syndrome. Erythroid hyperplasia with characteristic cytoplasmic vacuolization in both erythroid and granulocytic precursors is a hallmark finding

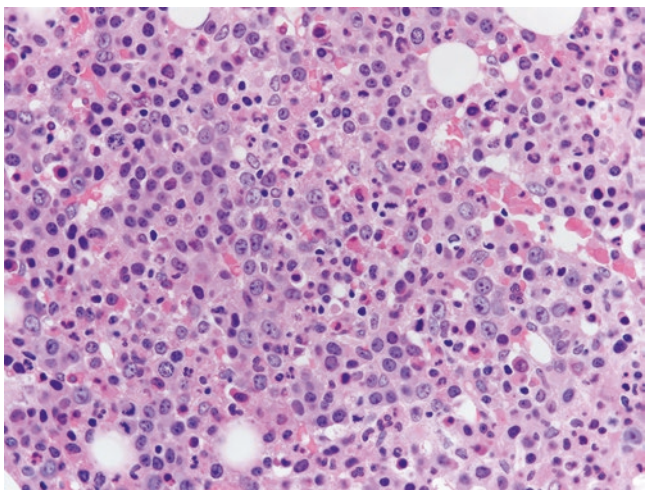

Fig. 2.15 The bone marrow core biopsy in vitamin B12 deficiency often is markedly hypercellular for the patient's age. Note the left-shifted appearance to the erythroid lineage, with prominent erythroblasts containing fine chromatin. Granulocytes are also left shifted, but with complete maturation. These features are nonspecific and could be misconstrued as a myeloid neoplasm

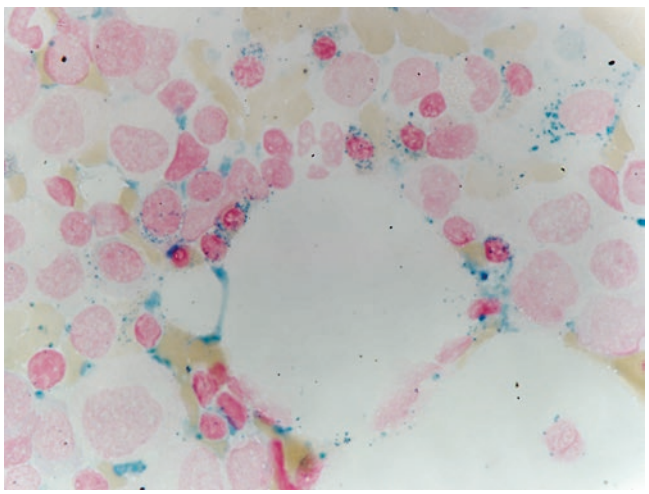

Fig. 2.17 Common findings in copper deficiency include increased storage iron and ring sideroblasts as shown in this Prussian blue stain, which can lead to misdiagnosis of myelodysplastic syndrome. Nonneoplastic causes of ring sideroblasts include alcoholism, medications (isoniazid), and lead poisoning, as well as congenital sideroblastic anemias [2] (*see* Chap. 4)

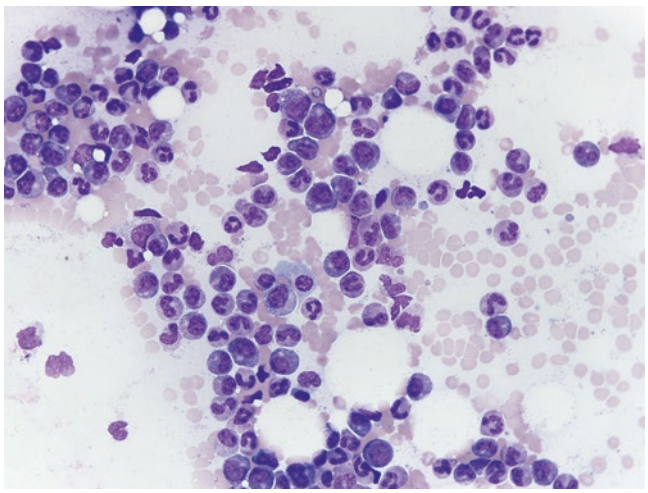

Fig. 2.18 An elevated myeloid to erythroid (M:E) ratio can occur if red cell production is depressed, often in autoimmune or paraneoplastic states. This bone marrow aspirate shows pure red cell aplasia in a patient with a thymoma

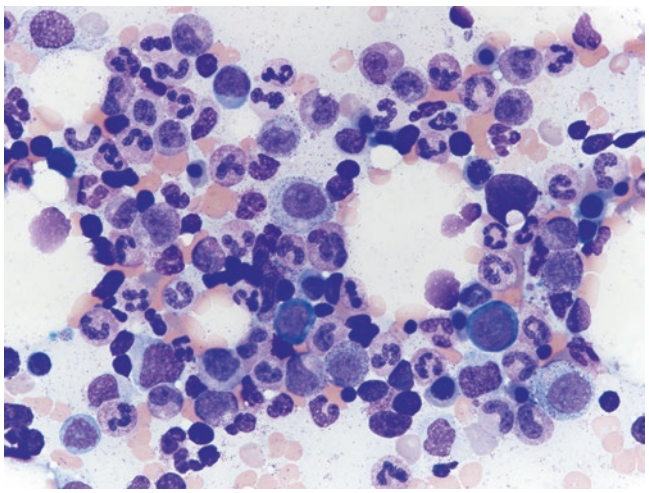

Fig. 2.20 Reactive granulocytic hyperplasia is characteristic of infections, especially bacterial sepsis, and can be seen in other inflammatory settings. Growth factor therapy, also described in Chap. 3, is also a common cause of granulocytic hyperplasia in patients receiving chemotherapy for hematopoietic neoplasms. This bone marrow aspirate shows granulocytic hyperplasia without significant left shift

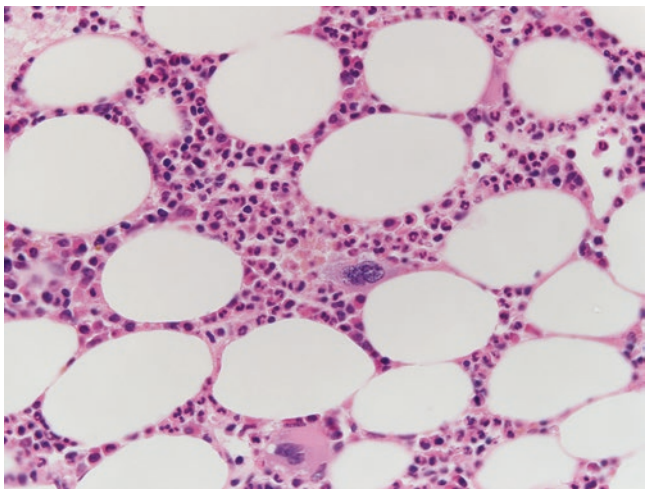

Fig. 2.19 The corresponding bone marrow biopsy specimen from Fig. 2.18 shows pure red cell aplasia in a patient with a thymoma

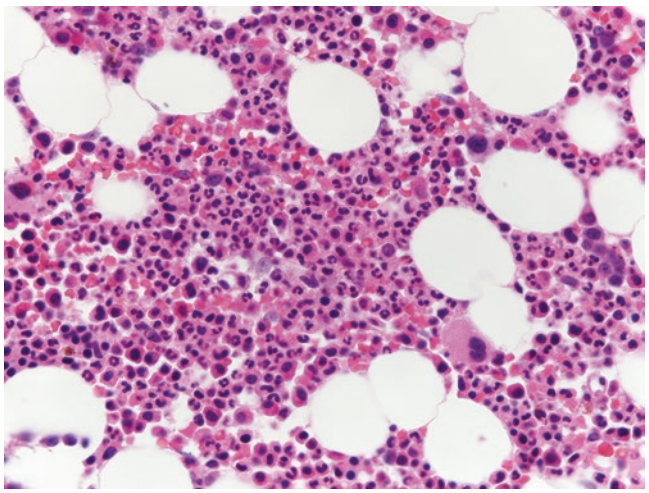

Fig. 2.21 This bone marrow biopsy from the same patient as shown in Fig. 2.20 shows granulocytic hyperplasia with increased numbers of mature granulocytes within the interstitium, away from the trabeculae. Erythroid precursors are also present but are relatively decreased in number

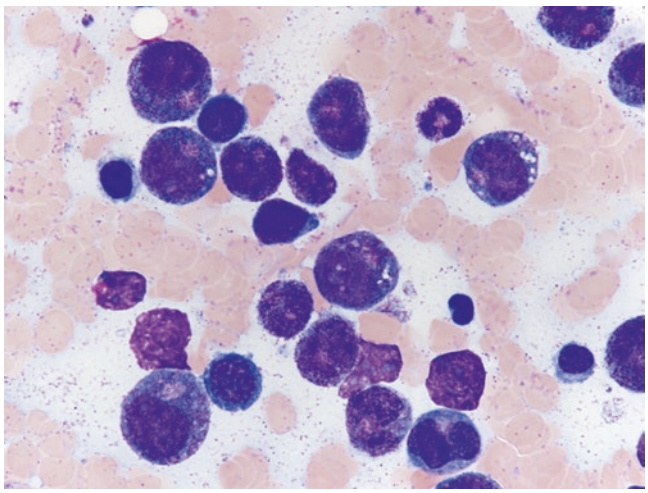

Fig. 2.22 Bone marrow aspirate from a patient with ongoing bacterial sepsis. Granulocytic hyperplasia and left shift are prominent. Toxic granulation and prominence of large, dark purple cytoplasmic granules, as well as vacuoles, are noted in the left-shifted granulocytic precursors

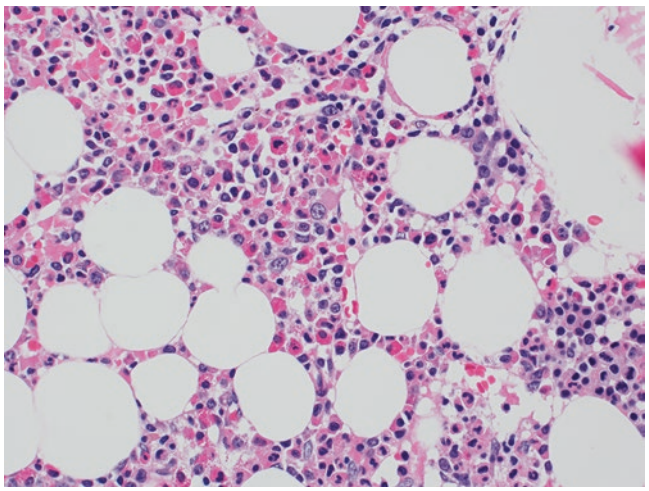

Fig. 2.24 Bone marrow biopsy showing eosinophilia, from the patient in Fig. 2.23

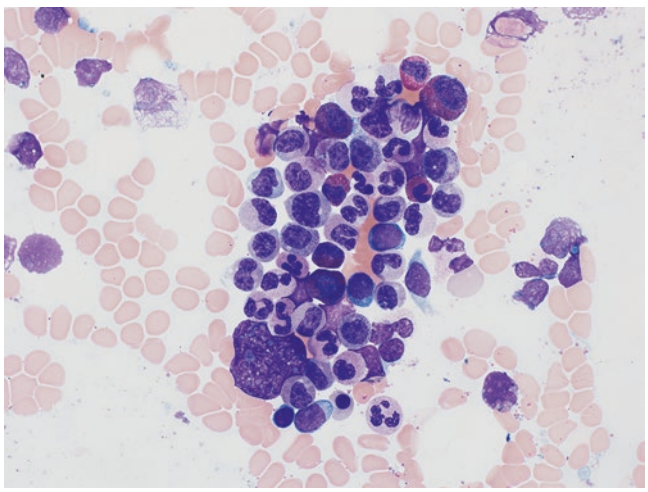

Fig. 2.23 Bone marrow aspirate showing eosinophilia. Eosinophils show normal maturation and cytology. This patient has a history of eosinophilic fasciitis and a peripheral eosinophilia. Increased eosinophils can be associated with a number of hematopoietic malignancies, but they also can be seen in infections, autoimmune disorders, and as a hypersensitivity to drugs or other substances

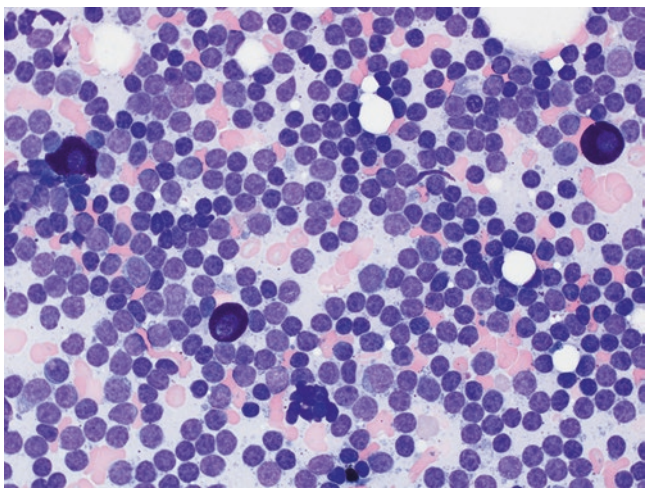

Fig. 2.25 Reactive increases in mast cells are rare in the bone marrow. Indications that mast cells are reactive include normal, round cytology with dense granulation, as depicted in this bone marrow aspirate smear, and a lack of aggregates on core biopsy. Lymphoplasmacytic lymphoma commonly shows a reactive mast cell infiltrate, as shown here

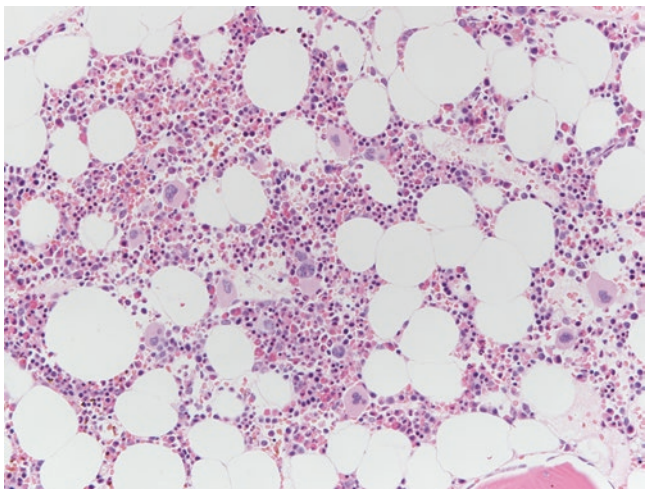

Fig. 2.26 Reactive megakaryocytic hyperplasia is typically seen in the setting of peripheral destruction or sequestration of platelets, such as in immune thrombocytopenic purpura (ITP). Though increased megakaryocytes are seen, they are in varying stages of maturation, lack bizarre cytologic features, and show at most focal loose clustering on biopsy. These features help distinguish a reactive megakaryocytic hyperplasia from that seen in myeloid neoplasms

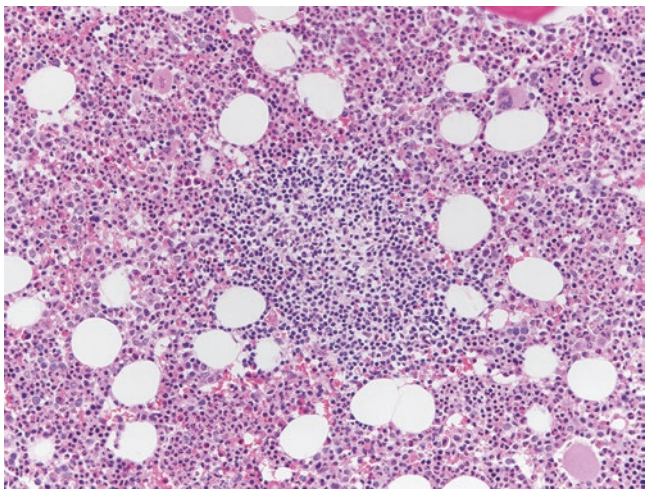

Fig. 2.27 In adults, lymphocytes typically comprise less than 20% of cells in the bone marrow. Reactive lymphoid aggregates in bone marrow increase in frequency with patient age and are typically an incidental finding. Patients with autoimmune disease or active viral infection are more likely to show reactive lymphoid aggregates. Reactive aggregates are typically non-paratrabecular in location and are well-circumscribed, as shown here. Cytologically, the cells are typically small, but there may be rare admixed larger cells, histiocytes, or plasma cells

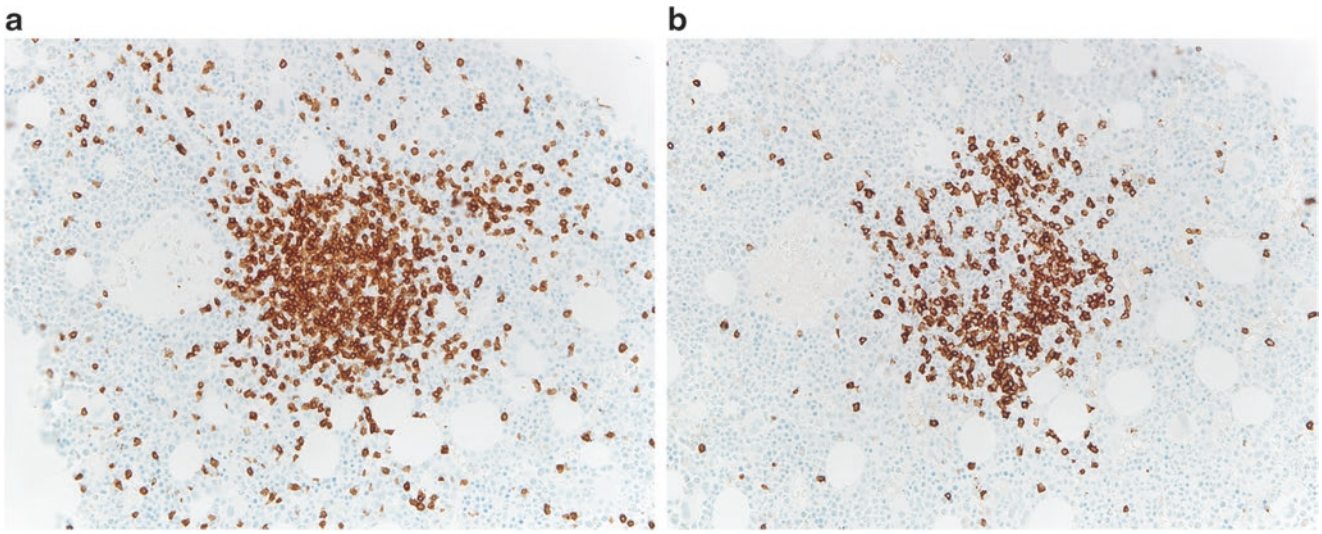

Fig. 2.28 CD3 immunohistochemical stain demonstrates a predominance of T cells (**a**) with fewer B cells staining with CD20 (**b**) in this reactive lymphoid aggregate

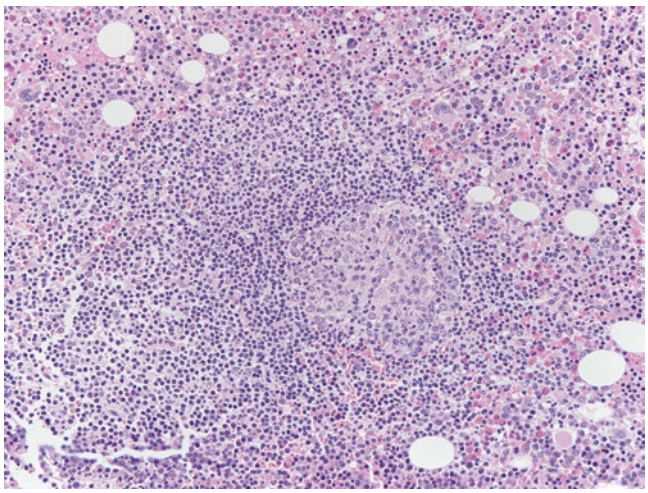

Fig. 2.29 Occasionally in reactive states, germinal center formation may occur in reactive lymphoid aggregates in the bone marrow, especially in autoimmune conditions

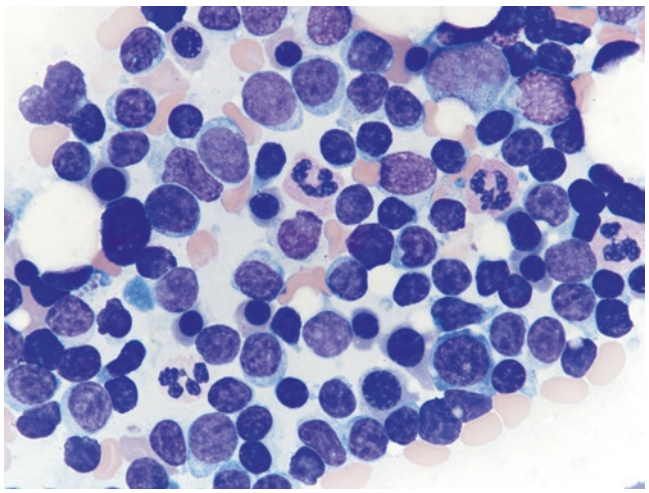

Fig. 2.31 Children may have large numbers of B-cell precursors called *hematogones*. Children (and less often adults) can show hematogone hyperplasia of the bone marrow under certain conditions that stress the bone marrow, including infections, underlying malignancy, and after chemotherapy or bone marrow transplantation. Hematogones can account for more than 50% of cells in rare instances [2]. This bone marrow aspirate demonstrates hematogone hyperplasia in a 64-year-old patient with a history of autoimmune neutropenia. A spectrum of maturation can be seen within the hematogones: some show more immature, blast-like chromatin, and others show more condensed chromatin, smaller size, and more abundant cytoplasm on this Wright-Giemsa-stained aspirate

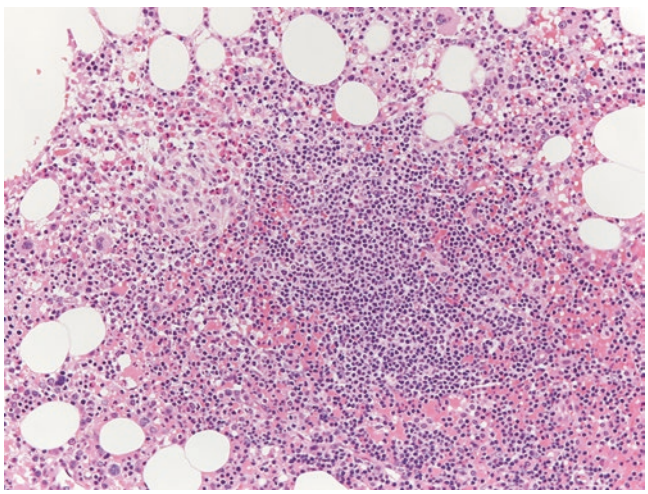

Fig. 2.30 In some instances, reactive lymphoid aggregates can be a clue to an underlying malignancy. Indolent systemic mastocytosis, shown here, often shows mast cell aggregates surrounded by a cuff of small, reactive lymphocytes

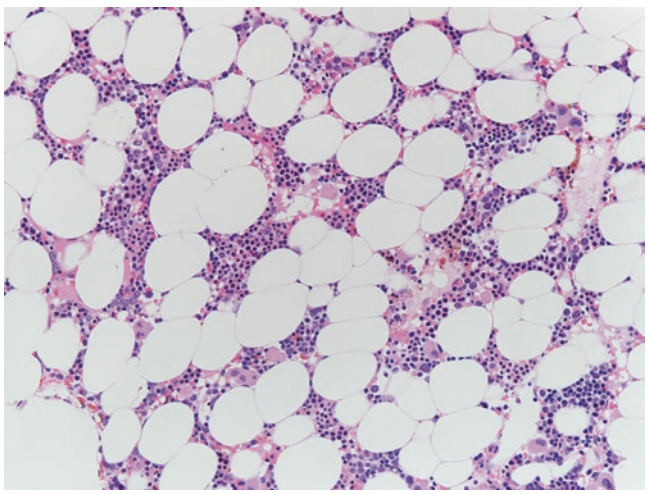

Fig. 2.32 Hematogone hyperplasia. Core biopsy from the same patient as depicted in Fig. 2.31 shows subtle interstitial lymphocytes, but no large aggregates

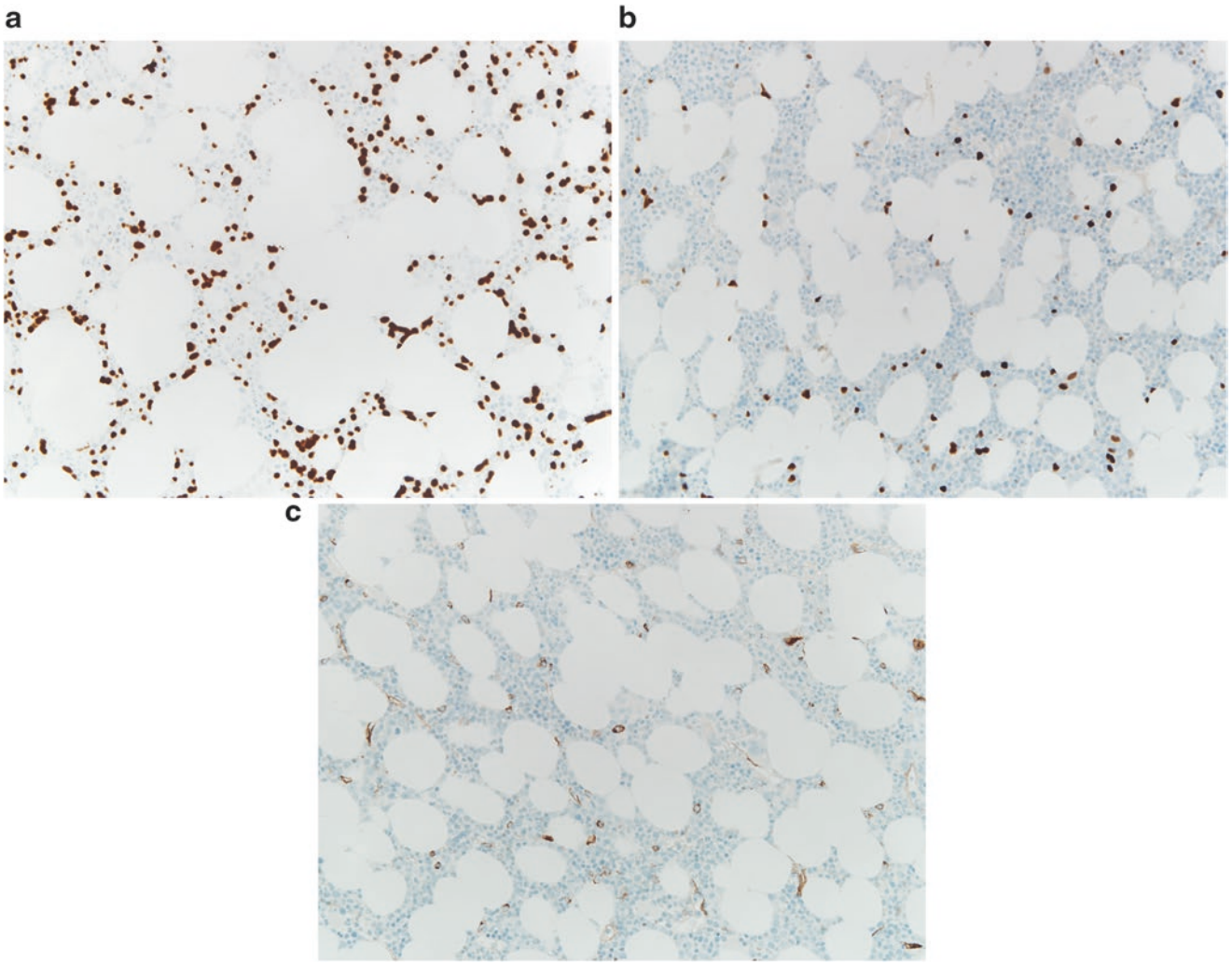

Fig. 2.33 Hematogone hyperplasia. PAX5 immunohistochemical stain shows an increased number of B-cell precursors within the marrow (**a**). In contrast, only rare cells are TdT-positive (**b**) or CD34-positive (**c**), highlighting the spectrum of maturation

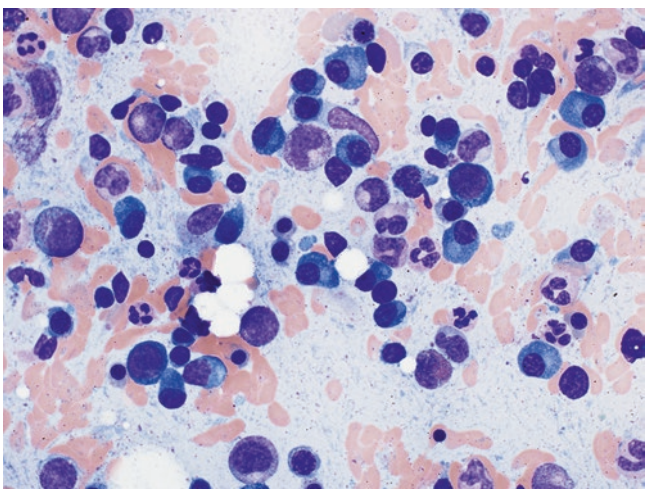

Fig. 2.34 Reactive polyclonal plasmacytosis can uncommonly occur in the bone marrow. Patients may have underlying infection, cirrhosis, autoimmune disease, or other malignancy. Cytologically, the plasma cells are typically bland, but mild atypia such as vacuolization or multinucleation can occur and does not necessarily indicate plasma cell neoplasia. Immunophenotyping is essential to assess for clonality. In this case, polytypic plasma cells account for at least 30% of the marrow cellularity in some areas. The patient had polyclonal hypergammaglobulinemia but no monoclonal protein. Angioimmunoblastic T-cell lymphoma was suspected, but definitive marrow involvement by lymphoma could not be proven

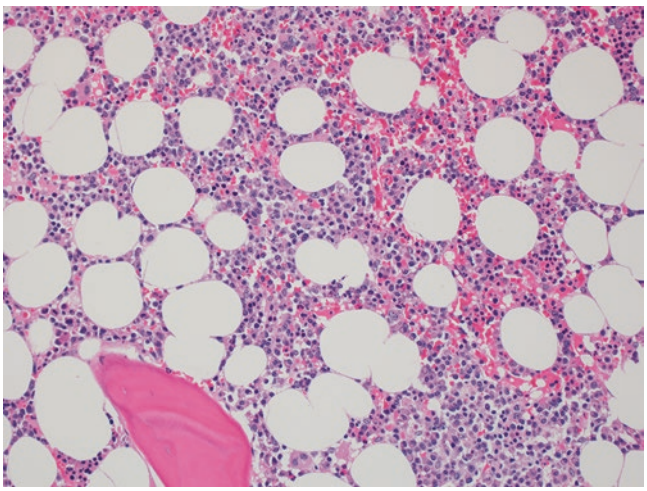

Fig. 2.35 Core biopsy from the patient in Fig. 2.34 shows polytypic plasmacytosis

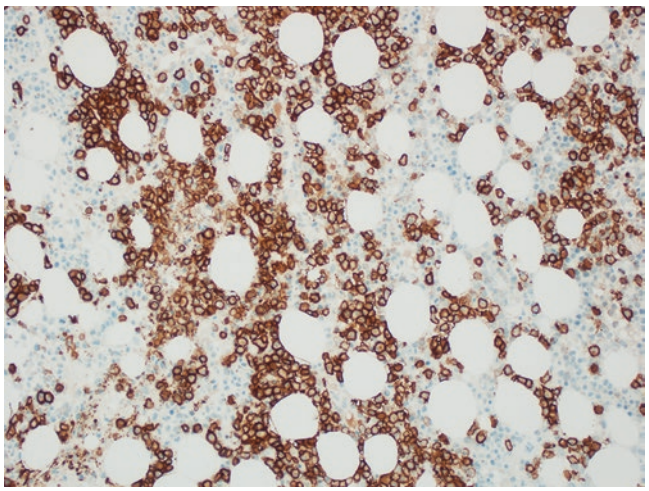

Fig. 2.36 Core biopsy from the patient in Fig. 2.34 shows polytypic plasmacytosis. CD138 immunohistochemistry highlights increased plasma cells

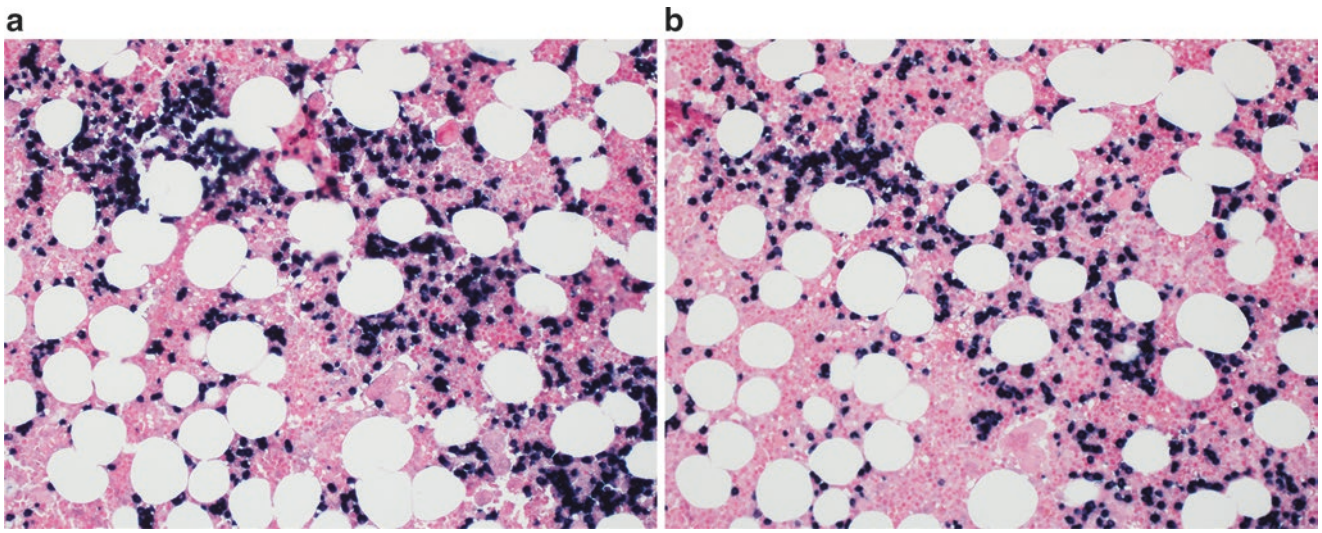

Fig. 2.37 Core biopsy from the patient in Fig. 2.34 shows polytypic plasmacytosis. Kappa (**a**) and lambda (**b**) in situ hybridization shows that the plasma cells are polytypic

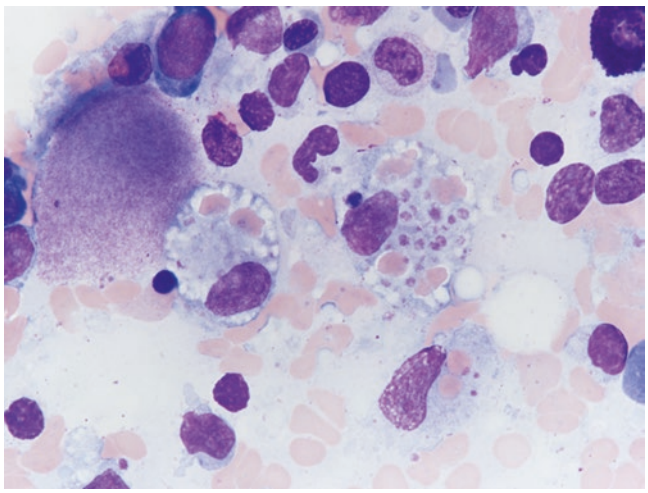

Fig. 2.38 Macrophages normally comprise less than 1% of bone marrow cells [2]. In states of high cell turnover, increased numbers of activated macrophages can be seen in aspirate smears. The presence of increased activated macrophages with ingested intact cells and cellular debris is termed *hemophagocytosis*. This reactive phenomenon can be due to a variety of neoplastic and nonneoplastic causes, including congenital syndromes, lymphoma, autoimmune disease, and viral infection. This aspirate smear shows hemophagocytosis in a patient who was diagnosed with hemophagocytic lymphohistiocytosis (HLH) associated with Epstein-Barr virus (EBV) infection. Examples of familial HLH can be found in Chap. 4 (Constitutional, Metabolic, and Related Disorders), with additional examples and discussion in Chap. 14 (Histiocytic Disorders)

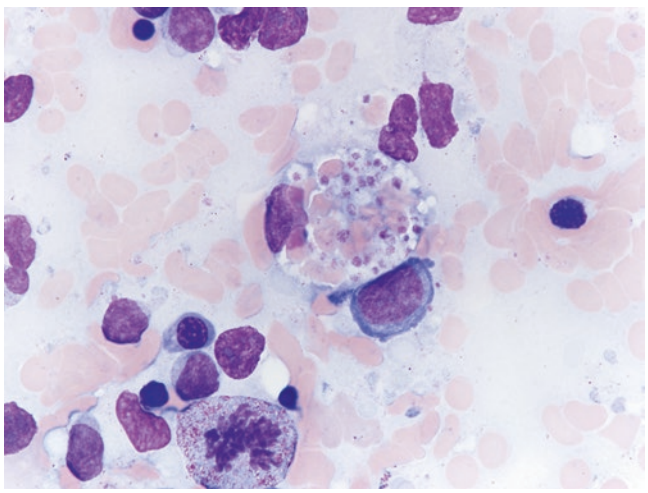

Fig. 2.39 Hemophagocytosis in a patient with HLH; activated macrophage is seen ingesting numerous platelets and RBCs

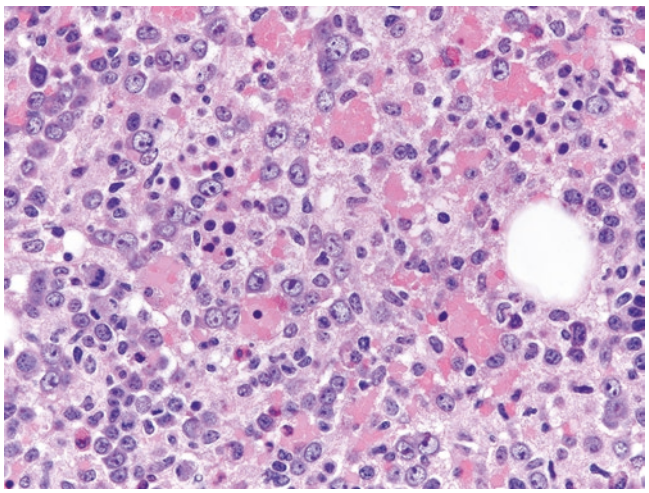

Fig. 2.40 Core biopsy in a patient with HLH, demonstrating increased interstitial macrophages containing ingested cells and cell debris. Especially prominent are macrophages ingesting numerous nonnucleated RBCs

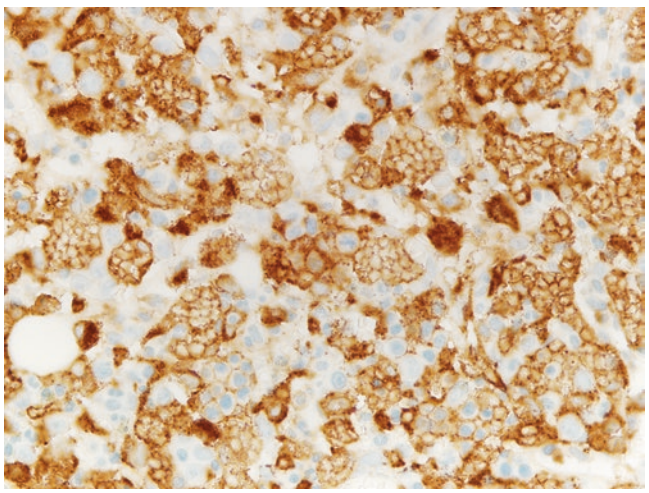

Fig. 2.41 CD163 immunohistochemical stain on the core biopsy stain macrophages and shows increased hemophagocytosis in HLH

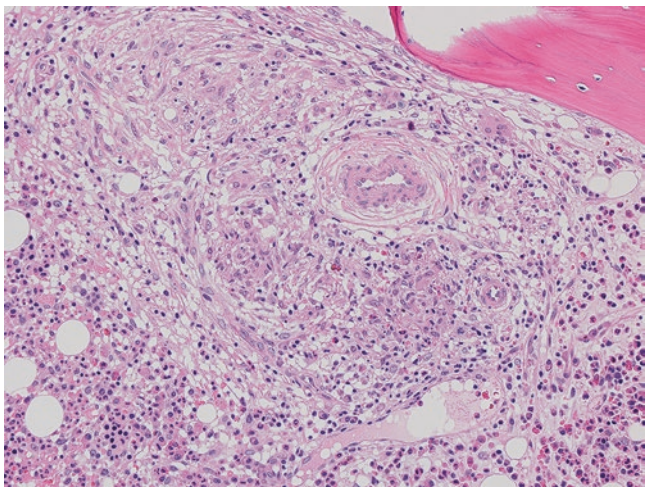

Fig. 2.42 Granulomatous inflammation in the marrow can indicate infection, underlying malignancy, or a systemic inflammatory disease such as sarcoidosis. Shown here are nonnecrotizing granulomas involving the marrow in a patient with sarcoidosis (see Chap. 14 for additional examples)

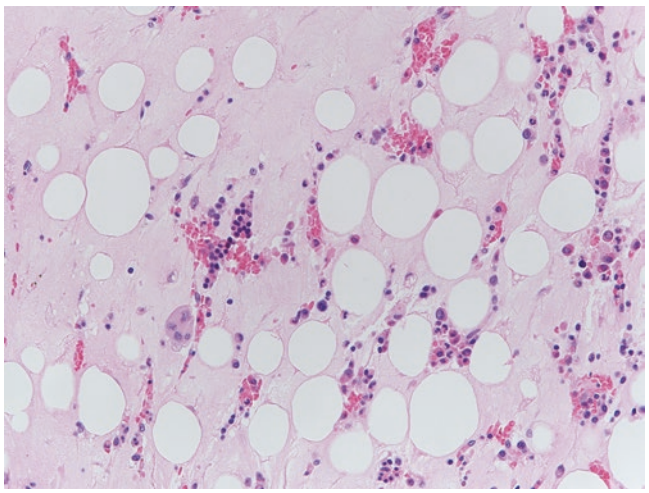

Fig. 2.44 Higher-power image of gelatinous transformation. Fat cell atrophy and loss of marrow elements are characteristic features

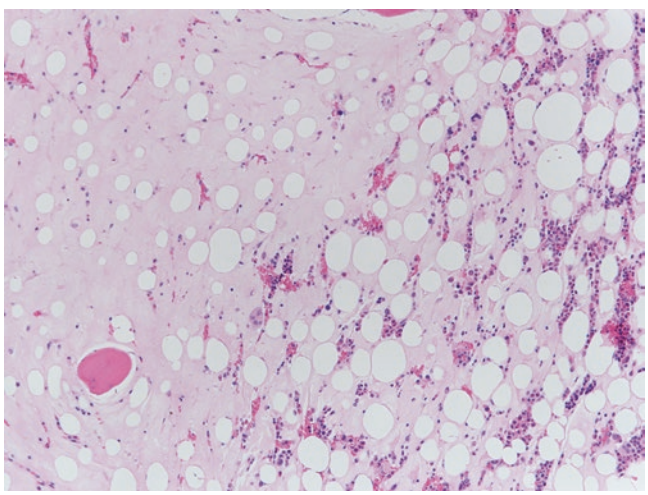

Fig. 2.43 Gelatinous transformation of bone marrow is seen in anorexia nervosa and other malnutritional states. Changes in the bone marrow stroma have been demonstrated to correlate with the degree of weight loss [3]. Bone marrow biopsy demonstrates loss of marrow elements and prominent extracellular deposition of an amorphous, gelatinous-appearing matrix

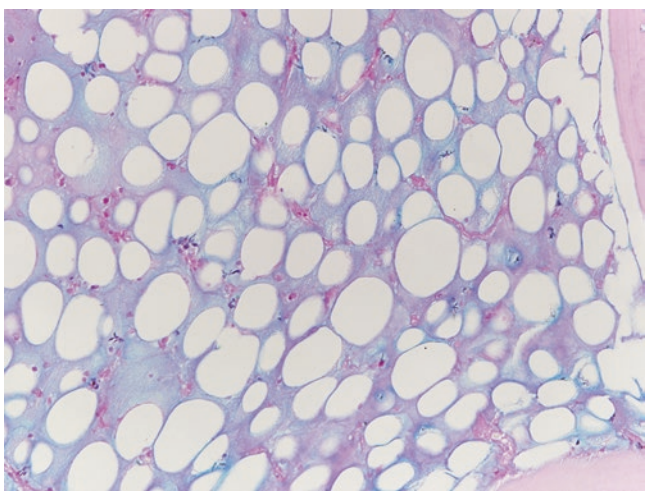

Fig. 2.45 Bone marrow biopsy from a patient with anorexia nervosa. The extracellular matrix seen in states of cachexia is composed of hyaluronic acid, which stains blue on Alcian blue stain as shown here [4]. This stain may aid in distinction from other extracellular deposits such as amyloid

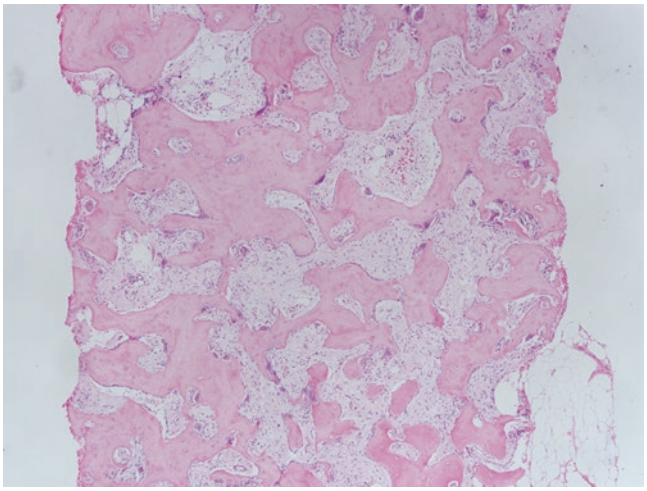

Fig. 2.46 Paget disease of bone (osteitis deformans) is a rare, progressive disease of unknown etiology resulting in accelerated bone remodeling. Bone marrow biopsy will show thickened trabeculae in a "jigsaw" pattern with prominent osteoclast and osteoblast activity. Marrow space shows replacement by fine fibrosis in the chronic stage of the disease. Clinical history is essential to avoid misdiagnosis as an end-stage myeloproliferative neoplasm

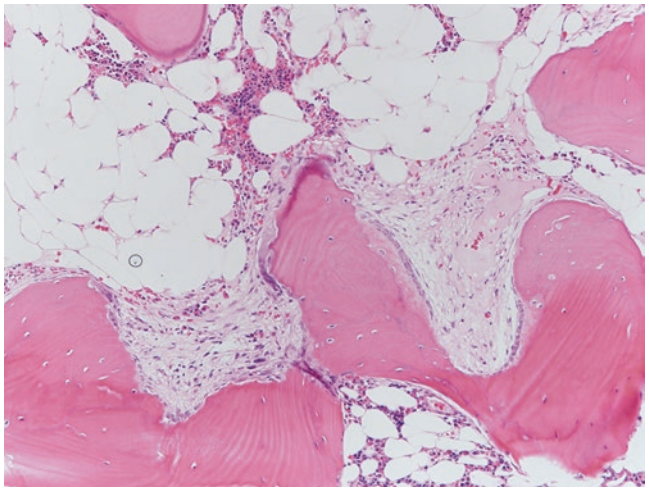

Fig. 2.48 Renal osteodystrophy typically accompanies chronic renal failure. Bone remodeling can be seen with increased osteoclast and osteoblast activity, as well as resulting osteosclerosis. In rare instances, a myelofibrosis-like picture may result [5]

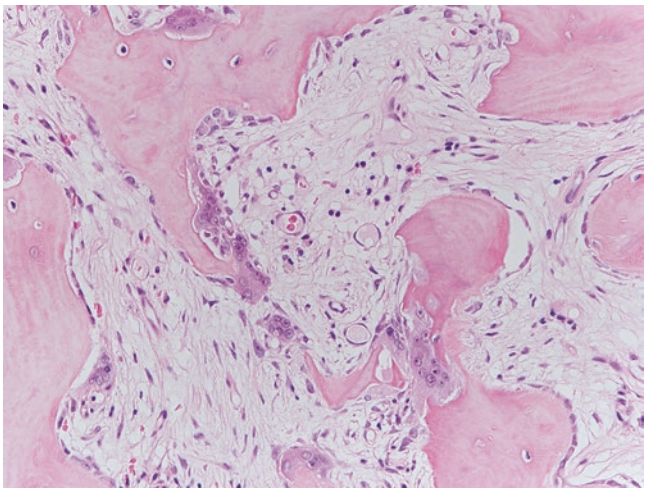

Fig. 2.47 Paget disease of bone (osteitis deformans) at higher power, showing prominent osteoclast and osteoblast activity. Marrow space shows replacement by fine fibrosis in the chronic stage of the disease

In many instances, the morphologic features are nonspecific with regard to etiology, emphasizing the importance of the clinical history in the interpretation of bone marrow pathology. In addition, many reactive changes overlap with those seen in neoplastic conditions, such as the striking erythroid atypia seen in erythroid regeneration in the setting of autoimmune hemolytic anemia (Figs. 2.3, 2.4, and 2.5). Finally, neoplastic conditions involving the marrow can result in a characteristic reactive alteration of other marrow elements, such as the reactive mast cell hyperplasia seen in lymphoplasmacytic lymphoma (Fig. 2.25).

References

1. Johnson-Wimbley TD, Graham DY. Diagnosis and management of iron deficiency anemia in the 21st century. Therap Adv Gastroenterol. 2011;4:177–84.
2. Foucar K, Reichard K, Czuchlewski D. Bone marrow pathology. 3rd ed. Chicago: ASCP Press; 2010.
3. Abella E, Feliu E, Granada I, Milla F, Oriol A, Ribera JM, et al. Bone marrow changes in anorexia nervosa are correlated with the amount of weight loss and not with other clinical findings. Am J Clin Pathol. 2002;118:582–8.
4. Mehta K, Gascon P, Robboy S. The gelatinous bone marrow (serous atrophy) in patients with acquired immunodeficiency syndrome. Evidence of excess sulfated glycosaminoglycan. Arch Pathol Lab Med. 1992;116:504–8.
5. Butt YM, Chen W. Myelofibrosis secondary to renal osteodystrophy. Blood. 2016;128:2104.

Post-therapy Marrow Changes

3

Jason H. Kurzer and Olga K. Weinberg

Bone marrow biopsies and aspirates from patients undergoing various forms of treatment can show a variety of histological and cytological findings, and it is therefore imperative that pathologists understand the array of associated therapy-related effects. Patients receiving induction chemotherapy for acute leukemia frequently have bone marrow aspirates and/or biopsies at specific intervals, allowing the pathologist to observe the immediate and long-term effects of the treatment regimen (Table 3.1).

Biopsies obtained after approximately 1 week of myeloablative therapy typically show marrow aplasia, loss of adipocytes, fibrinoid necrosis, and edema associated with dilated sinuses (Fig. 3.1) [1–3]. Two weeks after initiation of treatment, the fibrinoid necrosis persists, and the cellularity is composed of stromal cells, hemosiderin-laden macrophages, lymphocytes, and plasma cells (Figs. 3.2 and 3.3). At this time, adipocytes return, are frequently multiloculated, and are often accompanied by a loose network of reversible reticulin fibrosis (Fig. 3.4). By day 29 of induction therapy, erythropoiesis has typically returned, and may be accompanied by some degree of dyspoiesis (Fig. 3.5). Granulopoiesis typically follows, with megakaryopoiesis frequently appearing last (Figs. 3.6 and 3.7) [1].

It is important to recognize certain changes that may mimic residual disease after therapy. Hyperplasia of hematogones is often seen after treatment and can be particularly prominent in pediatric marrows following therapy and thus provide a diagnostic challenge when evaluating for residual lymphoblastic leukemia (Fig. 3.8). Other diagnostic challenges can arise when patients are treated with growth factors such as G-CSF. While early G-CSF therapy may show promyelocytic hyperplasia reminiscent of acute promyelocytic leukemia, these precursors typically show normal cytologic and histologic morphology (Figs. 3.9 and 3.10) [4–7]. Moreover, with time, the myeloid hyperplasia will demonstrate more mature precursors (Fig. 3.11). Another diagnostic challenge occurs in the setting of rituximab treatment. Therapy with rituximab can sometimes induce the formation of T-cell lymphoid aggregates in the marrow that may morphologically mimic persistent involvement by lymphoma (Fig. 3.12) [8].

Finally, certain diseases have specific therapies that show associated marrow findings. All *trans* retinoic acid (ATRA) treatment has been shown to promote differentiation of the atypical promyelocytes of acute promyelocytic leukemia (APL). Consequently, within a week of ATRA treatment, neutrophils may contain Auer rods. After several weeks, primary granules are diminished, but neutrophils may show deficiencies of secondary granule formation (Fig. 3.13) [9]. Chronic myeloid leukemia typically shows a hypercellular bone marrow with myeloid hyperplasia and frequent atypical megakaryocytes (Fig. 3.14). However, treatment for several months with a tyrosine kinase inhibitor such as imatinib can significantly reduce the marrow cellularity to normocellularity or even hypocellularity, as well as reduce the number of atypical megakaryocytes (Fig. 3.15) [10–12].

J.H. Kurzer (✉)
Stanford University School of Medicine, Stanford, CA, USA
e-mail: kurzer@stanford.edu

O.K. Weinberg
Pathology Department, Boston Children's Hospital,
Boston, MA, USA
e-mail: Olga.Weinberg@childrens.harvard.edu

T.I. George, D.A. Arber (eds.), *Atlas of Bone Marrow Pathology*, Atlas of Anatomic Pathology,
https://doi.org/10.1007/978-1-4939-7469-6_3

Table 3.1 Timeline of post-therapy changes in the bone marrow

Timepoint	Findings
One Week	Marrow aplasia
	Loss of adipocytes
	Fibrinoid necrosis
	Edema
	Dilated sinuses
Two Weeks	Fibrinoid necrosis
	Cellularity composed of stromal cells, hemosiderin-laden macrophages, lymphocytes, and plasma cells
	Return of adipocytes: multiloculated
	Loose network of reversible reticulin fibrosis
	Hematogone hyperplasia
Four Weeks	Erythroid precursors return
	Some granulopoiesis
	Clusters of megakaryocytes
	Reticulin fibrosis diminishes

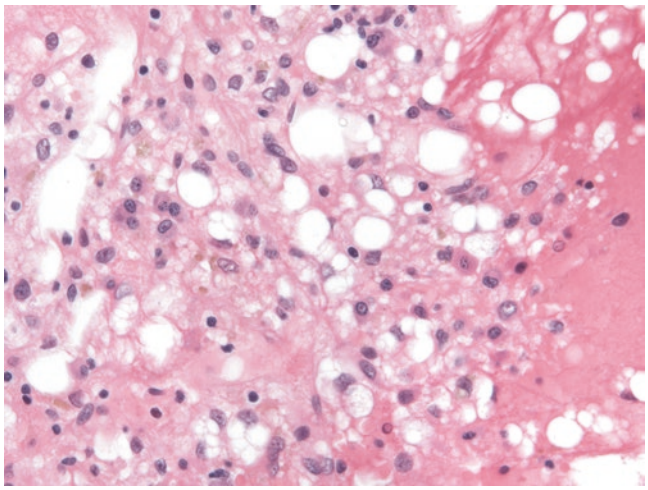

Fig. 3.2 This bone marrow biopsy of a 34-year-old man shows therapy-related changes on day 14, status post 7+3 induction therapy for acute myeloid leukemia. There continues to be prominent fibrinoid necrosis in the background. The cellularity is composed predominantly of lymphocytes, plasma cells, stromal cells, and histiocytes. A subset of histiocytes contains cellular debris and hemosiderin. By day 14, reemergence of adipocytes is appreciated, with many appearing multiloculated. A loose network of reticulin fibrosis can be appreciated in the background

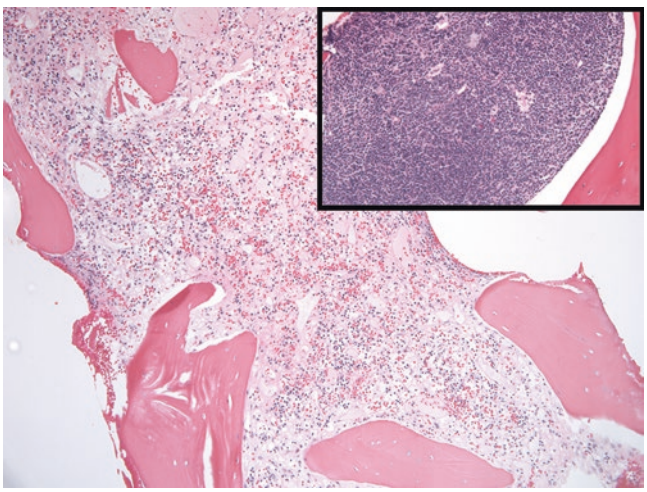

Fig. 3.1 This bone marrow biopsy of a 15-year-old female shows therapy-related changes on day 8 of induction chemotherapy for B-lymphoblastic leukemia. Prior to treatment, the marrow space is hypercellular and replaced by sheets of immature lymphoblasts (*inset*). On day 8 of induction therapy, the marrow is hypocellular and shows dilated sinuses with prominent edema, fibrinoid necrosis of stromal cells, an absence of hematopoietic precursors and adipocytes, and, in this case, multiple foci of residual scattered tumor cells

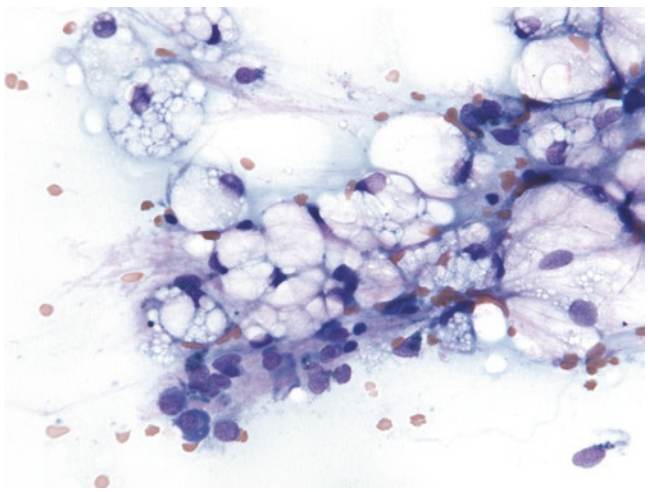

Fig. 3.3 This bone marrow aspirate from the patient in Fig. 3.2 shows multiloculated adipocytes, stromal cells, plasma cells, and occasional hemosiderin-laden macrophages

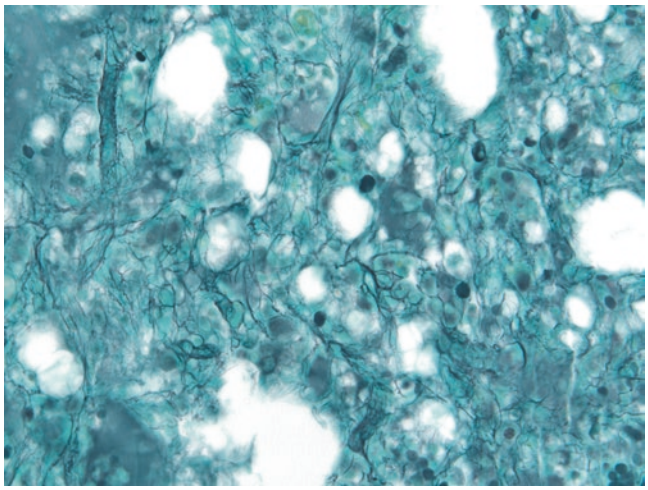

Fig. 3.4 This reticulin stain of the bone marrow biopsy of the patient from Fig. 3.2 shows increased fibrosis. Reversible reticulin fibrosis may sometimes be seen after high-dose chemotherapy

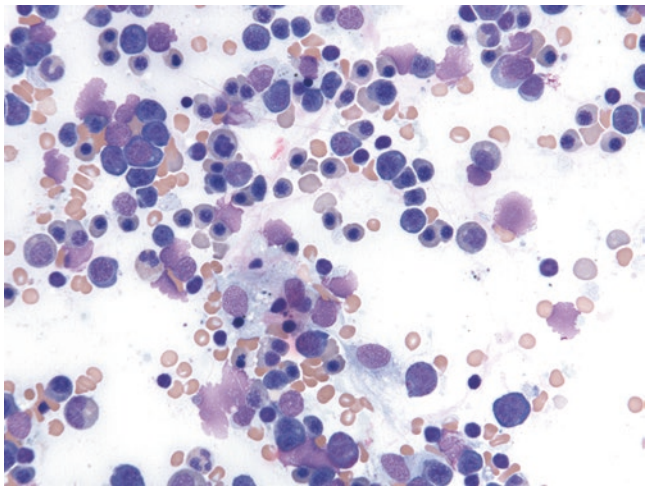

Fig. 3.6 This bone marrow aspirate of a 2-year-old boy shows therapy-related changes on day 29 of induction therapy for B-lymphoblastic leukemia. Erythroid-predominant hematopoiesis is appreciated, with occasional dyspoietic erythroblasts. Scattered immature granulocytes are also present in fewer numbers, indicative of returning myelopoiesis

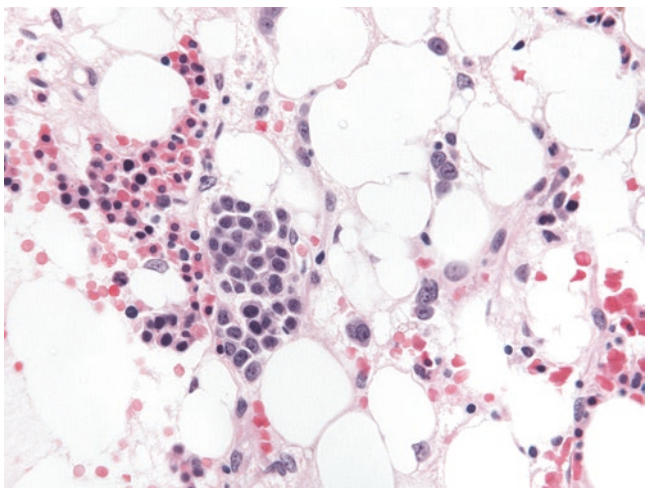

Fig. 3.5 This bone marrow biopsy of a 17-year-old male shows therapy-related changes on day 29 of induction therapy for B-lymphoblastic leukemia. As hematopoiesis returns, erythroid precursors are typically the first of the three lineages to reappear. It is not uncommon to find erythroid colonies scattered within a hypocellular marrow

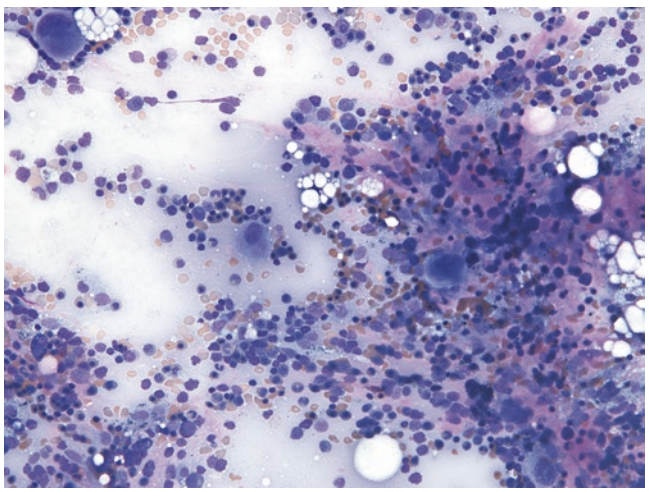

Fig. 3.7 This bone marrow aspirate of a 24-year-old man shows an erythroid hyperplasia on day 29 of induction therapy for B-lymphoblastic leukemia. Of note, regenerating megakaryocytes are present in clusters, with occasional hypolobated forms

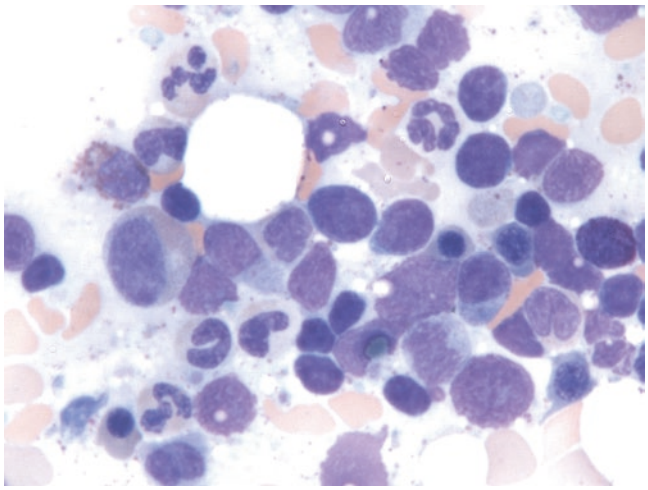

Fig. 3.8 This bone marrow aspirate of a 71-year-old man following treatment for acute myeloid leukemia shows a prominent hematogone hyperplasia admixed with maturing myeloid and erythroid precursors

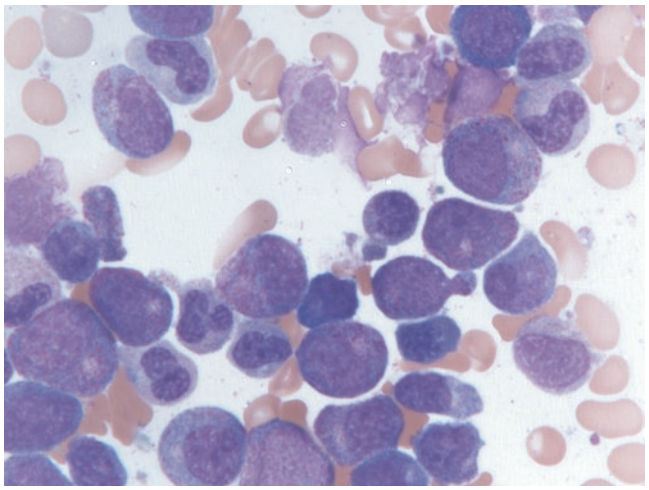

Fig. 3.10 The bone marrow aspirate from the same patient as Fig. 3.9 shows marked left-shifted maturation of the granulocytic precursors. A prominent Golgi apparatus is visible in the numerous normal-appearing promyelocytes, a finding that is commonly seen with G-CSF treatment

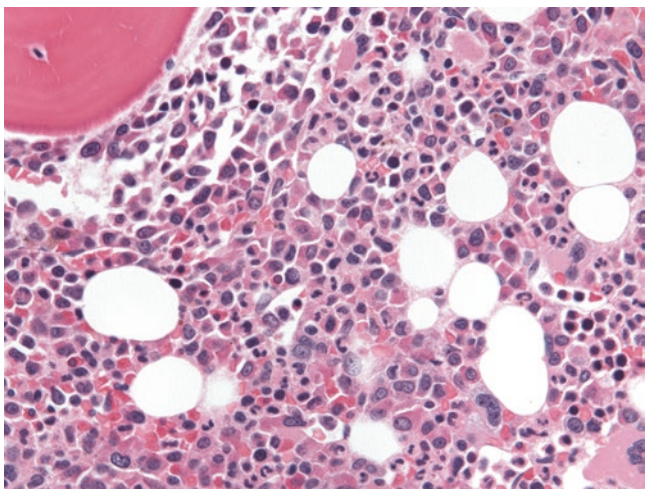

Fig. 3.9 This bone marrow from a 25-year-old woman treated with G-CSF 1 week prior to biopsy is hypercellular, with an increase in immature granulocytes. Nevertheless, a normal granulopoietic pattern is observed, proceeding outward from the bone trabeculae into the interstitium

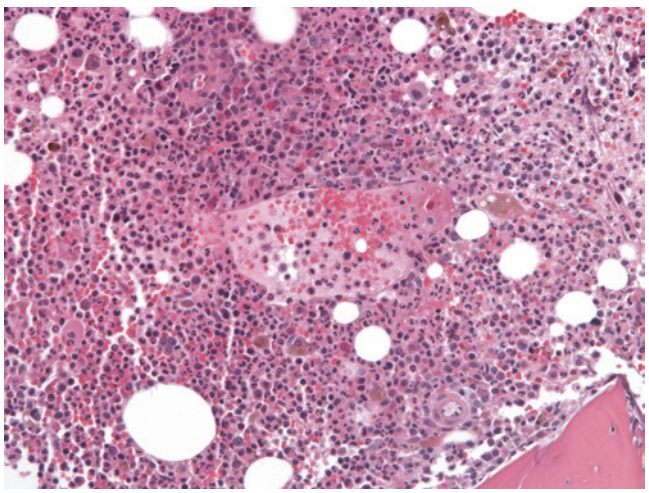

Fig. 3.11 This bone marrow from a 40-year-old man treated with G-CSF 2 weeks prior to biopsy shows a myeloid hyperplasia similar to Fig. 3.10 but with an increased percentage of fully mature granulocytes

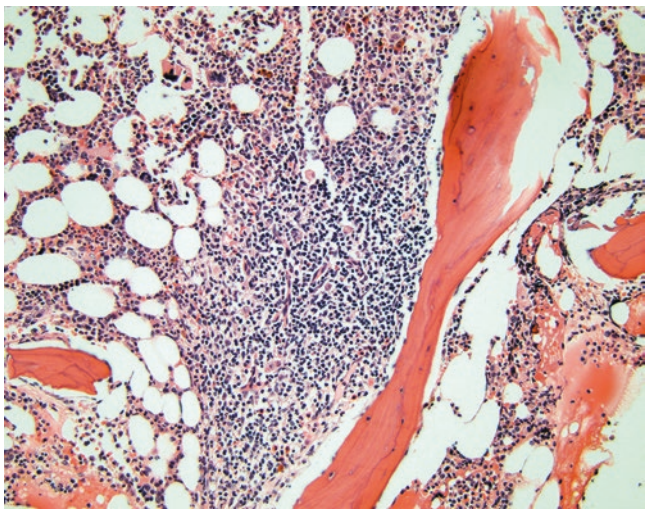

Fig. 3.12 This bone marrow biopsy from an 87-year-old woman with a history of diffuse large B-cell lymphoma shows prominent lymphoid aggregates in the marrow after receiving therapy that included rituximab. In this case, the lymphoid aggregates were shown to be composed of almost all T cells and virtually no B cells. As lymphoma cells with minimal CD20 expression may be present, it is important to stain for alternative B-cell markers such as PAX-5 or CD79a

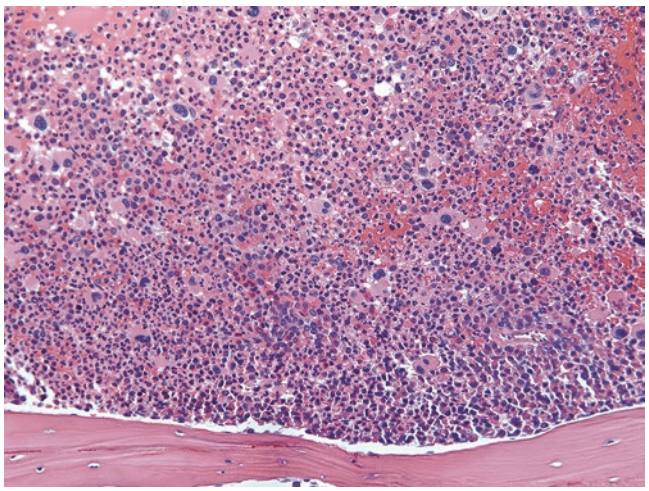

Fig. 3.14 This bone marrow biopsy from a 32-year-old woman with chronic myeloid leukemia shows the characteristic hypercellularity with associated myeloid hyperplasia. Loose clusters of atypical megakaryocytes are readily apparent

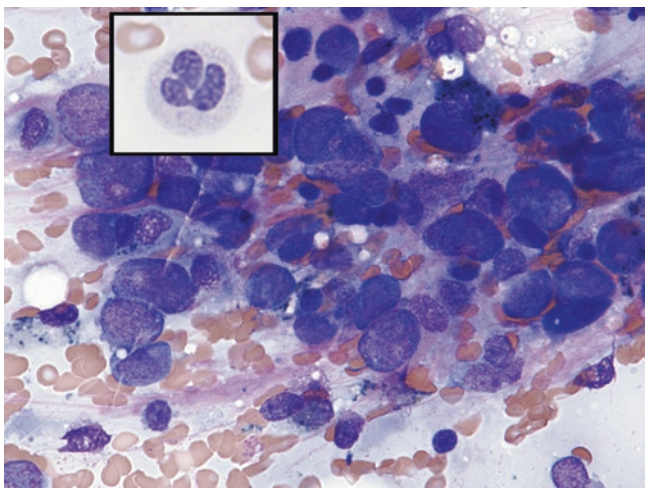

Fig. 3.13 This bone marrow aspirate from a 25-year-old woman treated with ATRA, idarubicin, and arsenic is hypocellular, with little differentiation of myeloid precursors past the promyelocytic stage, but the peripheral blood (inset) shows occasional neutrophils with a deficiency of secondary granules, likely resulting from ATRA-induced maturation of the initial neoplastic promyelocytes

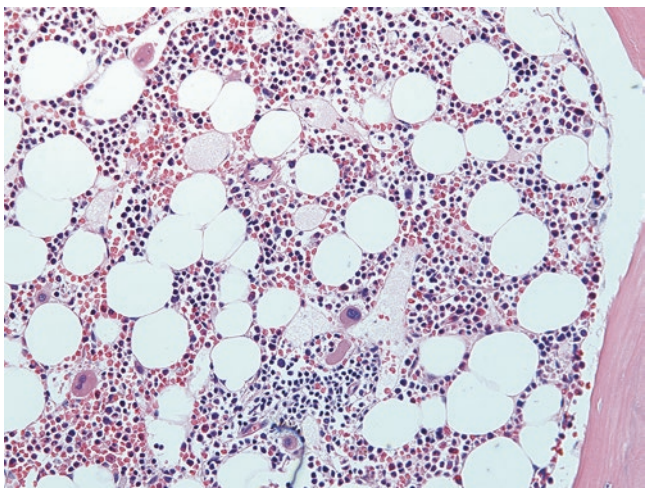

Fig. 3.15 This bone marrow biopsy from the same patient depicted in Fig. 3.14 reveals the effects of 6 months of imatinib treatment. The cellularity has returned to normal, with only scattered megakaryocytes

References

1. Islam A, Catovsky D, Galton DAG. Histological study of bone marrow regeneration following chemotherapy for acute myeloid leukemia and chronic granulocytic leukemia in blast transformation. Br J Haematol. 1980;45:535–40.
2. Dick FR, Burns CP, Weiner GJ, Heckman KD. Bone marrow morphology during induction phase of therapy for acute myeloid leukemia (AML). Hematol Pathol. 1995;9:95–106.
3. Kushwaha R, Kumar A, Aggrawal K, Nigam N, Kumar A. Post chemotherapy blood and bone marrow regenerative changes in childhood acute lymphoblastic leukemia: a prospective study. Indian J Pathol Microbiol. 2014;57:72–7. https://doi.org/10.4103/0377–4929.130903.
4. Campbell LJ, Maher DW, Tay DL, Boyd AW, Rockman S, McGrath K, et al. Marrow proliferation and the appearance of giant neutrophils in response to recombinant human granulocyte colony stimulating factor (rhG-CSF). Br J Haematol. 1992;80:298–304.
5. Ryder JW, Lazarus HM, Farhi DC. Bone marrow and blood findings after marrow transplantation and rhGM-CSF therapy. Am J Clin Pathol. 1992;97:631–7.
6. Schmitz LL, McClure JS, litz CE, Dayton V, Weisdorf DJ, Parkin JL, Brunning RD. Morphologic and quantitative changes in blood and marrow cells following growth factor therapy. Am J Clin Pathol. 1994;101:67–75.
7. Harris AC, Todd WM, Hackney MH, Ben-Ezra J. Bone marrow changes associated with recombinant granulocyte-macrophage and granulocyte colony-stimulating factors: discrimination of granulocytic regeneration. Arch Pathol Lab Med. 1994;118:624–9.
8. Raynaud P, Caulet-Maugendre S, Foussard C, Salles G, Moreau A, Rossi JF, et al. GOELAMS Group. T-cell lymphoid aggregates in bone marrow after rituximab therapy for B-cell follicular lymphoma: a marker of therapeutic efficacy? Hum Pathol. 2008;39:194–200.
9. Miyauchi J, Ohyashiki K, Inatomi Y, Toyama K. Neutrophil secondary-granule deficiency as a hallmark of all-trans retinoic acid-induced differentiation of acute promyelocytic leukemia cells. Blood. 1997;90:803–13.
10. Hasserjian RP, Boecklin F, Parker S, Chase A, Dhar S, Zaiac M, et al. ST1571 (imatinib mesylate) reduces bone marrow cellularity and normalizes morphologic features irrespective of cytogenetic response. Am J Clin Pathol. 2002;117:360–7.
11. Frater JL, Tallman MS, Variakojis D, Druker BJ, Resta D, Riley MB, et al. Chronic myeloid leukemia following therapy with imatinib mesylate (Gleevec). Bone marrow histopathology and correlation with genetic status. Am J Clin Pathol. 2003;119:833–41.
12. McNamara C, Grigg A, Szer J, Roberts A, Campbell L, Hoyt R, et al. Morphological effects of imatinib mesylate (STI571) on the bone marrow and blood of patients with Philadelphia chromosome (Ph) positive chronic myeloid leukaemia. Clin Lab Haematol. 2003;25:119–25.

Constitutional, Metabolic, and Related Disorders

4

Kristian T. Schafernak and Katherine R. Calvo

This chapter illustrates and describes the bone marrow features of inherited bone marrow failure syndromes (e.g., Fanconi anemia, Diamond-Blackfan anemia, Shwachman-Diamond syndrome, and dyskeratosis congenita), as well as acquired diseases such as aplastic anemia and paroxysmal nocturnal hemoglobinuria, which can have overlapping morphologic features and are often included in the differential diagnosis of young cytopenic patients) (Figs. 4.1, 4.2, 4.3, 4.4, 4.5, 4.6, and 4.7). Increasingly, it is recognized that adolescents and adults may harbor germline mutations in *GATA2* (Fig. 4.8), *RUNX1* (Fig. 4.23), and other genes, which predispose to marrow failure, myelodysplasia, and myeloid malignancy. The bone marrow features of other inherited diseases presenting with cytopenias and impaired immunity are also illustrated, including CTLA4 deficiency (Fig. 4.9), autoimmune lymphoproliferative syndrome (ALPS) (Fig. 4.10), activated PI3K-delta syndrome (Figs. 4.11, 4.12, 4.13, 4.14, 4.15, 4.16, and 4.17), Chédiak-Higashi syndrome (Figs. 4.18, 4.19, and 4.20), WHIM syndrome (Fig. 4.21), and chronic granulomatous disease (Fig. 4.22). Inherited diseases resulting primarily in single-lineage cytopenias involving erythroid (e.g., severe congenital neutropenia (Fig. 4.5)), myeloid (e.g., severe congenital neutropenia (Fig. 4.5)), and platelets (e.g., familial thrombocytopenia (Fig. 4.23)) are also presented. Marrow diseases associated with toxic and/or metabolic states and storage diseases (e.g., Gaucher disease (Fig. 4.24), Niemann-Pick disease (Figs. 4.25, 4.26, and 4.27), hemophagocytic lymphohistiocytosis (Fig. 4.28), megaloblastic anemia (Figs. 4.29, 4.30, and 4.31), arsenic toxicity (Fig. 4.32), renal osteodystrophy (Fig. 4.33), and osteopetrosis (Fig. 4.34) are included in this chapter.

K.T. Schafernak
Department of Pathology and Laboratory Medicine, Phoenix Children's Hospital, Phoenix, AZ, USA
e-mail: kschafernak@phoenixchildrens.com

K.R. Calvo, M.D. Ph.D. (✉)
Department of Laboratory Medicine, National Institutes of Health Clinical Center, 10 Center Dr. Bldg 10/2C306 Bethesda, MD 20892-1508, USA
e-mail: calvok@nih.gov

T.I. George, D.A. Arber (eds.), *Atlas of Bone Marrow Pathology*, Atlas of Anatomic Pathology,
https://doi.org/10.1007/978-1-4939-7469-6_4

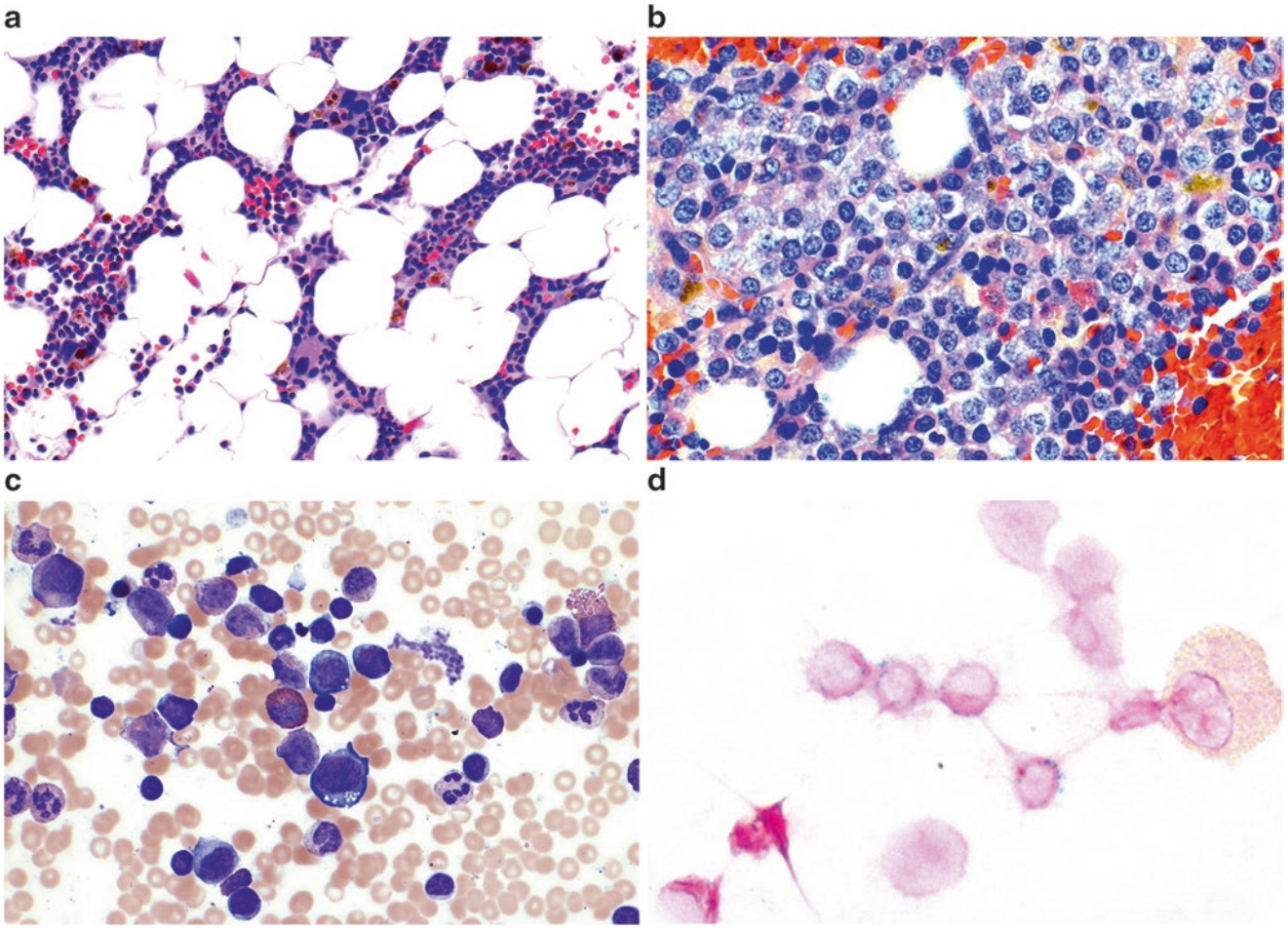

Fig. 4.1 Diamond-Blackfan anemia (DBA). DBA is an inherited bone marrow disorder caused by germline mutations in genes encoding ribosomal proteins (e.g., *RPS19*, *RPL5*). Onset is typically at birth or in early infancy. Initially, the bone marrow in DBA may be normocellular with only profound erythroid hypoplasia. (**a**) This 5-year-old's bone marrow is hypocellular and also has a decreased number of myeloid precursors. (**b**) This particle clot section shows a profound erythroid hypoplasia and increased storage iron as a sequela of blood transfusion. (**c**) Occasionally, the erythroid precursors in DBA contain cytoplasmic vacuoles. Note the full maturation of myeloid precursors and a few hematogones in the background. (**d**) Ring sideroblasts are sometimes seen in DBA, as in this case

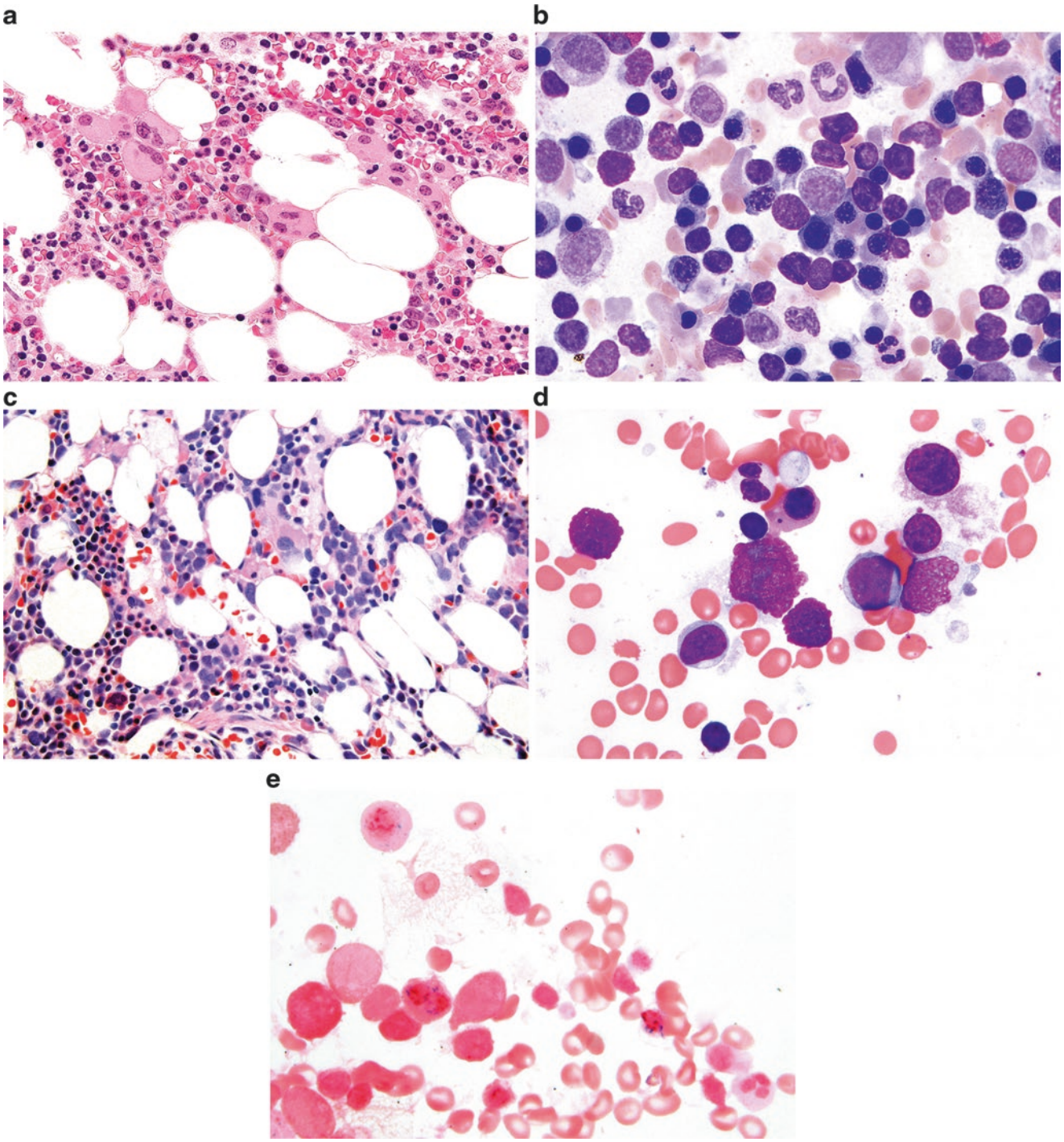

Fig. 4.2 Fanconi anemia. Fanconi anemia is caused by germline mutations in any 1 of currently 20 genes, the most common involving *FANCA*, *FANCC*, and *FANCG*. Patients develop bone marrow failure and have an increased risk of progression to myelodysplastic syndrome (MDS)/acute myeloid leukemia (AML). (**a**) This bone marrow core biopsy is from a 10-year-old boy with Fanconi anemia and pancytopenia. The bone marrow is hypocellular for the patient's age, with focal clustering of hypolobated megakaryocytes. (**b**) The aspirate smear shows a relative erythroid predominance and myeloid hypoplasia without increased blasts. Cytogenetic analysis showed a normal karyotype. About one third of Fanconi anemia patients go on to develop a hematologic malignancy, and some are even diagnosed with MDS or AML on their first bone marrow examination. In a different case, an 8-year-old boy with progressive fatigue was found to be anemic. He was previously healthy, with previous workups only for short stature/failure to thrive. His mother had died from breast cancer 5 years earlier. The bone marrow was hypocellular for age (**c**) and showed trilineage dysplasia with blasts in the 10–15% range (**d**) and numerous ring sideroblasts (**e**). The final diagnosis was MDS, refractory anemia with excess blasts-2 (RAEB-2) with complex cytogenetic abnormalities. A diepoxybutane (DEB) clastogen assay was positive, and genetic testing was also pursued, particularly in light of the family history

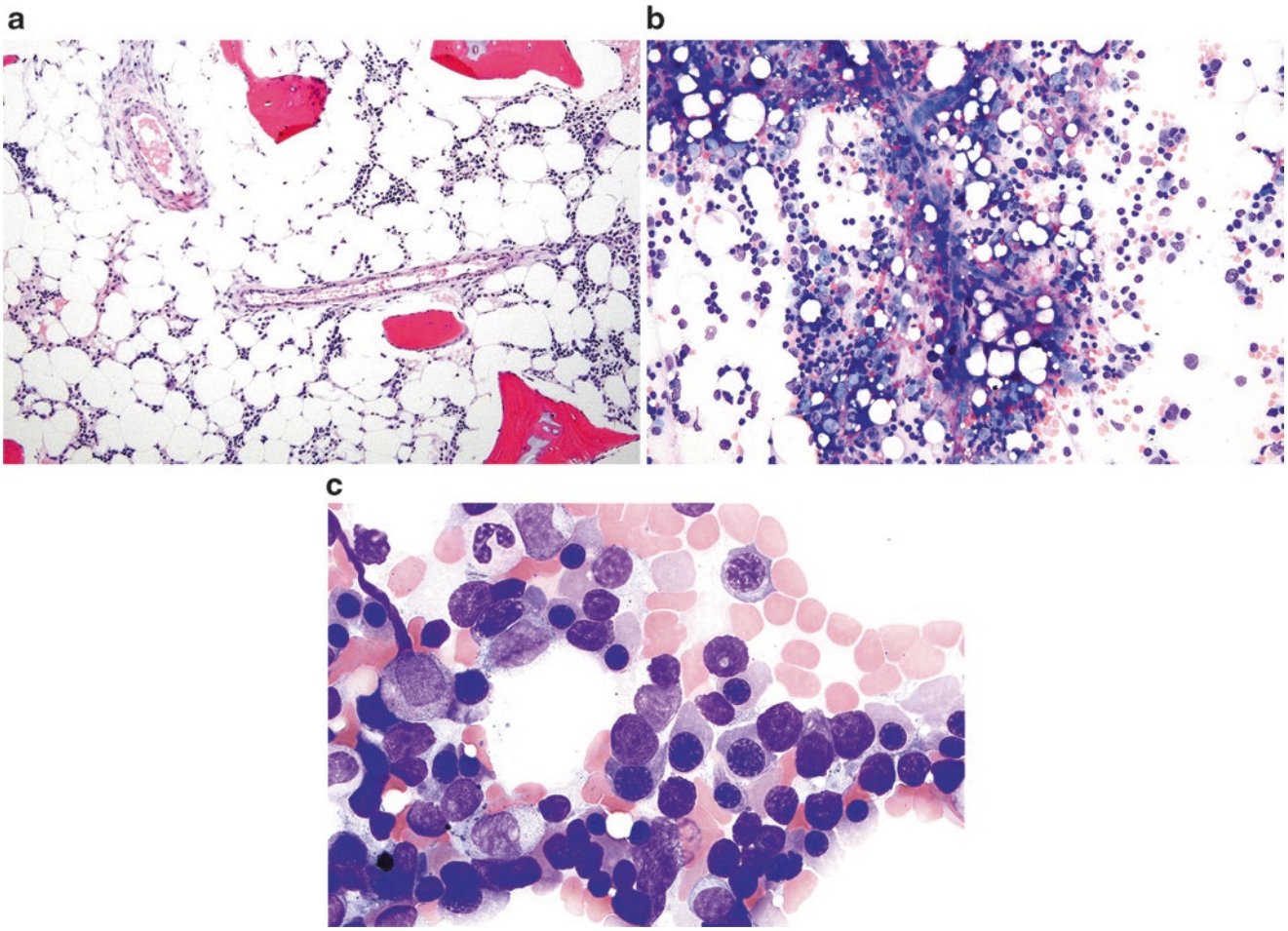

Fig. 4.3 Shwachman-Diamond syndrome (SDS). SDS is associated with germline mutations in the *SBDS* gene. Neutropenia is the most common cytopenia in SDS, although mild anemia and thrombocytopenia may also be present. Bone marrow cellularity is highly variable, ranging from hypoplastic to hypercellular, and does not correlate well with the degree of peripheral cytopenias. Children with SDS often present with bone marrows that are hypocellular for their age (**a**), with diminished multilineage hematopoiesis and relatively hypoplastic and left-shifted granulopoiesis (**b** and **c**). Because mild morphologic dysplasia is commonly seen in SDS, caution should be taken not to overinterpret it as MDS, although these patients are certainly at risk for MDS/AML. Furthermore, cytogenetic analysis in surveillance marrows may be associated with frequent appearance (and disappearance) of clones

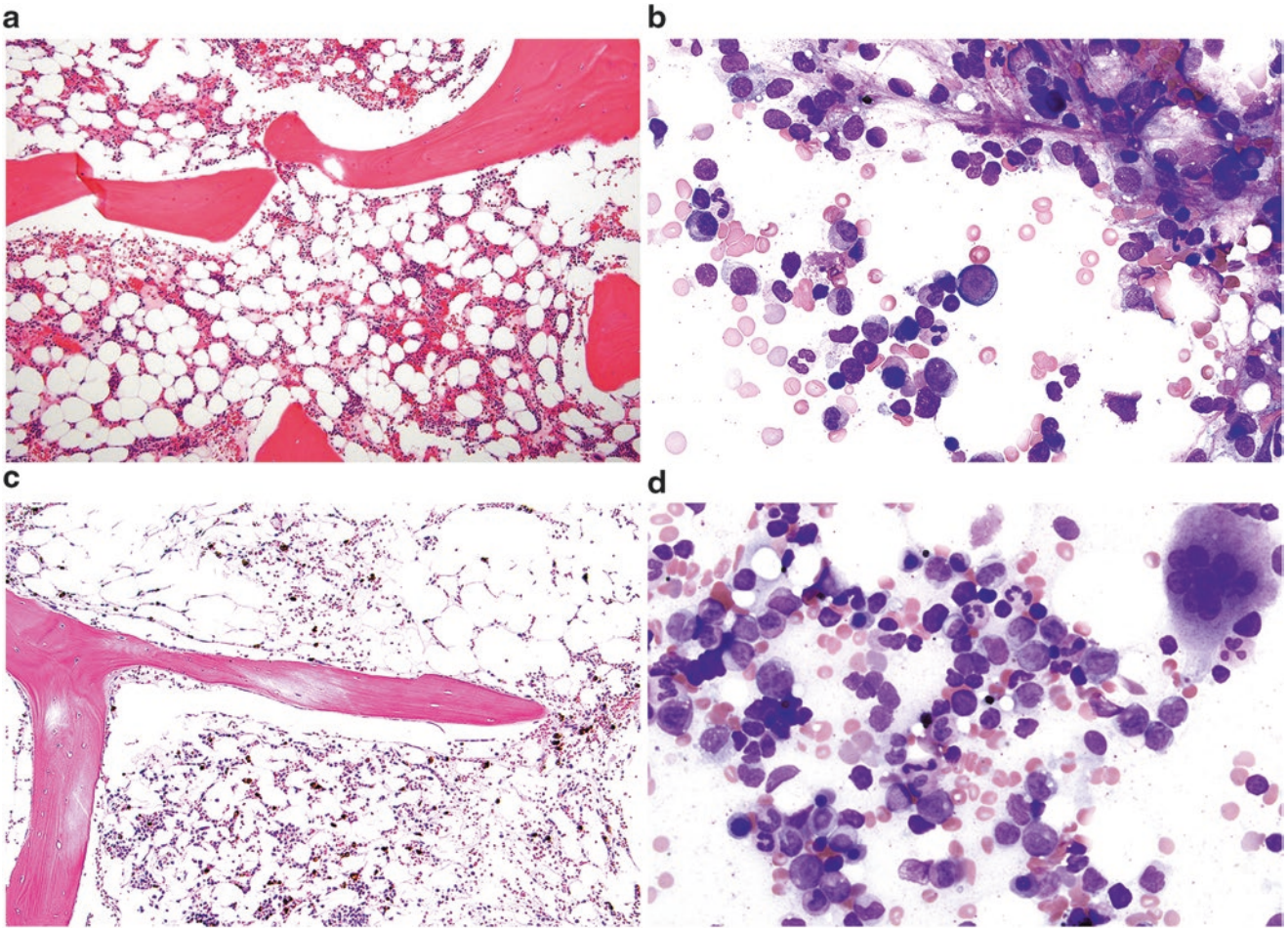

Fig. 4.4 Telomere diseases/dyskeratosis congenita. Dyskeratosis congenita and telomere diseases result from mutations in one of many genes, including *DKC1*, *TERT*, and *TERC*. Telomerase is a ribonucleoprotein complex that synthesizes/elongates telomeres to counteract the attrition that occurs with cell division. *TERT* encodes the telomerase enzyme, whereas *TERC* encodes the RNA template. *DKC1* is present on the X chromosome and encodes dyskerin, another protein associated with the complex, without which it becomes destabilized. Dyskeratosis congenita frequently refers to a bone marrow failure state with a classic triad of dystrophic nails, oral leukoplakia, and lacy, reticular skin pigmentation of the upper chest and neck, sometimes accompanied by mental retardation or other manifestations. Mutations in *TERT* and *TERC* and other genes in the telomere complex cause disease in children and adults characterized by bone marrow failure as well as pulmonary fibrosis, liver disease, and premature graying of hair. (**a**) and (**b**) Macrocytosis and thrombocytopenia were found in a previously healthy 16-year-old boy prior to surgery to repair a femur fracture sustained in a sports accident. Examination revealed that his bone marrow was hypocellular for age (30–35% cellular) with diminished multilineage hematopoiesis and a relative mild megaloblastoid erythroid hyperplasia but no increase in blasts. He was subsequently found to have extremely short telomeres and a heterozygous mutation in *TERT*. (**c**) and (**d**) A hypocellular marrow is present in a 9-year-old girl with a germline heterozygous mutation in *TERT* with moderate pancytopenia. The aspirate smear shows decreased progressive myelopoiesis and erythropoiesis without overt dysplasia. (**e**) Flow cytometry with fluorescence in situ hybridization (Flow-FISH) analysis demonstrates decreased telomere length in lymphocytes and granulocytes (black circle) from a young adult with pancytopenia and germline *TERC* mutation

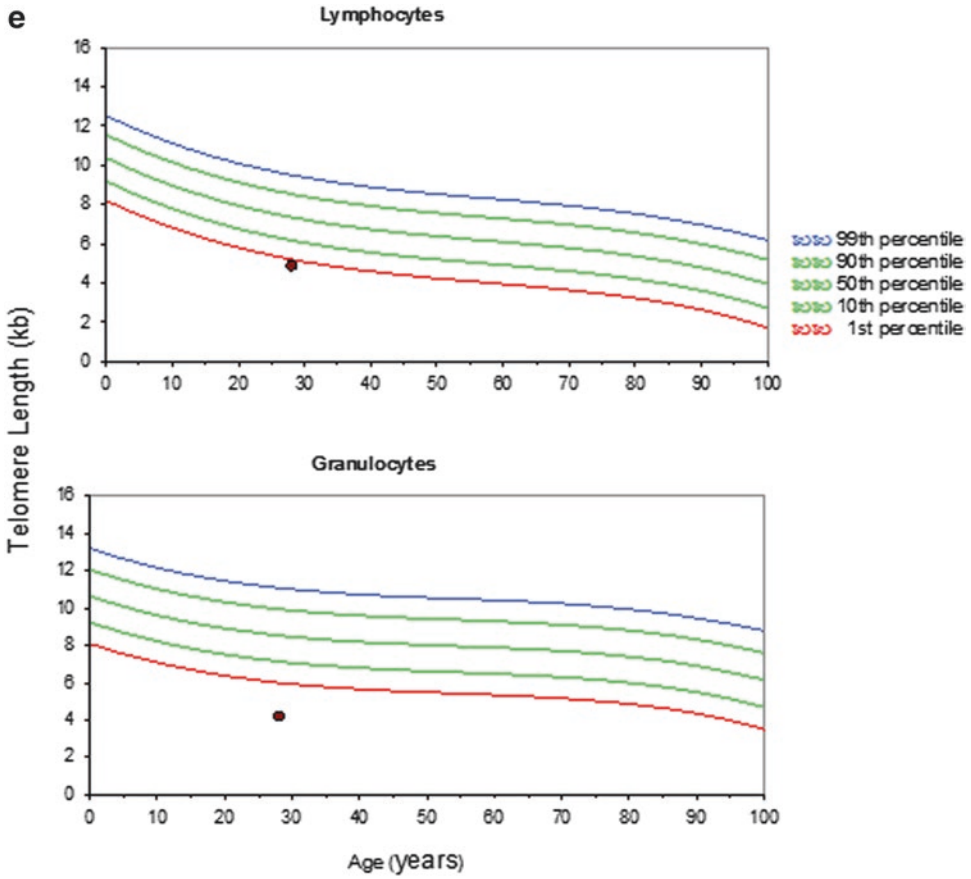

Fig. 4.4 (continued)

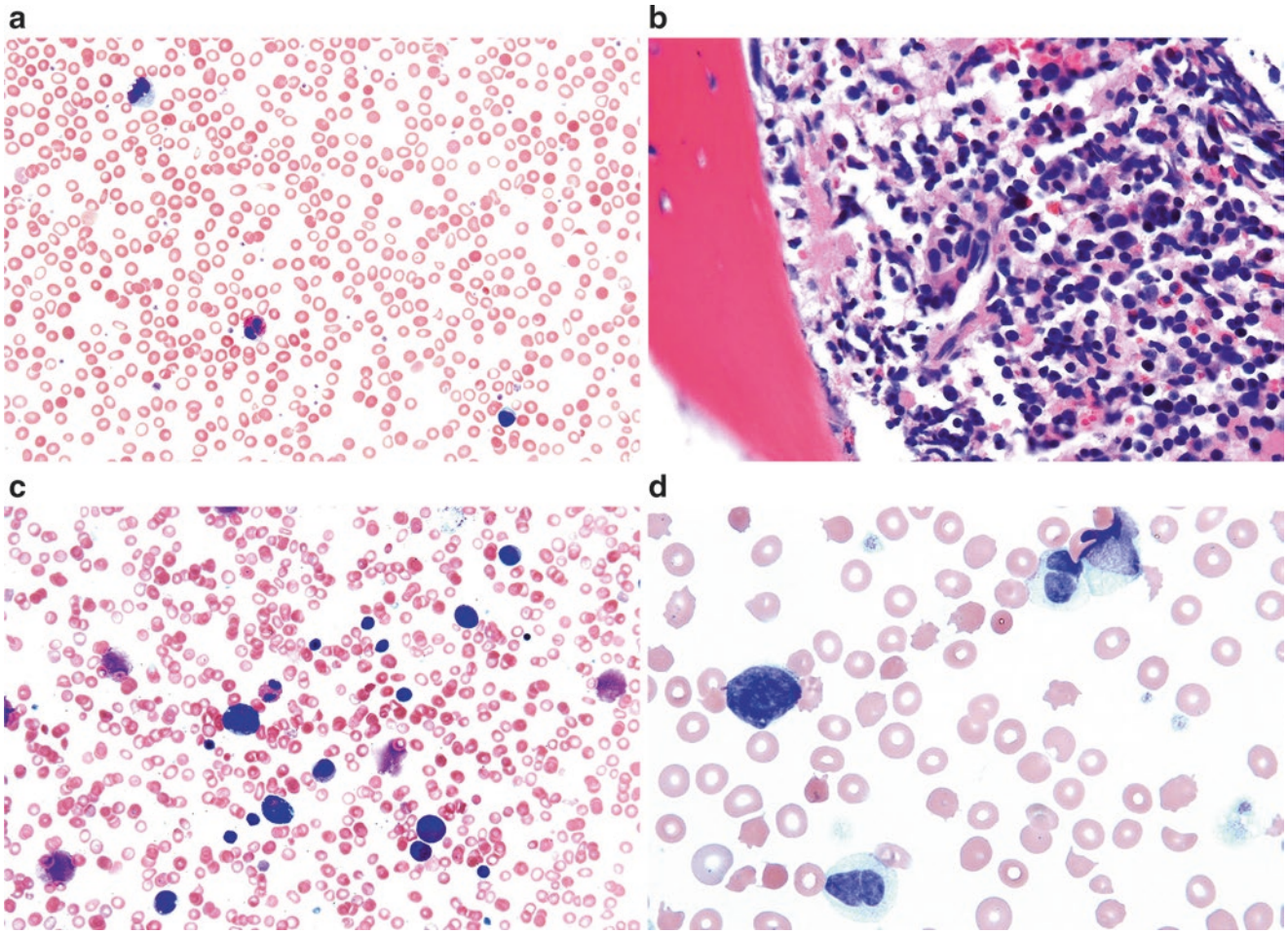

Fig. 4.5 Severe congenital neutropenia (SCN). In a 12-week-old boy, first-degree heart block, dermatitis, and neutropenia were all attributed to neonatal lupus erythematosus, as his mother had been diagnosed earlier with discoid lupus erythematosus. (**a**) No segmented neutrophils could be identified on his peripheral blood smear, although mature eosinophils were present. (**b**) and (**c**) Bone marrow examination revealed a prominent lymphoid component as physiologic hematogone hyperplasia, which typically occurs in the first month of life and persists for the first couple of years. However, a maturation arrest was observed in the neutrophil series; occasional promyelocytes and very rare neutrophilic myelocytes and metamyelocytes were seen without definite band forms or segmented neutrophils. We felt this might represent an alloimmune phenomenon associated with neonatal lupus erythematosus (which would be determined to some extent by a compatible clinical evolution but would tend to be associated with a later "block" in maturation), but we could not exclude severe congenital neutropenia/Kostmann syndrome. A mutation was found in his *ELANE* gene, which is associated with autosomal dominant severe congenital (static) neutropenia, as well as cyclic neutropenia. (**d**) A feared complication of SCN is shown here, with development of MDS/AML in a girl who had been receiving long-term therapy with granulocyte-colony stimulating factor

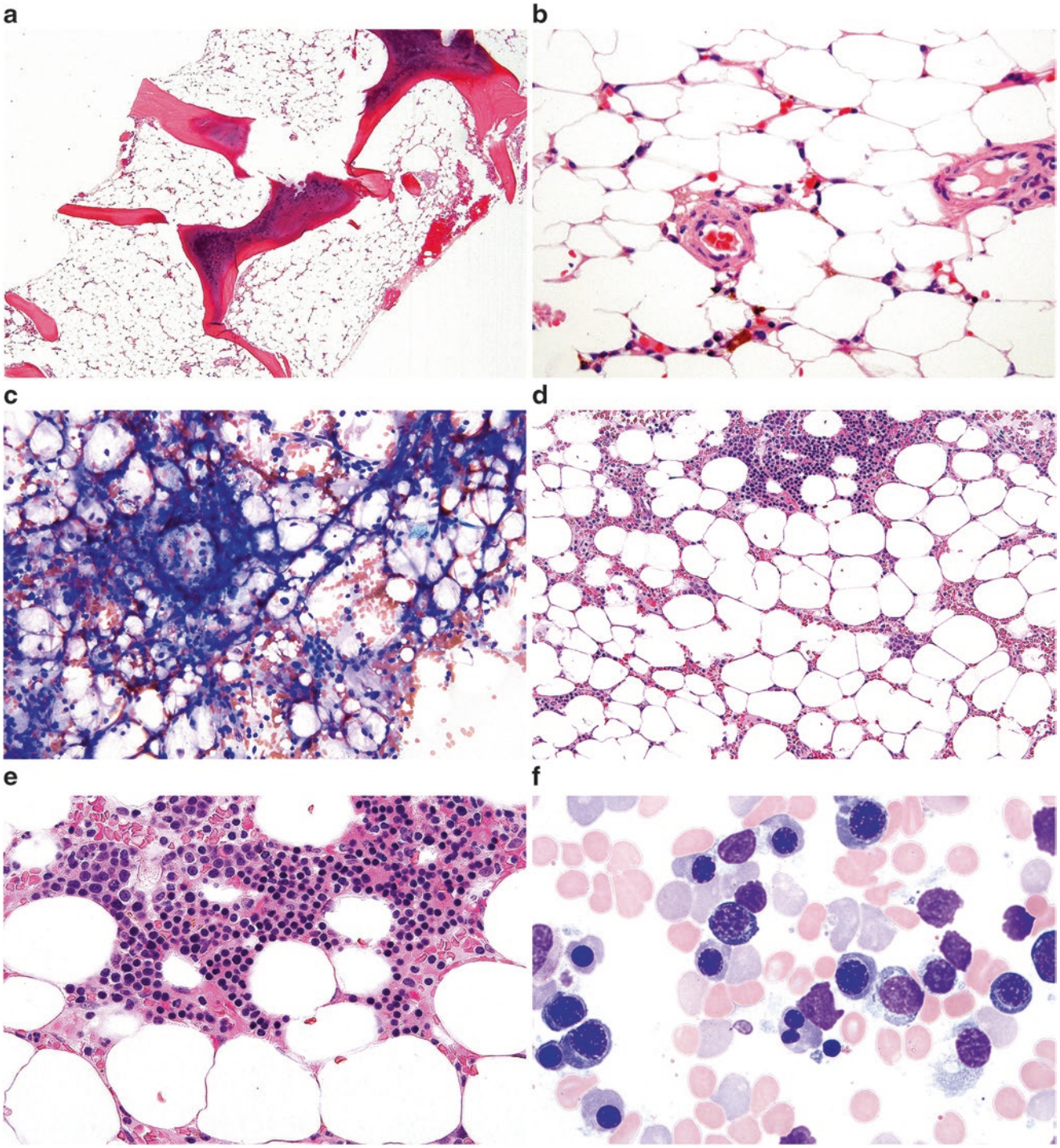

Fig. 4.6 Aplastic anemia (AA) and AA with a paroxysmal nocturnal hemoglobinuria (PNH) clone. Idiopathic AA is largely thought to be an acquired disease with autoimmune etiology, but the features overlap with many inherited bone marrow failure syndromes, and genetic testing may be required to rule out inherited bone marrow failure. Of patients with acquired AA, approximately 10–15% ultimately develop MDS, which suggests a component of underlying primary marrow disease in some patients. Patients with AA frequently harbor somatic mutations in *PIGA*, resulting in PNH clones. (**a**) This low-power image of a trephine biopsy from a teenage girl with AA whose marrow is diffusely and markedly hypocellular for age. (**b**) High-power image of an H&E-stained bone marrow biopsy section shows profound hypocellularity. The few remaining hematopoietic cells are lymphocytes, plasma cells, and macrophages with pigment in their cytoplasm. (**c**) Wright-Giemsa-stained bone marrow aspirate smear contains a profoundly hypocellular particle with prominent stromal elements including fat cells and capillaries lined by endothelial cells and few residual hematopoietic cells (mostly lymphocytes and macrophages). (**d**) Bone marrow from a 23-year-old man with AA and a PNH clone. The PNH clone was detected by flow cytometry analysis of the peripheral blood and involved 99% of neutrophils. (**e**) At higher magnification, note foci of erythropoiesis frequently seen in hypocellular marrows of patients with AA and PNH clones. (**f**) Aspirate smear shows an erythroid predominance and nuclear budding in occasional erythroid precursors from the same patient with AA and PNH. Occasional nuclear budding and binucleation of erythroid precursors (typically involving less than 10% of the erythroid precursors) can be seen in patients with PNH clones. Caution must be used not to overinterpret these changes as evidence of dysplasia in patients with PNH

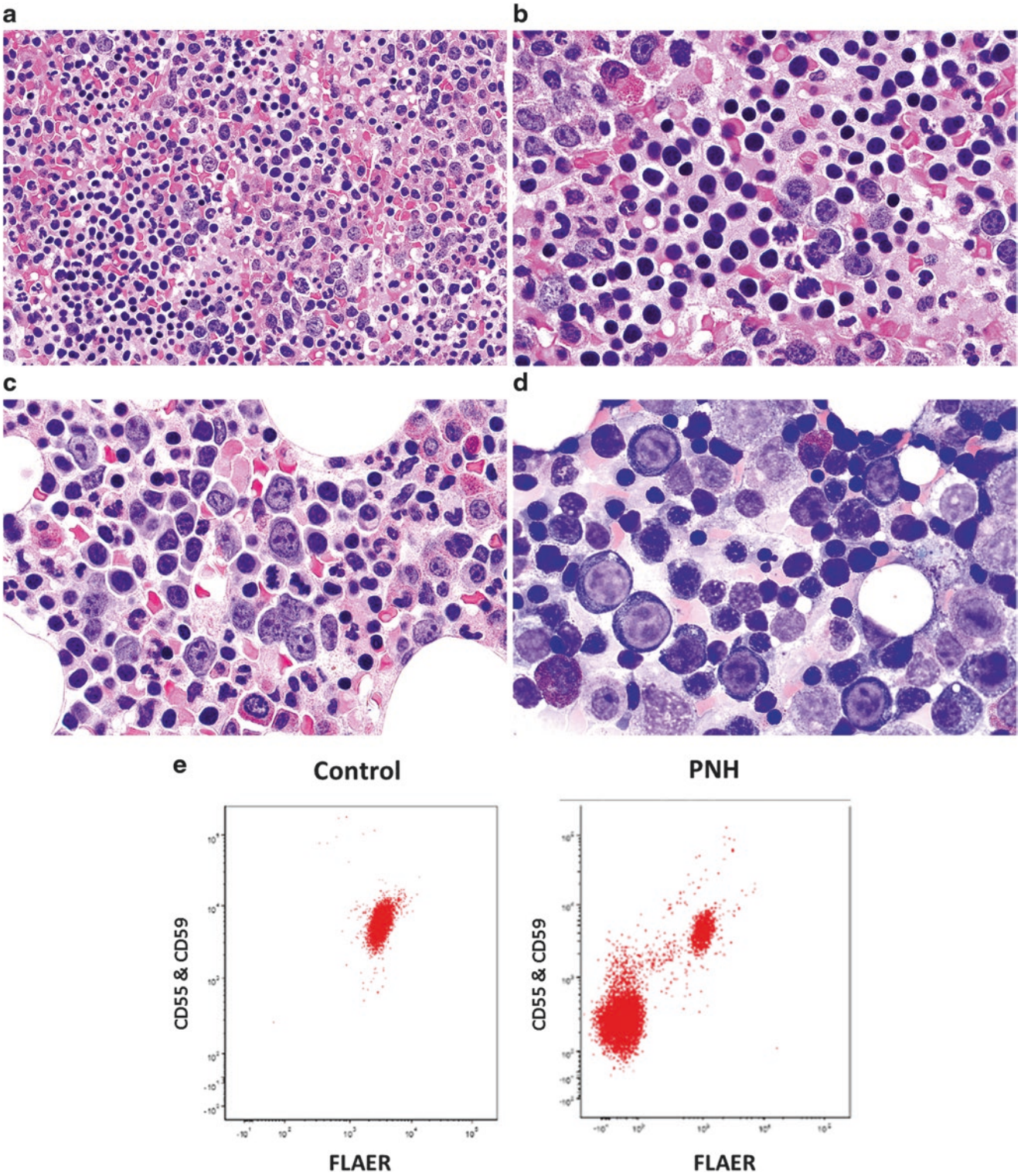

Fig. 4.7 Paroxysmal nocturnal hemoglobinuria. PNH is characterized by acquired somatic mutations in the *PIGA* gene, leading to loss of GPI-linked proteins on red blood cells (RBCs) and white blood cells, and subsequent destruction of RBCs by the complement system. Patients suffer from intravascular hemolysis, with an increased risk of thrombosis. (**a**) and (**b**) This bone marrow core biopsy from a woman with PNH shows a hypercellular marrow with erythroid hyperplasia. (**c**) Frequently, erythropoiesis is left-shifted with large cells with dispersed blast-like chromatin on H&E stain. (**d**) Aspirate smear shows left-shifted erythropoiesis and occasional nuclear budding consistent with stressed erythropoiesis. Flow cytometric analysis has largely replaced earlier tests (sucrose lysis test and Ham's acid hemolysis test) for PNH. (**e**) Peripheral blood neutrophils show normal expression of CD55, CD59, and FLAER in cells from a healthy control (left plot). In contrast, a large population of neutrophils in the patient with PNH has lost expression of CD55, CD59, and FLAER (*right plot*), representing a PNH clone of approximately 75% in this patient

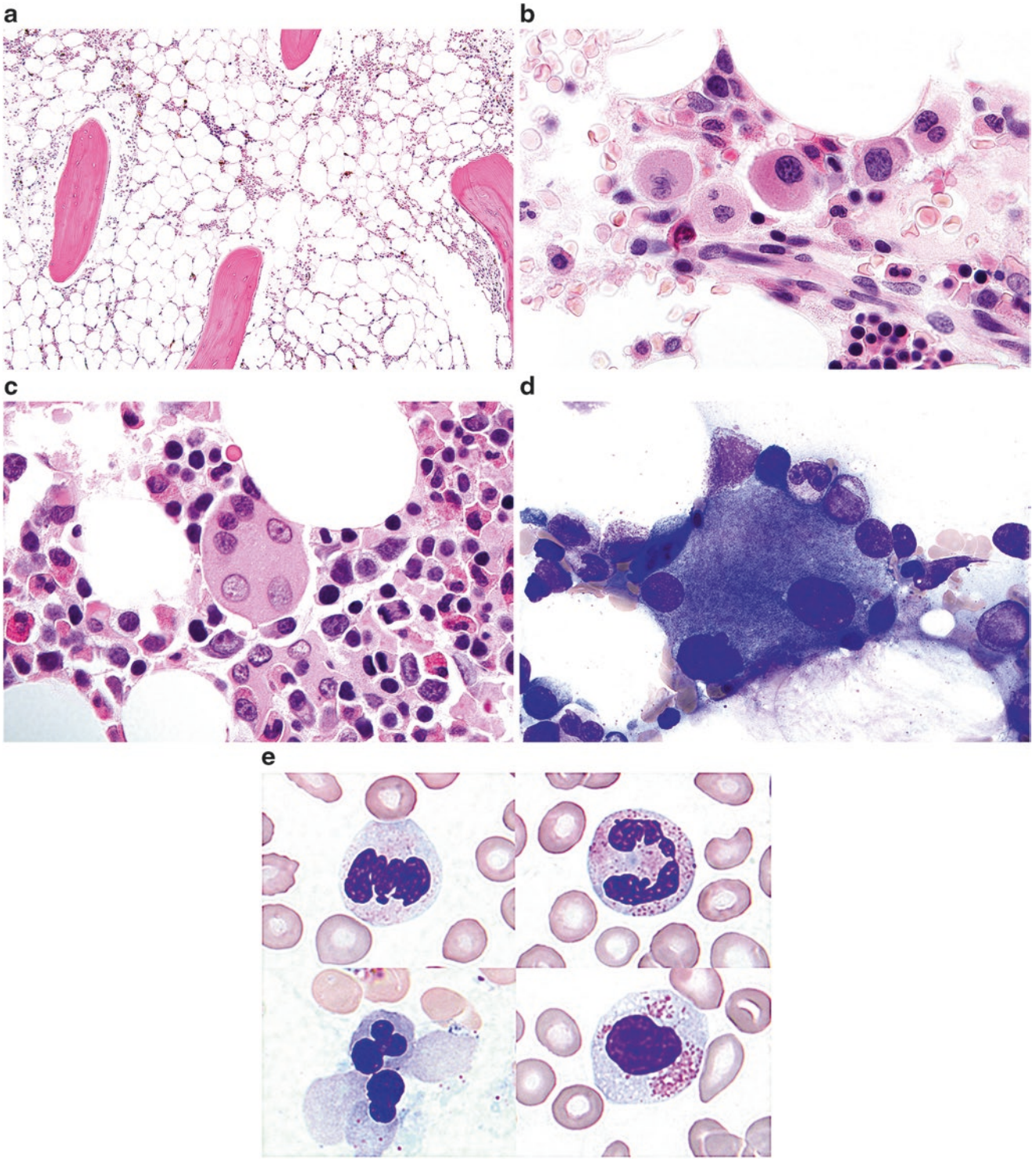

Fig. 4.8 GATA2 deficiency. GATA2 is a transcription factor that is critical for normal hematopoiesis. Germline heterozygous mutations in *GATA2* lead to a spectrum of bone marrow disease that overlaps with aplastic anemia (AA), hypocellular MDS/AML, and chronic myelomonocytic leukemia (CMML). Patients may have a family history of AA, MDS, AML, or CMML. Many patients present with a history of warts and/or severe immunodeficiency characterized by loss of monocytes, B cells, B-cell precursors, NK cells, and dendritic cells, with opportunistic infections such as *Mycobacterium avium* complex. (**a**) Bone marrow biopsy from a 19-year-old man with pancytopenia and a previous diagnosis of AA. The bone marrow is markedly hypocellular for the patient's age. (**b**) Close examination on higher power reveals clusters of atypical, hypolobated megakaryocytes. Cytogenetic analysis of this marrow specimen revealed monosomy 7, and a germline mutation in *GATA2* was identified. The final diagnosis was myelodysplasia with germline *GATA2* mutation. (**c**) and (**d**) Bone marrow from a 36-year-old man with a history of warts and recent cytopenias. Note the characteristic large, osteoclast-like megakaryocytes with multiple separated nuclear lobes on the core biopsy (**c**) and aspirate smear (**d**), which are common in patients with GATA2 deficiency. Cytogenetic analysis showed trisomy 8, and a germline *GATA2* mutation was identified. (**e**) Composite of atypical cells commonly seen in GATA2 deficiency, including hypogranular and/or hyposegmented granulocytes and dyserythropoietic red cell precursors

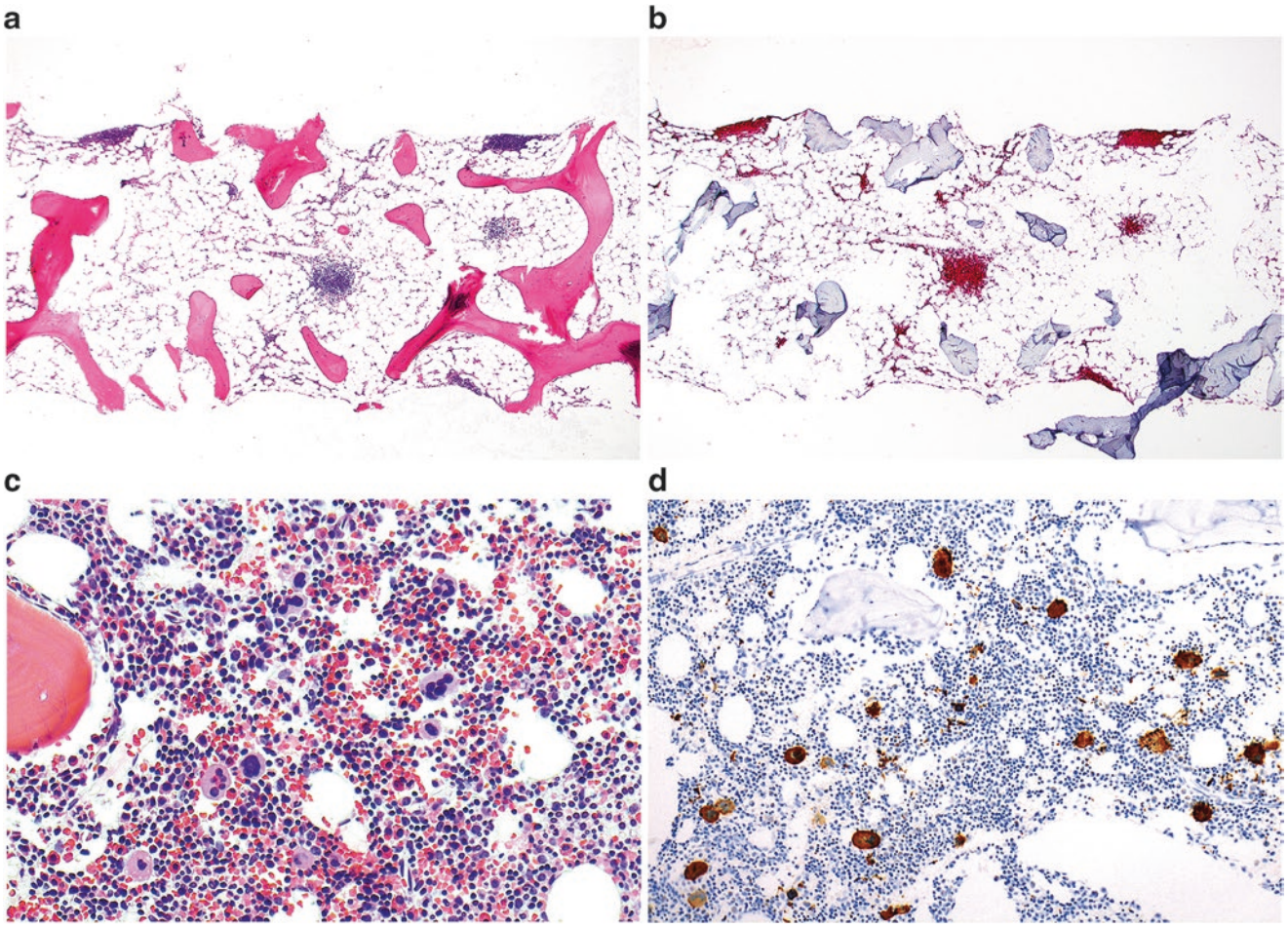

Fig. 4.9 CTLA4 deficiency. Patients with heterozygous germline mutations in the gene encoding cytotoxic T-lymphocyte antigen-4 (*CTLA4)* can present with severe immune dysregulation leading to autoimmune cytopenias, B-cell lymphopenia, and lymphocytic infiltrates in multiple organs. The bone marrow features show a morphologic spectrum overlapping with AA, large granular lymphocytic leukemia (LGL), and immune thrombocytopenic purpura (ITP). (**a**) Bone marrow core biopsy from an 18-year-old woman with pancytopenia. The marrow is markedly hypocellular for the patient's age, with trilineage hypoplasia resembling an aplastic marrow. Additionally, multiple distinct lymphoid aggregates are identified, which are composed of small- to medium-sized lymphocytes. (**b**) Immunohistochemistry (IHC) for CD3 showed that the lymphocytic aggregates were composed of T cells that were predominantly CD4-positive. IHC for CD8 revealed a subtle yet diffuse interstitial CD8-positive T-cell infiltrate (*not shown*). IHC for CD20 showed near absence of B cells (*not shown*). Molecular genetic studies showed an abnormal T-cell gene rearrangement pattern (oligoclonal). Genetic sequencing revealed a germline heterozygous mutation in *CTLA4*. (**c**) and (**d**) An 8-year-old boy initially presented at age 7 with marked thrombocytopenia with a high immature platelet fraction. He responded to two doses of intravenous immune globulin with brief but nonsustained normalization of the platelet count. In addition, there was an absolute neutropenia and mild anemia; the neutropenia resolved, but the anemia was stable. Bone marrow examination showed megakaryocytic hyperplasia (**C**, H&E stain; (**d**), CD61 IHC stain), consistent with the clinical diagnosis of ITP. Subsequently, platelet-specific and neutrophil antibodies were demonstrated; taken together with lymphadenopathy and splenomegaly, these results suggested autoimmune lymphoproliferative syndrome (ALPS). An ALPS panel by flow cytometry revealed 2.3% TCRαβ CD4,CD8 double-negative T cells (0.3–1.7). No mutations were identified in *FAS* (*TNFRSF6*), *FASLG* (*TNFSF6*), or *CASPASE 10*, three of the most common genes implicated in ALPS. Three years later, the patient presented with neurological symptoms and was found to have a large tumorlike inflammatory brain lesion, which led to sequencing and discovery of a heterozygous germline *CTLA4* mutation

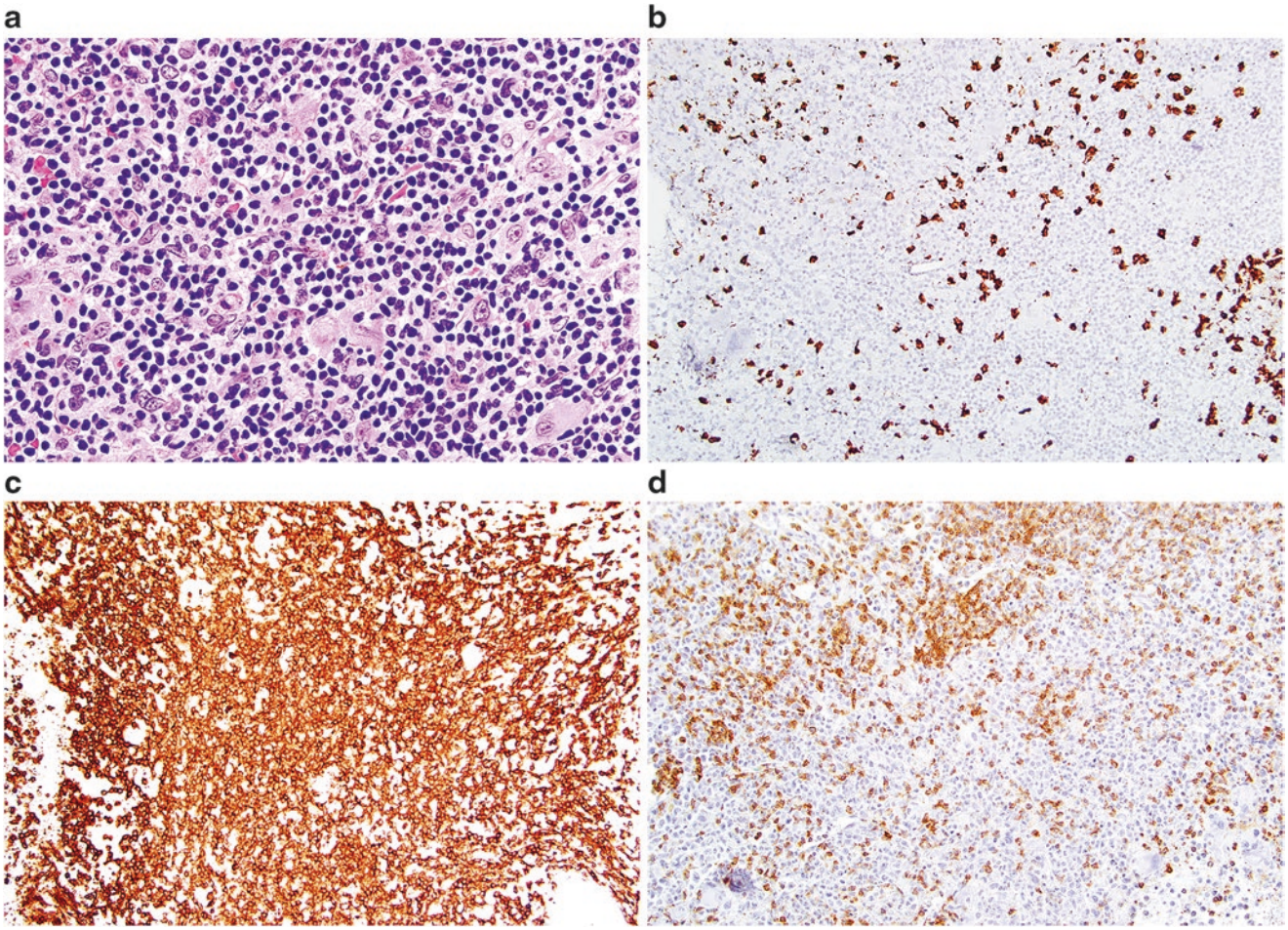

Fig. 4.10 Autoimmune lymphoproliferative syndrome (ALPS). Patients with ALPS have germline mutations in one of several genes critical for FAS-mediated lymphocyte apoptosis, including *FAS*, *FASL*, and *CASP 10*. Patients can present with autoimmune cytopenias, lymphadenopathy, splenomegaly, and hypergammaglobulinemia, and they have an increased risk of developing lymphoma. The hallmark of ALPS is increased numbers of CD4 and CD8 double-negative T cells (DNTs). The bone marrow in patients with ALPS typically shows lymphocytosis with non-paratrabecular lymphoid aggregates (**a**). In this case from a patient with a germline *FAS* mutation, the lymphoid aggregates are primarily composed of T cells highlighted by CD3 immunohistochemistry (IHC) (**c**), with occasional admixed B cells highlighted by CD20 IHC (**b**). CD45RO IHC staining (**d**) is significantly less than CD3, consistent with the presence of increased DNTs (*Courtesy of* Dr. Irina Maric)

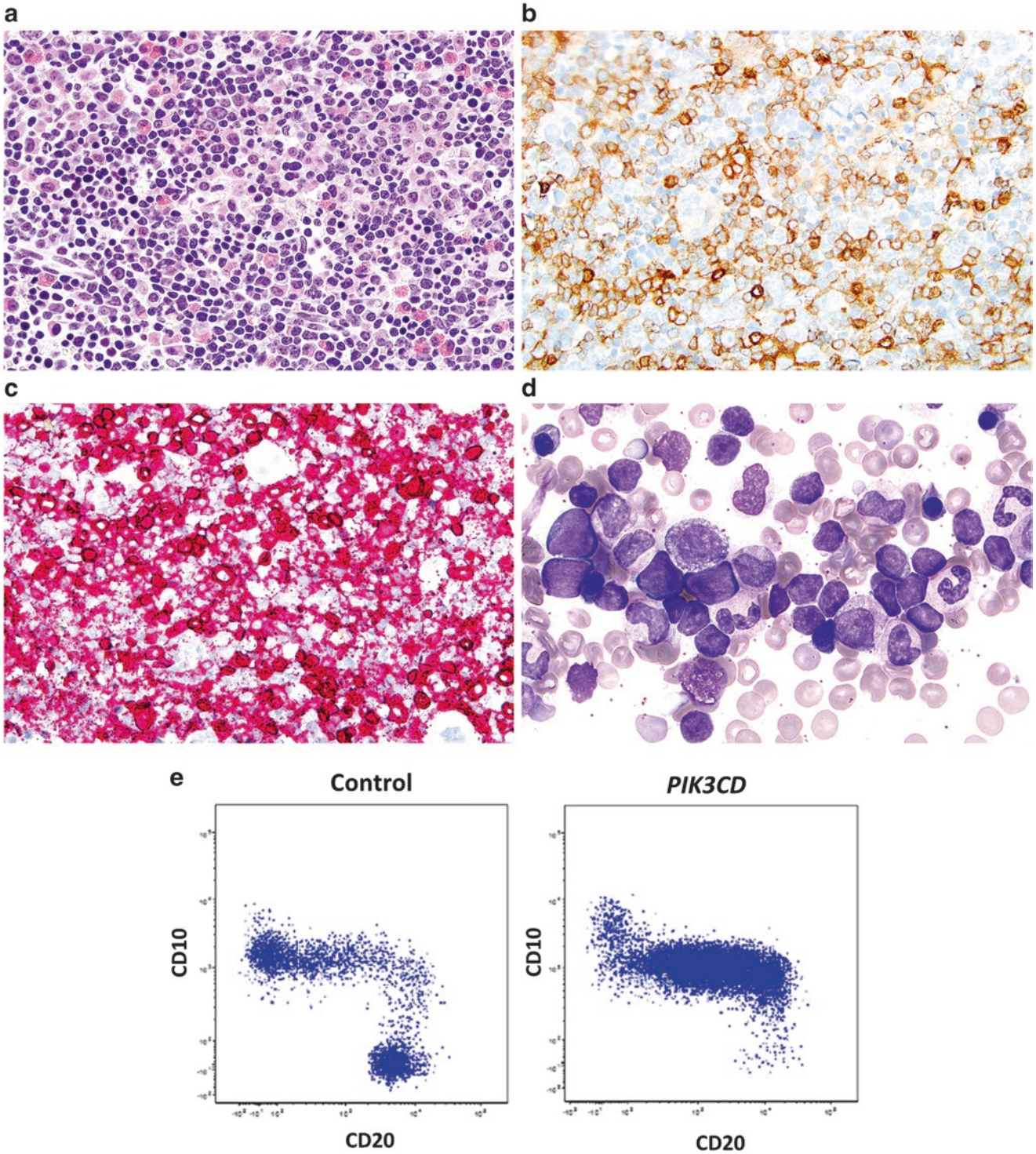

Fig. 4.11 Activated PI3K-delta syndrome. Germline gain-of-function mutations in *PIK3CD* can lead to a syndrome characterized by cytopenias, immunodeficiency, lymphoproliferation in tissues, lymphopenia in the peripheral blood, cytomegalovirus, and Epstein-Barr virus (EBV) viremia, with an increased risk of developing B-cell lymphomas. (**a**) This bone marrow is from a 5-year-old boy with cytopenias and a germline mutation in *PIK3CD*. The marrow is hypercellular, with hematogone or precursor B-cell hyperplasia. Immunohistochemistry for CD10 (**b**) and CD79a (**c**) shows an abundance of B-cell precursors. (**d**) The aspirate smear shows frequent immature lymphoid precursors, many of which have blast-like chromatin. Flow cytometric analysis shows an abnormal B-cell maturation pattern in the CD19+ lymphoid compartment. (**e**) Bone marrow from a healthy pediatric control, for comparison. The B-cell compartment of the patient with activated PI3K-delta syndrome shows an abundance of CD10+ B-cell precursors with a near absence of mature CD10−/CD20+ B cells. This pattern resembles a maturation arrest at the transitional B-cell or late hematogone stage. These findings may overlap with maturation arrest observed in an acute leukemia, so they should be interpreted with caution

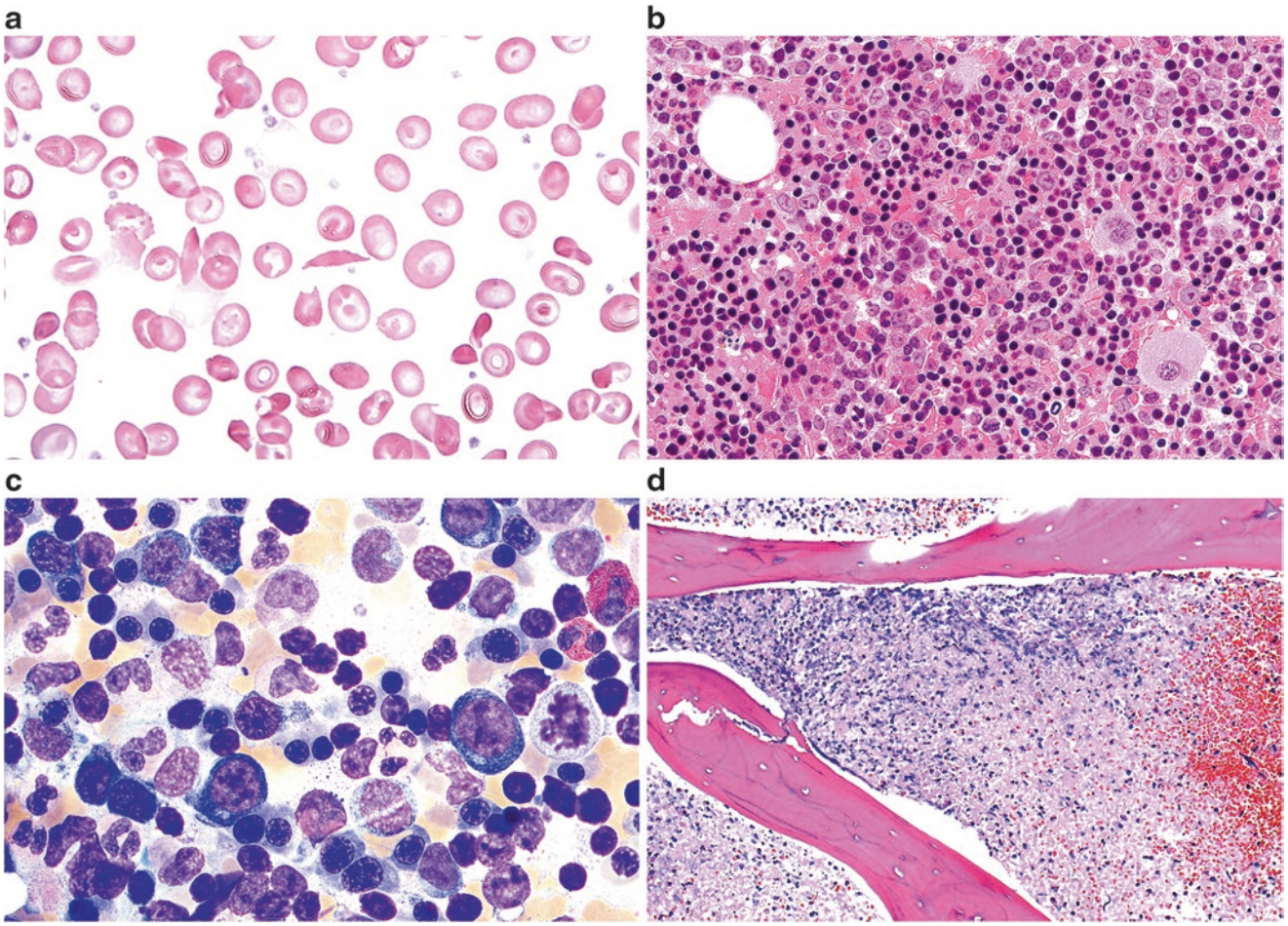

Fig. 4.12 Sickle cell anemia (SCA). SCA is an inherited hemoglobinopathy with RBCs that contain abnormal hemoglobin causing rigid sickling of the RBCs. (**a)** This peripheral smear from a 20-year-old man with hemoglobin SS shows RBCs with marked anisocytosis and poikilocytosis, sickle cells, numerous target cells, Howell-Jolly bodies, and Pappenheimer bodies. The bone marrow core biopsy is hypercellular (**b**). Evidence of erythroid hyperplasia is seen on both the core biopsy and the aspirate smear (**c**), as evidenced by an inverted M:E ratio. The bone marrow biopsy from a separate patient (**d**) shows necrosis and acute inflammation

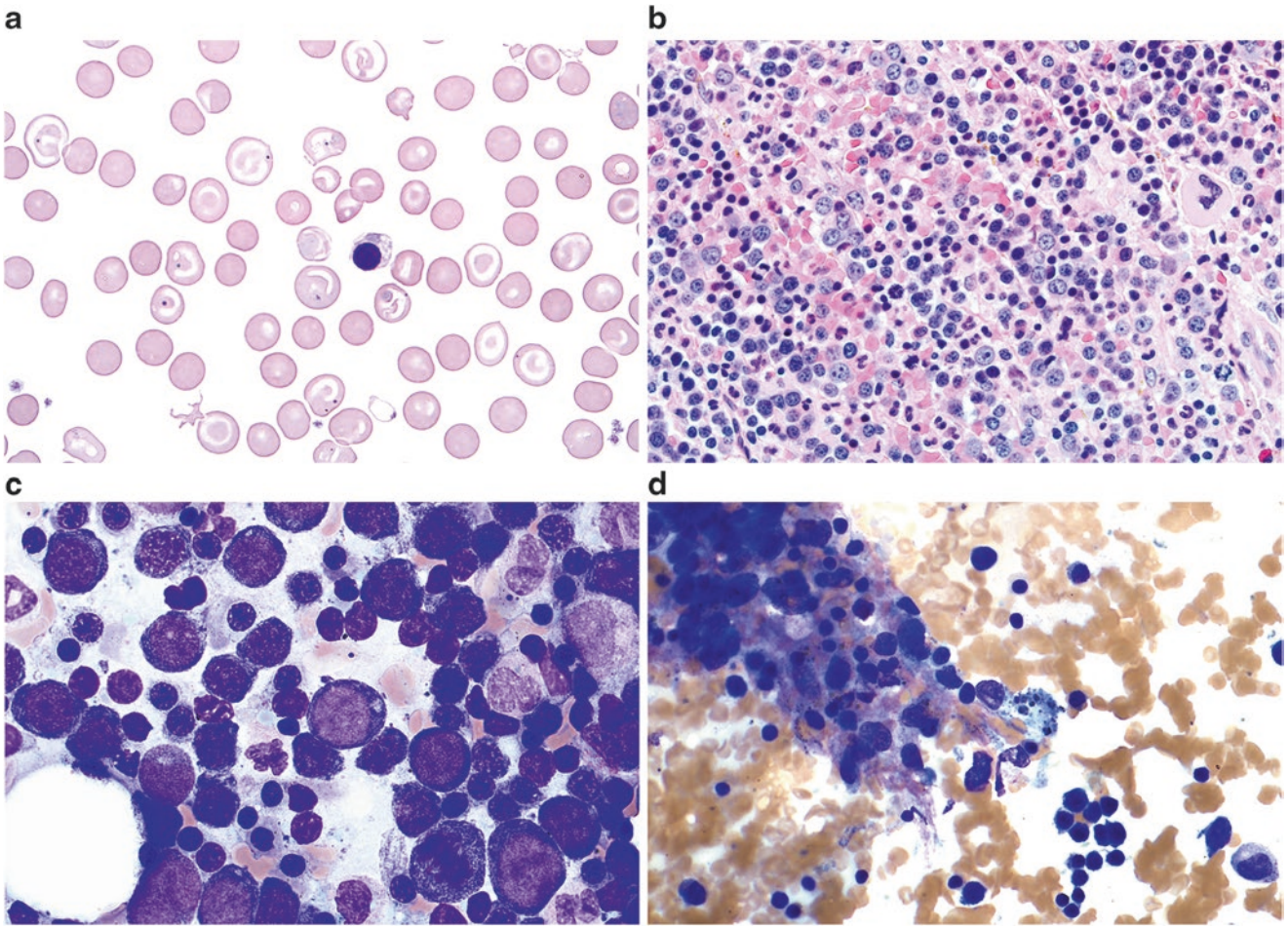

Fig. 4.13 Thalassemia. Thalassemia is an inherited blood disorder resulting from reduced production of hemoglobin. The two most common forms of thalassemia are β-thalassemia and α-thalassemia. (**a**) A peripheral smear from a 27-year-old woman with β-thalassemia intermedia showing severe anemia with nucleated RBCs, microcytes, target cells, and Pappenheimer bodies. (**b**) The bone marrow core biopsy shows a hypercellular marrow with an erythroid hyperplasia. Note the numerous cells with fine chromatin consistent with erythroid pronormoblasts and left-shifted erythropoiesis. (**c**) The aspirate smear confirms the marked erythroid predominance with frequent early erythroid progenitors. (**d**) A bone marrow aspirate smear from a teenage transfusion-dependent β-thalassemia patient shows erythroid hyperplasia and siderophages. Iron overload is a major cause of morbidity in thalassemia

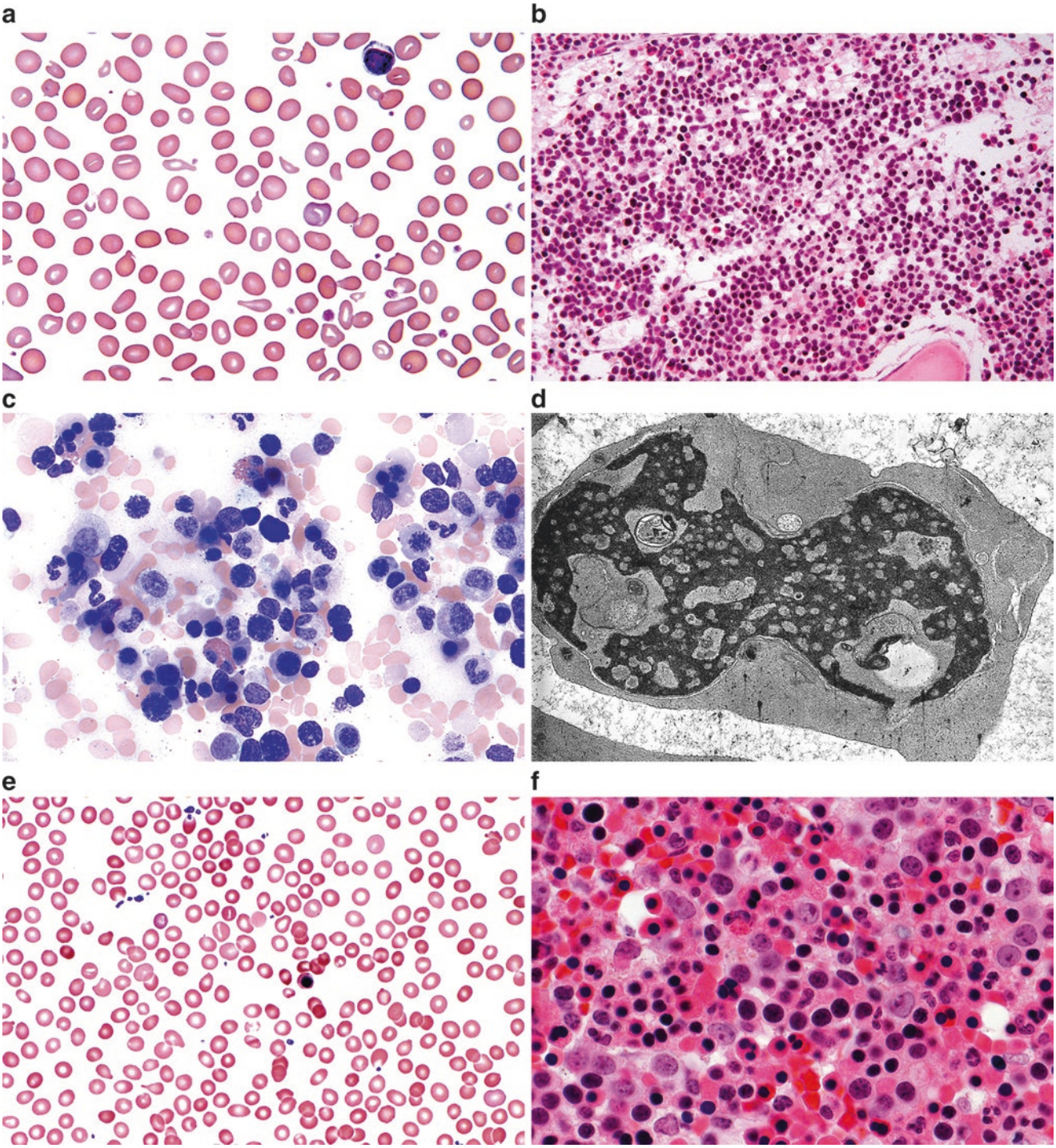

Fig. 4.14 Congenital dyserythropoietic anemia (CDA). (**a**) A peripheral blood smear in CDA type 1, a rare anemia caused by mutations in the *CDAN1* gene located at 15q15.1–15q15.3 and inherited in autosomal recessive fashion, typically shows macrocytic anemia with basophilic stippling. (**b**) As in all types of CDA, a marked erythroid hyperplasia is evident on histology. (**c**) In CDA type 1, the bone marrow aspirate demonstrates megaloblastic erythroid hyperplasia with an increase in binucleate erythroid precursors whose nuclei may partially fuse and be of unequal size. Internuclear chromatin bridges characteristically are seen between polychromatophilic erythroblasts (*not shown*). (**d**) Electron microscopy shows partially fused erythroid precursors with unequal nuclei and characteristic abnormalities of chromatin assembly in the dark-staining areas (heterochromatin) of their nuclei, resulting in a spongy or "Swiss cheese" appearance imparted by electron lucent "holes" (**e**) CDA type 2 is the most common type; it is caused by mutations in *CDAN2* at 20p11.23 and is also autosomal recessively inherited. The peripheral blood smear shows normocytic, normochromic anemia with moderate anisopoikilocytosis and basophilic stippling (*latter not shown*). (**f**) Trephine biopsy section shows an erythroid hyperplasia. Even on histology, binucleated erythroid precursors can be recognized.

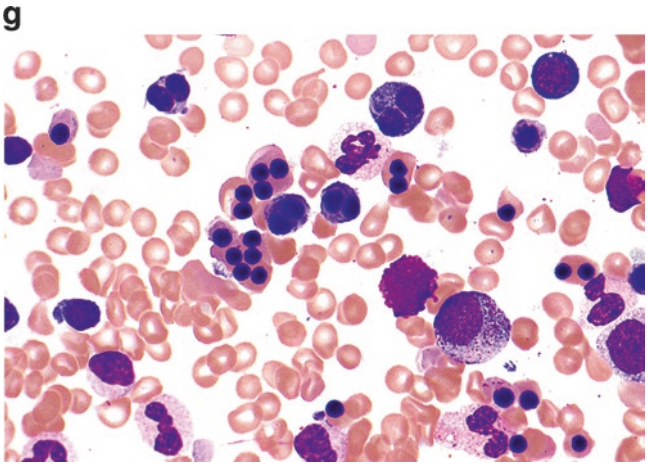

Fig. 4.14 (continued) (**g**) These direct smears from a middle-aged woman with lifelong anemia show a normoblastic erythroid hyperplasia; CDA type 2 is often diagnosed later in life than type 1. Rare early-stage and 10–35% of late-stage erythroid precursors are binucleate; a few are even trinucleate or multinuclear. CDA type 2 is also known as HEMPAS (hereditary erythroblastic multinuclearity with positive acidified serum test). The positive acidified serum lysis test (Ham test), whereby an antigen on CDA-2 red cells combines specifically with about 30% of fresh ABO-compatible normal sera, has been replaced by gel electrophoresis, which can be used to select who should undergo *CDAN2* gene testing, as the band 3 protein on CDA-2 red cells is underglycosylated and migrates faster than normal. CDA type 3 and other types are less common. CDA type 3 has both a familial form (*CDAN3*; autosomal dominant) and a sporadic form. Anemia is mild to moderate and usually macrocytic but sometimes is normocytic. Anisocytosis and poikilocytosis are present, as in CDA types 1 and 2. Like type 1, the bone marrow in CDA type 3 shows megaloblastic erythroid hyperplasia, but the distinguishing feature is the presence of 10–40% "gigantoblasts": large erythroid precursors with a single nucleus or up to 12 nuclei (*not shown*). Interestingly, CDA type 3 patients appear to have an increased risk of lymphoproliferative disorders, although the basis of this risk is unclear

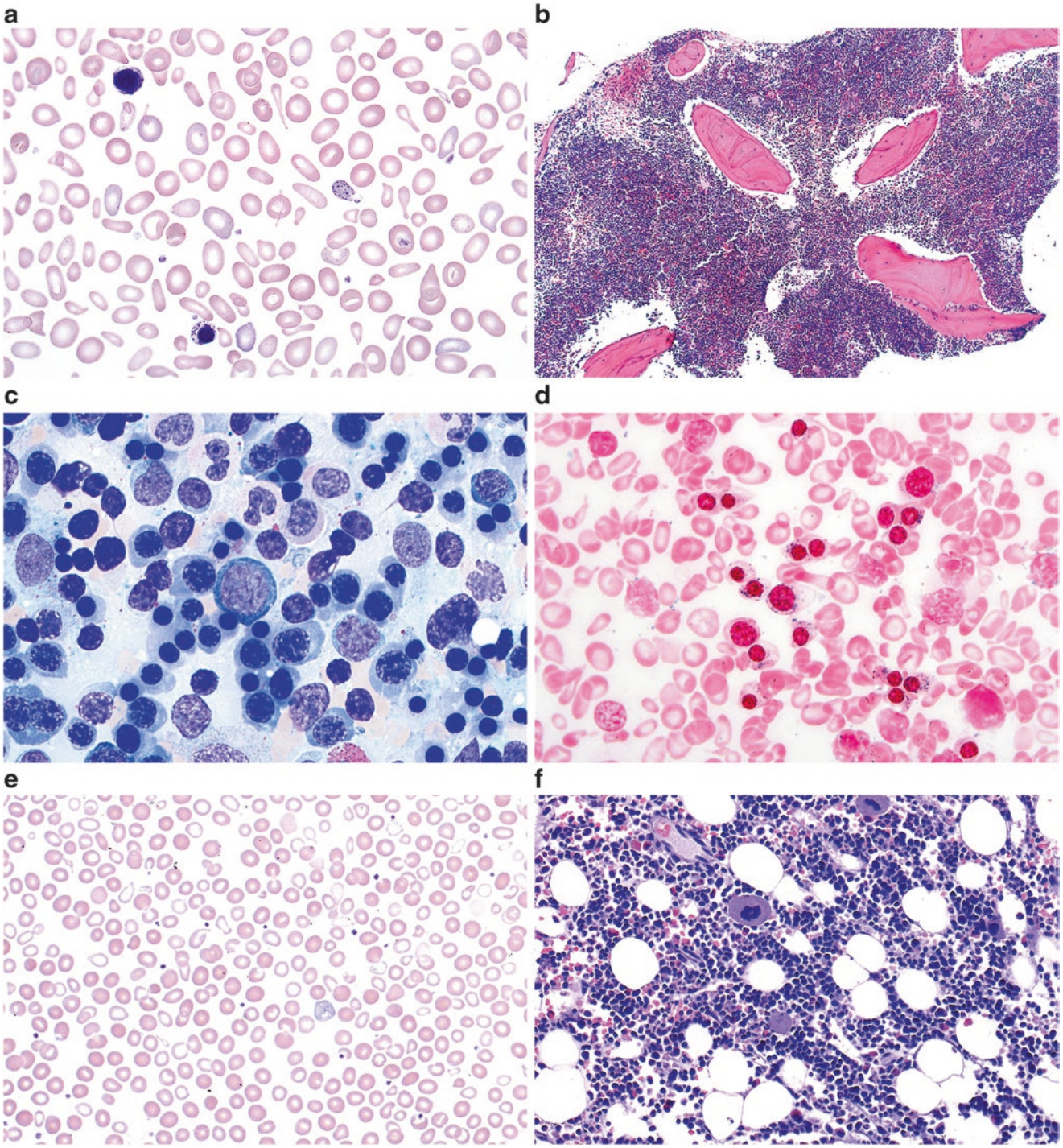

Fig. 4.15 Congenital sideroblastic anemia. (**a**) Peripheral smear from an 8-year-old girl with anemia and fevers, showing marked anisocytosis and poikilocytosis with increased polychromatophilic RBCs, nucleated RBCs, and basophilic stippling. (**b**) The bone marrow biopsy is hypercellular with a marked erythroid hyperplasia. (**c**) The aspirate smear also shows erythroid hyperplasia. (**d**) The iron stain reveals numerous ring sideroblasts. This patient also showed a paucity of B cells with abnormal B-cell maturation by flow cytometric analysis (*not shown*). Germline recessive mutations in *TRNT1* were identified. (**e**) Peripheral smear from a patient with X-linked sideroblastic anemia. The presence of a dimorphic red cell population with rare Pappenheimer bodies is a useful hint at the diagnosis of congenital sideroblastic anemia. (**f**) A bone marrow biopsy showed a hypercellular bone marrow. Although the lymphoid component is increased in this 17-year-old, one should note the predominance of erythroid precursors over granulocytic precursors. Ring sideroblasts were readily identified in the aspirate smears (*not shown*)

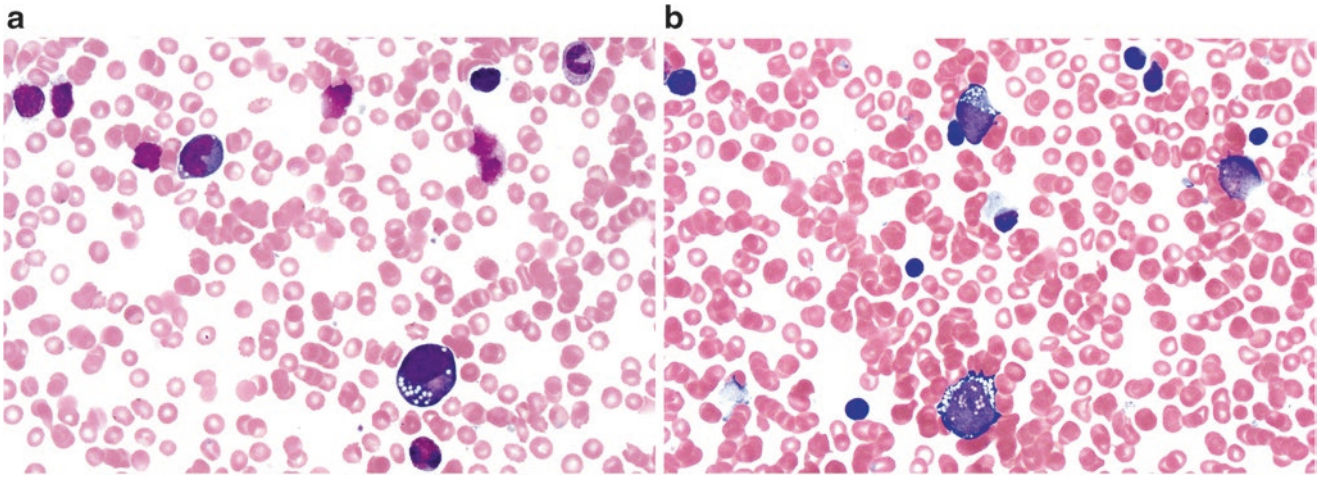

Fig. 4.16 Pearson syndrome. Pearson syndrome is a rare congenital mitochondrial cytopathy typically presenting during infancy. Bone marrow examination reveals vacuoles in both myeloid (**a**) and erythroid (**b**) precursors, with megaloblastic and hyperplastic dyserythropoiesis, including numerous ring sideroblasts (*not shown*) (*Photomicrographs courtesy of* Dr. Teresa Scordino)

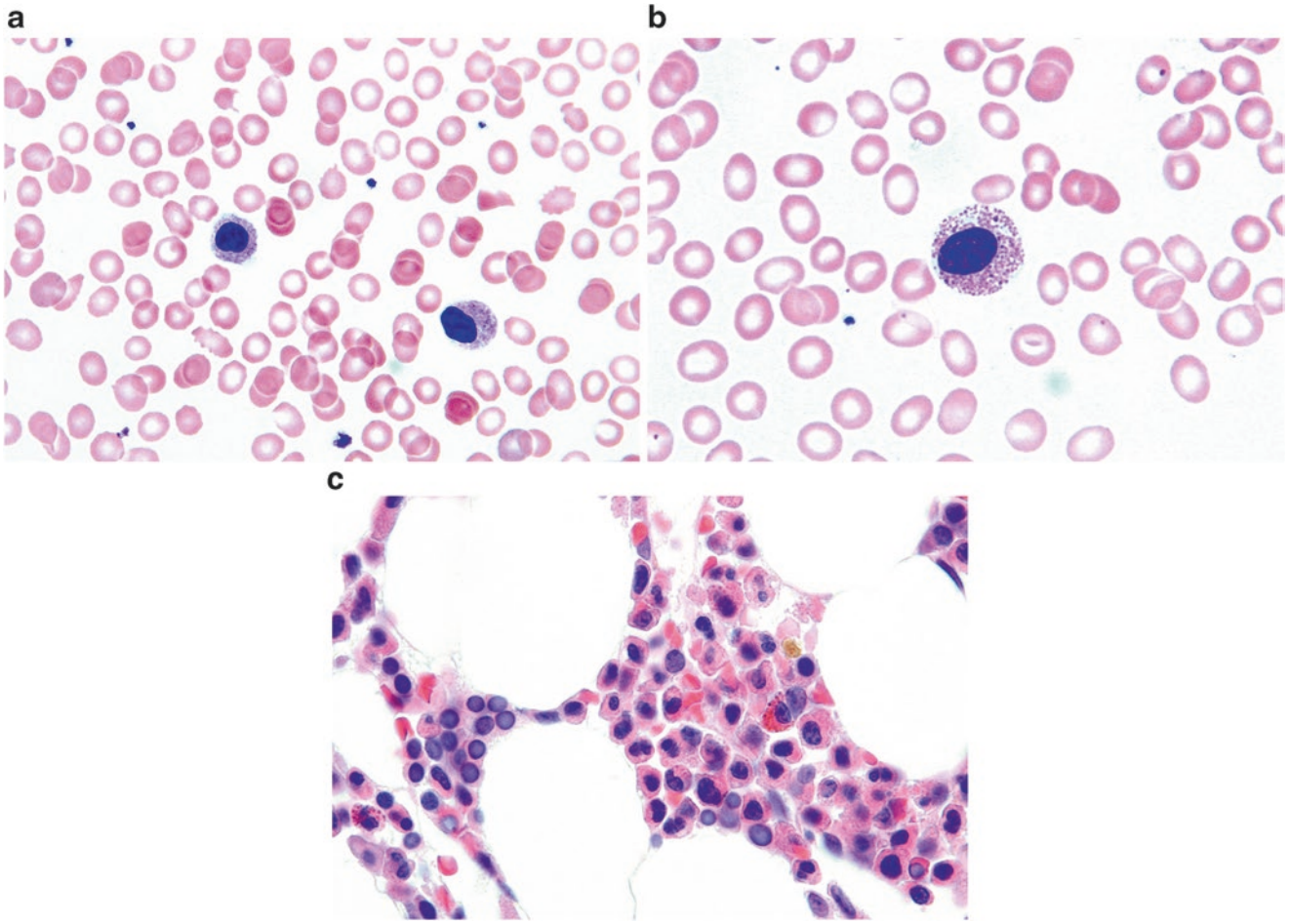

Fig. 4.17 Pelger-Huët anomaly. (**a**) In the Pelger-Huët anomaly, circulating neutrophils have condensed chromatin but hypolobate or monolobate nuclei and can potentially be misinterpreted as immature or dysplastic cells. In the acquired form, or pseudo-Pelger-Huët anomaly, only a subset of neutrophils has this appearance. (**b**) Eosinophils can also display abnormal nuclear segmentation in this disorder. (**c**) Bone marrow core biopsy shows many cells belonging to the neutrophil series, with nuclear lobulation that appears abnormally simple

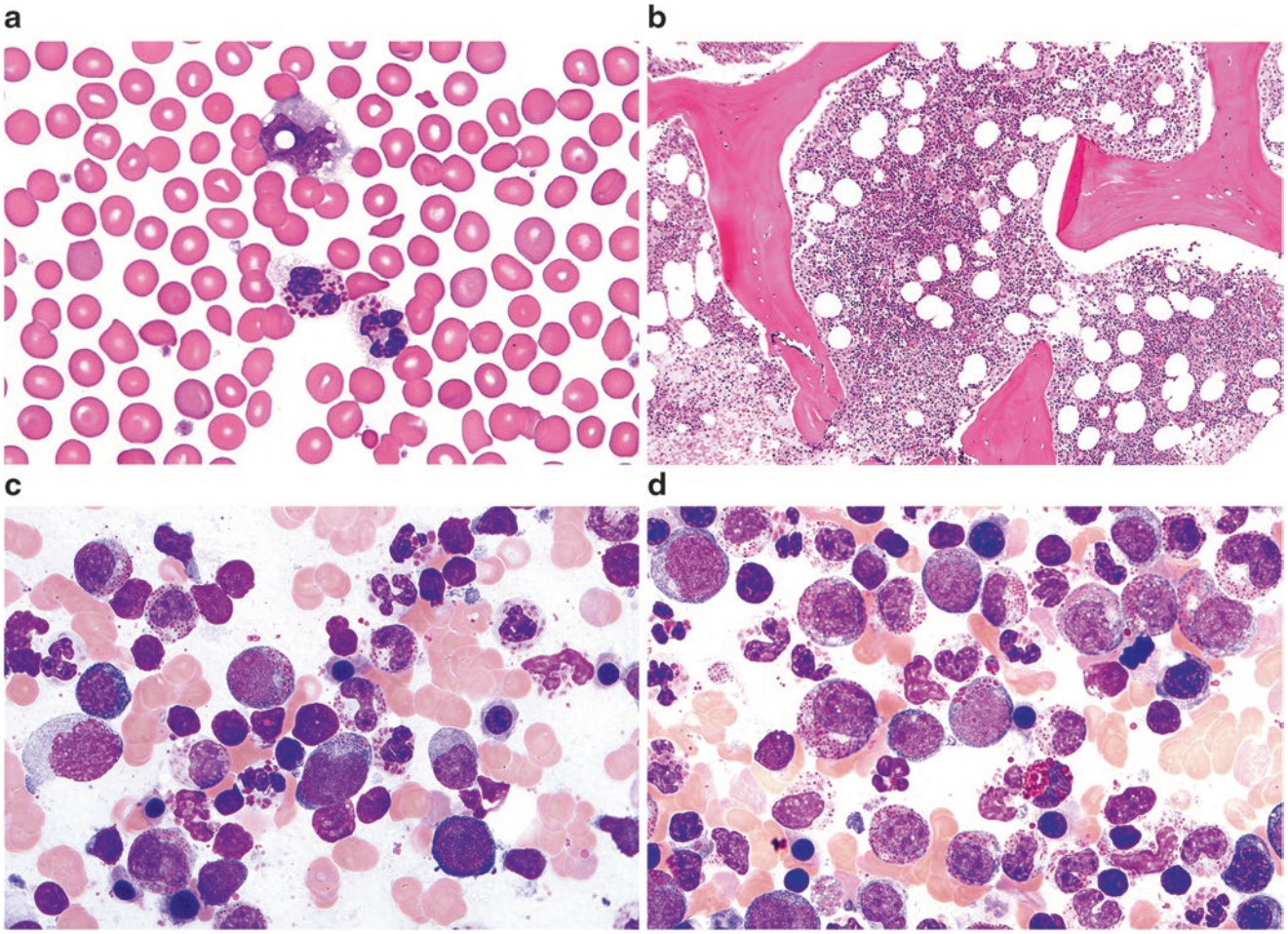

Fig. 4.18 Chédiak-Higashi syndrome. (**a**) This peripheral blood smear from a patient with Chédiak-Higashi syndrome shows the classic finding of giant granules in leukocytes. Although two neutrophils containing these granules are demonstrated here, granules are also seen in eosinophils (and granulocytic precursors), as well as large granular lymphocytes. (**b**) This bone marrow biopsy specimen came from an adolescent male with oculocutaneous albinism and germline autosomal recessive mutations in the *LYST* gene, which encodes a regulator of lysosomal trafficking. The marrow cellularity is normocellular for the patient's age. (**c**) and (**d**) Aspirate smear images show the presence of abnormal large/giant lysosomal granules in the full spectrum of myeloid maturation from blasts to mature neutrophils and eosinophils

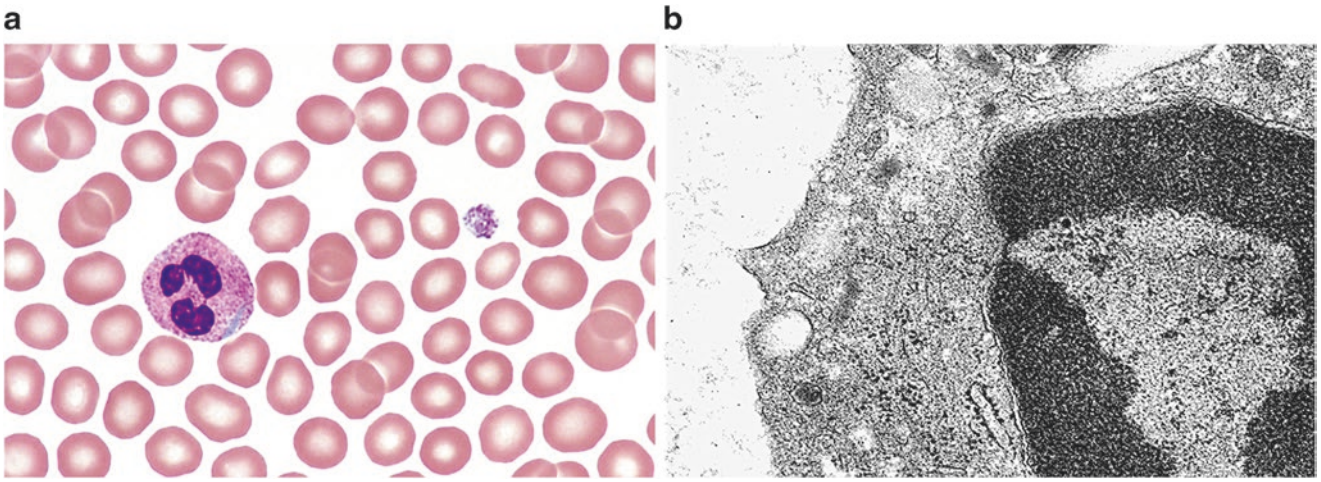

Fig. 4.19 May-Hegglin anomaly. (**a**) This peripheral blood smear is from a teenager with macrothrombocytopenia. Note that the neutrophil contains a basophilic structure that resembles a Döhle body but is larger. (**b**) Ultrastructure of a neutrophil from an infant with "congenital thrombocytopenia" found to have an *MHY9*-related disorder. The typical finding is clusters of randomly distributed ribosomes within highly dispersed filaments in neutrophils. Döhle-like bodies were observed in neutrophils and in occasional eosinophils in the blood (and can also be seen in monocytes and basophils), which also showed moderate thrombocytopenia with giant platelets; bone marrow examination did not contribute much to the diagnosis, aside from showing adequate megakaryocytes

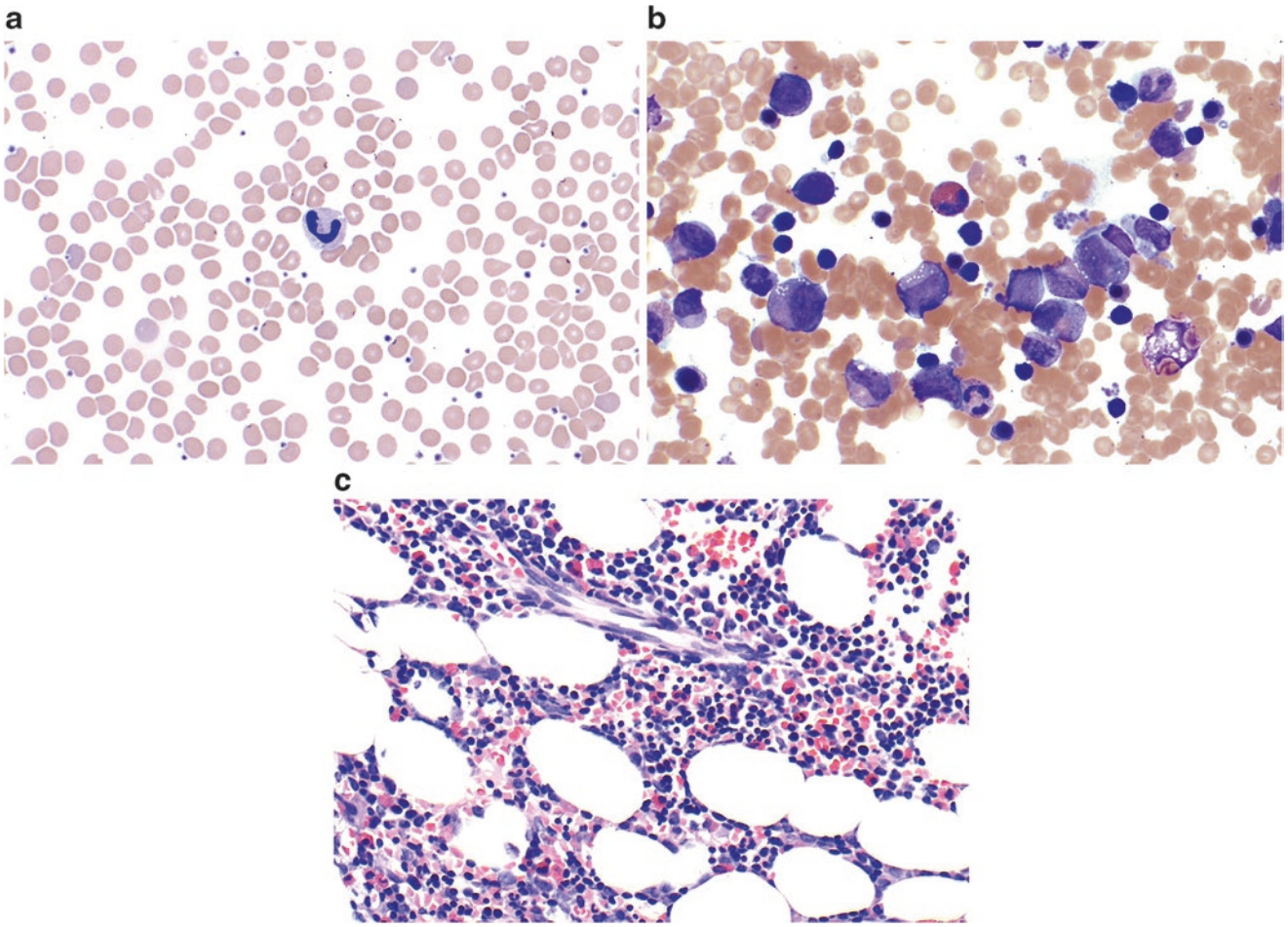

Fig. 4.20 Barth syndrome. Barth syndrome is a cardioskeletal myopathy with neutropenia and abnormal-appearing mitochondria caused by mutations in the *TAZ* gene at Xq28. (**a**) In the peripheral blood smear, vacuoles can be observed in neutrophils. In the original description of Barth syndrome, in addition to vacuoles in about one half of circulating neutrophils, a maturation arrest at the myelocyte stage was observed. (**b**) In this case, the neutrophil series is shifted to immaturity, and both neutrophil precursors and an eosinophil contain cytoplasmic vacuoles. (**c**) As in bone marrow biopsies from many young patients, the core biopsy shows a prominent lymphoid component, but as is characteristic of Barth syndrome, the neutrophil series is left-shifted, with only very rare mature neutrophils

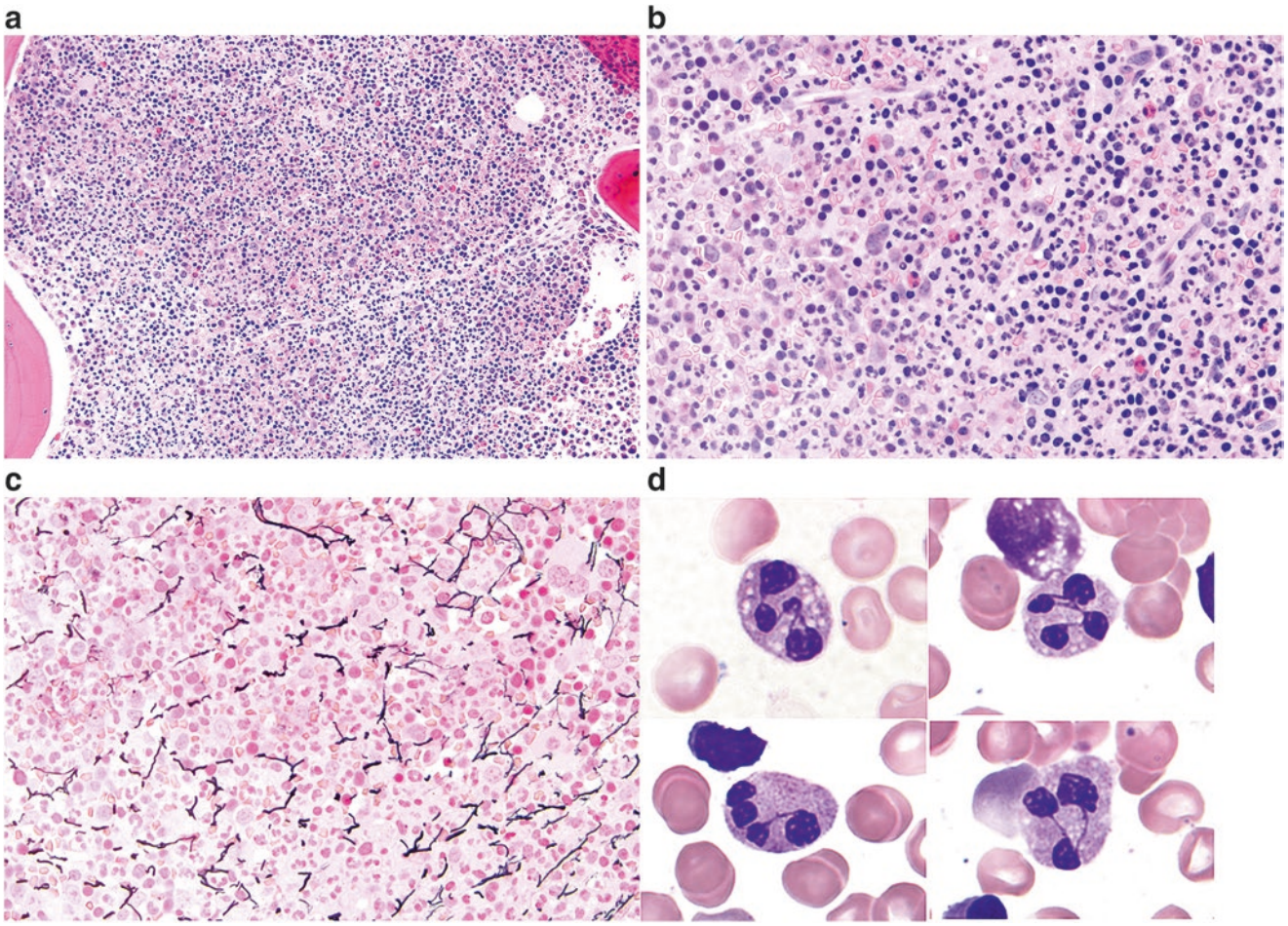

Fig. 4.21 Warts, hypogammaglobulinemia, infections, and myelokathexis (WHIM) syndrome. WHIM syndrome is a congenital immunodeficiency syndrome characterized by germline mutations in *CXCR4*. Patients with WHIM have chronic noncyclic neutropenia. (**a**) Despite the lack of neutrophils in the peripheral blood, the bone marrow is typically hypercellular, with an abundance of maturing myeloid precursors. (**b**) Mature neutrophils are unable to be released from the bone marrow (myelokathexis) and can be seen accumulating and undergoing apoptosis. (**c**) Increased reticulin fibers may be seen on reticulin staining of bone marrow core biopsies in WHIM. (**d**) Aspirate smears demonstrate the presence of unusual neutrophils with condensed nuclear segments connected by thin, wispy strands of chromatin and cytoplasmic vacuoles

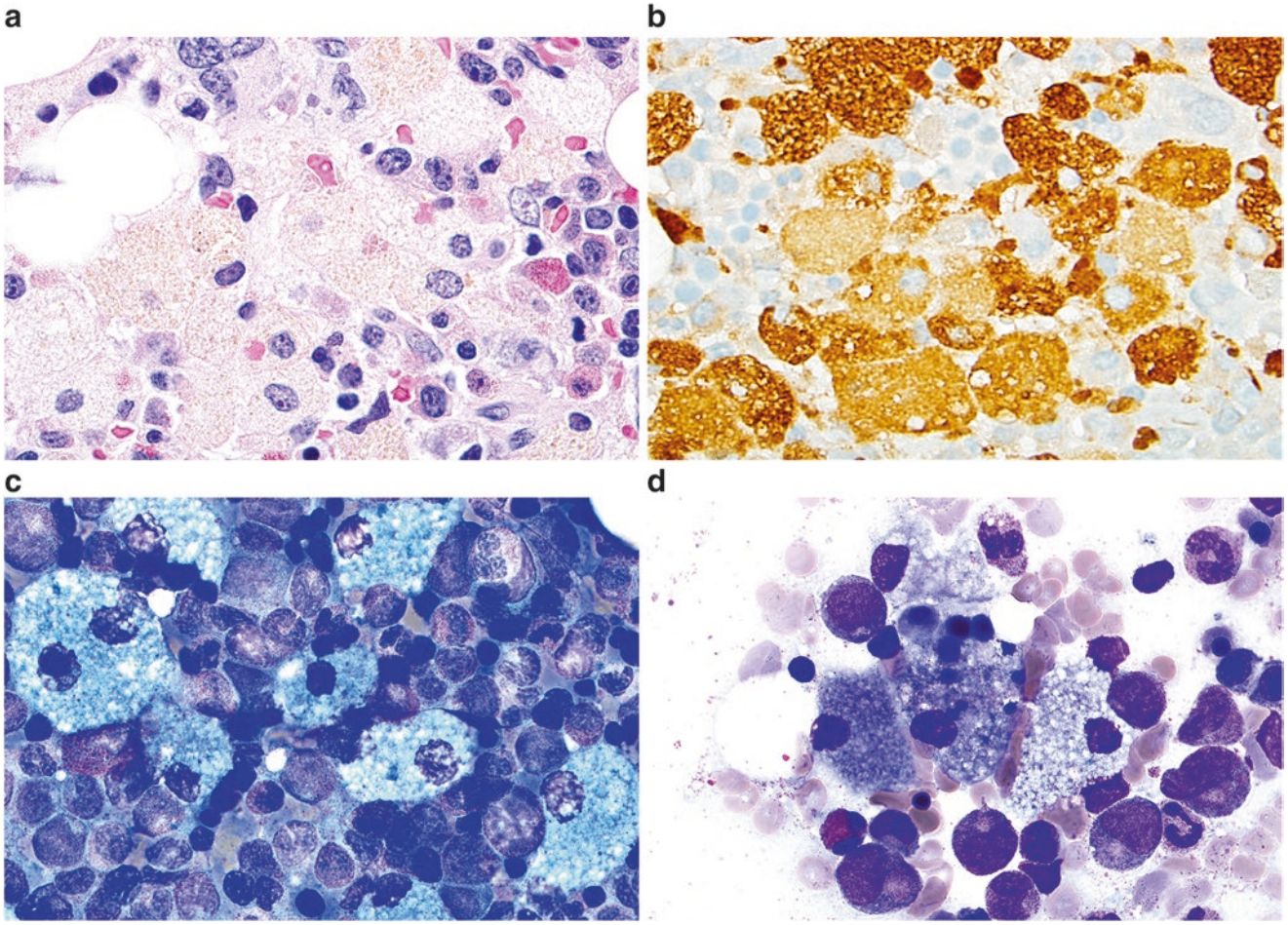

Fig. 4.22 Chronic granulomatous disease (CGD). CGD is an inherited immunodeficiency with germline mutations in genes encoding subunits of the NADPH oxidase complex, such as *CYBA*, *CYBB*, or *NCF1*. Inheritance may be autosomal recessive or X-linked recessive, depending on the gene that is mutated. Despite the presence of granulomas in the lung, skin, lymph nodes, and other tissues, granulomas are not typically seen in bone marrow specimens. However, other distinct features are common in the marrow, including pigmented macrophages (**a**) highlighted by CD68 immunohistochemical stain (**b**). Bone marrow aspirate smears often show the presence of sea-blue histiocytes (**c**) and increased vacuolated histiocytes (**d**), as seen on this marrow specimen from a young male with CGD

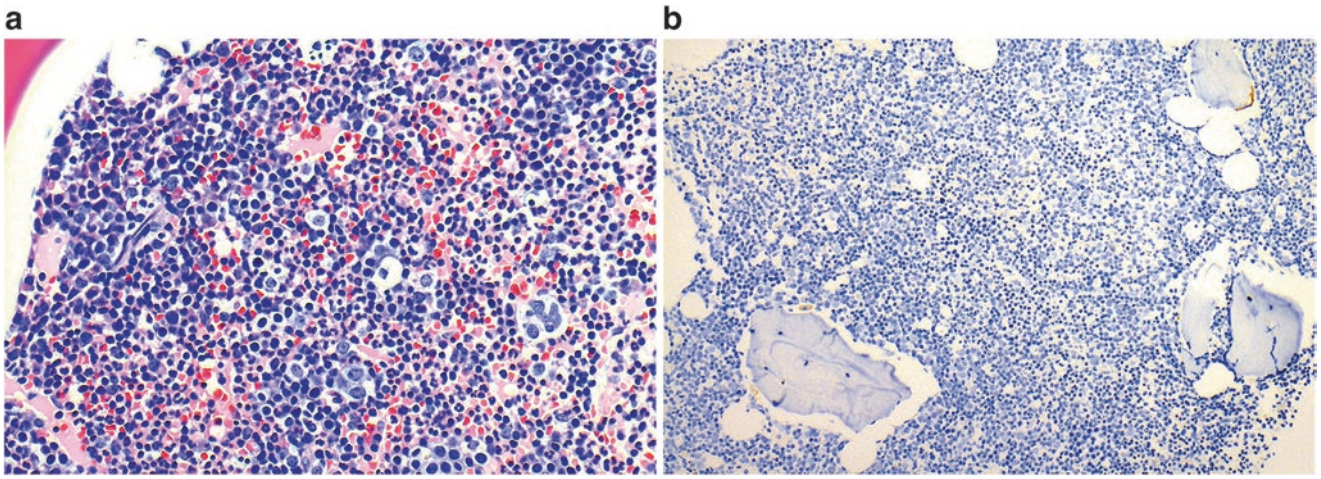

Fig. 4.23 Familial thrombocytopenia with predisposition to AML. This bone marrow comes from a 2-year-old boy with a platelet count of 1×10^9/L, sick contacts, and symptoms of a viral upper respiratory infection, which appeared about 1 week prior to development of bruising. In contrast to the much more common immune/idiopathic thrombocytopenic purpura (ITP), in which megakaryocytes are abundant and present at all stages of maturation, they are nearly absent in this case, with only one present in 17 mm of continuous bone marrow on the H&E-stained section (**a**) and none seen on the CD61 immunostain (**b**). The possibility of viral suppression could not be excluded, so we recommended gene sequencing if the platelet count did not recover, specifically to evaluate for X-linked thrombocytopenia with *GATA1* mutation, congenital amegakaryocytic thrombocytopenia due to *MPL* (thrombopoietin receptor) mutation, familial platelet disorder with associated myeloid malignancy (*RUNX1*), and/or Wiskott-Aldrich syndrome or its attenuated form, X-linked thrombocytopenia (*WAS*). A *germline RUNX1* mutation was found

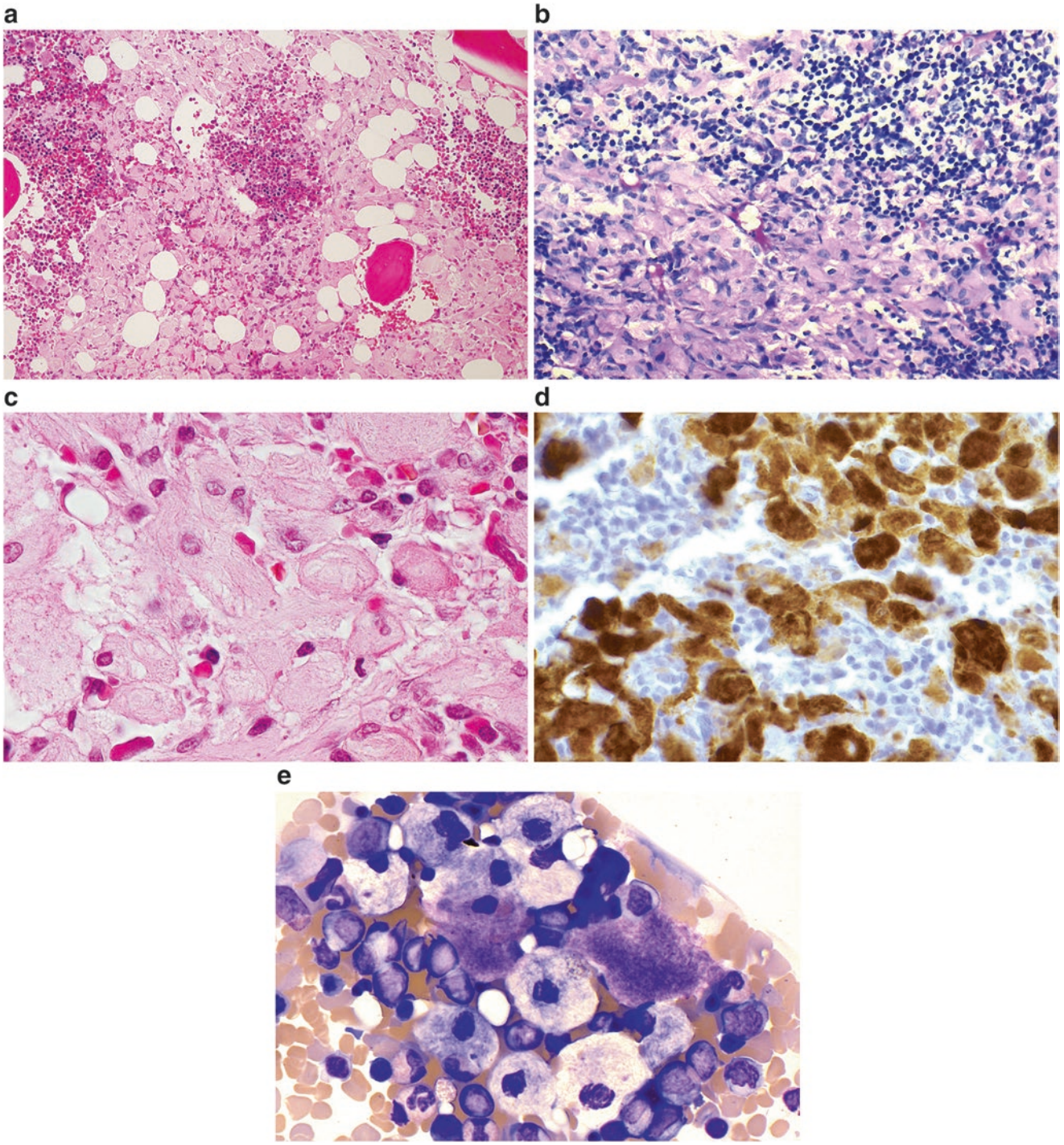

Fig. 4.24 Gaucher disease. (**a**) Bone marrow biopsy from a middle-aged man with thrombocytopenia shows extensive infiltrates of storage histiocytes with eosinophilic cytoplasm. (**b**) The macrophages in Gaucher disease are positive for PAS with and without diastase. (**c**) In this high-power photomicrograph of a core biopsy specimen, one can observe the subtle cytoplasmic striations or fibrillar structures that have caused Gaucher cells to be likened to "wrinkled tissue paper" or "crumpled silk." (**d**) Gaucher cells also stain positively for tartrate-resistant acid phosphatase (TRAP), although the test is now seldom performed. (**e**) Aspirate smear from an Ashkenazi Jewish teenage girl with numerous Gaucher cells demonstrating voluminous pale, basophilic cytoplasm and striations. Gaucher disease can affect people of any ethnic background, but up to 1 in 10 Jews of Eastern European descent are carriers, with a disease prevalence of about 1 in 450 in that population. It should be recognized, however, that pseudo-Gaucher cells can be seen in the bone marrow in a wide variety of other conditions

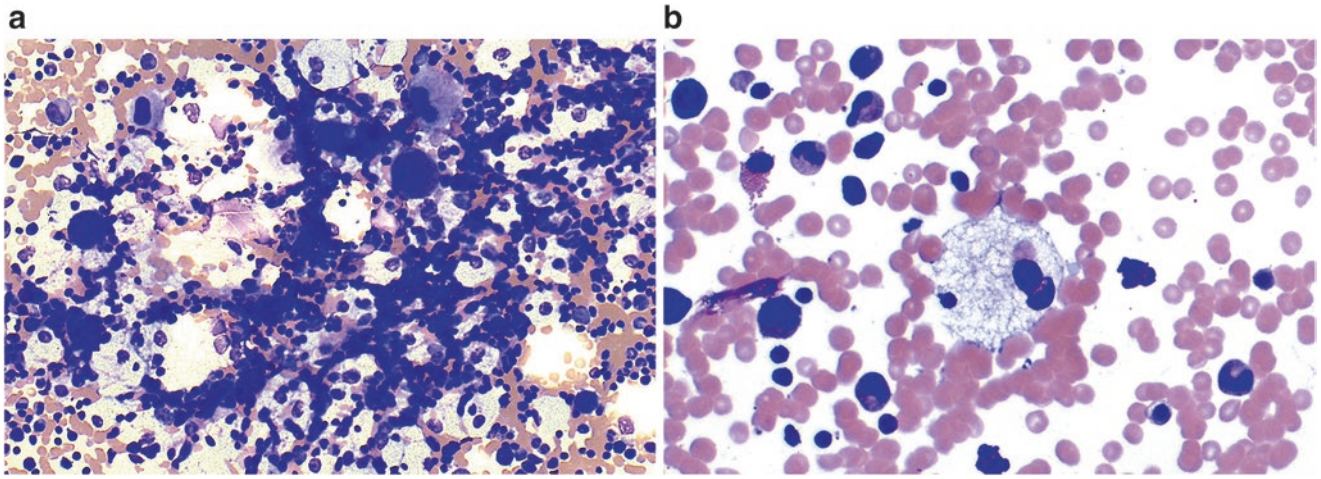

Fig. 4.25 Niemann-Pick disease. (**a**) and (**b**) The macrophages in Niemann-Pick disease have foamy cytoplasm with fine, round lipid-containing vacuoles having a "soap bubble" appearance. Although not depicted here, they are positive for PAS (with and without diastase), Sudan Black B, and oil red O. Similar macrophages can be observed in other storage diseases, such as Tangier disease, hyperlipidemia, fat necrosis, and bone marrow infarction

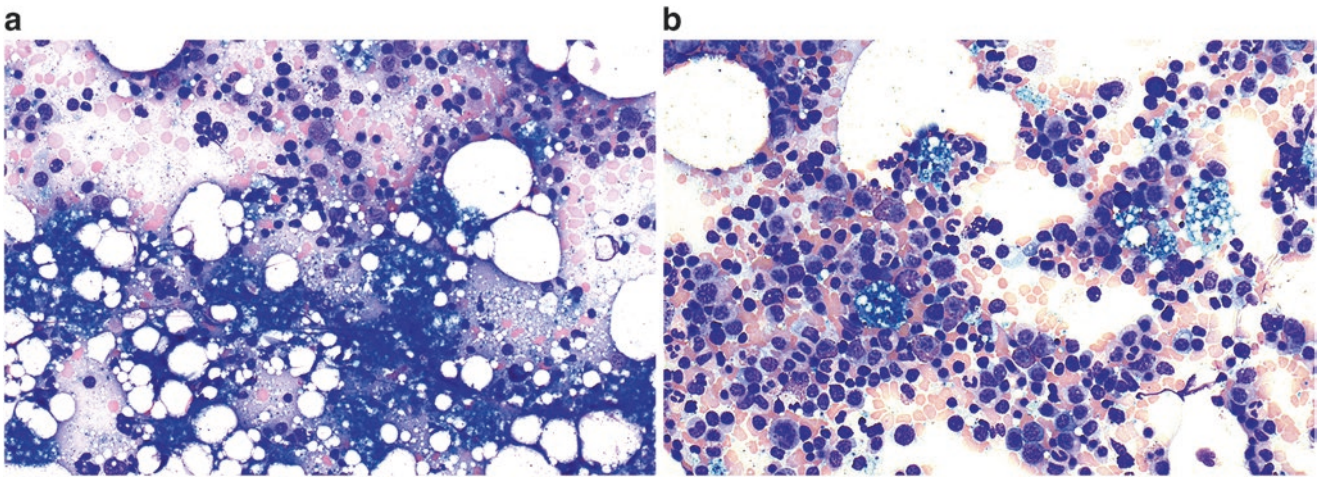

Fig. 4.26 Sea-blue histiocytosis/ceroid lipofuscinosis. (**a** and **b**) Now recognized as a variant of Niemann-Pick disease, the macrophages in sea-blue histiocytosis have coarse, sea-blue, or blue-green granules whose color is attributed to ceroid, which is composed of phospholipids and glycosphingolipids. The granules stain with oil red O and Sudan Black B, and as the pigment ages, it develops a yellow-green autofluorescence, followed by PAS positivity and then acid-fast positivity. But like the other storage diseases mentioned earlier, similar macrophages are seen in other conditions, including those with high cell turnover

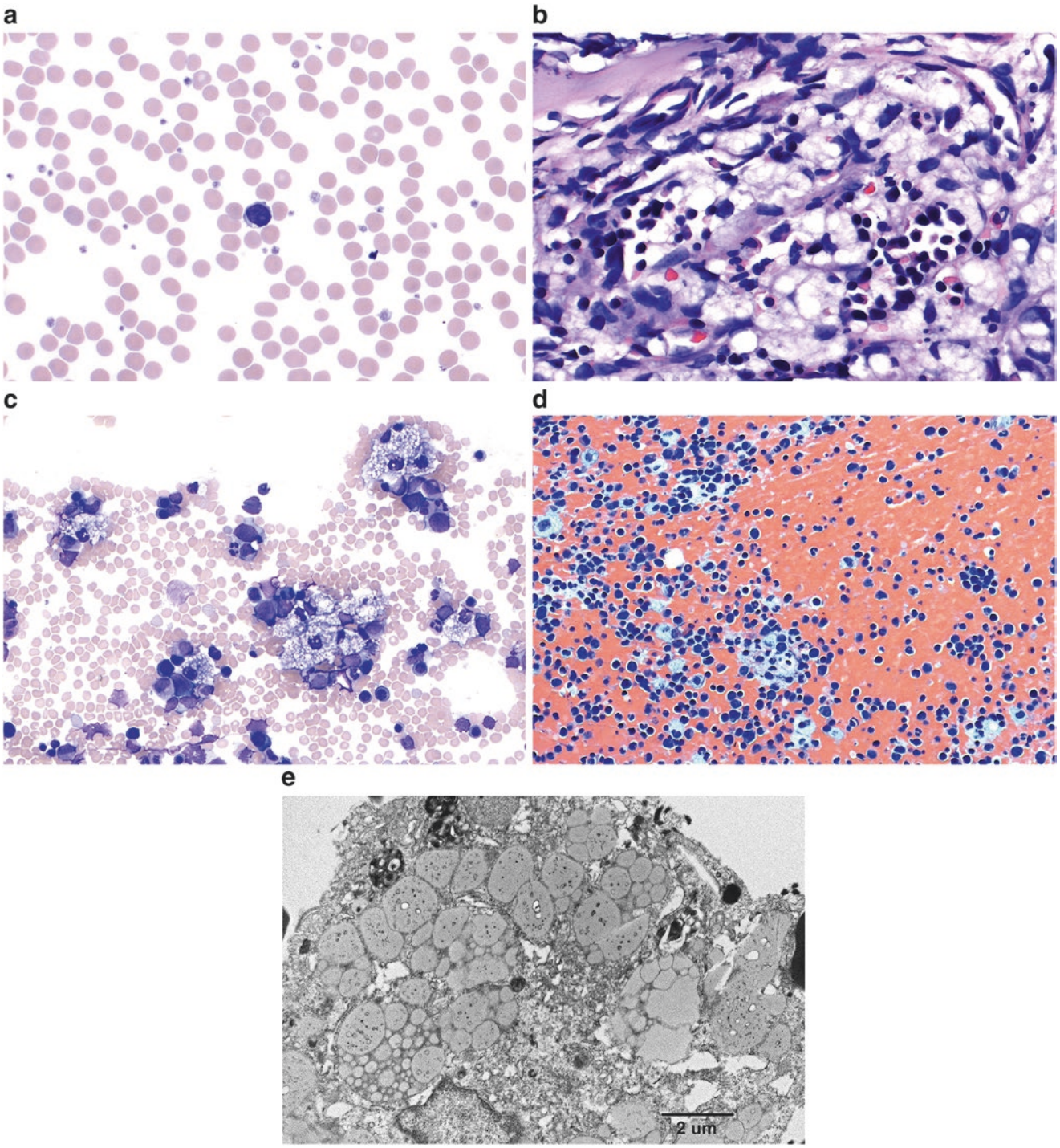

Fig. 4.27 Wolman disease/lysosomal acid lipase deficiency. (**a**) Vacuoles in a peripheral blood lymphocyte from a patient with Wolman disease are shown here. (**b**) High-power photomicrograph of a bone marrow core biopsy in Wolman disease shows an abundance of foamy macrophages. (**c**) Foamy macrophages are found in the bone marrow aspirate of a pediatric Wolman disease patient. Their cholesteryl ester storage content would be reflected by positive staining for oil red O and Cain's Nile blue. This patient had bilateral adrenal calcifications on imaging, a characteristic finding resulting after saponification of fatty acid esters that accumulate in and enlarge the adrenals. (**d**) Foamy macrophages in particle clot are seen in the same patient. (**e**) Electron microscopy shows numerous lipid inclusions

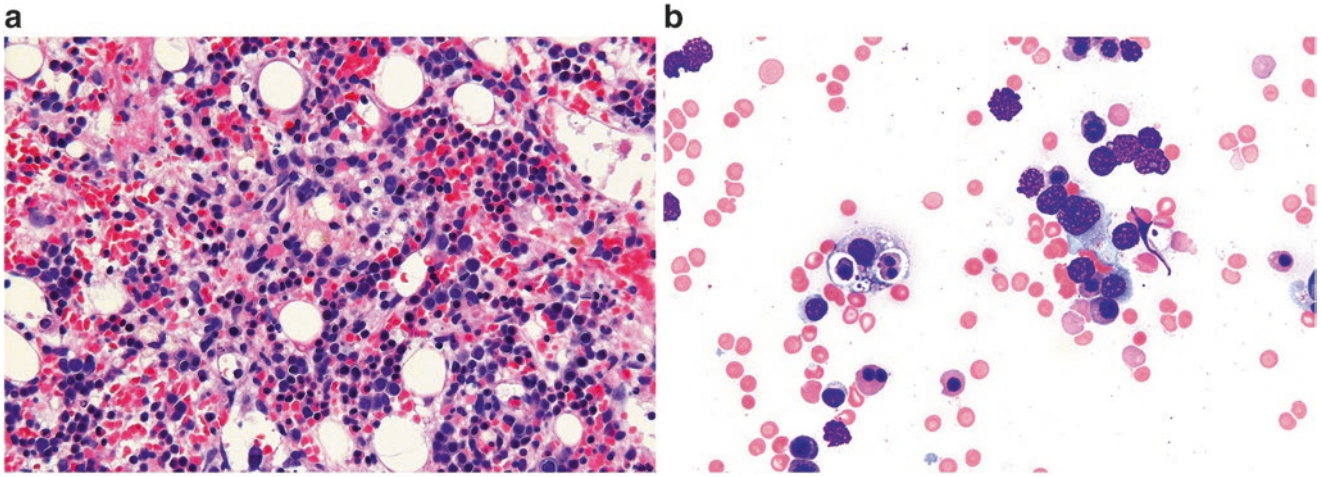

Fig. 4.28 Hemophagocytic lymphohistiocytosis (HLH). Interpretation of hemophagocytosis can be subjective and is neither sensitive nor specific; it is not even required for a diagnosis of HLH, but it was evident in the core biopsy (**a**) and aspirate smears (**b**) of this child with X-linked lymphoproliferative syndrome-1 (XLP1), who succumbed to fulminant EBV infectious mononucleosis. In suspected cases of HLH, bone marrow examination may be sought for treatable underlying causes, including malignancy or infection. Further discussion of HLH can be found in Chap. 14

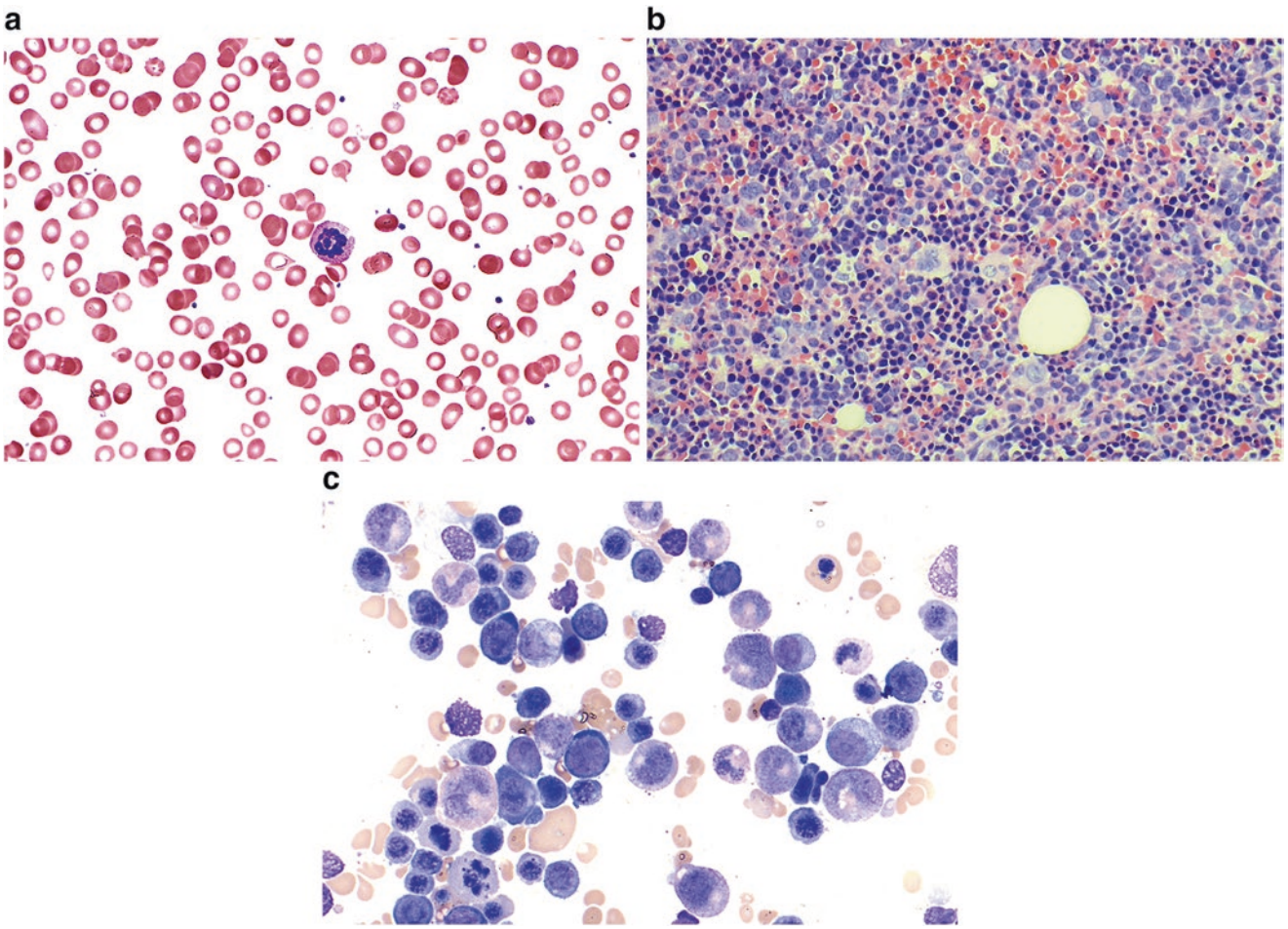

Fig. 4.29 Megaloblastic anemia. (**a**) Peripheral blood smear from a woman with megaloblastic anemia. Note the hypersegmented neutrophil. The second case is an older man who presented with fatigue and dyspnea on exertion, who was found to have hemoglobin of 3.5 g/dL and MCV of 117 fL. Vitamin B12 level was low at <50 pg/mL (normal, 181–914). (**b**) The bone marrow was hypercellular for age (90–95% cellular), with erythroid hyperplasia, megaloblastic maturation and significant dyspoiesis, and readily identifiable giant metamyelocyte and band neutrophils. (**c**)

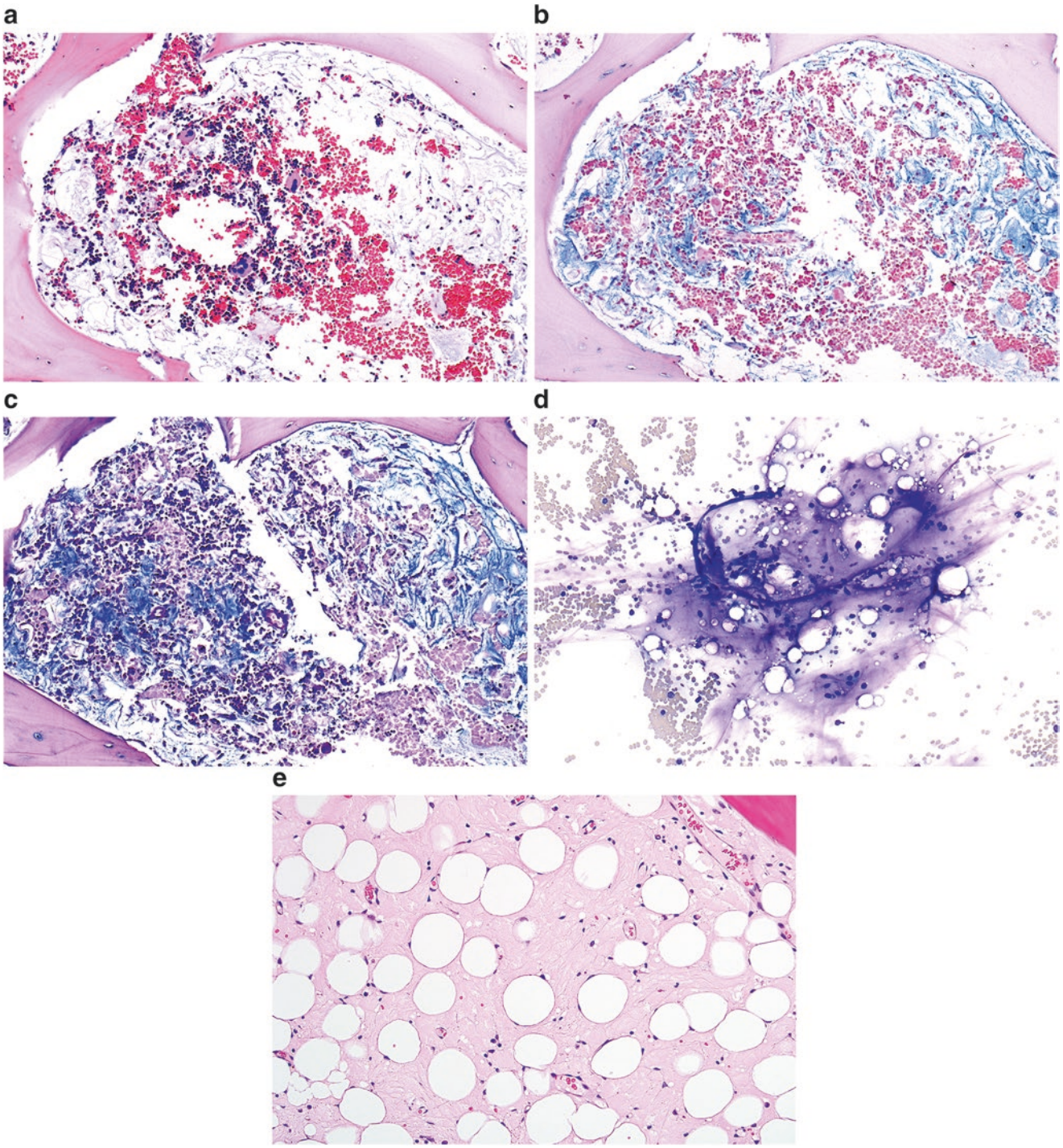

Fig. 4.30 Gelatinous transformation of the marrow/serous fat atrophy. These images come from the bone marrow of a 16-year-old girl with X-linked hypophosphatemic rickets, anorexia nervosa, and rumination syndrome with severe malnutrition. (**a**) The trephine biopsy displays amorphous, bluish, finely granular/fibrillar material with focal atrophy of fat cells and patchy residual hematopoiesis. Alcian blue (pH 2.5) (**b**) and Alcian blue-periodic acid-Schiff (**c**) stains confirm the acid mucosubstance composition of the amorphous material. (**d**) This stromal material shows a blue-pink appearance on Wright-Giemsa stain. Gelatinous transformation/serous fat atrophy is a nonspecific finding associated with anorexia nervosa or cachexia from chronic debilitating illnesses such as infections, malignancy, systemic lupus erythematosus, hypothyroidism, renal or heart failure, celiac disease, intestinal lymphangiectasia, and alcoholism; it also has been seen at sites of irradiation, and it can be seen in patients treated with chemotherapy (**e**). Images of gelatinous transformation are also found in Chap. 2 (Figs. 2.43, 2.44)

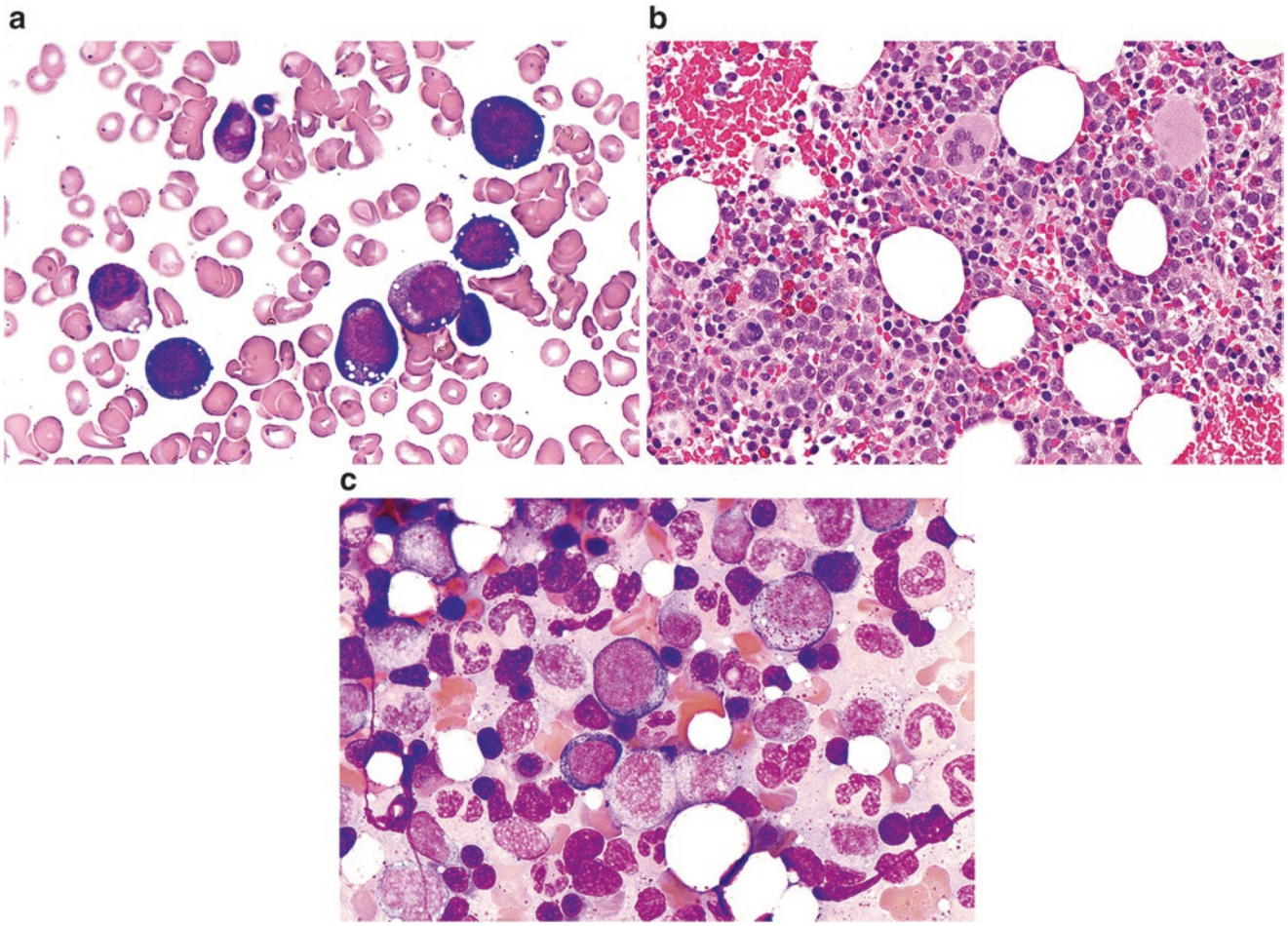

Fig. 4.31 Copper deficiency. Bone marrow aspirate smear (**a**) and core biopsy (**b**) from an elderly man referred to our institution to begin treatment for myelodysplastic syndrome. Vacuoles were seen in both myeloid and erythroid precursors; the serum copper level was found to be very low. The appearance of the bone marrow returned to normal following copper repletion (**c**) (*Images courtesy of* Dr. LoAnn Peterson)

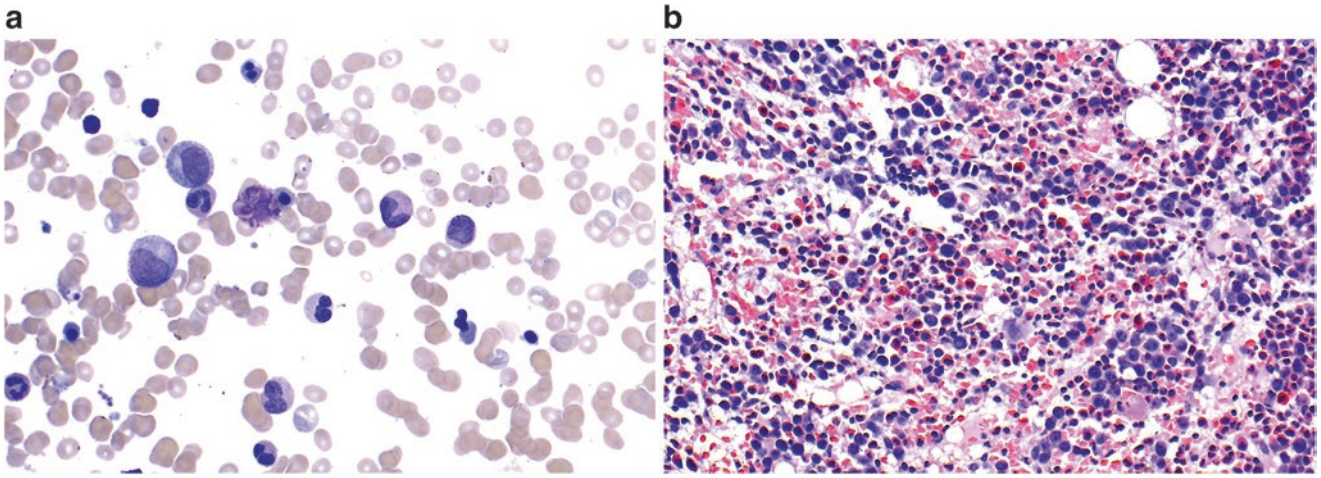

Fig. 4.32 Arsenic toxicity. Arsenic toxicity can result in unilineage or multilineage cytopenias. (**a** and **b**) Bone marrow examination in this case reveals bizarre, megaloblastic dyserythropoiesis with striking karyorrhexis, which can mimic myelodysplastic syndrome or megaloblastic anemia. Arsenic disappears from the blood within a few hours of acute ingestion (the body treats it like phosphate), but because it becomes concentrated by the kidneys, it can be detected for days in the urine. Arsenic has a high affinity for keratin due to high cysteine content, so Mees' lines (transverse white striae) may appear in the fingernails. Hair samples are useful for documenting exposure over the course of several months to a year

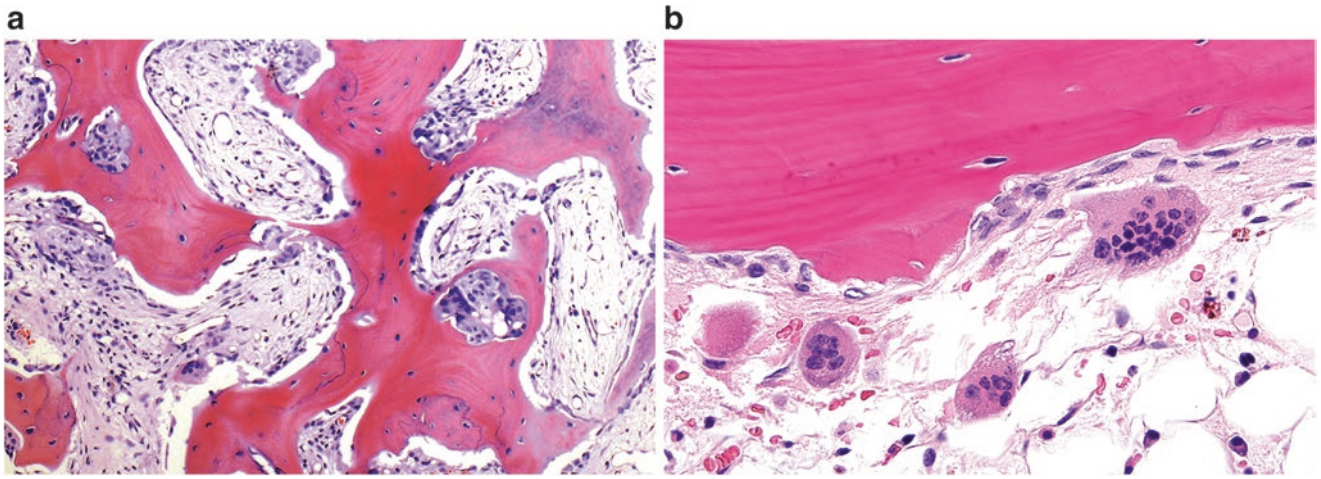

Fig. 4.33 Osteitis fibrosa/renal osteodystrophy. An 87-year-old woman with chronic kidney disease on darbepoetin alfa for several years for associated anemia developed progressive pancytopenia (WBC 1.5 × 10^9/L, hemoglobin 6.2 g/dL with an MCV of 117 fL and scattered dacrocytes, and platelets 30 × 10^9/L) over the course of several months. The bone marrow trephine biopsy (**a**) demonstrated nearly complete replacement by reticulin and collagen fibrosis and markedly thickened, anastomosing bony trabeculae with extensive features of remodeling (scalloped contours, osteoblastic rimming, and osteoclastic resorption, including in depressed resorption bays/Howship's lacunae). The differential diagnosis for such changes is broad and includes myeloid neoplasms (primary myelofibrosis, myelodysplastic syndrome with fibrosis, acute panmyelosis with myelofibrosis, acute megakaryoblastic leukemia), chronic renal failure (renal osteodystrophy) with or without secondary hyperparathyroidism, Paget's disease, systemic mastocytosis, metastatic tumor (carcinoma, classic Hodgkin lymphoma), osteosclerotic myeloma/POEMS syndrome, fracture or previous biopsy site, metabolic disorders, and autoimmune or infectious etiologies. The osteitis fibrosa was attributed to chronic renal disease after an unrevealing workup with normal/negative results of serum and urine protein electrophoresis and immunofixation, flow cytometry immunophenotyping, immunohistochemistry, and conventional cytogenetic analysis to exclude many of the above entities. (**b**) High-power image of osteoblasts and osteoclasts along the bony trabeculae is shown

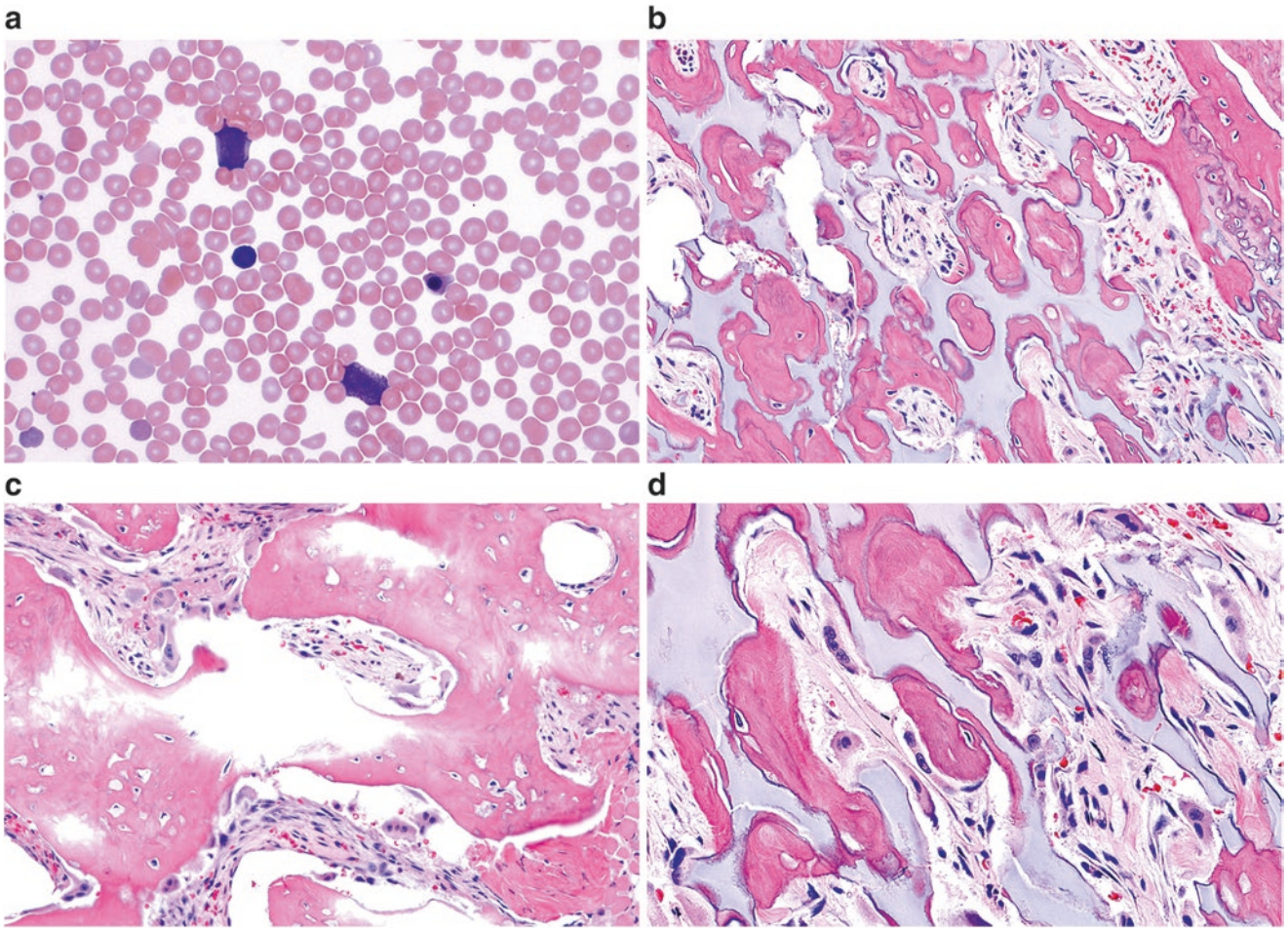

Fig. 4.34 Osteopetrosis. (**a**) Peripheral blood smear from a 10-week-old girl with autosomal recessive osteopetrosis due to two heterozygous pathogenic mutations in the *TCIRG1* gene shows a leukoerythroblastic reaction. Flow cytometry immunophenotyping revealed approximately 10% circulating transitional B cells and 4% myeloid blasts. It makes sense that the blood in osteopetrosis patients can contain elements typically found in the bone marrow, because excessive osteoblastic activity with decreased bone resorption (owing to functionally defective osteoclasts) leads to markedly thickened bone, which together with stromal fibrosis results in obliteration of the marrow space. The rationale for allogeneic hematopoietic stem cell transplantation is that progenitors that can differentiate into functional osteoclasts will promote bone remodeling and a reversal of pancytopenia and extramedullary hematopoiesis (**b**–**d**) Bone marrow biopsy images from a different patient with osteopetrosis illustrate the extent to which hematopoiesis is compromised in osteopetrosis. Note how excessive bone formation leads to obliteration of the marrow space (**b**). Although osteoclasts are abundant in this image of the subcortical marrow (**c** and **d**), they are functionally defective and cannot counterbalance osteoblastic activity (*Images B–D courtesy of* Dr. Tracy George)

Acknowledgment *Work in this chapter was in part supported by the Intramural Research Program of the National Institutes of Health and the NIH Clinical Center.*

Suggested Reading

1. Ansari S, Miri-Aliabad G, Saeed Y. Cystinosis: diagnostic role of bone marrow examination. Turk J Haematol. 2014;31:106.
2. Aprikyan AA, Khuchua Z. Advances in the understanding of Barth syndrome. Br J Haematol. 2013;161:330–8.
3. Bain BJ, Clark DM, Wilkins B. Bone marrow pathology. 4th ed. Wiley-Blackwell: Chichester; 2010.
4. Bakshi NA, Al-Zahrani H. Bone marrow oxalosis. Blood. 2012;120:8.
5. Boutin RD, White LM, Laor T, Spitz DJ, Lopez-Ben RR, Stevens KJ, et al. MRI findings of serous atrophy of bone marrow and associated complications. Eur Radiol. 2015;25:2771–8. https://doi.org/10.1007/s00330-015-3692-5.
6. Busuttil DP, Liu Yin JA. The bone marrow in hereditary cystinosis. Br J Haematol. 2000;111:385.
7. Calvo KR, Vinh DC, Maric I, Wang W, Noel P, Stetler-Stevenson M, et al. Myelodysplasia in autosomal dominant and sporadic monocytopenia immunodeficiency syndrome: diagnostic features and clinical implications. Haematologica. 2011;96:1221–5.
8. Cassinet B, Guardiola P, Chevret S, Schlageter MH, Toubert ME, Rain JD, et al. Constitutive elevation of serum alpha-fetoprotein in Fanconi anemia. Blood. 2000;96:859–63.
9. Colella R, Hollensead SC. Understanding and recognizing the Pelger-Huët anomaly. Am J Clin Pathol. 2012;137:358–66.
10. Cunningham J, Sales M, Pearce A, Howard J, Stallings R, Telford N, et al. Does isochromosome 7q mandate bone marrow transplant in children with Shwachman-Diamond syndrome? Br J Haematol. 2002;119:1062–9.
11. Dhanraj S, Matveev A, Li H, Lauhasurayotin S, Jardine L, Cada M, et al. Biallelic mutations in *DNAJC21* cause Shwachman-Diamond syndrome [letter]. Blood. 2017;129:1557–62.
12. Dror Y, Durie P, Ginzberg H, Herman R, Banerjee A, Champagne M, et al. Clonal evolution in marrows of patients with Shwachman-Diamond syndrome: a prospective 5-year follow-up study. Exp Hematol. 2002;30:659–69.
13. Dulau Florea AE, Braylan RC, Schafernak KT, Williams KW, Daub J, Goyal RK, et al. Abnormal B-cell maturation in the bone marrow of patients with germline mutations in *PIK3CD*. J Allergy Clin Immunol. 2017;139:1032–5.
14. Foucar K, Reichard K, Czuchlewski D. Bone marrow pathology. 3rd ed. Chicago: ASCP Press; 2010.
15. Foucar K, Viswanatha DS, Wilson CS. Non-neoplastic disorders in bone marrow. Washington, DC: American Registry of Pathology in collaboration with the Armed Forces Institute of Pathology; 2008.
16. Ganapathi KA, Townsley DM, Hsu AP, Arthur DC, Zerbe CS, Cuellar-Rodriguez J, et al. GATA2 deficiency-associated bone marrow disorder differs from idiopathic aplastic anemia. Blood. 2015;125:56–70.
17. Gregg XT, Reddy V, Prchal JT. Copper deficiency masquerading as myelodysplastic syndrome. Blood. 2002;100:1493–5.
18. Hoffbrand AV, Pettit JE, Vyas P. Color atlas of clinical hematology. 4th ed. Philadelphia: Mosby/Elsevier; 2010.
19. Hsu AP, Sampaio EP, Khan J, Calvo KR, Lemieux JE, Patel SY, et al. Mutations in GATA2 are associated with the autosomal dominant and sporadic monocytopenia and mycobacterial infection (MonoMAC) syndrome. Blood. 2011;118:2653–5.
20. Ireland RM. Morphology of Wolman cholesterol ester storage disease. Blood. 2017;129:803.
21. Keel SB, Scott A, Sanchez-Bonilla M, Ho PA, Gulsuner S, Pritchard CC, Abkowitz JL, King MC, Walsh T, Shimamura A. Genetic features of myelodysplastic syndrome and aplastic anemia in pediatric and young adult patients. Haematologica. 2016;101:1343–50.
22. Koca E, Buyukasik Y, Cetiner D, Yilmaz R, Sayinalp N, Yasavul U, Uner A. Copper deficiency with increased hematogones mimicking refractory anemia with excess blasts. Leuk Res. 2008;32:495–9.
23. Kuehn HS, Ouyang W, Lo B, Deenick EK, Niemela JE, Avery DT, et al. Immune dysregulation in human subjects with heterozygous germline mutations in CTLA4. Science. 2014;345:1623–7.
24. Lo B, Zhang K, Lu W, Zheng L, Zhang Q, Kanellopoulou C, et al. Patients with LRBA deficiency show CTLA4 loss and immune dysregulation responsive to abatacept therapy. Science. 2015;349:436–40.
25. Maserati E, Pressato B, Valli R, Minelli A, Sainati L, Patitucci F, et al. The route to development of myelodysplastic syndrome/acute myeloid leukemia in Shwachman-Diamond syndrome: the role of ageing, karyotype instability, and acquired chromosome abnormalities. Br J Haematol. 2009;145:190–7.
26. Mellink CH, Alders M, van der Lelie H, Hennekam RH, Kuijpers TW. SBDS mutations and isochromosome 7q in a patient with Shwachman-Diamond syndrome: no predisposition to malignant transformation? Cancer Genet Cytogenet. 2004;154:144–9. https://doi.org/10.1016/j.cancergencyto.2004.02.001.
27. Minelli A, Maserati E, Nicolis E, Zecca M, Sainati L, Longoni D, et al. The isochromosome i(7)(q10) carrying c.258+2t>c mutation of the *SBDS* gene does not promote development of myeloid malignancies in patients with Shwachman syndrome. Leukemia. 2009;23:708–11.
28. Orchard PJ, Fasth AL, Le Rademacher J, He W, Boelens JJ, Horwitz EM, et al. Hematopoietic stem cell transplantation for infantile osteopetrosis. Blood. 2015;126:270–6.
29. Orkin SH, Nathan DG, Ginsburg D, Look AT, Fisher DE, Lux SE. Nathan and Oski's hematology of infancy and childhood. 7th ed. Philadelphia: Saunders/Elsevier; 2009.
30. Pereira I, George TI, Arber DA. Atlas of peripheral blood: the primary diagnostic tool. Philadelphia: Wolters Kluwer Health/Lippincott Williams & Wilkins; 2012.
31. Porta G, Mattarucchi E, Maserati E, Pressato B, Valli R, Morerio C, et al. Monitoring the isochromosome i(7)(q10) in the bone marrow of patients with Shwachman syndrome by real-time quantitative PCR. J Pediatr Hematol Oncol. 2007;29:163–5.
32. Porwit A, McCullough J, Erber WN. Blood and bone marrow pathology. 2nd ed. Churchill Livingstone/Elsevier: Edinburgh; 2011.
33. Pressato B, Marletta C, Montalbano G, Valli R, Maserati E. Improving the definition of the structure of the isochromosome i(7)(q10) in Shwachman-Diamond Syndrome. Br J Haematol. 2010;150:632–3.
34. Pressato B, Valli R, Marletta C, Mare L, Montalbano G, Curto FL, et al. Cytogenetic monitoring in Shwachman-Diamond syndrome: a note on clonal progression and a practical warning. J Pediatr Hematol Oncol. 2015;37:307–10.
35. Preis M, Lowrey CH. Laboratory tests for paroxysmal nocturnal hemoglobinuria. Am J Hematol. 2014;89:339–41.
36. Proytcheva MA. Diagnostic pediatric hematopathology. Cambridge: Cambridge University Press; 2011.
37. Renella R, Wood WG. The congenital dyserythropoietic anemias. Hematol Oncol Clin N Am. 2009;23:283–306.
38. Rezaei N, Aghamohammadi A, Notarangelo LD. Primary immunodeficiency diseases: definition, diagnosis, and management. Berlin: Springer; 2008.

39. Schafernak KT. Gelatinous transformation of the bone marrow from anorexia nervosa. Blood. 2016;127:1374.
40. Spinner MA, Sanchez LA, Hsu AP, Shaw PA, Zerbe CS, Calvo KR, et al. GATA2 deficiency: a protean disorder of hematopoiesis, lymphatics, and immunity. Blood. 2014;123:809–21.
41. Sutton L, Vusirikala M, Chen W. Hematogone hyperplasia in copper deficiency. Am J Clin Pathol. 2009;132:191–9.
42. Townsley DM, Dumitriu B, Young NS. Bone marrow failure and the telomeropathies. Blood. 2014;124:2775–83.
43. Vicari P, Sthel VM. Cystine crystals in bone marrow. N Engl J Med. 2015;373:e27.
44. Wang E, Boswell E, Siddiqi I, CM L, Sebastian S, Rehder C, et al. Pseudo-Pelger-Huët anomaly induced by medications: a clinicopathologic study in comparison with myelodysplastic syndrome-related pseudo-Pelger-Huët anomaly. Am J Clin Pathol. 2011;135:291–303.
45. Weinstein JL, Badawy SM, Bush JW, Schafernak KT. Deconstructing the diagnosis of hemophagocytic lymphohistiocytosis using illustrative cases. J Hematop. 2015;8:113–25.
46. Wickramasinghe SN, Wood WG. Advances in the understanding of the congenital dyserythropoietic anaemias. Br J Haematol. 2005;131:431–6.
47. Xie Y, Pittaluga S, Price S, Raffeld M, Hahn J, Jaffe ES, et al. Bone marrow findings in autoimmune lymphoproliferative syndrome with germline FAS mutation. Haematologica. 2017;102:364–72.

Bone Marrow Infections

5

Ahmad Monabati, Girish Venkataraman,
and Perikala Vijayananda Kumar

Bone marrow aspiration and biopsy is frequently performed to identify possible infectious causes for fevers of unknown origin. In developing countries, the success rate of such bone marrow studies is high, particularly in light of the increased prevalence of certain infectious diseases like *Mycobacteria* and *Leishmania*. Such specimens are also especially useful in patients with underlying immune compromise for any reason (viz., posttransplant state, human immunodeficiency virus infection).

Careful examination of the peripheral blood is essential to identify certain agents that often circulate in the blood (such as malaria, *Babesia*, *Trypanosoma*, *Ehrlichia*, and *Borrelia* spp.). This chapter, however, will focus on infectious agents that are more likely to be detected in the marrow compared to peripheral blood. The majority of infections lead to nonspecific changes in blood or marrow, such as neutrophilia, lymphocytosis, monocytosis, eosinophilia, leukopenia, hypercellular or hypocellular marrow, or dysplastic changes in marrow elements.

Bone marrow aspirate and biopsies both have complementary roles that aid in identifying microorganisms when present. Agents such as *Leishmania* and *Histoplasma* are better seen on aspirates, while infectious processes that cause granulomas and necrosis (such as *Mycobacteria*) are better identified on biopsies, which in turn lend themselves to staining with acid-fast stains. Simultaneous pulls of bone marrow aspirates for culture studies are also important, especially with *Mycobacteria*, and also serve as important sources for additional stains (such as acid-fast or silver stains) and even molecular techniques, to search for underlying causes and subtype infectious agents (Figs. 5.1, 5.2, 5.3, 5.4, 5.5, 5.6, 5.7, 5.8, 5.9, 5.10, 5.11, 5.12, 5.13, 5.14, 5.15, 5.16, 5.17, 5.18, 5.19, 5.20, 5.21, 5.22, 5.23, 5.24, 5.25, 5.26, 5.27, 5.28, 5.29, 5.30, 5.31, 5.32, and 5.33).

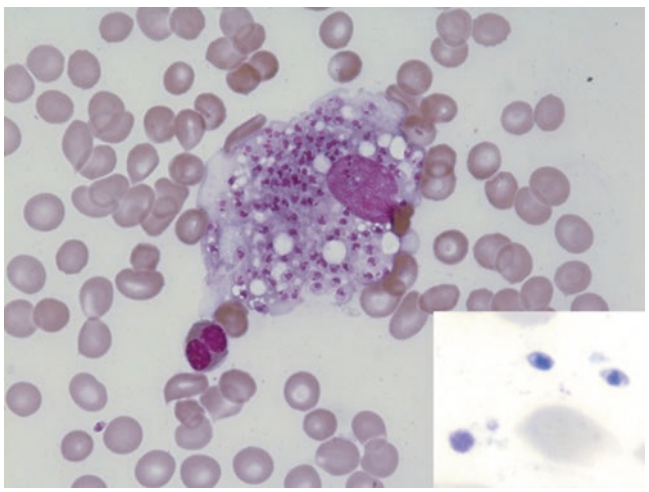

Fig. 5.1 A marrow macrophage stuffed with amastigote forms of *Leishmania donovani.* This patient is a 3-year-old boy with visceral leishmaniasis ("kala-azar") caused by *Leishmania donovani*, an intracellular parasite infecting the mononuclear phagocytic system in the liver, spleen, and bone marrow. This disease frequently presents with pancytopenia, prompting bone marrow biopsies. Inset shows two amastigote forms (top) with a platelet for comparison (bottom). Each amastigote ("Leishman-Donovan" [LD] body) has a nucleus and a kinetoplast near it

A. Monabati (✉) • P.V. Kumar
Department of Pathology, Shiraz Medical School,
Shiraz, Fars, Iran
e-mail: monabati.am@gmail.com; kumarv@sums.ac.ir

G. Venkataraman
Department of Pathology, University of Chicago Medical Center,
Chicago, IL, USA
e-mail: Girish.Venkataraman@uchospitals.edu

T.I. George, D.A. Arber (eds.), *Atlas of Bone Marrow Pathology*, Atlas of Anatomic Pathology,
https://doi.org/10.1007/978-1-4939-7469-6_5

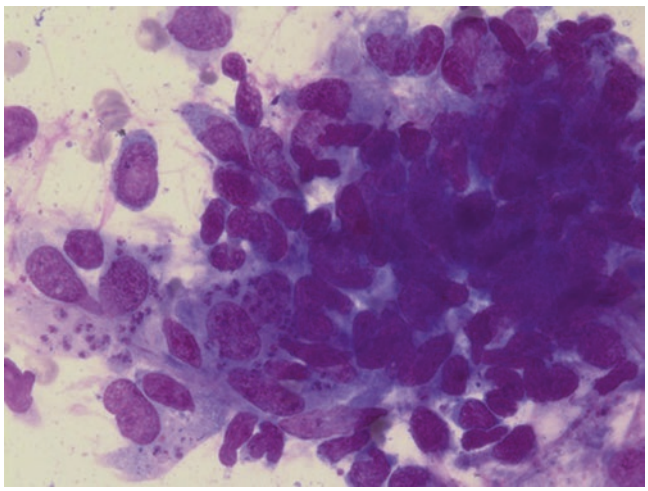

Fig. 5.2 A cluster of epithelioid histiocytes in this marrow aspirate contains entangled "LD" bodies of Leishmania. While bone marrow examination is a sensitive method to detect parasites, serologic and molecular tests performed on peripheral blood are good alternatives

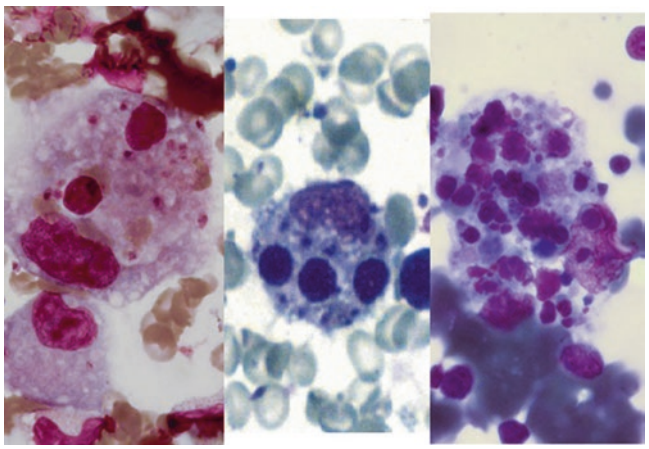

Fig. 5.4 Different forms and shapes of secondary hemophagocytic syndrome (hemophagocytic lymphohistiocytosis, HLH) in visceral leishmaniasis. HLH is a systemic disease that can be either inherited or acquired and is due to over-activation of immune cells. Secondary forms may be encountered in systemic infections such as kala-azar. Wright stain × 1000

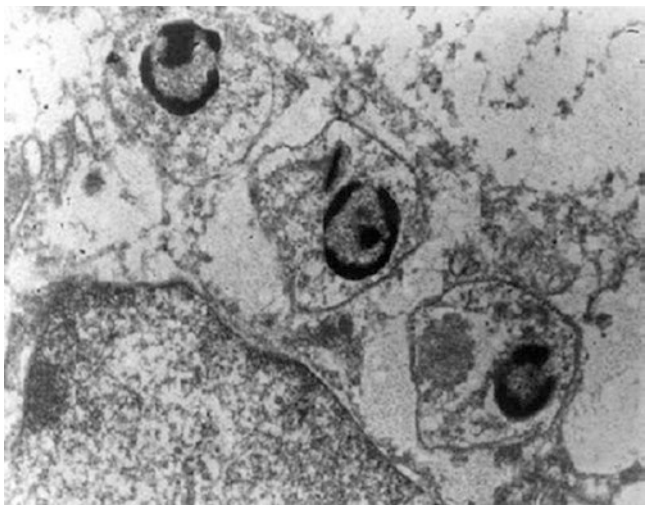

Fig. 5.3 Electron microscopy of Leishman bodies inside a macrophage. The middle one shows a kinetoplast adjacent to the nucleus. Kinetoplasts are large mitochondria filled by DNA and are only seen in protozoa of the class Kinetoplastida

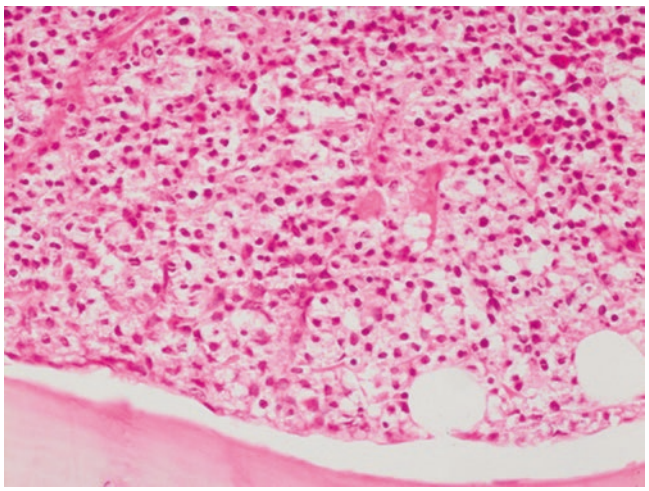

Fig. 5.5 Leishmaniasis triggers a granulomatous reaction in the marrow. There are several morphological patterns reflective of the varied host immunologic responses to the antigenic characteristics of the organism. This image shows a diffuse histiocytic reaction. Other reaction patterns, such as single-cell histiocytic reaction resembling a starry sky, may be seen in addition to frank bone marrow necrosis and lymphoid nodules

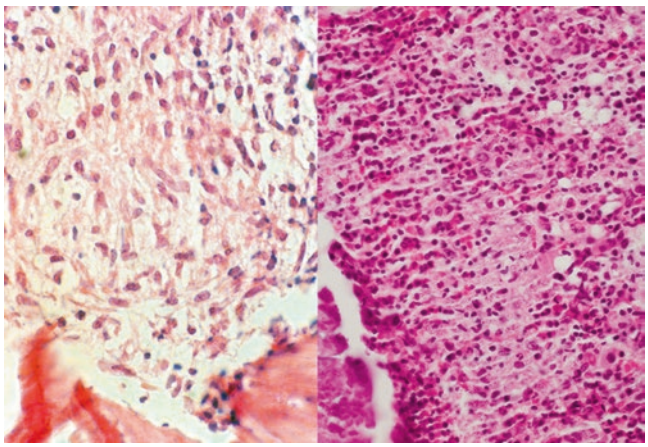

Fig. 5.6 The left side of the figure is notable for a tight tuberculoid type of granuloma, whereas on the right side, a diffuse histiocytic granuloma loaded with Leishman bodies is noted. When parasites are hard to find, PCR performed on bone marrow biopsies or aspirates is very efficient in confirming the diagnosis

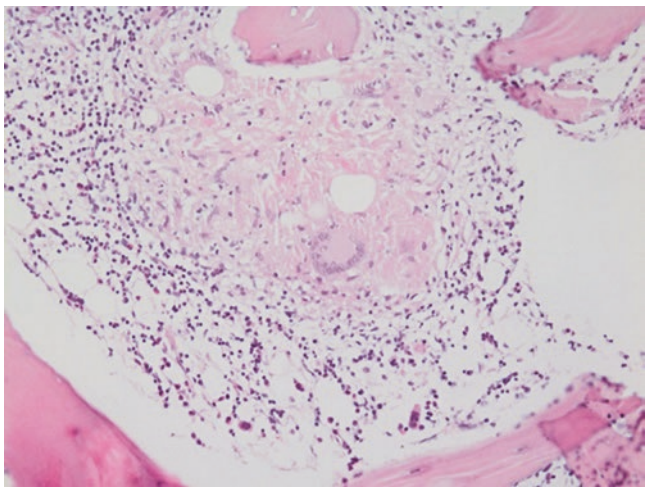

Fig. 5.8 Typical tuberculoid type of granuloma with Langhans giant cells in a 45-year-old man with miliary tuberculosis (TB). The majority of patients with this type of granuloma are ultimately diagnosed with tuberculosis. Acid-fast (Ziehl-Neelsen) cytochemical stain is a specific but not sensitive stain that should be done on all cases with granulomas given the high prevalence of TB. Molecular studies and culture may provide confirmatory results in such cases

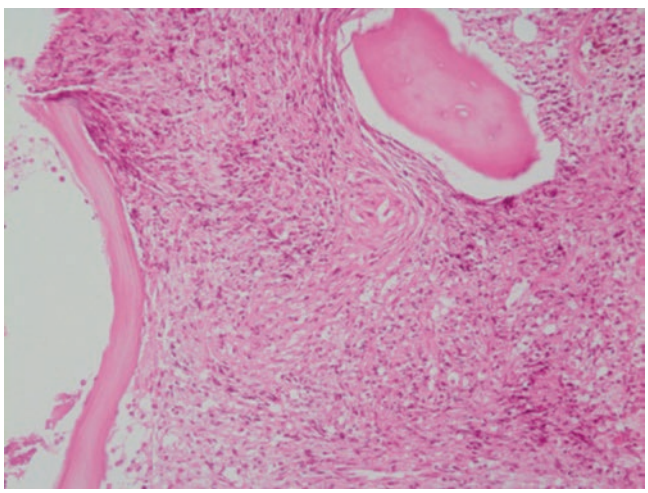

Fig. 5.7 Bone marrow fibrosis in Leishmaniasis

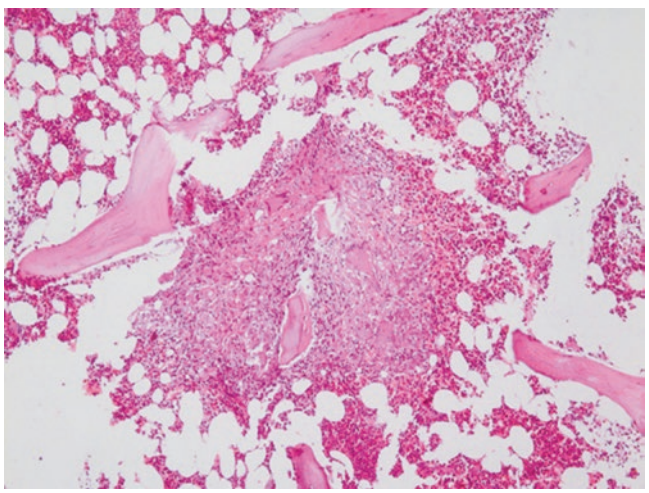

Fig. 5.9 Another discrete TB granuloma amid marrow with normal multilineage hematopoiesis. Acid-fast stain was positive. The differential diagnosis of bone marrow granulomas is large and includes noninfectious conditions including sarcoidosis as well as medications [1]

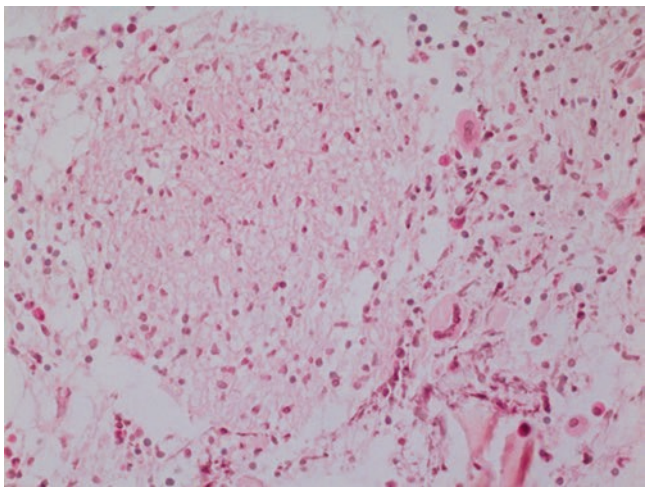

Fig. 5.10 A well-defined bone marrow granuloma in a patient with chronic brucellosis. This is a zoonotic type of infection transmitted by ingestion of unpasteurized milk of infected animals. Sacroiliitis and involvement of bony parts of lumbar spines are characteristic for brucellosis. Beside serologic tests, bone marrow culture and molecular methods such as PCR can be performed on a sample to reach a correct diagnosis

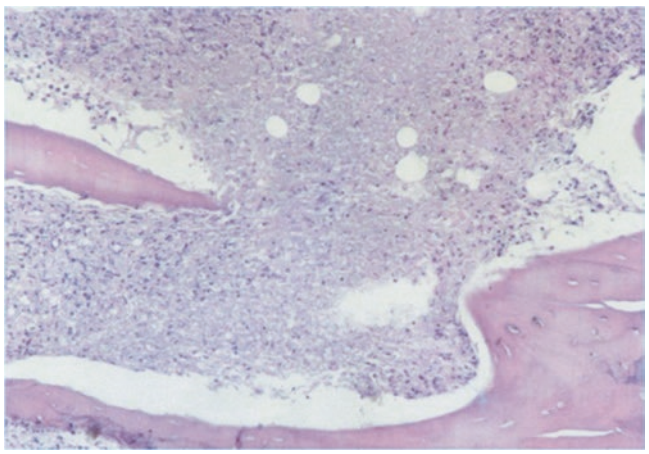

Fig. 5.12 Extensive bone marrow necrosis in a 3-month-old boy with disseminated bacille Calmette–Guerin (BCG) infection after vaccination with BCG. He was later identified to have underlying severe combined immunodeficiency (SCID) and succumbed to the BCG infection. Dissemination of mycobacterium after vaccination is a rare complication occurring in those with underlying immunodeficiency. Depending on the level of immune competence of the host, the presentation can vary from a localized skin nodule or axillary lymphadenopathy to severe disseminated disease with fever and multi-organ failure

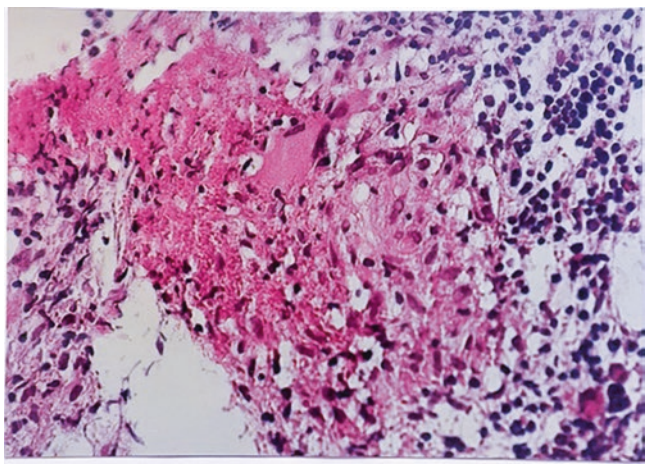

Fig. 5.11 Marrow granuloma caused by disseminated EBV infection after transplantation. Involvement of marrow by granulomas may be seen in acute or chronic phase of the disease. Sometimes fibrin ring granulomas are seen (not in this case)

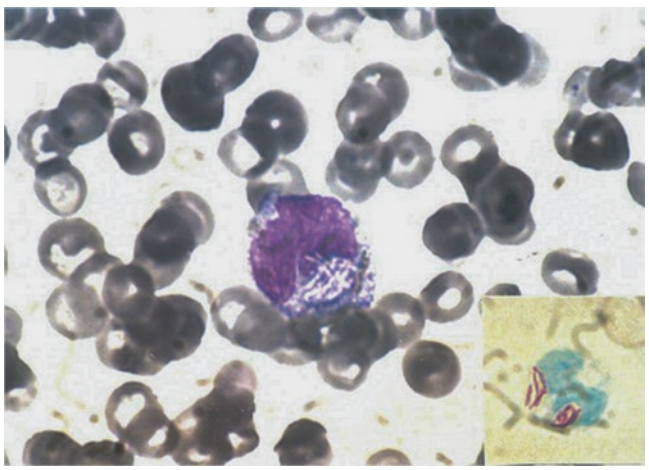

Fig. 5.13 A monocyte in peripheral blood with ghost tuberculous bacilli. Inset shows numerous acid-fast-stained bacilli in the cytoplasm. This is not a very frequent finding in these patients but when detected can be very helpful

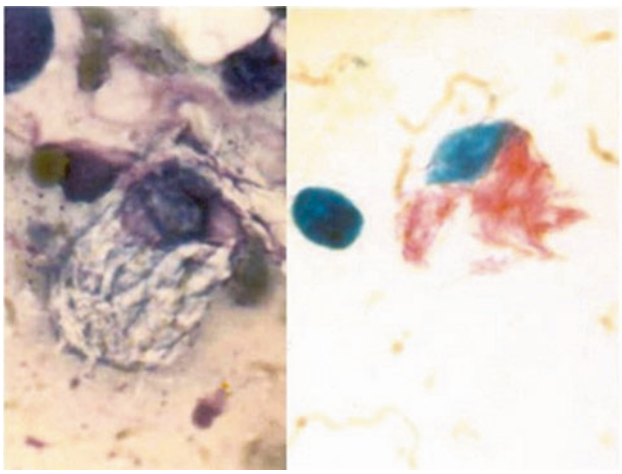

Fig. 5.14 A Gaucher-like histiocyte in marrow aspirate with multiple unstained linear structures representing multiple tuberculous bacilli (left) highlighted well in the acid-fast stain (right)

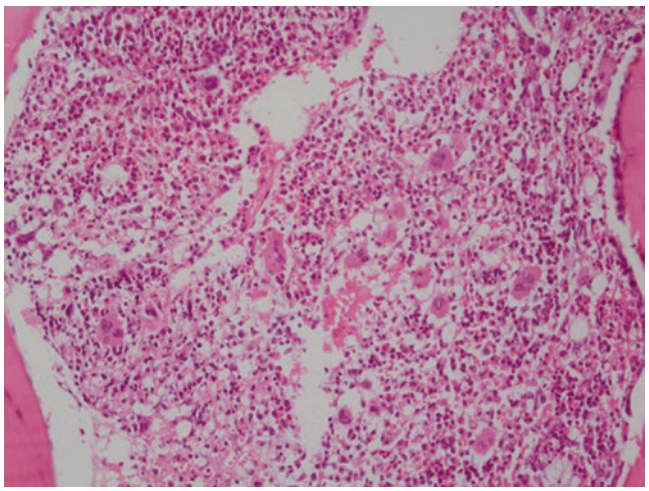

Fig. 5.16 Hypercellularity due to panmyelosis is another nonspecific change seen in HIV infection. This slide shows proliferation, clustering, and paratrabecular aggregation of megakaryocytes with occasional dysplastic forms, including small megakaryocytes and separated nuclei [2]. HIV patients are at increased risk for MDS, especially when not taking anti-retroviral therapy

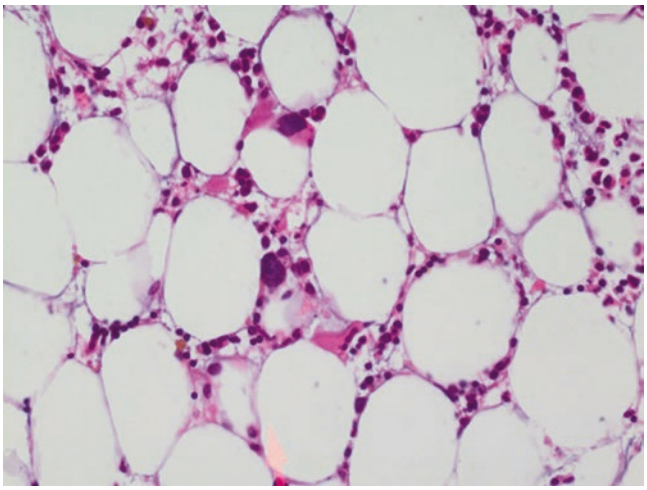

Fig. 5.15 Hypocellular marrow in a 34-year-old man with HIV. Decreased cellularity is one of the most common manifestations of this disease, particularly at advanced stage. Sometimes concomitant infections such as hepatitis viruses may lead to bone marrow suppression

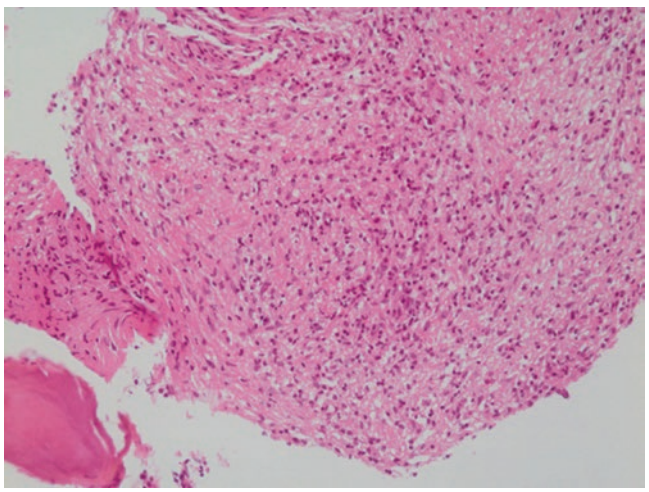

Fig. 5.17 Bone marrow granuloma in a man with HIV infection. The granulomas are typically diffuse with ill-defined borders as epithelioid histiocytes are not able to make a tuberculoid form

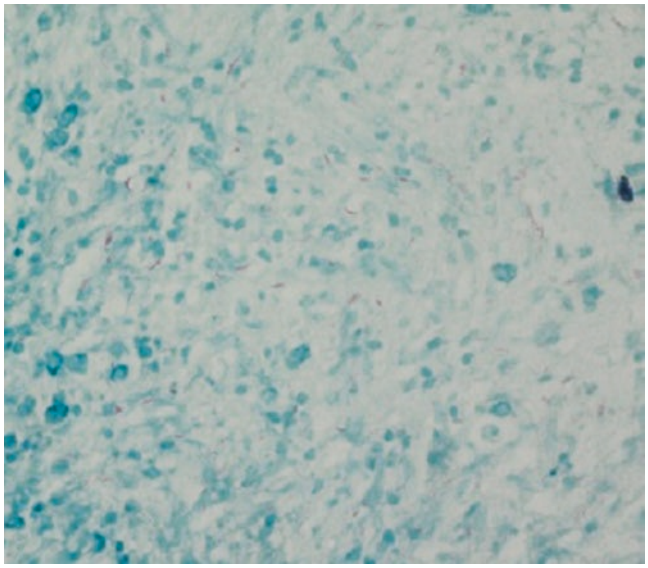

Fig. 5.18 In the case from Fig. 5.17, many acid-fast bacilli are seen. The organism was proved to be MAC (*Mycobacterium* avium-intracellulare complex) through the use of molecular methods. Ziehl-Neelsen stain

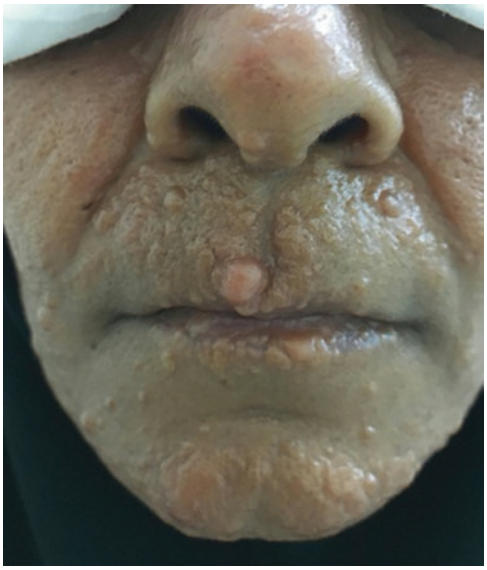

Fig. 5.20 Clinical photograph of patient from Fig. 5.19 depicting multiple nodular skin lesions consistent with mucocutaneous leishmaniasis. Another differential in this setting is the post-kala-azar dermal leishmaniasis, which is notable for small papular rash resembling lepromatous leprosy [3]

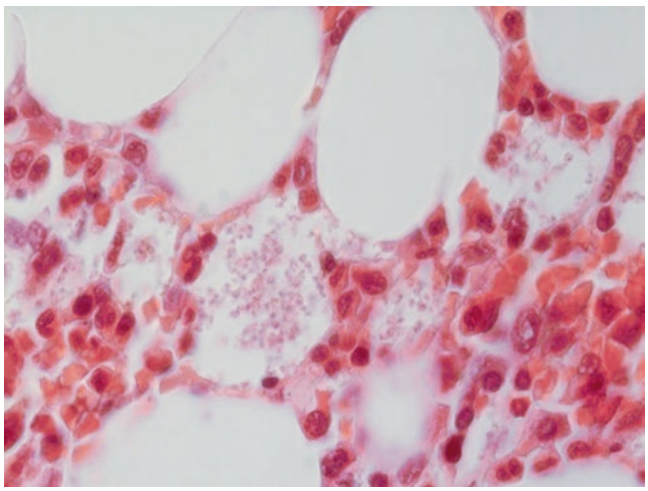

Fig. 5.19 Bone marrow in a 40-year-old woman with disseminated mucocutaneous and visceral leishmaniasis. In a survey for immune deficiency, she was proved to have unrecognized advanced HIV infection. The bone marrow biopsy is notable for numerous LD bodies spilling into the fat spaces

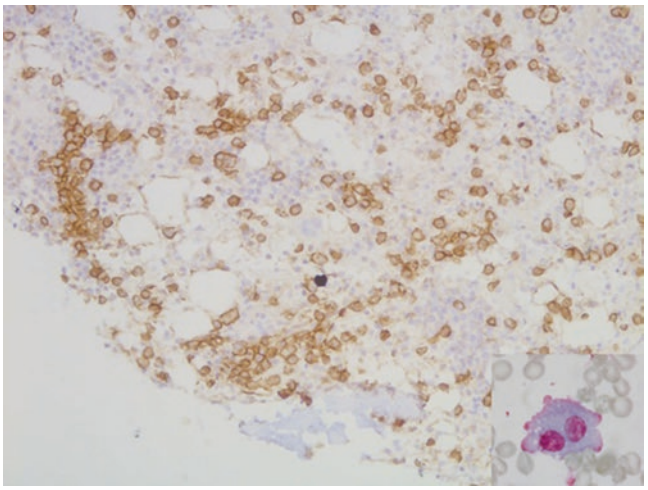

Fig. 5.21 Increase in number of plasma cells is a frequent finding in HIV infection. CD138 highlights plasma cells, which comprise around 20% of marrow cells in this case. They are, however, polyclonal. Inset shows binucleated form

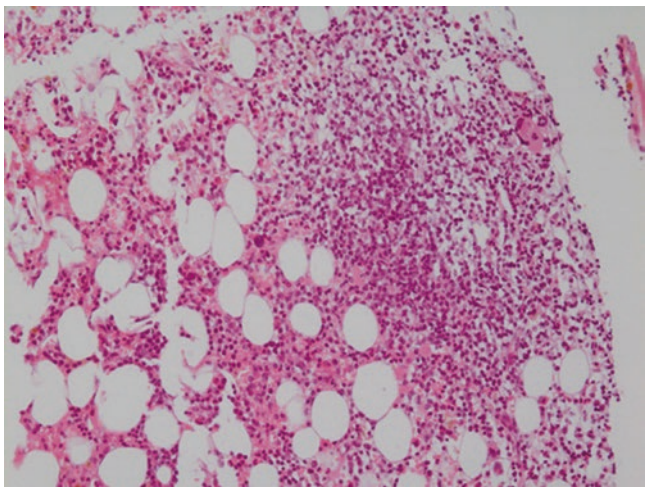

Fig. 5.22 Benign interstitial lymphoid nodule with a germinal center in the marrow of a young man with HIV infection. An important consideration in advanced HIV also includes multicentric Castleman disease (MCD) related to HHV8, which frequently presents with lymphoid nodules in the bone marrow with scattered HHV8+ mononuclear cells [4]

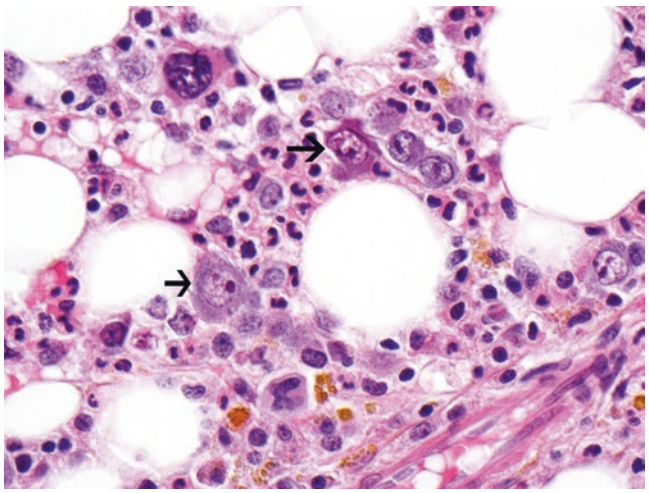

Fig. 5.24 Bone core biopsy in the same case (Fig. 5.23) showing scattered large pronormoblasts with eosinophilic nuclear viral inclusions (*arrows*)

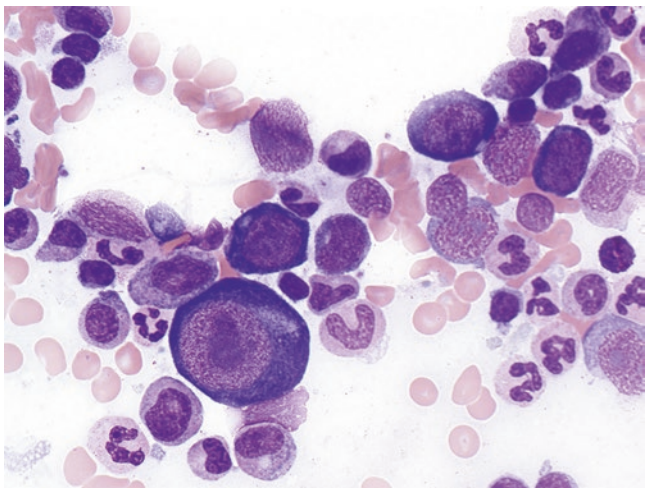

Fig. 5.23 *Parvovirus B19* infection in a patient with a history of renal transplantation. Large pronormoblast with ground-glass nuclear inclusion are present. These cells are often referred to as "lantern cells" due to the peculiar shape of the inclusion resembling a lantern. Frequently, cytoplasmic vacuolations and "dog-ear" cytoplasmic projections may also be observed. Note the paucity of more mature erythroid precursors in the surrounding areas. This virus causes self-limited childhood exanthem, called "fifth disease." This is very dangerous in those with underlying hemoglobin disorders, such as sickle cell anemia, wherein it might occur as a part of a crisis

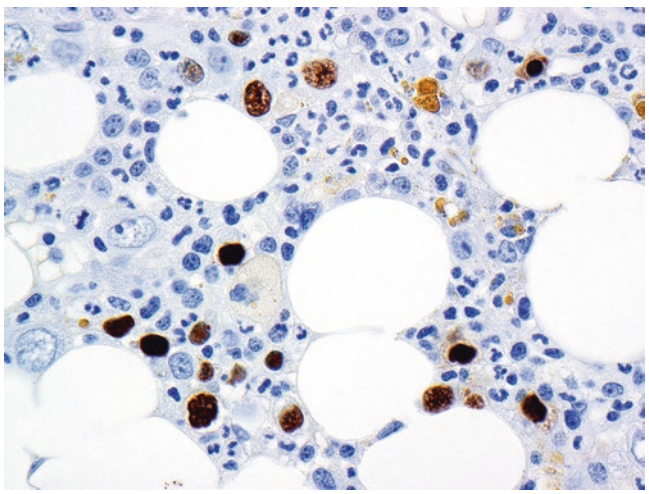

Fig. 5.25 Immunostain for parvovirus (same case as Fig. 5.23) is useful in highlighting the viral inclusions when the cells are hard to visualize

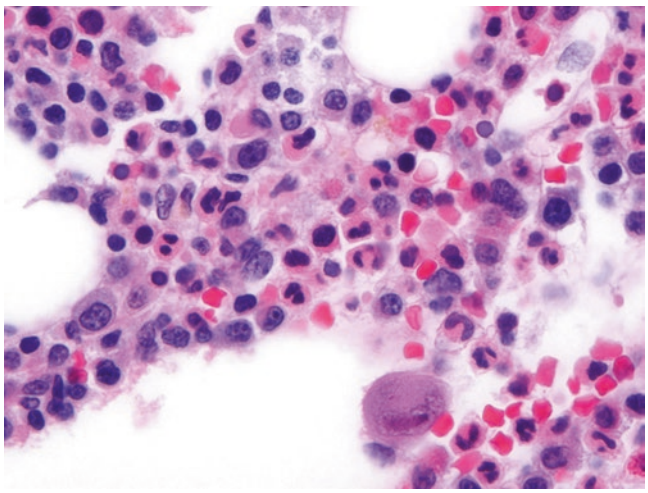

Fig. 5.26 Eosinophilic CMV viral inclusions in bone marrow. The infected cell is typically enlarged due to the viral cytopathic effect

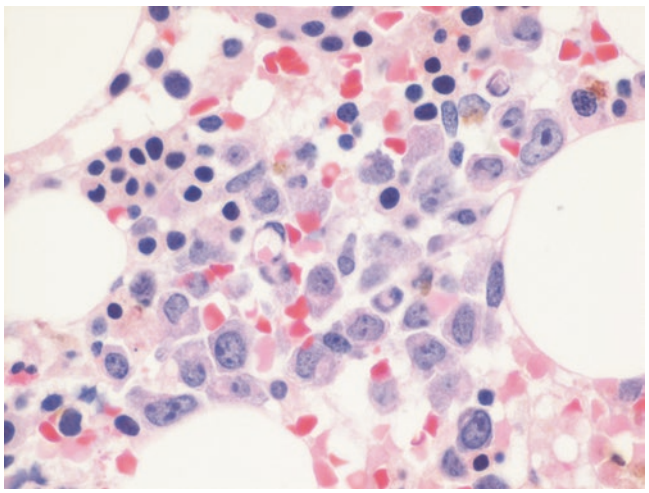

Fig. 5.28 Marrow findings in a patient with HHV6 viremia. This is a 7-year-old girl who, after allogeneic bone marrow transplantation for B-ALL, presented with neutropenia. Note the marked maturation arrest in the myeloid series with large left-shifted myeloid precursors consistent with HHV6 infection. Rarely medications are responsible for maturation arrest

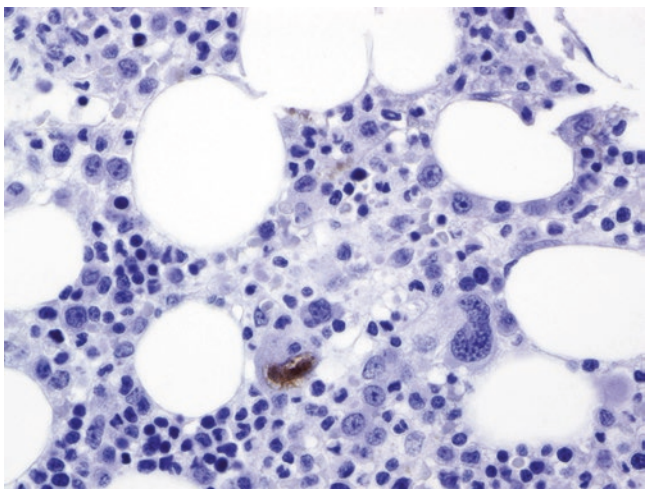

Fig. 5.27 Immunostaining highlights the CMV-infected cells

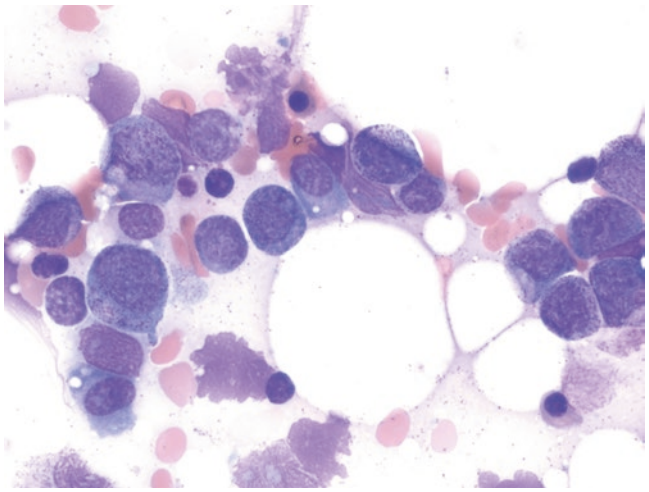

Fig. 5.29 Bone marrow aspirate in the patient from Fig. 5.28, with HHV6 infection showing large left-shifted myeloid precursors and scattered hematogones

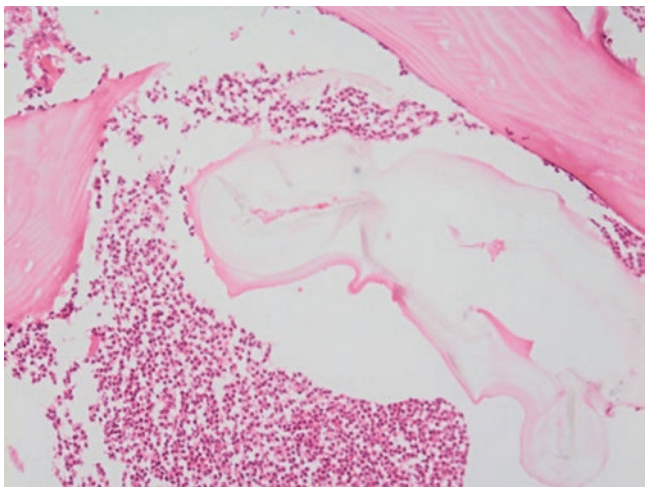

Fig. 5.30 Laminated membrane of *Echinococcus granulosus* adjacent to bone trabecula. A protoscolex was not identified in this case, as old infected cysts seldom show scolices and laminated membrane is proof of the diagnosis. This is a parasitic infection caused by tapeworms of the genus Echinococcus that infect humans who ingest foods or water contaminated by carnivores' fecal material containing eggs. Diagnosis is also made by serologic and radiologic tests

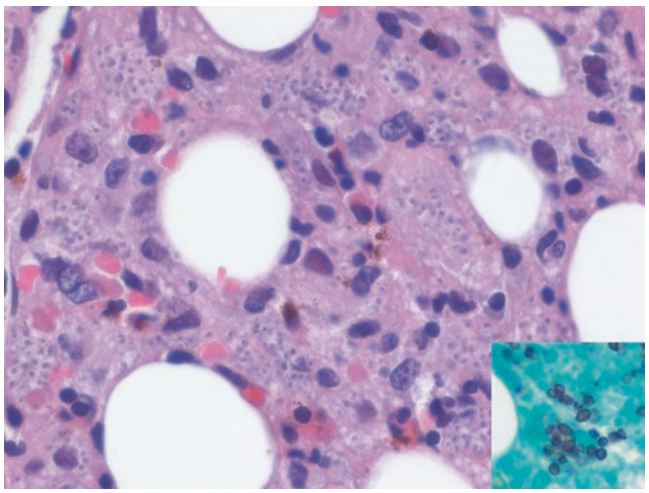

Fig. 5.32 Histoplasmosis involving marrow. This is a 44-year-old renal transplant recipient who presented with pancytopenia and fevers 8 years after transplantation. Numerous yeast forms are apparent within histiocytes percolating diffusely through the interstitium and are highlighted by the fungal stain (Grocott's methenamine silver, inset)

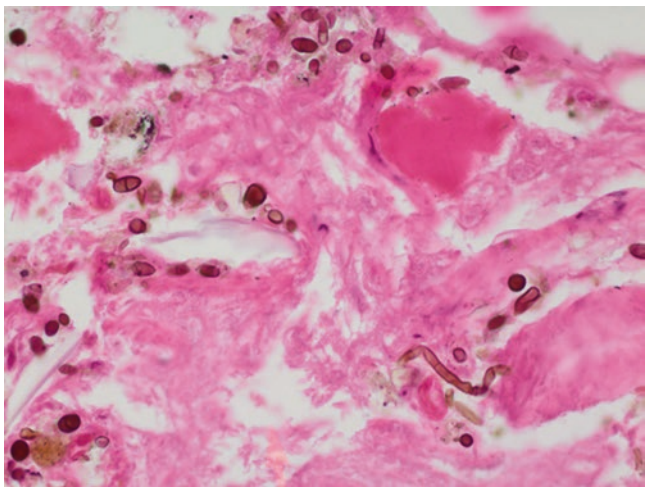

Fig. 5.31 Chromoblastomycosis involving bone trabecula in a patient with a long-standing history of skin lesions. This is a slow-growing fungal infection mainly involving subcutaneous tissue. Histologic examination shows pigmented yeast amid necrotic marrow tissue resembling "copper pennies" with pseudohyphae infiltrating between bone trabeculae

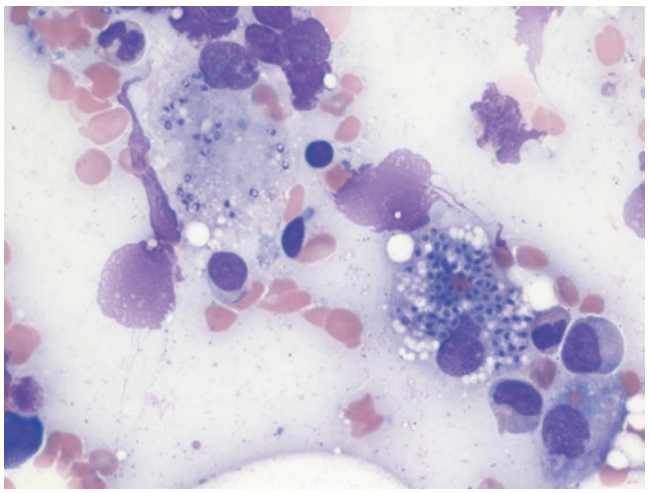

Fig. 5.33 Bone marrow aspirate in case above (*Histoplasma*) highlighting histiocytes filled with yeast forms. This case was also notable for concurrent hemophagocytosis (visible in the histiocytes at the bottom right)

References

1. Bodem CR, Hamory BH, Taylor HM, Kleopfer L. Granulomatous bone marrow disease. A review of the literature and clinicopathologic analysis of 58 cases. Medicine (Baltimore). 1983;62(6):372–83.
2. Karcher DS, Frost AR. The bone marrow in human immunodeficiency virus (HIV)-related disease. Morphology and clinical correlation. Am J Clin Pathol. 1991;95(1):63–71.
3. Zijlstra EE. PKDL and other dermal lesions in HIV co-infected patients with Leishmaniasis: review of clinical presentation in relation to immune responses. PLoS Negl Trop Dis. 2014;8(11):e3258.
4. Venkataraman G, Uldrick TS, Little R, Yarchoan R, Pittaluga S, Maric I. Bone marrow histology in a cohort of HIV plus patients with multicentric Castleman's disease (MCD) associated with Kaposi's sarcoma-associated herpesvirus. Mod Pathol. 1458:23.

Bone Marrow Lymphoma

6

Megan Parilla and Girish Venkataraman

Lymphomas are malignant hematopoietic neoplasms arising from mature lymphoid cells that typically reside within extramedullary lymphoid tissues, including the lymph nodes and spleen. However, lymphomas can frequently involve the extranodal tissues, including peripheral blood (leukemia) and/or the bone marrow. There are even rare instances in which the bone marrow is the sole location of involvement by lymphoma [1]. A variety of infiltration patterns may be observed (paratrabecular, interstitial, or sinusoidal) in the various B and T cell lymphomas, besides varying background microenvironment inflammatory cells (e.g., in Hodgkin lymphoma, T cell lymphomas). Both pattern and microenvironment are useful features that assist in characterizing marrow involvement by providing clues to the nature of the lymphoma in cases where marrow involvement is the presenting feature. Ancillary studies such as flow cytometry and immunohistochemistry are both complementary studies in evaluating for marrow involvement.

From a clinical perspective, however, vastly improved imaging techniques such as PET/CT have facilitated better identification of marrow involvement, decreasing the need to perform staging bone marrow biopsies in lymphomas, particularly in Hodgkin lymphoma [2]. Excluding diffuse large B cell lymphoma, a bone marrow biopsy is required when staging all non-Hodgkin lymphomas. In general, the presence of lymphoma within the bone marrow signifies advanced stage disease [3].

In this chapter, we will focus on bone marrow infiltrated by both non-Hodgkin and Hodgkin lymphoma: the histologic patterns of involvement and cellular cytomorphology, with significant focus on the immunohistochemical markers pertinent for diagnosis and prognostication in light of certain newly recognized entities in the WHO 2016 revision (such as the EBV+ diffuse large B cell lymphoma, not otherwise specified) [4]. See Figs. 6.1, 6.2, 6.3, 6.4, 6.5, 6.6, 6.7, 6.8, 6.9, 6.10, 6.11, 6.12, 6.13, 6.14, 6.15, 6.16, 6.17, 6.18, 6.19, 6.20, 6.21, 6.22, 6.23, 6.24, 6.25, 6.26, 6.27, 6.28, 6.29, 6.30, 6.31, 6.32, 6.33, 6.34, 6.35, 6.36, 6.37, 6.38, 6.39, 6.40, 6.41, 6.42, 6.43, 6.44, 6.45, 6.46, 6.47, 6.48, 6.49, 6.50, 6.51, 6.52, 6.53, 6.54, 6.55, 6.56, 6.57, 6.58, 6.59, 6.60, 6.61, 6.62, 6.63, 6.64, 6.65, 6.66, 6.67, 6.68, 6.69, 6.70, 6.71, 6.72, 6.73, 6.74, 6.75, 6.76, 6.77, 6.78, 6.79, 6.80, and 6.81 for details.

M. Parilla (✉) • G. Venkataraman
Department of Pathology, University of Chicago Medical Center, Chicago, IL, USA
e-mail: Megan.Parilla@uchospitals.edu; Girish.Venkataraman@uchospitals.edu

T.I. George, D.A. Arber (eds.), *Atlas of Bone Marrow Pathology*, Atlas of Anatomic Pathology,
https://doi.org/10.1007/978-1-4939-7469-6_6

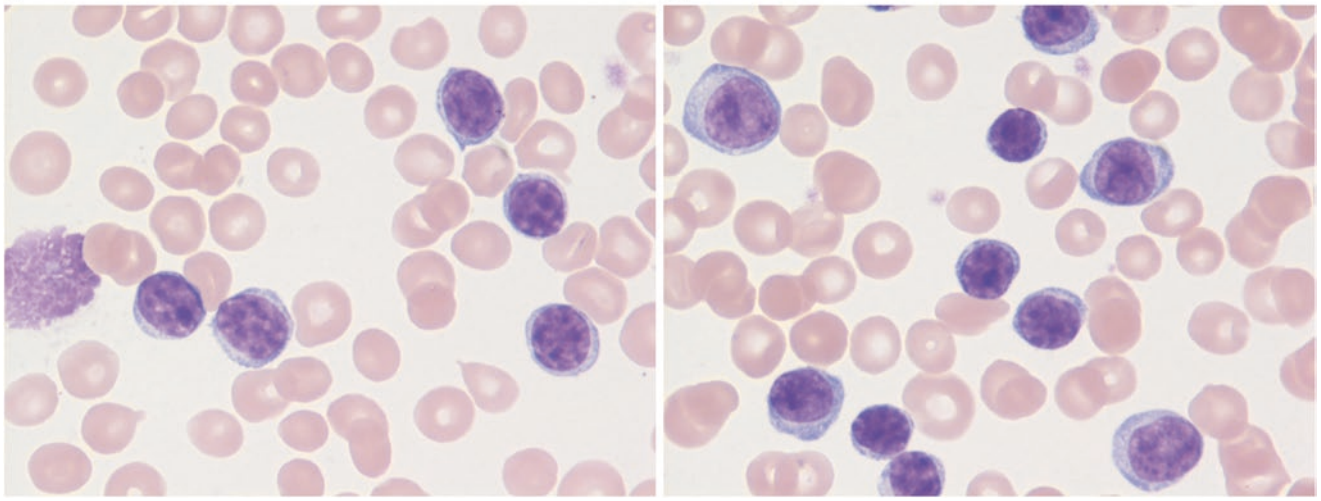

Fig. 6.1 Circulating chronic lymphocytic leukemia/small lymphocytic lymphoma (CLL/SLL) cells are fragile and often rupture in peripheral blood smear preparation resulting in "smudge cells" seen here on the left (**a**). The intact SLL/CLL cells within a peripheral blood smear are small with clumped chromatin and minimal cytoplasm; atypical CLL is often associated with larger cells with more open chromatin and is commonly seen in cases with a trisomy 12 chromosomal alteration pictured in this image (**b**). Circulating larger cells in CLL/SLL are prolymphocytes, identified by a single central prominent nucleolus. A diagnosis of B cell prolymphocytic leukemia (B-PLL) is favored if prolymphocytes exceed 55% of total cellularity

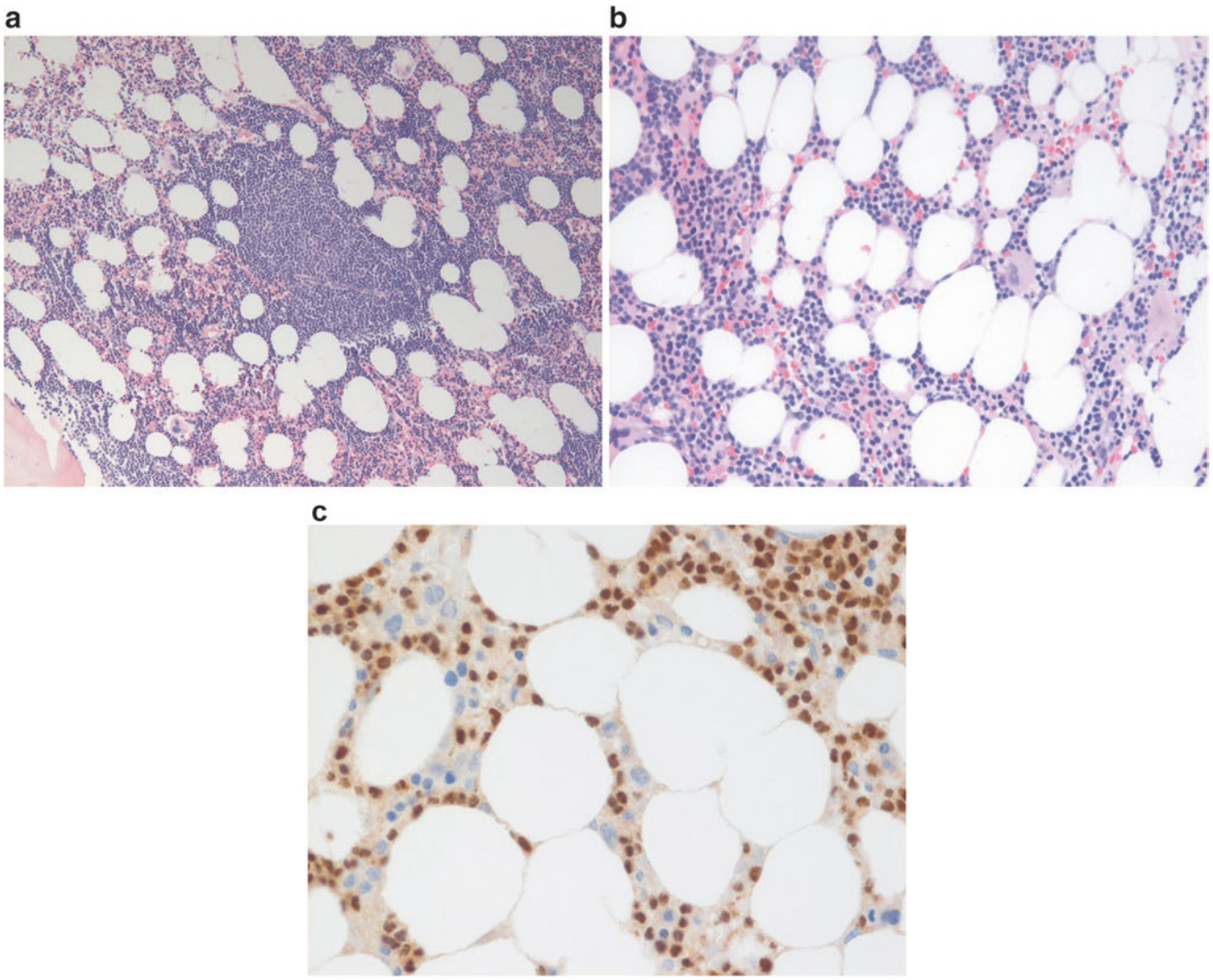

Fig. 6.2 When CLL/SLL involves the bone marrow, it may produce a nodular pattern (**a**) and/or an interstitial pattern histologically at higher power (**b**). The interstitial pattern of infiltration can be overt or subtle and better demonstrated with immunohistochemical stains. PAX5 may assist in assessing the extent of disease in inconspicuous cases (**c**)

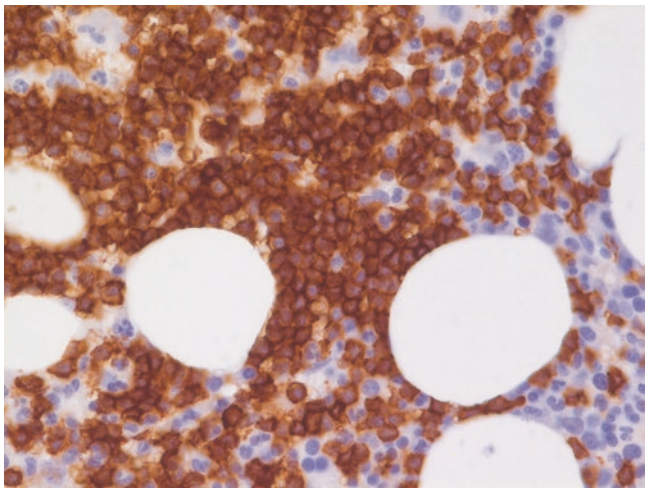

Fig. 6.3 CD20, pictured here, is positive in SLL/CLL reflective of B cell lineage although frequently CD20 is downregulated along with several other B cell lineage markers (CD79b, CD22) as well as surface light chains (by flow cytometry). CD5 (not shown) was also positive, while cyclin D1 was negative, allowing exclusion of mantle cell lymphoma

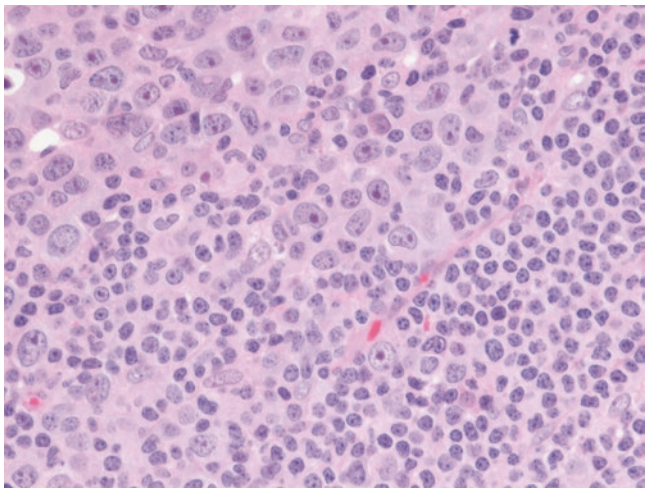

Fig. 6.5 Richter's transformation of CLL/SLL resulting in diffuse large B cell lymphoma (DLBCL-RT). A substantial proportion of this bone marrow biopsy is replaced by this biphasic neoplastic proliferation. The small, round CLL/SLL cells are best seen in the bottom right, while the large, transformed DLBCL cells with immunoblastic cytomorphology (prominent nucleoli) are more prevalent in the top left

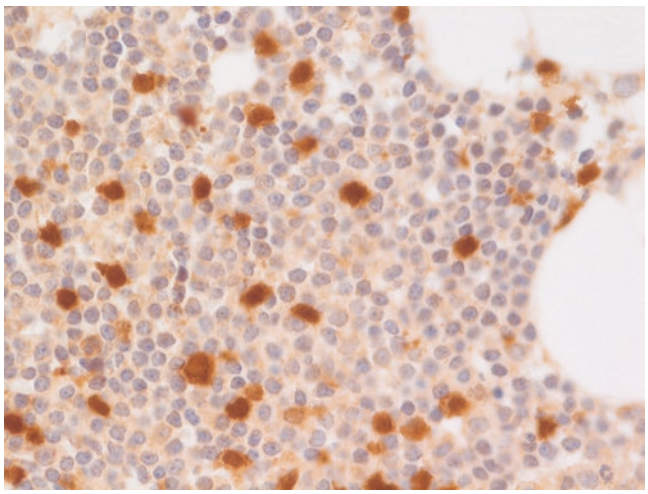

Fig. 6.4 ZAP-70 immunohistochemistry is negative in the CLL cells, while scattered background normal T cells demonstrate strong cytoplasmic expression. Lack of ZAP-70 correlates with a mutated *IGHV*, and such cases carry a better prognosis compared to ZAP-70+ cases with unmutated *IGHV* [5]. Cases with a purely nodular pattern were noted in one study to be mostly ZAP-70 negative by IHC [6]

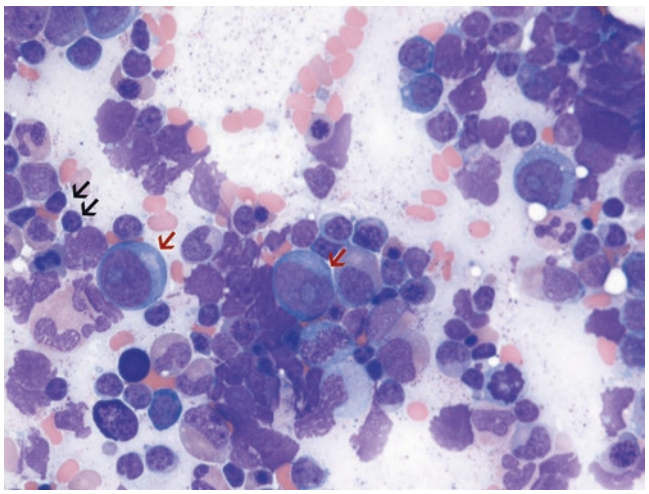

Fig. 6.6 Bone marrow aspirate of the same sample in Fig. 6.5 reveals both small inconspicuous lymphocytes consistent with SLL/CLL (black arrows) and large transformed cells with prominent nucleoli (red arrows) in this case of Richter's transformation. Note the small size of the background early erythroid precursors compared to the large lymphoma cells. DLBCL-RT is generally associated with poor prognosis with a median survival of less than 8 months [7], and its incidence is apparently increased in CLL after ibrutinib therapy (Bruton's tyrosine kinase inhibitor)

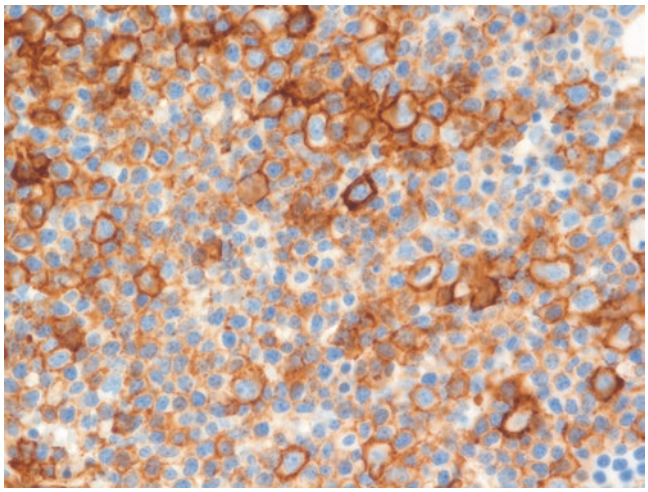

Fig. 6.7 This CD20 immunohistochemical stain on the same bone marrow biopsy with Richter's transformation reveals a biphasic pattern of CD20 expression. The small lymphoid CLL/SLL component has weak CD20 staining with interspersed clusters of large, brightly staining, transformed lymphoma cells of the DLBCL component

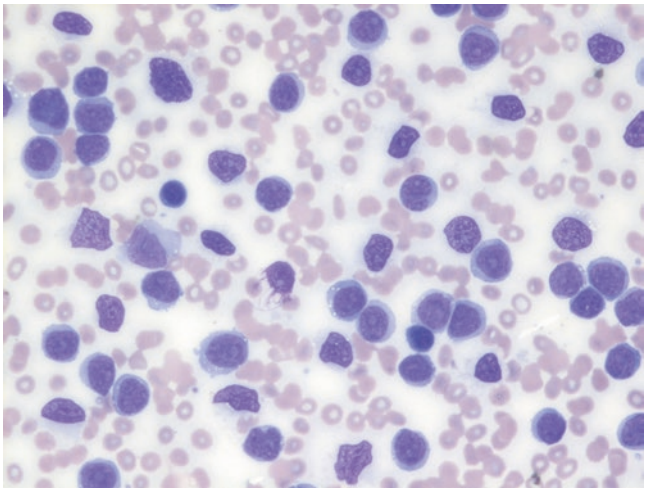

Fig. 6.8 B cell prolymphocytic leukemia (B-PLL) is a rare neoplasm predominately composed of prolymphocytes. The circulating prolymphocytes are "medium in size" or approximately twice a normal lymphocyte and display a prominent central nucleolus. As this image demonstrates, analysis of the peripheral blood in a patient with B-PLL will often reveal a markedly elevated lymphocyte count with anemia and thrombocytopenia

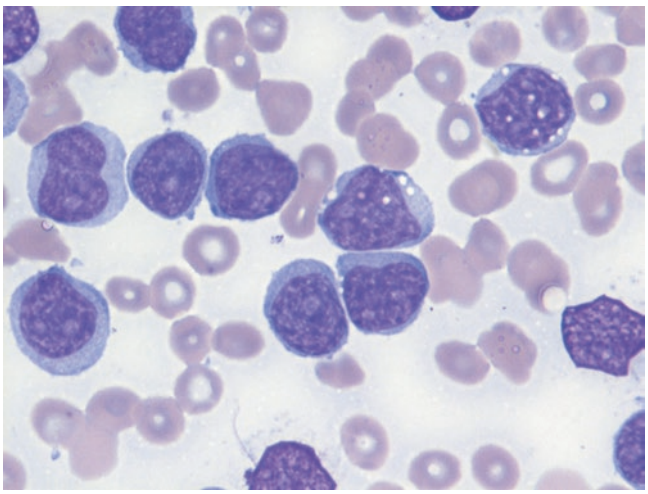

Fig. 6.9 At higher magnification, the nuclear features of B-PLL are better appreciated. The nuclear chromatin is more open than a normal mature circulating lymphocyte; however, it is also more condensed than lymphoblastic cells. The nuclear membrane is typically regular and the prominent vesicular nucleoli should be striking. Importantly, cytogenetic analysis must be done to rule out leukemic/blastoid variants of mantle cell lymphoma. A leukemic variant of mantle cell lymphoma will appear similar both by morphology and immunohistochemistry (CD20 and CD5); however, it will demonstrate the classic t(11;14) in contrast to B-PLL. In this illustrated case, cytogenetic analysis for t(11;14) was negative

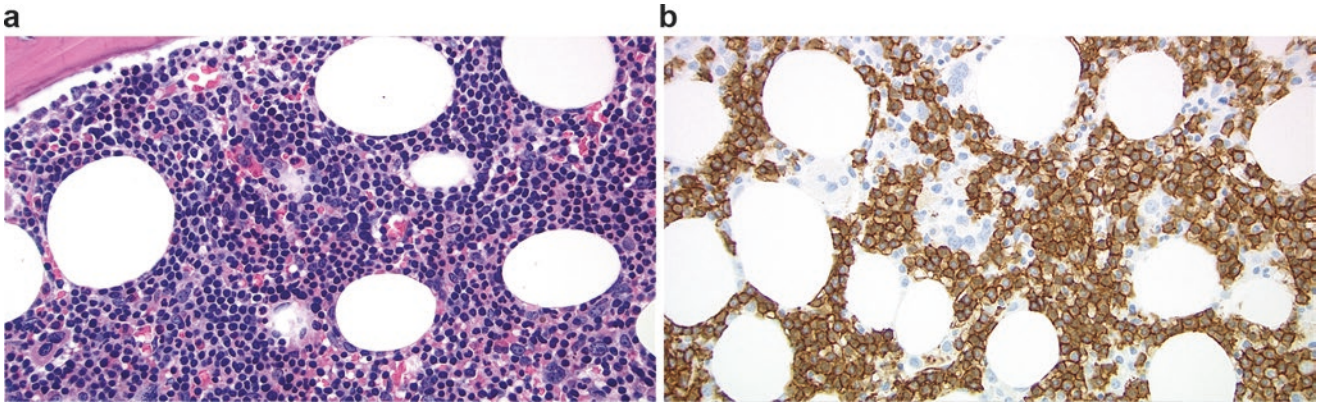

Fig. 6.10 This bone marrow biopsy demonstrates a diffuse infiltrate B-PLL cells with strong CD20 expression (**a** and **b**). Immunohistochemical staining for ZAP-70 was negative (*not shown*) with only background T cell staining. ZAP-70 and CD38 expressions in CLL/SLL are poor prognostic markers; however, in B-PLL, neither ZAP-70 nor CD38 are considered useful markers for prognostication [8, 9]

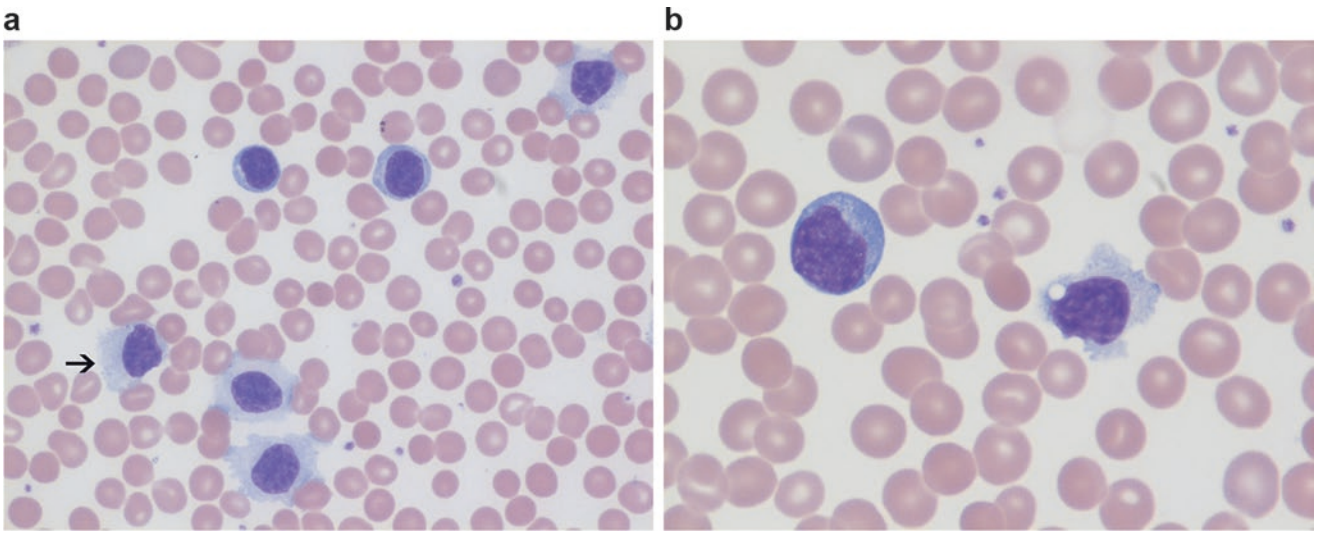

Fig. 6.11 Splenic marginal zone lymphoma (SMZL) cells in this peripheral blood smear are notable for numerous lymphoid cells with cytoplasmic projections that are variably circumferential with some heterogeneity between cells at high power (**a** and **b**). A subset of such cases may exhibit "polar villi" but only a minority of cases demonstrates typical polar villi. Both splenic and nodal marginal zone lymphoma can involve the bone marrow

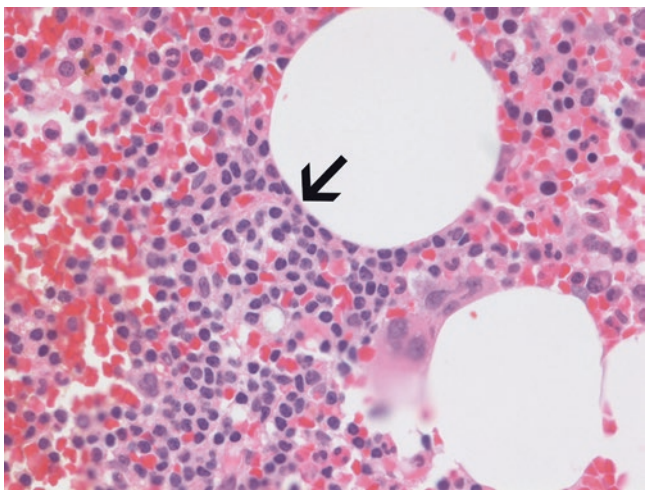

Fig. 6.12 When the bone marrow is involved in SMZL, the lymphoma cells are often seen in sinusoids where the histologic findings can be quite subtle, as in this image and best noted in the center with vague interstitial small lymphoid infiltrate adjacent to the fat space

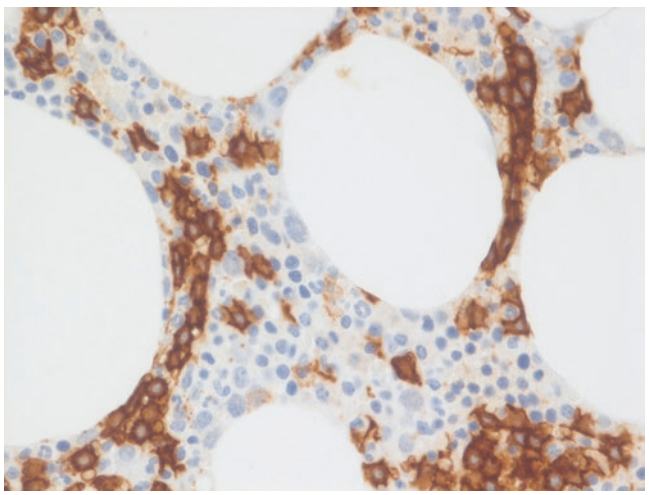

Fig. 6.13 CD20 immunohistochemical stain highlights the predominantly sinusoidal pattern of infiltration in SMZL, which is not easily appreciated with traditional H&E staining

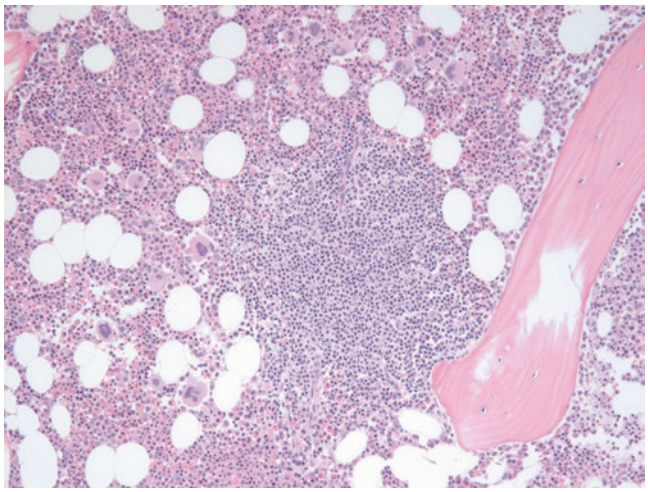

Fig. 6.14 Although identifying intrasinusoidal lymphoma cells can assist in making the diagnosis of MZL, the histology can be interstitial, sinusoidal, nodular, or mixed. In this bone marrow biopsy, the lymphoma cells have formed discrete nodules. The nodular pattern on bone marrow biopsy mostly excludes hairy cell leukemia, which may be in the differential based on the cytoplasmic projections of villous lymphocytes of SMZL

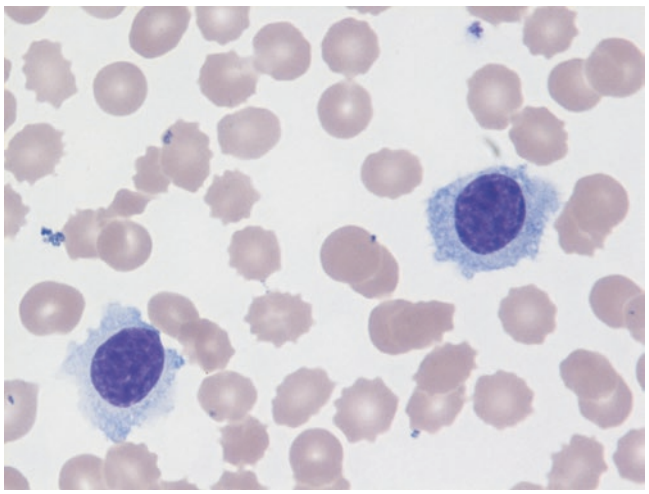

Fig. 6.16 Hairy cell leukemia (HCL) in peripheral blood. The leukemic cells exhibit abundant pale blue cytoplasm with circumferential projections that resemble fine hairs. The cells are typically medium-sized with an oval nucleus and inconspicuous nucleoli. Occasionally, the nucleus is more monocytoid with a reniform appearance

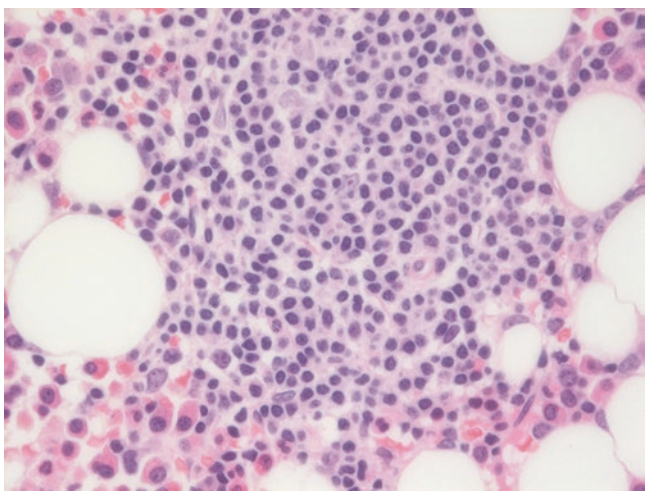

Fig. 6.15 On higher power, this lymphoid aggregate of MZL is cytologically composed of medium-sized monocytoid cells with a moderate amount of clear cytoplasm. More recently, cases of primary bone marrow cold agglutinin disease have been described that exhibit near-exclusive nodular pattern in association with clonal CD5-/CD10- B cells producing clonal immunoglobulin [10]

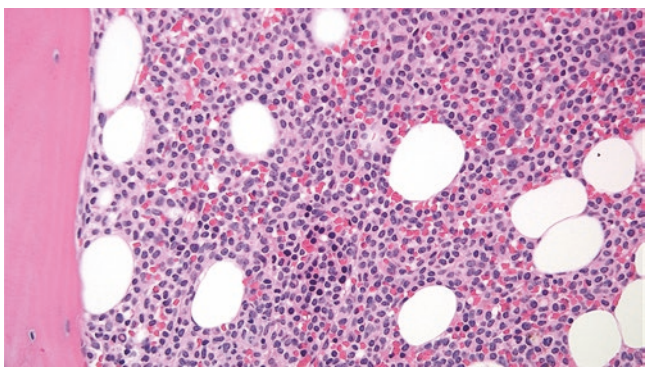

Fig. 6.17 Within the bone marrow, hairy cell leukemia is identified by collections of monomorphic lymphoid cells. The pattern of involvement is predominantly sinusoidal, but here there is diffuse involvement. On low power the crisp oval nuclei, lack of mitotic figures, and regular wide spacing of nuclei clue the observant pathologist to inspect these lymphoid cells more closely

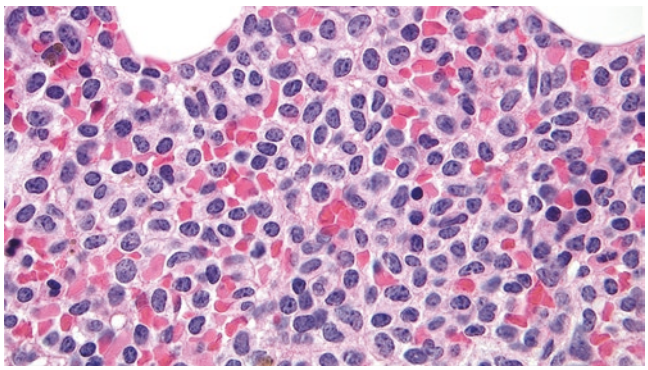

Fig. 6.18 On higher magnification, one can readily appreciate the "fried-egg" appearance with a central nucleus surrounded by abundant cytoplasm with prominent cell boarders in hairy cell leukemia. In this image, the infiltrate has nearly effaced all normal hematopoiesis with only rare scattered dark erythroid progenitors remaining in disrupted clusters seen on the right side

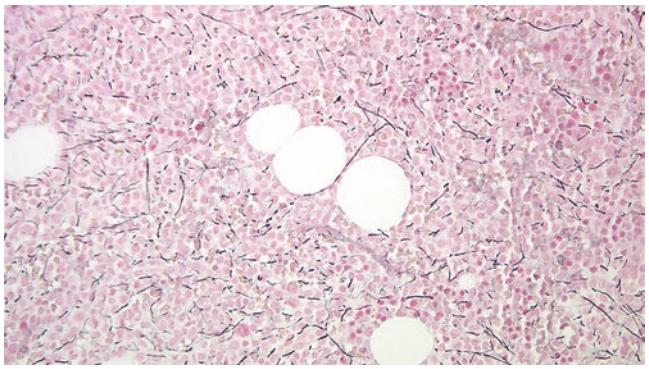

Fig. 6.19 Reticulin fibrosis is increased in hairy cell leukemia due to factors secreted by leukemic cells. This fibrosis is responsible for trapping the leukemic cells within the marrow, resulting in a "dry tap" with attempted bone marrow aspiration despite high cellularity seen within a bone marrow core biopsy

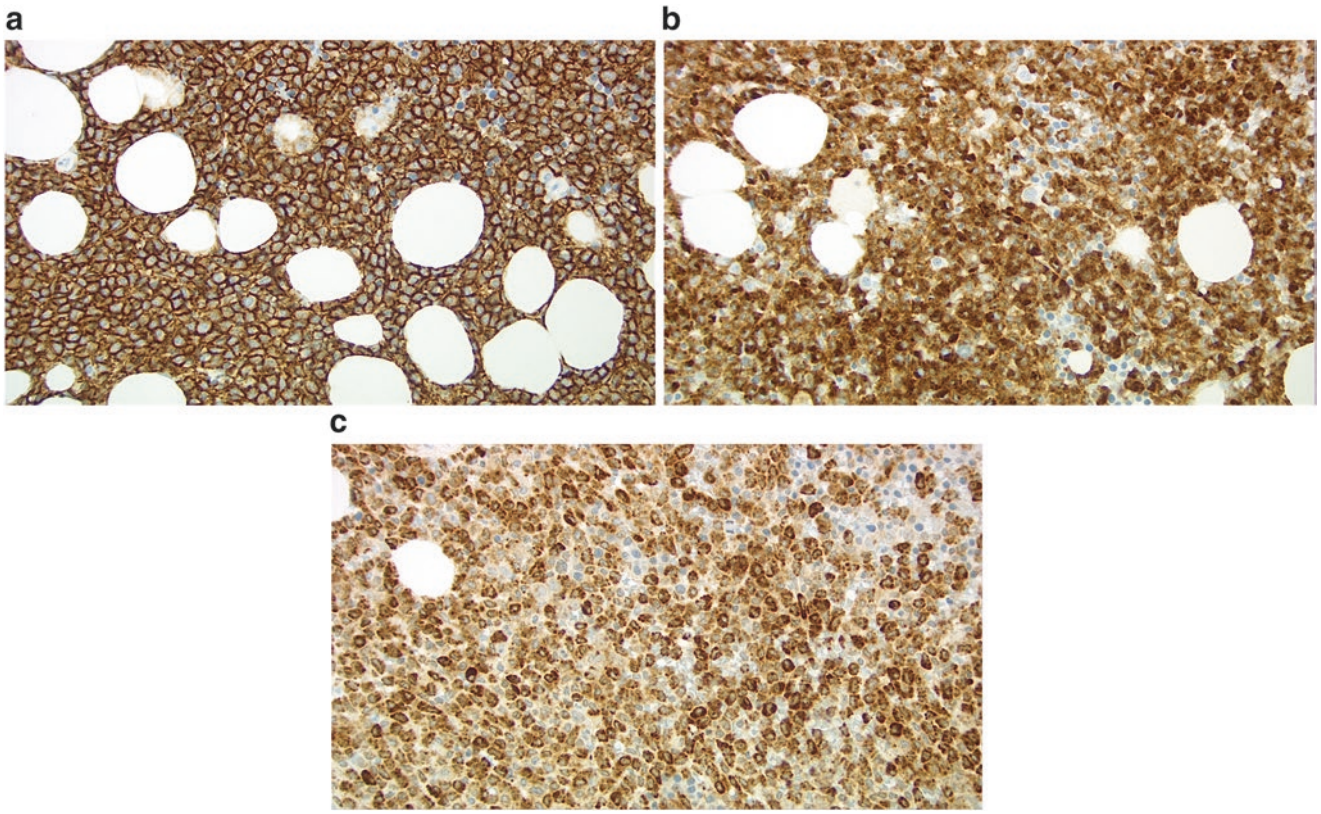

Fig. 6.20 Hairy cell leukemia is a mature B cell neoplasm and as such will express bright CD20 (**a**). Additionally, it classically expresses bright CD11c (**b**). Hairy cells will be positive when stained with the cytochemical stain, tartrate-resistant acid phosphatase (TRAP). More recently, immunohistochemical staining is possible for TRAP, and this shows strong and granular staining within the cytoplasm of the hairy cells (**c**)

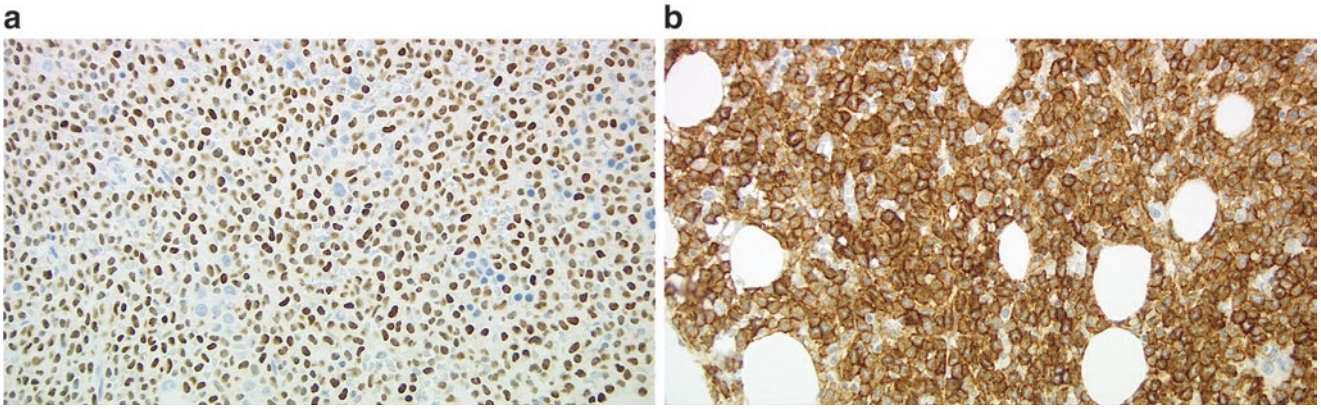

Fig. 6.21 Immunohistochemical staining for transcription factor T-box expressed in T cells (T-bet), a transcription factor expressed in normal reactive Th1 T cells, also has strong nuclear positivity in the B cells of hairy cell leukemia [11] and is useful for detecting minimal residual disease (**a**). CD123 positivity is an additional useful marker of hairy cell leukemia [12]; however, it is not specific to only hairy cell leukemia (**b**)

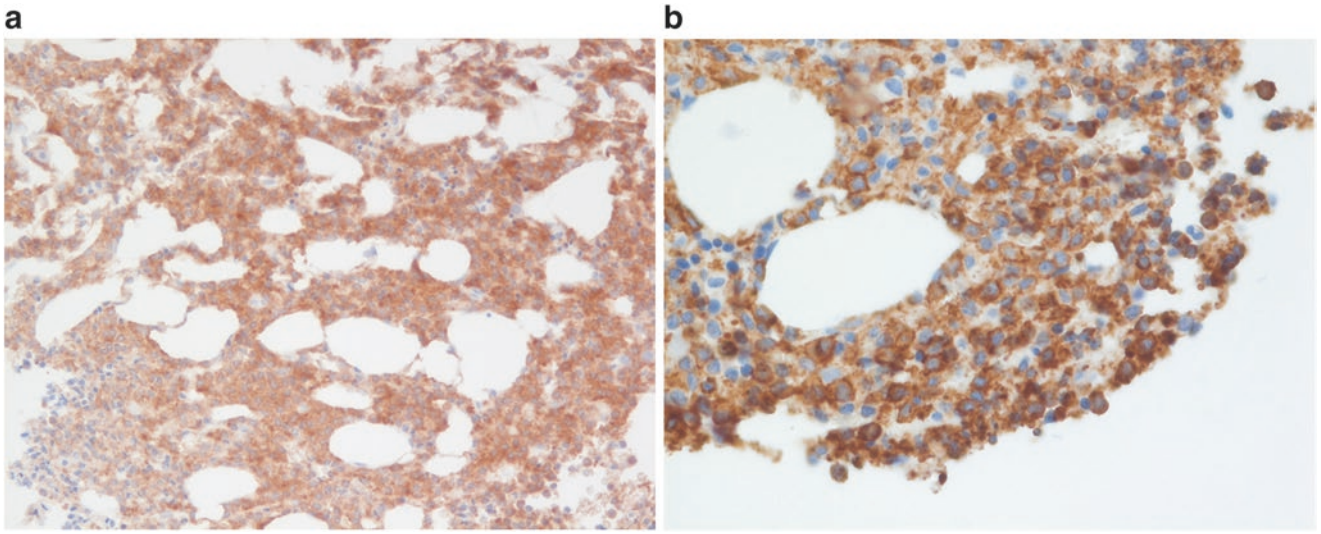

Fig. 6.22 The *BRAF*V600E mutation is found in almost all cases of hairy cell leukemia and is not seen in variant hairy cell leukemia [13]. This specific immunohistochemical stain for the mutated *BRAF* with the V600E mutation is positive, indicating classic hairy cell leukemia (**a**). Immunohistochemical stain for DBA44 (normally positive in benign mantle zone lymphocytes of hyperplasic follicles) is positive in hairy cell leukemia, along with some other lymphomas. In hairy cell leukemia, the staining is more intense at the margins of the cytoplasm/projections as seen in this image (**b**)

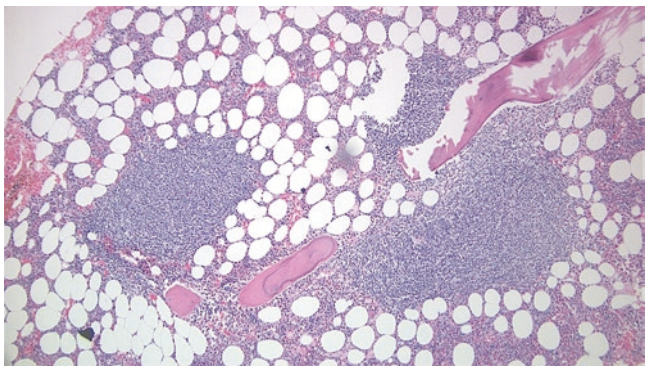

Fig. 6.23 Follicular lymphoma within the lymph nodes, unsurprisingly, has a follicular pattern of nodal effacement. Within the bone marrow, however, a follicular growth pattern is rare, and more often, the growth pattern is paratrabecular with paratrabecular aggregates, exemplified in this image. Follicular lymphoma involves the bone marrow in 40–70% of cases, and low-grade follicular lymphoma is paradoxically more likely to involve marrow compared to high-grade follicular lymphoma

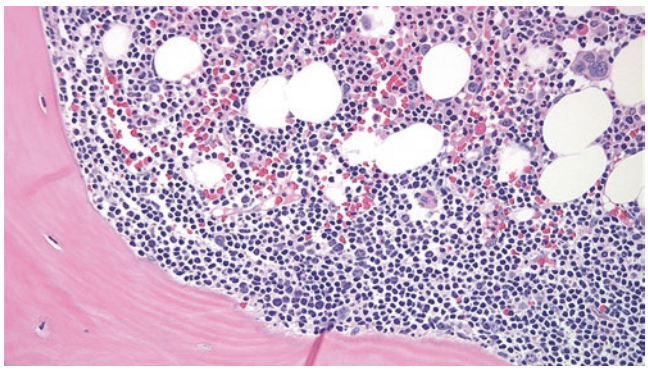

Fig. 6.24 The classic paratrabecular growth displaces normal hematopoiesis. Follicular lymphoma is composed of two cell types: the centrocyte, with small, irregular, dark nuclei, and the centroblast, which are slightly larger and have vesicular chromatin, less irregular contours, and peripheral nucleoli (classically three)

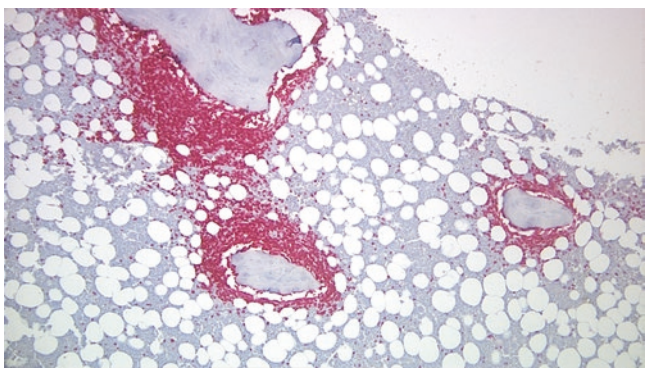

Fig. 6.25 Follicular lymphoma (FL) is a B cell neoplasm and thus expresses typical B cell markers such as CD20, seen in red. Immunohistochemical stains can assist in highlighting the spread of neoplastic cells into the interstitial areas from the more overt paratrabecular areas

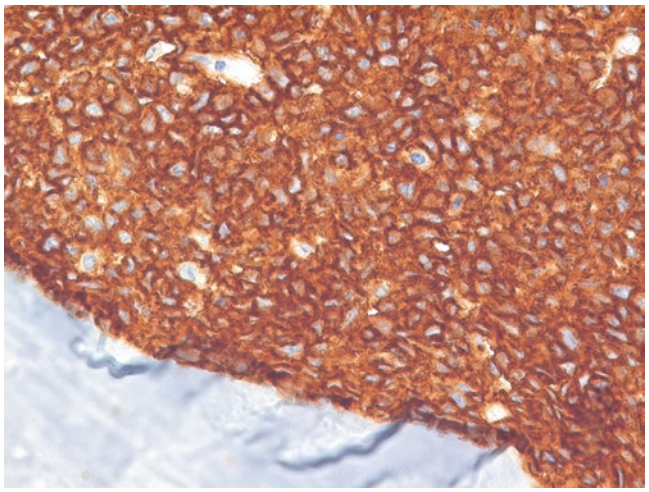

Fig. 6.26 The immunophenotype of these FL neoplastic cells is that of the B cells within a normal germinal center, including positive expression for CD10 (*above*) and BCL6 (not pictured). However, unlike normal germinal centers, these neoplastic cells will typically show strong positivity for BCL2, an antiapoptotic protein (not pictured). Rarely high-grade follicular lymphoma may be CD10 negative, and such cases are often reported to involve the marrow in elderly patients [14]

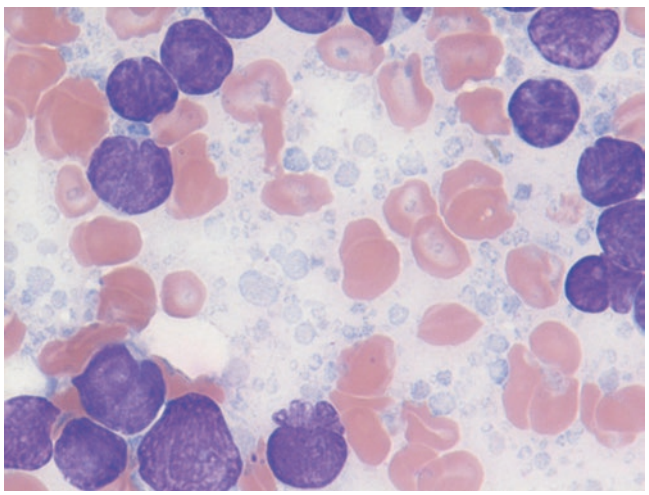

Fig. 6.27 Lymphoid cells with cleaved cytomorphology are prominent in this bone marrow aspirate. These cells have the same morphology as FL cells circulating in peripheral blood. In both instances, they are appropriately termed "buttock cells." Numerous so-called "lymphoglandular" bodies are also noted in the background representing detached fragile cytoplasmic fragments avulsed from the lymphoma cells

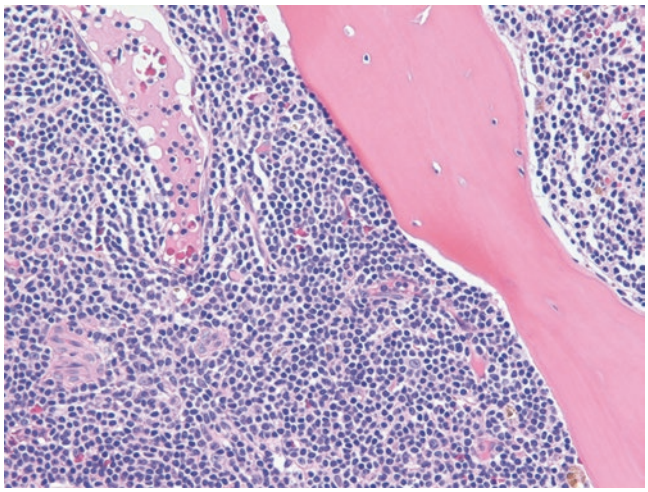

Fig. 6.28 Lymphoplasmacytic lymphoma (LPL) is theorized to arise from a post-follicular B cell committed to plasma cell differentiation, and thus the morphology of this neoplasm is variable from small B cells to plasmacytoid lymphocytes to mature-appearing plasma cells. Bone marrow involvement is identified in most cases of LPL. This bone marrow biopsy involved by LPL has a dilated sinus filled with eosinophilic plasma protein from excessive immunoglobulin. Although not exclusive to LPL, Waldenstrom macroglobulinemia, an IgM paraprotein-producing disease, is found in a large proportion of LPL cases

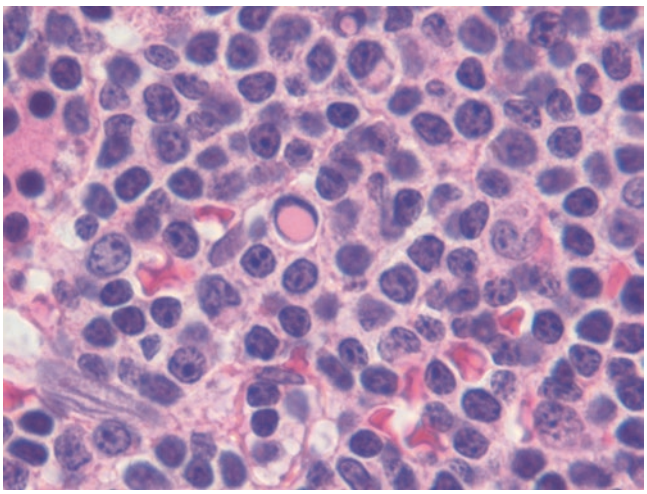

Fig. 6.29 Although the cells of LPL are predominantly of the small lymphoid type, a Dutcher body, seen here, provides evidence of their true differentiation. A Dutcher body is a cytoplasmic inclusion protruding within the nuclei theorized to be filled with immunoglobulin. These inclusions are seen in disease entities of plasma cells, such as myeloma, as well as neoplasms with plasmacytic differentiation, such as LPL

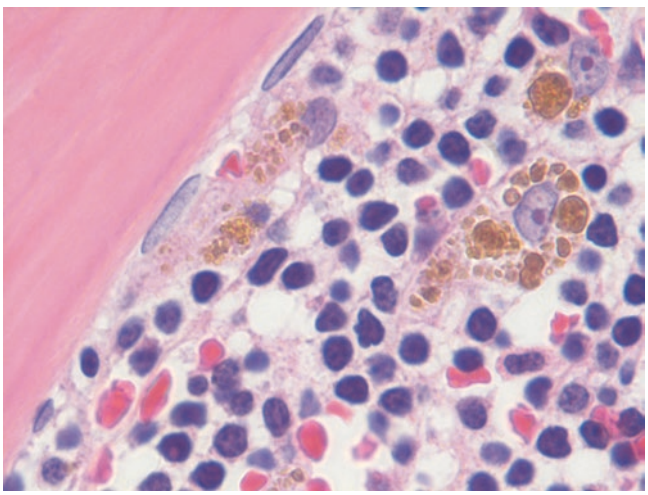

Fig. 6.30 LPL is commonly admixed with histiocytes in the background. These histiocytes seen here in the marrow biopsy are filled with hemosiderin, a characteristic finding often noted in tissues involved by LPL, offering diagnostic clues to the diagnosis

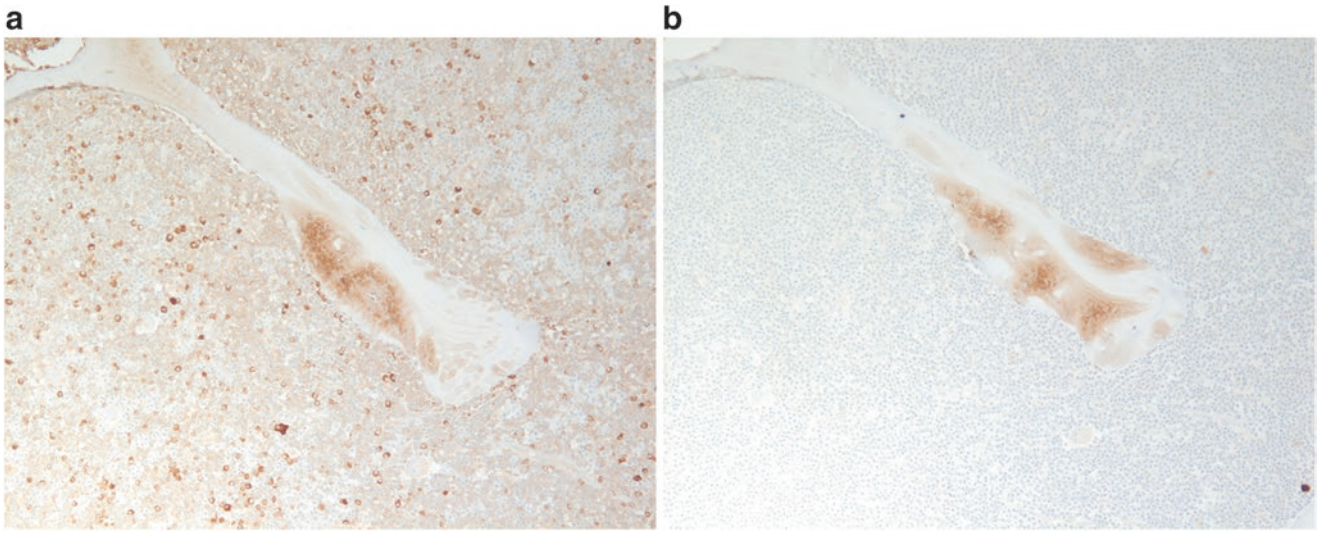

Fig. 6.31 Light chain restriction confirms the clonal nature of this disease. Kappa light chain immunohistochemical stain is positive (**a**), while lambda is entirely negative (**b**). Recently a specific mutation within *MYD88* was identified in the majority of cases [15]. The *MYD88*L265P mutation causes unchecked proliferation through Bruton's tyrosine kinase (Btk). Ibrutinib, a drug which targets Btk, is thus a highly effective treatment for most LPL cases. Most other non-LPL small lymphoid proliferations are negative for the mutation, thus allowing diagnostic discrimination in most instances

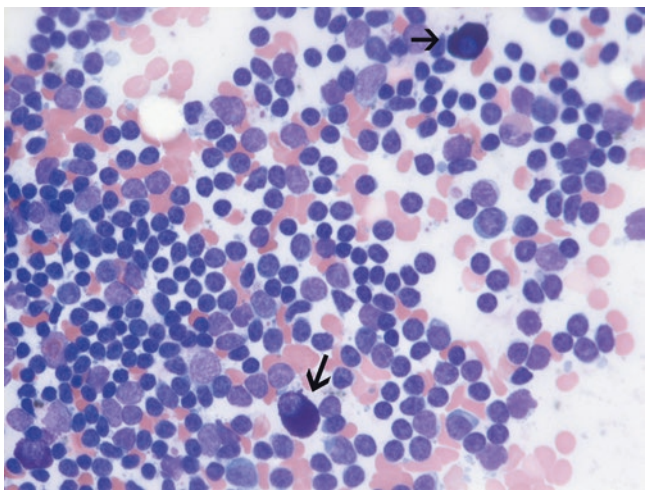

Fig. 6.32 Bone marrow aspirate in LPL showing scattered mast cells (black arrows) associated with the lymphoid cells. These mast cells are in response to the LPL and are not part of the malignant clone

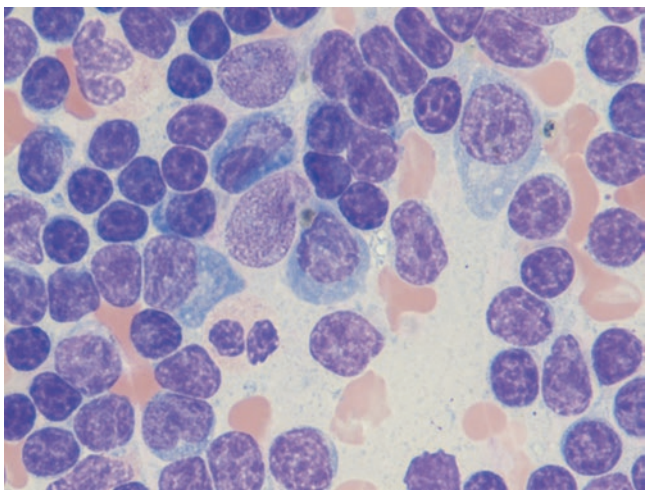

Fig. 6.33 The bone marrow aspirate highlights the atypical lymphocytes and plasma cells in LPL as well as cells with hybrid lymphoplasmacytic cytomorphology. Demonstration of identical clonal light chains in both lymphoid (CD19+/CD20+) and plasmacytic (CD138+/CD38+) compartments by flow cytometry is also useful in ascertaining the diagnosis in difficult cases prior to molecular studies for *MYD88* mutation

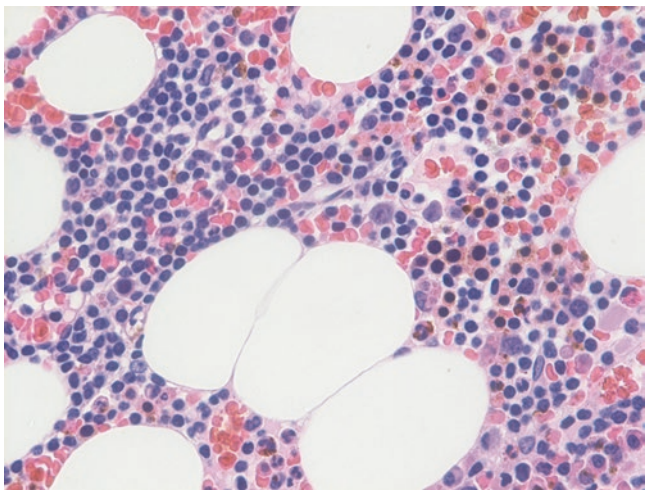

Fig. 6.34 Mantle cell lymphoma (MCL), which commonly involves the bone marrow, is yet another lymphoma composed of small- to medium-sized lymphoid cells [16]. The classic form seen here is composed of small, irregular, dark nuclei resembling normal centrocytes

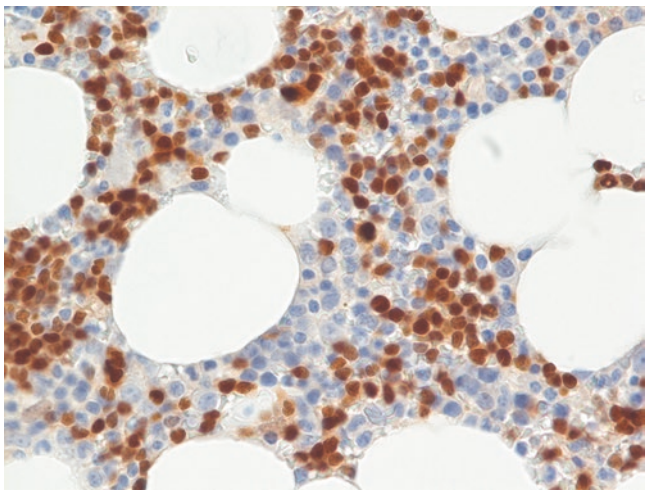

Fig. 6.36 This bone marrow biopsy from the same patient shows nuclear immunoreactivity for cyclin D1. This immunostain within the MCL cells is unequivocally positive, although it has variability in intensity from nucleus to nucleus, reflecting the different phases of the cell cycle each cell is in at the time of biopsy. Nearly all forms of MCL have cyclin D1 overexpression as a result of the t(11;14)

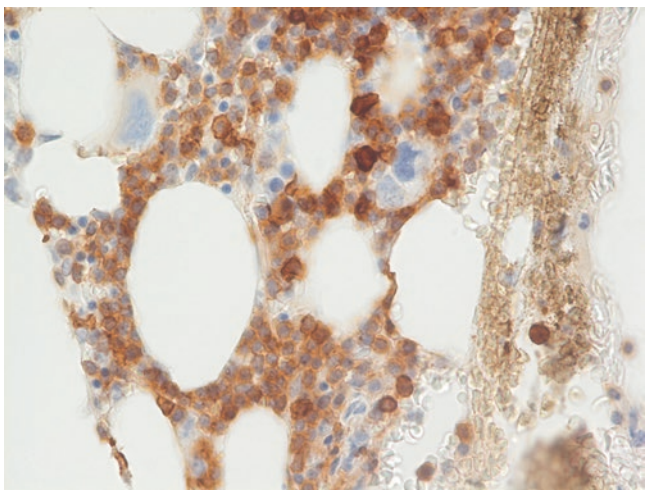

Fig. 6.35 MCL B cells are positive for CD5 (weak) compared to scattered background T cells with brighter CD5 expression. Immunohistochemical staining highlights the infiltrative interstitial neoplastic cells. In the bone marrow, MCL may histologically be nodular, interstitial, paratrabecular, or diffuse

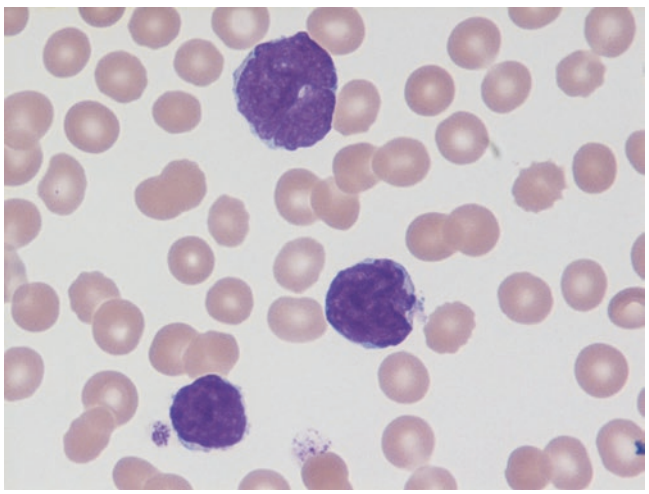

Fig. 6.37 The blastoid variant of MCL is an uncommon but aggressive form of MCL with complex karyotype and poor prognosis. The term blastoid mantle cell leukemia is used when the peripheral blood is involved by a blastoid mantle cell lymphoma. In this case, the peripheral blood demonstrates circulating large leukemic cells with open chromatin and deeply clefted nuclear contours

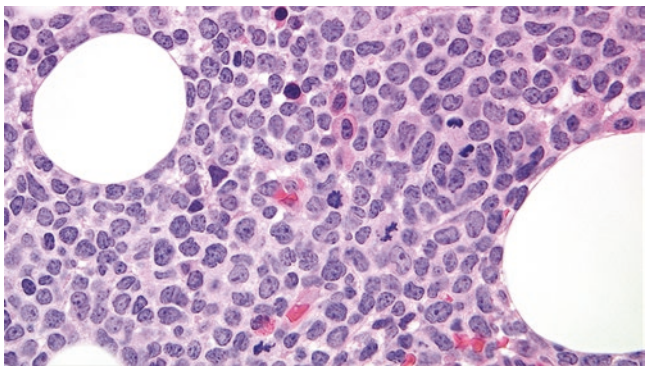

Fig. 6.38 Bone marrow biopsy in the blastoid variant of MCL shows a diffuse proliferation of blastoid lymphoid cells with an extremely high mitotic count. Blastoid MCL often resembles a lymphoblastic proliferation or Burkitt lymphoma on cytologic grounds. Importantly, mitotic count is the best prognostic indicator in all forms of MCL. High mitotic activity, common in blastoid MCL, portends a poor prognosis

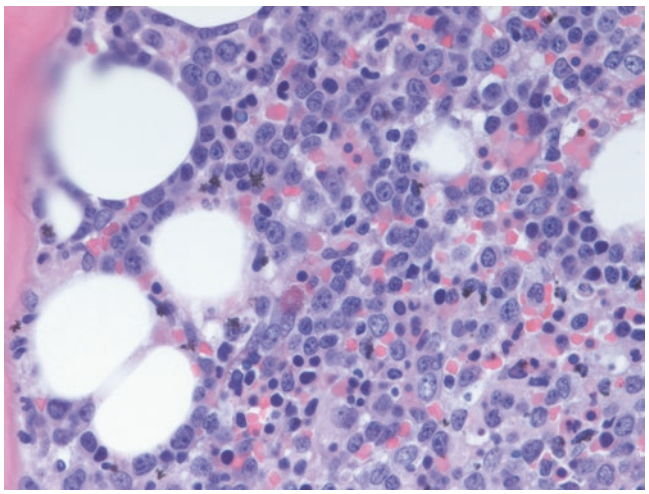

Fig. 6.40 Diffuse large B cell lymphoma (DLBCL) involves the bone marrow in approximately a quarter of cases. The cytology of the lymphoma cells can be centroblastic, immunoblastic, or pleomorphic. The large cells in this bone marrow biopsy are predominately vesicular with 1–3 nucleoli consistent with centroblastic cytomorphology

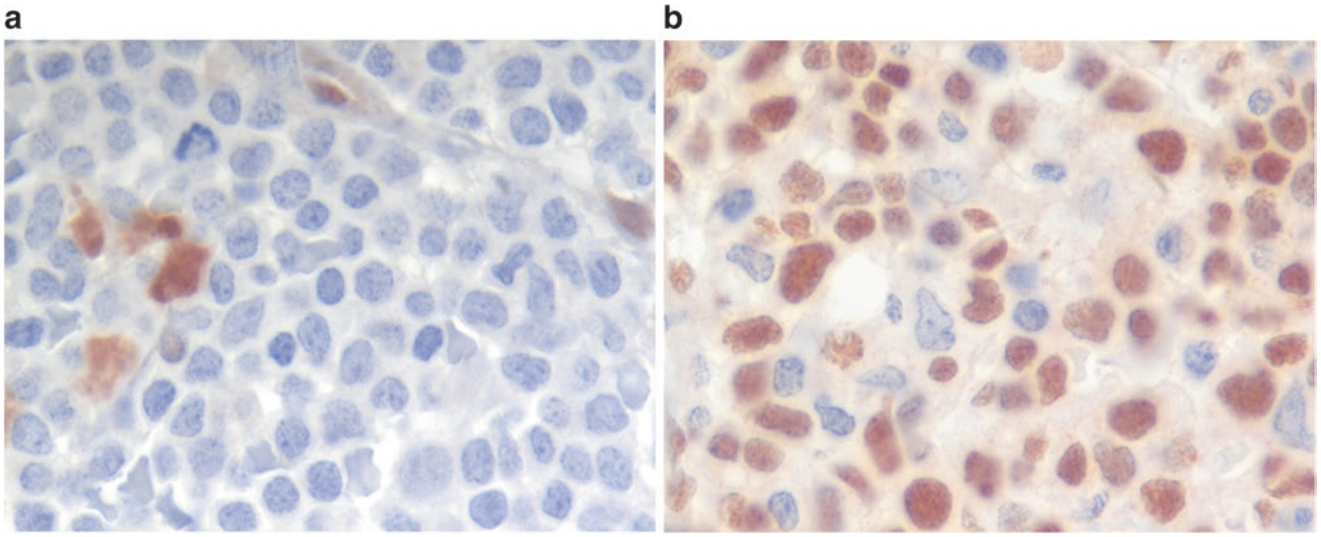

Fig. 6.39 This blastoid MCL was a cyclin D1-negative (**a**), SOX11-positive (**b**) variant. The positive staining in this cyclin D1 immunohistochemical stain is normal histiocytes and endothelial cells, not the lymphoma cells (**a**). Rearrangements in *CCND2*, which encodes the cyclin D2 protein required for the cell cycle G1 to S transition, are seen in 50% of cyclin D1-negative MCLs, most of which are positive for SOX11 [17, 18]

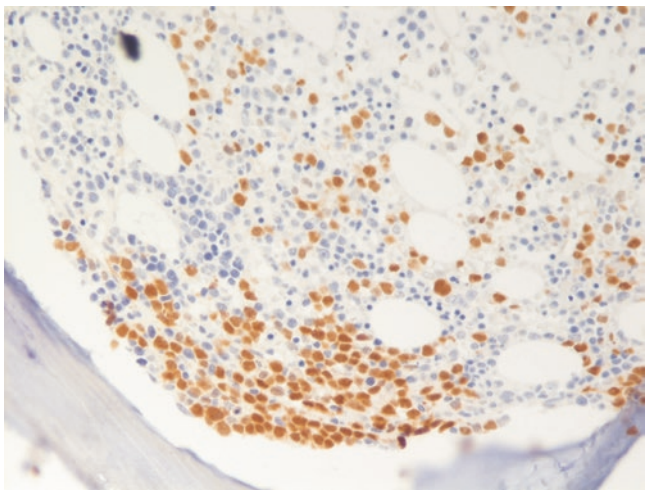

Fig. 6.41 In this example of DLBCL, PAX5 highlights a prominent paratrabecular lymphoid aggregate, reminiscent of bone marrow involvement by follicular lymphoma. Although this case demonstrated other areas compatible with a diffuse interstitial lymphoma component, rare cases can demonstrate isolated paratrabecular involvement (so-called discordant histology). Cases with marrow involvement showing discordant paratrabecular small lymphoid histology (reminiscent of follicular lymphoma) can often be seen, but this is not a negative prognostic factor independent of the IPI score [19]

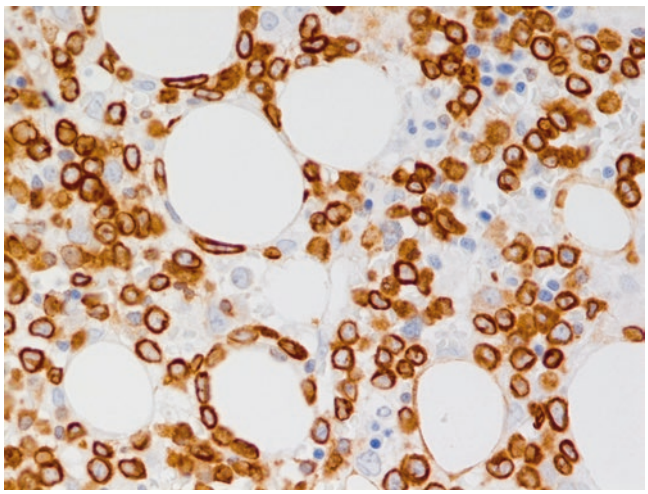

Fig. 6.42 This case of DLBCL is also BCL2 positive. Routine testing for c-MYC and BCL2 by immunohistochemistry is important in the light of the new WHO 2016 revisions to identify cases of "double-expresser" diffuse large B cell lymphomas, which have a worse clinical outcome and suboptimal response to standard therapy. These findings, however, do not entirely correlate with the presence of actual *MYC* and *BCL2* translocations

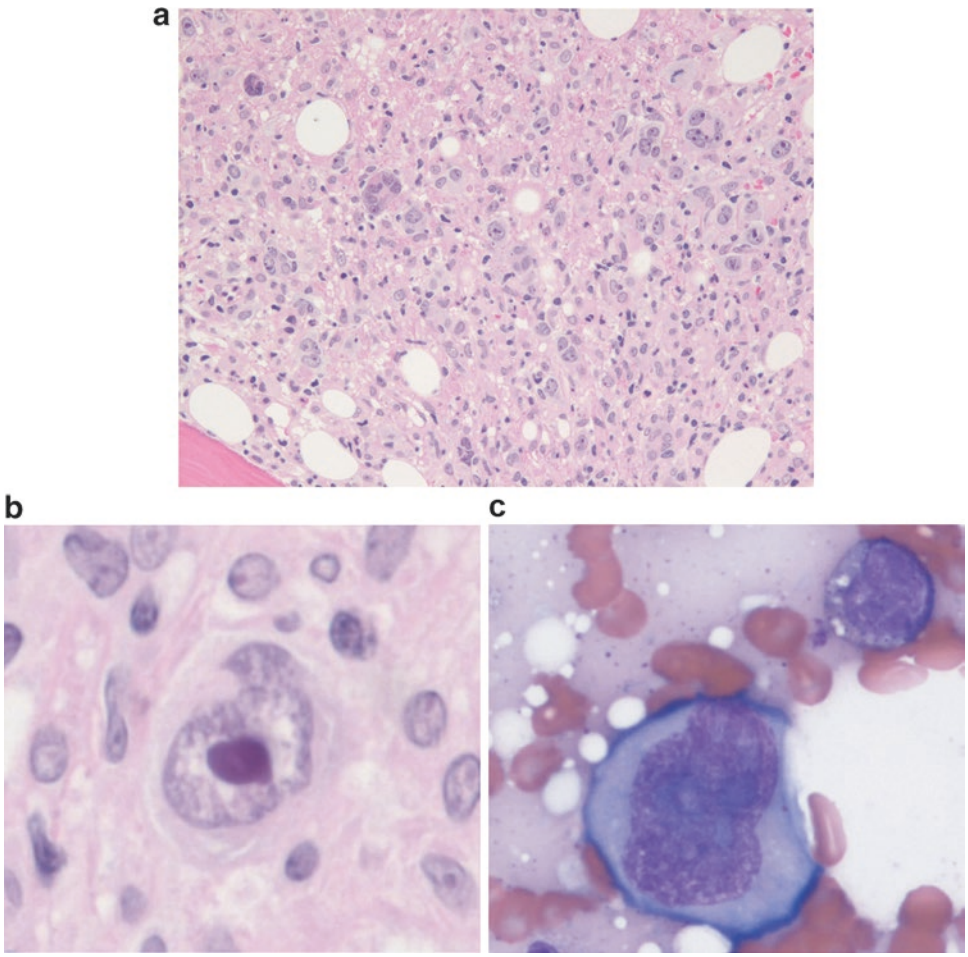

Fig. 6.43 The entity "EBV-positive DLBCL of the elderly" not infrequently is found in younger patients and thus has been renamed to "EBV-positive DLBCL NOS" in the WHO 2016 update [4]. In this case, a proliferation of large, pleomorphic cells extensively involved the marrow with Reed-Sternberg-like cells (**a**, **b**) associated with a background rich in histiocytes. Inset (**c**) shows scattered large lymphoma cells on the aspirate with prominent nucleoli

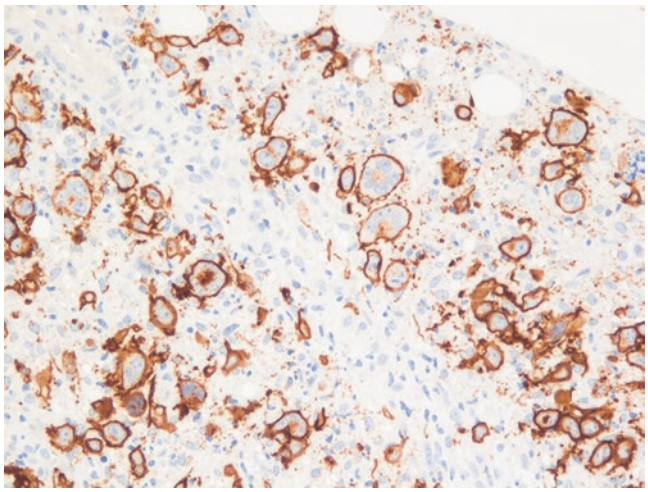

Fig. 6.44 CD20 is strongly positive in the large cells of EBV-positive DLBCL NOS, uniformly allowing distinction from classical Hodgkin lymphoma, which shows downregulation of CD20. EBV+ DLBCL typically has a non-germinal center/activated B cell immunophenotype with positive MUM1 as well as negative CD10 and BCL6 (not shown). Often there is downregulation of surface light chain expression in the lymphoma cells as a result of EBV coinfection

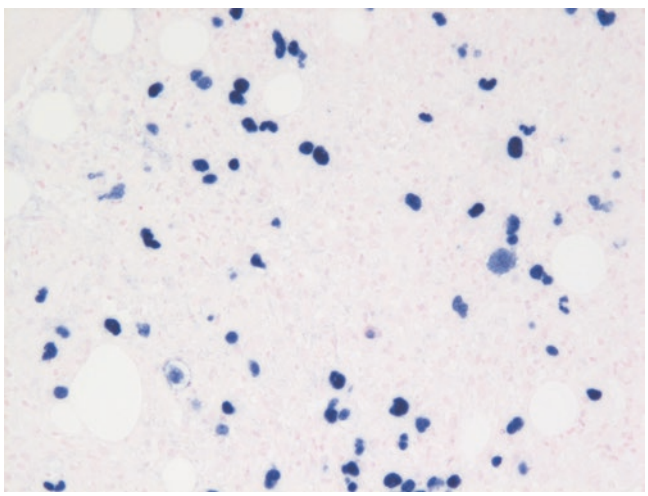

Fig. 6.45 In situ hybridization for EBV is positive in the neoplastic cells of EBV-positive DLBCL NOS, sparing the background normal hematopoietic elements. Neoplasms associated with EBV positivity are hardly unique to EBV+ DLBCL, and positivity may also be seen in angioimmunoblastic T cell lymphoma and classical Hodgkin lymphoma. Positive signals in EBV-DLBCL correspond to large and small lymphoid cells as opposed to classical Hodgkin lymphoma, where EBV is restricted to the HRS cells only

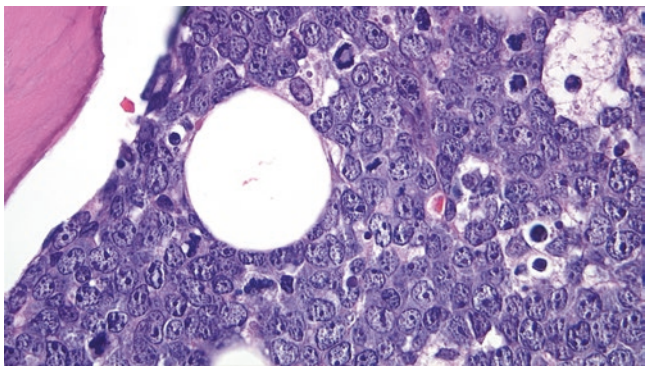

Fig. 6.46 Burkitt lymphoma (BL) is a "medium-sized" mature B cell lymphoma with an extraordinarily short doubling time. Mitotic figures and scattered macrophages are readily apparent, imparting a starry sky appearance at low power that is identical to nodal involvement by BL. Immunohistochemical stains for mitotic activity, such as Ki-67/MIB1, stain nearly 100% of tumor cells; however, the decalcification process used for bone marrow core biopsies can frequently lead to false low Ki-67 staining due to loss of antigenicity

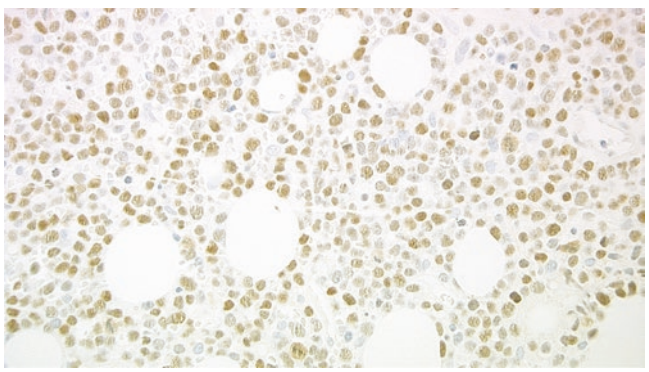

Fig. 6.47 Burkitt lymphoma is characterized by translocations in *MYC*, most often arising from t(8,14)(q24;q32); controversy still exists regarding whether true Burkitt lymphoma without any *MYC* translocation exists. c-MYC immunohistochemistry with the Y69 clone illustrated here demonstrates the expected high nuclear expression levels in this case of Burkitt lymphoma involving the bone marrow

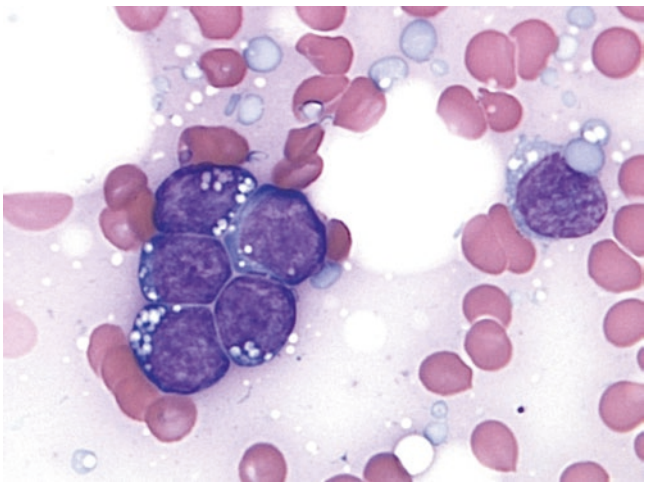

Fig. 6.48 In this bone marrow touch imprint, the cytology of Burkitt cells is well demonstrated with many clear lipid vacuoles within a dark blue cytoplasm

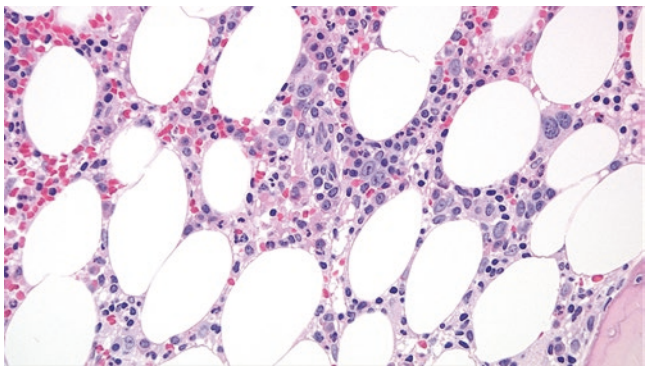

Fig. 6.50 T-LGL leukemia is clinically associated with cytopenias; despite this, however, the bone marrow is slightly hypercellular with appropriate hematopoiesis. Neoplastic cells comprise only a minority of the bone marrow cellularity in most cases. T-LGLs within the bone marrow are either interstitial or within sinusoids and are subtle on H&E alone

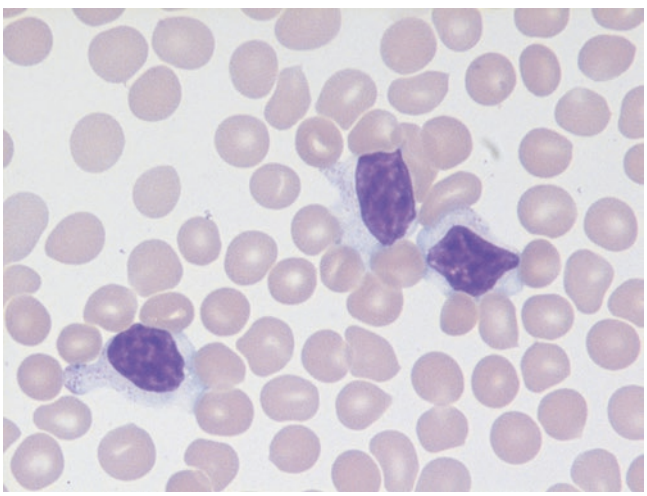

Fig. 6.49 Large granular lymphocytes (LGLs) are often seen in normal peripheral blood smears and represent normal activated cytotoxic T cells or natural killer cells. These LGLs, with abundant cytoplasm and large azurophilic granules, are a response to immune stimulation from infection or autoimmune disease. However, persistently high numbers of T cell LGLs (>2x10^9/L, >6 months) without a clear cause support a diagnosis of a clonal neoplasm with a large granular lymphocyte morphology. This blood smear shows circulating large granular lymphocytes in a case of a T-LGL leukemia

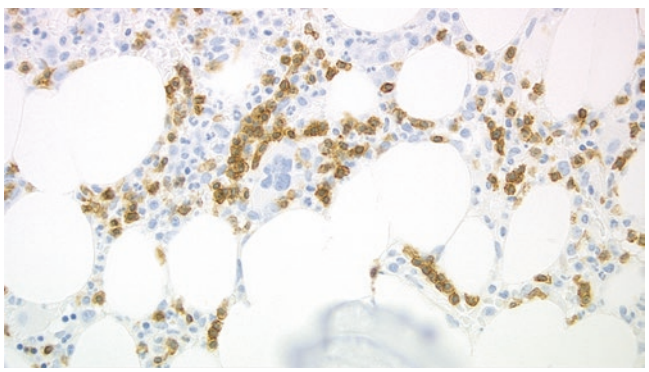

Fig. 6.51 A CD3 stain will highlight the intrasinusoidal linear collections of CD3-positive T cells. T-LGLs also express cytotoxic proteins, such as TIA-1 and granzyme B (not shown), and are typically CD8 positive (not shown). Recently *STAT3* and *STAT5B* mutations have been found in a substantial number of T-LGL cases, and these mutations are associated with a more aggressive clinical course that is atypical for T-LGL generally [20]

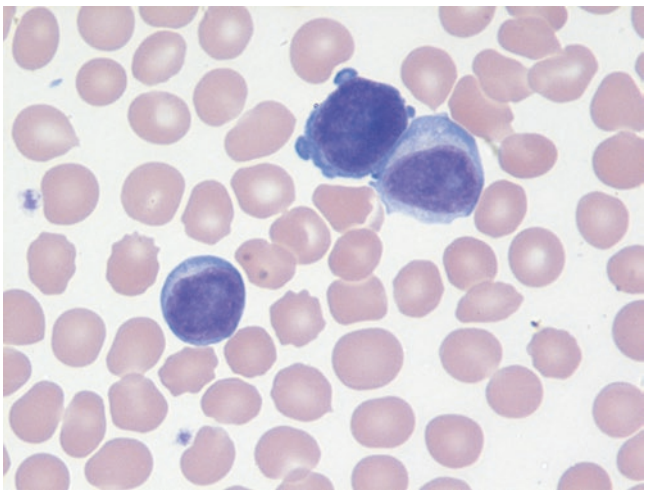

Fig. 6.52 Peripheral blood smears are key for the diagnosis of T cell prolymphocytic leukemia (T-PLL). The cytology is that of small- to medium-sized cells with cytoplasmic blebbing and a round-to-oval nucleus with a nucleolus. The cytoplasm is often dark blue in Wright-Giemsa preparation as opposed to B-PLL, where the cytoplasm is usually clear to pale blue. Clinically, this disease presents with a high white blood cell count (>100×10^9 /L) and in older adults

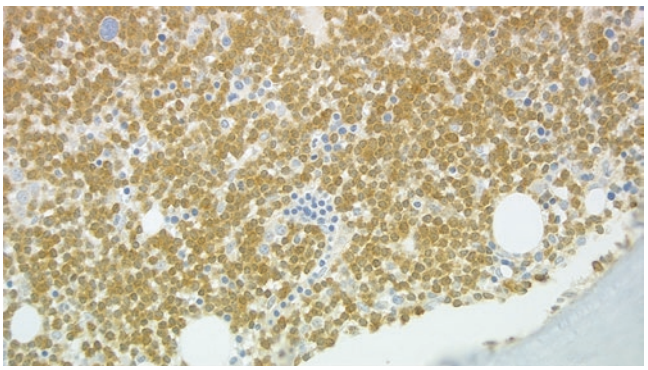

Fig. 6.54 T-PLL cells are notable for strong TCL1 immunoreactivity, as illustrated here. Most cases are CD4+ and frequently express bright CD7 as well. TCL1 overexpression stems from the juxtaposition of the *TCL1* adjacent to the *TCR* alpha-delta locus on chromosome 14 [21]. These cells express high levels of surface CD52 (via flow cytometry), which explains the favorable response to alemtuzumab (an anti-CD52 monoclonal antibody)

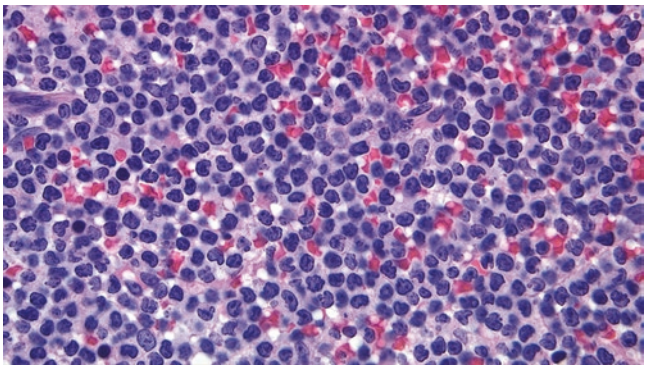

Fig. 6.53 In T-PLL, the bone marrow is almost always diffusely infiltrated by sheets of medium-sized lymphoid cells with small distinct nucleoli and irregular nuclear contours

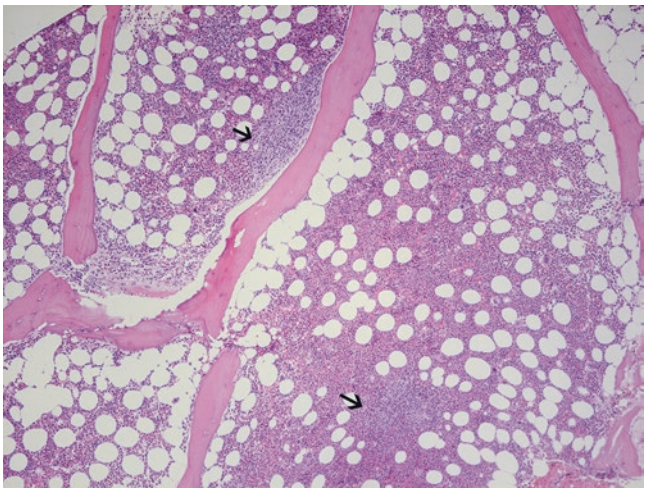

Fig. 6.55 Angioimmunoblastic T cell lymphoma (AITL) frequently involves marrow with a nodular and/or interstitial pattern and may frequently be paratrabecular, as seen here in hypercellular marrow

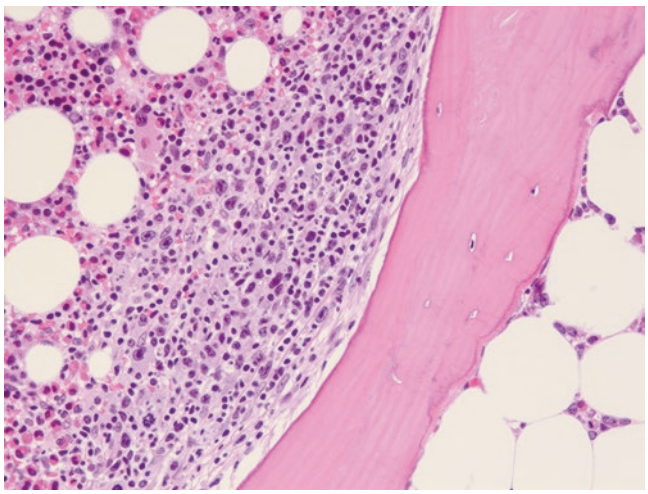

Fig. 6.56 On high power, the paratrabecular aggregate of AITL is notable for numerous large atypical lymphoid cells admixed with small lymphocytes with a background rich in eosinophils outside the aggregates. T cell receptor polymerase chain reaction studies, however, demonstrated clonal T cell gene rearrangement pattern in this marrow supporting T cell lymphoma with an associated large B cell proliferation (see Figs. 6.57 and 6.58)

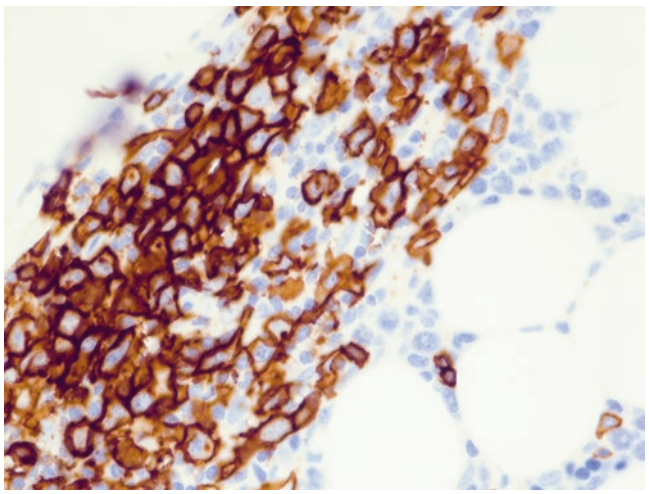

Fig. 6.58 The large atypical cells within the paratrabecular aggregates are positive for CD20 supporting a concurrent large B cell proliferation that can coexist in AITL, as shown here with CD20 immunohistochemical stain [22]. Such B cell populations are often EBV positive; however, this specific case was negative for EBV

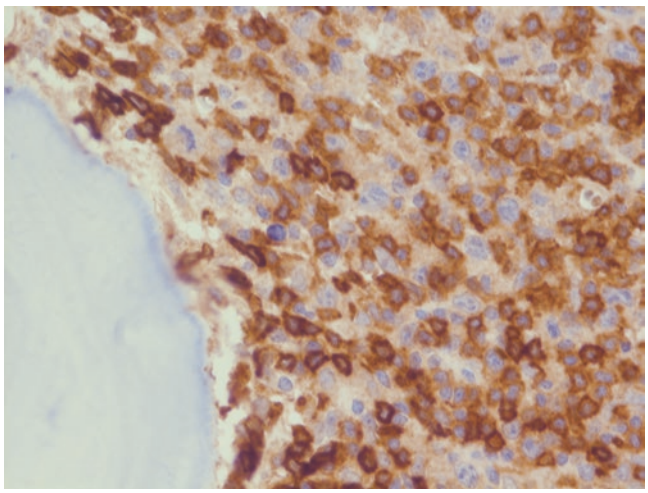

Fig. 6.57 Programmed death receptor-1 (PD-1), a marker of follicular helper T cells, is positive in the small lymphoid CD4 + T cell of AITL within the aggregates (above), as was CD10 and CXCL13 (not pictured) in keeping with derivation of AITL from follicular helper T cells

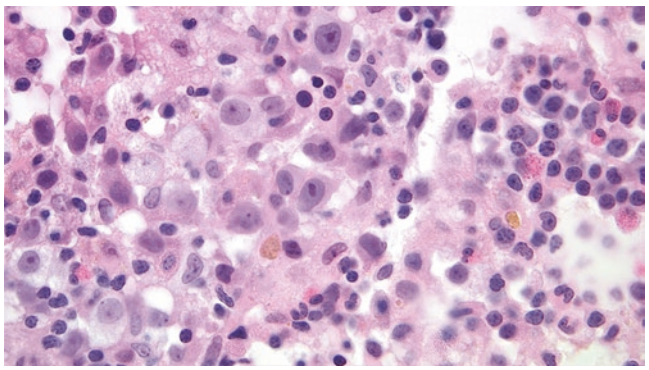

Fig. 6.59 Bone marrow involvement can be patchy and subtle in anaplastic large cell lymphoma (ALCL). The large, epithelioid, and cohesive cell clusters make metastatic carcinoma a diagnostic consideration. Concurrent hemophagocytic syndrome is not uncommon, and careful examination for hemophagocytic histiocytes is necessary after the diagnosis of ALCL is rendered. This patient rapidly deteriorated shortly after this biopsy with a concurrent hemophagocytic syndrome secondary to the lymphoma

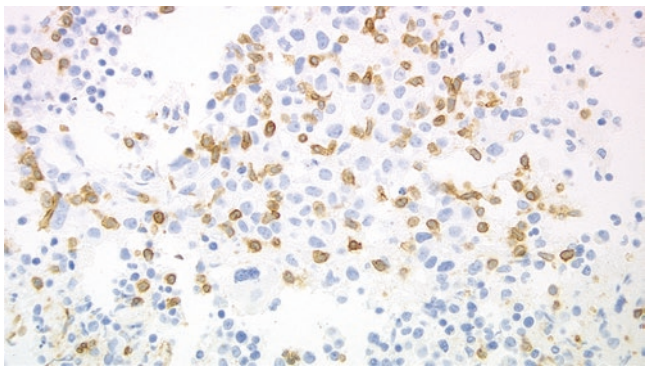

Fig. 6.60 This case of ALCL was negative for most T cell markers including CD3 (pictured here) with only cytotoxic marker positivity. Both ALK-positive and ALK-negative ALCL commonly show loss of multiple pan-T cell antigens (CD2, CD5, CD7) and express a "null" phenotype making lineage determination difficult

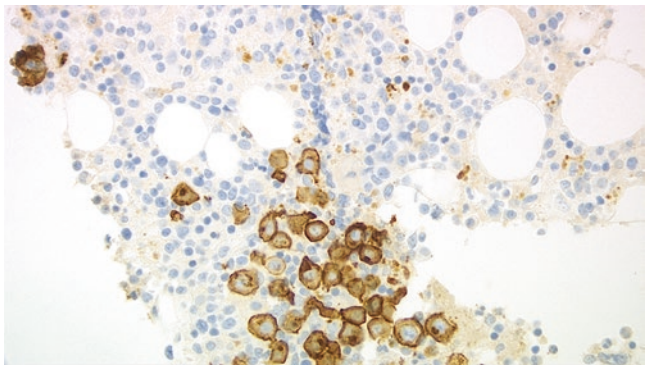

Fig. 6.61 Strong expression of CD30 confirms the diagnosis of ALCL. The CD30 stain is strongest at the cell membrane and within the Golgi region of lymphoma cells

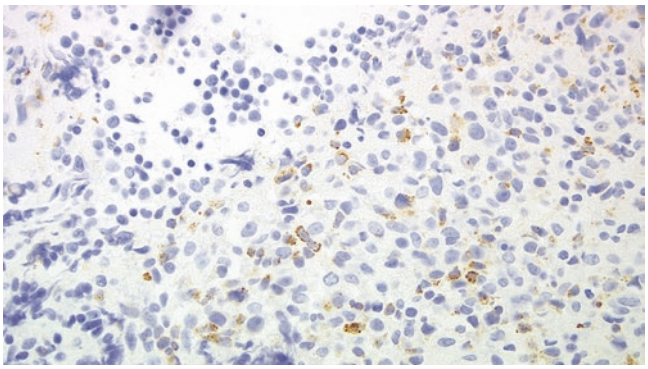

Fig. 6.62 This ALCL was negative for most cytotoxic markers, including granzyme B (shown here) with staining restricted to background small lymphoid cells corresponding to CD8 T cells. In cases that do not express any cytotoxic markers, caution must be exercised to exclude alternative malignancies that are or could be CD30 positive, such as classical Hodgkin lymphoma. However, this case was negative for PAX5, helping to exclude classical Hodgkin lymphoma

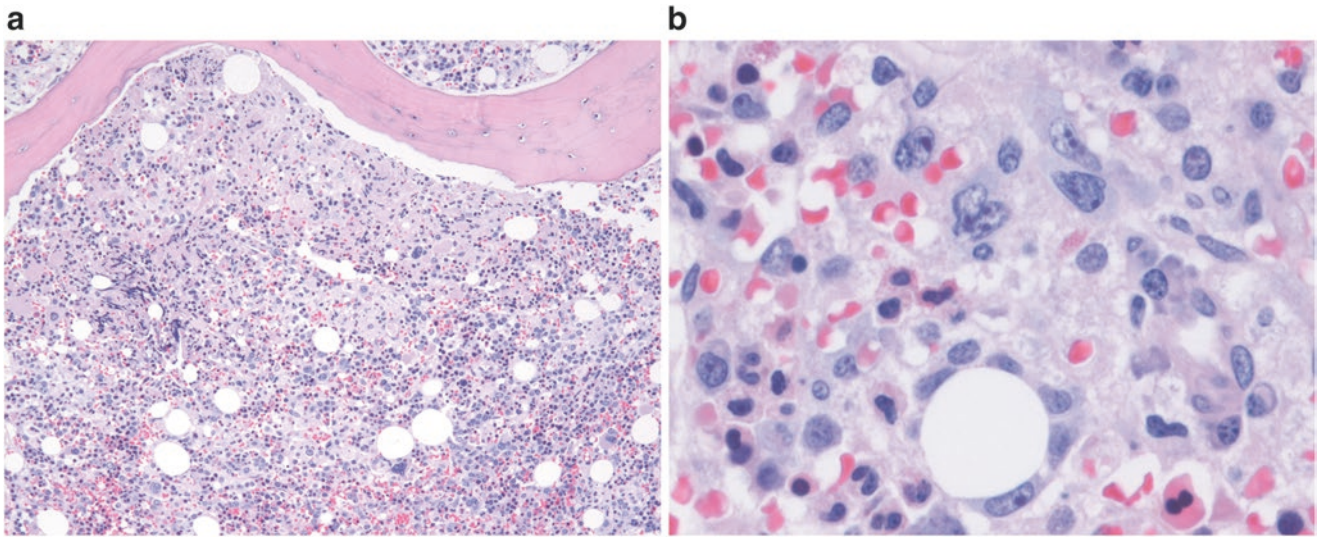

Fig. 6.63 Hepatosplenic T cell lymphoma (HSTL) involving the bone marrow. This case has only patchy ill-defined clusters of paratrabecular atypical lymphohistiocytic aggregates (**a**). At higher power (**b**), there are pleomorphic large lymphoid cells interspersed amid the histiocytes. This case is an αβ variant of HSTL which is much less common than the γδ variant. The morphologic features of αβ HSTL are largely similar to the γδ variant except it shows more pleomorphism [23]

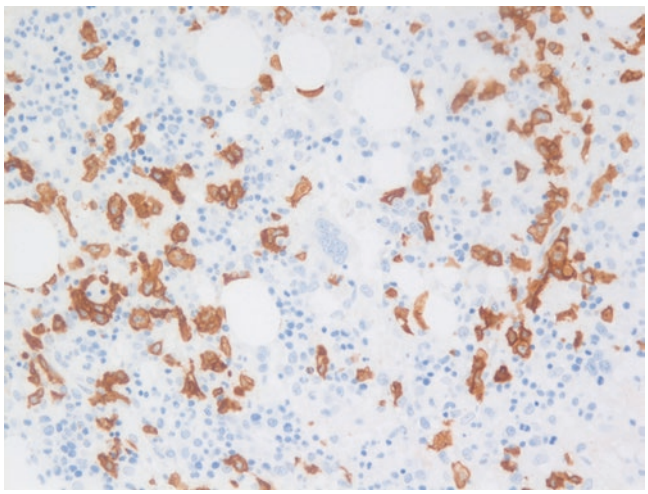

Fig. 6.64 HSTL cells in the spleen are home to the splenic sinusoids and recapitulate this pattern within the bone marrow sinusoids (like SMZL and T-LGL leukemia, both of which show an intrasinusoidal distribution). CD3 immunostain highlights linearly arranged neoplastic T cells within sinusoids on this biopsy. These cases are additionally positive for CD56, but usually negative for CD4 and CD8 (gamma-delta variant)

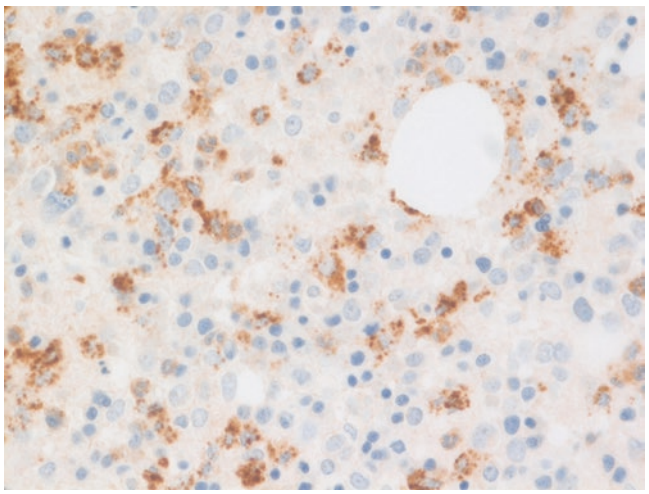

Fig. 6.66 All forms of HSTL are typically positive for the cytotoxic marker, T cell intracellular antigen (TIA-1) with a granular cytoplasmic pattern, but negative for the other cytotoxic markers (granzyme B and perforin, not shown) consistent with a nonactivated cytotoxic phenotype. Both variants of HSTL (alpha-beta and gamma-delta) are thought to be derived from T cells with cytolytic properties

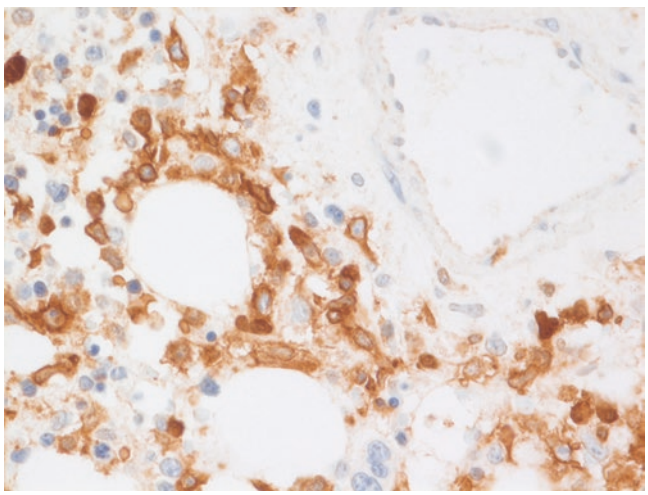

Fig. 6.65 TCR-β immunostaining is positive and supportive of the αβ variant of HSTL

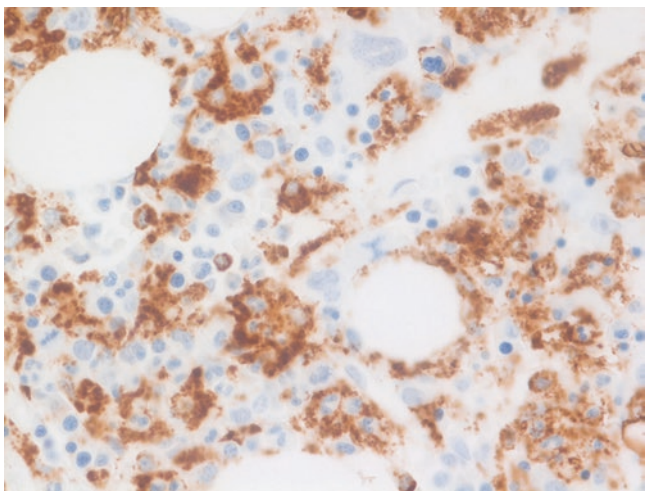

Fig. 6.67 CD68 immunostain highlights the abundant adjacent histiocytes in this case. It also confirms the concurrent hemophagocytosis. Clinically, HSTL is an aggressive disease with a poor prognosis

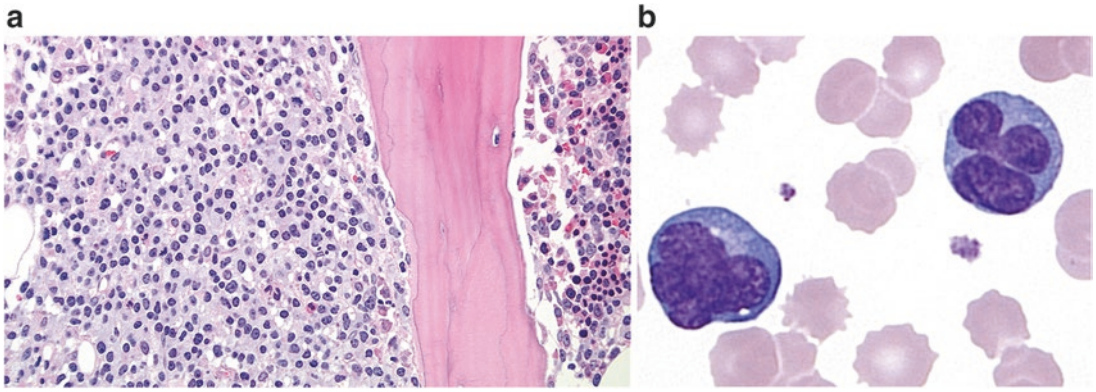

Fig. 6.68 Adult T cell leukemia/lymphoma involving marrow. This biopsy (**a**) was from a middle-aged man of Nigerian origin. There is diffuse interstitial involvement by large somewhat cohesive lymphoma cells with irregular nuclear contours. Numerous circulating peripheral blood lymphoma cells with deeply clefted, polylobate nuclei ("flower cells," inset) are noted (**b**). The deep clefts and basophilic cytoplasm allow distinction from Sezary cells in the blood. Marrow involvement is often less frequent than expected despite frequent stage 4 disease at presentation. Occasionally, prominent osteoclastic activity around the bony trabeculae may be seen, although this case showed only minimal osteoclastic bone resorption

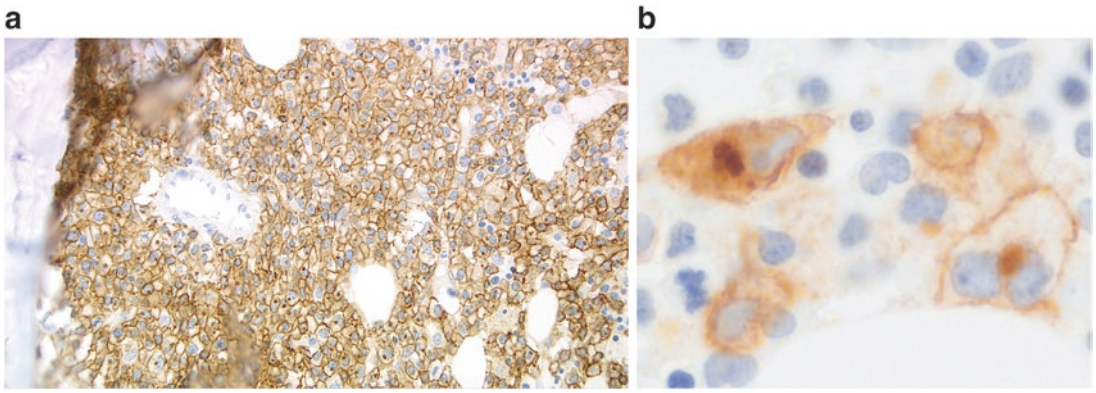

Fig. 6.69 This ATLL case was positive for CD3, CD4 (**a**), as well as CD25 (**b**) and TCRβ. Occasionally these cases may be CD30 positive, but they are negative for ALK as well as cytotoxic markers aiding in the exclusion of ALCL

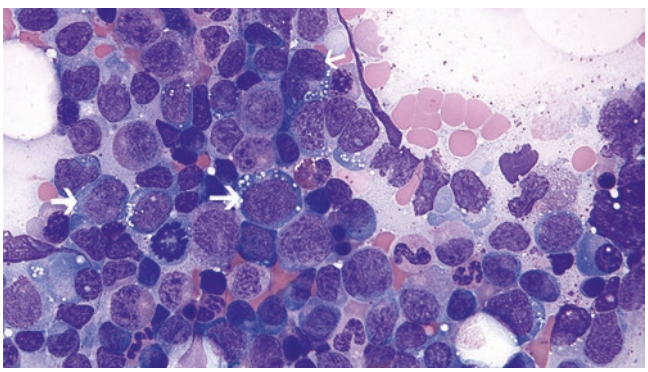

Fig. 6.70 Aspirate smears show numerous large lymphoma cells with vacuolated cytoplasm (arrows) and irregular nuclear contours intermingled with the normal hematopoietic elements in a patient with ATLL

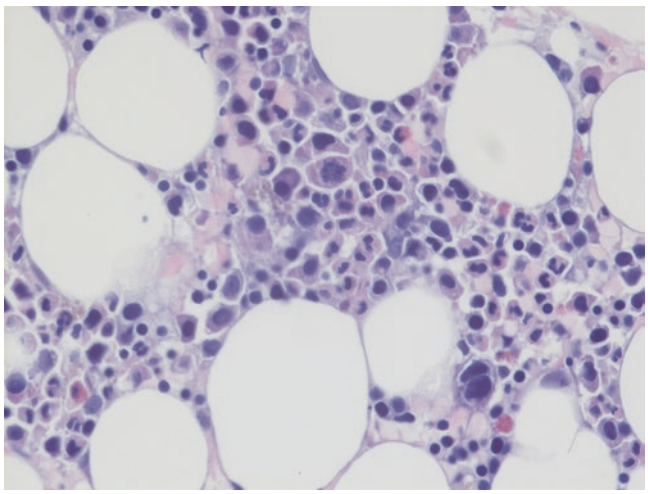

Fig. 6.71 Intravascular large B cell lymphoma (IVLBCL) involving marrow of a 60-year-old woman of Asian-Indian origin presenting with pancytopenia. The biopsy demonstrates rare large, atypical lymphoid cells within the bone marrow. These cells are within vessels, although the vessel walls are hard to appreciate without special stains. IVLBCL has two variants: (1) The "Asian variant" affects Asian populations and is a clinically aggressive disease with poor response to treatment, found throughout many body organs/systems. (2) The "Western variant" affects mostly Caucasian population in the Western countries, is often limited to the skin, and has a better prognosis [24]

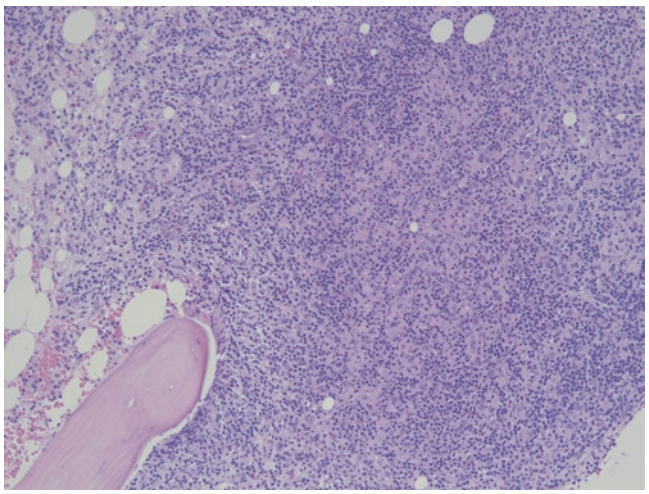

Fig. 6.73 Classical Hodgkin lymphoma (cHL) is a B cell neoplasm notable for marked paucity of neoplastic cells in a background predominated by an inflammatory infiltrate comprising lymphocytes, eosinophils, neutrophils, histiocytes, and plasma cells. Bone marrow involvement here shows disruption of the architecture by vaguely nodular infiltrates of inflammatory cells with scattered Hodgkin/Reed-Sternberg cells. The frequency of bone marrow involvement is higher in patients with HIV [10]. However, improved PET/CT techniques have largely obviated the need to perform routine staging marrow biopsies in Hodgkin lymphoma at diagnosis

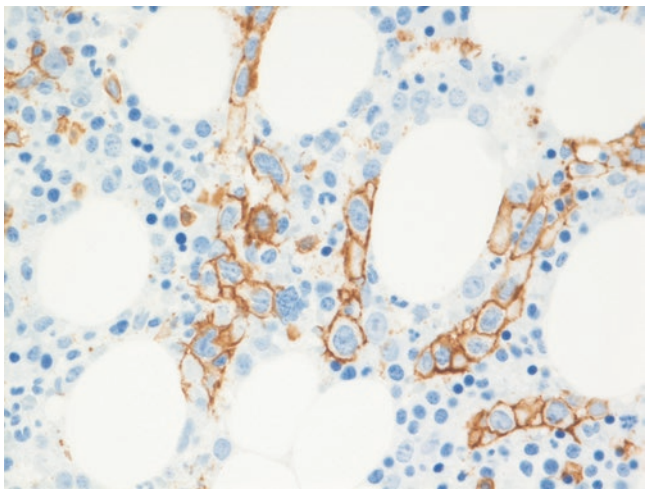

Fig. 6.72 CD20 immunostain in IVLBCL highlights the linear arrangement of the large intravascular lymphoma cells in this case

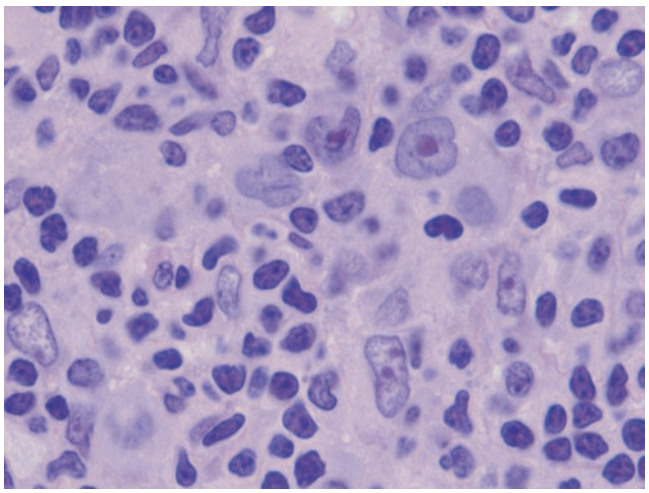

Fig. 6.74 In this higher power image, large mononuclear (Hodgkin) cells with prominent eosinophilic nucleoli are identified in a background milieu of mixed inflammatory cells rich in histiocytes within the bone marrow

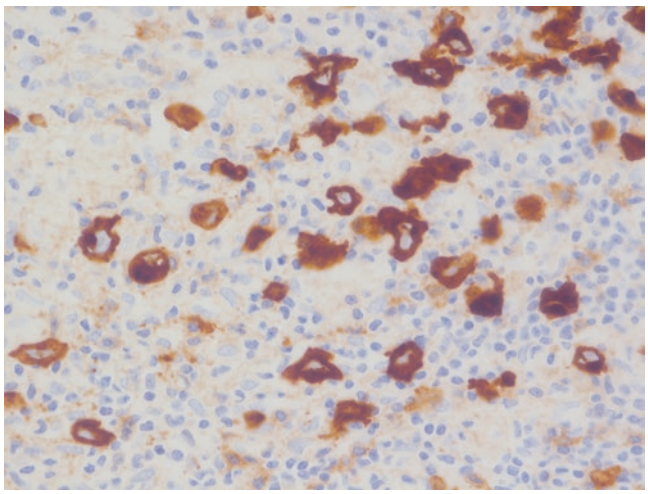

Fig. 6.75 CD30, a cytokine receptor, is strongly positive in the neoplastic B cells of cHL. CD30 staining is localized to the cell membrane as well as cytoplasm with Golgi zone accentuation. Normal bone marrow does not contain any CD30+ cells. Targeted therapy against CD30 antigen (brentuximab) is used more often in the relapsed setting in cHL

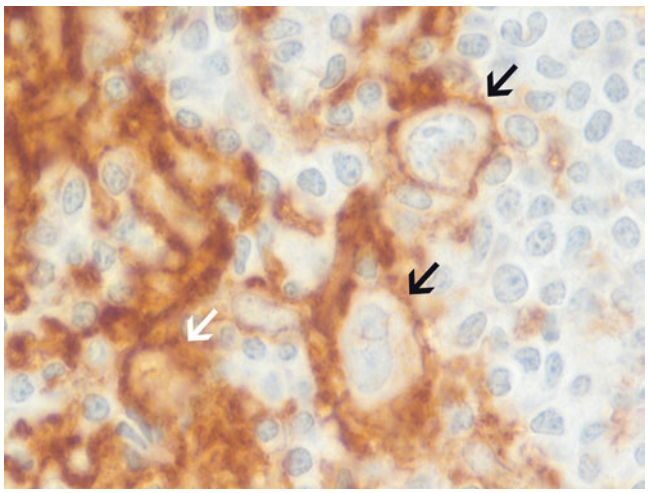

Fig. 6.77 Programmed death receptor ligand 1 (PD-L1) is strongly positive in these neoplastic cells of cHL (black arrows) and also within the reactive histiocytes (white arrows). Most cHL demonstrate overexpression of PD-L1, as seen here, and recent studies have noted near-universal amplification of the PD-L1 locus in cHL which led to the approval of checkpoint inhibitors in relapsed cHL [25, 26]

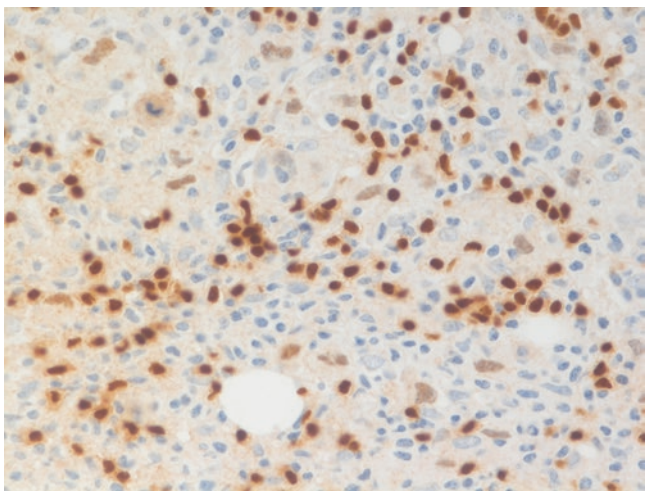

Fig. 6.76 Immunohistochemical stain for PAX5 is strongly positive in background nonneoplastic small B cells but is weak within the Hodgkin lymphoma B cells. Nearly 95% of all Hodgkin lymphomas are PAX5 positive, albeit weakly, consistent with the downregulation with the B cell and germinal center program in classical Hodgkin lymphoma. The Hodgkin cells should not stain for T cell markers, and this helps in the differentiation from anaplastic large T cell lymphoma

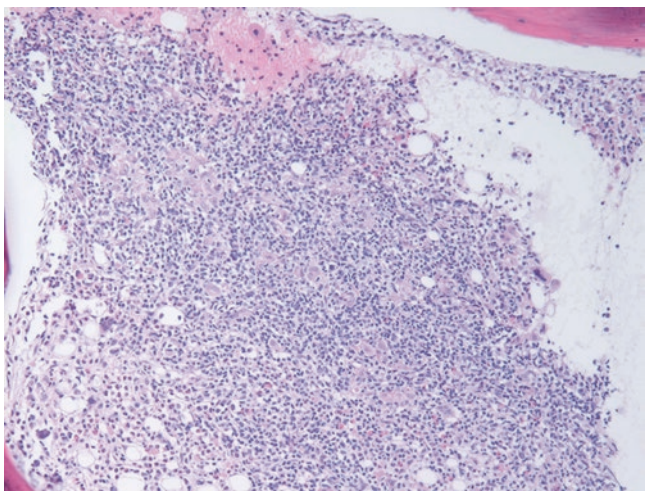

Fig. 6.78 T cell-/histiocyte-rich large B cell lymphoma (T/HRLBCL) involving the bone marrow of a 61-year-old man with pancytopenia and splenomegaly. On careful inspection, bone marrow involvement in T/HRLBCL shows scattered epithelioid granulomas with very few large atypical lymphoid cells within the granulomas. This case was the micronodular variant of T/HRLBCL that has been described in the spleen presenting in older patients with frequent marrow involvement [27]

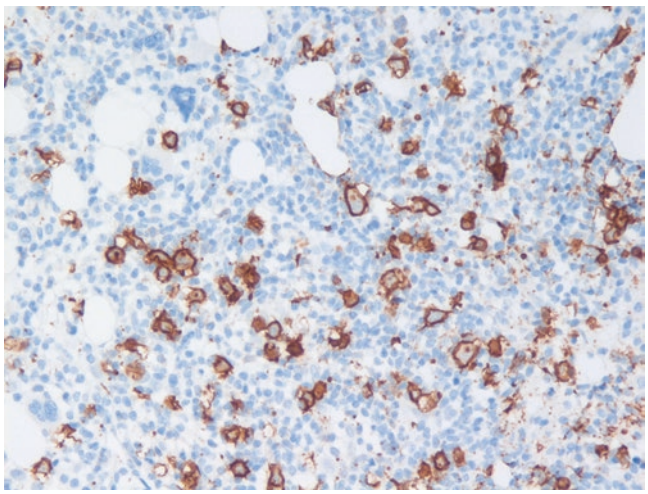

Fig. 6.79 Immunohistochemical staining for CD20 highlights the scattered large B cells within the background of T cells and histiocytes in T/HRLBCL. These cells may mimic the B cells seen in nodular lymphocyte-predominant Hodgkin lymphoma (NLPHL); however, T/HRLBCL do not have the usual "popcorn morphology" and show more size variability. Furthermore, marrow involvement is much less frequent in NLPHL

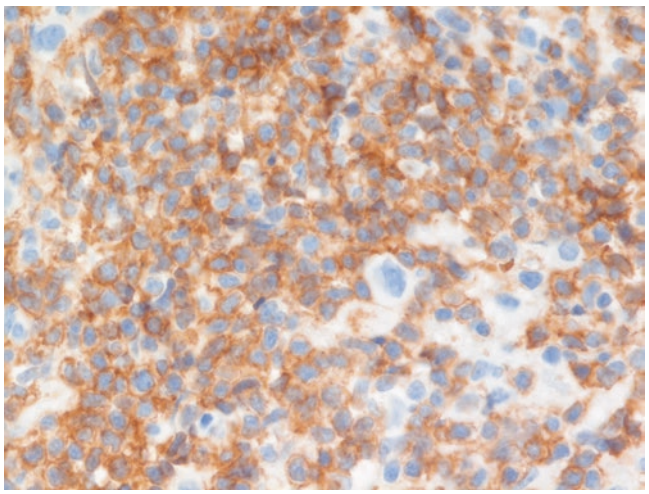

Fig. 6.81 Most of the background lymphoid cells in this case or T/HRLBCL are CD3+/CD4+ T cells expressing PD-1 (shown). The large neoplastic B cells are negative for PD-1. These small PD-1-positive T cells are not part of the neoplastic clone and are background CD4 T cells with immune exhaustion. This case showed a clonal T cell receptor gene rearrangement initially which led to an erroneous diagnosis of T cell lymphoma

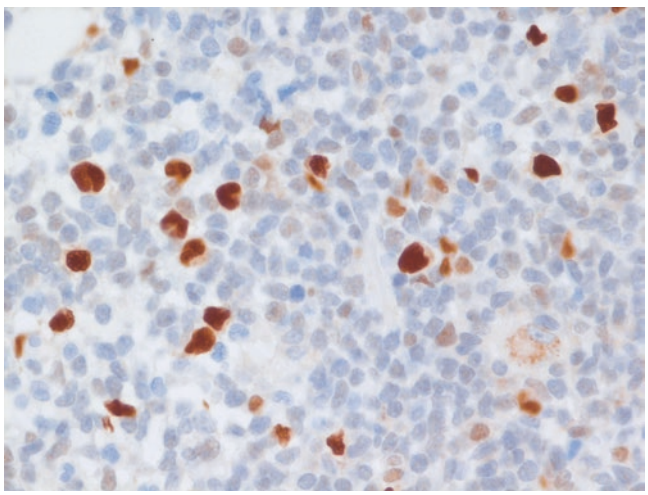

Fig. 6.80 OCT-2 nuclear immunostain for the B cell transcription factor marks the atypical B cells and demonstrates the marked size variation between neoplastic cells in T/HRLBCL. Also, note the paucity of associated background small B cells which is an important feature in distinguishing from NLPHL

References

1. Chang H, Hung YS, Lin TL, Wang PN, Kuo MC, Tang TC, et al. Primary bone marrow diffuse large B cell lymphoma: a case series and review. Ann Hematol. 2011;90(7):791–6.
2. Zwarthoed C, El-Galaly TC, Canepari M, Ouvrier MJ, Viotti J, Ettaiche M, et al Prognostic value of bone marrow tracer uptake pattern in baseline PET scan in Hodgkin Lymphoma: results from an International Collaborative Study. J Nucl Med. 2017. pii: jnumed.116.184218. doi: https://doi.org/10.2967/jnumed.116.184218.
3. Cheson BD, Fisher RI, Barrington SF, Cavalli F, Schwartz LH, Zucca E, et al. Recommendations for initial evaluation, staging, and response assessment of Hodgkin and non-Hodgkin lymphoma: the Lugano classification. J Clin Oncol. 2014;32(27):3059–68.
4. Swerdlow SH, Campo E, Pileri SA, Harris NL, Stein H, Siebert R, et al. The 2016 revision of the World Health Organization classification of lymphoid neoplasms. Blood. 2016;127(20):2375–90.
5. Wiestner A, Rosenwald A, Barry TS, Wright G, Davis RE, Henrickson SE, et al. ZAP-70 expression identifies a chronic lymphocytic leukemia subtype with unmutated immunoglobulin genes, inferior clinical outcome, and distinct gene expression profile. Blood. 2003;101(12):4944–51.

6. Schade U, Bock O, Vornhusen S, Jäger A, Büsche G, Lehmann U, et al. Bone marrow infiltration pattern in B-cell chronic lymphocytic leukemia is related to immunoglobulin heavy-chain variable region mutation status and expression of 70-kd zeta-associated protein (ZAP-70). Hum Pathol. 2006;37(9):1153–61.
7. Swords R, Bruzzi J, Giles F. Recent advances in the diagnosis and therapy of Richter's syndrome. Med Oncol. 2007;24(1):17–32.
8. Del Giudice I, Davis Z, Matutes E, Osuji N, Parry-Jones N, Morilla A, et al. IgVH genes mutation and usage, ZAP-70 and CD38 expression provide new insights on B-cell prolymphocytic leukemia (B-PLL). Leukemia. 2006;20(7):1231–7.
9. Del Giudice I, Osuji N, Dexter T, Brito-Babapulle V, Parry-Jones N, Chiaretti S, et al. B-cell prolymphocytic leukemia and chronic lymphocytic leukemia have distinctive gene expression signatures. Leukemia. 2009;23(11):2160–7.
10. Randen U, Trøen G, Tierens A, Steen C, Warsame A, Beiske K, et al. Primary cold agglutinin-associated lymphoproliferative disease: a B-cell lymphoma of the bone marrow distinct from lymphoplasmacytic lymphoma. Haematologica. 2014;99(3):497–504.
11. Johrens K, Stein H, Anagnostopoulos I. T-bet transcription factor detection facilitates the diagnosis of minimal hairy cell leukemia infiltrates in bone marrow trephines. Am J Surg Pathol. 2007;31(8):1181–5.
12. Venkataraman G, Aguhar C, Kreitman RJ, Yuan CM, Stetler-Stevenson M. Characteristic CD103 and CD123 expression pattern defines hairy cell leukemia: usefulness of CD123 and CD103 in the diagnosis of mature B-cell lymphoproliferative disorders. Am J Clin Pathol. 2011;136(4):625–30.
13. Tiacci E, Trifonov V, Schiavoni G, Holmes A, Kern W, Martelli MP, et al. BRAF mutations in hairy-cell leukemia. N Engl J Med. 2011;364(24):2305–15.
14. Karube K, Guo Y, Suzumiya J, Sugita Y, Nomura Y, Yamamoto K, et al. CD10-MUM1+ follicular lymphoma lacks BCL2 gene translocation and shows characteristic biologic and clinical features. Blood. 2007;109(7):3076–9.
15. Treon SP, Xu L, Yang G, Zhou Y, Liu X, Cao Y, et al. MYD88 L265P somatic mutation in Waldenstrom's macroglobulinemia. N Engl J Med. 2012;367(9):826–33.
16. Cohen PL, Kurtin PJ, Donovan KA, Hanson CA. Bone marrow and peripheral blood involvement in mantle cell lymphoma. Br J Haematol. 1998;101(2):302–10.
17. Salaverria I, Royo C, Carvajal-Cuenca A, Clot G, Navarro A, Valera A, et al. CCND2 rearrangements are the most frequent genetic events in cyclin D1(-) mantle cell lymphoma. Blood. 2013;121(8):1394–402.
18. Wlodarska I, Dierickx D, Vanhentenrijk V, Van Roosbroeck K, Pospísilová H, Minnei F, et al. Translocations targeting CCND2, CCND3, and MYCN do occur in t(11;14)-negative mantle cell lymphomas. Blood. 2008;111(12):5683–90.
19. Sehn LH, Scott DW, Chhanabhai M, Berry B, Ruskova A, Berkahn L, et al. Impact of concordant and discordant bone marrow involvement on outcome in diffuse large B-cell lymphoma treated with R-CHOP. J Clin Oncol. 2011;29(11):1452–7.
20. Rajala HL, Porkka K, Maciejewski JP, Loughran TP Jr, Mustjoki S. Uncovering the pathogenesis of large granular lymphocytic leukemia-novel STAT3 and STAT5b mutations. Ann Med. 2014;46(3):114–22.
21. Herling M, Patel KA, Teitell MA, Konopleva M, Ravandi F, Kobayashi R, et al. High TCL1 expression and intact T-cell receptor signaling define a hyperproliferative subset of T-cell prolymphocytic leukemia. Blood. 2008;111(1):328–37.
22. Higgins JP, van de Rijn M, Jones CD, Zehnder JL, Warnke RA. Peripheral T-cell lymphoma complicated by a proliferation of large B cells. Am J Clin Pathol. 2000;114(2):236–47.
23. Macon WR, Levy NB, Kurtin PJ, Salhany KE, Elkhalifa MY, Casey TT, et al. Hepatosplenic alphabeta T-cell lymphomas: a report of 14 cases and comparison with hepatosplenic gammadelta T-cell lymphomas. Am J Surg Pathol. 2001;25(3):285–96.
24. Ponzoni M, Ferreri AJ, Campo E, Facchetti F, Mazzucchelli L, Yoshino T, et al. Definition, diagnosis, and management of intravascular large B-cell lymphoma: proposals and perspectives from an international consensus meeting. J Clin Oncol. 2007;25(21):3168–73.
25. Roemer MG, Advani RH, Ligon AH, Natkunam Y, Redd RA, Homer H, et al. PD-L1 and PD-L2 Genetic Alterations Define Classical Hodgkin Lymphoma and Predict Outcome. J Clin Oncol. 2016;34(23):2690–7.
26. Ansell SM, Lesokhin AM, Borrello I, Halwani A, Scott EC, Gutierrez M, et al. PD-1 blockade with nivolumab in relapsed or refractory Hodgkin's lymphoma. N Engl J Med. 2015;372(4):311–9.
27. Dogan A, Burke JS, Goteri G, Stitson RN, Wotherspoon AC, Isaacson PG. Micronodular T-cell/histiocyte-rich large B-cell lymphoma of the spleen: histology, immunophenotype, and differential diagnosis. Am J Surg Pathol. 2003;27(7):903–11.

Plasma Cell Neoplasms

7

Carla S. Wilson

Plasma cell neoplasms are interrelated by the finding of an expanded monoclonal plasma cell population. The degree of bone marrow involvement, the type and quantity of secreted monoclonal immunoglobulin (M protein), and associated laboratory, radiographic, and clinical findings help to classify these disorders into several entities:

- Monoclonal gammopathy of undetermined significance (MGUS) (Figs. 7.1, 7.2, 7.3, 7.4, 7.5, and 7.6)
- Solitary plasmacytoma
- Plasma cell myeloma (PCM) (Figs. 7.1, 7.7, 7.8, 7.9, 7.10, 7.11, 7.12, 7.13, 7.14, 7.15, 7.16, 7.17, 7.18, 7.19, 7.20, 7.21, 7.22, 7.23, 7.24, 7.25, 7.26, 7.27, 7.28, 7.29, 7.30, and 7.31)
- Monoclonal immunoglobulin deposition diseases (Figs. 7.1, 7.29, 7.30, and 7.31)·Techniques used to immunophenotype and risk stratify plasma cell neoplasms (Figs. 7.32, 7.33, 7.34, 7.35, 7.36, 7.37, 7.38, 7.39, 7.40, and 7.41)

MGUS is present in 3–4% of individuals over the age of 50 years and precedes the development of PCM. Progression of MGUS to PCM occurs at a rate of 1% per year indefinitely and is associated with random, secondary genetic hits. Smoldering (asymptomatic) PCM is an early form of myeloma with no plasma cell-related organ damage, amyloidosis, or biomarker of malignancy. Individuals convert from smoldering to symptomatic PCM that requires treatment at a rate of 10% per year in the first 5 years after diagnosis. More than 90% of (symptomatic) PCM is diagnosed in individuals >50 years old, many of whom present with the unique triad of bone marrow plasmacytosis, osteolytic bone lesions, and monoclonal gammopathy. PCM accounts for 10–15% of hematopoietic neoplasms, although the incidence is increasing as the population ages. Table 7.1 lists the diagnostic criteria for classification of these entities per the WHO 2016 classification of hematopoietic neoplasms. New biomarkers of malignancy have been added to the more traditional criteria.

C.S. Wilson (✉)
Department of Pathology, University of New Mexico Health Sciences Center and Tricore Reference Laboratories, Albuquerque, NM, USA
e-mail: cswilson@salud.unm.edu

T.I. George, D.A. Arber (eds.), *Atlas of Bone Marrow Pathology*, Atlas of Anatomic Pathology,
https://doi.org/10.1007/978-1-4939-7469-6_7

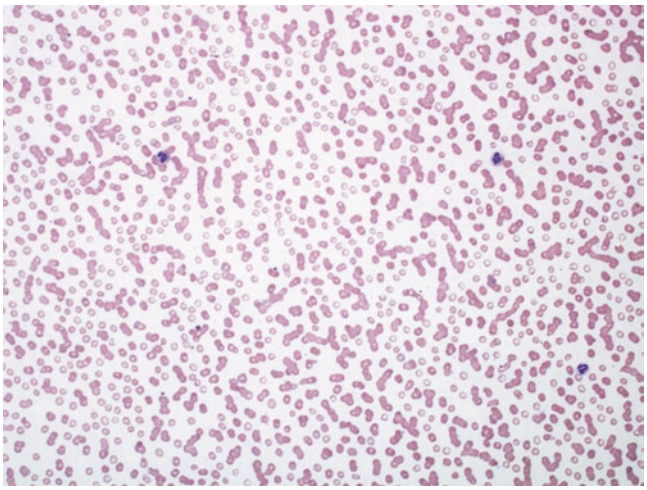

Fig. 7.1 Rouleaux formation is the linear arrangement of four or more red blood cells in the thin areas of the blood smear. This "stack of coins" appearance is caused by increased serum protein (i.e., globulins, fibrinogen). In monoclonal gammopathies, the quantity and type of secreted immunoglobulin is best determined by serum and urine protein electrophoresis (SPEP, UPEP) and immunofixation (IFE) studies

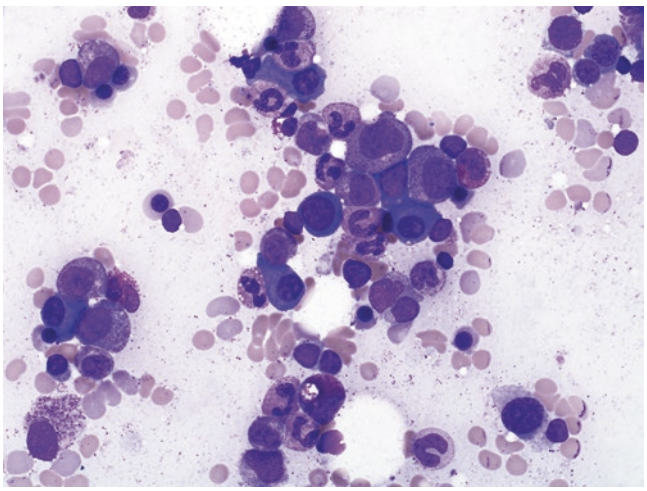

Fig. 7.2 The bone marrow aspirate smear from this 76-year-old man with persistent normochromic normocytic anemia has 4% mature-appearing plasma cells. Occasionally, enlarged and rare binucleated plasma cells are present, similar to what may be seen in a reactive plasmacytosis. This man was subsequently found to have an IgG lambda M component measuring 1.4 g/dL. The diagnosis of monoclonal gammopathy of undetermined significance (MGUS) was rendered when no evidence of end-organ damage or clinicopathological features attributable to the plasma cell proliferation was found. Three types of MGUS are recognized: non-IgM MGUS (plasma cell), IgM MGUS (lymphoid or lymphoplasmacytoid), and light chain MGUS (which progresses to light chain PCM). Approximately 15–20% of MGUS cases are of the IgM type, which (unlike the other types) progresses to lymphoplasmacytic lymphoma or chronic lymphocytic leukemia (CLL), not plasma cell myeloma (PCM), so this subtype will not be included in further discussion of MGUS in this chapter. Associated *MYD88* mutations may be seen

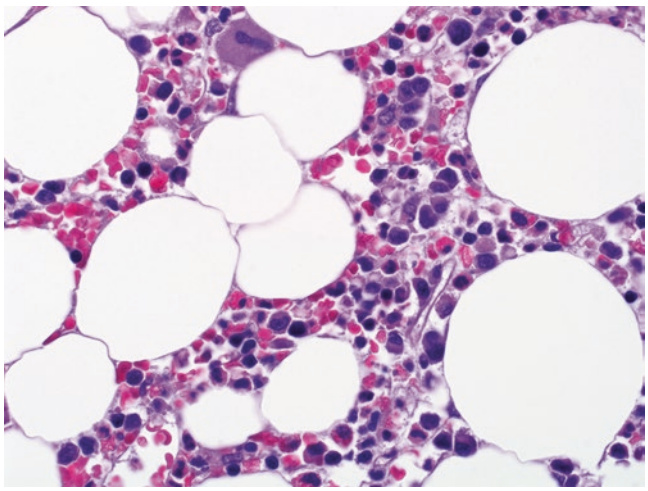

Fig. 7.3 The 76-year-old has a normocellular bone marrow with adequate trilineage hematopoiesis and no significant increase in lymphocytes. A scattered interstitial distribution of plasma cells is present, comprising <10% of the cellularity, characteristic of MGUS. MGUS is underdiagnosed in the general population and is frequently found incidentally during the workup of other clinical conditions. The lifelong risk of transformation to PCM or a related neoplasm is 1% per year for non-IgM MGUS and lower for light chain MGUS. The risk for an individual's progression can be further refined on the basis of three factors: serum M protein <1.5 g/dL, IgG subtype, and a normal free light chain ratio (0.26–1.65). Risk assessment scores for developing PCM consider the number of factors that differ from these standards: If all three factors differ, the patient has high risk (58%); any two differing indicate high-intermediate risk (37%); any one different represents low-intermediate risk (21%); if none differ, the risk is low (5%)

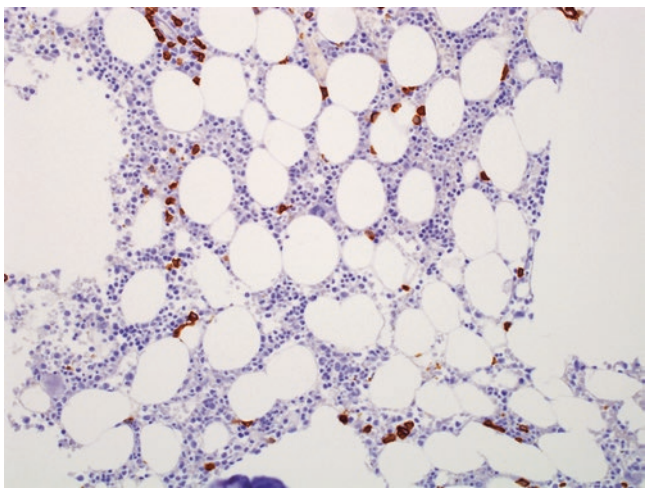

Fig. 7.4 CD138 immunohistochemical stain is the most specific marker for plasma cells but does not distinguish between reactive and neoplastic cells. CD138 immunohistochemistry helps to enumerate plasma cells in clot or trephine biopsy sections and to evaluate the pattern of infiltration. Plasma cells are interstitial in distribution and comprise 5% of the cellularity in this trephine biopsy from the 76-year-old man with MGUS. MUM1 is an alternative marker for assessing benign and neoplastic plasma cells

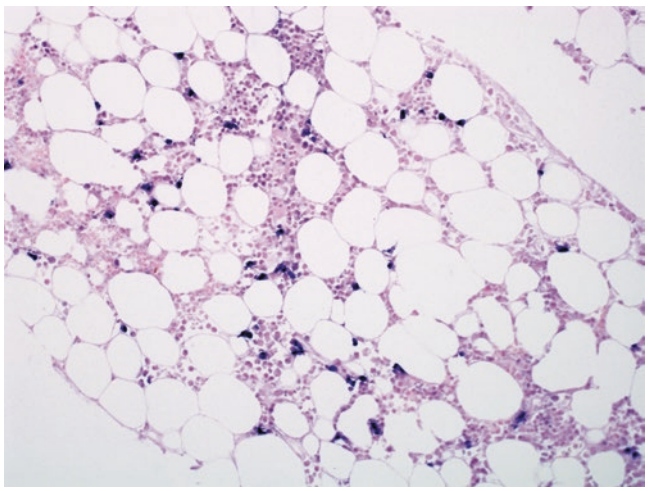

Fig. 7.5 Immunoglobulin light chain evaluation is required to determine plasma cell clonality. Most plasma cells in this case of MGUS express lambda light chain when assessed by in situ hybridization (the preferred method) as shown in this image. Lambda light chain restriction corresponds to the IgG lambda paraprotein identified in the 76-year-old

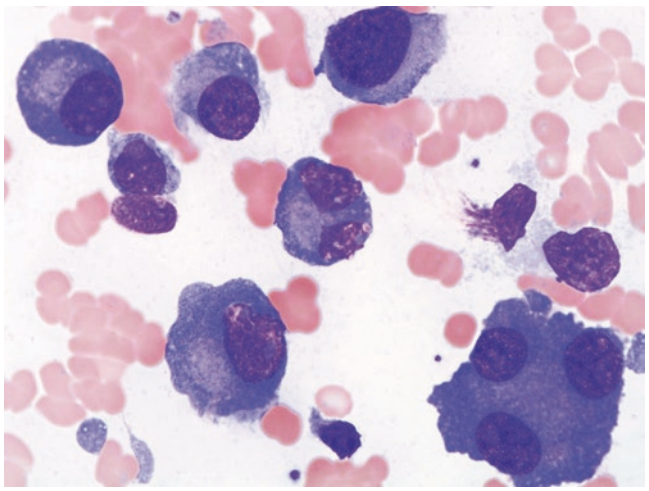

Fig. 7.7 Plasma cell cytology is best appreciated on aspirate smears and touch imprints. Marked plasma cell atypia is unusual in MGUS and likely represents PCM. Scattered cells with recognizable plasma cell features are found in smears from even the most unusual-appearing PCMs. Features of plasma cell atypia are seen in this Wright-stained aspirate, including cellular and nuclear enlargement, nuclear pleomorphism, multinucleation, dispersed nuclear chromatin, prominent nucleoli, and cytoplasmic fraying or shedding

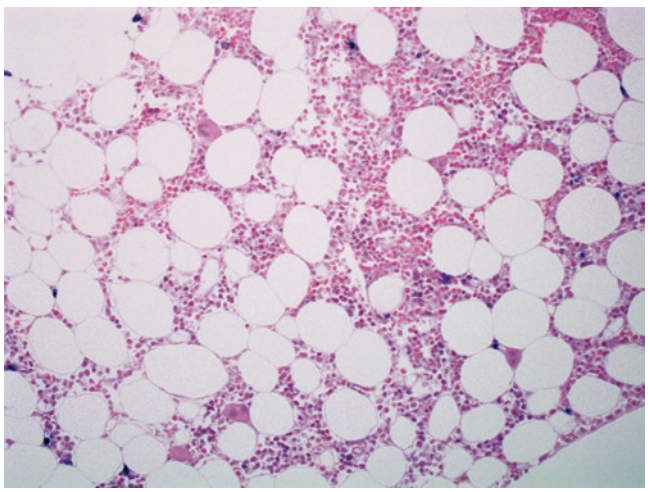

Fig. 7.6 The same bone marrow evaluated with kappa light chain by in situ hybridization shows only rare kappa-positive plasma cells. The laboratory findings of an M protein <1.5 g/d, IgG subtype, and serum free light chain ratio of 0.5 are diagnostic of low-risk MGUS in this 76-year-old, asymptomatic male

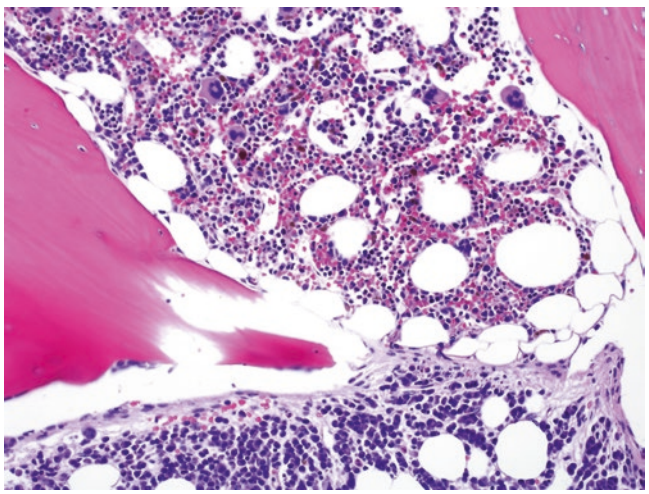

Fig. 7.8 Adequate bone marrow sampling is essential in the workup of PCM, as focal lesions may be widely spaced and irregularly distributed. This trephine biopsy has myeloma only in the lower portion of a long biopsy. Unlike MGUS, PCM often fills the interfatty spaces. Homogenous sheets of plasma cells displacing normal stroma and comprising more than one-half of a 40× high-power field indicate PCM. One problem with the 2016 WHO criteria for PCM is that the requirement of plasma cells ≥10% of bone marrow cellularity is not met in cases such as this, which has considerable bone marrow sparing. Additional sampling of preferably radiographically identified lesions is needed to fulfill this diagnostic criterion

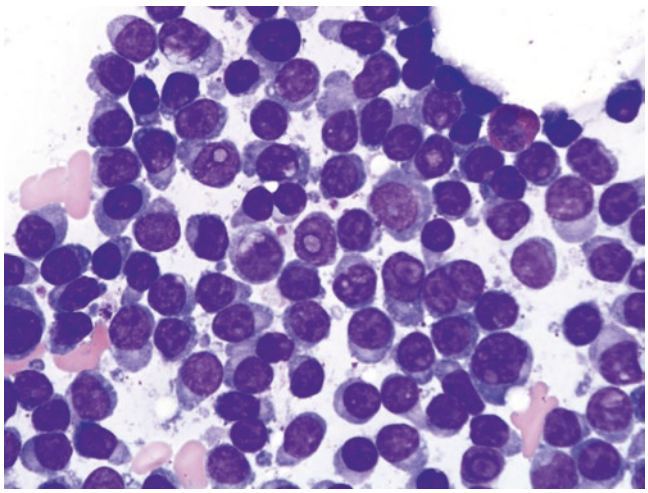

Fig. 7.9 Intranuclear and a variety of cytoplasmic inclusions may be seen in PCM but are not pathognomonic of neoplasia. Plasma cells with increased or blocked immunoglobulin secretions form cytoplasmic vacuoles that invaginate into the nucleus. These Dutcher bodies appear as nuclear globules, although the nuclear membrane is intact. The presence of frequent Dutcher bodies should prompt evaluation for a plasma cell neoplasm or lymphoplasmacytic lymphoma

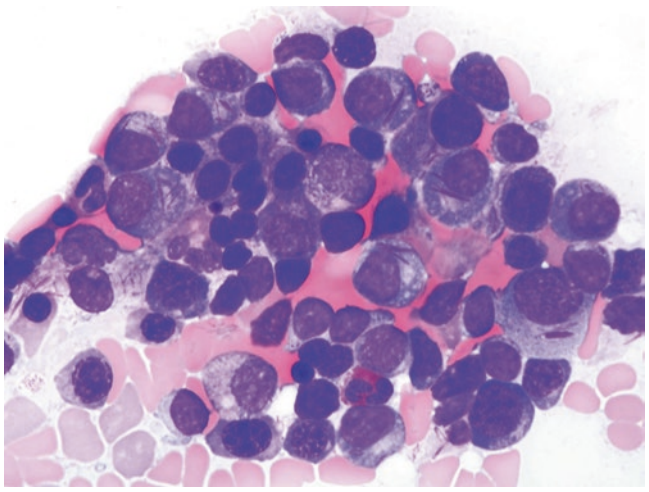

Fig. 7.11 Immunoglobulins crystalize or combine with other compounds to form crystals in the cytoplasm of some myeloma cells. Crystals stain blue, purple, or red, and when they are spindled or elongated in shape, they may resemble Auer rods. This PCM has numerous cytoplasmic crystals concerning for acute promyelocytic leukemia. Immunohistochemical stains confirm the plasma cell phenotype of this unusual myeloma

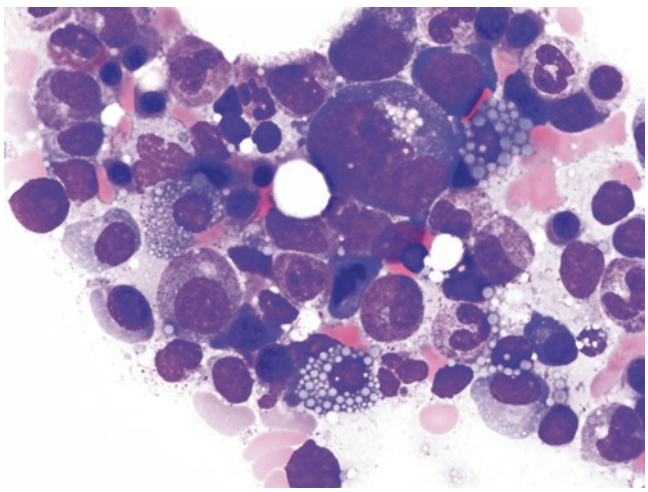

Fig. 7.10 The abundant endoplasmic reticulin in plasma cells leads to cytoplasmic immunoglobulin accumulations that appear as uniformly round, colorless globules called Russell bodies. When multiple Russell bodies are in the cytoplasm of myeloma cells, the cells are referred to as *Mott cells* or less commonly *morula cells* or *grape cells*

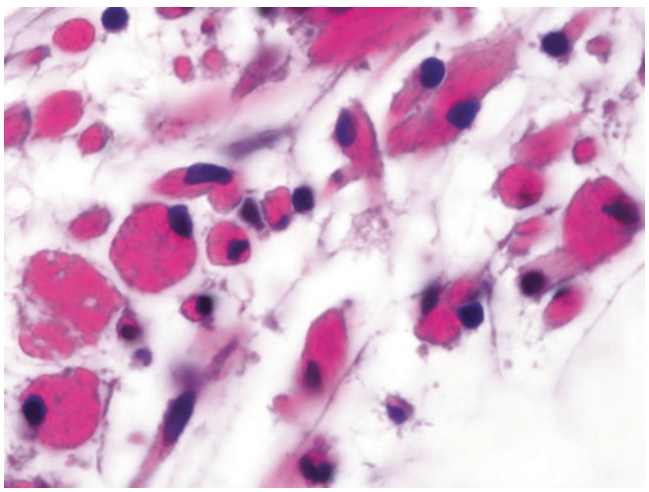

Fig. 7.12 Red crystals with diamond shapes or more elongated rod shapes pack the cytoplasm of these myeloma cells. Similar findings may be seen when crystals are taken up by histiocytes (referred to as crystal-storing histiocytosis). Immunostains (not shown) confirm that these crystal-containing cells are plasma cells and not histiocytes

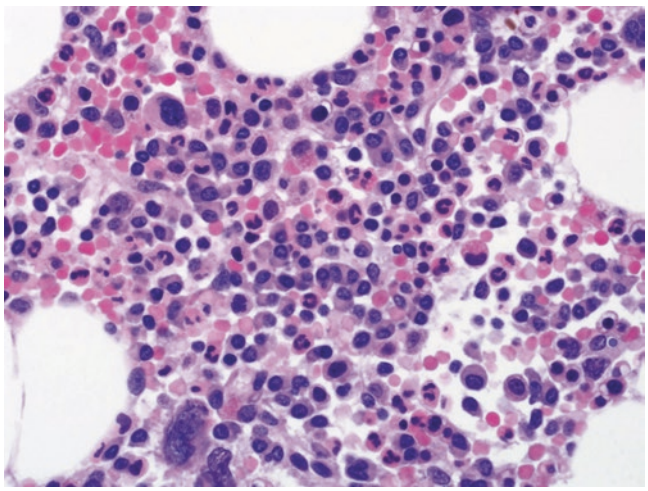

Fig. 7.13 Different PCM classification schemes have used the degree of plasma cell differentiation to predict patient outcome. The association of plasma cell appearance with prognosis is partly due to genetic abnormalities being associated with some morphologies. Myeloma cells that have the appearance of reactive plasma cells, as observed in this image, are considered to be of lower risk. The plasma cells have eccentrically placed, round nuclei with a cartwheel appearance and few nucleoli. This PCM has an interstitial pattern of bone marrow infiltration, which is usually more favorable than a nodular or diffuse pattern

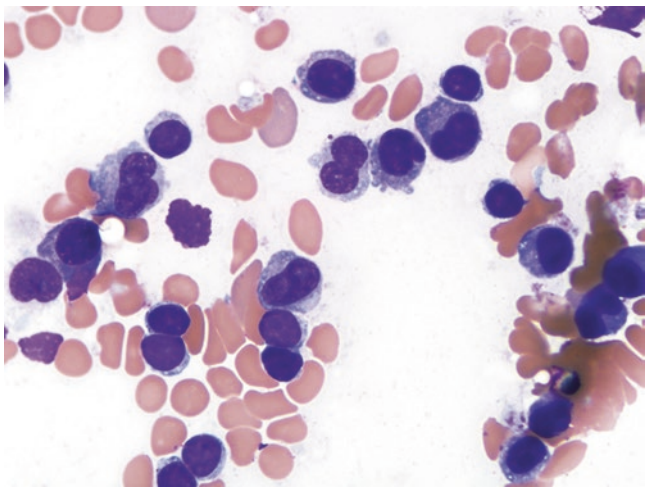

Fig. 7.15 As PCM is a heterogeneous disease with karyotypic abnormalities that are unusual in their complexity, it is not surprising that neoplastic plasma cells have a variety of appearances. This cleaved type of PCM has many cells with notched, cleaved, or convoluted nuclei of variable size

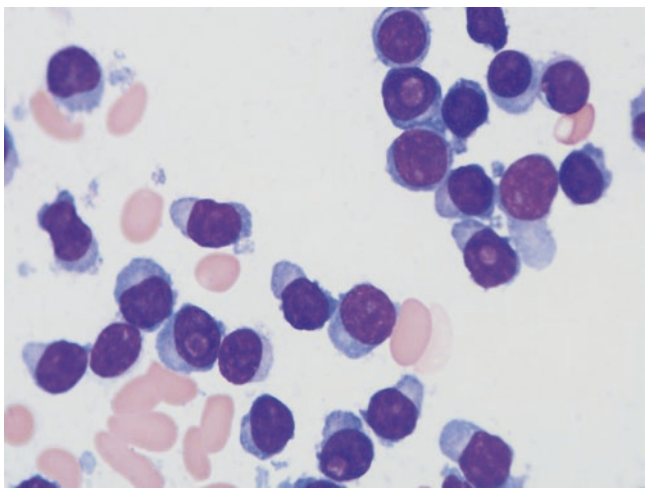

Fig. 7.14 The lymphoid or small-cell type of PCM has round, lymphocyte-like nuclei, usually a perinuclear hof or area of clearing, and a scant to moderate rim of cytoplasm. Occasional Dutcher bodies are present. This type of PCM is associated with a better prognosis when it is also CD20-positive with a t(11;14) translocation, findings that are not exclusive to this PCM variant

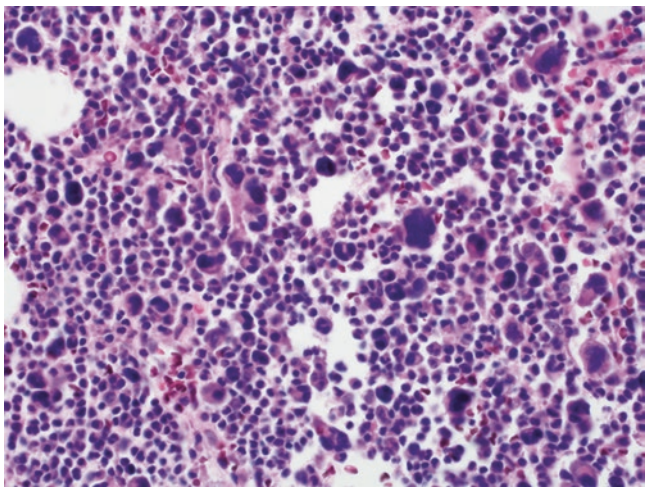

Fig. 7.16 This trephine biopsy section shows sheets of cleaved myeloma cells. Occasional larger myeloma cells are difficult to separate from intermixed megakaryocytes in this H&E-stained bone marrow section

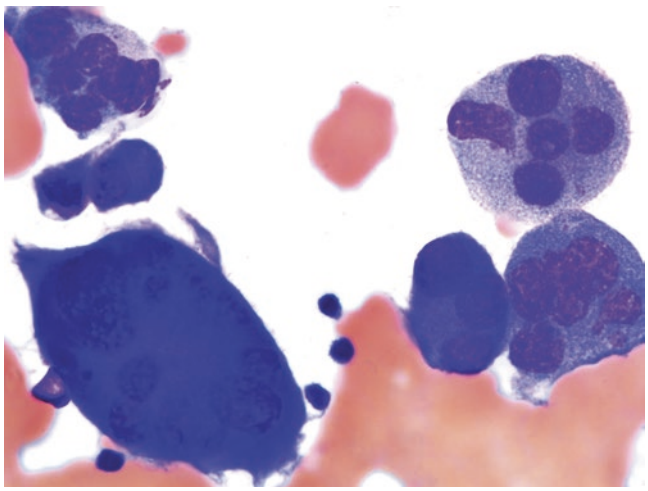

Fig. 7.17 The bone marrow aspirate smears in this PCM have many large, oddly shaped plasma cells. Marked cellular pleomorphism, multinucleation, and cells with prominent nucleoli are characteristic of this polymorphous type of PCM. The term "anaplastic" myeloma is not recommended for this type of case; this is not considered an entity in different classification schemes. Cells are not considered immature in the absence of fine or blastic-appearing nuclear chromatin

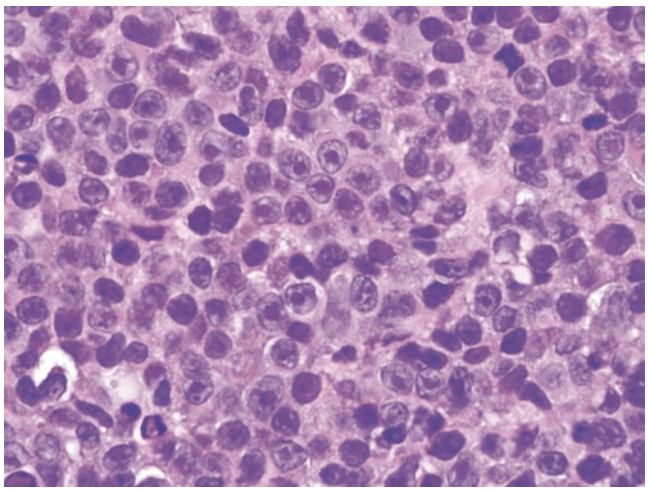

Fig. 7.19 Plasmablastic morphology is most predictive of an aggressive PCM. Although plasmablastic myeloma is an independent prognostic factor for survival in multiple studies, concurrent high-risk cytogenetic abnormalities are characteristically present, including del(17p13). Plasmablasts are described historically as having large concentric nuclei, prominent centrally located nucleoli, dispersed chromatin, and a rim of basophilic cytoplasm that is less than one-half the nuclear area. Plasmablastic areas in biopsies are frequently packed and fibrotic with increased mitoses, so plasmablasts are poorly represented in aspirate smears. Plasmablastic myeloma resembles immunoblastic or plasmablastic lymphoma in tissue sections

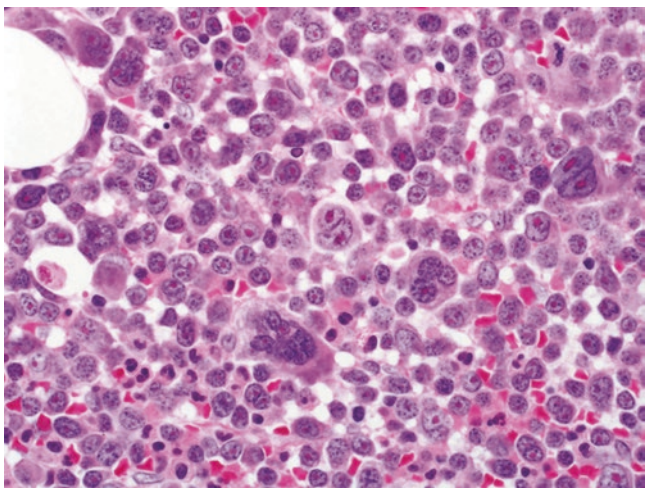

Fig. 7.18 The trephine biopsy section of the polymorphous type of PCM highlights the marked cellular pleomorphism, including the presence of large, multinucleated cells with prominent nucleoli, some of which resemble Reed-Sternberg cells or anaplastic large-cell lymphoma. A clue to correctly diagnosing this type of PCM is the presence of recognizable plasma cells in the background infiltrate; these are easiest to appreciate in aspirate smears or touch preparations

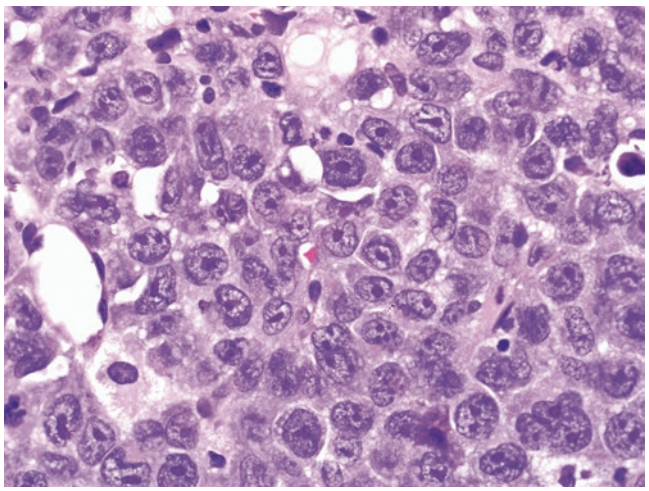

Fig. 7.20 This case of plasmablastic lymphoma has an appearance similar to plasmablastic myeloma in bone marrow. In contrast to myeloma, plasmablastic lymphoma is usually Epstein-Barr virus (EBV) positive and cyclin D1 negative

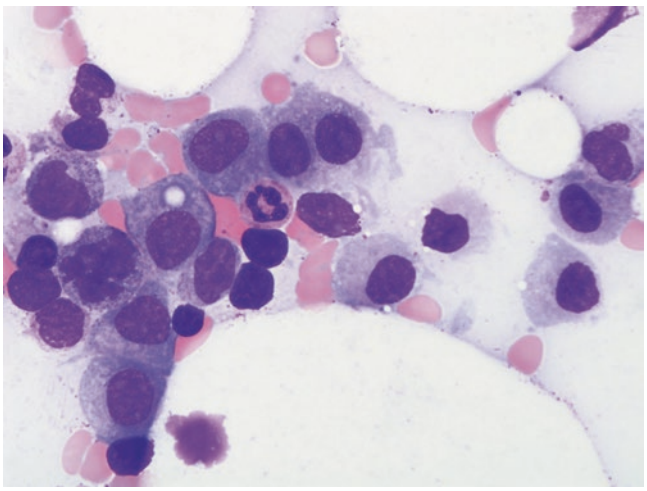

Fig. 7.21 Myeloma cells may be difficult to delineate from other hematopoietic cells in the bone marrow. Myeloma cells with abundant cytoplasm resembling histiocytes are scattered in this bone marrow aspirate smear

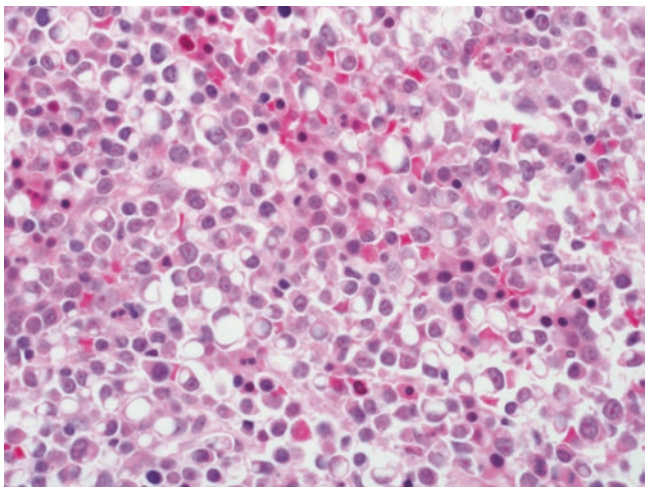

Fig. 7.23 Myelomatous infiltrates in biopsy sections have a variety of appearances and must be considered in the differential diagnosis of any morphologically unusual bone marrow infiltrate. This PCM has a signet-ring appearance owing to abundant cytoplasmic secretions that mimic the appearance of a signet-ring carcinoma. Immunohistochemical stains are essential for the correct identification of PCM in such infiltrates

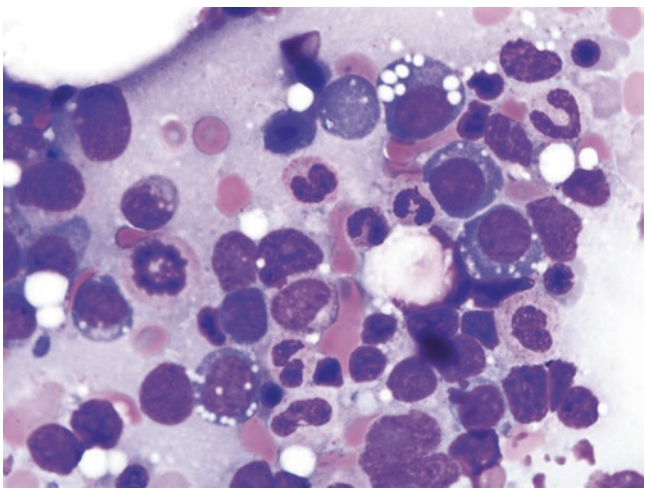

Fig. 7.22 Myeloma cells may be difficult to differentiate from erythroid or megakaryocytic precursors in bone marrow preparations. Cytoplasmic vacuoles in these myeloma cells help to distinguish them from surrounding erythroid precursors

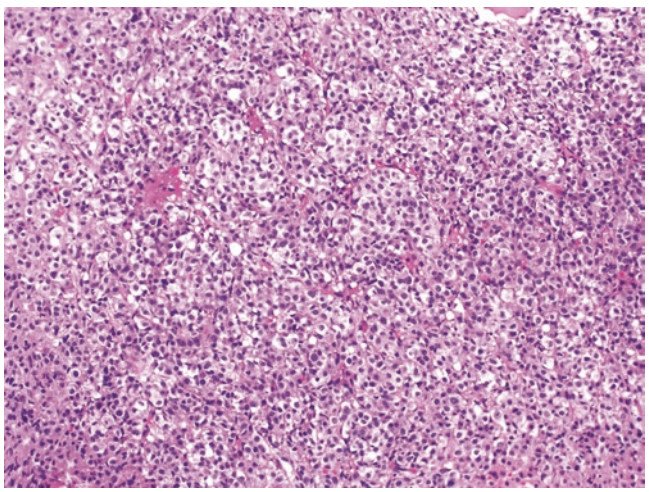

Fig. 7.24 This H&E-stained bone marrow is extensively involved by large cells with abundant pale to clear cytoplasm that appears to be forming nests mimicking metastatic carcinoma. These cells are cytokeratin negative and are positive for CD138, CD56, and kappa light chain, diagnostic of PCM

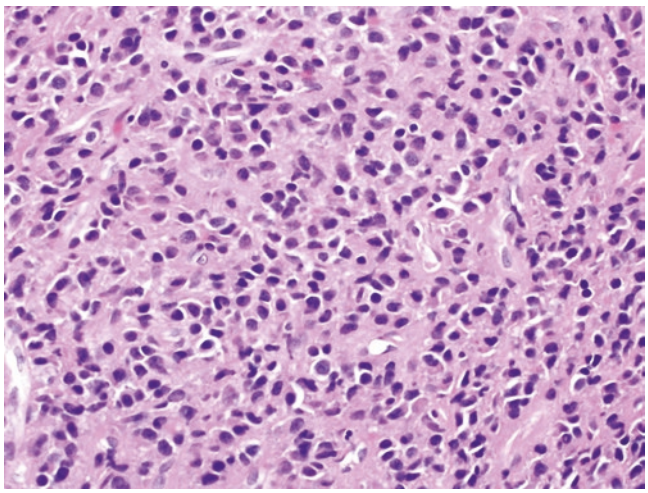

Fig. 7.25 Neoplastic plasma cells are difficult to delineate from other neoplastic infiltrates in fibrotic bone marrows. At diagnosis, approximately 9% of PCM has accompanying background fibrosis that appears as pink stroma and is difficult to aspirate

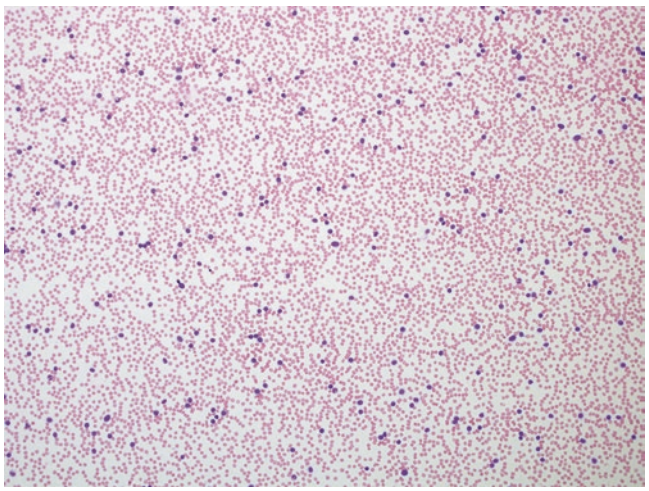

Fig. 7.27 This peripheral blood smear came from a patient presenting with leukocytosis, anemia, thrombocytopenia, and new-onset renal failure. Rouleaux formation and an increased population of plasma cells are present

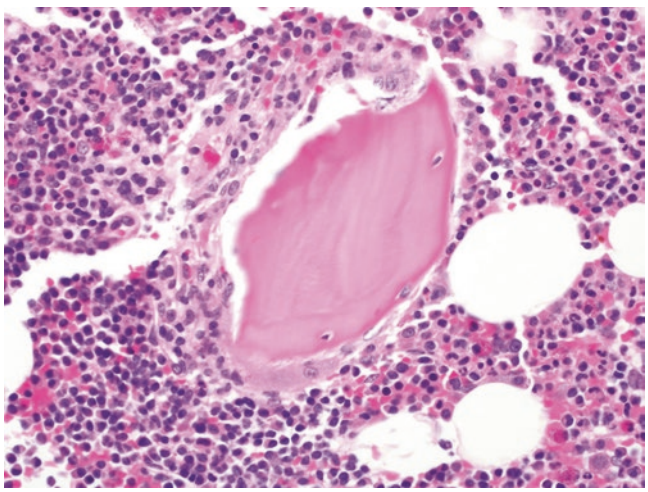

Fig. 7.26 Myeloma cell binding to bone marrow stroma induces osteoclastogenic factors. Bone lesions are caused by increased production and activation of osteoclasts and impaired osteoblast function. Bone lesions are found mainly in areas with adjacent myeloma cells, as observed in the lower portion of this image. Myeloma bone disease plays a profound role in patient morbidity

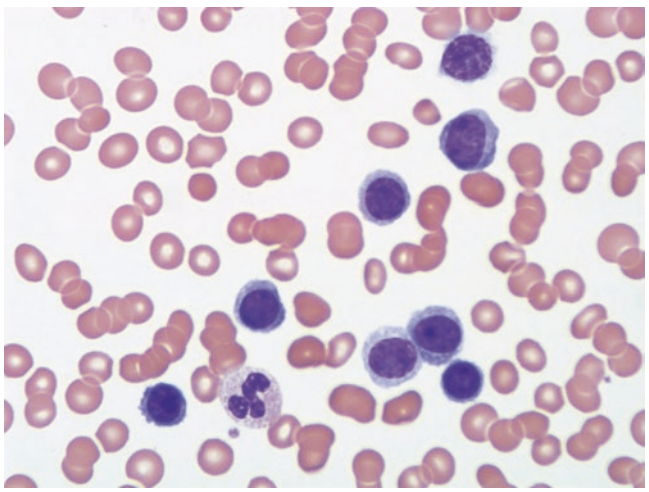

Fig. 7.28 The majority of leukocytes are small- to intermediate-sized plasma cells with round nuclei, indistinct nucleoli, and moderately abundant cytoplasm. The plasma cells comprise at least 20% of circulating white blood cells and are $>2 \times 10^9$/L, diagnostic of plasma cell leukemia (PCL). This de novo presentation may be confused with lymphoma, as circulating leukemic cells often have a lymphoid appearance and may express CD20 with lack of CD56. Patients present with extramedullary involvement, stage 3 disease, and frequently immunoglobulin light chain (Bence-Jones protein) disease. PCL has genetic abnormalities similar to those of high-risk PCM. Complex chromosomal karyotypes are common, and a majority are hypodiploid or have diploid DNA. IGH rearrangements, including t(11;14) and t(14;16), are found in 33% and 13% of cases, respectively

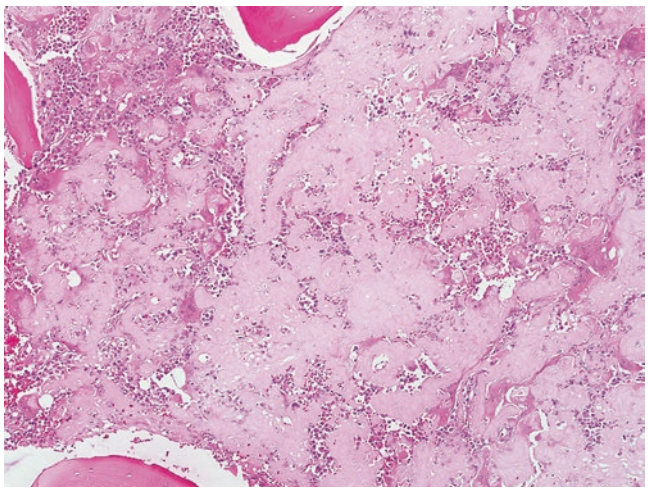

Fig. 7.29 Extensive amyloid deposition is observed in a patient with systemic immunoglobulin light chain (AL) amyloidosis. Primary amyloidosis (AL) is caused by monoclonal plasma cells that oversynthesize free immunoglobulin light chains, which are deposited in tissue. AL amyloid is most commonly formed by lambda light chains with reduced folding stability. The light chains self-associate into oligomers and fibrils that form distinct, beta-pleated sheets. Only 20% of patients with AL amyloidosis progress to overt PCM. Patients usually die of amyloid-related organ dysfunction prior to the development of myeloma

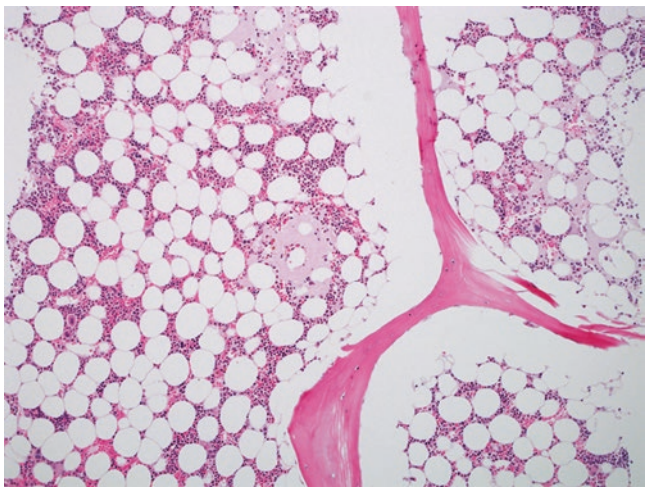

Fig. 7.31 Bone marrow biopsies in patients with PCM must be evaluated for vascular and stromal amyloid deposits, as seen in this H&E-stained biopsy and confirmed by Congo red staining. Although 10–15% of PCM patients have coexisting amyloid, the amyloid may be missed on bone marrow sampling and will require a fat pad aspirate or end-organ biopsy (kidney, gastrointestinal tract, heart) to identify. Therapy requires treatment of the underlying plasma cell neoplasm

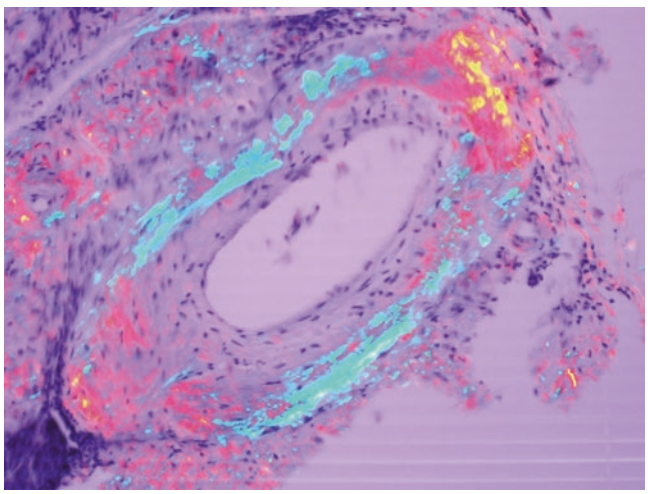

Fig. 7.30 Amyloid fibrils take up Congo red stain and exhibit apple-green birefringence under polarized light. This Congo red stain of a vessel wall is positive for amyloid

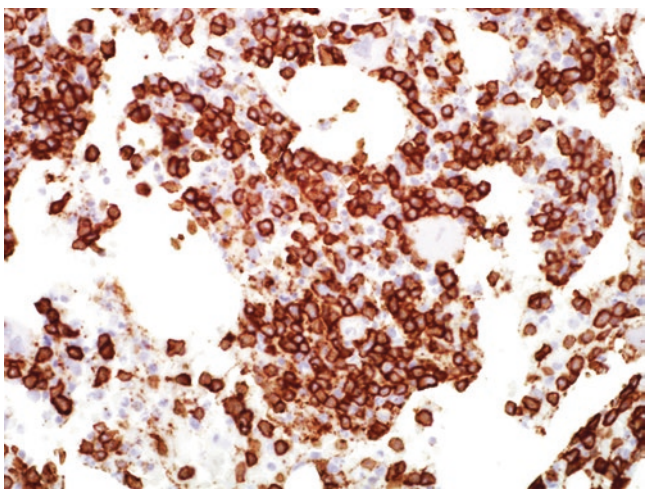

Fig. 7.32 CD138 immunohistochemical stain, as shown here, is the most specific marker for plasma cells in the bone marrow, but it may be expressed on non-hematopoietic neoplasms that metastasize to marrow. Immunohistochemistry helps to evaluate for the percentage of myelomatous involvement when plasma cells are unevenly distributed in clot and trephine biopsy sections

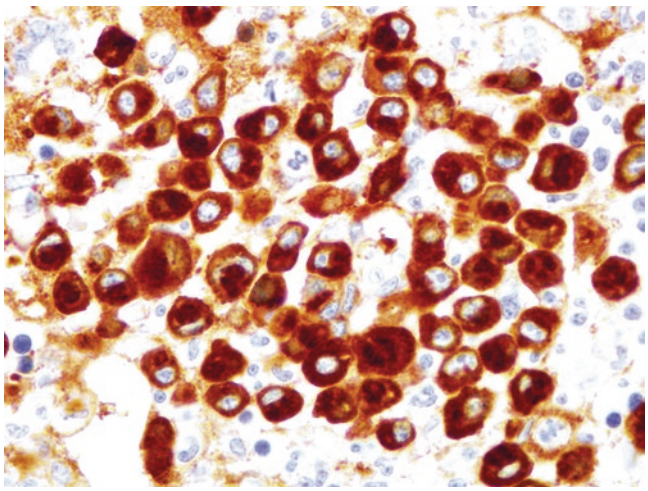

Fig. 7.33 Plasma cell clonality is best determined by light chain evaluation. The kappa-positive light chain expression in this case also confirms a neoplastic plasma cell process, as CD138 stains a variety of undifferentiated epithelial and mesenchymal neoplasms. In the few cases where light chain expression is difficult to interpret, evaluation of heavy chains (IgG, IgA, IgM, IgD) may help to clarify the presence of a clonal population

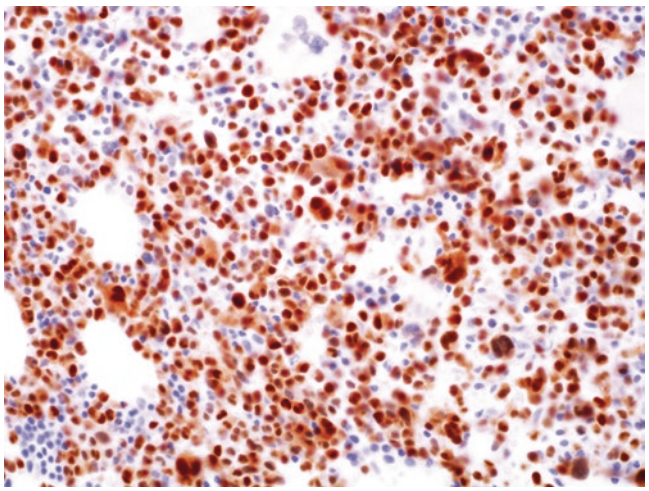

Fig. 7.35 Cyclin D1 expression in plasma cells confirms a clonal process. Positivity for cyclin D1 is found in at least one-third of cases of PCM and MGUS, including many that lack t(11;14)(q13;q32). The presence of cyclin D1(+), CD20(+), and t(11;14) with small-cell-type PCM confers a better prognosis. Cyclin D1 cannot be assessed by flow cytometry because of technical constraints

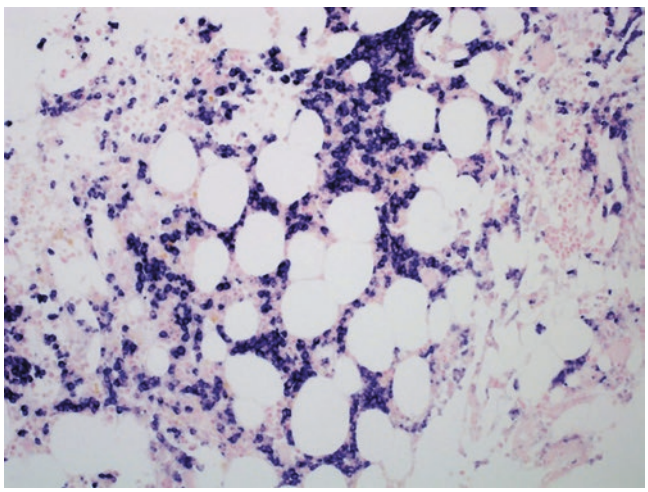

Fig. 7.34 In situ hybridization is often more reliable than immunohistochemistry for light chain assessment. This case of PCM shows kappa light chain restriction as shown here, with only rare positive cells seen by lambda in situ hybridization. Aberrant immunophenotypes are observed in more than 80% of PCM cases at diagnosis. CD20 expression is seen in 15–20% of PCM and needs to be distinguished from B-cell lymphoma, particularly lymphoplasmacytic lymphoma. B-cell lymphoma, unlike the majority of CD20-positive PCM, coexpresses CD19 and surface immunoglobulin

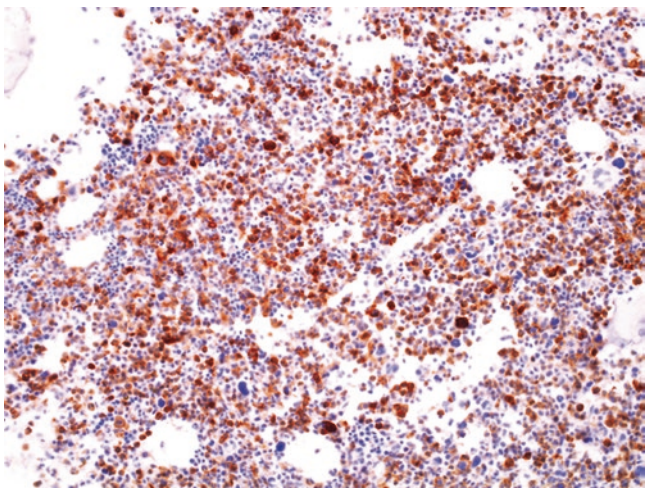

Fig. 7.36 Lineage infidelity is a feature of PCM; aberrant expression of myeloid, T-cell, and B-cell antigens occurs. This PCM is immunoreactive for CD117, which is detected in about 30% of cases of PCM

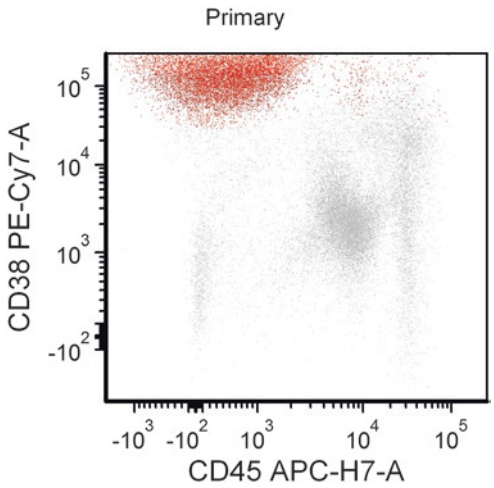

Fig. 7.37 Flow cytometric analysis routinely underestimates plasma cell percentages by as much as 70%. Although the specific cause is unclear in many cases, culprits include pre-analytical loss of plasma cells, shedding of antigen epitopes during handling, and stickiness of plasma cells to other cell types, altering expression patterns. The myeloma cells (red) in this flow cytometry histogram show bright CD38 expression and loss of CD45. Activated and immature T cells, hematogones, and monocytes may be brightly CD38 positive but are CD45 positive and CD138 negative

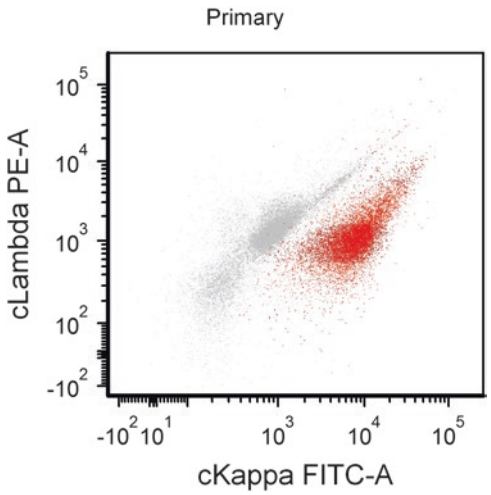

Fig. 7.39 Plasma cells require permeabilization of cell membranes to allow antibodies against immunoglobulins to enter the cytoplasm. Clonality is established in this case by finding cytoplasmic kappa light chain restriction in the plasma cell population (red)

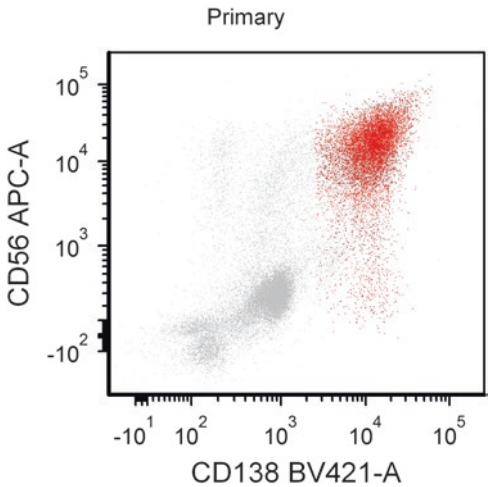

Fig. 7.38 Myeloma cells (red) in this histogram are CD138 and CD56 positive. CD138 identifies the plasma cell population, whereas aberrant CD56 expression supports a neoplastic process. Loss of the adhesion marker CD56 occurs in late-stage PCM, allowing plasma cells to leave the marrow stroma and develop extramedullary disease or secondary plasma cell leukemia. Some of the additional lineage antigens aberrantly expressed in PCM include CD19 (<5%), CD20 (15–20%), CD28 (40%), CD33 (15%), and CD52 (30%). CD138 may be falsely negative by flow cytometric analysis if the extracellular portion of the molecule containing the binding site for the antibody is shed during handling

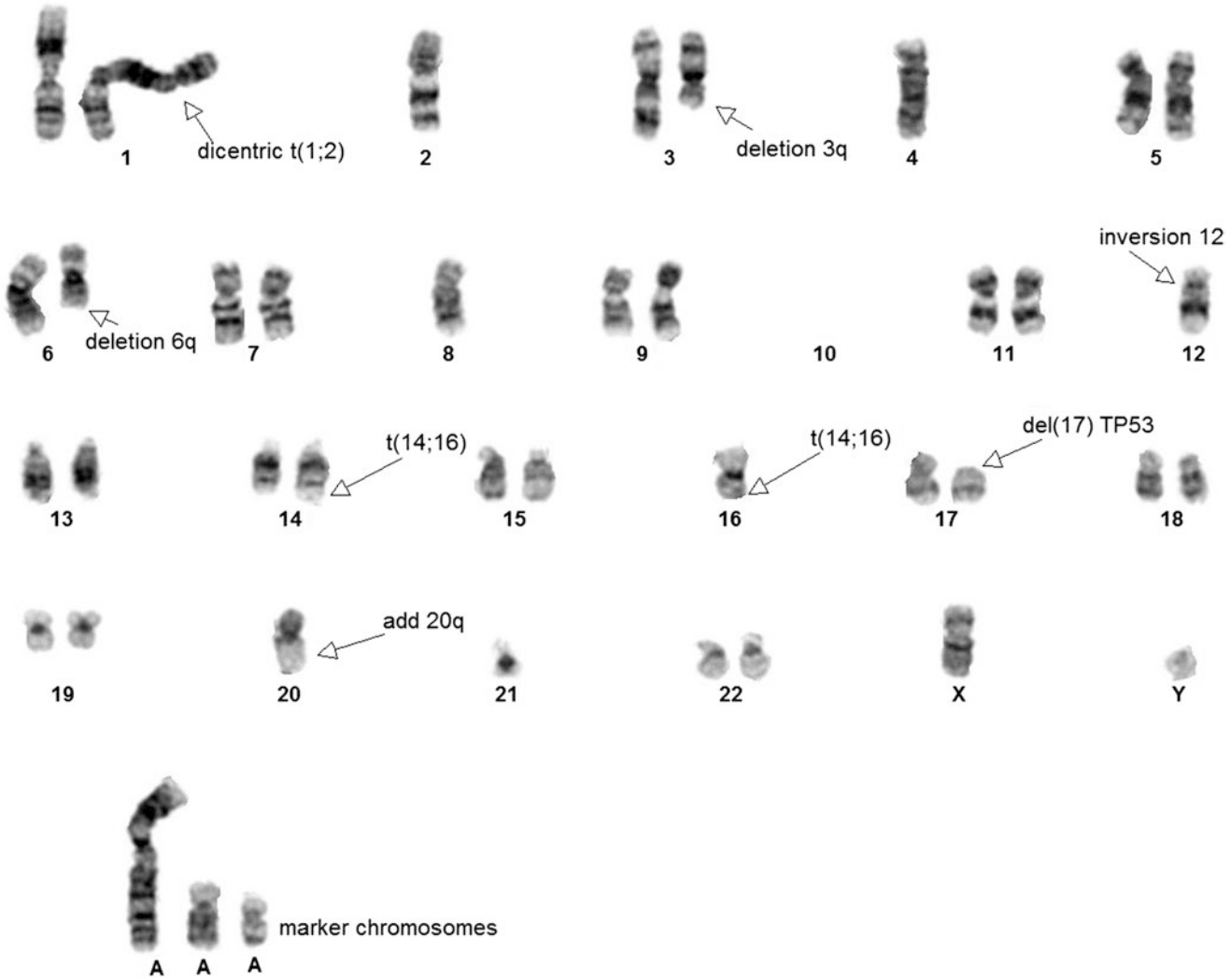

Fig. 7.40 PCM commonly has a hyperdiploid karyotype with multiple trisomies of the odd-numbered chromosomes. In contrast, this karyotype is from a plasmablastic myeloma and shows abnormalities in all 20 mitotic cells analyzed, including loss of chromosomes 4, 8, 10, 12, 16, 20, and 21; deletion 6q; deletion 17p; complex, unbalanced rearrangements of chromosomes 1, 2, 3, 8, and 20; and gain of three to five marker chromosomes. The 14;16 translocation results in an *IGH-MAF* gene rearrangement, which occurs in roughly 3% of patients with PCM. This poor-prognosis translocation has been linked with *MAF* and *CCND2* upregulation, resulting in apoptosis resistance and aggressive disease

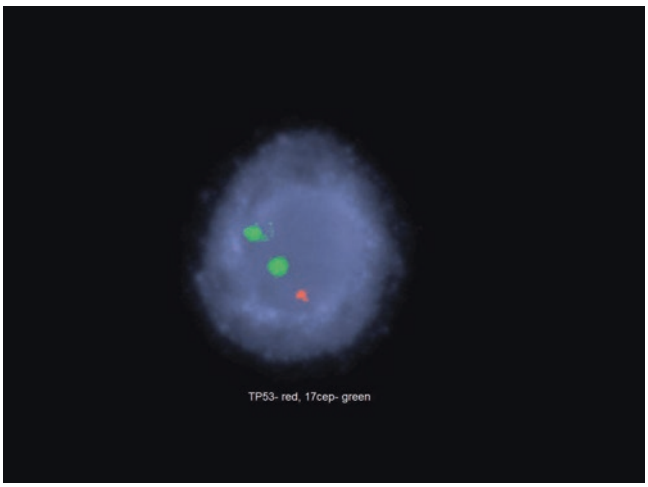

Fig. 7.41 Interphase fluorescence in situ hybridization (FISH) analysis shows two normal copies of the chromosome 17 centromeric region (green) and a deletion of the 17p13.1 region (red). Deletions of 17p13, including *TP53*, are found in approximately 10% of PCM cases. This high-risk cytogenetic marker is commonly associated with high proliferative disease, drug resistance, and worse outcomes, especially when present in the majority of plasma cells. The *TP53* deletion is unfavorable regardless of the presence of other cytogenetic abnormalities. Additional FISH analysis on the plasmablastic myeloma confirmed imbalances of 1p/1q, t(14;16), and a variant *MYC* gene rearrangement in at least 50% of the interphase cells scored (not shown)

Table 7.1 2016 WHO classification of plasma cell neoplasms

Criteria	Monoclonal gammopathy of undetermined significance (MGUS)	Smoldering myeloma	Plasma cell myeloma (PCM)
Clonal bone marrow plasma cells	<10%	≥10% and <60% or biopsy-proven plasmacytoma and/or fulfilling criteria below for monoclonal (M) protein	≥10% or biopsy-proven plasmacytoma
Monoclonal (M) protein in serum or urine	<30 g/L or <500 mg/24 h	≥30 g/L or ≥500 mg/24 h	Usually
Additional requirement	Absence of amyloidosis, lymphoma, or CRAB*	Absence of amyloidosis or CRAB*	Either CRAB* or 1 myeloma biomarker listed below
Myeloma-defining biomarkers	No	No	Clonal bone marrow plasma cells ≥60% Involved/uninvolved serum free light chain ratio ≥ 100 >1 focal lesion on MRI (each ≥5 mm in size)

*International Myeloma Working Group updated diagnostic criteria for CRAB:
Calcium (in serum) > 0.25 mmol/L (>1 mg/dL) above upper limit of normal or >2.75 mmol/L (>11 mg/dL)
Renal insufficiency with creatinine clearance <40 mL/min or serum creatinine >177 μmol/L (>2 mg/dL)
Anemia with hemoglobin >2 g/dL below lower limit of normal or <10 g/dL
Bone lesions with ≥1 lytic lesions on skeletal x-ray, CT, or PET/CT

Plasma cell leukemia (PCL) is a rare, aggressive form of PCM, which may occur de novo (primary PCL) or as a terminal event in progressive PCM (secondary PCL). Criteria for the diagnosis of PCL are peripheral blood plasma cell count $>2 \times 10^9$/L and/or plasma cells ≥20% of white blood cells. Solitary plasmacytoma is an uncommon, localized proliferation of clonal plasma cells involving a single bone (50% of cases) or extramedullary soft tissue (often the head and neck area). Strict staging with radiographic and laboratory studies to exclude myeloma or lymphoma with plasmacytic differentiation is required. A random bone marrow biopsy must contain no clonal plasma cell population; if <10% clonal plasma cells are present, the diagnosis is changed to "solitary plasmacytoma with minimal marrow involvement."

The most common monoclonal immunoglobulin deposition disease is systemic amyloid light chain (AL) amyloidosis. This amyloid-related systemic syndrome (involving the kidneys, liver, heart, gastrointestinal system, and peripheral nerves) is a monoclonal plasma cell proliferation disorder that may progress to PCM.

The basic genetic events that lead to plasma cell oncogenesis are similar in the different plasma cell neoplasms. Underlying genetic variations likely explain the heterogeneous clinical behavior in patients with these different disorders.

Clinical and biologic implications of recurrent genomic aberrations, best examined in PCM, have led to major advances in risk stratification and treatment approaches to this currently incurable neoplastic disorder.

Suggested Reading

1. Ahn JS, Okal R, Vos JA, Smolkin M, Kanate AS, Rosado FG. Plasmablastic lymphoma versus plasmablastic myeloma: an ongoing diagnostic dilemma. J Clin Pathol 2017;70:775-80.
2. Bartl R, Frisch B, Fateh-Moghadam A, Kettner G, Jaeger K, Sommerfeld W. Histologic classification and staging of multiple myeloma. A retrospective and prospective study of 674 cases. Am J Clin Pathol. 1987;87:342–55.
3. Bayer-Garner IB, Sanderson RD, Dhodapkar MV, Owens RB, Wilson CS. Syndecan-1 (CD138) immunoreactivity in bone marrow biopsies of multiple myeloma: shed syndecan-1 accumulates in fibrotic regions. Mod Pathol. 2001;14:1052–8.
4. Chesi M, Bergsagel PL. Advances in the pathogenesis and diagnosis of multiple myeloma. Int J Lab Hematol. 2015;37(Suppl 1):108–14.
5. Heerema-McKenney A, Waldron J, Hughes S, Zhan F, Sawyer J, Barlogie B, Shaughnessy JD Jr. Clinical, immunophenotypic, and genetic characterization of small lymphocyte-like plasma cell myeloma: a potential mimic of mature B-cell lymphoma. Am J Clin Pathol 2010;133:265–270.
6. Jelinek T, Kryukov F, Rihova L, Hajek R. Plasma cell leukemia: from biology to treatment. Eur J Haematol. 2015;95:16–26.
7. Małyszko J, Kozłowska K, Małyszko JS. Amyloidosis: a cancer-derived paraproteinemia and kidney involvement. Adv Med Sci. 2017;62:31–8.
8. Muchtar E, Dispenzieri A, Lacy MQ, Buadi FK, Kapoor P, Hayman SR, et al. Overuse of organ biopsies in immunoglobulin light chain amyloidosis (AL): the consequence of failure of early recognition. Ann Med. 2017;49:545-51.
9. Paiva B, Puig N, Cedena MT, de Jong BG, Ruiz Y, Rapado I, et al. Differentiation stage of myeloma plasma cells: biological and clinical significance. Leukemia. 2017;31:382–92.
10. Rajkumar SV, Dimopoulos MA, Palumbo A, Blade J, Merlini G, Mateos MV, et al. International Myeloma Working Group updated criteria for the diagnosis of multiple myeloma. Lancet Oncol. 2014;15:e538–48.
11. Rajkumar SV. Multiple myeloma: 2016 update on diagnosis, risk-stratification, and management. Am J Hematol. 2016;91:719–34.
12. Ravindran A, Bartley AC, Holton SJ, Gonsalves WI, Kapoor P, Siddiqui MA, et al. Prevalence, incidence and survival of smoldering multiple myeloma in the United States. Blood Cancer J. 2016;6:e486.
13. Stella F, Pedrazzini E, Agazzoni M, Ballester O, Slavutsky I. Cytogenetic alterations in multiple myeloma: prognostic significance and the choice of frontline therapy. Cancer Investig. 2015;33:496–504.

Immunodeficiency-Associated Lymphoproliferative Disorder

8

Juehua Gao and Yi-Hua Chen

Immunodeficiency-associated lymphoproliferative disorders (LPDs) can occur in the setting of HIV infection, after transplantation (posttransplant lymphoproliferative disorder, PTLD), or in other clinical conditions including primary immunodeficiency or the use of immunosuppressive drugs (iatrogenic immunodeficiency-associated LPD). LPDs in the setting of immunodeficiency share similar morphologic features, with a broad spectrum of findings from polymorphous lymphoplasmacytic proliferations to aggressive lymphoma. In patients diagnosed with an immunodeficiency-associated LPD, a staging bone marrow is recommended as part of the initial workup.

Lymphoproliferative Disorders in HIV Patients

LPDs in HIV patients are heterogeneous and range from polyclonal hyperplastic lesions to aggressive lymphomas. At one end of the spectrum are the early and polymorphic lesions that typically show a heterogeneous cellular proliferation composed of small lymphocytes, plasma cells, and immunoblasts resembling polymorphic PTLD (Fig. 8.1). Bone marrow involvement by early and polymorphic LPDs may show features overlapping with reactive changes commonly seen in HIV-infected patients. The frequency of early and polymorphic LPDs in HIV patients is unknown, but they seem much less common than in the PTLD setting. At the other end of the spectrum is HIV-associated lymphoma, which includes lymphomas also occurring in immunocompetent patients, such as diffuse large B-cell lymphoma, Burkitt lymphoma, and Hodgkin lymphoma, as well as lymphomas occurring much more commonly in HIV patients, such as primary effusion lymphoma and plasmablastic lymphoma. HIV-associated lymphomas are usually aggressive and often spread to the bone marrow; in some cases, the bone marrow may be the primary or initial diagnostic site (Figs. 8.2, and 8.3) [1, 2]. The morphologic features of HIV-associated lymphomas are similar to their counterparts in the immunocompetent population, but Epstein-Barr virus (EBV) is more often positive. HIV-related Hodgkin lymphoma, for example, is almost always associated with EBV [3]. The reported frequency of bone marrow involvement by HIV-related lymphoma varies. In one of the largest series, the German HIV Lymphoma Cohort reported bone marrow involvement in 25 (16%) of 154 diffuse large B-cell lymphomas, 32 (31%) of 103 Burkitt lymphomas, and 6 (18%) of 34 plasmablastic lymphomas [4]. Primary effusion lymphoma almost always occurs in immunodeficient patients, with universal association with human herpesvirus 8 (HHV8) infection and common EBV coinfection, but bone marrow involvement is uncommon (11%) [5]. The features of bone marrow involvement by HIV-associated LPD are summarized in Table 8.1.

Posttransplant Lymphoproliferative Disorders

PTLD comprises another major group of immunodeficiency-associated LPDs and includes four categories based on the current WHO classification: early lesions, polymorphic PTLD, monomorphic PTLD (B- and T-cell lymphomas), and classical Hodgkin lymphoma (Table 8.2). The frequency of bone marrow involvement by PTLDs after solid organ transplant varies from 14% to 40% [6–13]; monomorphic (23.5%) and polymorphic (15.7%) types predominate [13]. The bone marrow involvement by monomorphic PTLD can be either B-cell or T-cell type (Fig. 8.4) [13]. Among all types of monomorphic PTLDs involving the bone marrow, diffuse large B-cell lymphoma is the most common, but other types such as Burkitt lymphoma, plasmacytoma-like lesions,

J. Gao (✉) • Y.-H. Chen
Department of Pathology, Northwestern University Feinberg School of Medicine, Chicago, IL, USA
e-mail: j-gao@northwestern.edu; y-chen5@northwestern.edu

T.I. George, D.A. Arber (eds.), *Atlas of Bone Marrow Pathology*, Atlas of Anatomic Pathology,
https://doi.org/10.1007/978-1-4939-7469-6_8

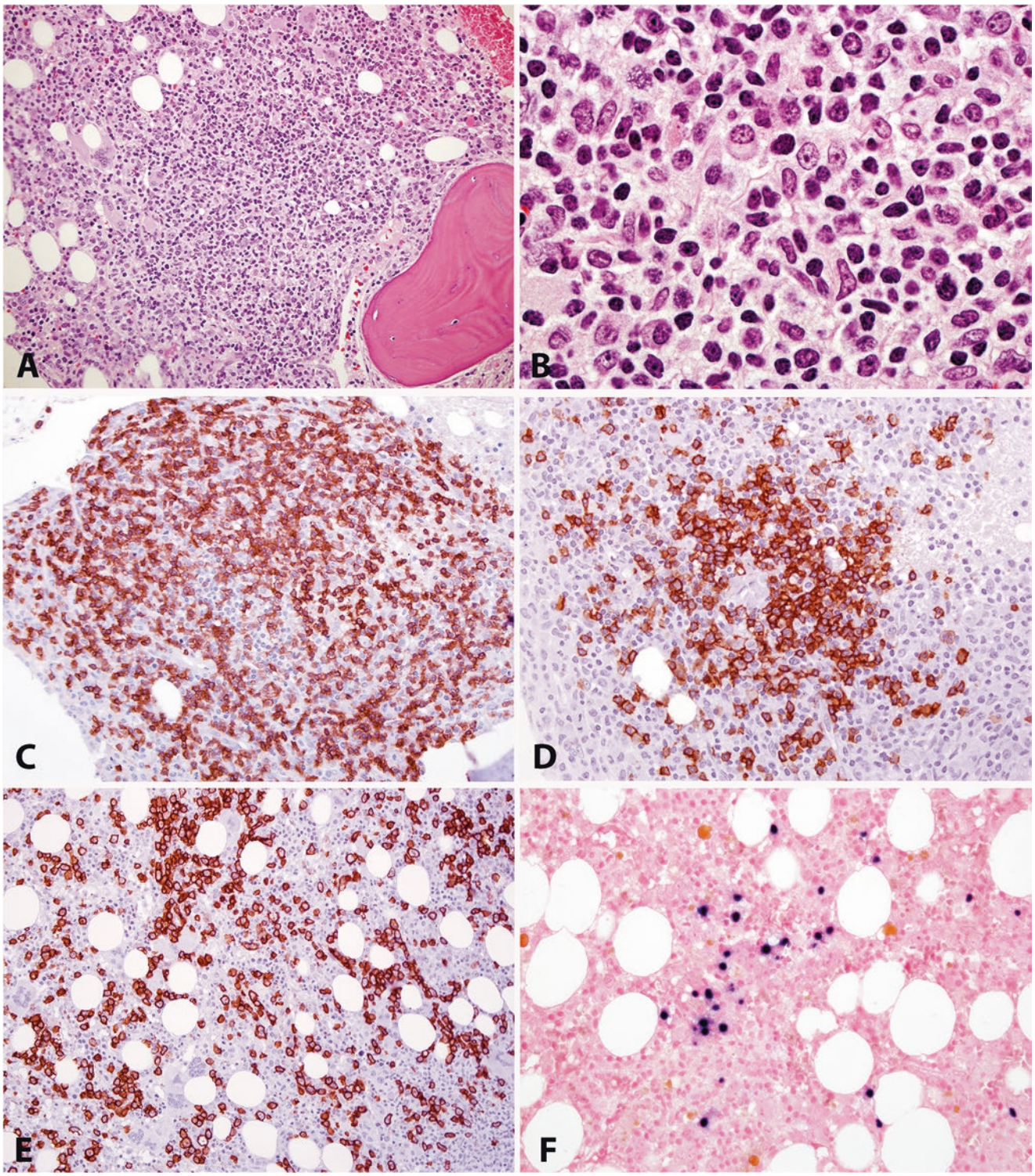

Fig. 8.1 Polymorphic lymphoid proliferation involving the bone marrow in a 43-year-old woman with HIV infection. (**a**) The bone marrow core biopsy shows multiple lymphoid aggregates and interstitial lymphoplasmacytic infiltrates. (**b**) The infiltrate is composed of a mixture of lymphocytes, plasma cells, and histiocytes. The lymphocytes are predominantly small to intermediate in size, but occasional large immunoblasts are also present. (**c**) The majority of lymphocytes are CD3+ T cells. (**d**) CD20+ B cells are present but are much less numerous than T cells. (**e**) Frequent plasma cells are seen and highlighted by CD138 staining. These plasma cells show a polytypic staining pattern for cytoplasmic kappa and lambda light chains (not shown). (f) In situ hybridization for EBV-encoded RNA (EBER) shows scattered positive cells. Flow cytometric analysis revealed a predominant T-cell population without immunophenotypic abnormality except for an inverted CD4-to-CD8 cell ratio. The B-cell population showed a polyclonal staining pattern for surface kappa and lambda light chains

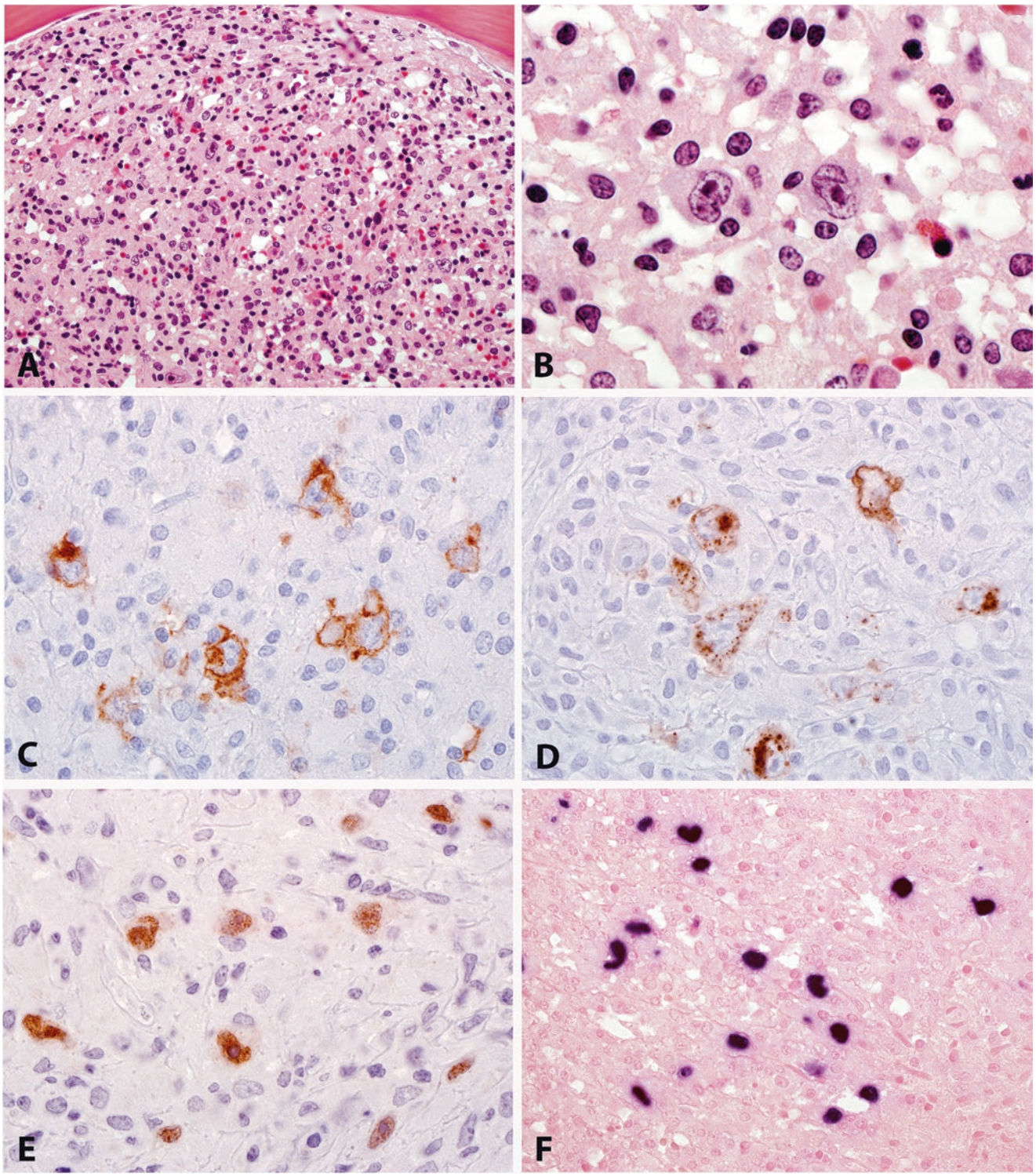

Fig. 8.2 Classical Hodgkin lymphoma identified initially in a bone marrow biopsy of a 40-year-old man with HIV infection. (**a**) The bone marrow is focally effaced by fibrosis and a polymorphous infiltrate composed of small lymphocytes, histiocytes, plasma cells, eosinophils, and scattered large, atypical cells. (**b**) The large cells contain large nuclei and prominent eosinophilic nucleoli, consistent with Hodgkin cells. The large cells are positive for CD30 (**c**), CD15 (**d**), PAX-5 (**e**), and EBER (**f**) and negative for CD45, CD20, and CD3 (not shown)

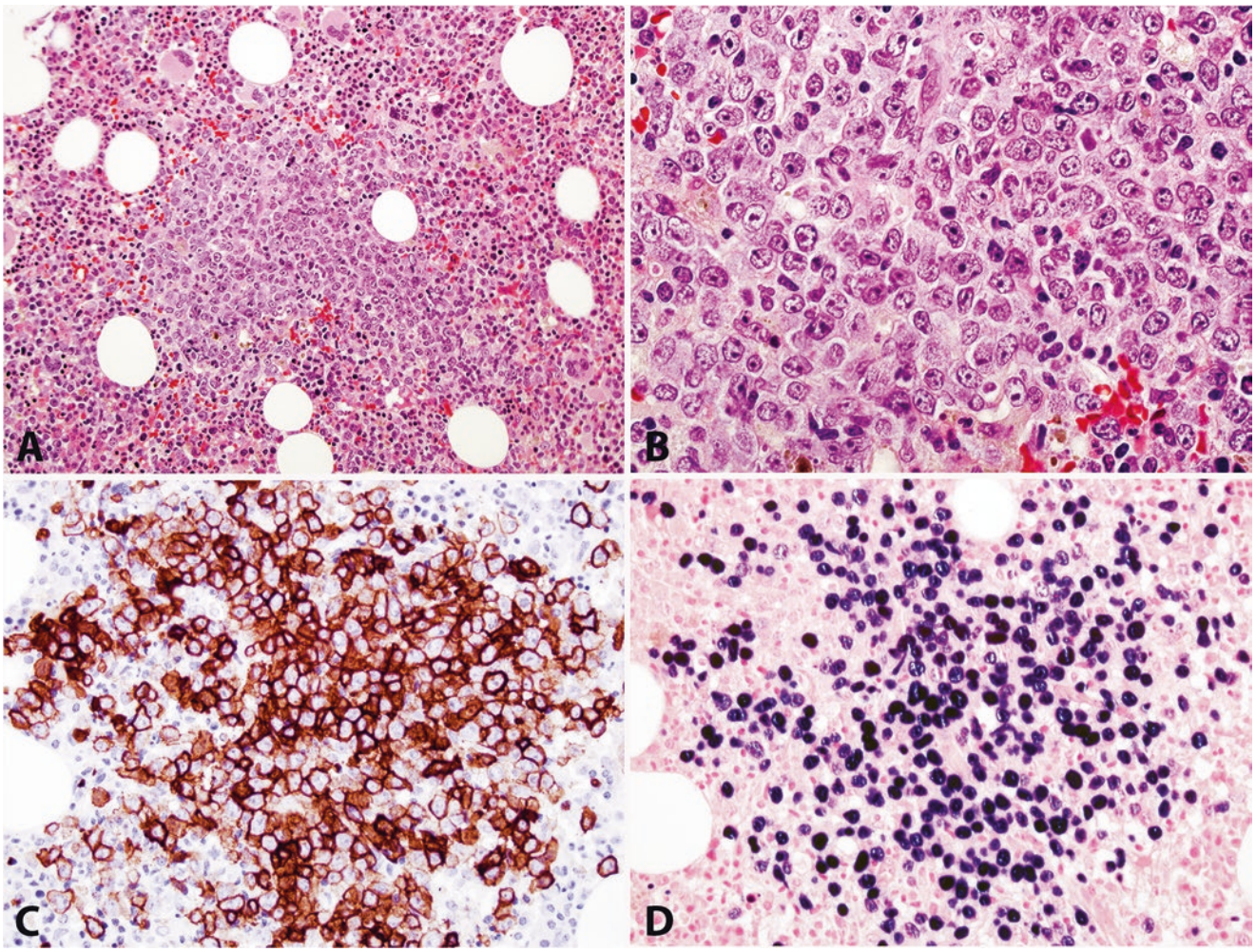

Fig. 8.3 High-grade B-cell lymphoma involving the bone marrow in a 50-year-old woman with HIV infection and a newly diagnosed high-grade B-cell lymphoma with *MYC* gene rearrangement. (a) The bone marrow core biopsy shows lymphoid aggregates composed of large lymphoid cells. (b) The large cells have distinct to prominent nucleoli and ample amphophilic cytoplasm. The large cells are positive for CD20 (**c**) and EBER (**d**). Cytogenetic studies revealed a complex karyotype with three separate clones, and each clone had t(8;14)(q24,1;q32)

plasma cell myeloma, and rare NK/T-cell lymphoma have also been reported) (Figs. 8.5, 8.6, 8.7, and 8.8) [13]. Neither EBV status, based on in situ hybridization for EBV-encoded RNA (EBER), nor the type of organ transplanted is statistically significant in predicting the presence or absence of bone marrow involvement [13]. The morphologic findings of bone marrow involvement by PTLD vary from lymphoid aggregates, interstitial infiltration, and increased plasma cells to architectural, destructive lesions consisting of sheets of atypical lymphocytes [13–15]. The bone marrow involvement by early lesions or polymorphic PTLD can be subtle and may overlap with reactive or infectious conditions. The positive EBER is seen in scattered hematopoietic cells or in aggregates, co-localized with lymphocytes, plasmacytoid lymphocytes, or plasma cells [14]. In cases with subtle morphologic findings such as small lymphoid aggregates and mild plasmacytosis, the presence of rare EBER-positive cells could be expected in posttransplant immunodeficiency; this is not considered definitive evidence of bone marrow involvement by PTLD [14]. However, the presence of cytologic atypia, extensive necrosis or increased large transformed cells, and detection of clonality or chromosomal aberrancies favor a lymphoproliferative process [14, 16]. The morphologic findings of monomorphic PTLD are similar to the corresponding lymphoma occurring in immunocompetent patients; the bone marrow involvement ranges from subtle interstitial infiltrates highlighted by immunohistochemistry to overt nodular or diffuse infiltrates [13, 15].

Table 8.1 Bone marrow involvement by HIV-associated lymphoproliferative disorders

Type of lesions	Histologic subtypes	Frequency of involvement	Viral status	Morphology
Polymorphic lymphoid proliferation	Polymorphous lymphoid proliferation	Less common than in PTLD setting	Often EBV+	A range of lymphoid cells from small plasmacytoid to immunoblasts
Lymphomas also occurring in immunocompetent patients	Diffuse large B-cell lymphoma	12–16% [4, 19]	30–90% EBV+ [20]	Numerous centroblasts or immunoblasts with plasmacytoid features
	Burkitt lymphoma	31% [4]	30–70% EBV+ [20]	Similar to Burkitt lymphoma in immunocompetent patients, some with more plasmacytoid features
	Classical Hodgkin lymphoma	14% [2]	Nearly all EBV+ [20]	Space-occupying lesions with polymorphous infiltrates and Reed-Sternberg cells or variants
Lymphomas occurring specifically in HIV patients	Primary effusion lymphoma	11% [5]	Universally HHV8+, commonly EBV+	Sheets of large cells with plasmablastic or immunoblastic morphology
	Plasmablastic lymphoma	6–39% [21, 22]	91% EBV+ [21]	Sheets of large cells with plasmablastic morphology

EBV, Epstein-Barr virus; HHV8, human herpesvirus 8; PTLD, posttransplant lymphoproliferative disorder

Table 8.2 Bone marrow involvement by posttransplant lymphoproliferative disorders

Type of lesions	Frequency of involvement	EBV status	Morphology	Treatment and outcome
Early lesions	Rare	Virtually all EBV+	Lymphoid aggregates; polyclonal plasma cell hyperplasia	Tend to regress spontaneously or with reduction of immunosuppressant
Polymorphic PTLD	15.7% [13]	Majority EBV+	Polymorphous proliferation with a full spectrum of B-cell differentiation admixed with immunoblasts	Tapering of immunosuppressant with or without rituximab
Monomorphic PTLD	23.5% [13]	EBV+/−	Diffuse large B-cell lymphoma, Burkitt lymphoma, plasmacytoma-like lesion, plasma cell myeloma, NK/T-cell lymphoma	Chemotherapy; bone marrow involvement is associated with worse outcomes
Classical Hodgkin lymphoma	Rare	Majority EBV+	Morphologic features similar to classical Hodgkin lymphoma in immunocompetent patients	Chemotherapy; bone marrow involvement is associated with worse outcomes

EBV, Epstein-Barr virus; PTLD, posttransplant lymphoproliferative disorder

Iatrogenic Immunodeficiency-Related Disorders

Analogous to what has been observed in PTLDs, iatrogenic immunodeficiency-associated LPDs may occur in patients with rheumatologic diseases or inflammatory conditions treated with immune modulatory drugs (Fig. 8.9). Immunodeficiency-associated LPDs arising in clinical settings other than transplantation are morphologically similar to PTLDs, though extranodal involvement is frequent and bone marrow involvement is uncommon [17, 18]. Overall, the information regarding bone marrow involvement by immunodeficiency-associated LPDs in non-transplant patients is limited.

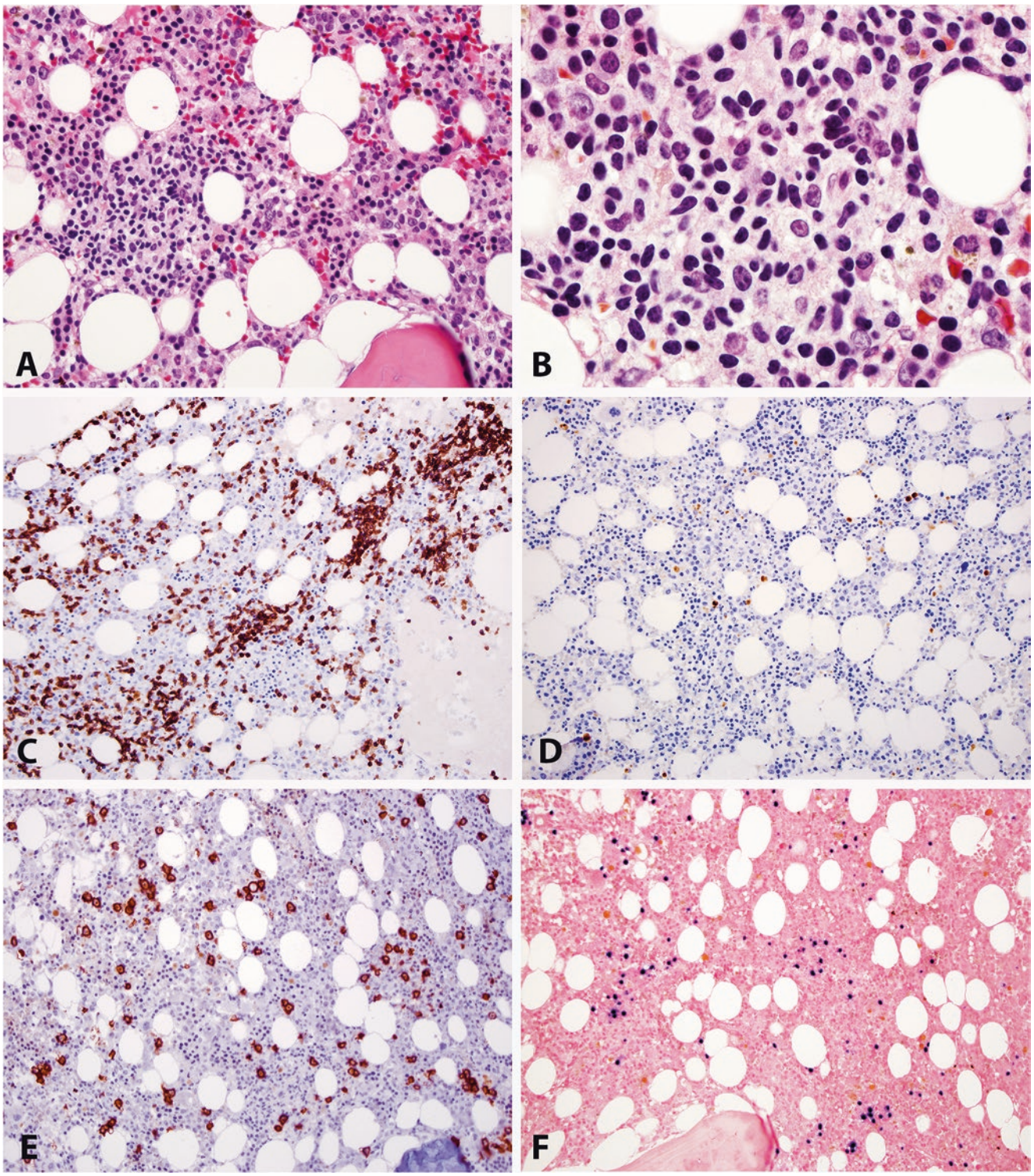

Fig. 8.4 Polymorphic posttransplant lymphoproliferative disorder (PTLD) involving the bone marrow in a 32-year-old man with history of hematopoietic stem cell transplantation for aplastic anemia 4 months ago, now with increasing lymphadenopathy and EBV titers. (**a**) The bone marrow core biopsy shows an abnormal lymphoid infiltrate in aggregates and with an interstitial infiltration pattern. (**b**) The lymphocytes are predominantly small; admixed histiocytes and occasional plasma cells are present. (**c**) Immunostaining for CD3 shows that the lymphoid infiltrate is composed predominantly of CD3+ T cells. (**d**) Very rare CD20+ B cells are seen (<1%). (**e**) Increased plasma cells (CD138+) are also present but show a polytypic staining pattern for cytoplasmic kappa and lambda light chains. (**f**) In situ hybridization for EBER shows scattered positive cells throughout the bone marrow section. Flow cytometric analysis identified a very small, monotypic B-cell population (<1% of total cells) that was negative for CD5 and CD10. The T cells showed an inverted CD4-to-CD8 cell ratio

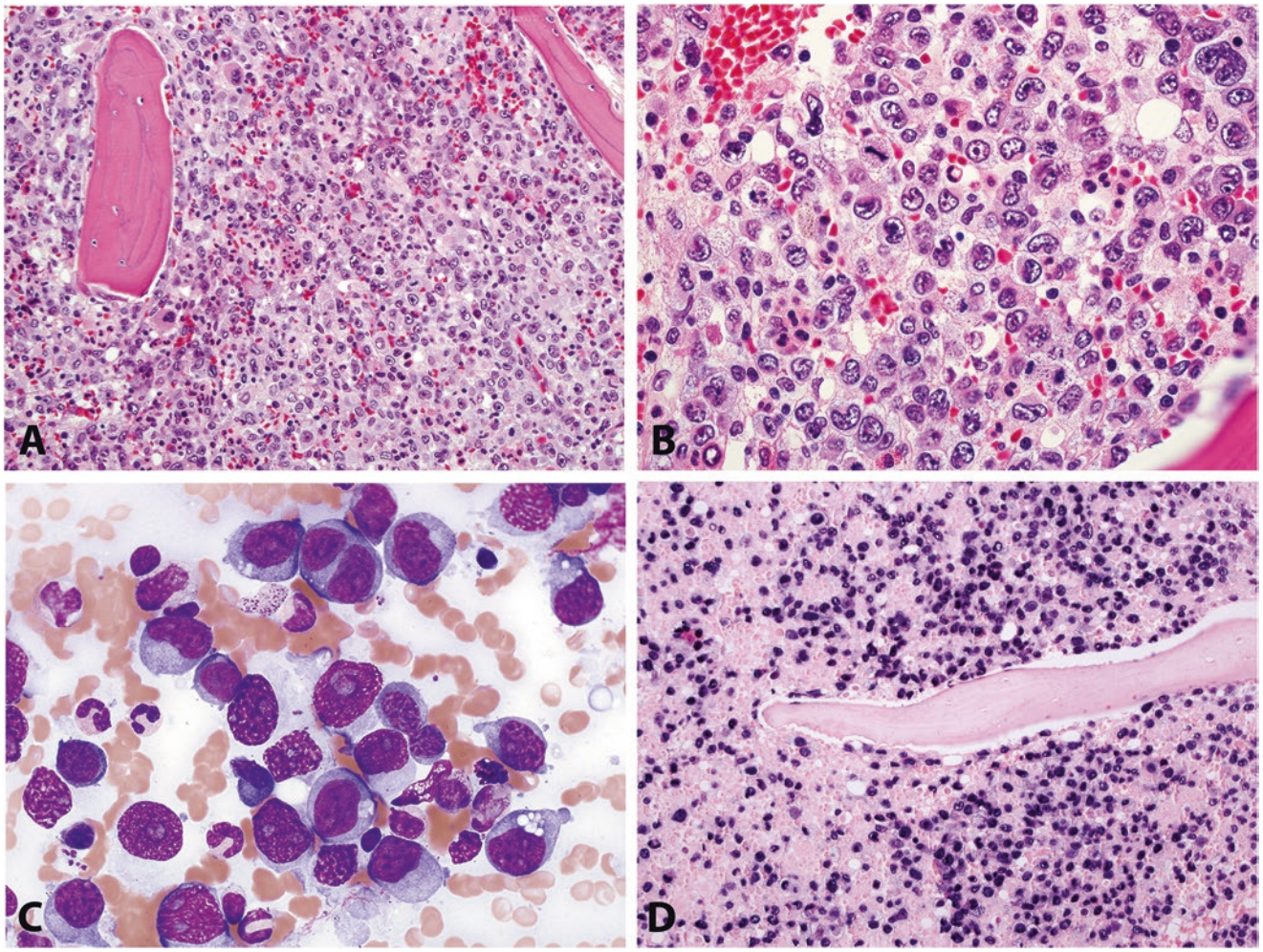

Fig. 8.5 Monomorphic posttransplant lymphoproliferative disorder (PTLD), diffuse large B-cell lymphoma (DLBCL), involving the bone marrow in a 23-year-old man with history of heart transplantation for restrictive cardiomyopathy 20 years ago. (**a**) The bone marrow core biopsy shows diffuse infiltration by large lymphoid cells. (**b**) The large cells have large nuclei, prominent nucleoli, and ample amphophilic cytoplasm. (**c**) The bone marrow aspirate smear shows large lymphoid cells with large nuclei, prominent nucleoli, and abundant basophilic cytoplasm. (**d**) The large cells are positive for EBER by in situ hybridization

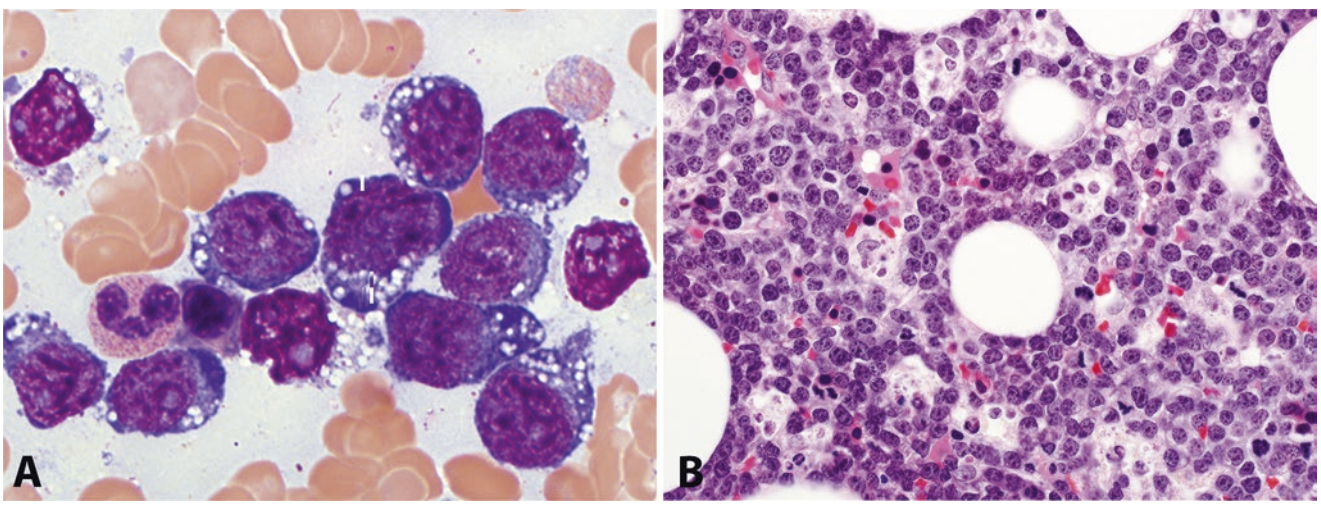

Fig. 8.6 Monomorphic posttransplant lymphoproliferative disorder (PTLD) , Burkitt lymphoma, involving the bone marrow in a 65-year-old man with history of orthotopic renal transplantation 6 years ago and a recent diagnosis of monomorphic PTLD, Burkitt lymphoma, in a lymph node biopsy. (**a**) The bone marrow aspirate smear shows medium-sized lymphocytes with high nuclear-to-cytoplasmic ratio and deeply basophilic and vacuolated cytoplasm. (**b**) The bone marrow core biopsy shows a lymphoid infiltrate composed of a monotonous population of medium-sized lymphocytes with admixed scattered, tingible body macrophages, with a "starry sky" appearance. EBER is negative (not shown). Cytogenetic analysis is positive for t(2;8)(p11.2;q24.1), a variant *MYC* gene rearrangement involving the *IGK* gene

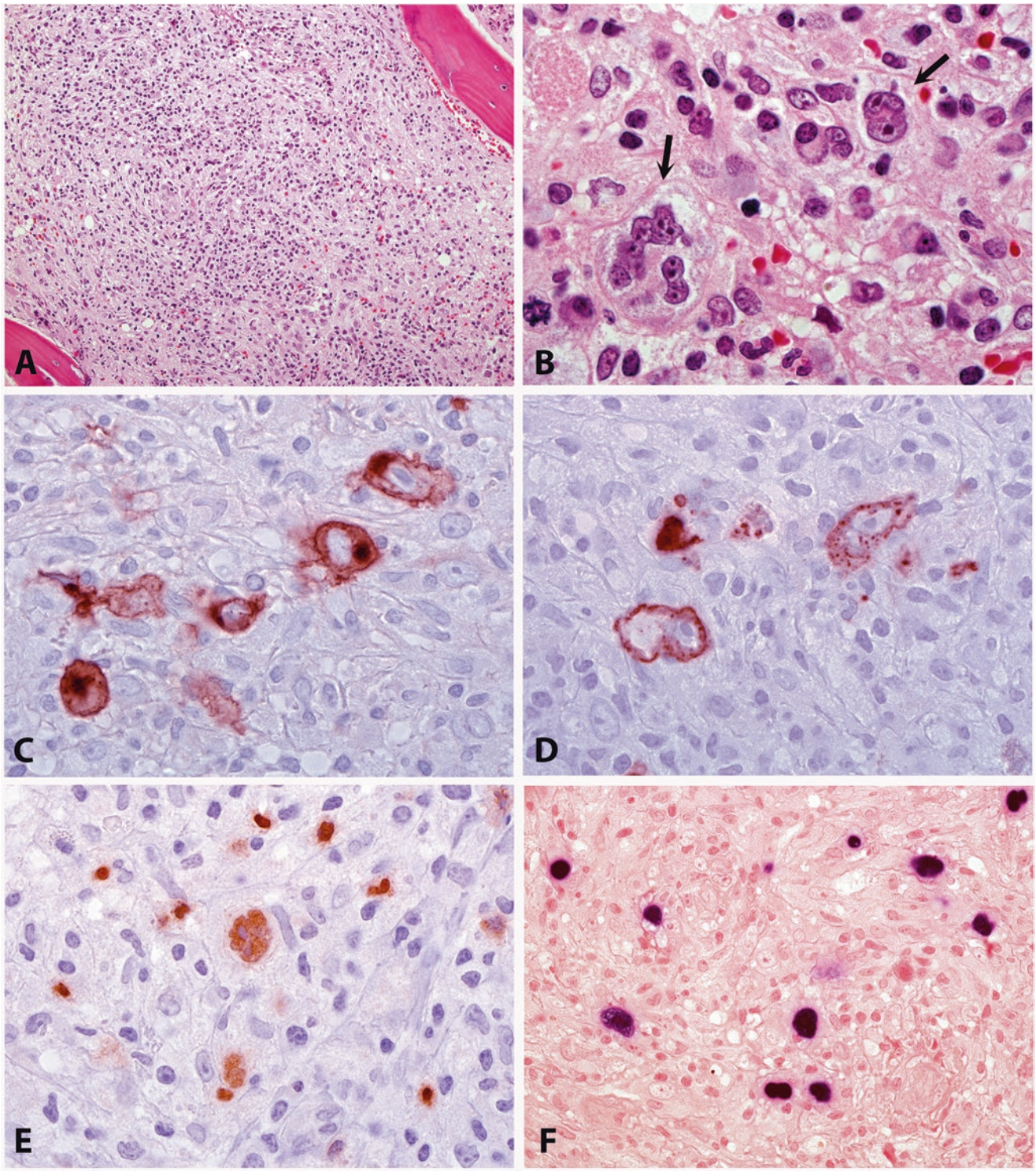

Fig. 8.7 Monomorphic posttransplant lymphoproliferative disorder (PTLD) , classical Hodgkin lymphoma type, involving the bone marrow in a 42-year-old man with history of orthotopic liver transplantation for autoimmune hepatitis with new-onset anemia and thrombocytopenia. (**a**) The bone marrow core biopsy shows extensive polymorphous cellular infiltrates in a background of fibrosis. (**b**) There are occasional mononuclear Hodgkin cells and bilobed or multinucleated Reed-Sternberg cells (*arrows*) in a background of fibrosis and inflammatory infiltrates composed of small lymphocytes, plasma cells, histiocytes, and occasional eosinophils. The large cells are positive for CD30 (**c**), CD15 (**d**), PAX-5 (**e**), and EBER (**f**)

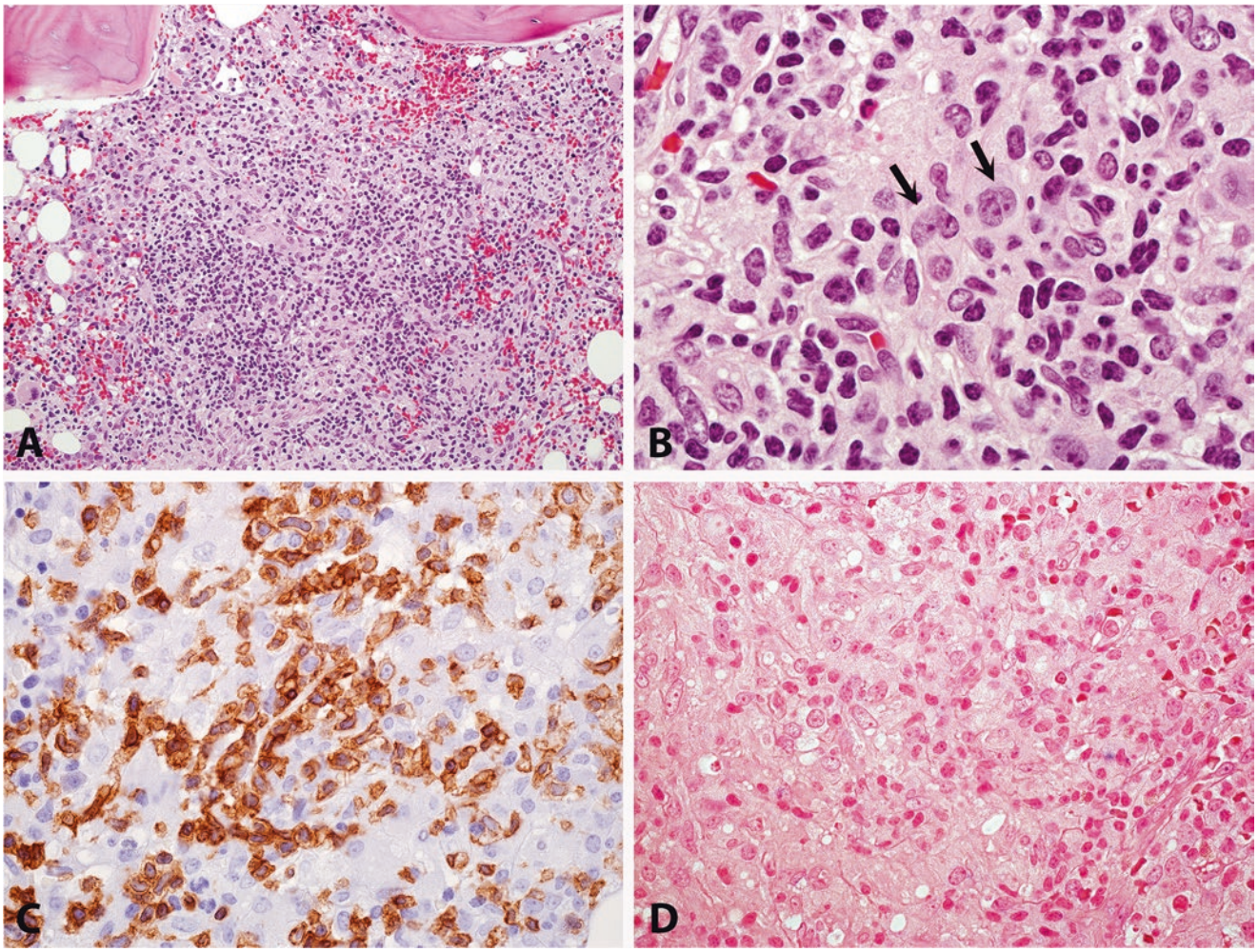

Fig. 8.8 Monomorphic posttransplant lymphoproliferative disorder (PTLD) , peripheral T-cell lymphoma, not otherwise specified (PTCL-NOS), involving the bone marrow in a 50-year-old man with a history of renal transplantation 15 months ago for end-stage renal disease secondary to hypertension and a recently diagnosed PTLD, PTCL-NOS, in a lymph node biopsy. (**a**) The bone marrow core biopsy shows multifocal lymphohistiocytic infiltrates. (**b**) The lymphocytes are predominantly small with irregular nuclei; rare Hodgkin-like cells are also present (arrows). (**c**) The vast majority of lymphocytes are CD3+ T cells. (**d**) EBER is negative. Flow cytometric analysis showed T cells with loss of CD7, similar to the lymph node biopsy

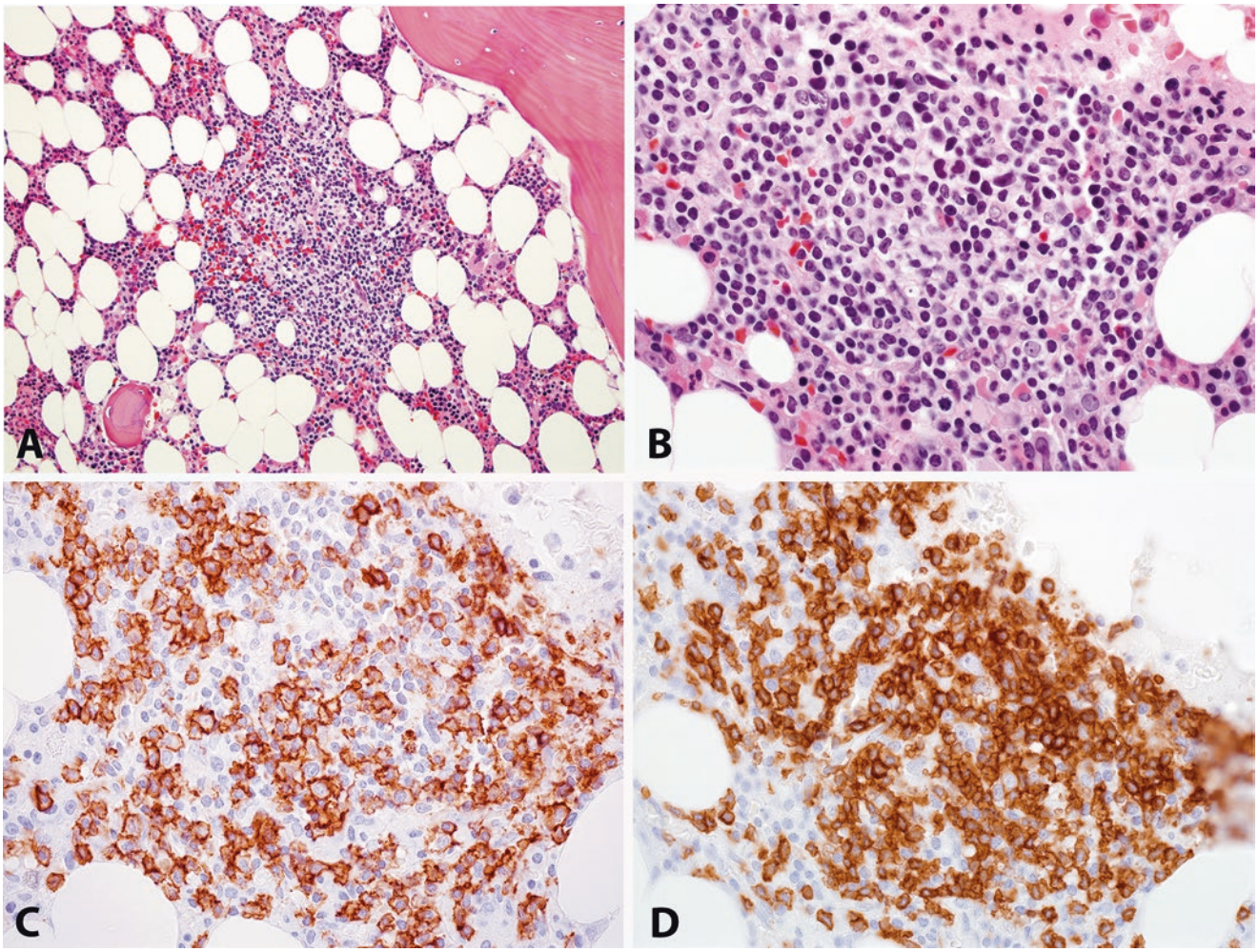

Fig. 8.9 Polymorphic-type LPD involving the bone marrow in a 47-year-old woman with a history of systemic lupus erythematosus treated with methotrexate and a recent diagnosis of polymorphic-type iatrogenic immunodeficiency-associated lymphoproliferative disorder in a lymph node biopsy. (**a**) The bone marrow core biopsy shows lymphoid aggregates and interstitial infiltration of lymphocytes with admixed histiocytes. (**b**) The lymphocytes are predominantly small, with slightly irregular nuclei and scant cytoplasm. (**c**) Immunostaining for CD20 shows many B cells ranging from small to medium in size. (**d**) Abundant CD3+ T cells are present. Occasional EBER+ cells were seen (not shown). Flow cytometric analysis did not identify monotypic B cells or immunophenotypically abnormal T cells

References

1. Corti M, Villafane M, Minue G, Campitelli A, Narbaitz M, Gilardi L. Clinical features of AIDS patients with Hodgkin's lymphoma with isolated bone marrow involvement: report of 12 cases at a single institution. Cancer Biol Med. 2015;12:41–5.
2. Ponzoni M, Fumagalli L, Rossi G, Freschi M, Re A, Vigano MG, et al. Isolated bone marrow manifestation of HIV-associated Hodgkin lymphoma. Mod Pathol. 2002;15:1273–8.
3. Said JW. Immunodeficiency-related Hodgkin lymphoma and its mimics. Adv Anat Pathol. 2007;14:189–94.
4. Schommers P, Hentrich M, Hoffmann C, Gillor D, Zoufaly A, Jensen B, et al. Survival of AIDS-related diffuse large B-cell lymphoma, Burkitt lymphoma, and plasmablastic lymphoma in the German HIV Lymphoma Cohort. Br J Haematol. 2015;168:806–10.
5. Boulanger E, Agbalika F, Maarek O, Daniel MT, Grollet L, Molina JM, et al. A clinical, molecular and cytogenetic study of 12 cases of human herpesvirus 8 associated primary effusion lymphoma in HIV-infected patients. Hematol J. 2001;2:172–9.
6. Morrison VA, Dunn DL, Manivel JC, Gajl-Peczalska KJ, Peterson BA. Clinical characteristics of post-transplant lymphoproliferative disorders. Am J Med. 1994;97:14–24.
7. Maecker B, Jack T, Zimmermann M, Abdul-Khaliq H, Burdelski M, Fuchs A, et al. CNS or bone marrow involvement as risk factors for poor survival in post-transplantation lymphoproliferative disorders in children after solid organ transplantation. J Clin Oncol. 2007;25:4902–8.
8. Dotti G, Fiocchi R, Motta T, Mammana C, Gotti E, Riva S, et al. Lymphomas occurring late after solid-organ transplantation: influence of treatment on the clinical outcome. Transplantation. 2002;74:1095–102.
9. Muti G, Cantoni S, Oreste P, Klersy C, Gini G, Rossi V, et al. Post-transplant lymphoproliferative disorders: improved outcome after clinico-pathologically tailored treatment. Haematologica. 2002;87:67–77.
10. Akar Ozkan E, Ozdemir BH, Yilmaz Akcay E, Terzi A, Karakus S, Haberal M. Bone marrow involvement by lymphoproliferative disorders after solid-organ transplant. Exp Clin Transplant. 2015;13(Suppl 1):183–7.

11. Hourigan MJ, Doecke J, Mollee PN, Gill DS, Norris D, Johnson DW, et al. A new prognosticator for post-transplant lymphoproliferative disorders after renal transplantation. Br J Hematol. 2008;141:904–7.
12. Knight JS, Tsodikov A, Cibrik DM, Ross CW, Kaminski MS, Blayney DW. Lymphoma after solid organ transplantation: risk, response to therapy, and survival at a transplantation center. J Clin Oncol. 2009;27:3354–62.
13. Montanari F, O'Connor OA, Savage DG, Zain JM, Venkatraman S, McCormick EK, et al. Bone marrow involvement in patients with posttransplant lymphoproliferative disorders: incidence and prognostic factors. Hum Pathol. 2010;41(8):1150.
14. Koeppen H, Newell K, Baunoch DA, Vardiman JW. Morphologic bone marrow changes in patients with posttransplantation lymphoproliferative disorders. Am J Surg Pathol. 1998;22:208–14.
15. Perry AM, Aoun P, Coulter DW, Sanger WG, Grant WJ, Coccia PF. Early onset, EBV(−) PTLD in pediatric liver–small bowel transplantation recipients: a spectrum of plasma cell neoplasms with favorable prognosis. Blood. 2013;121:1377–83.
16. Frizzera G, Hanto DW, Gajl-Peczalska KJ, Rosai J, McKenna RW, Sibley RK, et al. Polymorphic diffuse B-cell hyperplasias and lymphomas in renal transplant recipients. Cancer Res. 1981;41:4262–79.
17. Salloum E, Cooper DL, Howe G, Lacy J, Tallini G, Crouch J, et al. Spontaneous regression of lymphoproliferative disorders in patients treated with methotrexate for rheumatoid arthritis and other rheumatic diseases. J Clin Oncol. 1996;14:1943–9.
18. Hoshida Y, JX X, Fujita S, Nakamichi I, Ikeda J, Tomita Y, et al. Lymphoproliferative disorders in rheumatoid arthritis: clinicopathological analysis of 76 cases in relation to methotrexate medication. J Rheumatol. 2007;34:322–31.
19. Baptista MJ, Garcia O, Morgades M, Gonzalez-Barca E, Miralles P, Lopez-Guillermo A, et al. HIV-infection impact on clinical-biological features and outcome of diffuse large B-cell lymphoma treated with R-CHOP in the combination antiretroviral therapy era. AIDS. 2015;29:811–8.
20. Raphael M, Said J, Borisch B, Cesarman E, Harris NL. Lymphomas associated with HIV infection. In: Swerdlow SH, Campo E, Harris NL, Jaffe ES, Pileri SA, Stein H, et al., editors. WHO classification of tumours of haematopoietic and lymphoid tissues. 4th ed. Lyon: WHO Publications Center; 2008. p. 340–2.
21. Koizumi Y, Uehira T, Ota Y, Ogawa Y, Yajima K, Tanuma J, et al. Clinical and pathological aspects of human immunodeficiency virus-associated plasmablastic lymphoma: analysis of 24 cases. Int J Hematol. 2016;104:669–81.
22. Loghavi S, Alayed K, Aladily TN, Zuo Z, Ng SB, Tang G, et al. Stage, age, and EBV status impact outcomes of plasmablastic lymphoma patients: a clinicopathologic analysis of 61 patients. J Hematol Oncol. 2015;8:65.

Lymphoblastic Leukemia/Lymphoma

9

Qian-Yun Zhang

Lymphoblastic leukemia/lymphoma (i.e., acute lymphoblastic leukemia/lymphoma or ALL) is the most common type of cancer in childhood. The age-adjusted incidence rate is 3.1/100,000 in children, so approximately 2500–3000 children are diagnosed with acute lymphoblastic leukemia (ALL) each year in the United States). Approximately 80–85% of the cases are B-ALL and 10–15% are T-ALL (Table 9.1). Approximately 75% of ALL occurs in children under 6 years old, but it can occur at any age [1, 2]. Genetic factors play important roles in cancer initiation. ALL with t(12;21) *ETV6-RUNX1* fusion is found in newborn blood spots from Guthrie cards in patients who developed ALL later. Patients with Down syndrome have an increased risk for ALL, and twins and siblings of ALL patients also have an increased incidence of ALL [3]. Other factors that may contribute to the risk of developing ALL include radiation exposure, increased maternal age, male sex, and Caucasian race. Patients typically present with anemia, thrombocytopenia, and/or neutropenia-related signs and symptoms such as fatigue, weakness, shortness of breath, easy bruising, bleeding, and infection. A typical diagnostic workup for ALL patients is listed in Tables 9.2 and 9.3, with findings illustrated in Figs. 9.1, 9.2, 9.3, 9.4, 9.5, 9.6, 9.7, 9.8, 9.9, 9.10, 9.11, 9.12, 9.13, 9.14, 9.15, 9.16, 9.17, 9.18, 9.19, 9.20, 9.21, 9.22, 9.23, 9.24, 9.25, 9.26, 9.27, 9.28, 9.29, 9.30, 9.31, 9.32, 9.33, 9.34, 9.35, and 9.36.

Although ALL is primarily a disease of blood and bone marrow, some patients may present with extramedullary disease and have less than 25% blasts in the marrow; those patients meet criteria for lymphoblastic lymphoma (LBL). The definition of acute lymphoblastic leukemia (ALL) requires greater than 25% of blasts in the bone marrow, but this definition is arbitrary. ALL and LBL are biologically similar but differ in their clinical manifestations; they are collectively called ALL. Both B-ALL and T-ALL may exhibit a spectrum of maturation. Tables 9.4 and 9.5 summarize the immunophenotypic characteristics of the different stages.

The prognosis of ALL depends on clinical features, laboratory findings, genetic aberrations, and responsiveness to chemotherapy (Tables 9.6, 9.7, and 9.8 and Figs. 9.37, 9.38, and 9.39) [2, 4–6]. The overall complete remission rate in children is greater than 95% but it is much lower (60–85%) in adults. The survival rate is greater than 90% in children, 40% for ages 25 to 59 years, and less than 20% in older patients [7–10].

Q.-Y. Zhang (✉)
Department of Pathology, University of New Mexico,
Albuquerque, NM, USA
e-mail: qzhang@salud.unm.edu

T.I. George, D.A. Arber (eds.), *Atlas of Bone Marrow Pathology*, Atlas of Anatomic Pathology,
https://doi.org/10.1007/978-1-4939-7469-6_9

Table 9.1 2017 WHO classification of ALL

B-lymphoblastic leukemia/lymphoma, NOS
B-lymphoblastic leukemia/lymphoma with t(9;22)(q34.1;q11.2); *BCR-ABL1*
B-lymphoblastic leukemia/lymphoma with t(v;11q23.3); *KMT2A* rearranged
B-lymphoblastic leukemia/lymphoma with t(12;21)(p13.2;q22.1); *ETV6-RUNX1*
B-lymphoblastic leukemia/lymphoma with hyperdiploidy
B-lymphoblastic leukemia/lymphoma with hypodiploidy (hypodiploid ALL)
B-lymphoblastic leukemia/lymphoma with t(5;14)(q31.1;q32.3); *IL3-IGH*
B-lymphoblastic leukemia/lymphoma with t(1;19)(q23;p13.3); *TCF3-PBX1*
B-lymphoblastic leukemia/lymphoma, *BCR-ABL1–like*
B-lymphoblastic leukemia/lymphoma with *iAMP21*
T-lymphoblastic leukemia/lymphoma
Early T-cell precursor lymphoblastic leukemia
Provisional entity: Natural killer (NK) cell lymphoblastic leukemia/lymphoma

Table 9.2 Common tests recommended at the diagnosis and follow-up of ALL

Tests	When to do	Value of the test
Complete blood count	At diagnosis and follow-up	For diagnosis and to assess hematopoiesis
Bone marrow aspiration and core biopsy	At diagnosis and follow-up	For diagnosis and to assess residual disease and hematopoiesis
Flow cytometric study	At diagnosis and optional at follow-up	To detect leukemic cells and to monitor minimal residual disease
COG FISH panel in pediatric patients	At diagnosis and optional at follow-up	For prognosis and monitoring if there is established abnormality
Cytogenetic analysis	At diagnosis and optional at follow-up	For prognosis, for monitoring if there is established abnormality, for detection of clonal evolution
Molecular study for *BCR-ABL1* fusion	At diagnosis and follow-up	For monitoring
Ph-like workup[a]	At diagnosis	For prognosis
Metabolic panel	At diagnosis and optional at follow-up	To assess physiological status
Tumor lysis syndrome workup	At diagnosis and optional at follow-up	To assess the presence and severity of tumor lysis syndrome
Cerebrospinal fluid	At diagnosis and follow-up	For prognosis and monitoring
Radiographic study	At diagnosis, optional	To assess extramedullary involvement

COG Children's Oncology Group; *FISH* fluorescence in situ hybridization
[a]Ph-like (*BCR-ABL1*-like): ALL with gene expression profile similar to Ph + ALL but without *BCR-ABL1* fusion

Table 9.3 Bone marrow staging at follow-up; cerebrospinal fluid staging

BM stages	*BM findings*
M1 marrow	<5% blasts
M2 marrow	5% to <25% blasts
M3 marrow	≥25% of blasts
CSF stages	*CSF findings*
CNS1	No detectable leukemia cells in the CSF
CNS2	<5 white blood cells per microliter of blood and a positive cytospin preparation for blasts
CNS3	>5 white blood cells per microliter and a positive cytospin

BM bone marrow; *CSF* cerebrospinal fluid

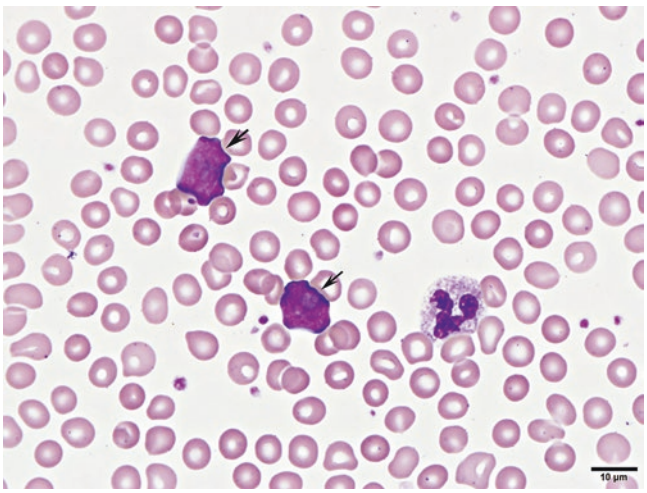

Fig. 9.1 A complete blood count (CBC) is an essential part of the workup for acute lymphoblastic leukemia/lymphoma (ALL) (Table 9.2). Peripheral blood smear review often reveals circulating blasts. This peripheral blood from a 5-month-old boy with a recent diagnosis of B-lymphoblastic leukemia shows two blasts and a neutrophil. The blasts are small to intermediate in size and have scant blue cytoplasm, fine to slightly clumped chromatin, and one or two prominent nucleoli. Scattered platelets are seen in the background. When caught early, the patient may not have peripheral blood cytopenias, such as in this case, but most patients will present with cytopenia-related signs and symptoms such as fatigue, weakness, dizziness, or shortness of breath secondary to anemia; infection secondary to neutropenia; bleeding or bruising secondary to thrombocytopenia; pain in arms, legs, or joints due to leukemic cell infiltrate; and systemic symptoms such as unexplained weight loss

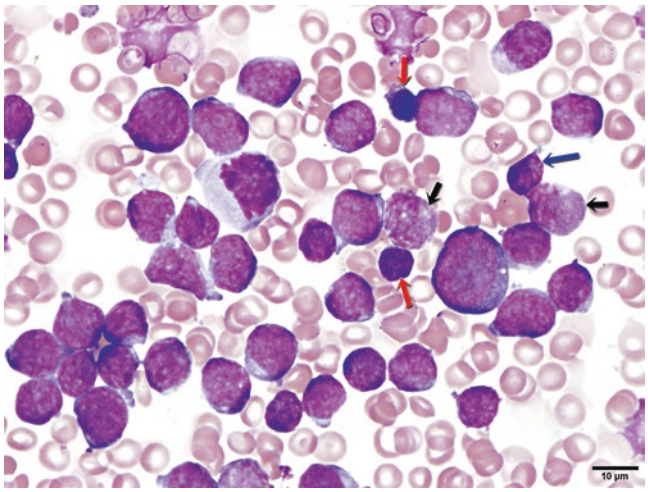

Fig. 9.3 Typically the bone marrow aspirate reveals predominantly lymphoblasts of variable size ranging from small to large. Normal hematopoietic elements are markedly reduced. In this image, a lonely erythroid precursor (red arrow), two myelocytes (black arrows), and two lymphocytes (blue arrows) are admixed with lymphoblasts

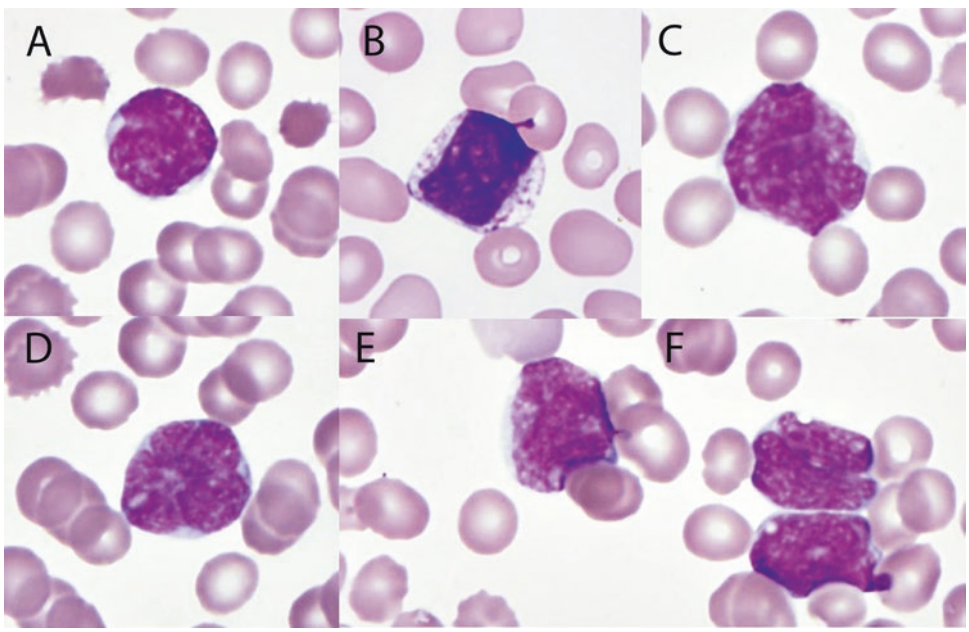

Fig. 9.2 ALL blasts can exhibit various morphology, such as seen in this composite image. The blasts can range from small to large in size. The nuclei can be round or slightly cleaved (**a**). Most blasts have scant blue cytoplasm, but rarely the blast can have moderately abundant cytoplasm with coarse azurophilic granules (**b**). Blasts can have deeply cleaved nuclei (**c**,**e**,**f**) or flower-shaped nuclei (**d**)

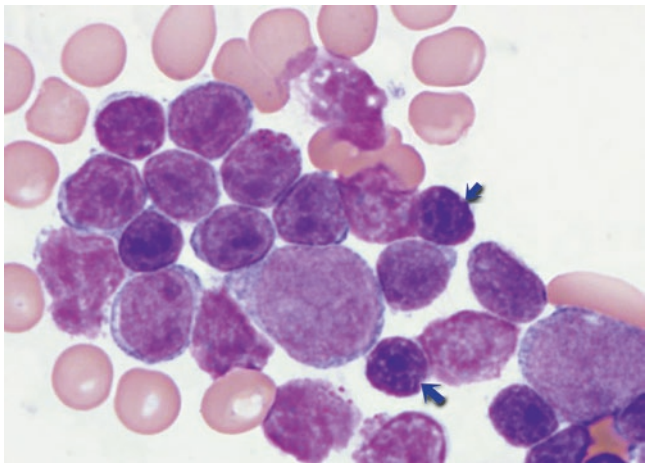

Fig. 9.4 Higher-power view of the bone marrow aspirate reveals lymphoblasts with slightly clumped chromatin pattern in the small blasts, to open and fine chromatin in the large blasts. In comparison, two small mature lymphocytes (blue arrows) are also present

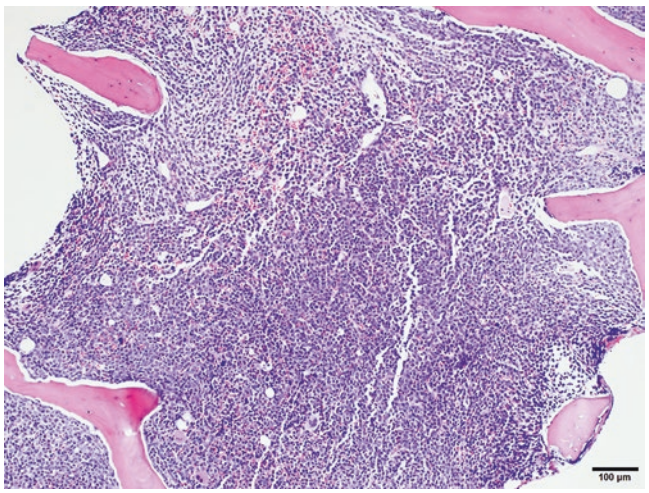

Fig. 9.5 Low-power view of a bone marrow core biopsy shows that the marrow is diffusely replaced by lymphoblasts. Admixed is markedly reduced trilineage hematopoiesis. Rare megakaryocytes can be seen at this low power

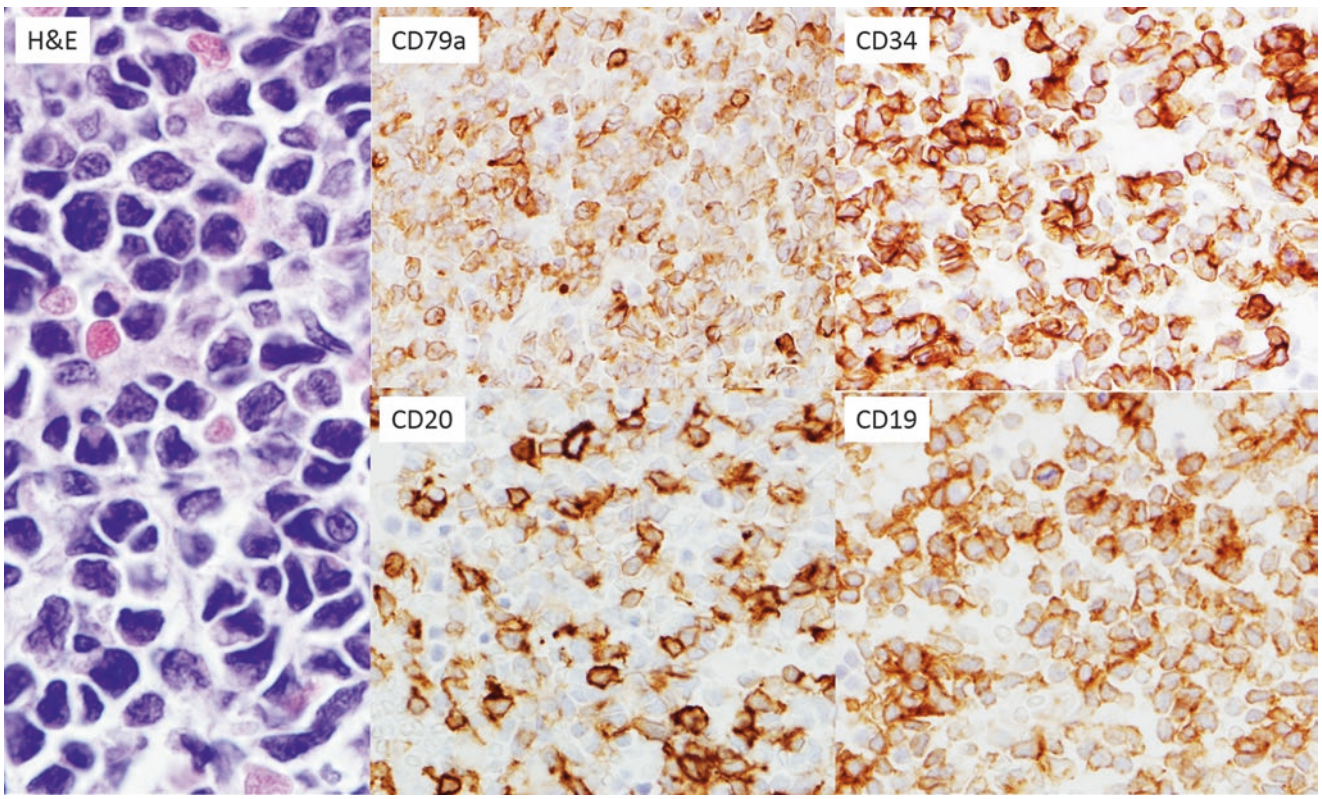

Fig. 9.6 High-power view of the bone marrow core biopsy demonstrates the lymphoblasts in detail. The blasts exhibit variation in size and have condensed to open chromatin, round to deeply cleaved nuclear contours, and inconspicuous to prominent nucleoli. Immunohistochemical stains demonstrate that the blasts express CD79a, CD34, and CD19, and a subset of cells also express CD20

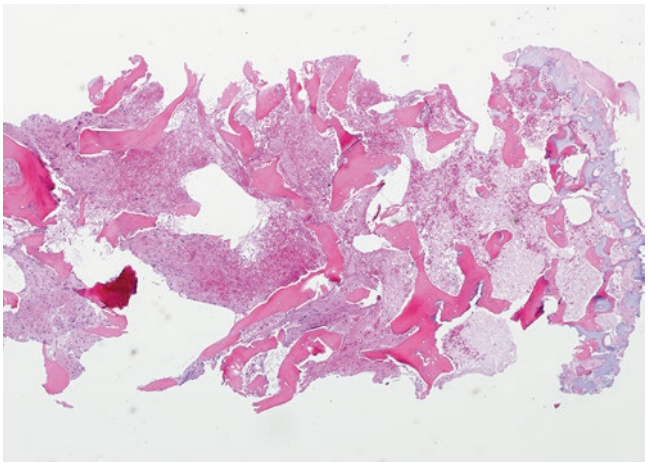

Fig. 9.7 Rarely, the marrow can be necrotic. As shown in this case, the marrow is completely necrotic, and the immunophenotype by both flow cytometry and immunohistochemical stains failed to establish the diagnosis. There were no circulating blasts in the peripheral blood. The patient had to undergo repeated bone marrow biopsy to finally reach the diagnosis of B-ALL

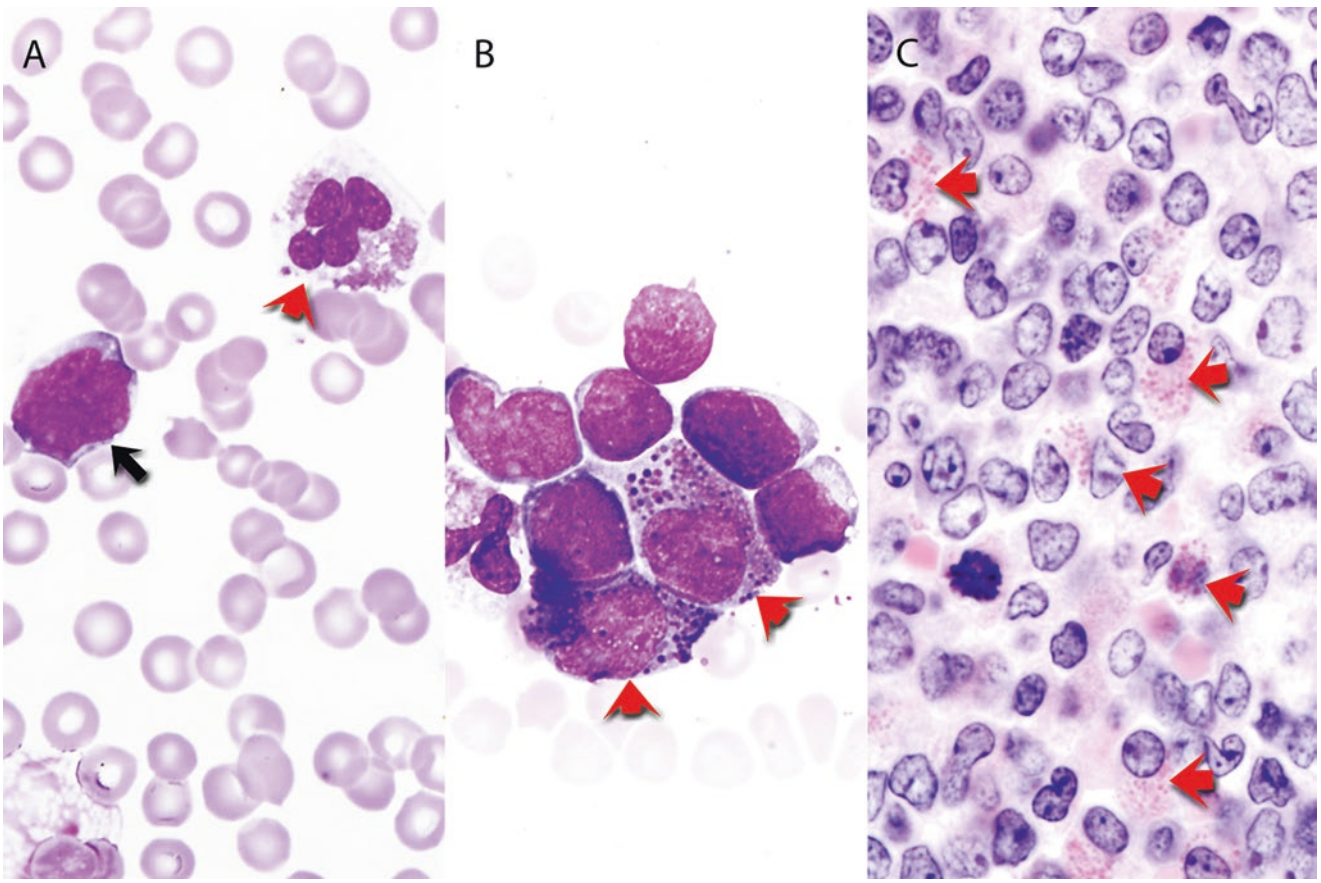

Fig. 9.8 (**a**) This patient had significant absolute eosinophilia in the peripheral blood (red arrow) in addition to circulating blasts (black arrow). (b) In the bone marrow aspirate, there were markedly increased eosinophilic precursors with mixed, coarse eosinophilic and basophilic granules (red arrows). (c) The bone marrow core biopsy showed the presence of numerous lymphoblasts with admixed eosinophilic precursors (red arrows). Cytogenetic study revealed translocation t(5;14) (q31;q32) *IL3-IGH*. This translocation involves the *IL3* gene and *IGH* gene, resulting in constitutive overexpression of the *IL3* gene, which leads to reactive eosinophilia. The eosinophils are not part of the neoplastic clone. The clinical aspects, blast morphology, and prognosis are no different from those of other types of B-ALL. The caveat regarding this type of B-ALL is that the patient may present with eosinophilia without circulating blasts. Therefore, a high index of suspicion is required in patients with eosinophilia without an apparent etiology. Bone marrow biopsy may be required to establish the diagnosis

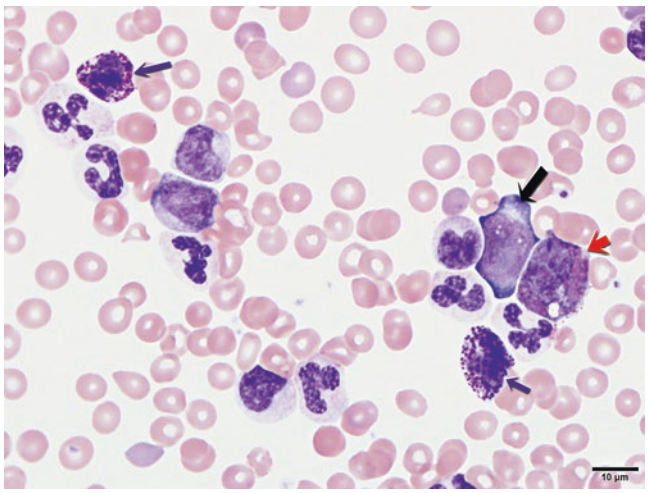

Fig. 9.9 ALL predominantly presents as de novo disease but occasionally can present as a blast crisis in patients with chronic myeloid leukemia (CML). This blood smear is from a 28-year-old man who presented with CML in chronic phase in the peripheral blood. Bone marrow biopsy revealed a blast phase with B-ALL. *BCR-ABL1* transcript is shown in Fig. 9.26

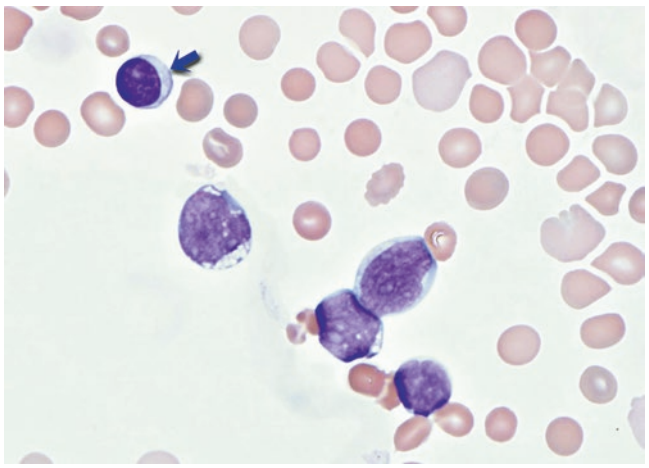

Fig. 9.11 Not infrequently, lumbar puncture may be traumatic and produce samples with peripheral blood (PB) contamination, as depicted in this image. Four blasts are present in a background of numerous red blood cells and a mature lymphocyte (blue arrow). It is not possible to distinguish whether the blasts come from PB or CSF. In this situation, a concurrent review of a PB smear is paramount to exclude a blood origin. If there are no blasts present in the PB, it is safe to assume that the blasts are from the CSF. If blasts are also present in the PB, a repeat CSF in a week or so should be recommended for further assessment

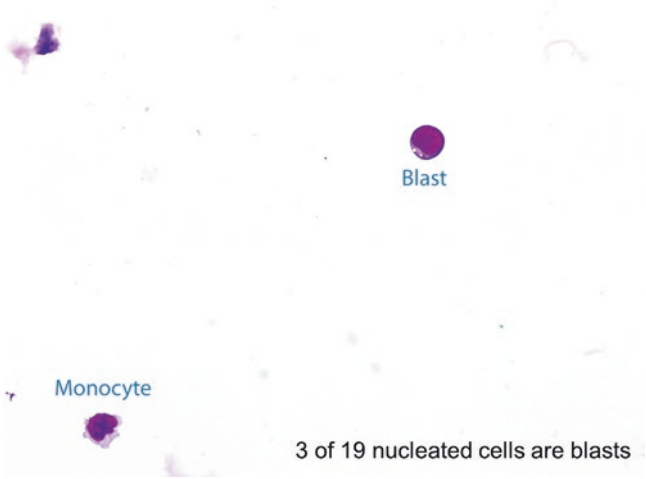

Fig. 9.10 Cerebrospinal fluid (CSF) testing is part of the standard workup for ALL (Tables 9.2 and 9.3). It is done at the time of diagnosis and periodically thereafter. A positive CSF as depicted in this image predicts an adverse prognosis. A monocyte with a moderate amount of pale cytoplasm is also seen in this image. Continuous monitoring of CSF (and testicular examination) will detect relapse of ALL, as the CNS and testes are sanctuary sites for the leukemic cells and are often the sites of relapse. Lumbar puncture also allows intrathecal delivery of chemotherapy such as methotrexate as standard of care for ALL patients

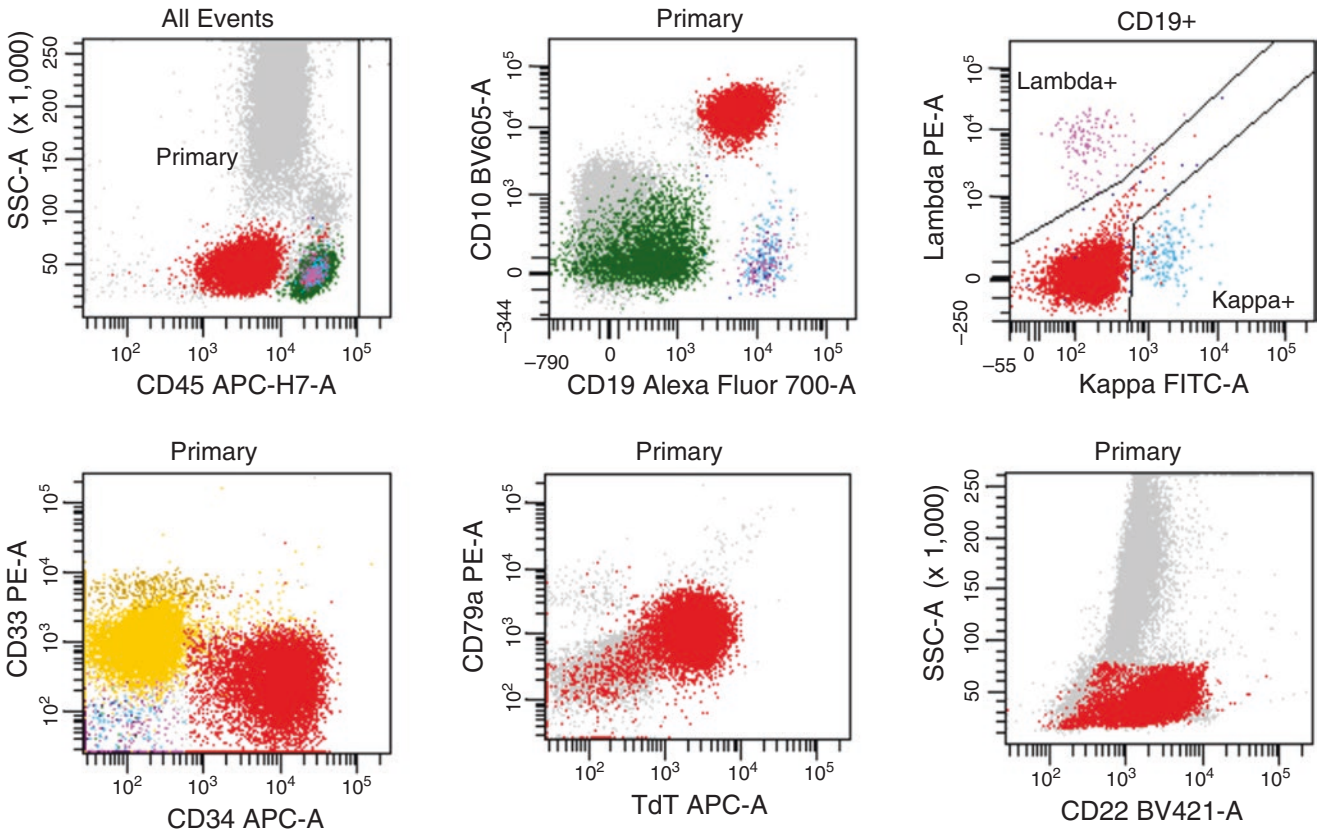

Fig. 9.12 Flow cytometric study of the blood and/or bone marrow should be performed whenever possible. Flow allows detection of six to ten antibodies simultaneously. It also allows one to detect aberrant expression of antigens with a much broader antibody panel and a sensitivity that is much superior to immunohistochemistry. It is an excellent tool for detecting minimal residual disease in the follow-up samples. ALL may arise from precursors at different maturation stages, as shown in Tables 9.4 and 9.5. Some cases of ALL have an immature immunophenotype, whereas others may exhibit mature immunophenotype. This composite flow plot illustrates a typical B-ALL flow finding, which is seen in most cases of B-ALL. The *red* population represents ALL cells that are positive for weak CD45; B-cell markers CD10, CD19, CD79a, and CD22; and immature cell markers CD34 and TdT. The blasts are negative for surface immunoglobulin light chains and the myeloid marker CD33

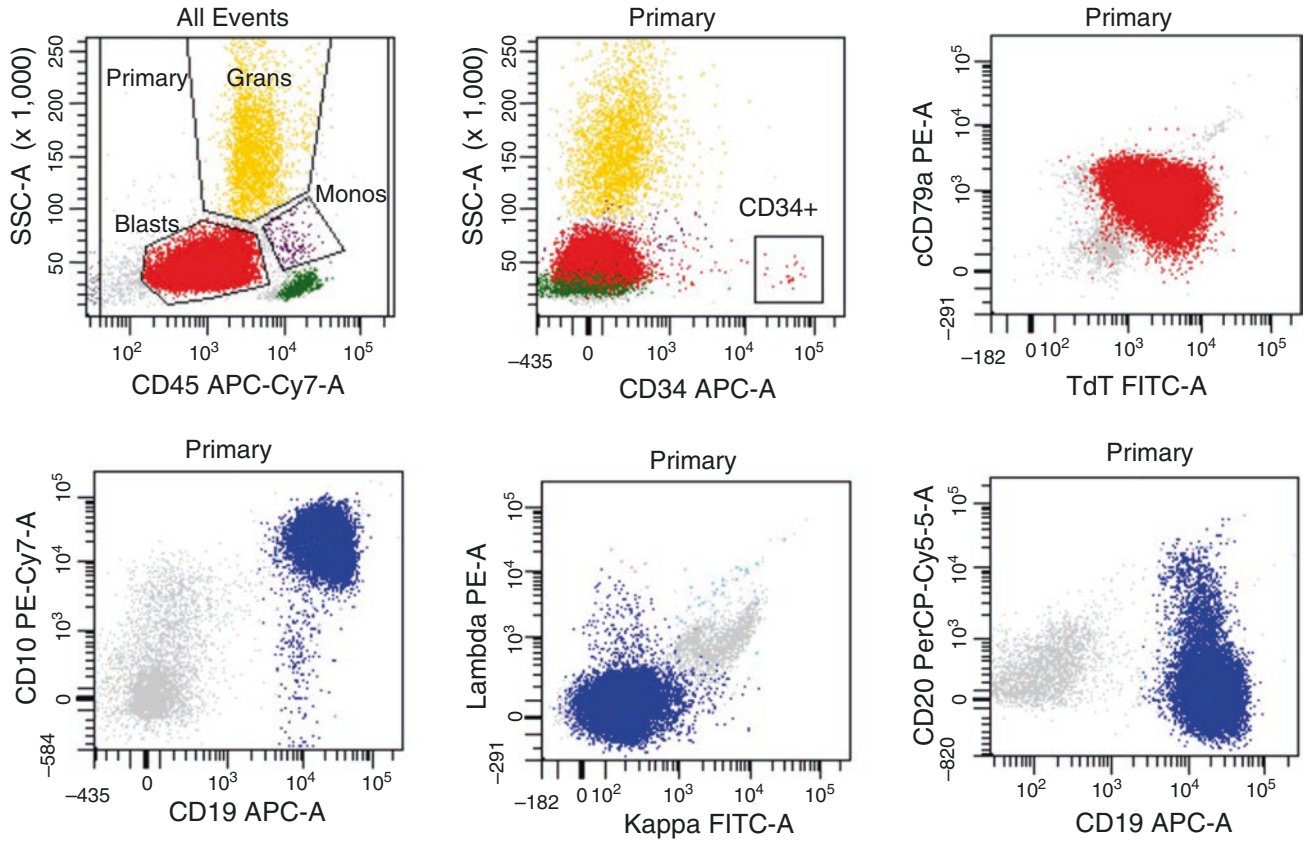

Fig. 9.13 Immunophenotype is closely associated with cytogenetic findings in certain types of ALL. Cytogenetic study is paramount in the workup of ALL, as cytogenetic abnormalities predict prognosis (Tables 9.6 and 9.7). This is an example of B-ALL with translocation (1;19) (q23;p13.3) *TCF3-PBX1*. The blast population is painted *red* on the upper panel and blue on the lower panel. Characteristically, ALLs with this translocation have a mature immunophenotype (i.e., negative for CD34). The blasts often express cytoplasmic μ chain (not done in this case) and a spectrum of CD20. The other markers expressed by the blasts include CD10, CD79a, TdT, and dim CD45. ALL with t(1;19) *TCF3-PBX1* accounts for 6% of B-ALL cases in children, but it is less common in adults. The clinical and morphologic features are indistinguishable from other types of ALL. *TCF3-PBX1* fusion has an oncologic effect. Patients with *TCF3-PBX1* ALL have an intermediate prognosis and a higher chance of CNS relapse

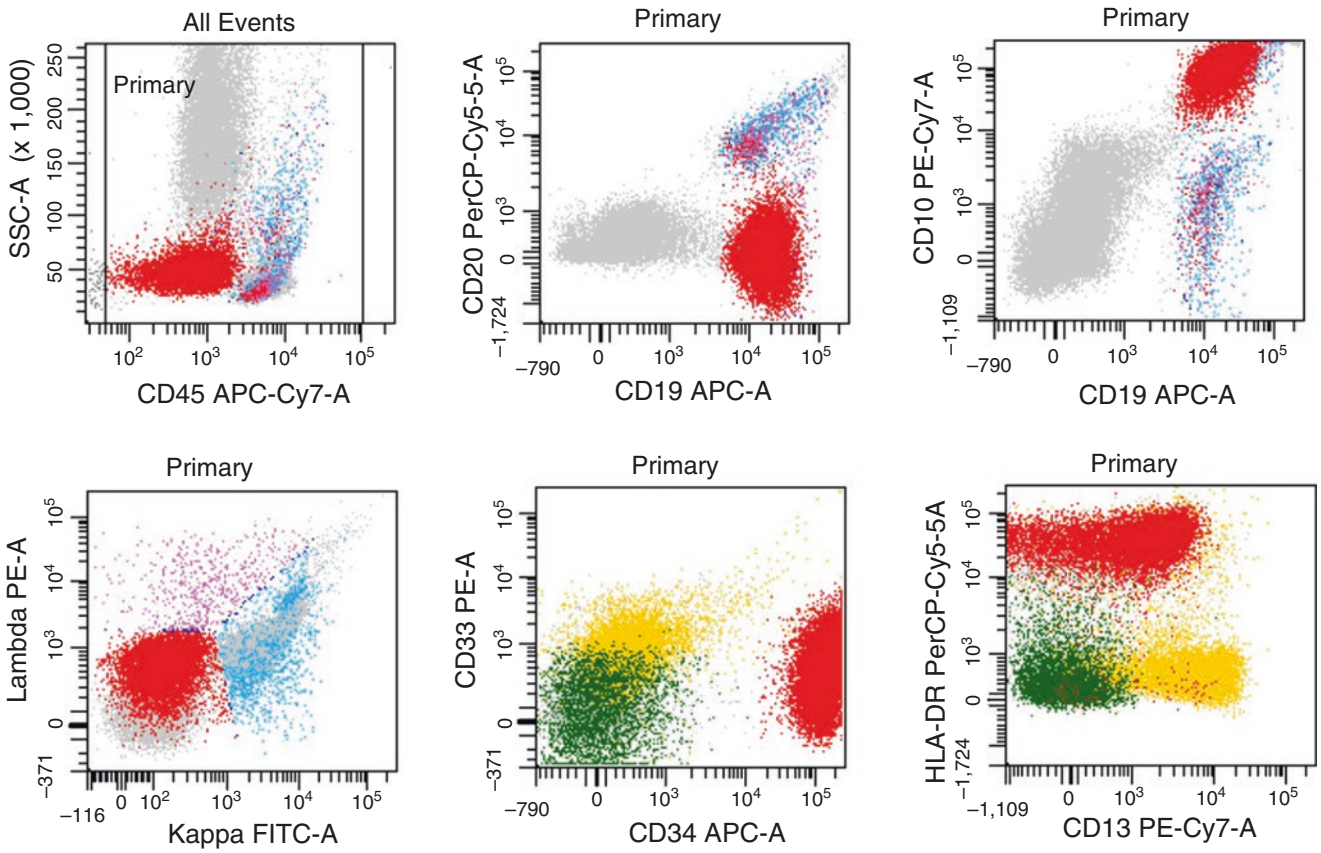

Fig. 9.14 ALL can occasionally express myeloid markers such as CD13 and CD33. This is especially prevalent in ALL with *BCR-ABL1* fusion-associated translocation 9;22 (Ph + ALL). Therefore, it is important to perform cytogenetic and/or fluorescence in situ hybridization (FISH) and/or polymerase chain reaction (PCR)-based molecular studies to exclude the translocation, as *BCR-ABL1* fusion-positive ALL carries the worst prognosis of all types of ALL. Ph + ALL accounts for 25% of adult ALL and only 2% to 4% of pediatric ALL. Most Ph + ALL cases in children produce a p190 *BCR-ABL1* fusion (see Fig. 9.27 A and B, red curve; black curve is housekeeping gene). About half of adult ALL cases produce p190 *BCR-ABL1* fusion, and the other half produce p210 *BCR-ABL1* fusion (see Fig. 9.26 A–C, green curve. The black curve is housekeeping gene. The red curve is p190 transcript, which is often seen at a low copy number at the diagnosis and often disappears after treatment). Ph + ALL tends to have hyperleukocytosis and poor response to therapy. Patients often have concurrent *IKZF1* mutation. Treatment of Ph + ALL has included a tyrosine kinase inhibitor such as imatinib, dasatinib, and nilotinib

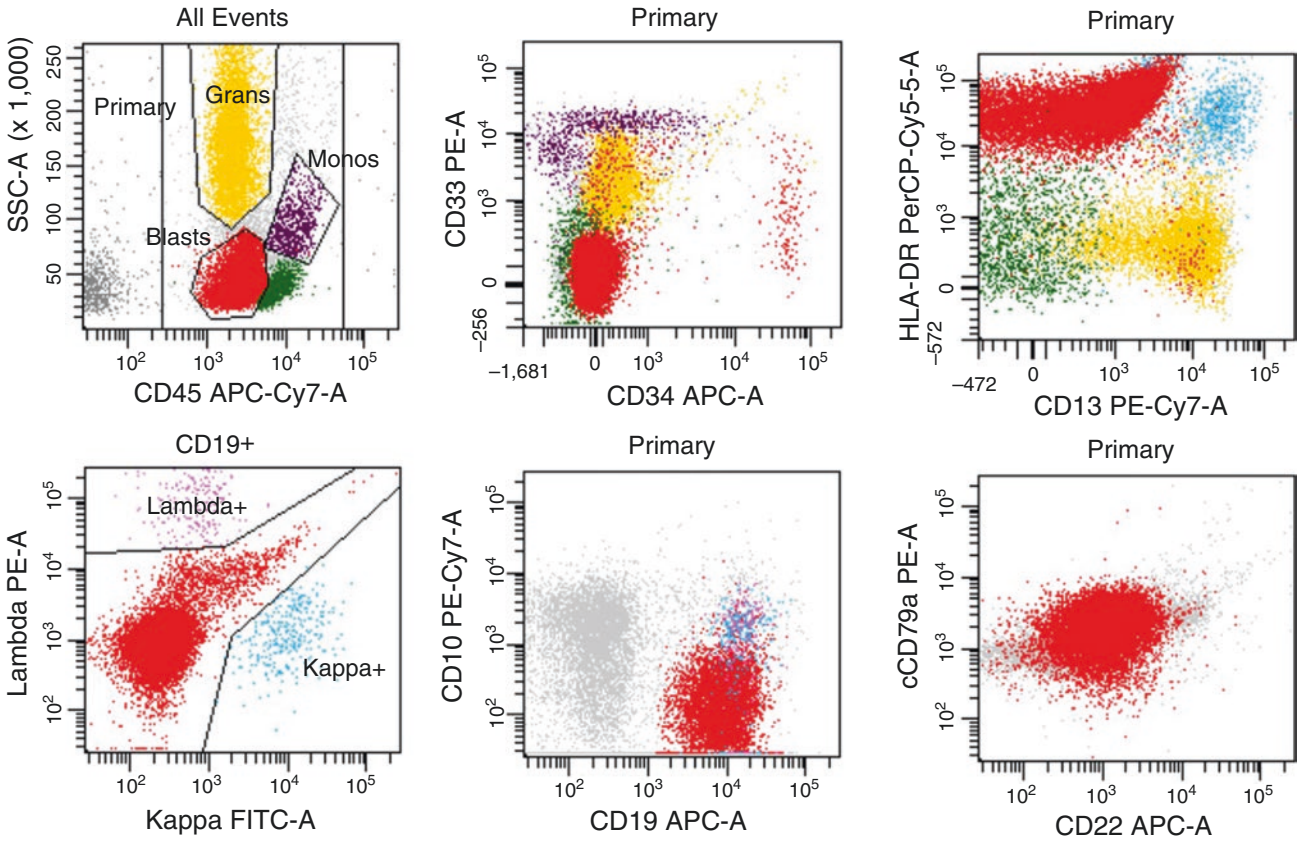

Fig. 9.15 Another type of ALL with a unique immunophenotype is ALL with *KMT2A* (i.e., *MLL*) gene rearrangement. *KMT2A* has many translocation partner genes, with t(4;11)(q21;q23) involving *AF4* and *KMT2A* genes being the most common. This translocation may occur in utero with a short latency between the translocation and the development of disease. Approximately 80% of ALLs in infants less than a year old have the *KMT2A* rearrangement. There is an increased risk of CNS involvement. The lymphoblasts are early precursors and are characteristically negative for CD10. They express CD19, CD79a, and CD22. They can also express myeloid markers such as CD13 and CD15. Leukemia with *KMT2A* translocation has a poor prognosis [11]

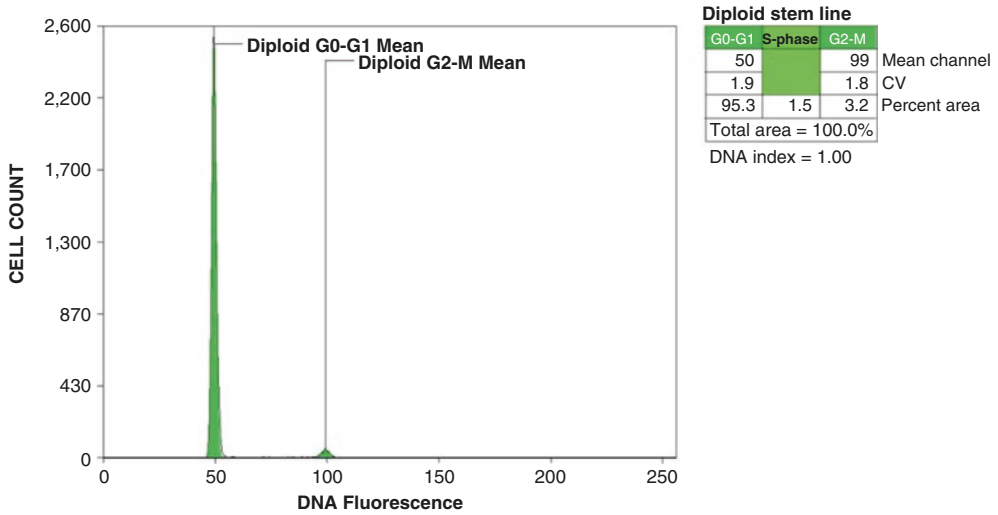

Fig. 9.16 As a routine test at the time of diagnosis, DNA index reflects the number of chromosomes in the cells (Table 9.2). This flow-based test measures DNA index with an internal diploid standard (DNA index of 1.0). As illustrated in this example, the leukemic cells are diploid, and therefore the leukemic cell peak overlaps completely with the control population; thus a single peak is seen (diploid G0-G1 mean) and the DNA index of the blasts is 1.0. The method also measures the percentages of cells in the S phase, G2 phase, and metaphase (diploid G2-M mean), although they do not have prognostic significance

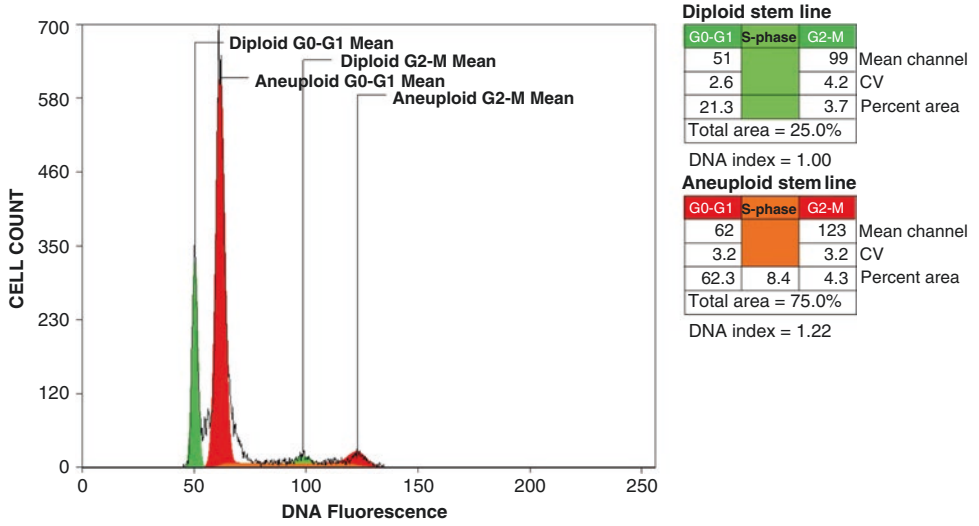

Fig. 9.17 In this DNA index study, the leukemic cells are aneuploidy with a DNA index of 1.22 (i.e., hyperdiploidy). The leukemic cell DNA content forms a separate peak (red peak, aneuploid G0-G1 mean). The diploid G0-G1 mean peak can be seen on the left as an internal control (green peak, diploid G0-G1 mean)

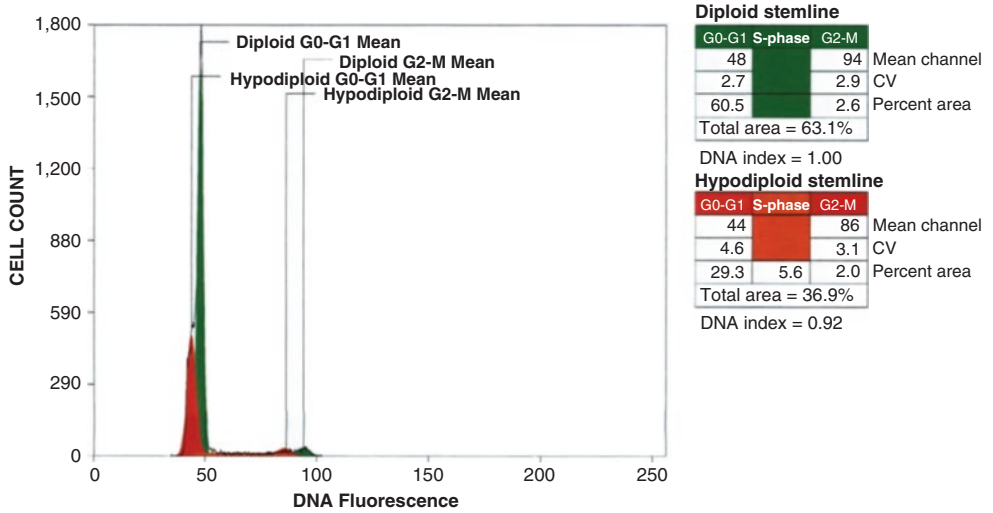

Fig. 9.18 A hypodiploid DNA index (red peak, hypodiploid G0-G1 mean) is illustrated here. The internal control diploid peak is seen on the right (green peak, diploid G0-G1 mean). The DNA index is 0.92

63~64,XY,+2,+3,+4,+5,+6,+7,+8,+10,+11,+12,+13,+14,+17,+18,+19,+21,+21,+22[cp6]/46,XY[14]

FISH reveals three copies of chromosome 4, 10, and 17

Fig. 9.19 The hyperdiploid karyotype depicted in this image (left) including triple trisomy of chromosomes 4, 10, and 17 is from a 2-year-old boy who presented with low white blood cell (WBC) count and a negative CSF; this is predictive of a good prognosis. On the right is FISH for centromeres of chromosomes 4, 10, and 17. Three copies of each chromosome (red, green, and aqua) are demonstrated here

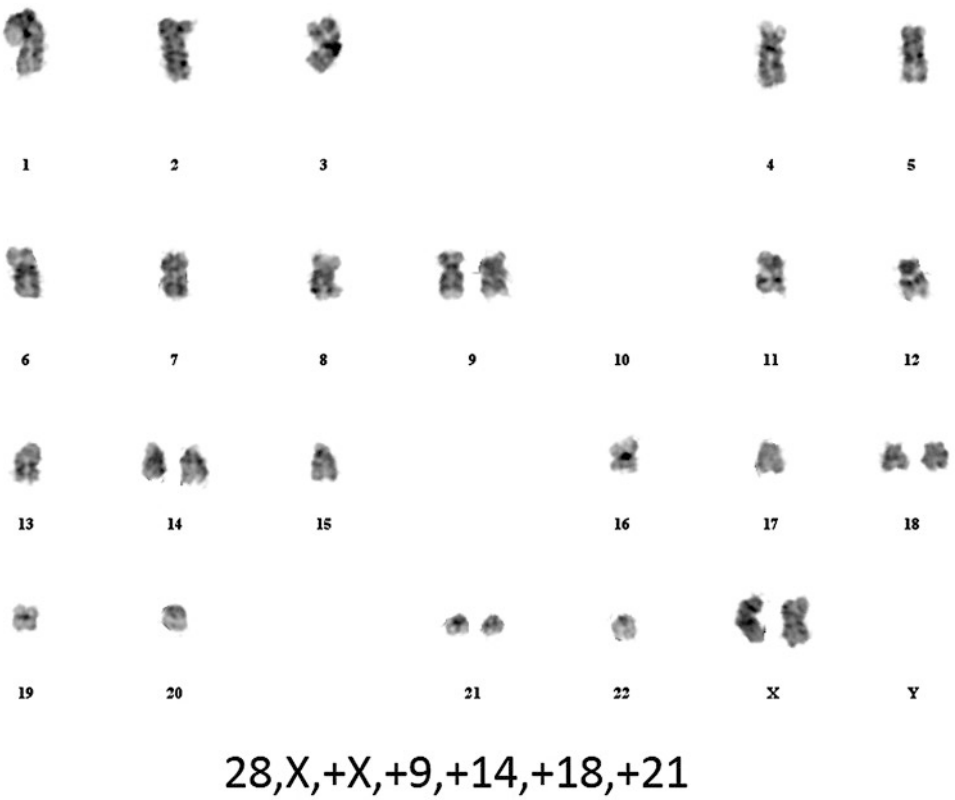

Fig. 9.20 On the contrary, this hypodiploid karyotype is indicative of a poor outcome [12]. This karyotype reveals a near-haploid cell line with two copies of chromosomes X, 9, 14, 18, and 21

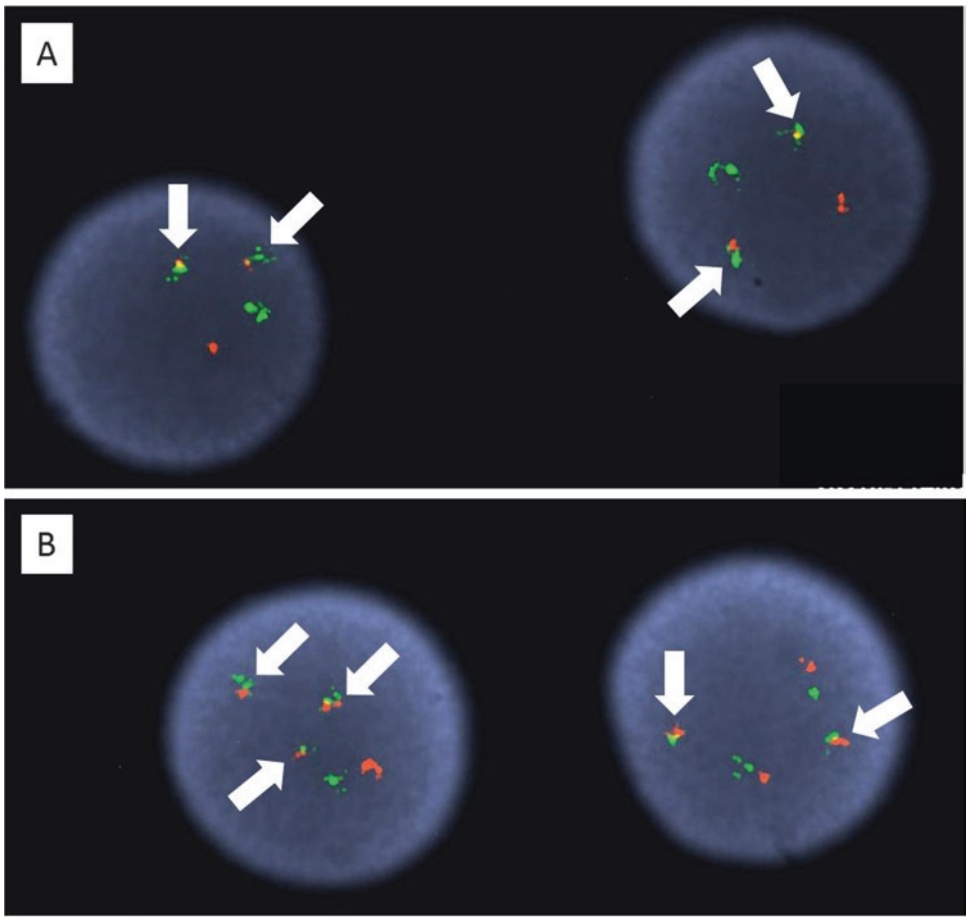

Fig. 9.21 Fluorescence in situ hybridization (FISH) is often used in conjunction with karyotype and molecular studies to identify cytogenetic abnormalities such as translocations, deletions, duplications, or chromosome numeric abnormalities. The advantage of FISH is that it can be performed on interphase cells and can detect deletions and additions that are submicroscopic on karyotype. In patients with a dry tap or when the cells fail to grow, FISH can be done on the touch preparations or direct smears. In this 48-year-old woman with ALL, conventional karyotype failed owing to a lack of growth. (**a**) FISH on the aspirate smear illustrates two copies of *BCR-ABL1* fusion (white arrows), one copy of the normal *BCR* gene (green) and one copy of normal *ABL1* (red) in the majority of the cells. (**b**) However, a small subset of cells demonstrates three fusion signals (white arrows) in the cells on the left. This finding is indicative of a clonal evolution in a minor subset of blasts

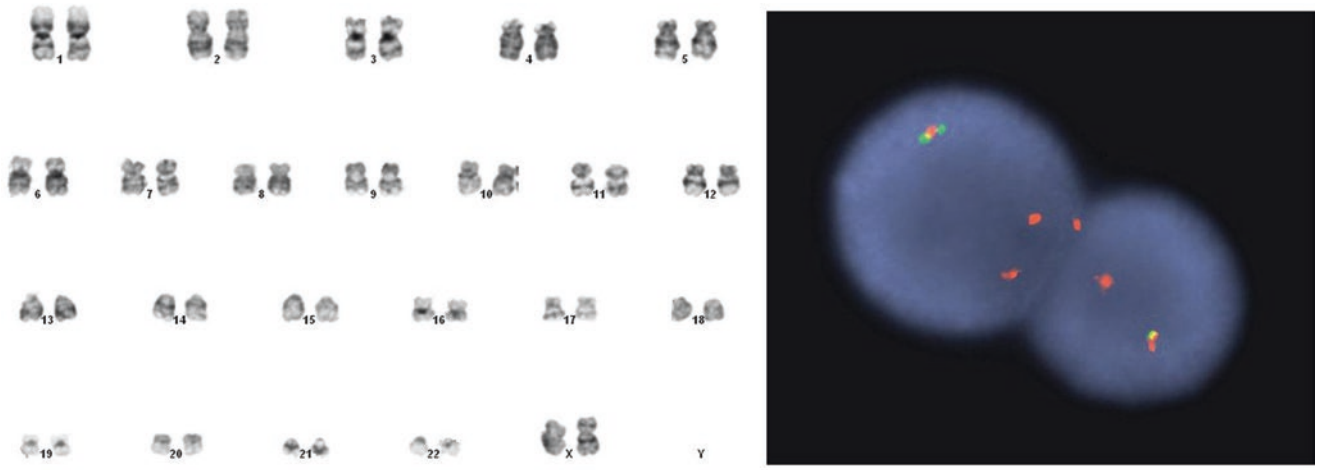

Fig. 9.22 Translocation 12;21 in ALL is regarded as a good prognostic indicator. However, this translocation is cryptic and cannot be detected by karyotype (*left*). FISH is required to establish the diagnosis (right). The t(12;21) translocation is the most common translocation in pediatric ALL, accounting for 20% of cases. It is not seen in infant ALL, and it is rare in adult ALL. The clinical and morphologic findings resemble other ALLs. Immunophenotype is similar to other ALLs, except for frequent CD13 expression. In this image, the left panel is a chromosomal study that reveals a normal karyotype 46,XX. FISH study shows an abnormal signal consistent with *ETV6/RUNX1* (i.e., *TEL/AML1*) fusion. The finding is atypical, as only one fusion signal is present. In addition, there is loss of the normal ETV6 region (no normal green signal). These atypical findings can be seen in FISH and are most likely secondary to loss of a fragment of DNA, or the remaining portion of the gene is too small for the FISH probes to hybridize. ALL with translocation of t(12;21) carries good prognosis

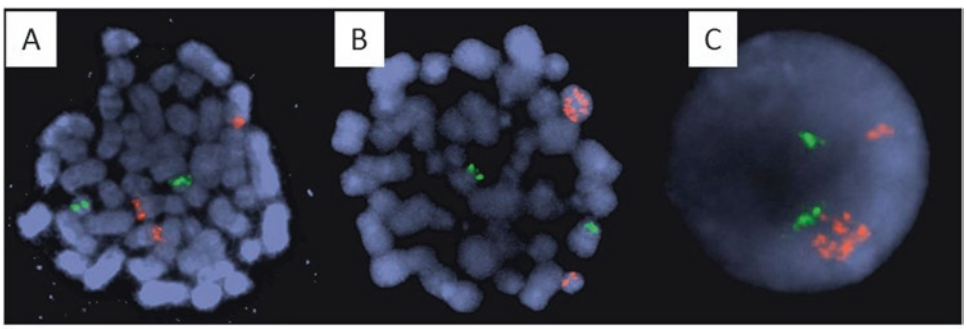

A. FISH with BCR (green) and ABL1 (red) probes on metaphase cell. B. FISH with ETV6 (green) and RUNX1 (red) probes on metaphase cell. C. FISH with ETV6 (green) and RUNX1 (red) probes on interphase cell

Fig. 9.23 Cytogenetic study in this 12-year-old girl shows a karyotype of complex abnormalities. On the Children's Oncology Group (COG) FISH panel, there are three copies of the *ABL1* gene (**a**) and multiple copies of the *RUNX1* gene (i.e., intrachromosomal amplification of the *RUNX1* gene or iAMP21) (**b**, **c**). Further workup for the *ABL1* abnormality is required, as the *ABL1* rearrangement is considered Ph-like ALL and carries a poor prognosis similar to that of Ph + ALL (Table 9.8) [13–21]. Nonetheless, this patient would be stratified as having poor prognosis based on age, complex karyotype, and iAMP21. ALL with iAMP21 tends to occur in older patients, presents with a low WBC count, and carries a poor prognosis [22]

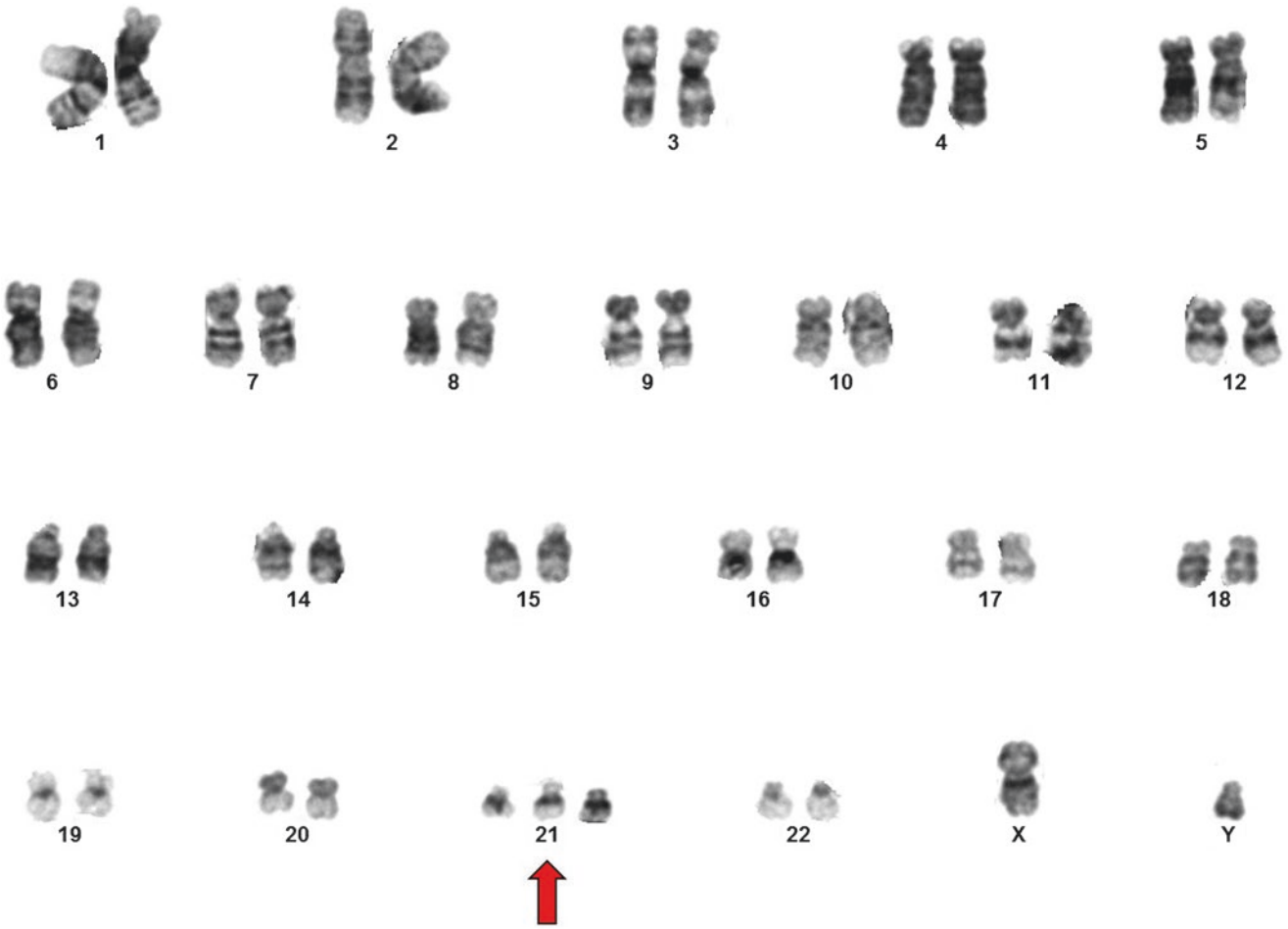

Fig. 9.24 Patients with Down syndrome (DS) may exhibit benign hematologic abnormalities such as transient abnormal myelopoiesis in neonates and persistent macrocytosis without anemia. They also have a tenfold to 20-fold increase in the incidence of hematologic malignancies, namely, acute myeloid leukemia of megakaryocytic lineage and B-ALL. Some postulate that *RUNX1*, *CRLF2*, and/or *CBS* genes on chromosome 21 may play a role in clonal transformation in DS; others have suggested that many other genes also may be involved. B-ALL in DS is often associated with a hypodiploid karyotype and occasionally favorable karyotypes [23, 24]. DS patients with ALL usually have a good clinical outcome. These patients are particularly sensitive to chemotherapy, so appropriate dosage is important. CRLF2 abnormalities, often associated with JAK mutations, are seen in over 50% of DS-ALL (Table 9.8). Cytogenetic study on this 25-year-old man with DS shows constitutional trisomy 21 (red arrow). No other abnormality was detected

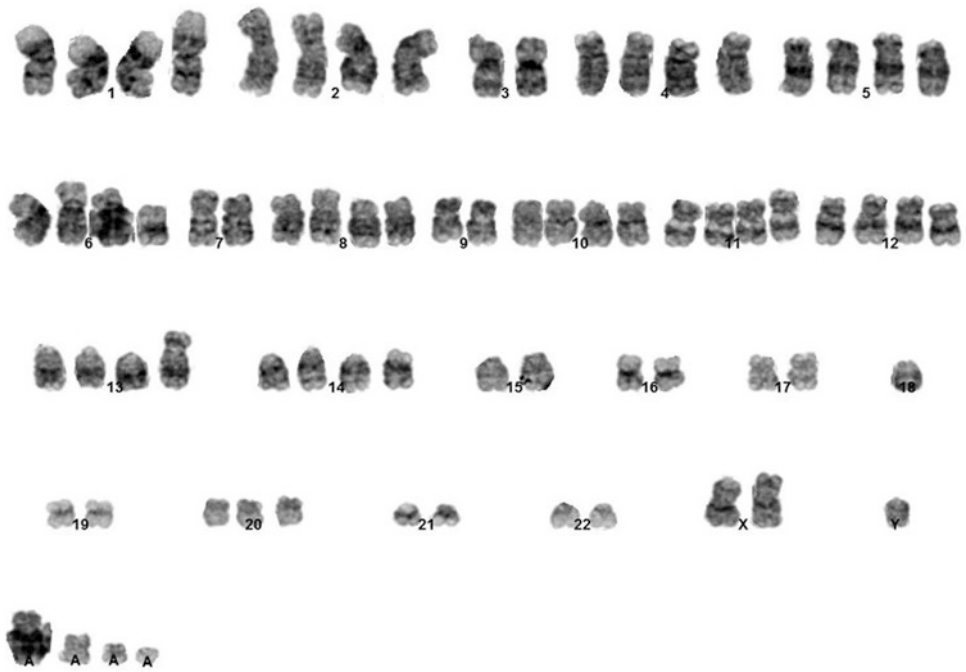

73~76<3n>,XXY,+1,+2,-3,+4,+5,+del(6)(q21),-7,+8,-9,+10,+11,add(11)(q23),add(11)(p14),+12,+13,rob(13;21)(q10;q10),+add(14)(p11.2),-15,-16,-17,-18,-19,+20,-21,-22,+2~7mar

Fig. 9.25 Occasionally, the karyotype can be highly complex, as illustrated here with 72 chromosomes. However, this is not a hyperdiploidy karyotype. On careful examination, this is a hypertriploid male chromosome complement. There are extensive structural and numerical abnormalities consisting of extra copies of chromosomes, loss of chromosomes, deletion, additional materials, a translocation, and two to seven marker chromosomes of unknown origin. This complement represents endoreduplication of a hypodiploid karyotype and predicts a poor outcome in this patient. Hypodiploid ALL tends to have a higher chance of relapse

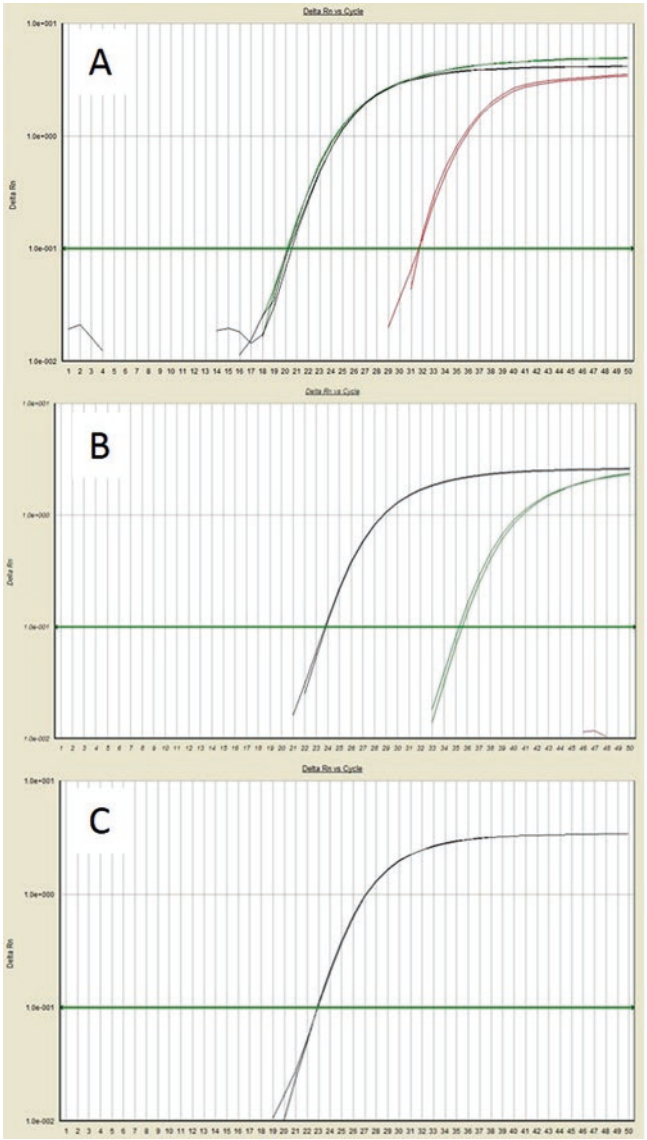

A. p210 BCR/ABL1 fusion at diagnosis

B. p210 BCR/ABL1 fusion at low level

C. BCR/ABL1 fusion negative

Fig. 9.26 In patients with Ph + ALL, the role of assessing the *BCR-ABL1* fusion transcript is not as well established as in chronic myeloid leukemia. However, data indicate that molecular response assessed by quantitative polymerase chain reaction (qPCR) is associated with outcome. Complete molecular response (CMR) is defined as the absence of detectable *BCR-ABL1* transcript with an assay sensitivity of 0.01%. Major molecular response (MMR) is defined as *BCR-ABL1*:*ABL1* ratio $\leq 0.1\%$ on the international scale (IS) for p210 *BCR-ABL1* or a three-log reduction for p190 *BCR-ABL1*, but not meeting criteria for CMR. Studies show that MMR at 3 to 6 months and sustained CMR correlates with superior survival and excellent long-term outcomes [25, 26]. In this illustration, the black curve is the transcript of the housekeeping gene *ABL1*, the green curve is the p210 *BCR-ABL1* transcript, and the red curve is the p190 *BCR-ABL1* transcript. (**a**) At the time of B-ALL diagnosis in this 48-year-old woman, a p210 *BCR-ABL1*/ABL1 transcript ratio of 0.86 is present, which indicates a high copy number of *BCR-ABL1* fusion transcript, typically seen at the time of diagnosis (green curve). Black curve is housekeeping gene, used as internal quality control. A minor product of p190 *BCR-ABL1* (red curve) at a very low level is commonly present in the background, only seen at diagnosis when the major transcript level is high; it often disappears after treatment. This transcript may represent a product of alternative splicing. (**b**) *BCR-ABL1* transcript at 3 months with a *BCR-ABL1*/ABL1 ratio of 0.00031. It fulfills the criteria for MMR, but not CMR, as there are still detectable transcripts. **C** At the 5-month mark, the patient has achieved CMR with no detectable transcript, no more green or red curves. Only the housekeeping gene (black curve) is present

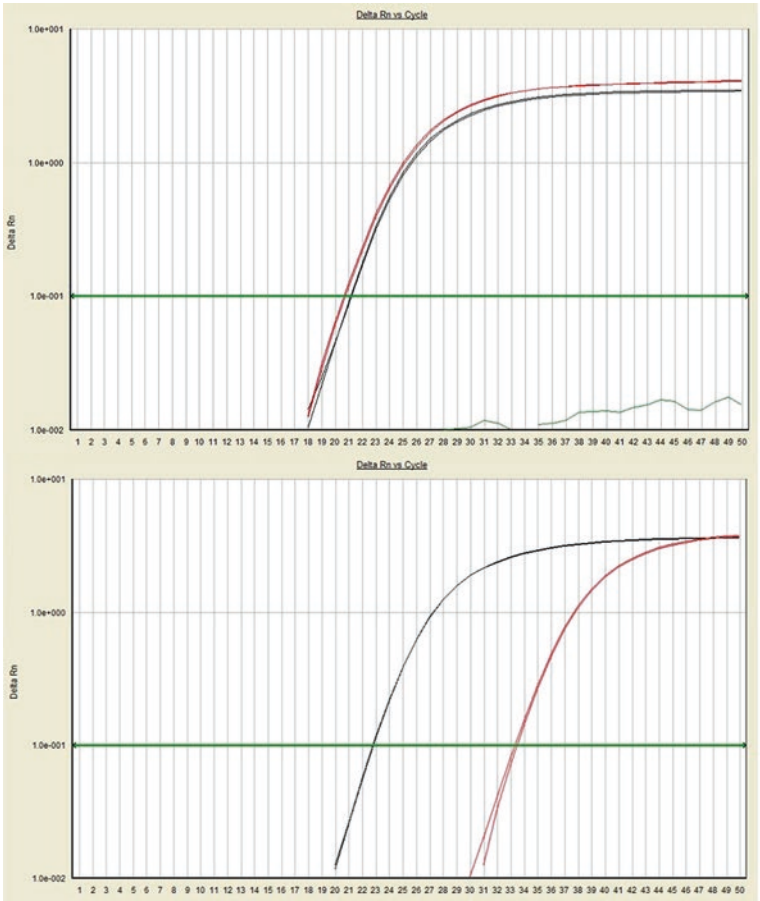

Fig. 9.27 A 13-year-old boy diagnosed with Ph ± B-ALL had a p190 *BCR-ABL1/ABL1* ratio of 1.01 (red curve), a level typically seen at diagnosis (**a**). One month later (**b**), the transcript has dropped to 0.00053, a more than three-log reduction, which meets the criteria for MMR

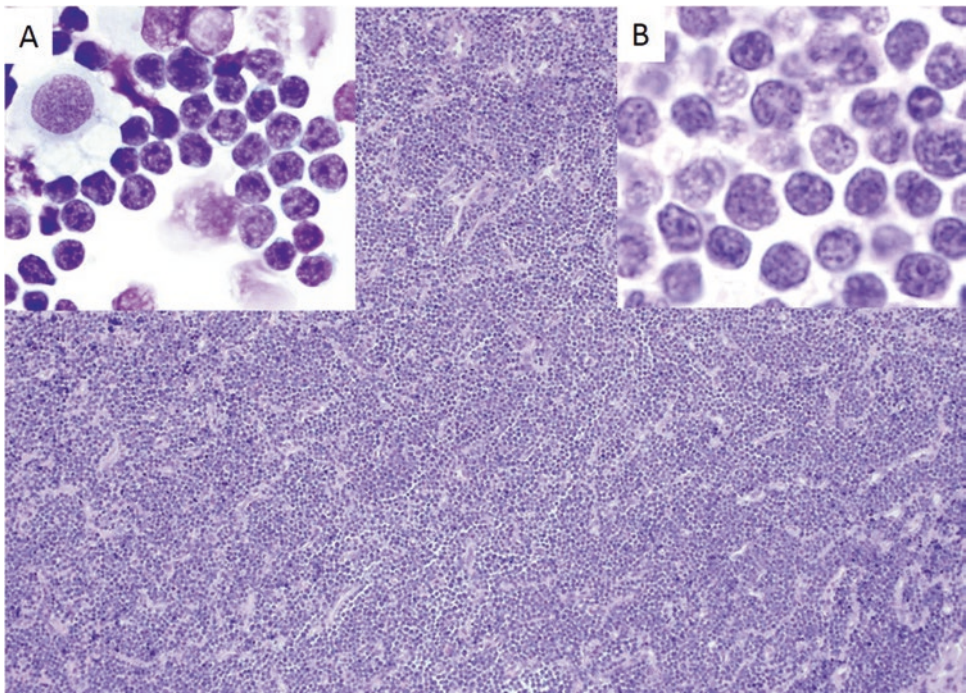

Fig. 9.28 The classic presentation of T-ALL/lymphoblastic lymphoma (LBL) is mediastinal lymphadenopathy in an adolescent or a young adult man [27, 28]. T-ALL is more common in adults, accounting for 20–25% of adult ALL. There is a male predominance, and it often presents with high WBC count, as well as lymphadenopathy, organomegaly, and an anterior mediastinal mass. The lymph node biopsy illustrated here was taken from a 15-year-old boy with a mediastinal mass and cervical lymphadenopathy, as well as pleural effusion. The low-power view exhibits a diffuse lymphoid infiltrate replacing the entire lymph node. On high power (**Inset B**), the blasts have scant cytoplasm, round to slightly irregular nuclear contours, relatively condensed to open chromatin, and occasional prominent nucleoli. On the cytospin preparation of the pleural fluid (**Inset A**), numerous blasts are seen surrounding a macrophage

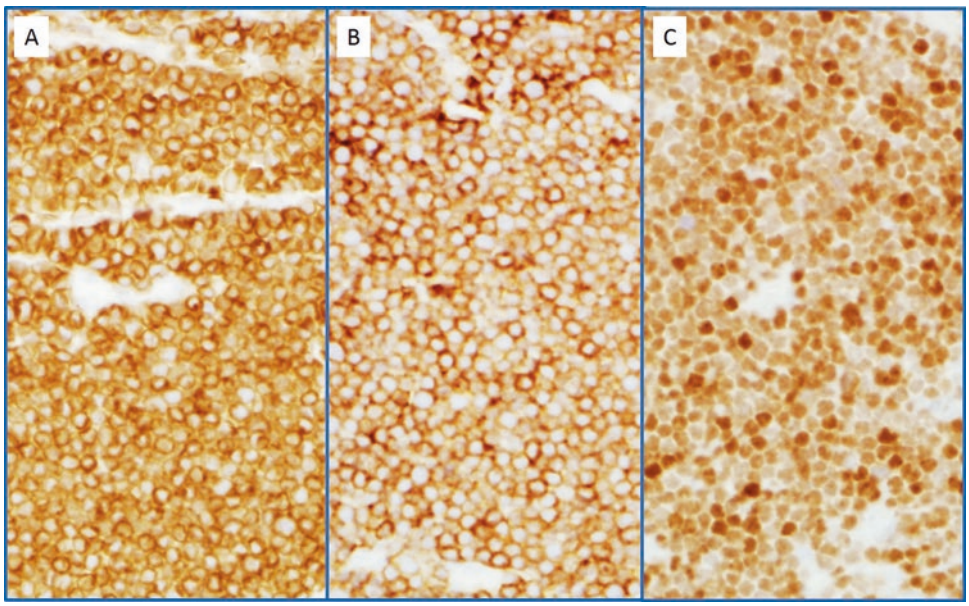

Fig. 9.29 This is the same patient as Fig. 9.28. The blasts express CD3 (**a**), TIA1 (**b**), and TdT (**c**) by immunohistochemical stains. Flow cytometric study is shown in Fig. 9.33

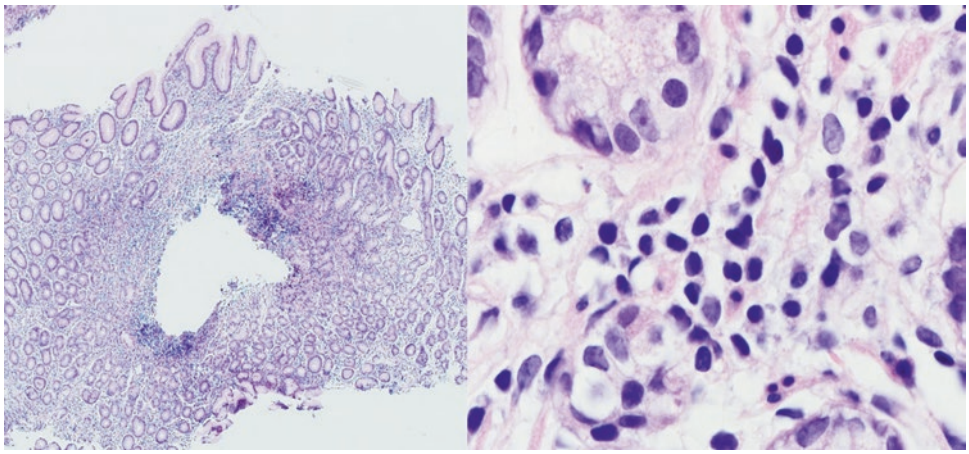

Fig. 9.30 Although T-ALL/LBL typically manifests as nodal or bone marrow disease, extranodal involvement can occur with or without mediastinal involvement. This 11-year-old boy with a history of chronic constipation presented to the emergency room with fever, vomiting, and progressing abdominal pain. Esophagogastroduodenoscopy identified multiple grape-like masses throughout the duodenum. Additional radiographic studies detected an anterior mediastinal mass. In this duodenal biopsy, there is a mild mucosal and submucosal lymphoid infiltrate (left image), which focally destroys duodenal glands, as depicted in the high-power view on the right

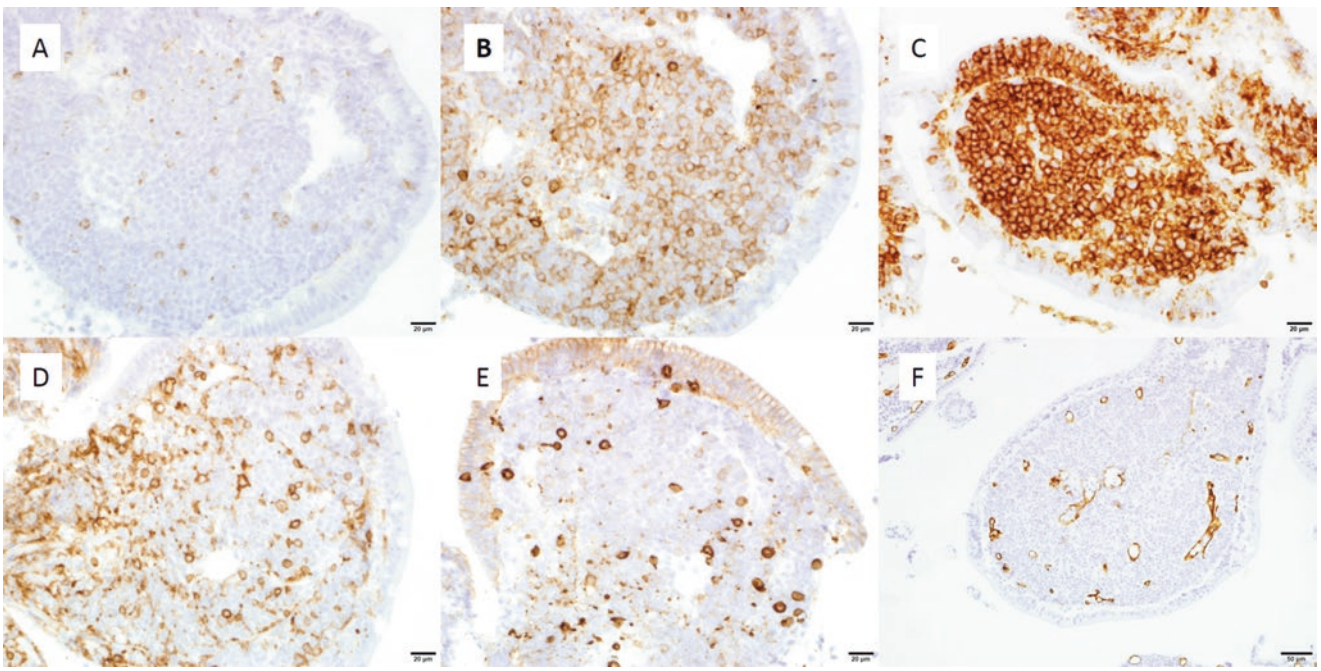

Fig. 9.31 Immunohistochemistry on the same patient as Fig. 9.30 shows that the T-ALL cells express CD3, CD5, CD7, CD43, CD45, and BCL2. They are negative for CD2, CD4, CD8, CD34, TIA, EBER, BCL6, and lysozyme. Representative immunohistochemical stains are illustrated: CD2 (**a**), CD5 (**b**), CD7 (**c**), CD4 (**d**), CD8 (**e**), and CD34 (**f**)

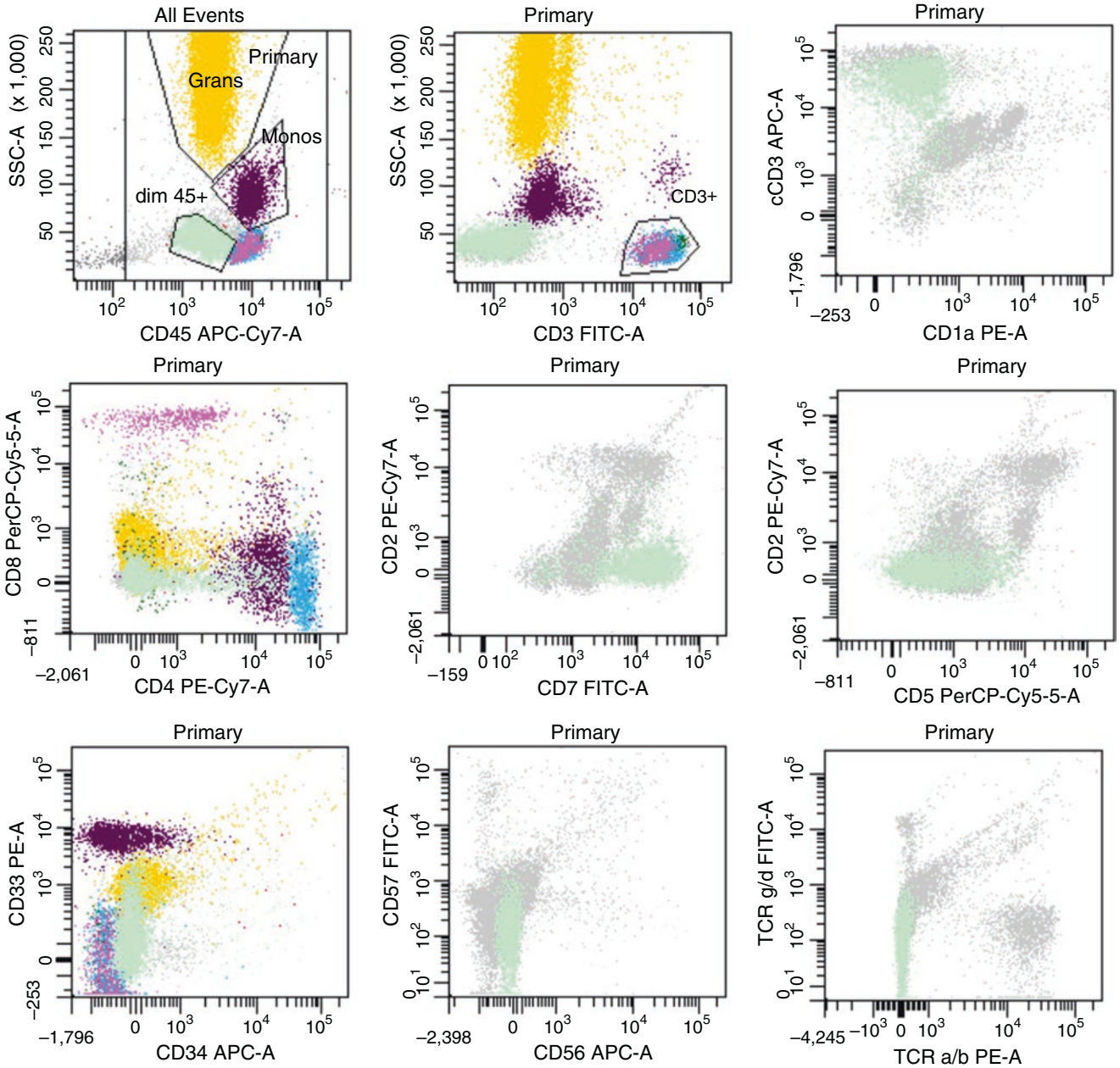

Fig. 9.32 Flow cytometry study on the peripheral blood sample from the same patient as Figs. 9.30 and 9.31 shows an abnormal population of T cells (light aquamarine), which express cytoplasmic CD3 and CD7 and are weakly positive for CD45 and a minor subset weakly positive for CD4, CD5, and CD33. They are negative for surface CD3, CD2, CD8, CD34, CD56, CD57, TCR a/b, and TCR g/d

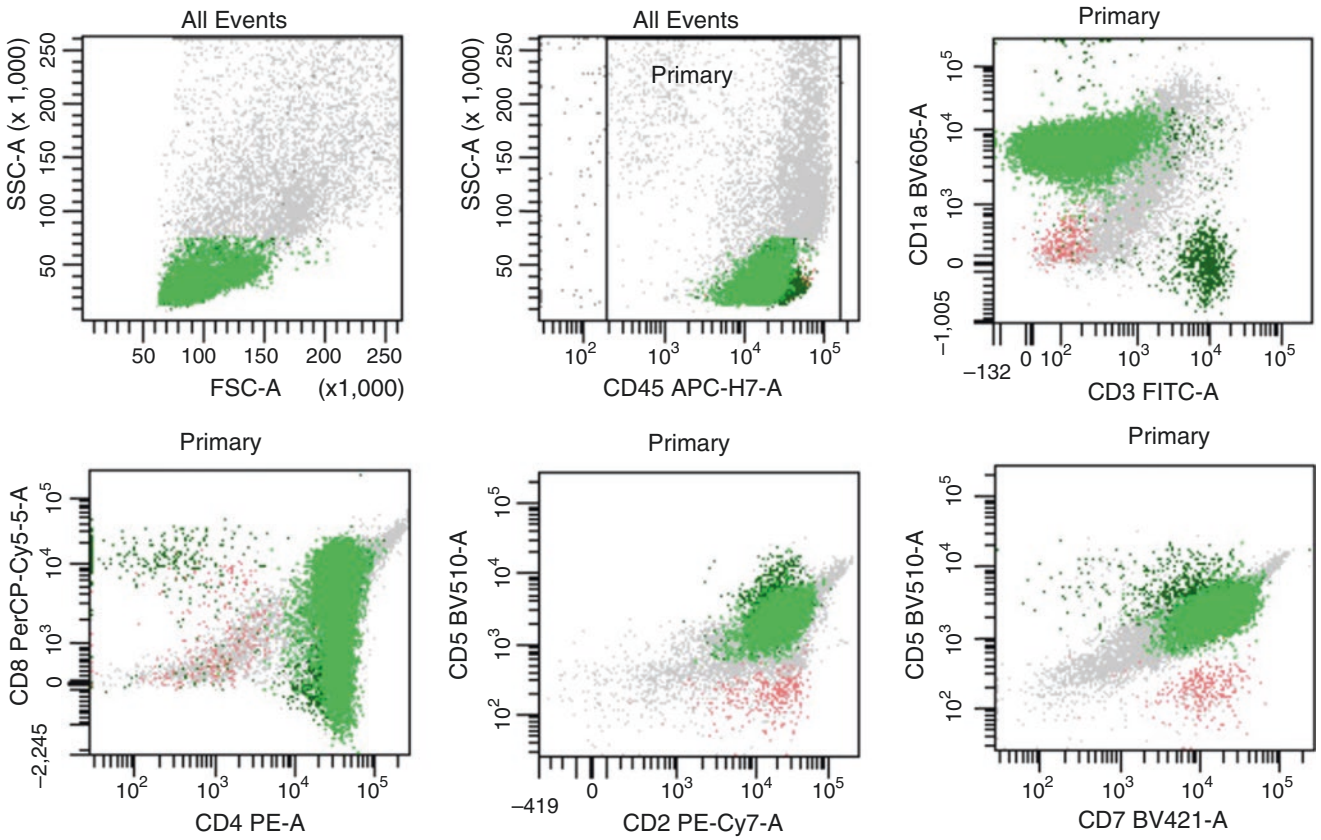

Fig. 9.33 Typical T-ALL/LBL immunophenotype, from the patient in Figs. 9.28 and 9.29, reveals that the lymphoblasts (bright green population) express CD1a, CD2, CD5, CD7, CD4, spectrum of CD8, and fairly bright CD45. They are negative for surface CD3. This immunophenotype is called "double positive" for CD4 and CD8. Along with the positive CD1a, it corresponds to the cortical thymocyte (i.e., common thymocyte) stage in T-cell development (Table 9.5)

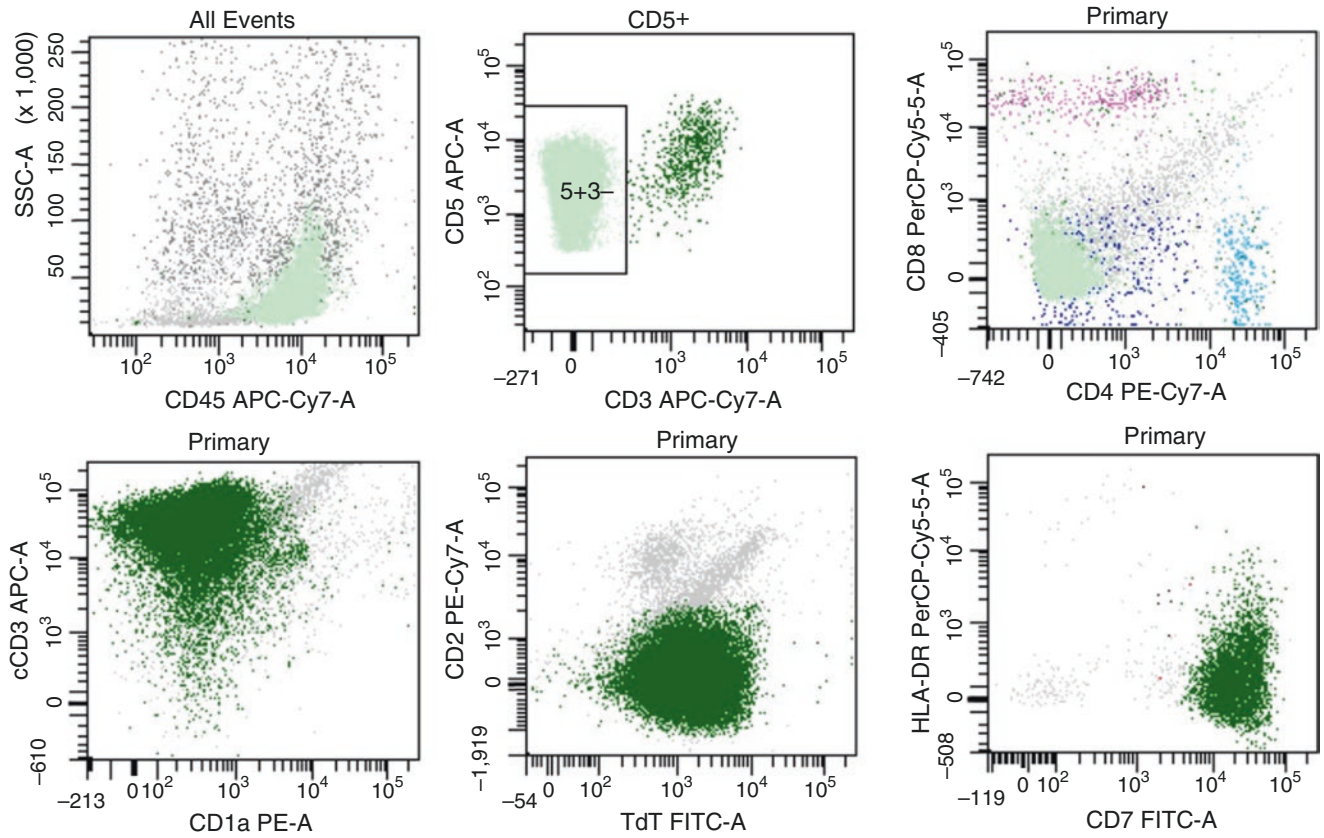

Fig. 9.34 T-ALL/LBL can exhibit a "double negative" immunophenotype. This flow cytometry panel demonstrates that the lymphoblasts (*aquamarine* on top panel, deep green on the lower panel) express CD5, CD7, cytoplasmic CD3, TdT, and CD45. They are negative for CD2, CD4, CD8, HLA-DR, and CD34 (not shown). This immunophenotype most likely represents immature thymocytes (i.e., pre-T cells) (Table 9.5)

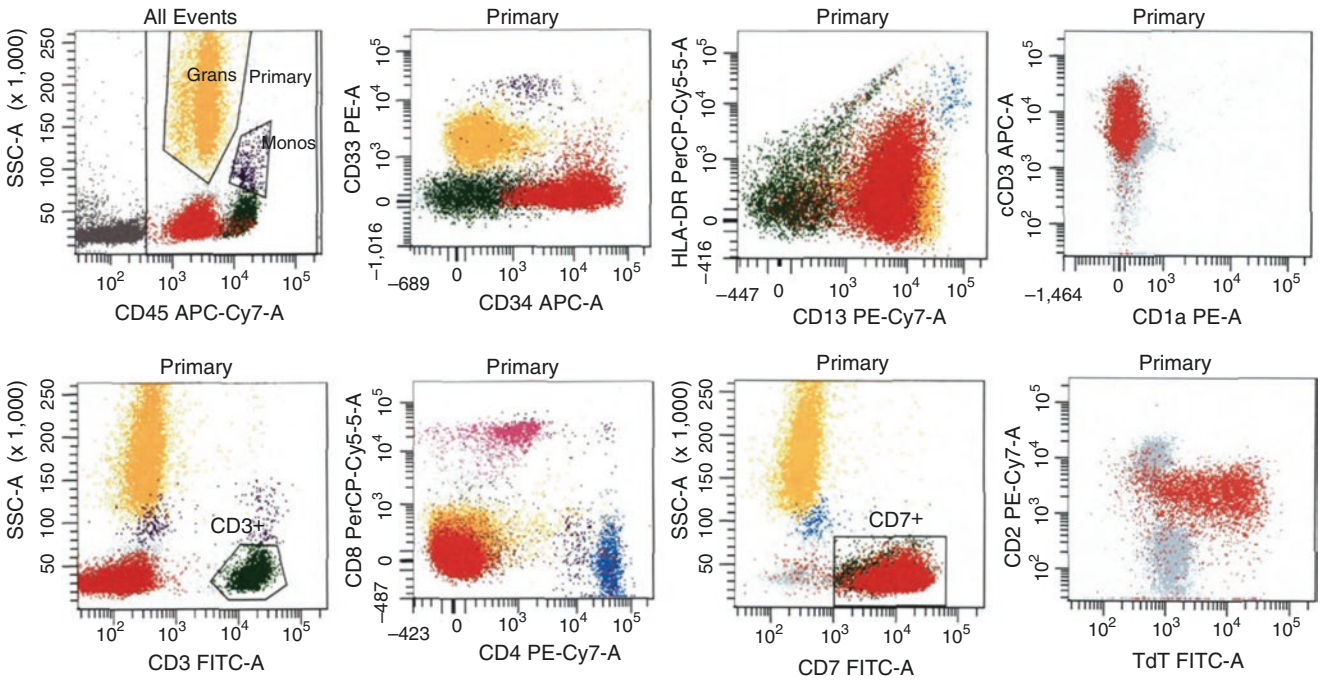

Fig. 9.35 Early T precursor (ETP) T-ALL/LBL has a unique immunophenotype and occurs in older patients. It is significant to recognize ETP T-ALL/LBL, as it carries a poor prognosis. By definition, blasts express CD7. They can also express CD2 and cytoplasmic CD3. The blasts can have CD4 but are negative for CD8. They characteristically express one or more of the myeloid or stem cell markers CD34, CD117, HLA-DR, CD13, CD33, CD11b, or CD65. This flow cytometry plot illustrates a typical finding in ETP T-ALL/LBL. The blasts are positive for CD7, CD2, cytoplasmic CD3, CD34, CD13, TdT, and subset HLA-DR. They are negative for surface CD3, CD4, CD8, and CD1a

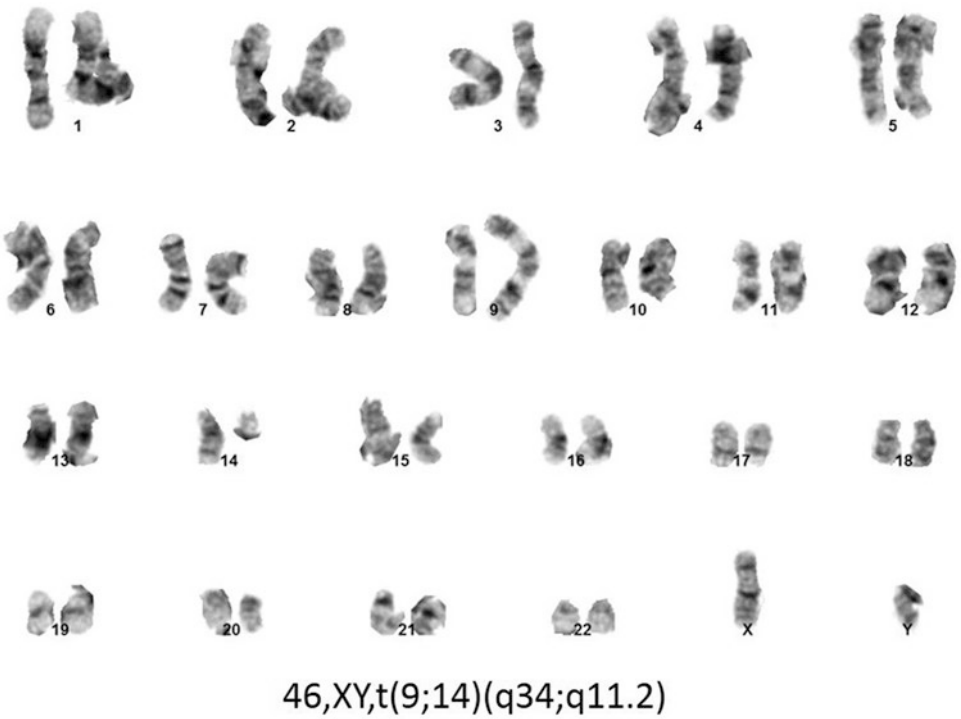

Fig. 9.36 Abnormal karyotype is found in up to 55–70% of T-ALL/LBL, including translocations and deletions [28]. The most common abnormality involves the T-cell receptor (TCR) loci (α and δ at 14q11.2, β at 7q34, and γ at 7p14), deletion of 6q, loss of 9p material through deletions or unbalanced translocations, trisomy 8, deletion of 11q, and loss of 12p (Table 9.7) [29–32]. In addition, amplifications and point mutations are commonly seen by molecular techniques. *NOTCH1* activation mutation is seen in about 50% of T-ALL and likely contributes to T-ALL pathogenesis, but it is of unknown prognostic significance [33]. *NOTCH1* encodes a transmembrane signaling protein that plays key roles in development and neoplasia. The karyotype in the image depicted is t(9;14)(q34;q11.2), *NOTCH1/TRA* (*TCR*). *NOTCH1-TRA* fusion is a rare occurrence in T-ALL [34]

Table 9.4 Clinical, pathologic, and genetic findings in B-ALL of different stages

Characteristic	Early precursor	"Common" type	Mature precursor
Clinical	Infant	Children and adults	Children, less common in adults
Pathologic finding	CD10 negative	CD10 positive	Cytoplasmic μ heavy chain, often CD34 negative
Cytogenetics	*KMT2A* (*MLL*) rearrangement	All types	t(1;19)
Prognosis	Poor	All types	Intermediate

Table 9.5 Markers expressed in T-ALL at different stages

Early T precursor (ETP)
CD7 plus one or more of the immature or myeloid markers CD34, TdT, CD117, HLA-DR, CD13
Can express cCD3 and CD2
Immature thymocyte (pre-T cell, double negative)
TdT, CD7, CD2, cCD3, variable CD34, variable HLA-DR
Common thymocyte (cortical thymocyte, double positive)
CD1a, CD2, CD5, CD7, CD4, CD8
Mature thymocyte (medullary thymocyte, either CD4 or CD8)
sCD3, CD2, CD5, CD7, CD4, or CD8

Table 9.6 Risk stratification based on clinical findings, initial laboratory tests, and cytogenetic aberrations

Characteristics	Favorable	Unfavorable
Age at diagnosis	1–10 y	<1 y or ≥10 y
Sex	Female	Male
WBC at diagnosis	$<50 \times 10^9$/L	$\geq 50 \times 10^9$/L
CNS stage	CNS1	CNS2, CNS3
Cytogenetics	Hyperdiploid > 50 chromosomes; triple trisomy of chromosomes 4, 10, and 17; t(12;21) *EVT6-RUNX1*	Hypodiploid; t(9;22) *BCR-ABL1*, *KMT2A* rearrangement, iAMP21, t(17;19) *TCF3-HLF*
Response to therapy		
Morphology	M1 at end of induction	M2, M3 at end of induction
Flow analysis	MRD < 0.1% by flow	MRD > 0.1% by flow
qPCR for *BCR-ABL1* transcript	MMR or CMR by 6 months	Did not achieve MMR by 6 months

CMR complete molecular response; *MMR* major molecular response; *MRD* minimal residual disease; *qPCR* quantitative polymerase chain reaction; *WBC* white blood cell count

Table 9.7 Common types of cytogenetic abnormalities

Abnormality	Tumor type	Frequency	Prognosis
Hyperdiploid	B-ALL	25%	Favorable
t(12;21) *ETV6-RUNX1*	B-ALL	20%	Favorable
Ph-like ALL (*BCR-ABL1*-like)	B-ALL	9%	Unfavorable
KMT2A rearrangement	B-ALL	6%	Unfavorable
t(1;19) *TCF3-PBX1*	B-ALL	4%	Intermediate
t(9;22) *BCR-ABL1*	B-ALL	3%	Unfavorable
iAMP21	B-ALL	2%	Unfavorable
Hypodiploid	B-ALL	1%	Unfavorable
Translocation *TCR* loci	T-ALL	30% of aberrant cases	Unclear
Del 6p	T-ALL	20%	Unclear
Loss of 9p	T-ALL	15%	Unclear
Trisomy 8, del11q, del12p	T-ALL	5–10%	Unclear
NUP214-ABL1 fusion	T-ALL	4–6%	Unclear
NOTCH1 activation mutation	T-ALL	50%	Unclear

TCR T-cell receptor

Table 9.8 Features of Ph-like (*BCR-ABL1*-like) ALL

Feature	Comments		
Frequency	~10% childhood ALL, ~15% high-risk ALL, 27% young adult ALL		
Characteristics	Increases with age		
	Higher WBC count at presentation		
	More common among males		
	Higher MRD at the end of induction		
	Inferior survival rate		
NGS-based test	Identifies fusions, point mutations, and expression levels from RNA input (81 genes associated with ALL, including all recurrent Ph-like ALL fusion events)		
FISH-based test	Identifies rearrangement of *CRLF2, ABL1, ABL2, PDGFRB, CSF1R, JAK2, EPOR*		
Major genes involved			
Genes	**Gene function**	**Frequency**	**Potential TKI**
CRLF2	Associated with mutant *JAK* in 50% of cases; constitutive JAK-STAT activation	<3% pediatric B-ALL	JAK inhibitor ruxolitinib
		~10% in adult ALL	
		>50% in DS-ALL	
JAK1/2	Constitutive JAK-STAT activation	Up to 35% of DS-ALL	JAK inhibitor ruxolitinib
EPOR	Constitutive JAK-STAT activation	3.9%	JAK inhibitor ruxolitinib
ABL1	*ABL* class tyrosine kinase	5% T-ALL	ABL class inhibitors: imatinib, dasatinib, nilotinib
ABL2	*ABL* class tyrosine kinase	–	ABL class inhibitors: imatinib, dasatinib, nilotinib
PDGFRB	*ABL* class tyrosine kinase	8% Ph-like ALL	ABL class inhibitors: imatinib, dasatinib, nilotinib
CSF1R	*ABL* class tyrosine kinase	–	ABL class inhibitors: imatinib, dasatinib, nilotinib
IKZF1	Kinase, a hallmark of Ph + ALL	15% pediatric ALL, 30% adult ALL, > 60% Ph + ALL	–

DS-ALL Down syndrome-associated ALL; *FISH* fluorescence in situ hybridization; *MRD* minimal residual disease; *NGS* next-generation sequencing; *TKI* tyrosine kinase inhibitor; *WBC* white blood cell

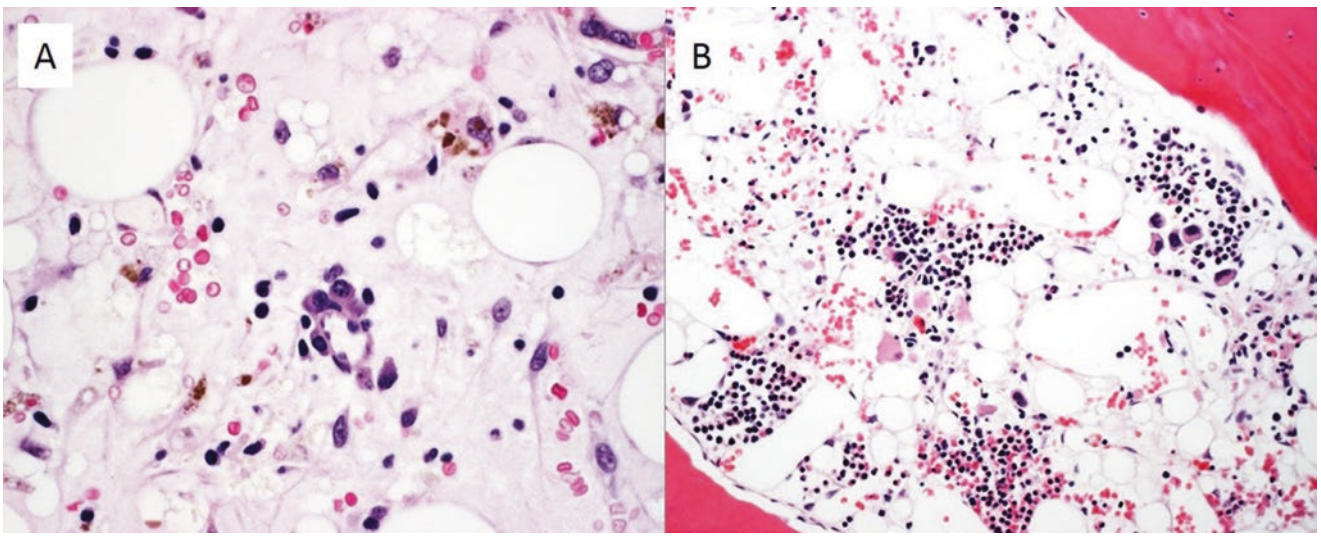

Fig. 9.37 Response to chemotherapy is significant in predicting prognosis. Early responders have superior outcome. (**a**) Bone marrow biopsy at day 14 of chemotherapy was routinely done years ago but is no longer required, given the improved sensitivity of detecting minimal residual disease (MRD) from peripheral blood by flow cytometric analysis. At day 14, the typical finding in patients responding to chemotherapy is essentially an acellular marrow with a few scattered fibroblasts, endothelial cells, plasma cells predominantly around vessels, scattered lymphocytes, and macrophages with hemosiderin pigment in a background of profound fibrinoid necrosis (chemotherapy effect). The hematopoietic cells are absent. (**b**) Bone marrow biopsy at day 29. It illustrates the beginning of bone marrow recovery, with a predominance of erythroid precursors. A few megakaryocytes can be appreciated. Myeloid lineage will soon follow

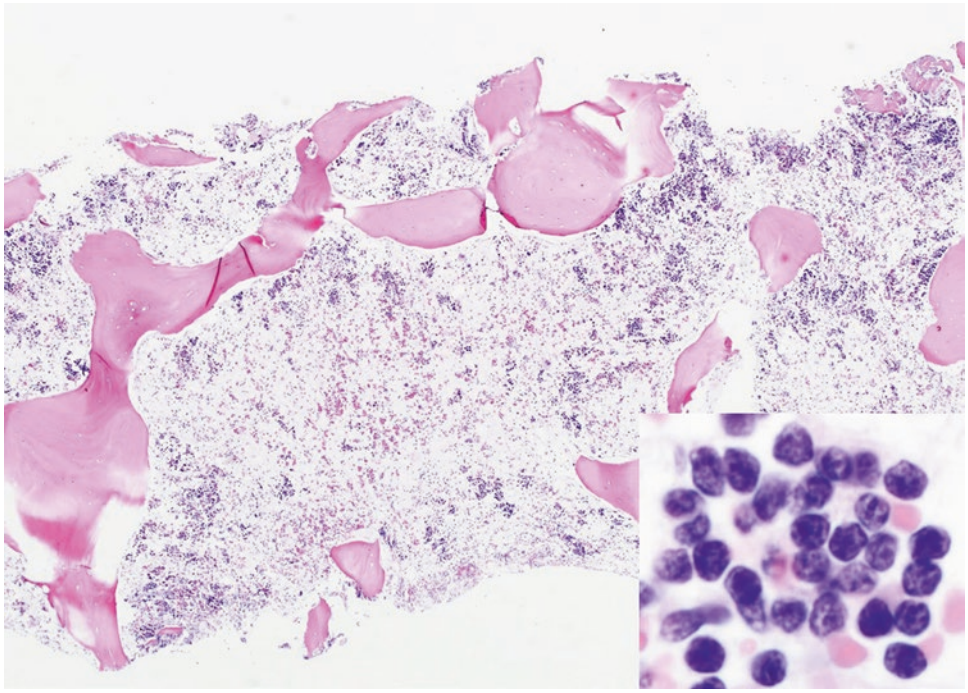

Fig. 9.38 Day 15 marrow from a 17-year-old female with residual disease. The marrow is markedly hypocellular, indicating response to chemotherapy. However, there are clusters of cells present, and on high power (**inset**), the cells are morphologically similar to the diagnostic blasts. Flow cytometric study confirms residual disease. This finding is predictive of a less favorable prognosis

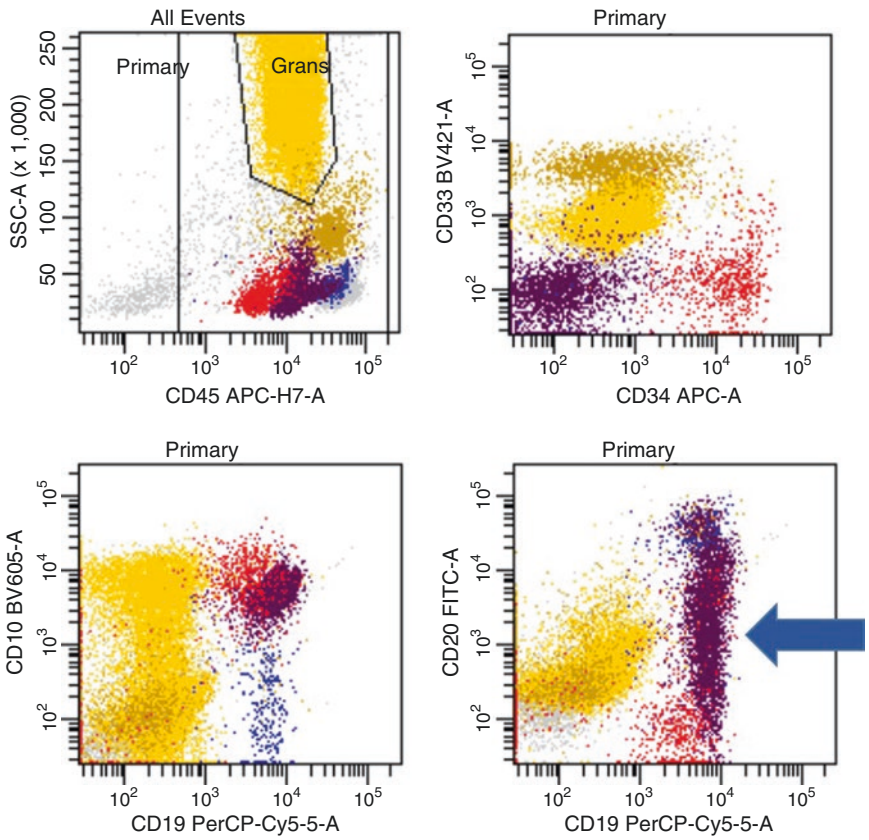

Fig. 9.39 A challenge during MRD assessment is to distinguish lymphoblasts from hematogones, which can be prominent in post-chemotherapy marrows. Lymphoblasts usually form a cluster on the flow cytometry plot. Hematogones characteristically exhibit a spectrum of maturation on CD20 expression and often loss of CD34 expression in the majority of cells. The differences between lymphoblasts and hematogones are illustrated in this composite flow plot. A 16-year-old boy diagnosed with *BCR-ABL1*-positive B-ALL experienced a slow response and eventually went into morphologic remission after 3 months of treatment. Two months after he finished his 2-year ALL protocol treatment, his BCR-ABL1 transcript started to rise. A bone marrow biopsy and flow cytometric study were performed. A population of blasts confirms relapse of his disease. The lymphoblasts form a tight cluster (red population) and express CD34, CD10, and CD19. They are negative for CD20. Hematogones (purple population) express both CD19 and CD10, but have lost CD34 expression in most cells and show a characteristic spectrum of CD20 expression (blue arrow). In contrast, the mature B cells (blue) express both CD19 and CD20, but are CD10 negative. Also seen are granulocytes (yellow) and monocytes (brown)

References

1. Swerdlow SH, Campo E, Harris NL, Jaffe ES, Pileri SA, Stein H, et al. WHO classification of tumours of haematopoietic and lymphoid tissues. 4th ed. IARC: Lyon; 2008. p. 168–78.
2. Bassan R, Maino E, Cortelazzo S. Lymphoblastic lymphoma: an updated review on biology, diagnosis, and treatment. Eur J Haematol. 2016;96:447–60. https://doi.org/10.1111/ejh.12722.
3. Moriyama T. Familial acute lymphoblastic leukemia. Rinsho Ketsueki. 2016;57:900–9. 10.11406/rinketsu.57.900.
4. Pulte D, Gondos A, Brenner H. Improvement in survival in younger patients with acute lymphoblastic leukemia from the 1980s to the early 21st century. Blood. 2009;113:1408–11. https://doi.org/10.1182/blood-2008-06-164863.
5. Pui CH, Mullighan CG, Evans WE, Relling MV. Pediatric acute lymphoblastic leukemia: where are we going and how do we get there? Blood. 2012;120:1165–74. https://doi.org/10.1182/blood-2012-05-378943.
6. Madhusoodhan PP, Carroll WL, Bhatla T. Progress and prospects in pediatric leukemia. Curr Probl Pediatr Adolesc Health Care. 2016;46:229–41. https://doi.org/10.1016/j.cppeds.2016.04.003.
7. Sorensen JT, Gerald K, Bodensteiner D, Holmes FF. Effect of age on survival in acute leukemia. 1950-1990. Cancer. 1993;72:1602–6.
8. Irken G, Oren H, Gülen H, Duman M, Uçar C, Atabay B, et al. Treatment outcome of adolescents with acute lymphoblastic leukemia. Ann Hematol. 2002;81:641–5.
9. Jacobson S, Tedder M, Eggert J. Adult acute lymphoblastic leukemia: a genetic overview and application to clinical practice. Clin J Oncol Nurs. 2016;20:E147–54.
10. Paul S, Kantarjian H, Jabbour EJ. Adult acute lymphoblastic leukemia. Mayo Clin Proc. 2016;91:1645–66. https://doi.org/10.1016/j.mayocp.2016.09.010.
11. Guest EM, Stam RW. Updates in the biology and therapy for infant acute lymphoblastic leukemia. Curr Opin Pediatr. 2017;29:20–6. https://doi.org/10.1097/MOP.0000000000000437.
12. Safavi S, Paulsson K. Near-haploid and low-hypodiploid acute lymphoblastic leukemia: two distinct subtypes with consistently poor prognosis. Blood. 2017;129:420–3. https://doi.org/10.1182/blood-2016-10-743765.
13. Bhojwani D, Kang H, Menezes RX, Yang W, Sather H, Moskowitz NP, *et al.*; Children's Oncology Group Study; Dutch Childhood Oncology Group; German Cooperative Study Group for Childhood Acute Lymphoblastic Leukemia. Gene expression signatures predictive of early response and outcome in high-risk childhood acute lymphoblastic leukemia: a Children's Oncology Group Study [corrected]. J Clin Oncol 2008;26:4376–4384. doi: https://doi.org/10.1200/JCO.2007.14.4519
14. Moorman AV, Schwab C, Ensor HM, Russell LJ, Morrison H, Jones L, et al. IGH@ translocations, CRLF2 deregulation, and microdeletions in adolescents and adults with acute lymphoblastic leukemia. J Clin Oncol. 2012;30:3100–8. https://doi.org/10.1200/JCO.2011.40.3907.
15. Roberts KG, Morin RD, Zhang J, Hirst M, Zhao Y, Su X, et al. Genetic alterations activating kinase and cytokine receptor signaling in high-risk acute lymphoblastic leukemia. Cancer Cell. 2012;22:153–66. https://doi.org/10.1016/j.ccr.2012.06.005.
16. Mullighan CG. The genomic landscape of acute lymphoblastic leukemia in children and young adults. Hematology Am Soc Hematol Educ Program. 2014;2014(1):174–80. https://doi.org/10.1182/asheducation-2014.1.174.
17. Roberts KG, Li Y, Payne-Turner D, Harvey RC, Yang YL, Pei D, et al. Targetable kinase-activating lesions in Ph-like acute lymphoblastic leukemia. N Engl J Med. 2014;371:1005–15. https://doi.org/10.1056/NEJMoa1403088.
18. Boer JM, Steeghs EM, Marchante JR, Boeree A, Beaudoin JJ, Beverloo HB, et al. Tyrosine kinase fusion genes in pediatric BCR-ABL1-like acute lymphoblastic leukemia. Oncotarget. 2017;8:4618–28. 10.18632/oncotarget.13492.
19. Den Boer ML, van Slegtenhorst M, De Menezes RX, Cheok MH, Buijs-Gladdines JG, Peters ST, et al. A subtype of childhood acute lymphoblastic leukaemia with poor treatment outcome: a genome-wide classification study. Lancet Oncol. 2009;10:125–34. https://doi.org/10.1016/S1470-2045(08)70339-5.
20. Jain N, Roberts KG, Jabbour E, Patel K, Eterovic AK, Chen K, et al. Ph-like acute lymphoblastic leukemia: a high-risk subtype in adults. Blood. 2017;129:572–81. https://doi.org/10.1182/blood-2016-07-726588.
21. Roberts KG, Gu Z, Payne-Turner D, McCastlain K, Harvey RC, Chen IM, et al. High frequency and poor outcome of Philadelphia chromosome–like acute lymphoblastic leukemia in adults. J Clin Oncol. 2017;35:394–401. https://doi.org/10.1200/JCO.2016.69.0073.
22. Ryan SL, Matheson E, Grossmann V, Sinclair P, Bashton M, Schwab C, et al. The role of the RAS pathway in iAMP21-ALL. Leukemia. 2016;30:1824–31. https://doi.org/10.1038/leu.2016.80.
23. Buitenkamp TD, Izraeli S, Zimmermann M, Forestier E, Heerema NA. van den Heuvel-Eibrink MM, *et al.* Acute lymphoblastic leukemia in children with Down syndrome: a retrospective analysis from the Ponte di Legno study group. Blood. 2014;123:70–7. https://doi.org/10.1182/blood-2013-06-509463.
24. Lee P, Bhansali R, Izraeli S, Hijiya N, Crispino JD. The biology, pathogenesis and clinical aspects of acute lymphoblastic leukemia in children with Down syndrome. Leukemia. 2016;30:1816–23. https://doi.org/10.1038/leu.2016.164.
25. Zhang L, Ramjit RT, Hill CE, Arellano M, Khoury HJ, Mann KP. Clinical significance of quantitative monitoring and mutational analysis of *BCR-ABL1* transcript in Philadelphia chromosome positive B lymphoblastic leukemia. Leuk Lymphoma. 2015;57:364–9. https://doi.org/10.3109/10428194.2014.1003059.
26. Short NJ, Jabbour E, Sasaki K, Patel K, O'Brien SM, Cortes JE, et al. Impact of complete molecular response on survival in patients with Philadelphia chromosome–positive acute lymphoblastic leukemia. Blood. 2016;128:504–7. https://doi.org/10.1182/blood-2016-03-707562.
27. Belver L, Ferrando A. The genetics and mechanisms of T cell acute lymphoblastic leukaemia. Nat Rev Cancer. 2016;16:494–507. https://doi.org/10.1038/nrc.2016.63.
28. Karrman K, Johansson B. Pediatric T-cell acute lymphoblastic leukemia. Genes Chromosomes Cancer. 2017;56:89–116. https://doi.org/10.1002/gcc.22416.
29. Heerema NA, Sather HN, Sensel MG, Kraft P, Nachman JB, Steinherz PG, et al. Frequency and clinical significance of cytogenetic abnormalities in pediatric T-lineage acute lymphoblastic leukemia: a report from the Children's Cancer Group. J Clin Oncol. 1998;16:1270–8.
30. Schneider NR, Carroll AJ, Shuster JJ, Pullen DJ, Link MP, Borowitz MJ, et al. New recurring cytogenetic abnormalities and association of blast cell karyotypes with prognosis in childhood T-cell acute lymphoblastic leukemia: a pediatric oncology group report of 343 cases. Blood. 2000;96:2543–9.
31. Karrman K, Forestier E, Heyman M, Andersen MK, Autio K, Blennow E, et al. Clinical and cytogenetic features of a population-based consecutive series of 285 pediatric T-cell acute lymphoblastic leukemias: rare T-cell receptor gene rearrangements are associated with poor outcome. Genes Chromosomes Cancer. 2009;48:795–805. https://doi.org/10.1002/gcc.20684.

32. Girardi T, Vicente C, Cools J, De Keersmaecker K. The genetics and molecular biology of T-ALL. Blood. 2017;129:1113–23. https://doi.org/10.1182/blood-2016-10-706465.
33. Reichard K. Precursor B- and T-cell acute lymphoblastic leukemia/lymphoma (aka lymphoblastic leukemia/lymphoma). In: Foucar K, Reichard K, Czuchlewski D, editors. Bone marrow pathology. 3rd ed. Chicago: ASCP; 2010. p. 591–615.
34. Suzuki S, Nagel S, Schneider B, Chen S, Kaufmann M, Uozumi K, et al. A second NOTCH1 chromosome rearrangement: t(9;14)(q34.3;q11.2) in T-cell neoplasia. Leukemia. 2009;23:1003–6. https://doi.org/10.1038/leu.2008.366.

Myelodysplastic Syndrome

10

Sandeep Gurbuxani

The myelodysplastic syndromes (MDS) are clonal hematopoietic stem cell diseases characterized by cytopenia(s) due to ineffective hematopoiesis accompanied by dysplasia in one or more myeloid cell lines and an increased risk of development of acute leukemia. A correct diagnosis and classification of MDS requires integration of morphology with clinical data and ancillary studies including cytogenetics and next-generation sequencing to detect submicroscopic pathogenic variants. Assessment of morphologic dysplasia relies on review of adequately stained peripheral blood smear, bone core biopsy, and bone marrow aspirate smears. In addition, the blast count is predictive of progression to acute leukemia and should be obtained from a careful assessment of 200 cells in the peripheral blood and 500 cells on the bone marrow aspirate. The chapter summarizes morphologic dysplasia for each of the lineages in the context of the diagnostic criteria for the WHO-defined MDS categories (see Table 10.1 and reference [1]). It is now recognized that cytopenia is invariably implicit in the diagnosis of MDS and the clinical behavior is influenced by the number of dysplastic lineages and the blast count [2]. The WHO revision therefore proposes to change the nomenclature to eliminate the use of refractory anemia and refractory cytopenia and replace it with "myelodysplastic syndrome" with further subclassification relying on the dysplastic lineages and the blast count (Table 10.1 (Figs. 10.1, 10.2, 10.3, 10.4, 10.5, 10.6, 10.7, 10.8, 10.9, 10.10, 10.11, 10.12, 10.13, 10.14, 10.15, 10.16, 10.17, 10.18, 10.19, 10.20, 10.21, 10.22, 10.23, 10.24, 10.25, 10.26, 10.27, 10.28, 10.29, 10.30, 10.31, 10.32, 10.33, 10.34, 10.35, 10.36, 10.37, 10.38, 10.39, and 10.40).

S. Gurbuxani (✉)
Department of Pathology, Section of Hematopathology, University of Chicago, Chicago, IL, USA
e-mail: sandeep.gurbuxani@uchospitals.edu

T.I. George, D.A. Arber (eds.), *Atlas of Bone Marrow Pathology*, Atlas of Anatomic Pathology,
https://doi.org/10.1007/978-1-4939-7469-6_10

Table 10.1 WHO classification of MDS

Subtype	Dysplastic lineage	Cytopenias	PB and BM blasts	Comment
MDS with single lineage dysplasia (MDS-SLD)	1	1 or 2	PB < 1%, BM <5%, no Auer rods	Exclude MDS with isolated del5(q)
MDS with multilineage dysplasia (MDS-MLD)	2 or 3	1–3	PB < 1%, BM <5%, no Auer rods	Exclude MDS with isolated del(5q)
MDS with ring sideroblasts (MDS-RS)				
MDS-RS with SLD	1	1 or 2	PB < 1%, BM <5%, no Auer rods	RS ≥ 15% if *SF3B1* mutation not present or not evaluated, ≥5% if *SF3B1* mutation present; exclude MDS with isolated del(5q)
MDS-RS with MLD	2 or 3	1–3	PB < 1%, BM <5%, no Auer rods	RS ≥ 15% if *SF3B1* mutation not present or not evaluated, ≥5% if *SF3B1* mutation present; exclude MDS with isolated del(5q)
MDS with excess blasts (MDS-EB)				
MDS-EB-1	1–3	1–3	PB 2–4%, BM 5–9%, no Auer rods	
MDS-EB-2	1–3	1–3	PB 5–19%, BM 10–19%, or Auer rods	
MDS with isolated del(5q)	1–3	1–2	PB < 1%, BM <5%, no Auer rods	1 additional cytogenetic abnormality except -7 or del(7q)
MDS, unclassifiable (MDS-U)				
1% PB blasts	1–3	1–3	PB = 1%, BM <5%, no Auer rods	1% blasts should be documented on 2 separate occasions
Pancytopenia and single lineage dysplasia	1	3	PB < 1%, BM <5%, no Auer rods	
Cytopenia without dysplasia but with MDS-defining cytogenetic abnormality	0	1–3	PB < 1%, BM <5%, no Auer rods	
Refractory cytopenia of childhood (provisional entity)	1–3	1–3	PB < 2%, BM <5%, no Auer rods	

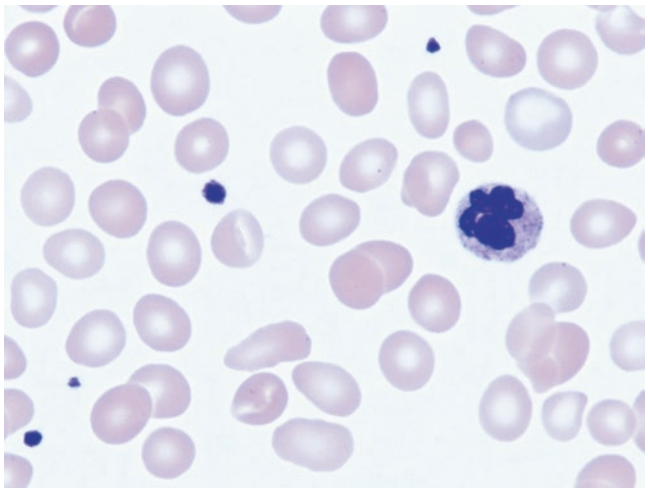

Fig. 10.1 Peripheral blood smear from a 67-year-old gentleman with a diagnosis of refractory anemia (now classified as MDS with single lineage dysplasia [MDS-SLD]) showing dimorphic red blood cells including some macrocytic ovalocytes. The neutrophil in the field has appropriate nuclear lobation and cytoplasmic granularity. Blasts were not seen in the peripheral blood. The patient presented with anemia of 9 g/dL and normal white cell count and platelet count, normal B12 and folic acid levels. A diagnosis of MDS-SLD can be made with cytopenia of two lineages as long as dysplasia is restricted to a single lineage. Patients presenting with pancytopenia tend to have a different clinical outcome and are classified as myelodysplastic syndrome, unclassifiable (see Fig. 10.40)

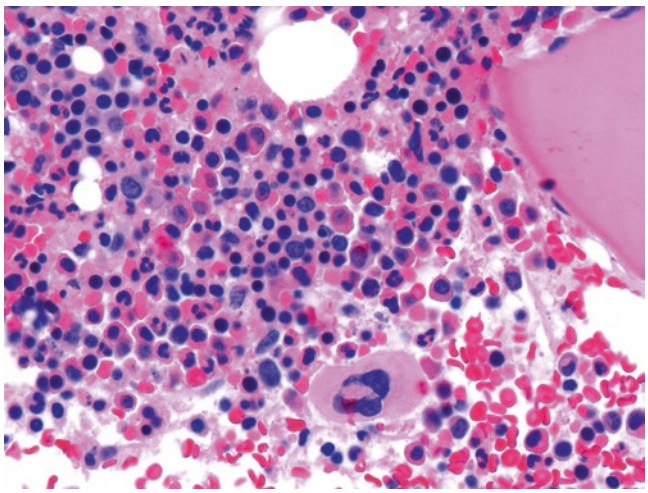

Fig. 10.2 Bone marrow biopsy shows a hypercellular bone marrow with increased erythroid precursors. There is no increase in bone marrow blasts, and progressively maturing granulopoiesis is present along with normal megakaryocytes (bottom of the field). Other patients can have normocellular and, less commonly, hypocellular bone marrows

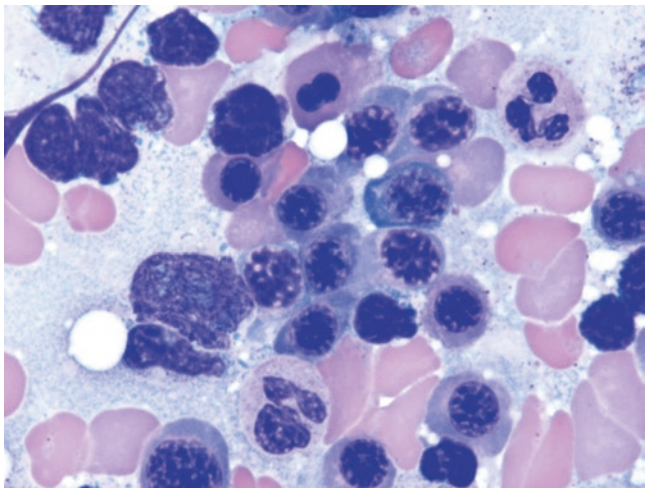

Fig. 10.3 Bone marrow aspirate shows modest erythroid dysplasia manifest by megaloblastoid erythroid maturation with occasional erythroid precursors with a bilobed nucleus (top). The two neutrophils in the field show normal nuclear chromatin, normal nuclear lobation, and appropriate cytoplasmic granularity

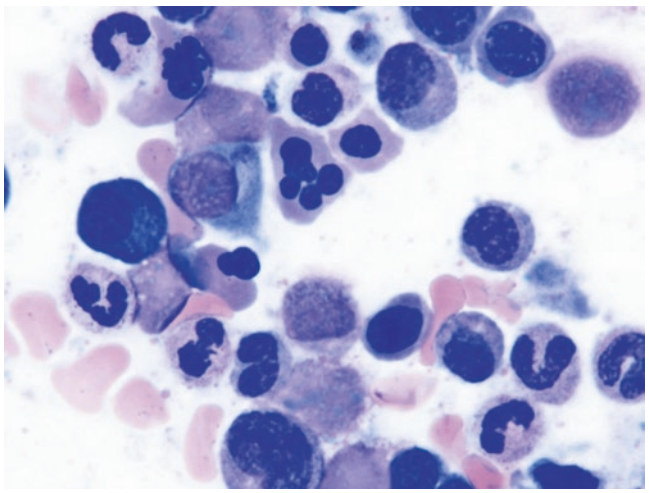

Fig. 10.4 Bone marrow aspirate from a 71-year-old woman with a diagnosis of MDS-SLD shows more pronounced erythroid dysplasia. Nuclear budding, multinuclearity, and nuclear hyperlobation can be seen in addition to megaloblastoid erythroid maturation. Granulocytic dysplasia is equivocal and manifests as occasional neutrophils with nuclear hypolobation and nuclear excrescences. Less than 10% of the neutrophils were affected. The vast majority of the cases with a diagnosis of MDS-SLD will be cases with anemia and bone marrow dyserythropoiesis [3]. Isolated granulocytic dysplasia and isolated megakaryocyte dysplasia are uncommon and warrant meticulous exclusion of autoimmune phenomenon, exposure to drugs, and infectious etiologies that might result in secondary suppression of these lineages as well as morphologic changes mimicking dysplasia

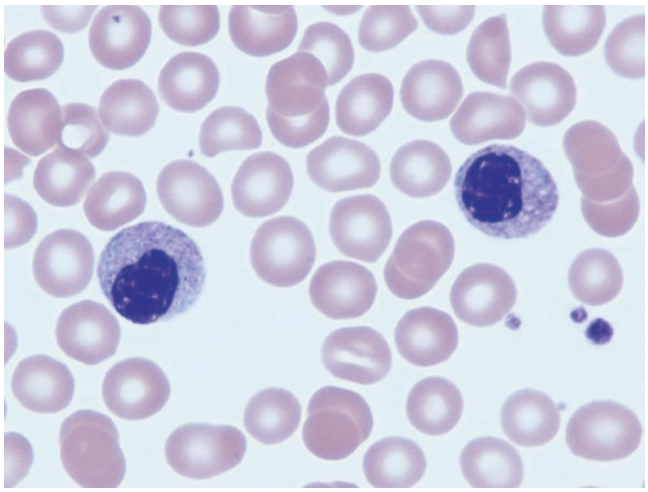

Fig. 10.5 Peripheral blood smear from a patient with a history of kidney transplant on valacyclovir and tacrolimus showing red cell macrocytosis and numerous hypolobated neutrophils in the peripheral blood. The case highlights the fact that the presence of morphologic dysplasia alone is not sufficient to establish a diagnosis of MDS and was secondary to the medications in this case

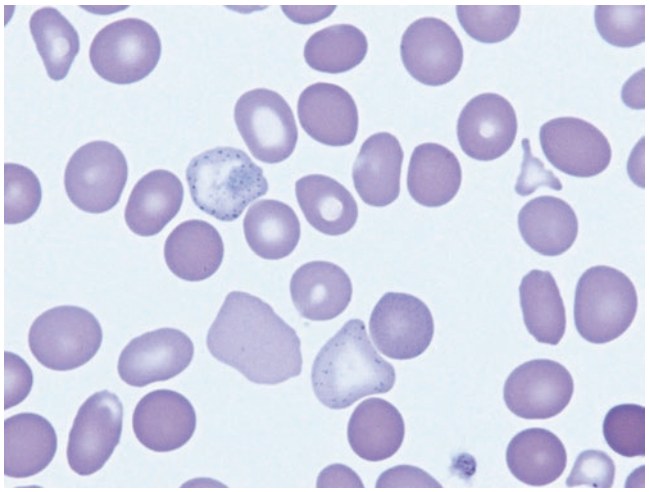

Fig. 10.7 Peripheral blood smear from a patient with myelodysplastic syndrome with single lineage dysplasia and ring sideroblasts (MDS-RSSLD) previously known as refractory anemia with ring sideroblasts (RARS). The red cells are macrocytic, and basophilic stippling noted in the red cells is a consequence of abnormal ribosomal maturation and retention in anucleate red cells

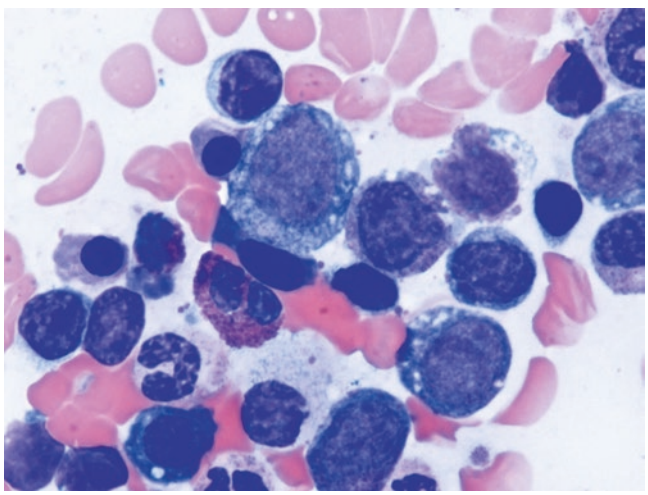

Fig. 10.6 Bone marrow aspirate smear from a 42-year-old female patient who presented with pancytopenia. Bone marrow aspirate showed cytoplasmic vacuoles in precursors of all lineages. There was no increase in bone marrow blasts. A karyotype analysis revealed a normal female karyotype. Additional history obtained was notable for bariatric surgery performed 2 years prior to her current presentation. Because of the history and bone marrow morphology notable for vacuolated cytoplasm of both erythroid and myeloid lineage, copper deficiency (an MDS mimic) was suspected and laboratory studies showed a copper level of less than 20 mcg/dL. In addition to bariatric surgery, copper deficiency can result from parenteral or tube feedings without copper supplementation, protein-losing enteropathies and excessive zinc intake (causes intestinal trapping of copper), zinc-containing denture adhesive, and nutritional supplements [4]

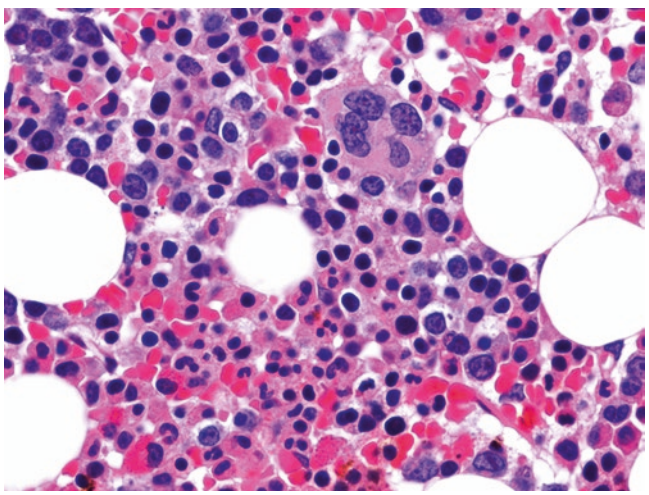

Fig. 10.8 Bone marrow core biopsy in MDS-RSSLD is mildly hypercellular and notable for erythroid proliferation. Blasts, by definition, account for less than 5% of the bone marrow cellularity. Normally maturing granulocytic cells and morphologically normal megakaryocytes are present

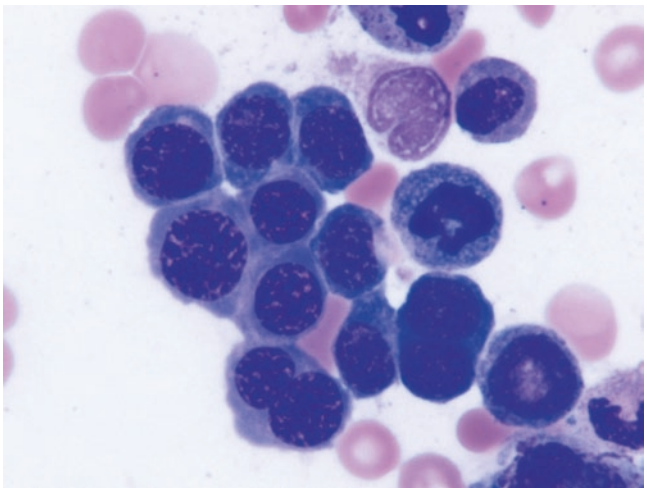

Fig. 10.9 Wright-Giemsa-stained preparation of the bone marrow aspirate of MDS-RSSLD shows megaloblastoid erythroid maturation and occasional binucleate erythroid precursors. There is no granulocytic or megakaryocyte dysplasia noted

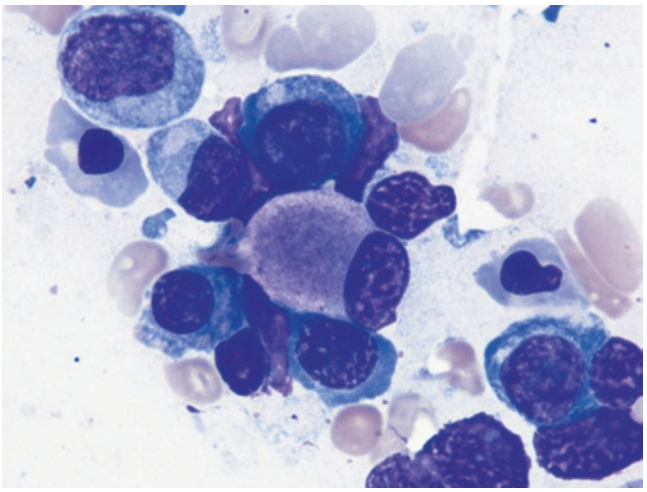

Fig. 10.11 In contrast to Fig. 10.9, this bone marrow aspirate shows a dysplastic unilobated megakaryocyte in addition to megaloblastoid erythroid precursors. A Prussian blue stain showed numerous ring sideroblasts and next-generation sequencing (NGS) was notable for an *SF3B1* mutation. In the absence of increased bone marrow blasts, the presence of *SF3B1* mutation is associated with a favorable outcome even in patients with multilineage dysplasia [6]. The 2016 revision of the WHO classification allows for recognition of patients with multilineage dysplasia and ring sideroblasts or *SF3B1* mutation as a distinct subtype designated MDS with multilineage dysplasia and ring sideroblasts (MDS-RSMLD)

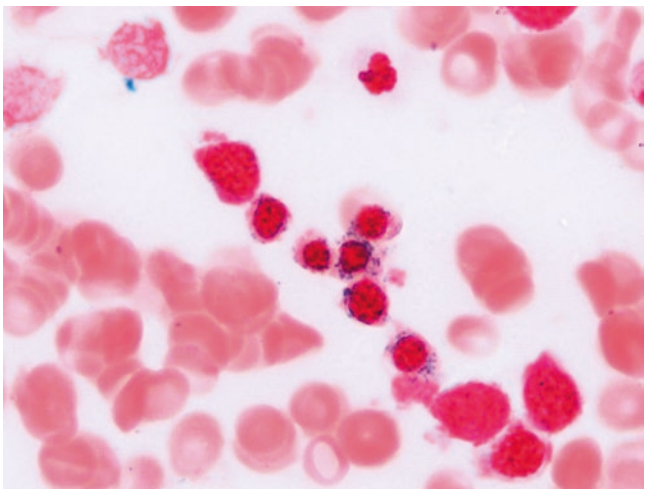

Fig. 10.10 Prussian blue stain of the bone marrow aspirate of MDS-RSSLD shows numerous ring sideroblasts. Ring sideroblasts are defined as red cell precursors with 5 or more granules encircling one-third or more of the nucleus. Historically, the diagnosis of refractory anemia with ring sideroblasts (RARS) was rendered in patients with peripheral blood anemia and dysplasia restricted to the erythroid lineage if 15% or more of the erythroid precursors were demonstrated to be ring sideroblasts. Recent data [5] has indicated a strong correlation between the presence of bone marrow ring sideroblasts and mutation in the spliceosome gene *SF3B1*. The upcoming revision of the WHO classification therefore allows for making the diagnosis with as few as 5% ring sideroblasts if an *SF3B1* mutation is present. In keeping with the revised nomenclature that eliminates the use of refractory anemia, the proposed new classification of RARS is MDS-RSSLD

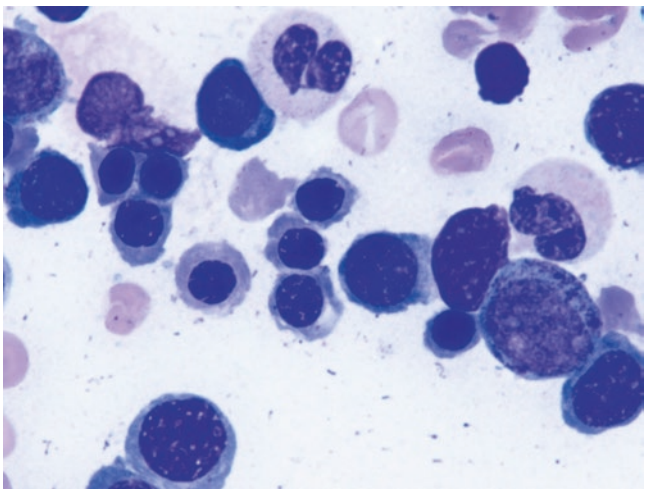

Fig. 10.12 MDS-RSMLD with megaloblastoid erythroid maturation and granulocytic dysplasia manifest as nuclear hypolobation and hypogranular cytoplasm in 20% of the neutrophil precursors and neutrophils. Blasts were less than 5% of the cells in the bone marrow. A Prussian blue stain showed ring sideroblasts and NGS showed *SF3B1* mutation

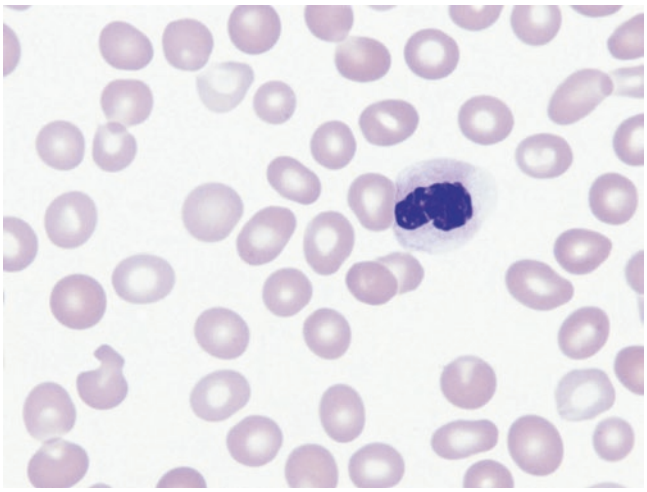

Fig. 10.13 MDS with multilineage dysplasia (MDS-MLD) is associated with variable cytopenias. In this example, all three lineages are affected. No blasts were appreciated in the peripheral blood. The neutrophil shown is dysplastic and shows hypolobated nucleus with abnormally condensed chromatin and hypogranular cytoplasm

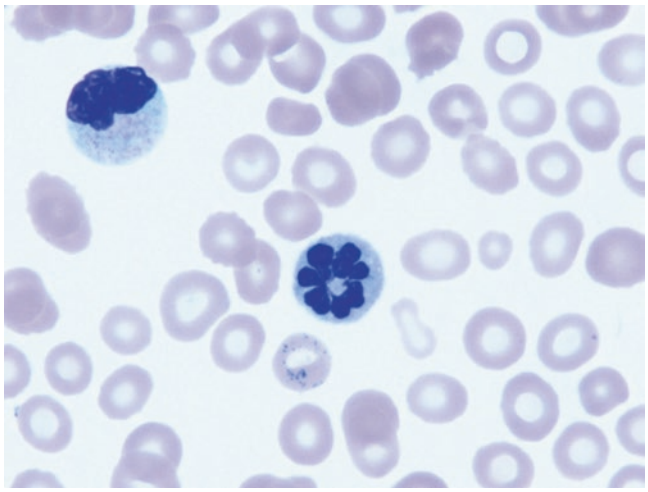

Fig. 10.15 MDS-MLD with additional granulocytic dysplasia manifest by irregular nuclear hypersegmentation and hypogranular cytoplasm

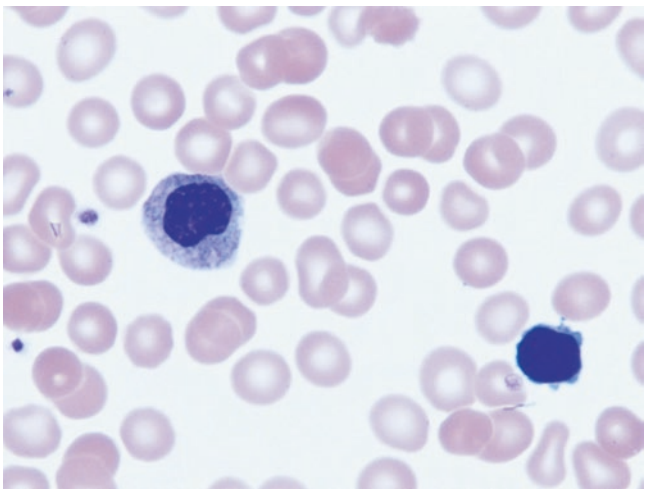

Fig. 10.14 MDS-MLD with preserved platelet count, macrocytic anemia, and unilobated neutrophils in the peripheral blood

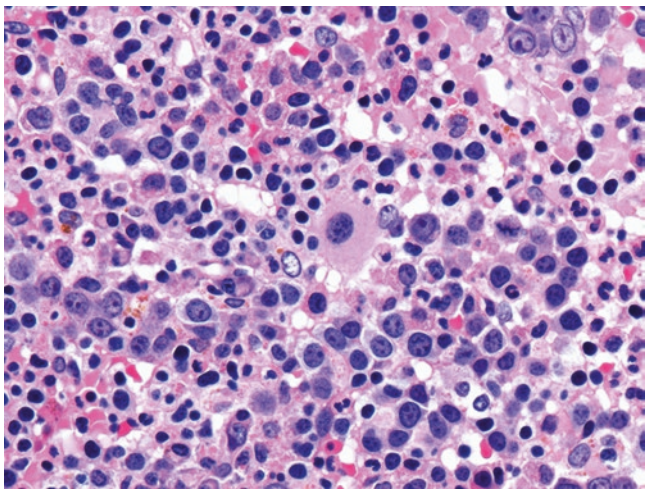

Fig. 10.16 MDS-MLD with hypercellular bone marrow indicative of ineffective hematopoiesis, which is a common underlying feature of all MDS. The biopsy is notable for megaloblastoid erythroid maturation and unilobated megakaryocytes. While granulocytic maturation is left shifted, blasts account for less than 5% of the marrow cellularity

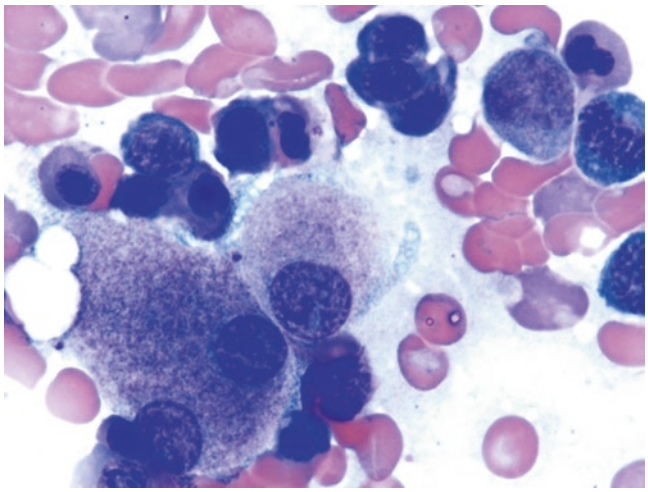

Fig. 10.17 The bone marrow aspirate smear shows dysplastic megakaryocytes that are small in size and have a single-lobed nucleus. Other megakaryocytes are larger and shows widely separated nuclear lobes. In addition, there is megaloblastoid erythroid maturation with nuclei notable for budding and bilobation consistent with dysplasia in two lineages and a diagnosis of MDS-MLD previously referred to as refractory cytopenia with multilineage dysplasia (RCMD)

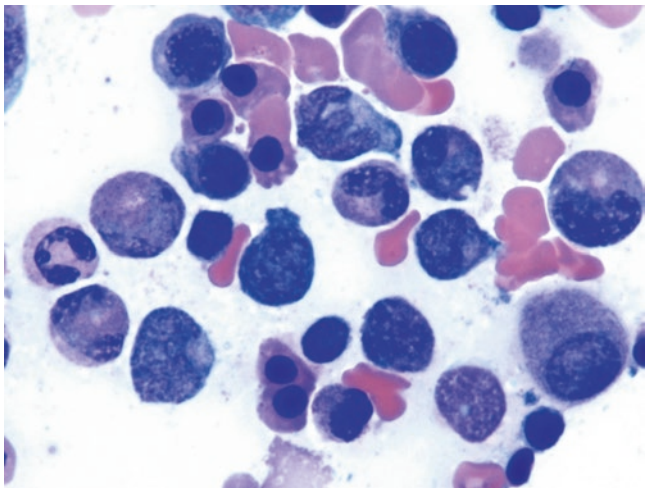

Fig. 10.19 MDS-MLD with dysplastic megakaryocyte and granulocytic dysplasia. While one blast is present in the field, the overall bone marrow blast count was less than 5%, and no blasts were appreciated in the peripheral blood

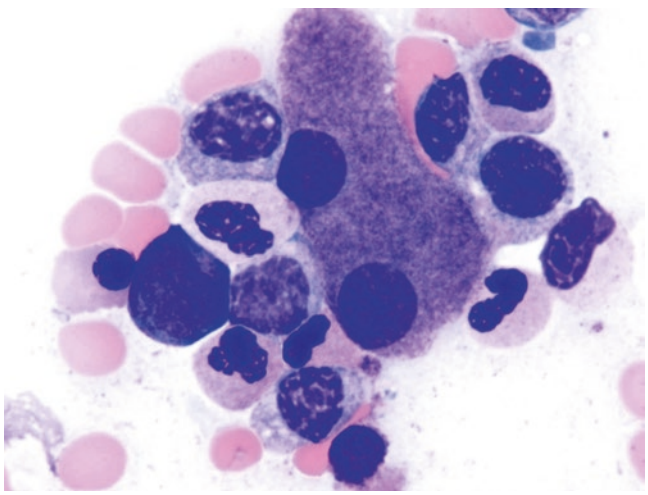

Fig. 10.18 MDS-MLD affecting granulocytic and megakaryocyte lineage. Neutrophil dysplasia is represented by nuclear hypolobation and cytoplasmic granularity. Megakaryocyte dysplasia is represented by abnormally separated nuclear lobes. Erythropoiesis is overall reduced and blasts were less than 5%. No ring sideroblasts were appreciated and the karyotype was notable for i(17q) resulting in deletion of the short arm of chromosome 17 with consequent loss of *TP53* gene

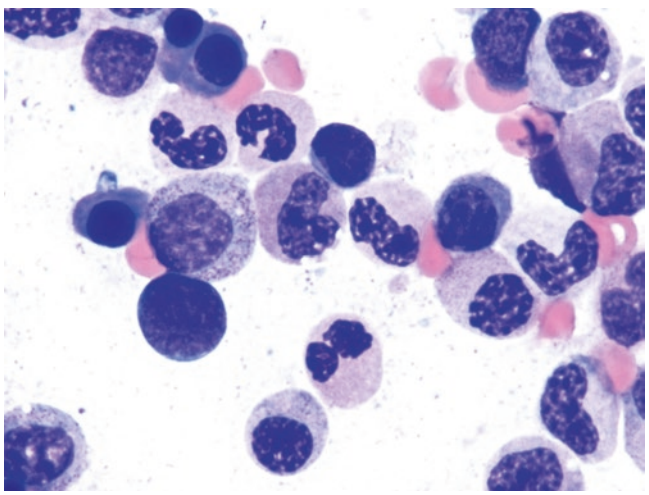

Fig. 10.20 The bone marrow aspirate smear is from a 71-year-old gentleman who presented with anemia and thrombocytopenia and 2% blasts in the peripheral blood. The bone marrow aspirate shows marked granulocytic dysplasia represented by unilobated and hypolobated neutrophils with cytoplasmic hypogranularity and 6% blasts in the bone marrow consistent with a diagnosis of MDS with excess blasts-1 (MDS-EB1) previously referred to as refractory anemia with excess blasts (RAEB)

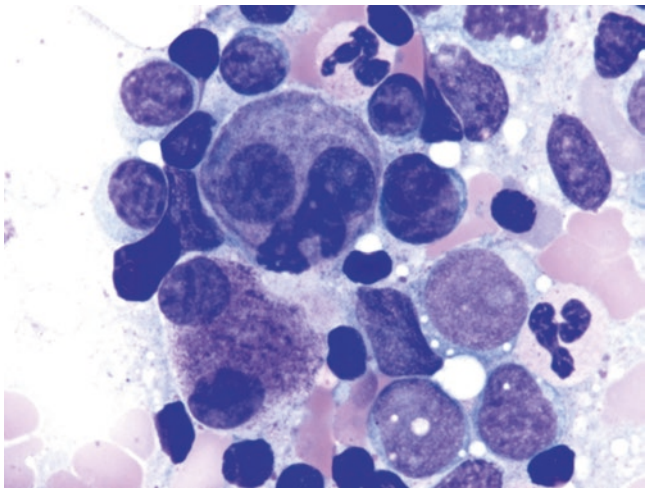

Fig. 10.21 The bone marrow aspirate smear is notable for presence of dysplastic megakaryocytes, dysplastic neutrophils, and 12% blasts consistent with a diagnosis of MDS-EB2. The karyotype was notable for -5 and del(20q). The clinical course was notable for progression to acute myeloid leukemia 3 months after initial diagnosis

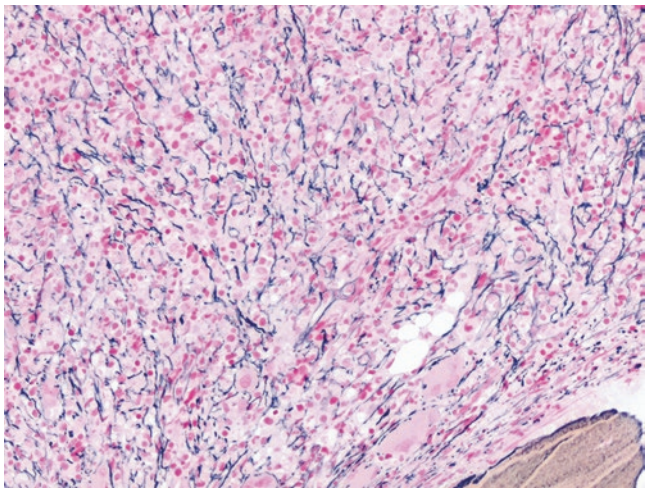

Fig. 10.23 A reticulin stain shows diffusely increased bone marrow fibrosis. Because bone marrow fibrosis (and concomitant cytopenias) can be seen in other conditions including therapy-related myeloid neoplasm and myeloproliferative neoplasms, these conditions should be excluded

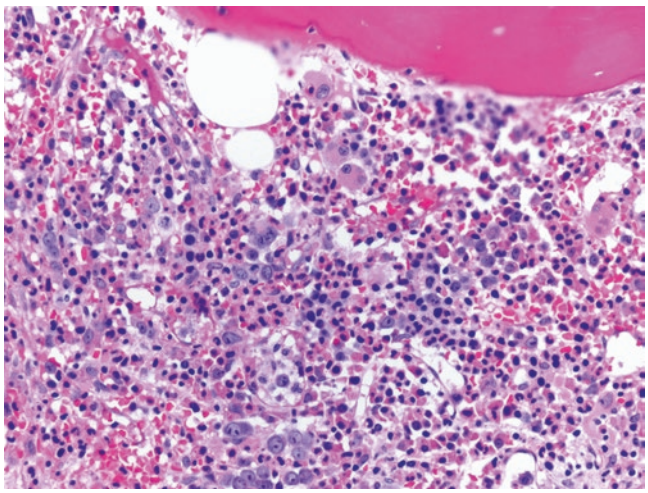

Fig. 10.22 In about 15% of patients with MDS, significant fibrosis can be seen in the bone marrow [7]. The bone core biopsy shown here is notable for streaming of cells and dilated sinuses suggestive of underlying fibrosis. Clearly dysplastic megakaryocytes are appreciated close to the boney trabeculum

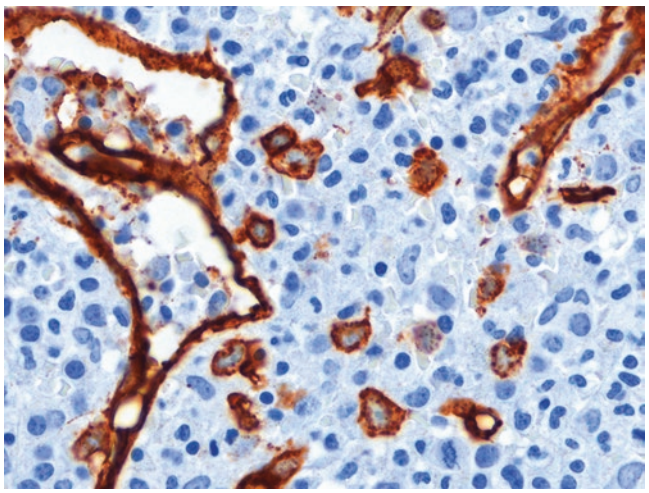

Fig. 10.24 CD34 immunostaining in a patient with MDS and increased bone marrow fibrosis. Most cases of MDS with fibrosis are associated with increased blasts. However, the bone marrow aspirate smears are inadequate for an accurate differential, and the demonstration of increased bone marrow blasts relies on immunohistochemistry

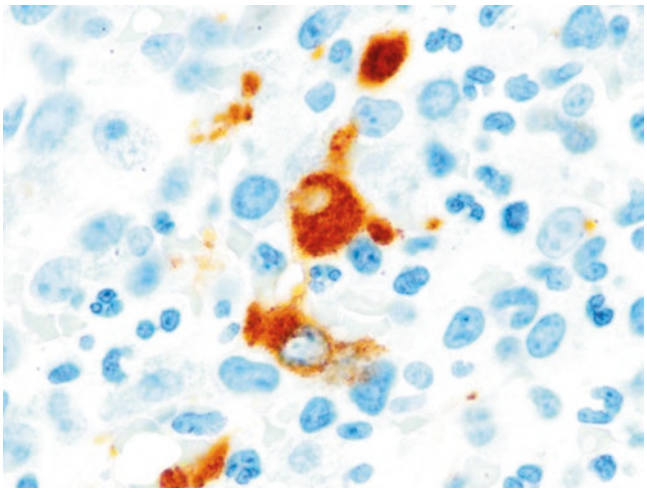

Fig. 10.25 CD61 immunostaining used to highlight small dysplastic megakaryocytes in a bone core biopsy in a patient with MDS and increased bone marrow fibrosis. These dysplastic megakaryocytes can be numerous in patients with increased bone marrow fibrosis and somewhat masked by numerous granulocytic precursors particularly when micromegakaryocytes are present

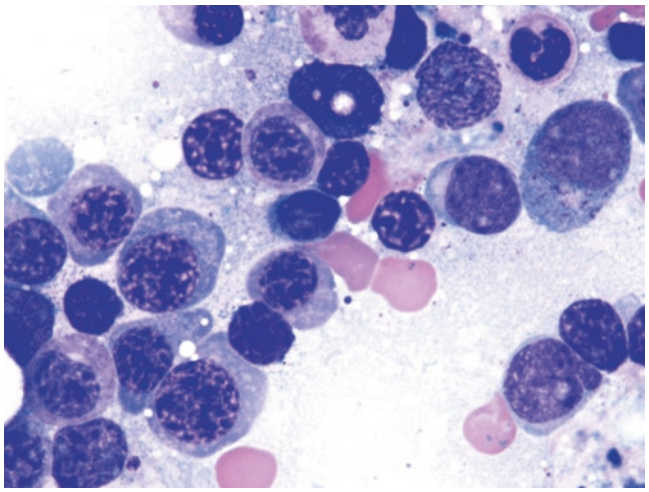

Fig. 10.27 The bone marrow aspirate shows increased blasts (6% of the marrow cellularity) along with increased erythroid precursors that account for 80% of the marrow cellularity. This would have resulted in enumeration of the blasts as a fraction of non-erythroid cells and a diagnosis of acute myeloid leukemia of the erythroid/myeloid type per the 2008 WHO classification. However, the clinical behavior and genetic profile of these cases are more closely aligned to MDS than AML [8]. Therefore the 2016 revision of the WHO classification recommends enumeration of the blast count from all nucleated cells in the bone marrow. The appropriate diagnosis for this bone marrow aspirate would therefore be MDS-EB1

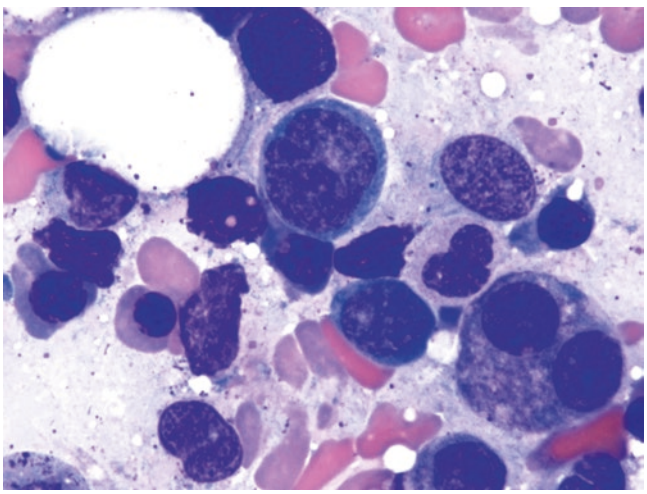

Fig. 10.26 MDS-EB with ring sideroblasts and *SF3B1* mutation as exemplified by this case with multilineage dysplasia and increased blasts is not associated with the favorable outcome noted in patients with *SF3B1* mutation but no increase in bone marrow blasts. Therefore, irrespective of *SF3B1* mutation, the diagnosis for these cases remains MDS with excess blasts

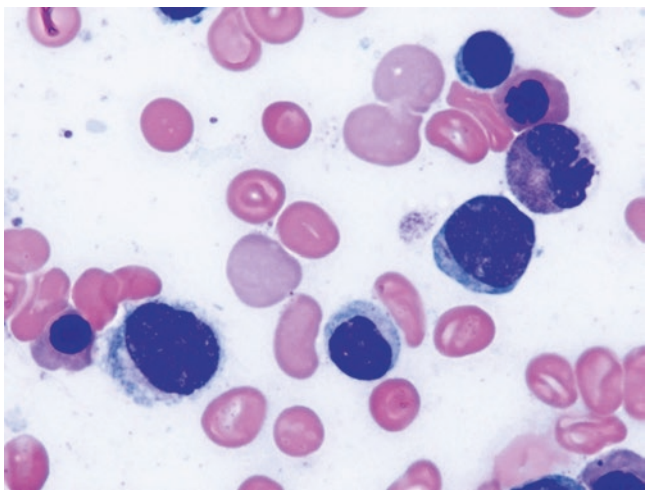

Fig. 10.28 The bone marrow aspirate smear illustrates an Auer rod in patient with megakaryocyte and erythroid dysplasia and bone marrow blast count of 3%. Irrespective of the peripheral blood or bone marrow blast count, the presence of Auer rods in the blasts tends to be associated with a more aggressive clinical course, and these cases are best classified as MDS-EB [9]

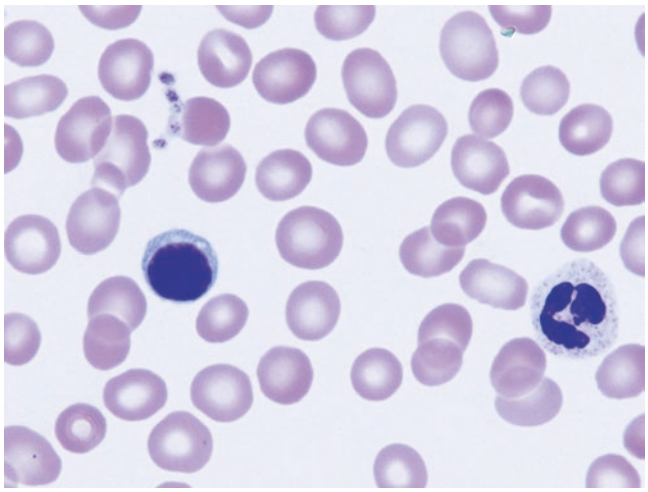

Fig. 10.29 Peripheral blood smear with macrocytic anemia, normal white cell and platelet count with no circulating blasts or granulocytic dysplasia, is the most common manifestation of patients with MDS with isolated del(5q)

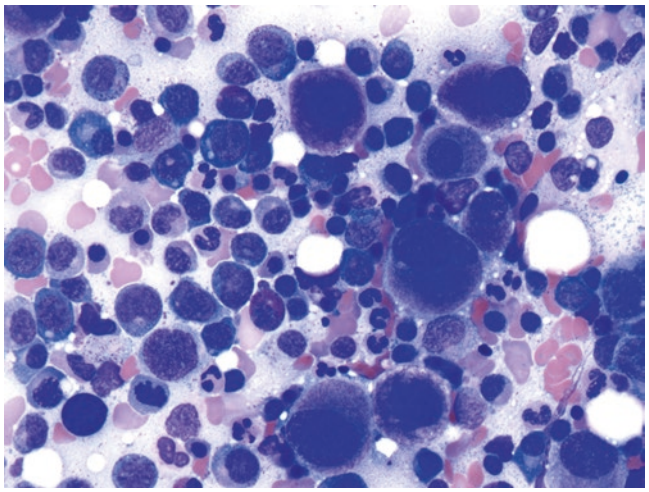

Fig. 10.31 Bone marrow aspirate smear shows several small, unilobated megakaryocytes and no dysplasia in the maturing granulocytic cells. The karyotype was notable for a single cytogenetic abnormality of del(5q). The term 5q- syndrome has been used to designate cases with macrocytic anemia, normal or elevated platelet count, and BM erythroid hyperplasia. By definition, the peripheral blood blast count is less than 1% and the bone marrow blast count is less than 5%. Recent literature has demonstrated that single additional, low-risk cytogenetic abnormalities do not influence the clinical behavior of the disease, and therefore the diagnosis of MDS with isolated del(5q) can be made even in the presence of one additional cytogenetic abnormality provided it is not monosomy 7 [10]

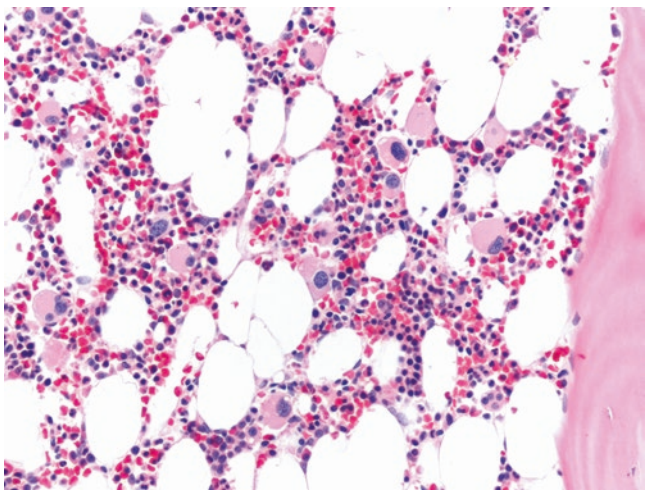

Fig. 10.30 The bone marrow biopsy in this case of MDS with isolated del(5q) is mildly hypocellular and notable for increased megakaryocytes that are somewhat small in size and have non-lobated nuclei. Bone marrow blasts are not increased

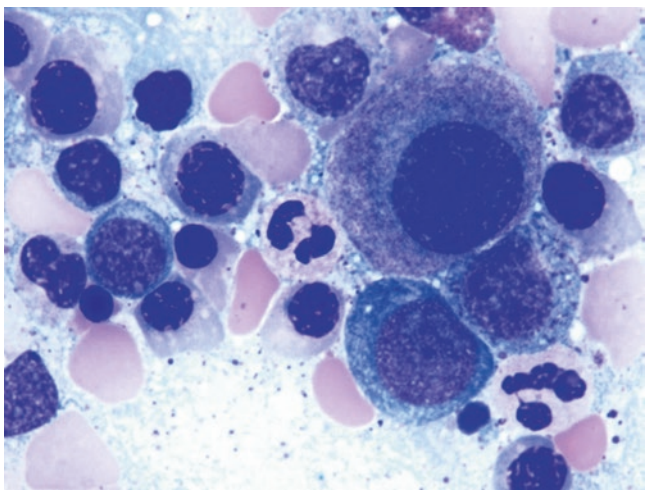

Fig. 10.32 Another example of bone marrow aspirate notable for megaloblastoid erythroid maturation and unilobated megakaryocyte. While rare neutrophils with hypogranular cytoplasm, as shown here, can be present, neutrophil dysplasia in more than 10% of the neutrophils or more than 5% bone marrow blasts precludes the diagnosis of MDS with isolated del(5q)

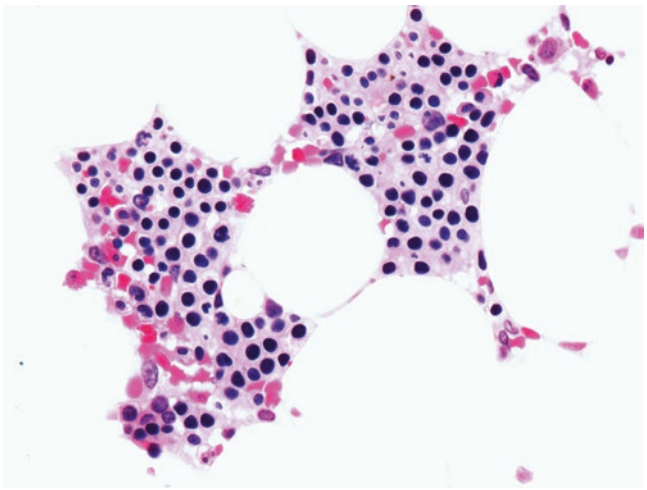

Fig. 10.33 MDS presenting in childhood is extremely uncommon and the diagnosis should always lead to careful exclusion of inherited bone marrow failure syndrome. Unlike the adult population, low-grade MDS in the childhood group frequently presents with very hypocellular bone marrow and needs to be distinguished from aplastic anemia. The presence of clusters of erythroid precursors with megaloblastoid erythroid maturation and increased mitoses as shown in this image are supportive of a diagnosis of refractory cytopenia of childhood (RCC) and help distinguish the condition from aplastic anemia [11, 12]

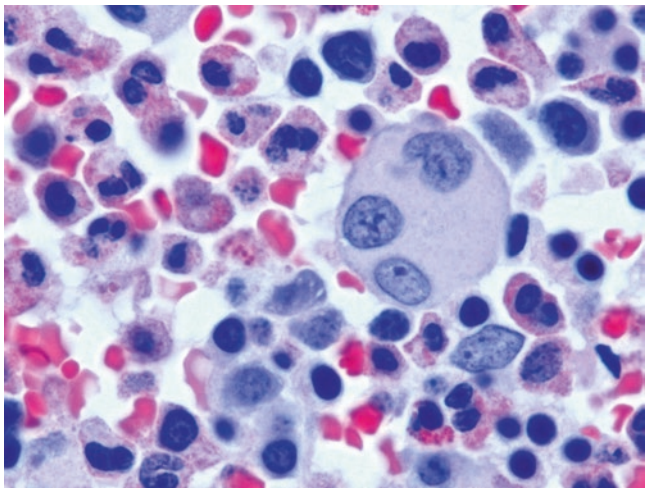

Fig. 10.35 The bone core biopsy with dysplastic megakaryocytes and increased blasts demonstrates another presentation of childhood MDS. In the context of increased bone marrow blasts, the presence of leukemia-defining cytogenetic abnormalities such as t(8;21) or inv(16) should be excluded. When present, these recurrent cytogenetic abnormalities allow the diagnosis of AML even with less than 20% bone marrow blasts

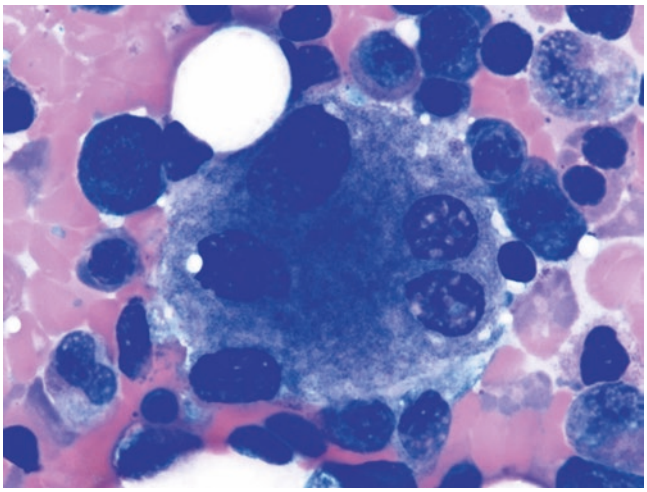

Fig. 10.34 Distinctly large megakaryocytes, when present, are also a distinctive feature of childhood MDS

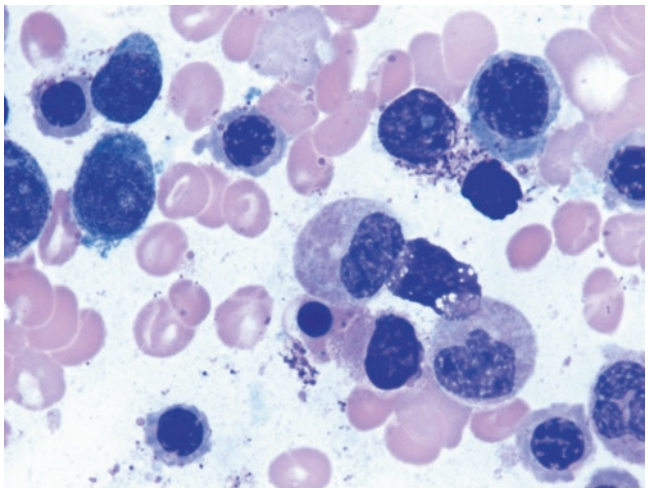

Fig. 10.36 The bone marrow aspirate shows increased blasts along with dysplastic neutrophils. The karyotype was notable for monosomy 7. Abnormal karyotype is seen in 55% of children with MDS with excess blasts with monosomy 7 being the most common cytogenetic abnormality followed by trisomy 8 and trisomy 21 [13]

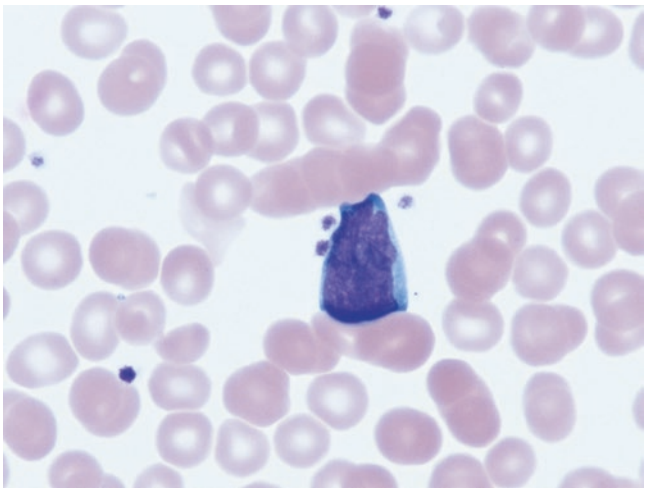

Fig. 10.37 Contrary to the name, MDS unclassifiable (MDS-U) as a category is a designation used for three specific situations. The peripheral blood illustrates one such example of the presence of 1% blasts on two repeat peripheral blood smears in a patient with peripheral pancytopenia and bone marrow notable for 2% blasts accompanied by dysgranulopoiesis and dyserythropoiesis. These patients tend to have a clinical course somewhat more aggressive than that observed when peripheral blood blasts are less than 1% resulting in a diagnosis of MDS-U

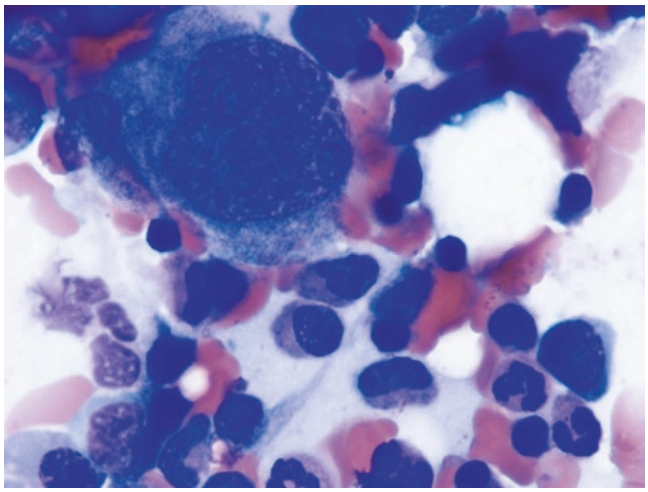

Fig. 10.39 Another example of MDS-U where the bone marrow aspirate smear shows a single hypolobated megakaryocyte and somewhat megaloblastoid erythroid precursors in a patient with anemia and thrombocytopenia. The karyotype was notable for presence of del(9q)

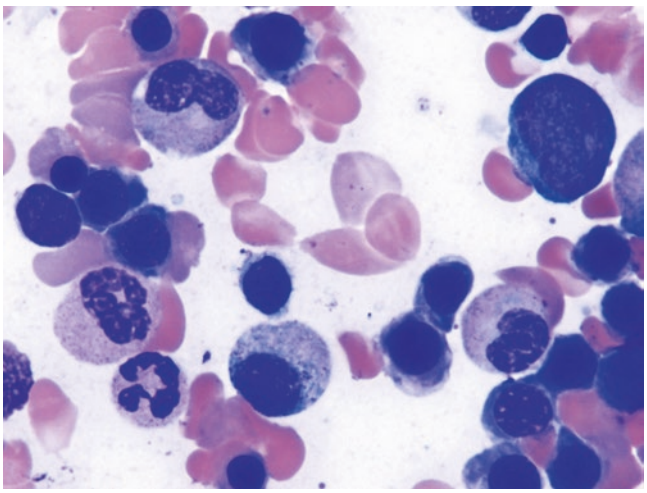

Fig. 10.38 More frequently, a diagnosis of MDS-U is made when, in the context of peripheral cytopenia(s), the bone marrow dysplasia is equivocal or affects less than 10% cells for a given lineage but is accompanied by an MDS-defining cytogenetic abnormality (see Table 10.2). This bone marrow aspirate showed occasional hypolobated neutrophils, 1% bone marrow blasts, and no erythroid or megakaryocyte dysplasia. The karyotype was notable for the presence of monosomy 13

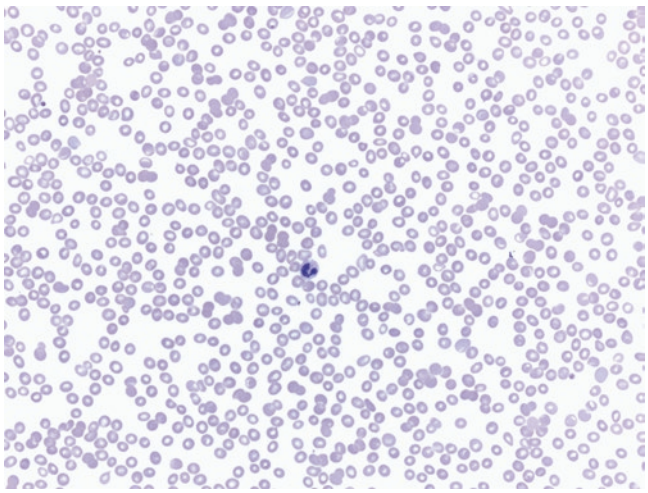

Fig. 10.40 The third category of MDS cases, in which diagnosis of MDS-U is preferred, is in the context of pancytopenia with unequivocal dysplasia in a single lineage in the bone marrow. The peripheral blood shown here is notable for pancytopenia with no circulating blasts. However, the bone marrow showed mostly hypolobated megakaryocytes but unremarkable neutrophils and erythroid precursors. The karyotype was notable for trisomy 8 and a normal chromosome 5

Table 10.2 Recurrent cytogenetic abnormalities in MDS

Unbalanced	Balanced
-7 or del(7q) (10%)	t(11;16)(q23;p13.3)
-5 or del(5q) (10–15%)	t(3;21)(q26.2;q22.1)
i(17q) or t(17p) (2–3%)	t(1;3)(p36.3;q21.2)
-13 or del(13q) (1–2%)	t(2;11)(p21;q23)
del(11q) (1–2%)	inv(3)(q21q26.2)
del(12p) or t(12p) (1–2%)	t(6;9)(p23;q34)
del(9q) (1%)	
idic(X)(q13) (1%)	

+8, -Y and del(20q) cannot be used to make a diagnosis of MDS without unequivocal dysplasia

References

1. Arber DA, Orazi A, Hasserjian R, Thiele J, Borowitz MJ, Le Beau MM, et al. The 2016 revision to the World Health Organization classification of myeloid neoplasms and acute leukemia. Blood. 2016;127:2391–405.
2. Arber DA, Hasserjian RP. Reclassifying myelodysplastic syndromes: what's where in the new WHO and why. Hematology Am Soc Hematol Educ Program. 2015;2015:294–8.
3. Germing U, Strupp C, Giagounidis A, Haas R, Gattermann N, Starke C, et al. Evaluation of dysplasia through detailed cytomorphology in 3156 patients from the Dusseldorf registry on myelodysplastic syndromes. Leuk Res. 2012;36:727–34.
4. Willis MS, Monaghan SA, Miller ML, McKenna RW, Perkins WD, Levinson BS, et al. Zinc-induced copper deficiency: a report of three cases initially recognized on bone marrow examination. Am J Clin Pathol. 2005;123:125–31.
5. Papaemmanuil E, Cazzola M, Boultwood J, Malcovati L, Vyas P, Bowen D, et al. Somatic SF3B1 mutation in myelodysplasia with ring sideroblasts. N Engl J Med. 2011;365:1384–95.
6. Malcovati L, Karimi M, Papaemmanuil E, Ambaglio I, Jädersten M, Jansson M, et al. SF3B1 mutation identifies a distinct subset of myelodysplastic syndrome with ring sideroblasts. Blood. 2015;126:233–41.
7. Vardiman JW. Hematopathological concepts and controversies in the diagnosis and classification of myelodysplastic syndromes. Hematology Am Soc Hematol Educ Program. 2006:199–204.
8. Grossmann V, Bacher U, Haferlach C, Schnittger S, Pötzinger F, Weissmann S, et al. Acute erythroid leukemia (AEL) can be separated into distinct prognostic subsets based on cytogenetic and molecular genetic characteristics. Leukemia. 2013;27:1940–3.
9. Willis MS, McKenna RW, Peterson LC, Coad JE, Kroft SH. Low blast count myeloid disorders with Auer rods: a clinicopathologic analysis of 9 cases. Am J Clin Pathol. 2005;124:191–8.
10. Germing U, Lauseker M, Hildebrandt B, Symeonidis A, Cermak J, Fenaux P, et al. Survival, prognostic factors and rates of leukemic transformation in 381 untreated patients with MDS and del(5q): a multicenter study. Leukemia. 2012;26:1286–92.
11. Baumann I, Führer M, Behrendt S, Campr V, Csomor J, Furlan I, et al. Morphological differentiation of severe aplastic anaemia from hypocellular refractory cytopenia of childhood: reproducibility of histopathological diagnostic criteria. Histopathology. 2012;61:10–7.
12. Niemeyer CM, Baumann I. Classification of childhood aplastic anemia and myelodysplastic syndrome. Hematology Am Soc Hematol Educ Program. 2011;2011:84–9.
13. Hasle H. Myelodysplastic and myeloproliferative disorders of childhood. Hematology Am Soc Hematol Educ Program. 2016;2016:598–604.

Acute Myeloid Leukemia

11

Daniel A. Arber

Acute myeloid leukemia (AML) represents a heterogenous group of disorders that are characterized by peripheral blood and bone marrow myeloblast proliferations that will kill the patient in weeks or months if untreated [1]. They show variable response to therapy, and some types are best treated by hematopoietic cell transplantation, while other types may be eligible for more targeted therapy. The 2016 World Health Organization (WHO) classification of acute myeloid leukemia includes a number of categories and many subtypes [2]. Most of these subtypes have distinctive morphologic features, which are illustrated in this chapter, but the complete diagnosis relies on correlation between morphology, immunophenotypic, cytogenetic, and molecular genetic studies. Although the detection of Auer rods—cytoplasmic granules that aggregate to form rod-shaped cytoplasmic inclusions—is specific for myeloid lineage, they are not present in many cases, and immunophenotyping is now routine in all cases of suspected acute leukemia. Cytochemical studies may also be useful but have been largely supplanted by flow cytometry immunophenotyping. While this chapter focuses on the morphology of the bone marrow in AML, correlation with peripheral blood findings is also essential, and some cases may have more myeloblasts in the blood than in the marrow; such cases may be diagnosed as AML based solely on the peripheral blood blast cell count.

Table 11.1 lists the various disease categories of AML in the 2016 WHO classification. Morphologic features are fairly specific for acute promyelocytic leukemia with *PML-RARA*, AML with t(8;21)(q22;q22.1), and AML with inv(16)(p13.1q22) or t(16;16)(p13;q22) (Figs. 11.1, 11.2, 11.3 and 11.4), but the molecular or cytogenetic abnormality in each must be confirmed [3]. These three disease groups are also considered as AML even when blast cells are less than 20% in the peripheral blood and bone marrow. The remaining categories of AML with recurrent genetic abnormalities (Figs. 11.5, 11.6, 11.7, 11.8, 11.9, 11.10, 11.11 and 11.12) are required to have 20% or more blood or marrow blasts to be diagnosed as AML. Cases in these groups with less than 20% blast cells are generally diagnosed as myelodysplastic syndrome (MDS).

Cases of AML with myelodysplasia-related changes (Figs. 11.13, 11.14 and 11.15) may be diagnosed with any of the three features, but many have more than one. They may have (1) multilineage dysplasia in blood or marrow, defined by dyspoiesis of 50% or more cells in a given lineage and at least two lineages affected (maturing myeloid cells, nucleated erythroid cells, or megakaryocytes/platelets), (2) myelodysplasia-related cytogenetic abnormalities (Table 11.2), or (3) a history of MDS or a myelodysplastic/myeloproliferative neoplasm. Cases diagnosed due to the presence of multilineage dysplasia alone, however, must not have mutations of *NPM1* or biallelic mutations of *CEBPA*, since dyspoiesis in those unique AML subtypes does not infer the poor prognosis usually associated with a diagnosis of AML with myelodysplasia-related changes [4].

A history of prior cytotoxic therapy (chemotherapy or radiation therapy) (Fig. 11.16) trumps all other AML categories in the 2016 WHO classification, and separating therapy-related cases based on blast cell count into AML or myelodysplastic syndrome is of limited prognostic significance [5]. Despite this, if one of the recurring cytogenetic abnormalities of other AML types (such as *PML-RARA*) is identified in a therapy-related case, the abnormality should be clearly noted in the diagnosis, as such findings may predict a survival difference compared to other therapy-related myeloid neoplasm types.

Acute myeloid leukemia, not otherwise specified (AML, NOS) (Figs. 11.17, 11.18, 11.19, 11.20, 11.21,

D.A. Arber (✉)
Department of Pathology, The University of Chicago,
Chicago, IL, USA
e-mail: darber@uchicago.edu

T.I. George, D.A. Arber (eds.), *Atlas of Bone Marrow Pathology*, Atlas of Anatomic Pathology,
https://doi.org/10.1007/978-1-4939-7469-6_11

Table 11.1 2016 WHO classification of acute myeloid leukemia (AML)

AML with recurrent genetic abnormalities
AML with t(8;21)(q22;q22.1); *RUNX1-RUNX1T1*
AML with inv(16)(p13.1q22) or t(16;16)(p13;q22); *CBFB-MYH11*
Acute promyelocytic leukemia with *PML-RARA*
AML with t(9;11)(p21.3;q23.3); *KMT2A-MLLT3*
AML with t(6;9)(p23;q34.1); *DEK-NUP214*
AML with inv(3)(q21.3q26.2) or t(3;3)(q21.3;q26.2); *GATA2, MECOM*
AML (megakaryoblastic) with t(1;22)(p13.3;q13.3); *RBM15-MKL1*
Provisional entity: AML with *BCR-ABL1*
AML with mutated *NPM1*
AML with biallelic mutations of *CEBPA*
Provisional entity: AML with mutated *RUNX1*
AML with myelodysplasia-related changes
Therapy-related myeloid neoplasms
AML not otherwise specified
AML minimally differentiated
AML without maturation
AML with maturation
Acute myelomonocytic leukemia
Acute monoblastic/monocytic leukemia
Pure erythroid leukemia
Acute megakaryocytic leukemia
Acute basophilic leukemia
Acute panmyelosis with myelofibrosis
Myeloid sarcoma
Myeloid proliferations related to Down syndrome

11.22, 11.23 and 11.24), contains morphologic subtypes that are not of prognostic significance, and subclassification is not necessary for most types [6]. Exceptions to this, however, are pure erythroid leukemia (Fig. 11.22) and acute panmyelosis with myelofibrosis (Fig. 11.24). Pure erythroid leukemia is a proliferation of nucleated erythroid cells (over 80%) with at least 30% normoblasts. The prior category of the erythroid/myeloid type of erythroleukemia, in which marrow-nucleated erythroid cells were 50% or more of marrow cells and myeloblasts were 20% or more of non-erythroid cells, has been eliminated from the AML classification [2]. Most of such cases are now diagnosed as myelodysplastic syndrome based on their absolute marrow blast cell count. Acute panmyelosis with myelofibrosis is extremely rare and may not actually exist as currently defined. Such cases have a panmyelosis of the marrow as well as at least 20% myeloblasts

Myeloid sarcoma is not illustrated in this atlas, since it represents a tissue manifestation of the various marrow disorders already illustrated. Some cases of AML, however, present as myeloid sarcomas without marrow involvement. Such cases should be further classified into a specific WHO category based on immunophenotypic, cytogenetic, and molecular genetic studies.

The myeloid proliferations related to Down syndrome (Fig. 11.25) include transient abnormal myelopoiesis, present at birth, and the later-occurring myeloid neoplasm of Down syndrome that may have features of AML or myelodysplastic syndrome [8, 9]. Megakaryoblasts are usually present in all types, and the morphologic features are not helpful in distinguishing the transient disorder from the later-occurring neoplasms that require therapy.

Because a variety of studies are necessary to arrive at a complete and accurate diagnosis of AML using the WHO classification, it is essential that the diagnosing physician correlates the immunophenotypic, cytogenetic, and molecular genetic findings with the morphology before issuing a final, consolidated report [10].

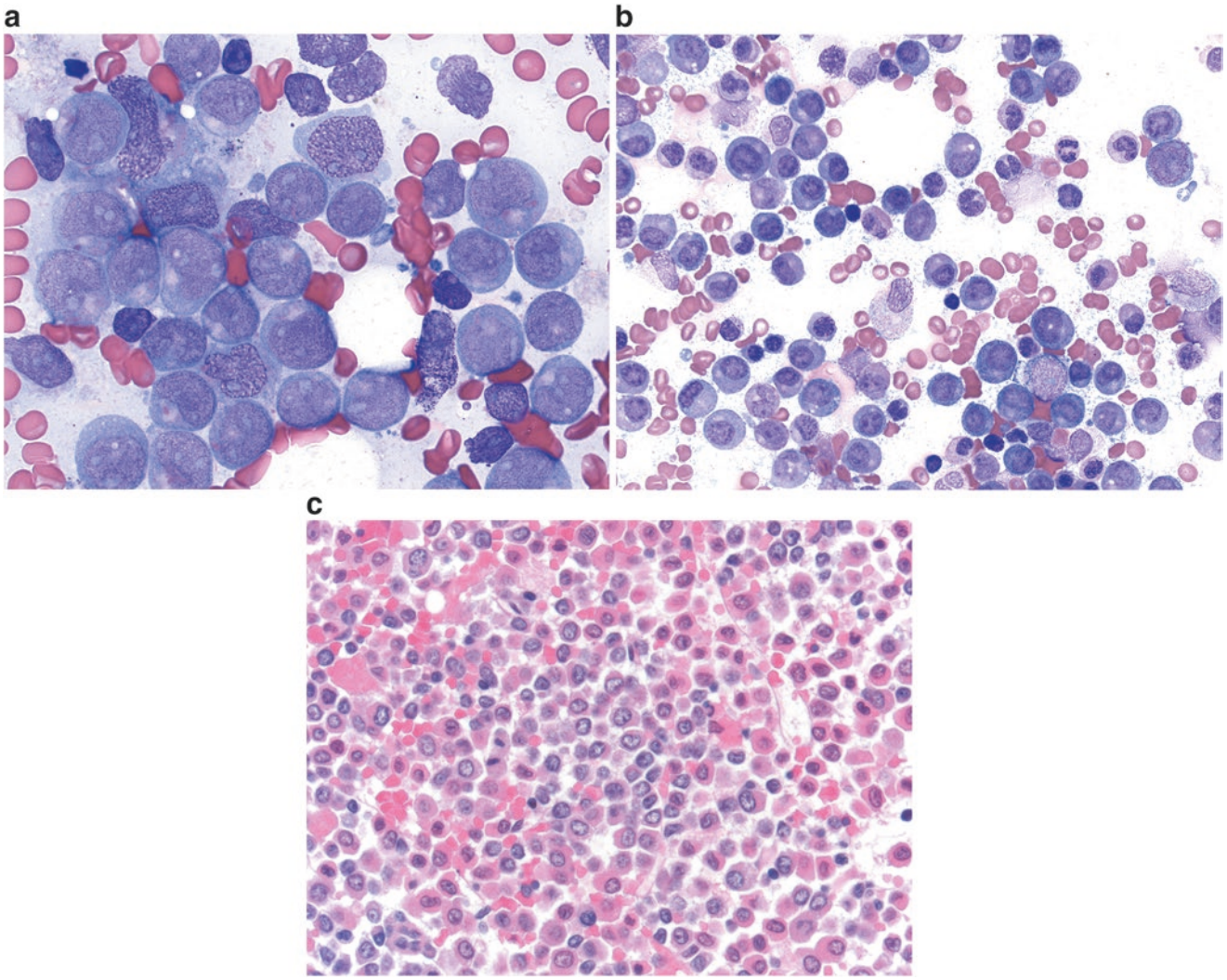

Fig. 11.1 AML with t(8;21)(q22;q22.1); *RUNX1-RUNX1T1*. (**a**) Bone marrow aspirate smear with many blasts with abundant cytoplasm, perinuclear hofs, and large pink or salmon-colored granules. These cells express myeloid antigens, including myeloperoxidase, as well as CD34, and are usually CD19 positive. Although they have similarities to promyelocytes, the presence of Auer rods, large pink granules, and the aberrant expression of CD19 are all features of leukemic cells, and such cells should be counted as blast equivalents. (**b**) Another case shows cells that may appear to be too mature for a diagnosis of AML, but such a case should be diagnosed as AML when this cytogenetic abnormality is present even when the blast count is below 20%. (**c**) This trephine biopsy also shows a proliferation of cells with abundant cytoplasm that may not clearly be identifiable as myeloblasts

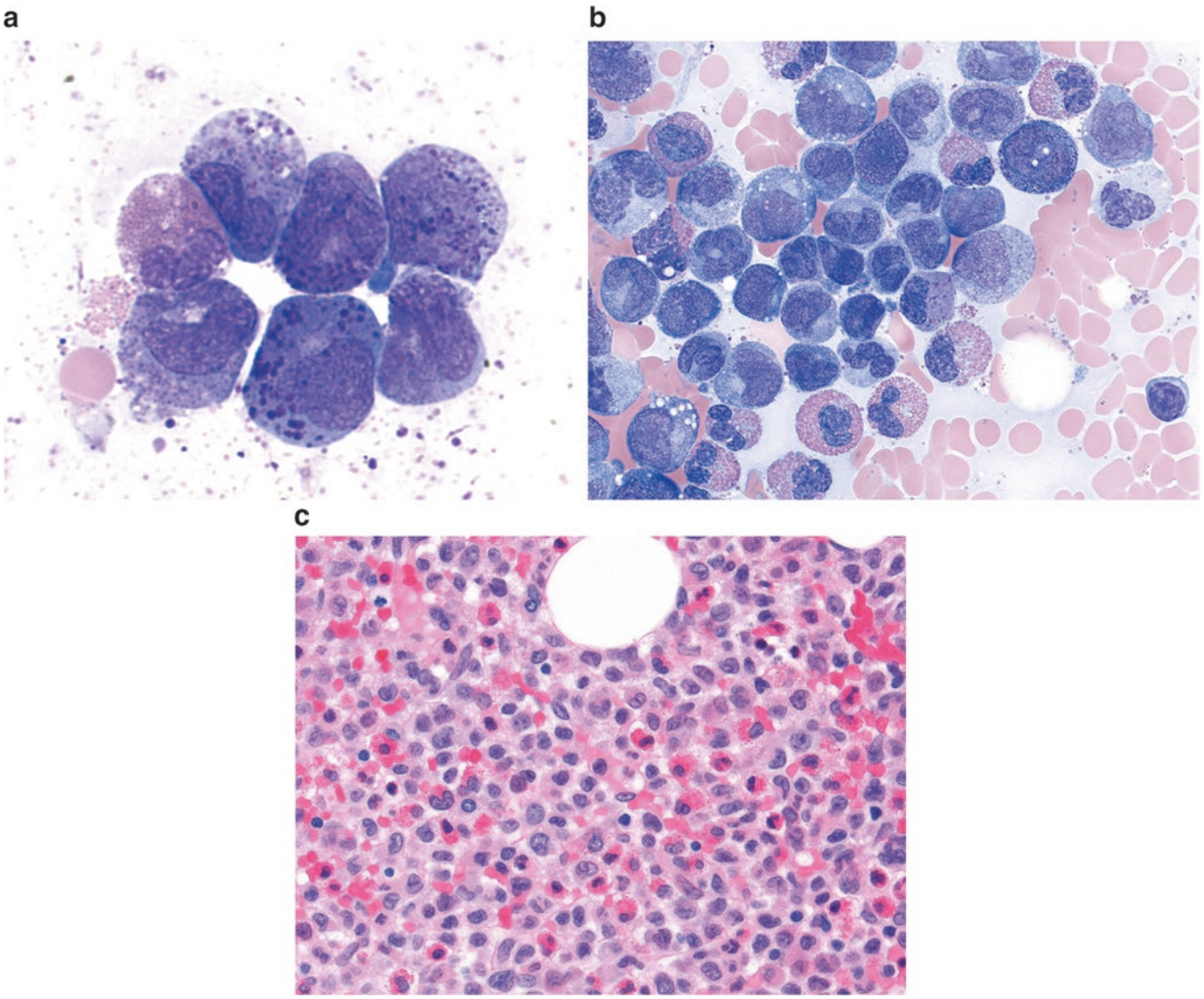

Fig. 11.2 AML with inv(16)(p13.1q22) or t(16;16)(p13.1;q22); *CBFB-MYH11*. (**a**) Abnormal eosinophils, defined as eosinophils and precursors that have eosinophil granules, but also dark, basophilic granules, are characteristic of this cytogenetic abnormality. The associated blast cell population may have a myelomonocytic appearance, and mature monocytes may be frequent. This mixture of cells may result in a blast cell count below 20%, but such cases should still be diagnosed as AML. (**b**) This leukemia has myelomonocytic blast cells as well as an increase in mostly normal eosinophil precursors. An abnormal eosinophil with a few basophilic granules is present near the center of the field. An increase in normal eosinophils may occur with other AML types and that finding alone is not sufficient to suggest an inv(16) or t(16;16). (**c**) The biopsy reveals sheets of cells with irregular nuclear contours, suggestive of myelomonocytic cells and an increase in eosinophil precursors. Abnormal eosinophils, however, cannot be detected in biopsy sections

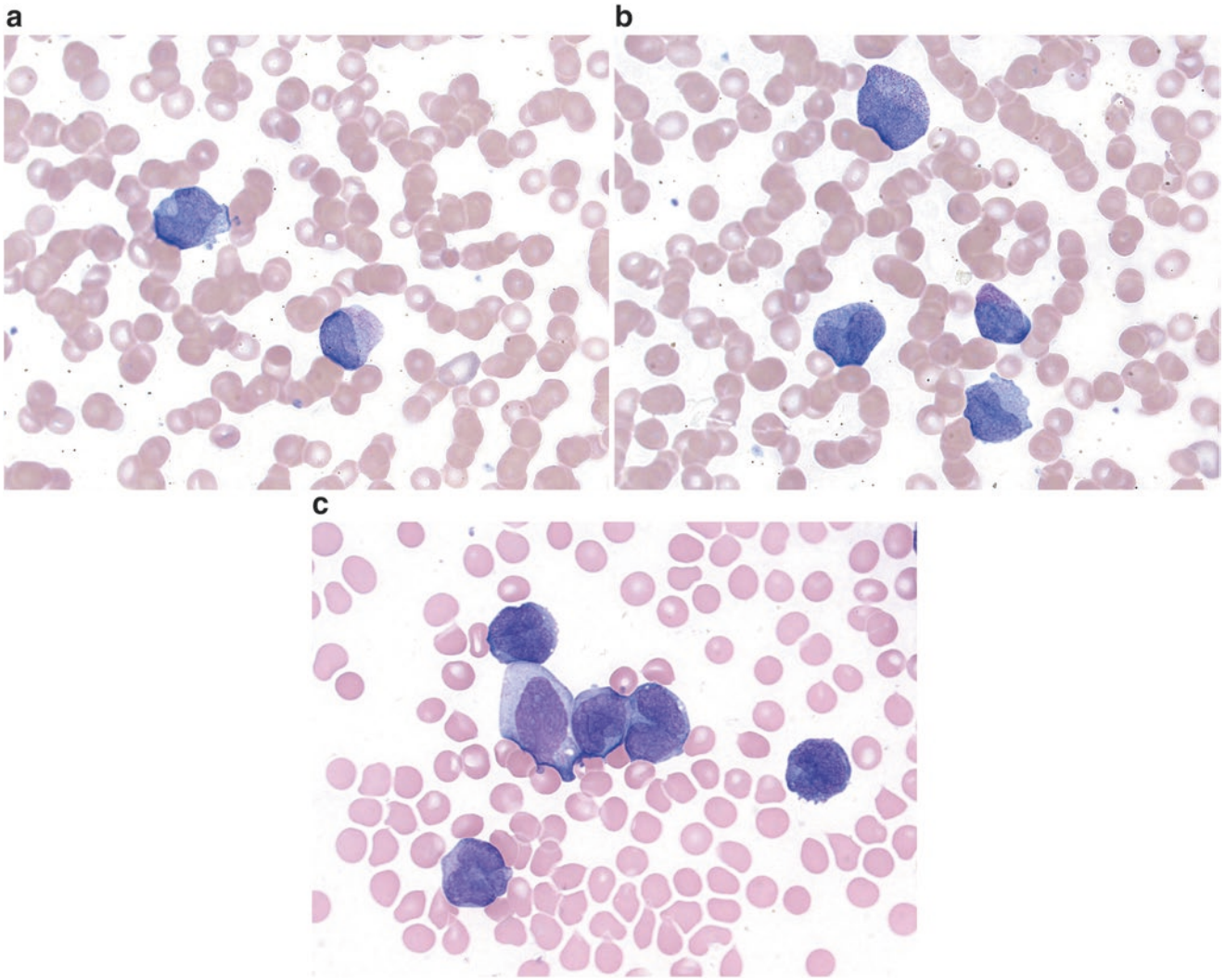

Fig. 11.3 Acute promyelocytic leukemia (APL) with *PML-RARA*. (**a–c**), The peripheral blood is often the first clue to the diagnosis of APL. While blasts with numerous Auer rods (**a**) or abundant cytoplasmic granules (**b**) are characteristic, they are often difficult to identify. Other, less granular blasts (**c**) have a characteristic bilobed or "butterfly-wing" nucleus, seen in all three cases. Identification of such cells in the blood should raise suspicion for APL even in the absence of cytoplasmic granules or Auer rods

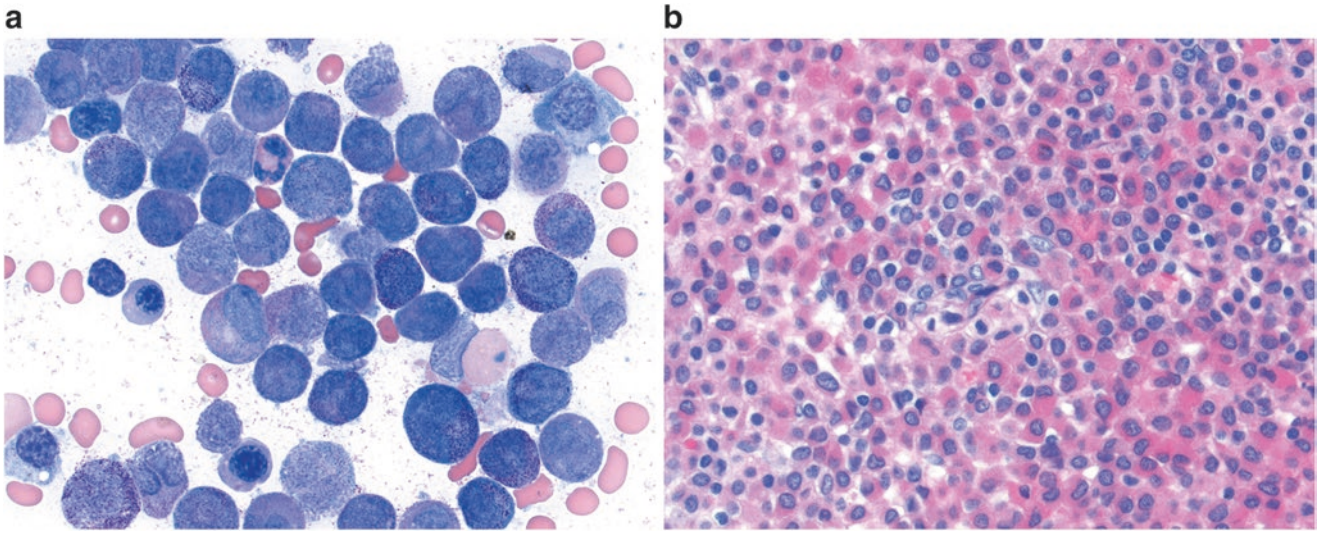

Fig. 11.4 Acute promyelocytic leukemia with *PML-RARA*. (**a**) Blasts with cytoplasmic granules are often more numerous in the marrow. APL is the third type of AML that can be diagnosed as acute leukemia with less than 20% blast cells in the blood or marrow, but the diagnosis should be confirmed by molecular studies that detect the *PML-RARA* fusion. (**b**) The core biopsy also reveals cells with abundant, granular cytoplasm

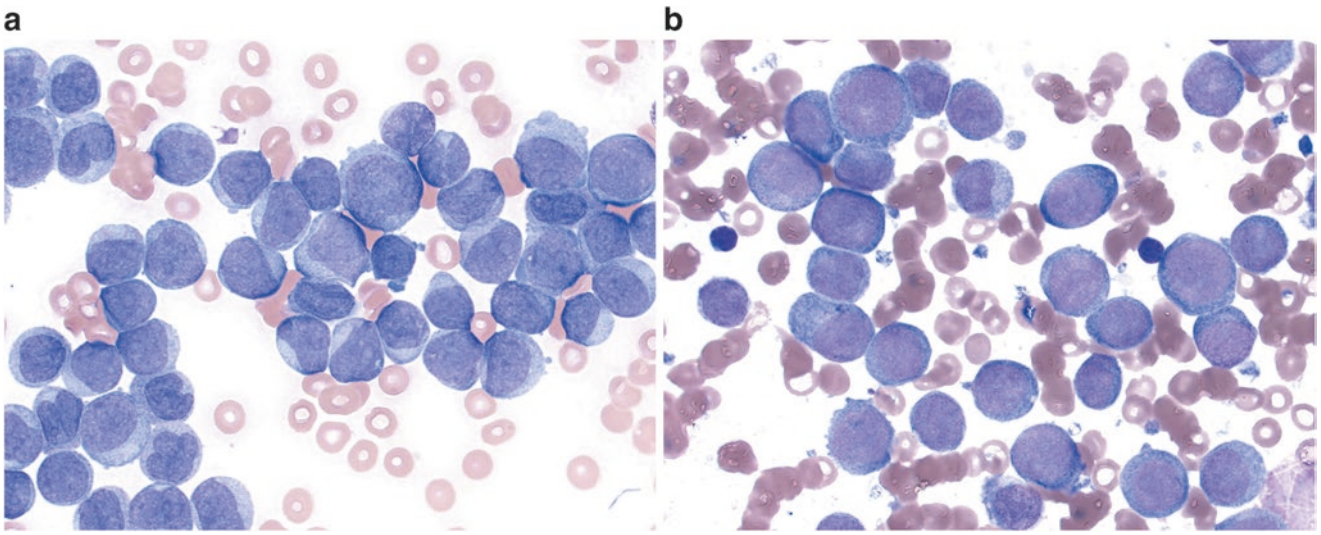

Fig. 11.5 AML with t(9;11)(p21.3;q23.3); *KMT2A-MLLT3*. (**a**) The blasts are often monocytic or myelomonocytic in this AML type. (**b**) Some cases, however, show less differentiation. This case failed to express myeloperoxidase or monocytic markers but was CD13 and CD33 positive, consistent with a more minimally differentiated myeloid leukemia. Therefore, there is really no distinctive morphologic feature to predict this cytogenetic abnormality. Some patients develop AML with t(9;11) after chemotherapy, especially after topoisomerase II inhibitor therapy. Such cases are considered to be therapy-related myeloid neoplasms and are not part of this category, which is restricted to de novo cases

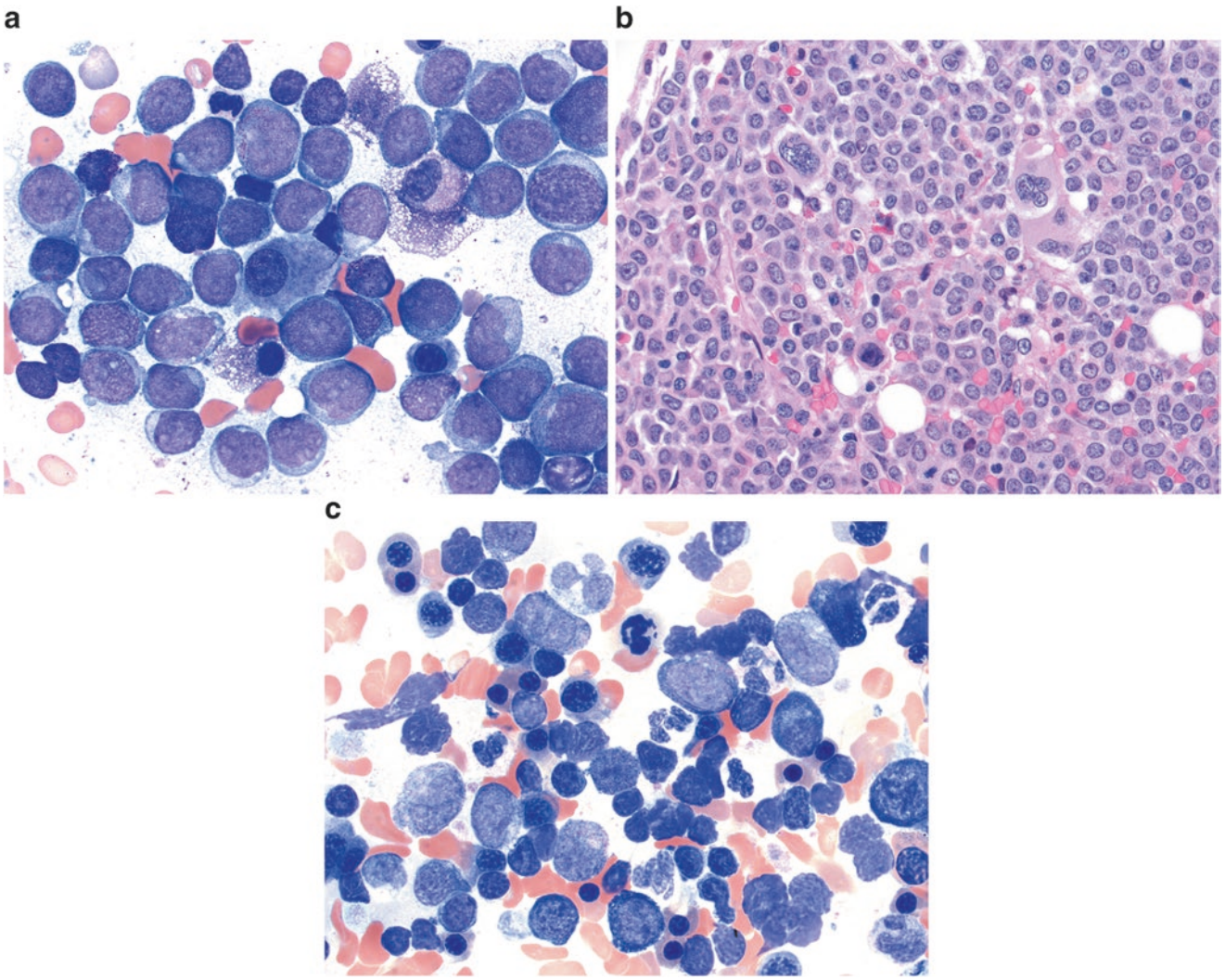

Fig. 11.6 AML with t(6;9)(p23;q34.1); *DEK-NUP214*. (**a**) This case shows a predominance of myeloblasts without specific morphologic features. Admixed basophils, however, are present. The presence of an increase in basophils is uncommon in AML but is relatively common in this AML type as well as AML with *BCR-ABL1*. (**b**) Dysplastic megakaryocytes are also commonly identified on the core biopsy. (**c**) Erythroid hyperplasia, often with background multilineage dysplasia, is also common with this AML type. Note the abnormal red blood cell maturation and the hypogranular neutrophils in the background. This case had sufficient blast cells for a diagnosis of AML, but cases with less than 20% blasts should be diagnosed as MDS. Despite the common presence of multilineage dysplasia, these cases are considered a distinct AML subtype and should not be diagnosed as AML with myelodysplasia-related changes

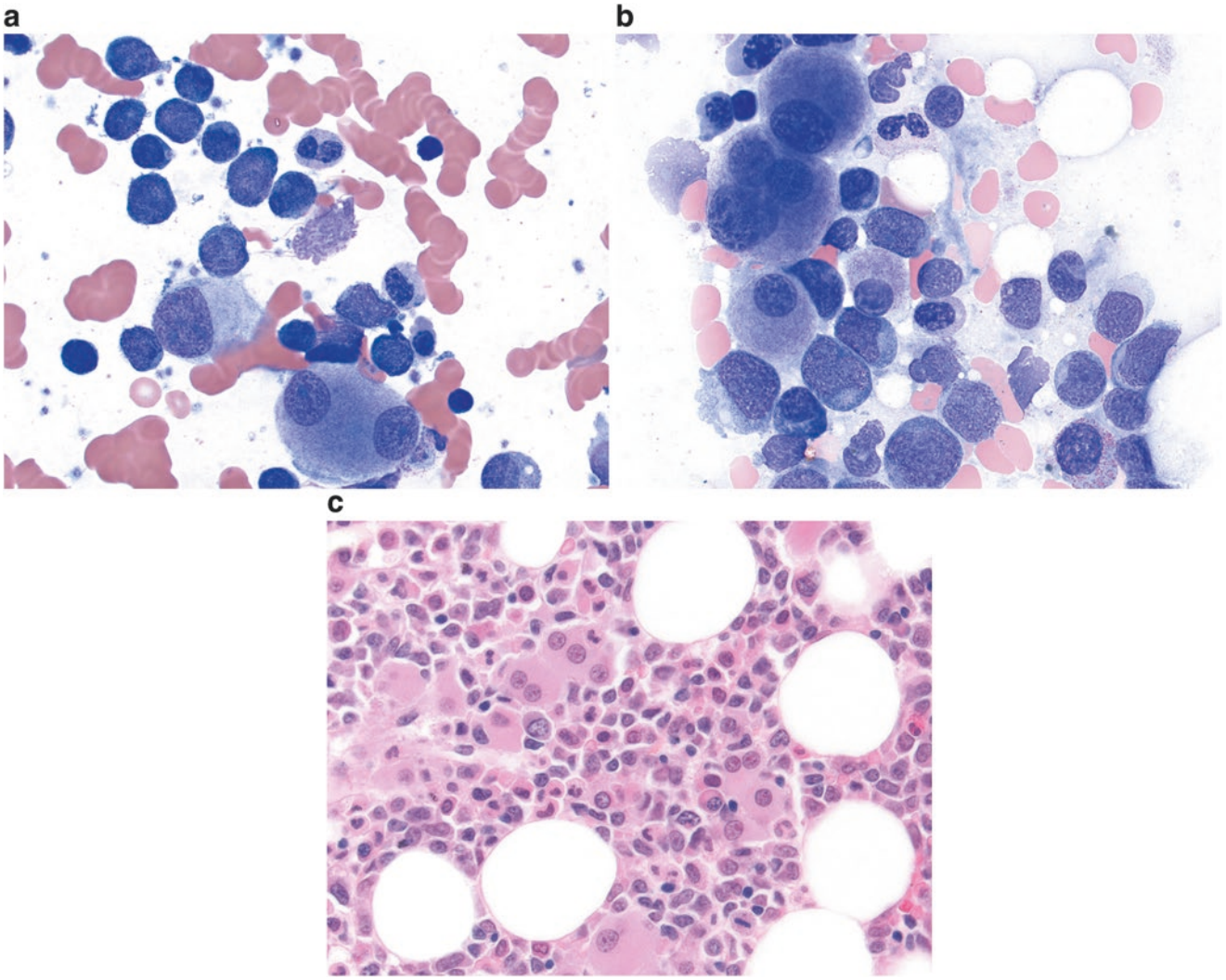

Fig. 11.7 AML with inv(3)(q21.3q26.2) or t(3;3)(q21.3;q26.2); *GATA2*, *MECOM*. This AML type is characterized by the presence of increased bilobed or non-lobed small megakaryocytes which are usually easy to recognize on aspirate smears (**a** and **b**) and core biopsies (**c**). Dysplasia of other background cell types may also be present but is less consistent. Patients may present in as myelodysplastic syndrome and should not be diagnosed as AML until blasts reach 20% in the blood or bone marrow

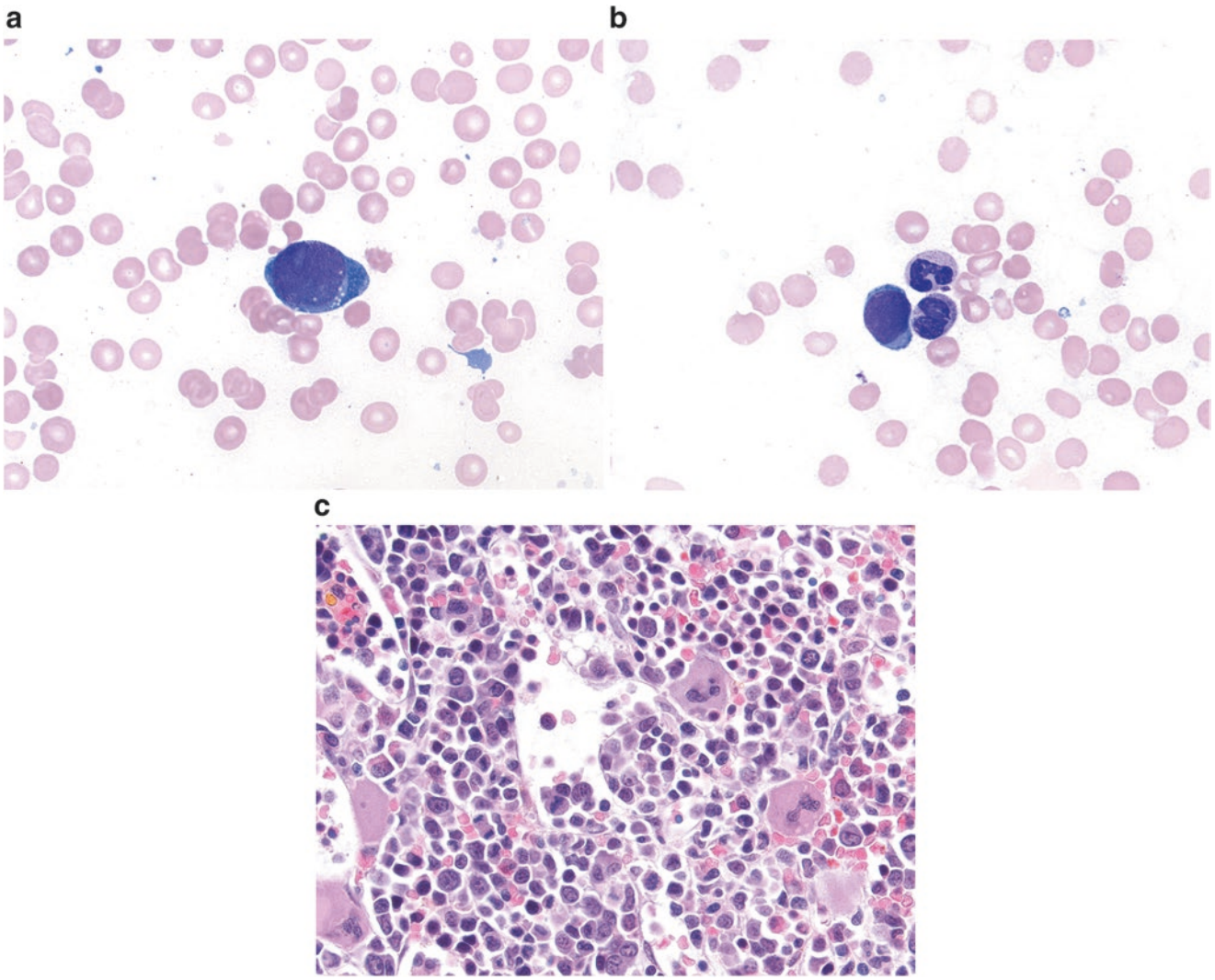

Fig. 11.8 AML (megakaryoblastic) with t(1;22)(p13.3;q13.3); *RBM15-MKL1*. This AML type is extremely uncommon and usually present in infants and very young children. The blasts typically express megakaryocyte markers, such as CD61 and CD41. The marrow is often fibrotic and inaspirable. Only rare blasts may be present, therefore, in aspirate smears. The blasts tend to have granular cytoplasm and may show cytoplasmic blebs (**a**), but this finding is not specific for megakaryocytic lineage and is not present in the blast in (**b**). The core biopsy (**c**) shows sheets of immature cells as well as atypical megakaryocytes and open sinuses due to marrow fibrosis

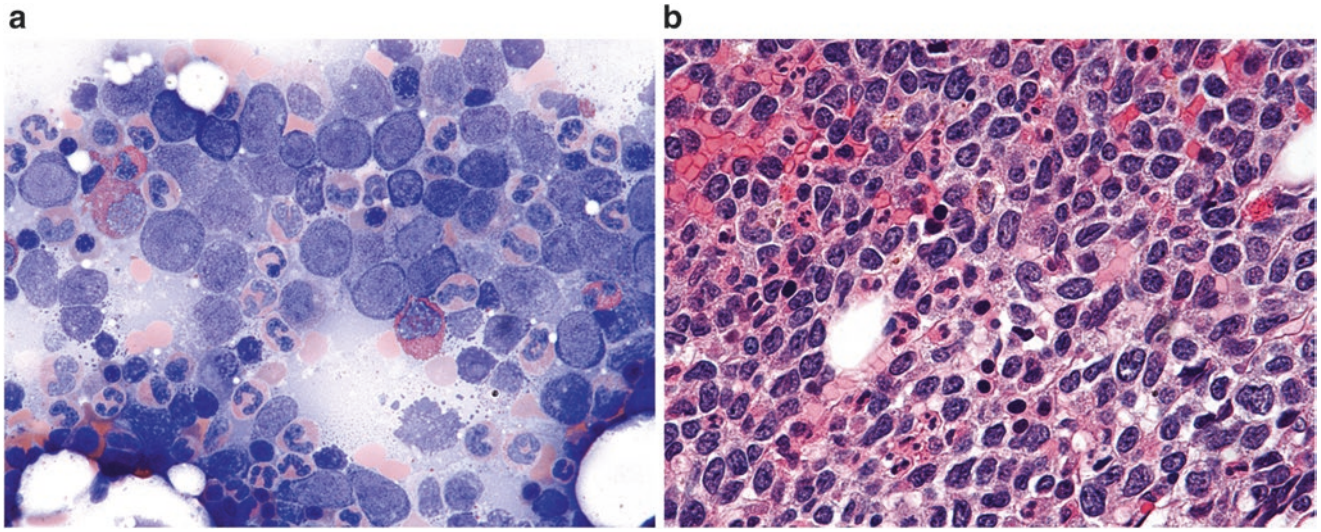

Fig. 11.9 AML with *BCR-ABL1*. This is an uncommon AML type that is a provision entity in the 2016 WHO classification. It may be difficult to impossible to distinguish from myeloid blast transformation of chronic myeloid leukemia (CML) unless there is documented absence of CML in the recent past. The bone marrow aspirate (**a**) and core biopsy (**b**) may show an increase in background neutrophils and basophils. (Images courtesy of Dr. Mark Ewalt, University of Colorado)

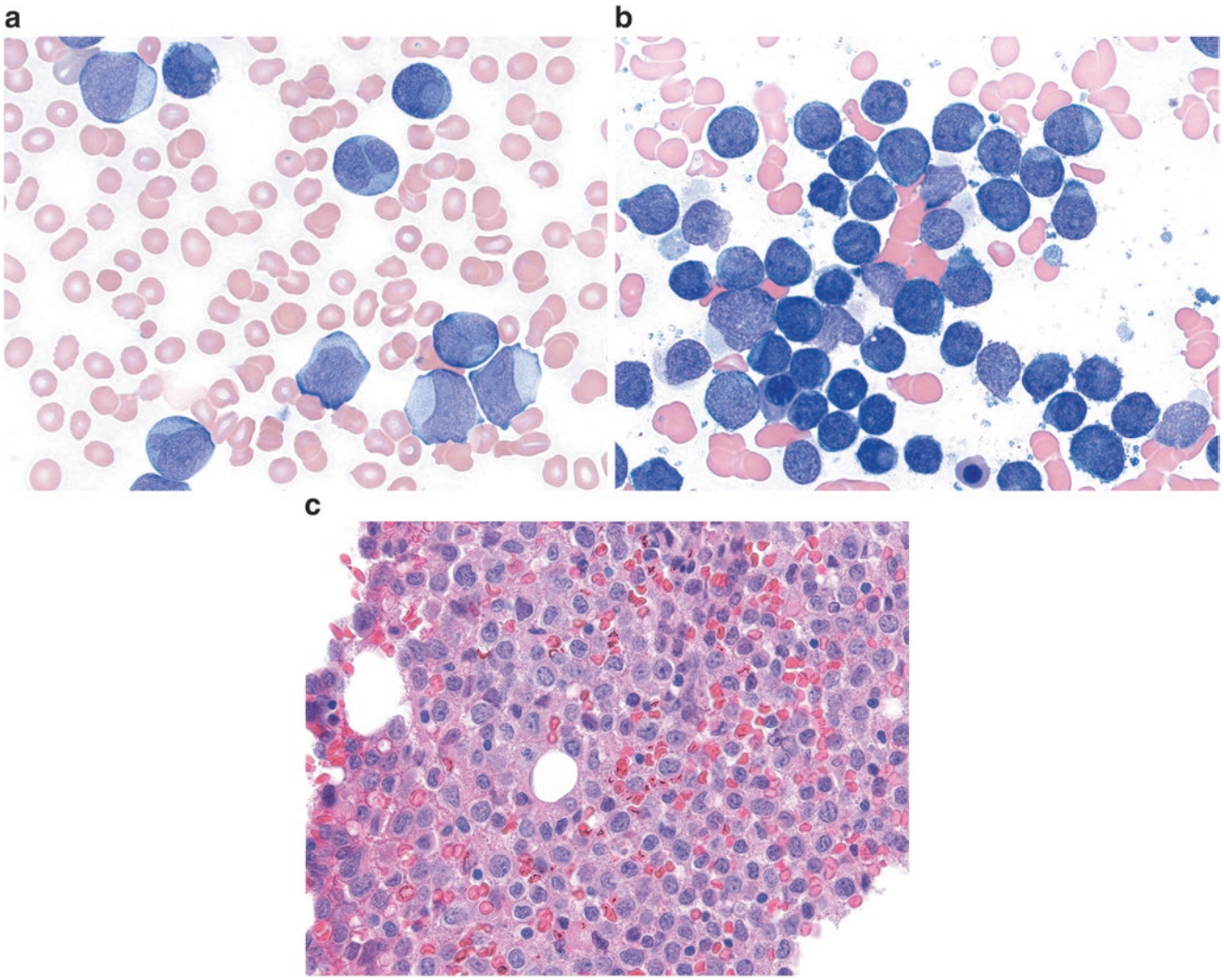

Fig. 11.10 AML with mutated *NPM1*. Many cases of this AML type demonstrate monocytic features. (**a**) Nuclear indentations that may give the appearance of a large nucleolus (upper right) or a cup-shaped (also called a fish mouth) nucleus are common, especially in cases that have mutations of both *NPM1* and *FLT3*-ITD, as was the case with the illustrated patient. (**b**) The morphologic features, however, are otherwise nonspecific. (**c**) The core biopsy features are also nonspecific, but the blasts have a monocytoid appearance in this sample

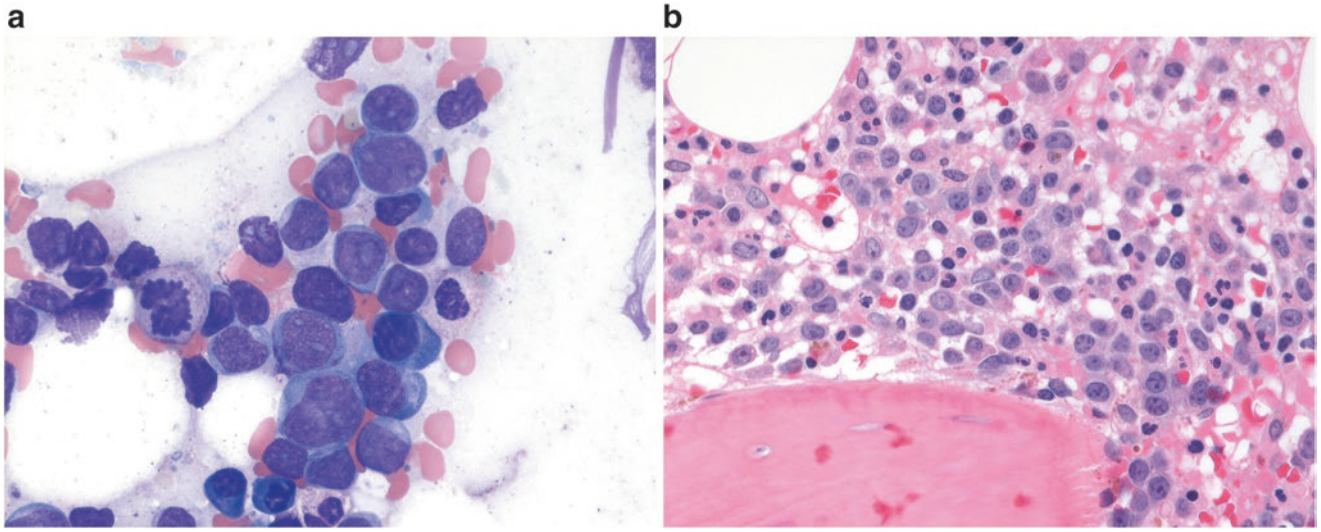

Fig. 11.11 AML with biallelic mutations of *CEBPA*. This AML type does not have specific morphologic features. In this case, the marrow aspirate (**a**) and core biopsy (**b**) show a predominance of relatively undifferentiated blasts, some of which have large nucleoli. Background neutrophils (**A**) show some hyposegmentation, but dyspoiesis in the absence of other myelodysplasia-related findings, such as a history of myelodysplastic syndrome or MDS-related cytogenetic abnormalities, has not been shown to have prognostic significance in this group or in AML with mutated *NPM1*. Some *CEBPA* mutations are germline abnormalities, and non-involved tissue should be studied when this mutation is detected. When a germline mutation is detected, family members should also be screened since the mutation confers an increased risk of developing a myeloid neoplasm (Images courtesy of Dr. Girish Venkataraman, University of Chicago)

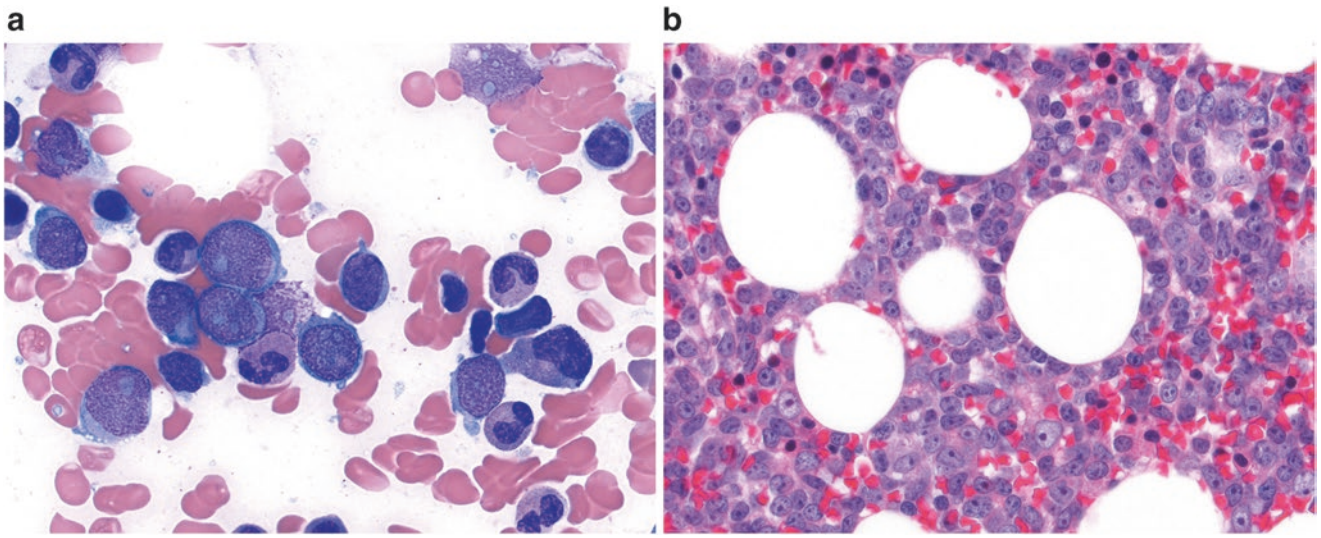

Fig. 11.12 AML with mutated *RUNX1*. This AML type is a provisional entity in the 2016 WHO classification and is restricted to de novo cases without MDS-related cytogenetic abnormalities. Many, but not all, cases are minimally differentiated myeloid leukemias lacking myeloperoxidase expression. The aspirate smear (**a**) and core biopsy (**b**) in this case show immature-appearing blasts without other specific morphologic features. Like *CEBPA* mutations, some *RUNX1* mutations are germline abnormalities. In such cases, family members should also be screened because the mutation confers an increased risk of developing a myeloid neoplasm

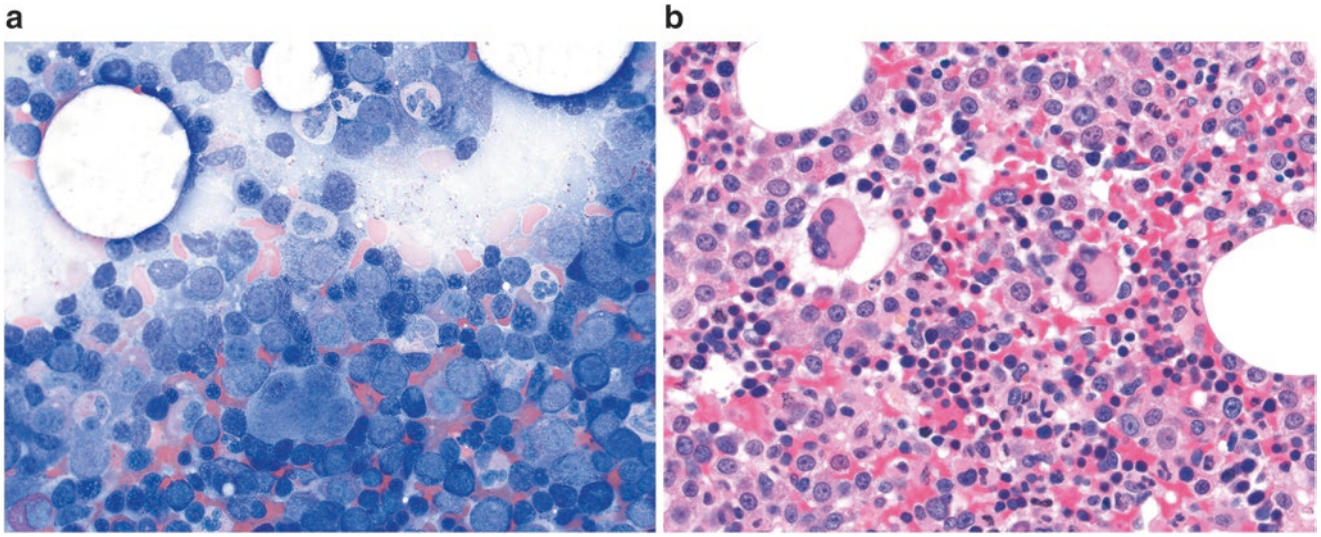

Fig. 11.13 AML with myelodysplasia-related changes. A heterogenous cell population is often present, including blasts cells, erythroid cells with nuclear cytoplasmic asynchrony, and maturing granulocytes with hypogranular cytoplasm or abnormal nuclear lobation. The dysplastic changes are best seen on the aspirate smear (**a**), but atypical megakaryocytes are usually easily recognized on the biopsy (**b**), as illustrated by this case

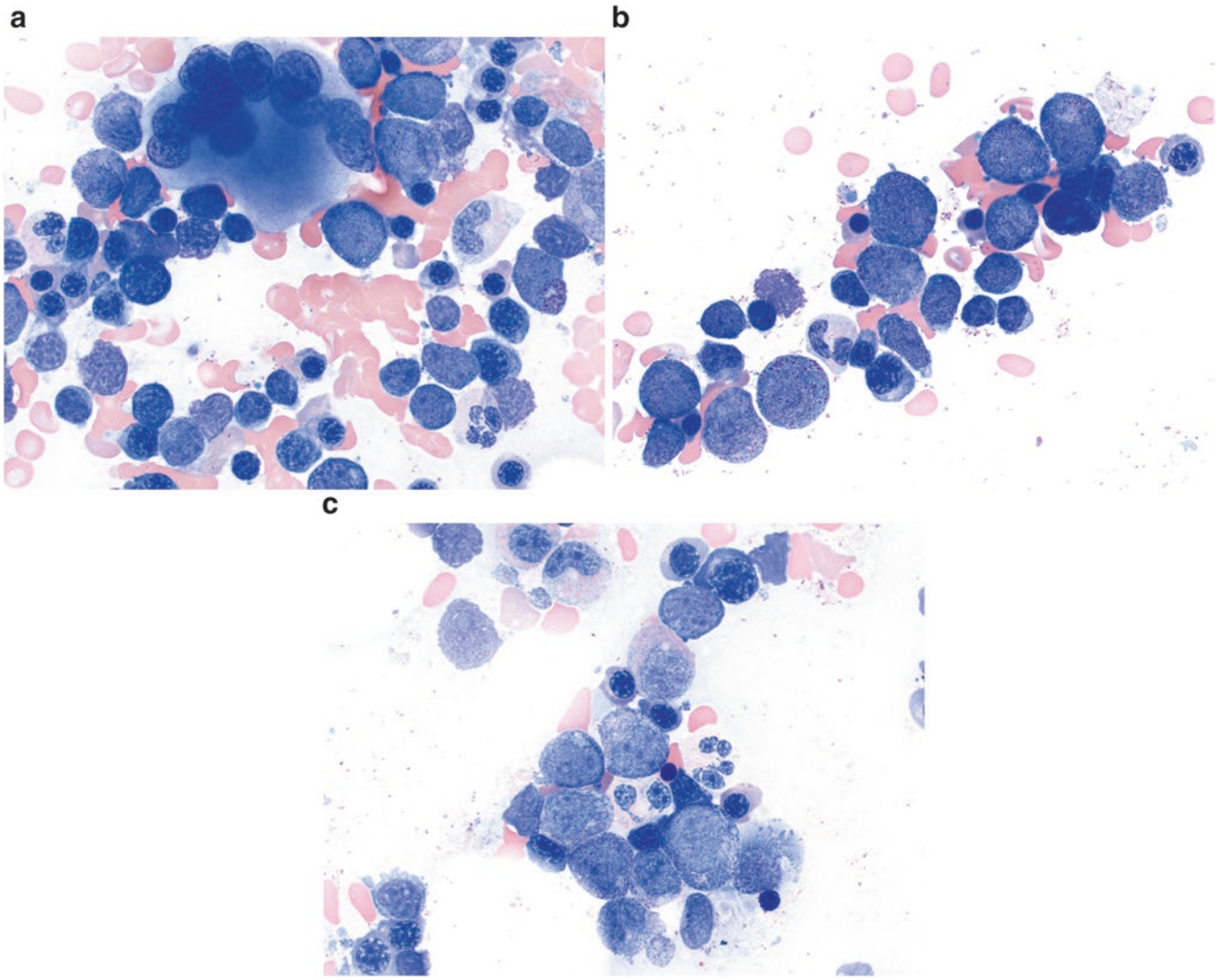

Fig. 11.14 AML with myelodysplasia-related changes. Megakaryocyte dysplasia may result in small, hypolobated forms, as illustrated in Fig. 11.7, or as hyperlobated forms, often with detached nuclear lobes as seen in (**a**). Erythroid dysplasia includes cells with irregular nuclear contours including the cells with flattened nuclear contours shown in the upper right of (**b**). Granulocytic dysplasia may result in hypogranular neutrophils or cells with irregular nuclear lobes (**c**)

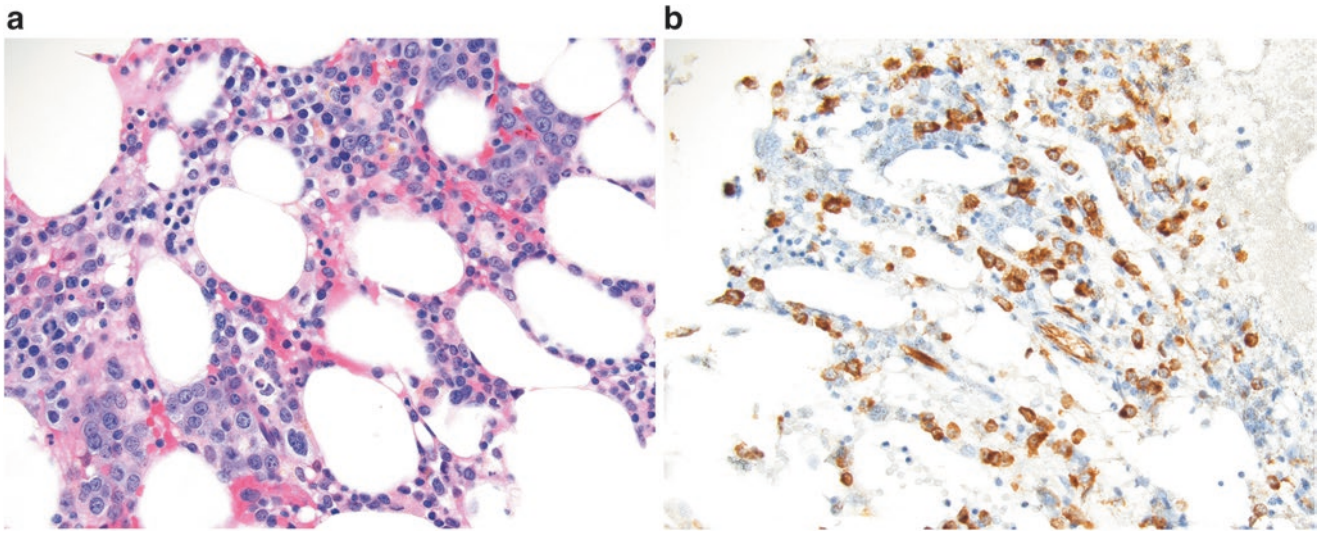

Fig. 11.15 AML with myelodysplasia-related changes. Some cases may be more hypocellular (**a**) with increased blasts identified by staining for CD34 (**b**)

Table 11.2 Cytogenetic abnormalities sufficient for a diagnosis of AML with myelodysplasia-related changes, in the absence of prior cytotoxic therapy, when bone marrow or blood blasts are 20% or more

Complex karyotype (3 or more abnormalities)
Unbalanced abnormalities
-7/del(7q)
del(5q)/t(5q)
i(17q)/t(17p)
-13/del(13q)
del(11q)
del(12p)/t(12p)
idic(X)(q13)
Balanced abnormalities
t(11;16)(q23.3;p13.3)
t(3;21)(q26.2;q22.1)
t(1;3)(p36.3;q21.2)
t(2;11)(p21;q23.3)
t(5;12)(q32;p13.2)
t(5;7)(q32;q11.2)
t(5;17)(q32;p13.2)
t(5;10)(q32;q21.2)
t(3;5)(q25.3;q35.1)

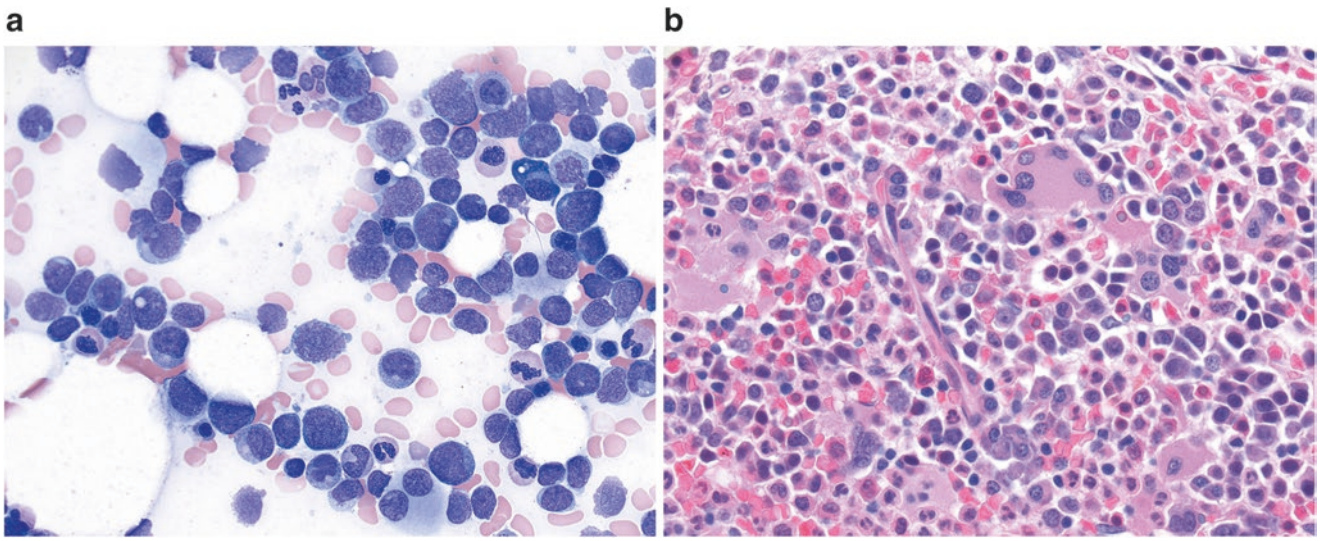

Fig. 11.16 Therapy-related myeloid neoplasms. There are two morphologic variations of therapy-related myeloid neoplasms. Those that present quickly usually show monocytic differentiation with a translocation involving *KMT2A*, with features virtually identical to what is illustrated in Fig. 11.5. The second type usually progresses over a 5–7-year period and has a feature of myelodysplastic syndrome or AML with myelodysplasia-related changes with background multilineage dysplasia as illustrated in the marrow aspirate (**a**) and biopsy (**b**) of this case

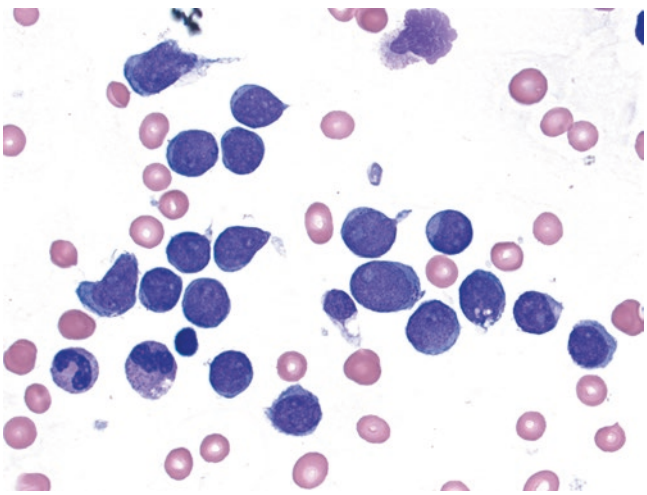

Fig. 11.17 AML not otherwise specified (AML minimally differentiated). The blasts cannot be morphologically distinguished from lymphoblasts with scant, agranular cytoplasm. They are, by definition, myeloperoxidase negative but positive by other myeloid antigens by flow cytometry or other immunophenotyping methods

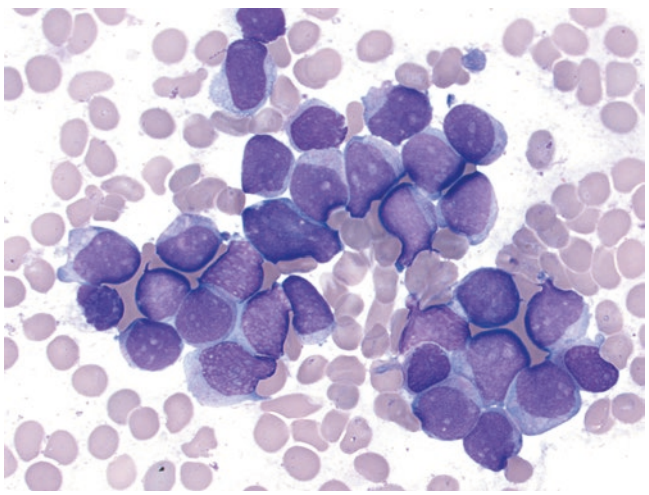

Fig. 11.18 AML not otherwise specified (AML without maturation). The blasts may be identical to those in minimally differentiated AML or may have some granules. By definition, they express myeloperoxidase

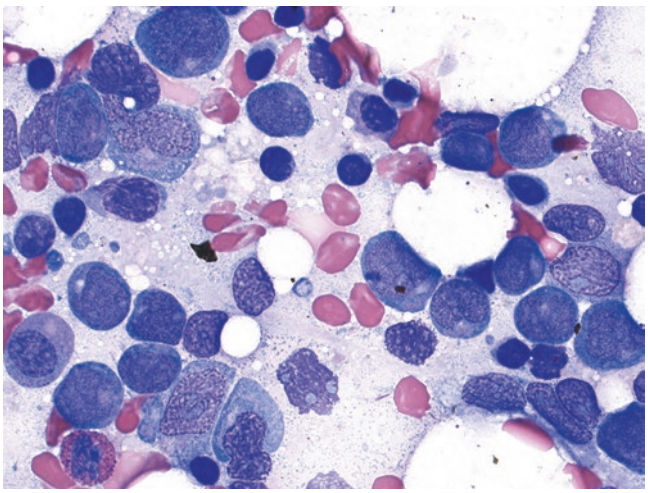

Fig. 11.19 AML not otherwise specified (AML with maturation). These blasts have more granules and more frequent Auer rods, with at least 10% of cells maturing to the promyelocyte stage of differentiation

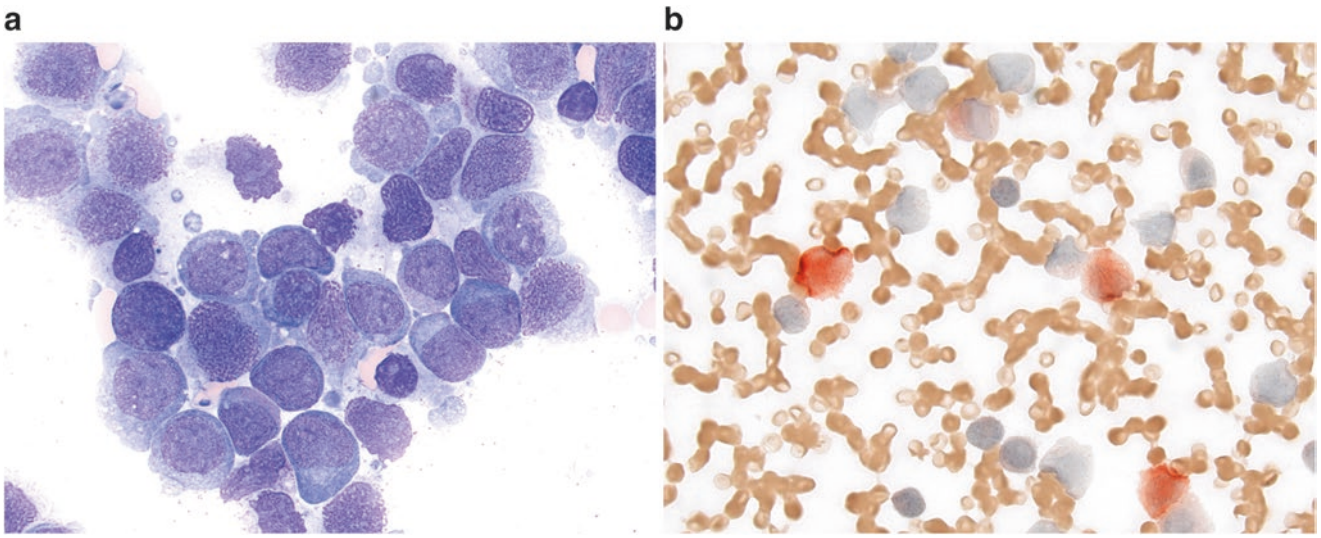

Fig. 11.20 AML not otherwise specified (acute myelomonocytic leukemia). These cases show a mix of cells that are myeloblasts and cells with a feature of monoblasts. In this case, some blasts have more abundant and vacuolated cytoplasm (**a**), and over 20% of the blast cells are positive for nonspecific esterase (**b**), which is indicated by weak-to-strong red staining of the cytoplasm of neoplastic cells in this figure

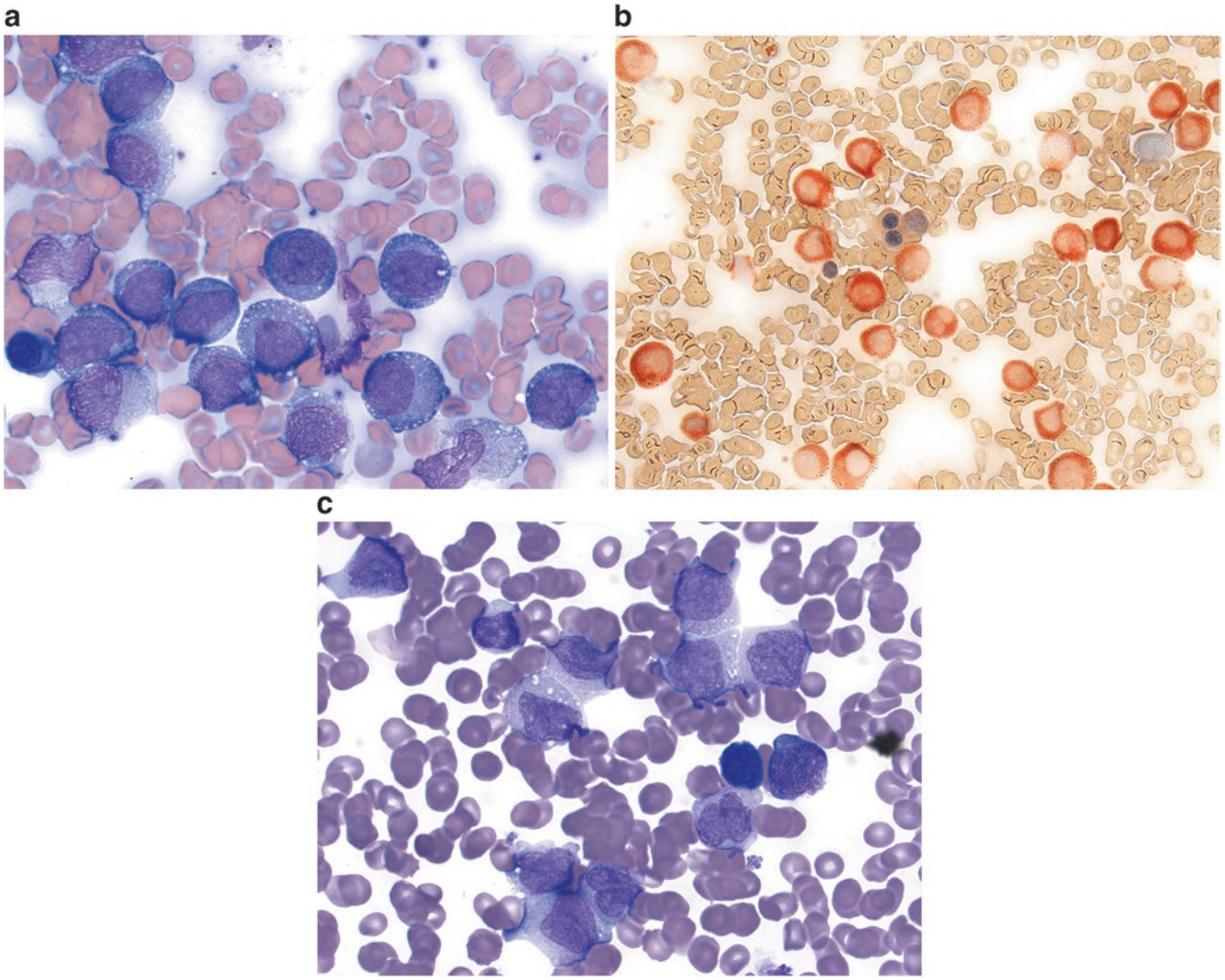

Fig. 11.21 AML not otherwise specified (acute monoblastic/monocytic leukemia). These cases have over 80% of blasts with monocytic features. The blasts in (**a**) have more immature, round nuclei but basophilic, vacuolated cytoplasms typical of monoblastic leukemia. The monocytic features are confirmed by the high number of positive cells on the nonspecific esterase stain (**b**). The case illustrated in (**c**) is more monocytic with folded nuclei more suggestive of maturing monocytes despite the immature, fine nuclear chromatin

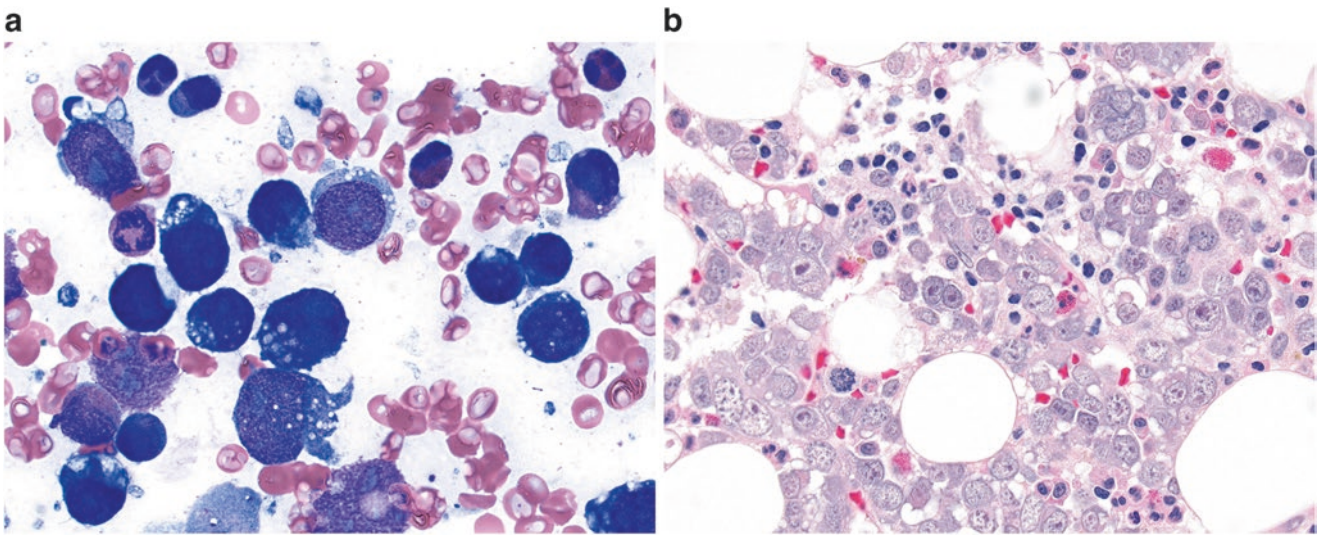

Fig. 11.22 AML not otherwise specified (pure erythroid leukemia). The immature cell proliferation in this case is composed entirely of immature erythroid precursors that tend to have darkly staining nuclear chromatin and vacuolated, basophilic cytoplasm (**a**). The vacuoles tend to be more crisply defined than the vacuoles of monoblasts. The erythroid lineage of the immature cells is less obvious on the core biopsy (**b**)

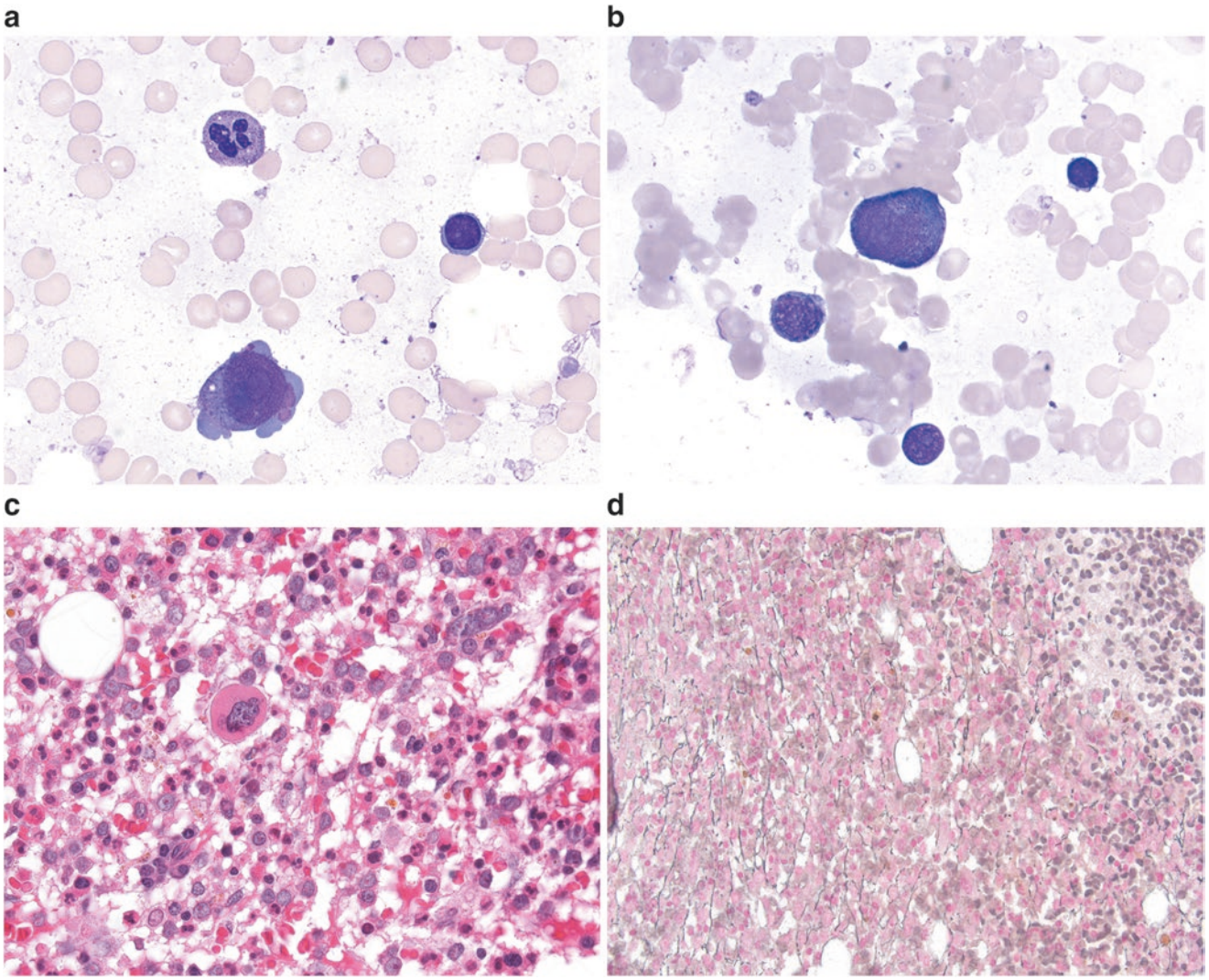

Fig. 11.23 AML not otherwise specified (acute megakaryocytic leukemia). The blasts are similar to the megakaryoblasts illustrated in Fig. 11.8. Some may have cytoplasmic granules and cytoplasmic blebbing (**a**), but blebbing is not always present (**b**) and is not specific for megakaryocytic lineage. Admixed dysplastic megakaryocytes are often present and are usually more easily seen on the core biopsy (**c**) since cellular aspirate smears are often difficult to obtain in this disorder. The lack of a good aspirate is usually due to increased reticulin fibrosis ((**d**) reticulin stain)

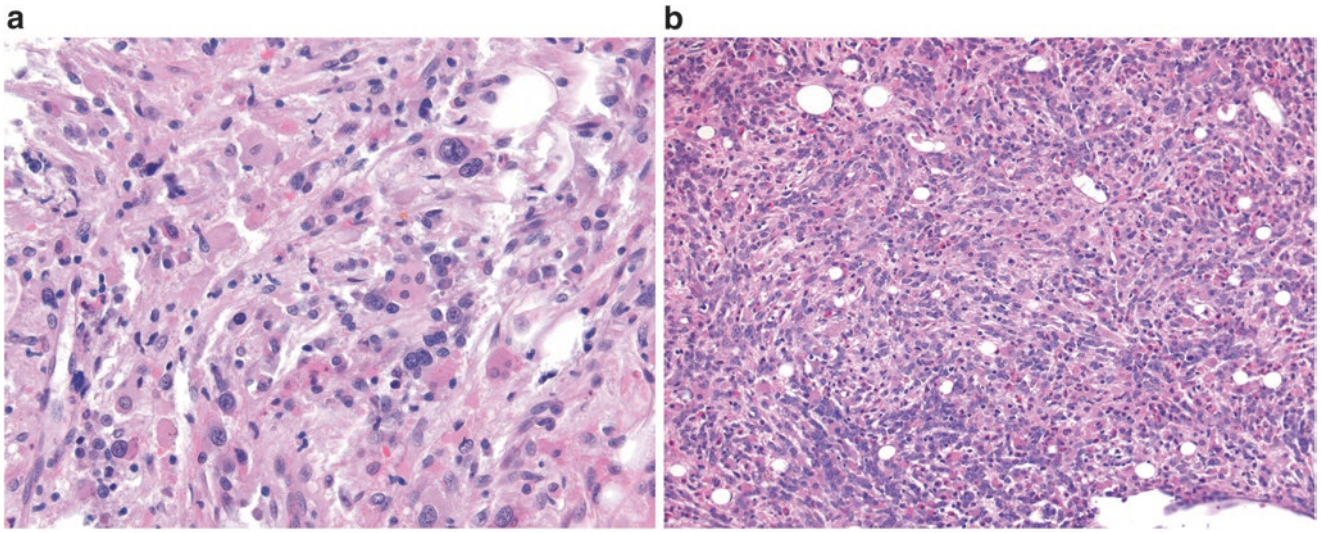

Fig. 11.24 AML not otherwise specified (acute panmyelosis with myelofibrosis). (**a**) This diagnosis is extremely rare and should be associated with marrow fibrosis with an increase in myeloblasts but also with an increase in all immature marrow cell types (erythroid and megakaryocytic). Some may represent transformation of a previously undetected myeloproliferative neoplasm and should be more accurately diagnosed as such. (**b**) Cases such as the one illustrated here were previously diagnosed as acute panmyelosis with myelofibrosis, but after immunophenotyping this case was correctly classified as acute megakaryocytic leukemia

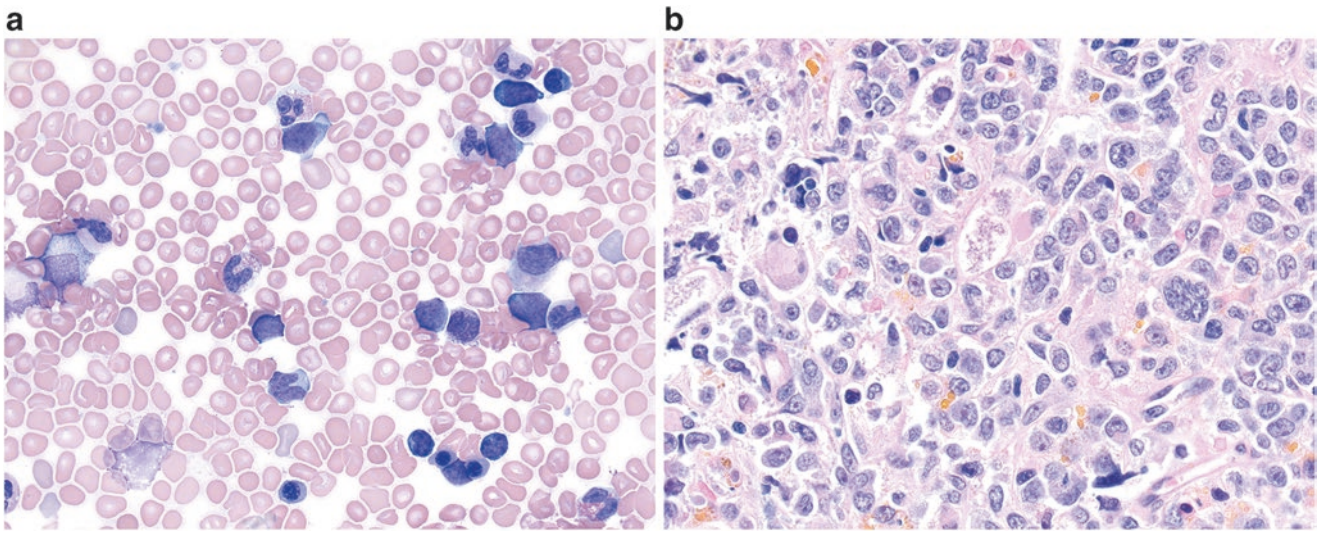

Fig. 11.25 Myeloid proliferations related to Down syndrome. Transient abnormal myelopoiesis (TAM) (**a**) and the myeloid neoplasm of Down syndrome (**b**) are morphologically similar. The aspirate shows a population of megakaryoblasts, but the percentage may be quite variable in both disorders. Bone marrow biopsies are usually not performed in TAM, but this example from an older child with Down syndrome shows an increase in blast cells as well as atypical mature megakaryocytes

References

1. Döhner H, Weisdorf DJ, Bloomfield CD. Acute Myeloid Leukemia. N Engl J Med. 2015;373(12):1136–52.
2. Arber DA, Orazi A, Hasserjian R, Thiele J, Borowitz MJ, Le Beau MM, et al. The 2016 revision to the World Health Organization classification of myeloid neoplasms and acute leukemia. Blood. 2016;127(20):2391–405.
3. Arber DA, Stein AS, Carter NH, Ikle D, Forman SJ, Slovak ML. Prognostic impact of acute myeloid leukemia classification. Importance of detection of recurring cytogenetic abnormalities and multilineage dysplasia on survival. Am J Clin Pathol. 2003;119(5):672–80.
4. Díaz-Beyá M, Rozman M, Pratcorona M, Torrebadell M, Camós M, Aguilar JL, et al. The prognostic value of multilineage dysplasia in de novo acute myeloid leukemia patients with intermediate-risk cytogenetics is dependent on NPM1 mutational status. Blood. 2010;116(26):6147–8.
5. Singh ZN, Huo D, Anastasi J, Smith SM, Karrison T, Le Beau MM, et al. Therapy-related myelodysplastic syndrome: morphologic subclassification may not be clinically relevant. Am J Clin Pathol. 2007;127(2):197–205.
6. Walter RB, Othus M, Burnett AK, Löwenberg B, Kantarjian HM, Ossenkoppele GJ, et al. Significance of FAB subclassification of "acute myeloid leukemia, NOS" in the 2008 WHO classification: analysis of 5848 newly diagnosed patients. Blood. 2013;121(13):2424–31.
7. Arber DA. Revisiting erythroleukemia. Curr Opin Hematol. 2017;24(2):146–51.
8. Roy A, Roberts I, Vyas P. Biology and management of transient abnormal myelopoiesis (TAM) in children with Down syndrome. Semin Fetal Neonatal Med. 2012;17(4):196–201.
9. Lange BJ, Kobrinsky N, Barnard DR, Arthur DC, Buckley JD, Howells WB, et al. Distinctive demography, biology, and outcome of acute myeloid leukemia and myelodysplastic syndrome in children with Down syndrome: Children's cancer group studies 2861 and 2891. Blood. 1998;91(2):608–15.
10. Arber DA, Borowitz MJ, Cessna M, Etzell J, Foucar K, Hasserjian RP, et al. Initial diagnostic workup of acute leukemia: guideline from the College of American Pathologists and the American Society of Hematology. Arch Pathol Lab Med. 2017;141(10):1342–93.

Myeloid Proliferations of Down Syndrome

12

Lee J. McGhan and Maria A. Proytcheva

Individuals with Down syndrome (DS) have a markedly increased risk of developing unique myeloid proliferations such as transient abnormal myelopoiesis (TAM) and myeloid leukemia associated with Down syndrome (ML-DS) [1, 2]. These proliferations occur in the first 3 years of life and are a result of several transforming genetic events that arise during the fetal and newborn period. The initial event, an additional chromosome 21, leads to increased megakaryocytic proliferation in the fetal liver. Subsequent mutation of *GATA*-binding protein *1* (*GATA1*) results in the development of TAM. Further acquisition of additional mutations of epigenetic regulators and common signaling pathways such as JAK family kinases, MPL, and multiple RAS pathway genes leads to the transformation to ML-DS [3].

While the time of presentation varies, TAM typically occurs shortly after birth, whereas ML-DS typically occurs between 3 months and 3 years of age. The morphologic and immunophenotypic features of the myeloid proliferations of DS are essentially indistinguishable, (Table 12.1, Figs. 12.1, 12.2, 12.3, 12.4, 12.5, 12.6, 12.7, 12.8, 12.9, 12.10, and 12.11).

Approximately 4% to 18% of individuals with DS develop TAM, although the true incidence of TAM is difficult to discern in view of the fact that most infants are asymptomatic, so blood counts or morphologic evaluation may not be performed [4]. TAM typically occurs at the time of birth (or within the first few days following birth) and is defined as an increase in peripheral blasts that have morphologic and phenotypic features of megakaryocytic lineage. There is no internationally agreed-upon definition of a percentage blast threshold for diagnosis, however, and circulating blasts are also frequently seen in DS individuals without TAM. The blasts in TAM harbor acquired N-terminal truncating mutations in the key hematopoietic transcription factor gene *GATA1* [5, 6]; this mutation is considered a molecular hallmark of these disorders. A subset of patients with so-called silent TAM may also have acquired *GATA1* mutations despite lacking clinical or overt hematologic manifestations of disease [7]. In most cases (75–90%), the peripheral blasts resolve spontaneously by approximately 3 months of age without the need for chemotherapy, although a few children may experience life-threatening or even fatal complications.

Approximately 20% of patients with clinically apparent TAM subsequently develop nonremitting acute myeloid leukemia (AML), when persistent *GATA1*-mutant cells acquire additional oncogenic mutations [8–12]. ML-DS encompasses cases of both myelodysplastic syndrome (MDS) and overt AML, which behave in a similar fashion regardless of the absolute blast count [1]. ML-DS occurs later than TAM, usually in the first 3 years of life, and is usually preceded by TAM. In most cases, the acute leukemia is a megakaryoblastic leukemia, in contrast to the relatively low incidence of this leukemia in non-DS individuals. ML-DS has a relatively favorable prognosis with enhanced chemotherapeutic responsiveness.

L.J. McGhan (✉) • M.A. Proytcheva
Department of Pathology, University of Arizona/Banner University Medical Center, Tucson, AZ, USA
e-mail: lee.mcghan@dignityhealth.org; mproytcheva@pathology.arizona.edu

T.I. George, D.A. Arber (eds.), *Atlas of Bone Marrow Pathology*, Atlas of Anatomic Pathology,
https://doi.org/10.1007/978-1-4939-7469-6_12

Table 12.1 The myeloid proliferations of Down syndrome

	Transient abnormal myelopoiesis (TAM)	Myeloid leukemia associated with Down syndrome (ML-DS)
Incidence in DS individuals	4–18%	1–2%
Onset	From birth to first few days of life; may also present in the fetal period	Usually <3 y (median age about 2 y)
Clinical features	Variable, ranging from asymptomatic (the majority) to disseminated leukemic infiltration; clinical manifestations may include hepatomegaly, jaundice, splenomegaly, pericardial/pleural effusions, and bleeding diatheses	Most cases have a history of preceding TAM and have an indolent presentation; organomegaly may be present
Laboratory features	Leukocytosis (30–50%) with peripheral blood blasts and granulocytic left shift; platelets may be increased, decreased, or normal (with large forms usually present); megakaryocyte fragments may be seen; significant anemia is uncommon, and marked polychromasia and circulating nucleated red cells may also be seen	Progressive pancytopenia with leukopenia, thrombocytopenia, and evidence of dysplasia; the circulating blast percentage is typically low
Immunophenotype	Variable, but usually involves expression of a combination of stem cell markers (CD34, CD117), myeloid markers (CD13, CD33), and platelet glycoproteins (CD36, CD41, CD61), with variable expression of CD4, CD7, and CD56; staining for nonspecific esterase is also usually positive and MPO is negative	
Molecular features	*GATA1* mutations present in all cases	*GATA1* mutations present in all cases; cytogenetic abnormalities include trisomy 8, trisomy 11, loss of chromosome 5 and 7 material, del(6q), del(7p), del(16q), and dup(1p); other mutations involve key cohesion component genes (*RAD21, STAG2, SMC3, SMC1A*), epigenetic regulators (*EZH2, KANSL1*), *CTCF*, RAS pathway genes, and somatic point mutations in *JAK1, JAK2, JAK3, PT53, FLT3,* and *MPL*
Prognosis	Most neonates (>80%) undergo spontaneous remission within 3–4 months; overall 5-year survival is 80%	Long-term survival has been reported, with outcomes better than non-DS AML (event-free survival of 80%); prognosis after relapse is poor

AML acute myeloid leukemia

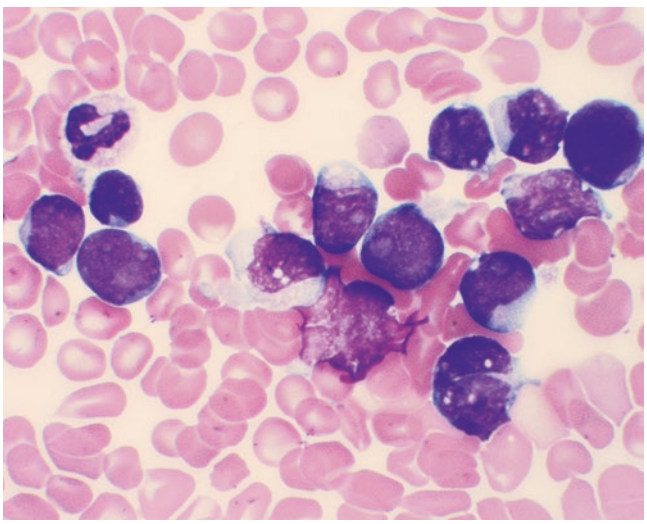

Fig. 12.1 The peripheral blood smear in transient abnormal myelopoiesis (TAM) typically shows leukocytosis, with increased blasts exhibiting megakaryoblastic morphology, although the morphology may be variable. The neoplastic cells characteristically show high N:C ratio, with fine chromatin and prominent nucleoli. The basophilic cytoplasm may be scant to moderate and may demonstrate occasional peripheral "blebs." Small vacuoles may also be present [Wright-Giemsa, 100×]

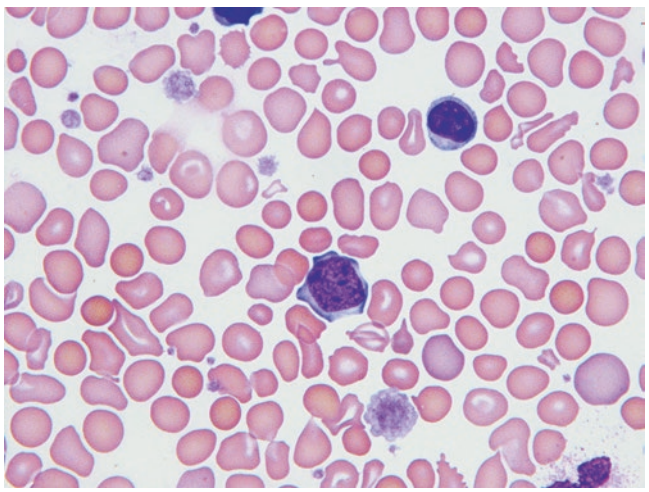

Fig. 12.2 The platelet count in TAM may be increased or decreased, and the peripheral blood smear may show numerous large platelets (pictured) in addition to megakaryocytic fragments. A circulating blast is also illustrated in the center of the image [Wright-Giemsa, 100×]

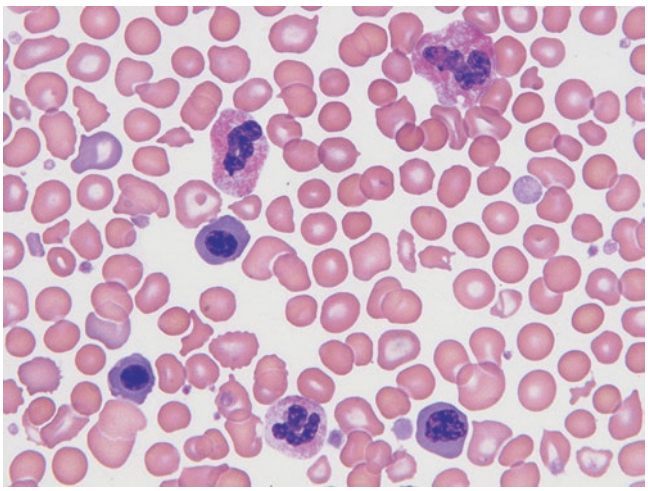

Fig. 12.3 Numerous polychromatophilic cells and circulating nucleated red cells are often seen in the peripheral blood in TAM. Other changes involving the red cells that may be seen in Down syndrome (in the absence of TAM) include an increase in the mean corpuscular hemoglobin (MCH) and mean cell volume (MCV), usually evident at 9 to 12 months of age [13, 14] [Wright-Giemsa, 100×]

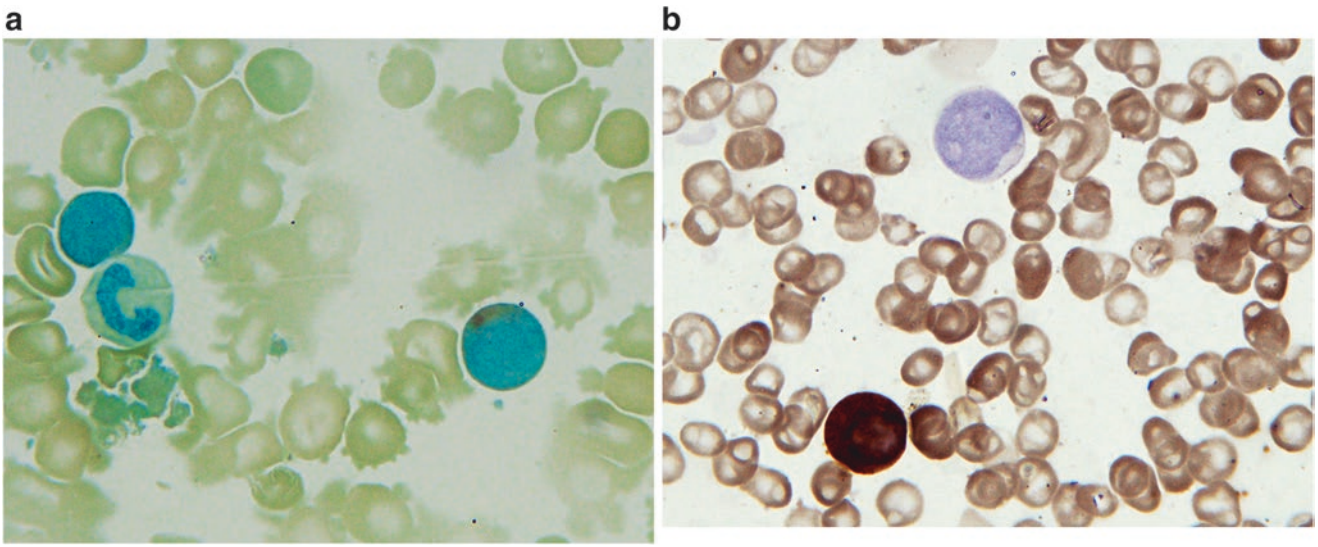

Fig. 12.4 The blasts in TAM are shown to be positive for nonspecific esterase (**a**) and negative for myeloperoxidase (**b**), with the latter showing strong positivity in an adjacent granulocyte precursor. Myeloperoxidase may show weak staining in some cases [nonspecific esterase and myeloperoxidase cytochemical stains, 100×]

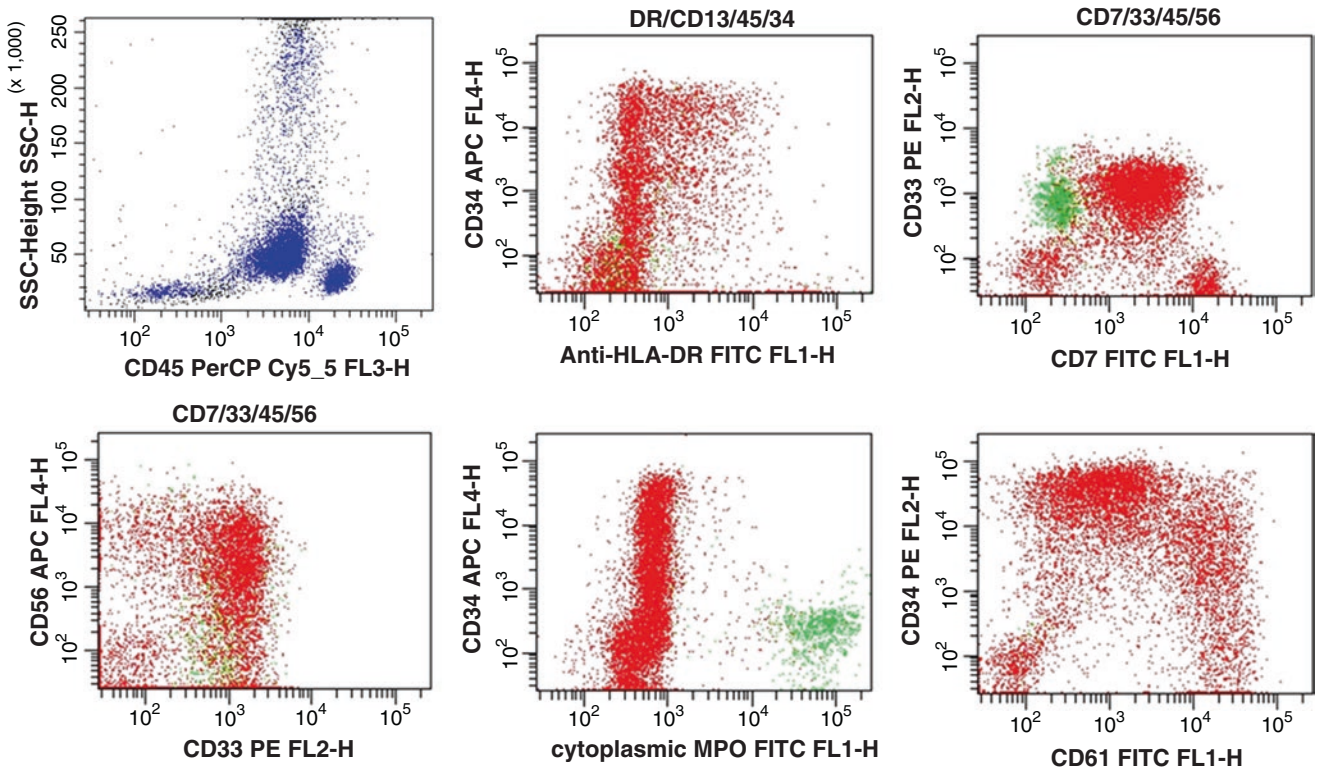

Fig. 12.5 By flow cytometry, the blasts in TAM show moderate to bright CD45 expression, in addition to expression of immature marker CD34, myeloid marker CD33, and megakaryocyte marker CD61. CD7 and CD56 are also aberrantly expressed on the blasts. HLA-DR and MPO are negative. The intensity of CD34 expression appears uniformly heterogeneous. Also demonstrated is a pattern of loss of CD34 expression with increasing expression of CD61 (bottom right plot), suggestive of "maturation" of the neoplastic cells. The phenotype is consistent overall with megakaryocytic differentiation

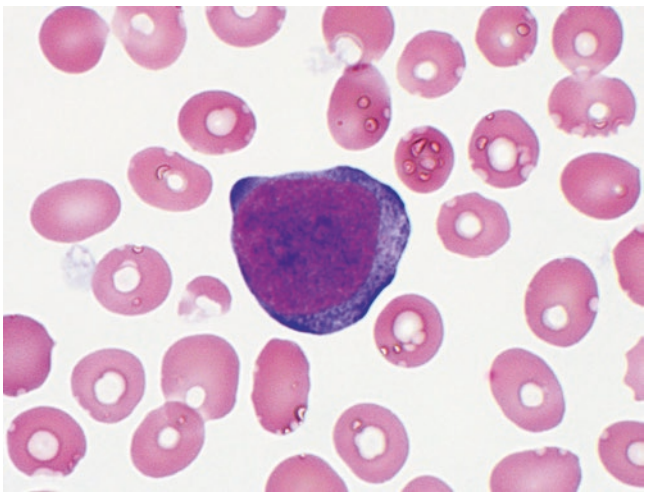

Fig. 12.6 The circulating blasts in myeloid leukemia associated with Down syndrome (ML-DS) also typically exhibit megakaryoblastic morphology, characterized by fine chromatin and prominent nucleoli. The cytoplasm is typically deeply basophilic and may show occasional cytoplasmic blebbing and vacuolation. The blasts usually circulate in relatively low numbers [Wright-Giemsa, 100×]

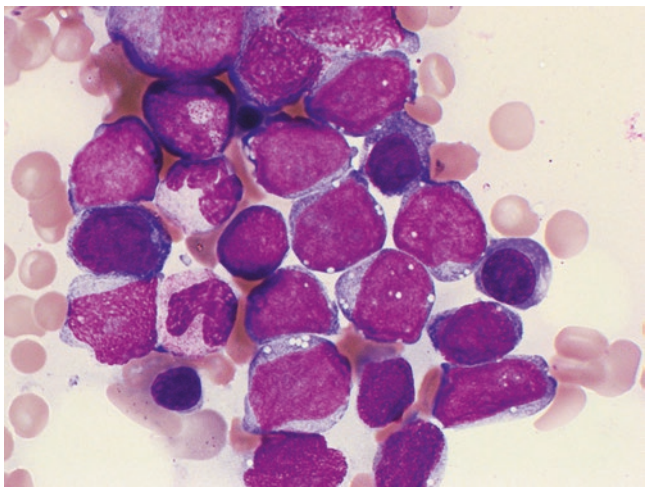

Fig. 12.7 The bone marrow aspirate in ML-DS shows increased numbers of megakaryoblasts, with relatively reduced background hematopoietic elements. In some instances, the presence of marked bone marrow fibrosis may produce a "dry tap" [Wright-Giemsa, 100×]

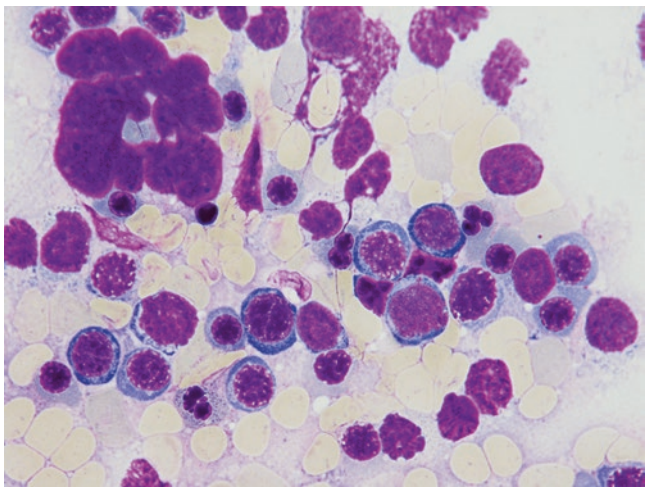

Fig. 12.8 There may be prominent dysplasia present in ML-DS, here shown to affect the red cell lineage in a bone marrow aspirate. Mature red cell precursors show multinucleation and nuclear budding [Wright-Giemsa, 100×]

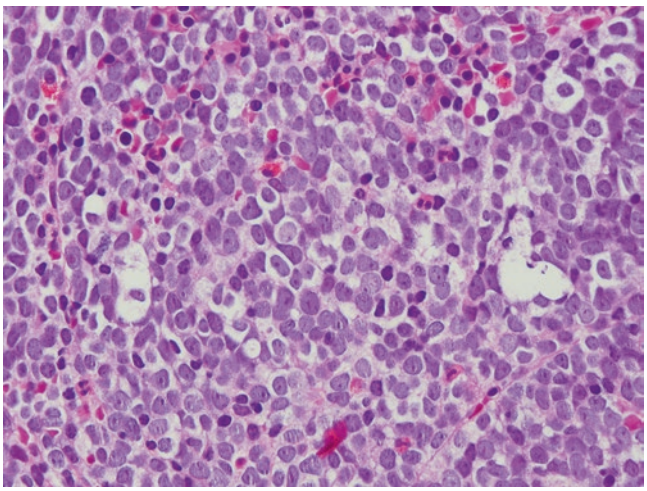

Fig. 12.9 The bone marrow core biopsy in acute megakaryoblastic leukemia typically shows a hypercellular bone marrow with sheets of blasts showing pale, fine chromatin, visible nucleoli, and variable amounts of cytoplasm. Background hematopoietic elements are reduced. Reticulin fibrosis may also be prominent in some cases (*not shown*) [H&E, 40×]

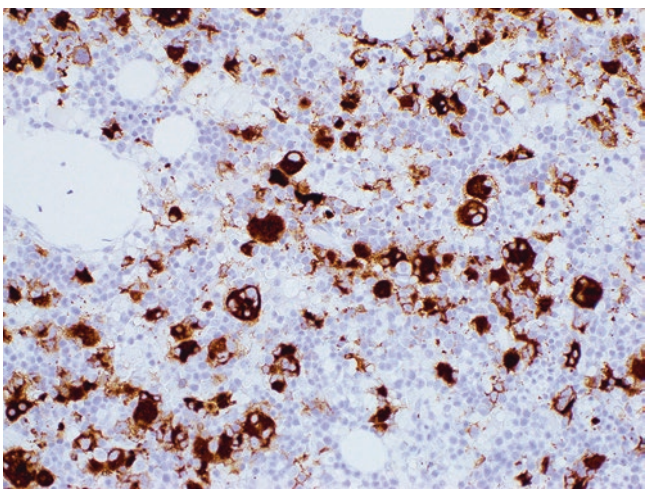

Fig. 12.10 The blasts in the bone marrow core biopsy in ML-DS can be highlighted by a CD61 immunostain, which also highlights occasional larger background megakaryocytes [CD61, 40×]

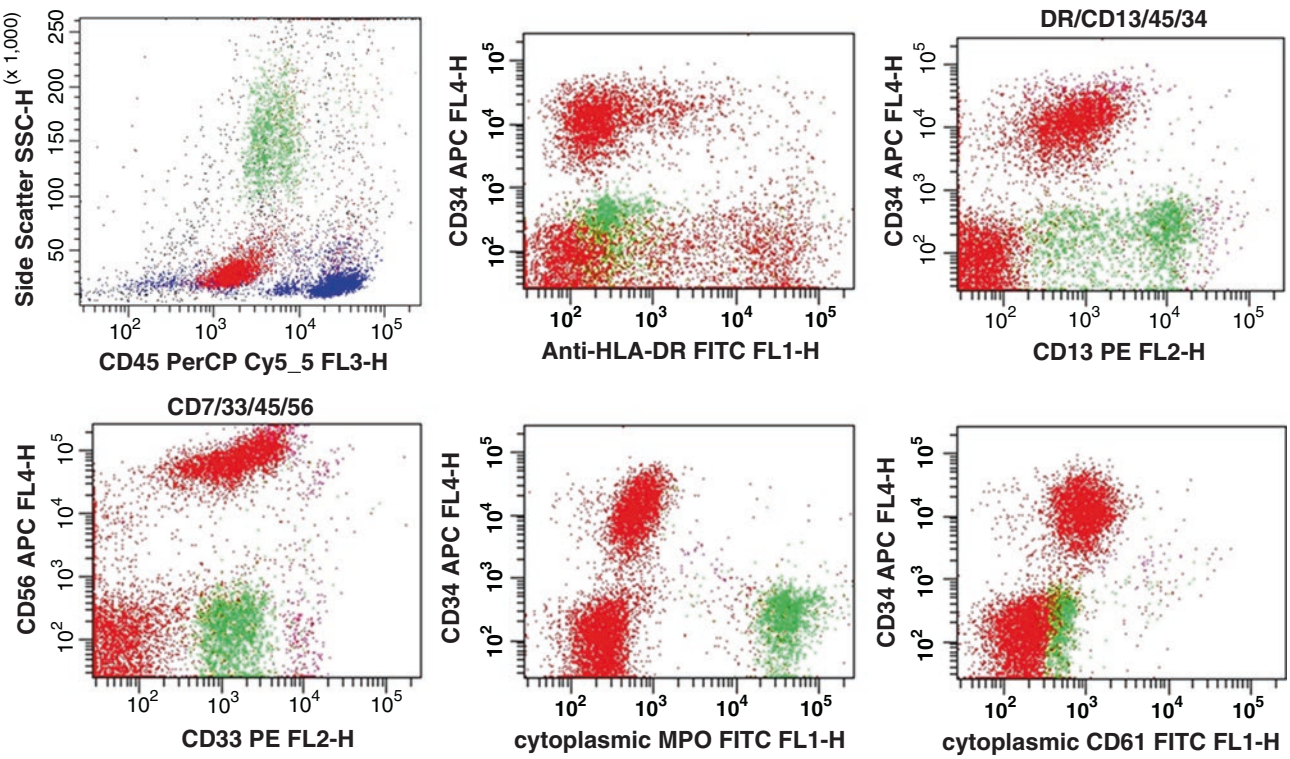

Fig. 12.11 The blasts in acute megakaryoblastic leukemia show a similar phenotype to that seen in TAM, here showing expression of immature marker CD34, myeloid markers CD13 and CD33, and megakaryocyte marker CD61. There is also bright aberrant expression of CD56. HLA-DR and MPO are negative. In contrast to TAM, the CD34 expression shown here is bright, with a more discrete population showing relatively little heterogeneity. Furthermore, there does not appear to be the same "phenotypic" maturation pattern (i.e., loss of CD34 with increasing CD61 expression) as illustrated previously in the case of TAM (Fig. 12.5)

References

1. Mateos MK, Barbaric D, Byatt SA, Sutton R, Marshall GM. Down syndrome and leukemia: insights into leukemogenesis and translational targets. Transl Pediatr. 2015;4:76–92.
2. Arber DA, Orazi A, Hasserjian R, Thiele J, Borowitz MJ, Le Beau MM, et al. The 2016 revision to the World Health Organization classification of myeloid neoplasms and acute leukemia. Blood. 2016;127:2391–405.
3. Yoshida K, Toki T, Okuno Y, Kanezaki R, Shiraishi Y, Sato-Otsubo A, et al. The landscape of somatic mutations in Down syndrome-related myeloid disorders. Nat Genet. 2013;45:1293–9.
4. Cantor AB. Myeloid proliferations associated with Down syndrome. J Hematop. 2015;8:169–76.
5. Bhatnagar N, Nizery L, Tunstall O, Vyas P, Roberts I. Transient abnormal myelopoiesis and AML in Down syndrome: an update. Curr Hematol Malig Rep. 2016;11:333–41.
6. Bombery M, Vergillo J. Transient abnormal myelopoiesis in neonates: GATA get the diagnosis. Arch Pathol Lab Med. 2014;138:1302–6.
7. Roberts I, Alford K, Hall G, Juban G, Richmond H, Norton A, et al. Oxford-Imperial Down Syndrome Cohort Study Group. *GATA1*-mutant clones are frequent and often unsuspected in babies with Down syndrome: identification of a population at risk of leukemia. Blood. 2013;122:3908–17.
8. Blink M, van den Heuvel-Eibrink MM, Aalbers AM, Balgobind BV, Hollink IH, Meijerink JP, et al. High frequency of copy number alterations in myeloid leukemias of Down syndrome. Br J Haematol. 2012;158:800–3.
9. Blink M, Zimmermann M, von Neuhoff C, Reinhardt D, de Haas V, Hasle H, et al. Normal karyotype is a poor prognostic factor in myeloid leukemia of Down syndrome: a retrospective, international study. Haematologica. 2014;99:299–307.
10. Blink M, Buitenkamp TD, van den Heuvel-Eibrink MM, Danen-van Oorschot AA, de Haas V, Reinhardt D, et al. Frequency and prognostic implications of *JAK 1-3* aberrations in Down syndrome acute lymphoblastic and myeloid leukemia. Leukemia. 2011;25:1365–8.
11. Walters DK, Mercher T, TL G, O'Hare T, Tyner JW, Loriaux M, et al. Activating alleles of *JAK3* in acute megakaryoblastic leukemia. Cancer Cell. 2006;10:65–75.
12. Malinge S, Ragu C, Della-Valle V, Pisani D, Constantinescu SN, Perez C, et al. Activating mutations in human acute megakaryoblastic leukemia. Blood. 2008;112:4220–6.
13. Kivivuori SM, Rajantie J, Siimes MA. Peripheral blood cell counts in infants with Down's syndrome. Clin Genet. 1996;49:15–9.
14. Akin K. Macrocytosis and leukopenia in Down's syndrome. JAMA. 1988;259:842.

Acute Leukemias of Ambiguous Lineage

13

Min Shi and Kaaren K. Reichard

Acute leukemias of ambiguous lineage are defined by the World Health Organization (WHO) classification as leukemias that either lack a specific lineage association or show features of concurrent multiple lineage associations [1, 2]. Ambiguous-lineage leukemias are more rare and more diagnostically challenging than conventional acute myeloid leukemias and lymphoblastic leukemias [1–11]. Given that the cytologic features of these leukemias are generally nonspecific, the diagnosis rests upon extensive immunophenotypic analysis. Multiparametric flow cytometric immunophenotyping is the preferred method for immunophenotyping, but in some cases, immunohistochemistry may be performed and may facilitate the recognition of two distinct blast populations in tissue sections. In addition to standard immunophenotypic studies, further evaluation should include cytogenetic studies to identify cases with t(9;22)(q34.1;q11.2); *BCR-ABL1* or t(v;11q23.3); *KMT2A* rearranged. Table 13.1 highlights the diagnostic subcategories of acute leukemias of ambiguous lineage, Table 13.2 lists the diagnostic criteria for lineage determination, and Table 13.3 compares lineage-specific and lineage-associated markers in acute leukemia. This chapter provides pathologic examples of various ambiguous-lineage leukemias and illustrates the key diagnostic challenges, considerations, and caveats in establishing these rare diagnoses (Figs. 13.1, 13.2, 13.3, 13.4, 13.5, 13.6, 13.7, 13.8, 13.9, 13.10, 13.11, 13.12, 13.13, 13.14, 13.15, 13.16, and 13.17).

M. Shi (✉) • K.K. Reichard
Department of Laboratory Medicine and Pathology, Division of Hematopathology, Mayo Clinic, Rochester, MN, USA
e-mail: shi.min@mayo.edu; reichard.kaaren@mayo.edu

T.I. George, D.A. Arber (eds.), *Atlas of Bone Marrow Pathology*, Atlas of Anatomic Pathology,
https://doi.org/10.1007/978-1-4939-7469-6_13

Table 13.1 Diagnostic subtypes of acute leukemias of ambiguous lineage

Subtype	Exemplary figures
Acute undifferentiated leukemia	Figs. 13.1, 13.2, 13.3 and 13.4
Mixed phenotype acute leukemia, T/myeloid, NOS	Figs. 13.5, 13.6 and 13.7
Mixed phenotype acute leukemia, B/myeloid, NOS	Figs. 13.8, 13.9 and 13.10
Mixed phenotype acute leukemia with t(9;22)(q34.1;q11.2); *BCR-ABL1*	Figs. 13.11, 13.12, 13.3 and 13.4
Mixed phenotype acute leukemia with t(v;11q23.3); *KMT2A* rearranged	Not illustrated
Mixed phenotype acute leukemia, NOS: rare types	Not illustrated

NOS—not otherwise specified

Table 13.2 Criteria for lineage assignment for a diagnosis of mixed phenotype acute leukemia

Myeloid lineage
Myeloperoxidase (flow cytometry, immunohistochemistry, or cytochemistry)
Monocytic differentiation (at least two of the following: nonspecific esterase cytochemistry, CD11c, CD14, CD64, lysozyme)
T lineage
Strong[a] cytoplasmic CD3 (with antibodies to CD3 ε chain)
Surface CD3
B lineage
Strong[a] CD19 with at least one of the following strongly expressed: CD79a, cytoplasmic CD22, or CD10
Weak CD19 with at least two of the following strongly expressed: CD79a, cytoplasmic CD22, or CD10

Adapted from Arber et al. [1]
[a]*Strong* is defined as equal to or brighter than the normal B cells or T cells

Table 13.3 Comparison of lineage-specific and lineage-associated markers in acute leukemia

	Lineage-specific markers	*Comments*
Myeloid lineage	Myeloperoxidase	Myeloid only
T lineage	cCD3 or sCD3 (with antibodies to CD3 ε chain)	T lineage only
B lineage	CD19	Can be seen in AML with t(8;21)
	Lineage-associated markers	*Comments*
Myeloid lineage	CD13, CD33, CD117	Can be seen in B-ALL and T-ALL
T lineage	CD2, CD5, CD7	Can be seen in AML and B-ALL
B lineage	CD10, cCD22, CD79a	Can be seen in AML and T-ALL

AML, acute myeloid leukemia; B-LL,B-lymphoblastic leukemia; T-LL, T-lymphoblastic leukemia

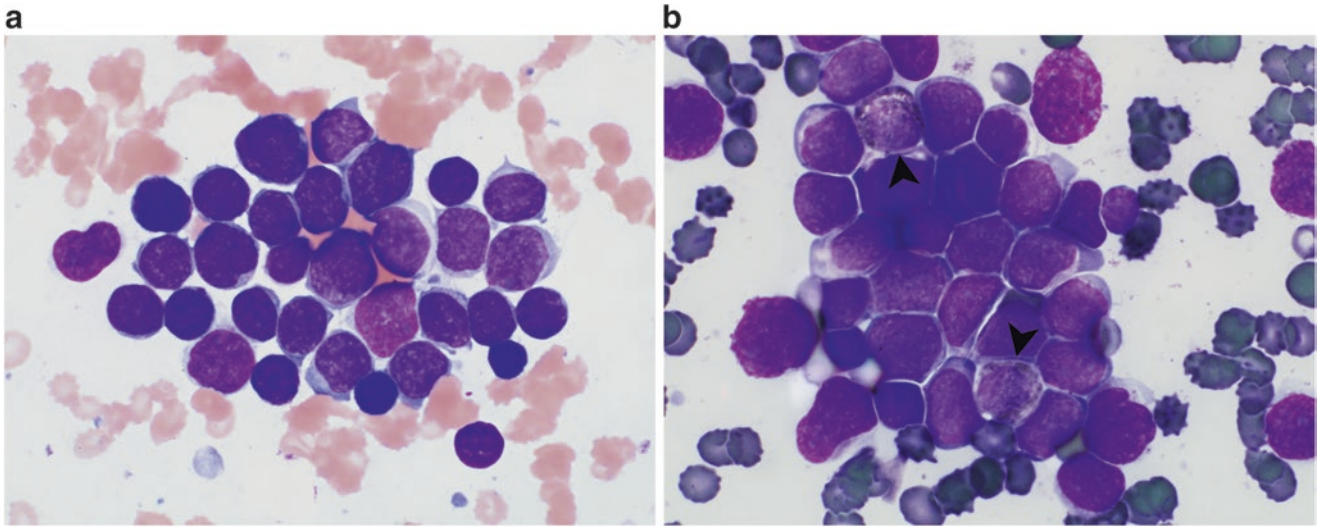

Fig. 13.1 Morphologic and cytochemical features in acute undifferentiated leukemia. (**a**) The morphologic features of the blasts in acute undifferentiated leukemia are generally nonspecific and, importantly, lack Auer rods. The blasts are small to intermediate in size, with round to slightly irregular nuclear contours, dispersed chromatin, and scant amounts of usually agranular cytoplasm. This morphologic appearance does not allow distinction of acute undifferentiated leukemia from acute myeloid leukemia with minimal differentiation and acute lymphoblastic leukemia, emphasizing the significant importance of extensive immunophenotyping for lineage determination. (**b**) Cytochemical testing for myeloperoxidase (MPO) is also a helpful tool to identify myeloid lineage. In this example of an acute undifferentiated leukemia, the blasts lack cytochemical MPO positivity, with admixed residual myelocytes (arrowheads) serving as internal positive controls. In contrast, a small fraction of MPO-positive blasts (<3%) may be seen in some cases of acute myeloid leukemia with minimal differentiation

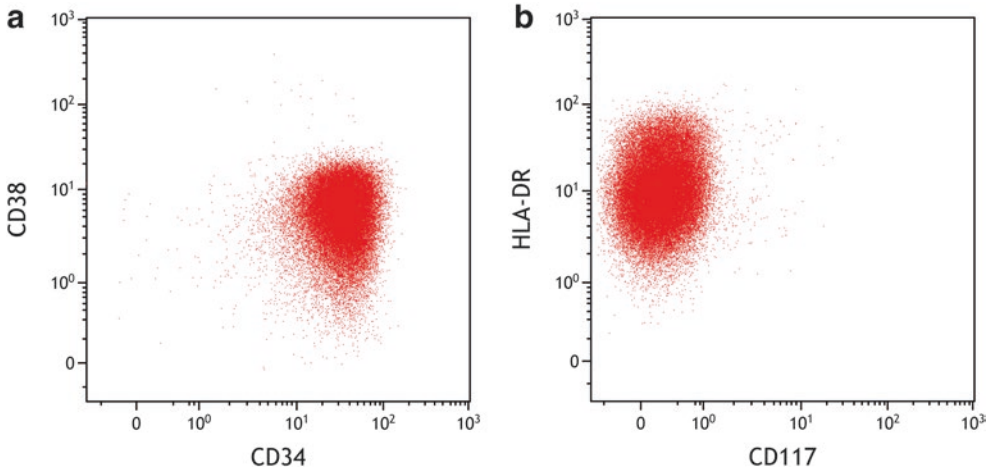

Fig. 13.2 Flow cytometric findings in acute undifferentiated leukemia. The blasts in acute undifferentiated leukemia, by definition, do not express any markers that are considered lineage specific (see Table 13.2). However, they are identified as blasts based on expression of early hematopoietic precursor markers, such as CD34 (**a**). Commonly they also express CD38 (**a**) and HLA-DR (**b**). The blast population is depicted in red

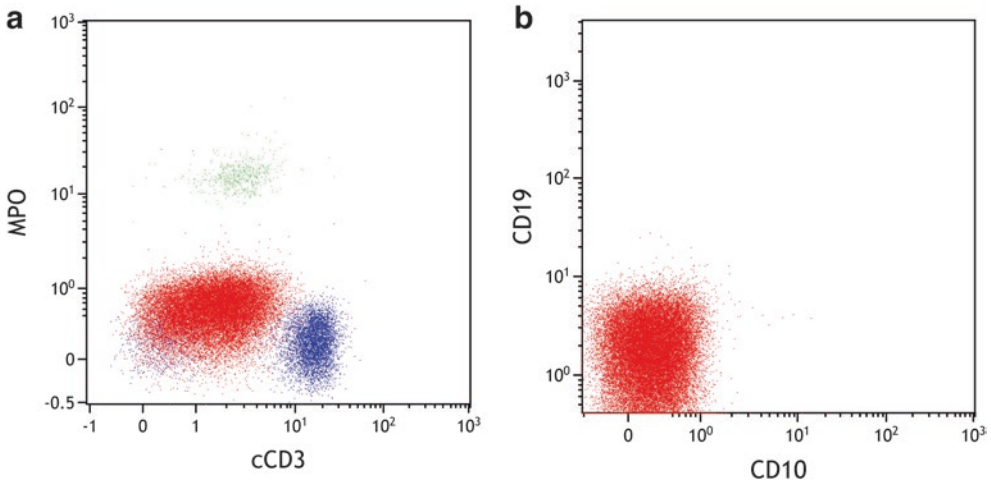

Fig. 13.3 Flow cytometric findings in acute undifferentiated leukemia. Comprehensive flow cytometric immunophenotyping is essential when diagnosing a case of acute undifferentiated leukemia. Specifically, commitment to a specific lineage(s) (myeloid, B, or T) must be excluded. To accurately determine whether lineage-specific markers are expressed or not, proper internal controls are crucial. (**a**) The blasts (red) are negative for MPO and cytoplasmic CD3 (cCD3); the internal granulocytic population (green) and mature T cells (blue) serve as internal positive controls. (**b**) Similarly, the blasts (red) lack expression of the B-lineage markers CD19 and CD10

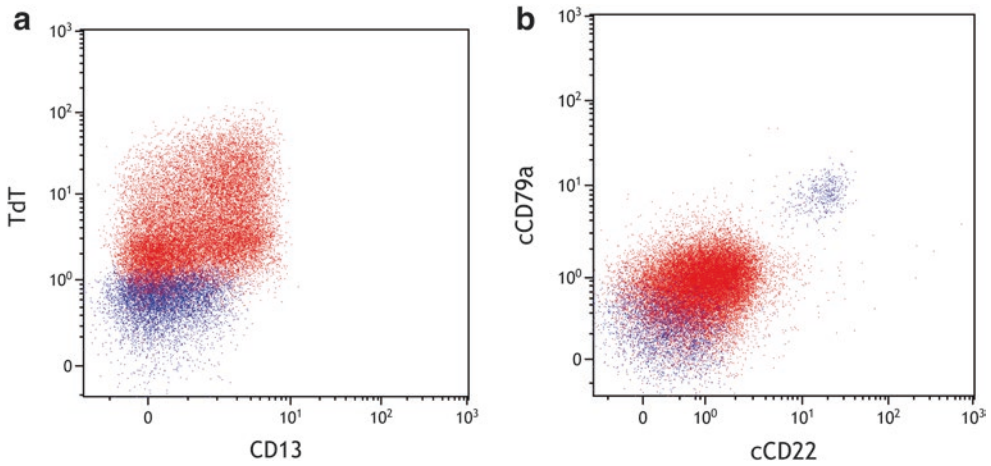

Fig. 13.4 Flow cytometric findings in acute undifferentiated leukemia. The blasts in acute undifferentiated leukemia may show positivity for terminal deoxynucleotidyl transferase (TdT) (blasts depicted in red) (**a**). TdT is not a lineage-specific marker and can be expressed in a variety of acute leukemia subtypes. In addition, acute undifferentiated leukemia may express some myeloid-associated markers (CD13, CD33, CD117), but typically no more than one of these markers is present. In this case, the blasts (*red*) express CD33 (not shown), but do not express CD117 (see Fig. 13.2b) or CD13 (*a*). The blasts lack both monocyte-associated markers (not shown) and the B-lineage-associated markers (cCD79a and cCD22) (blasts shown in red; mature B cells in blue [upper right]) (**b**)

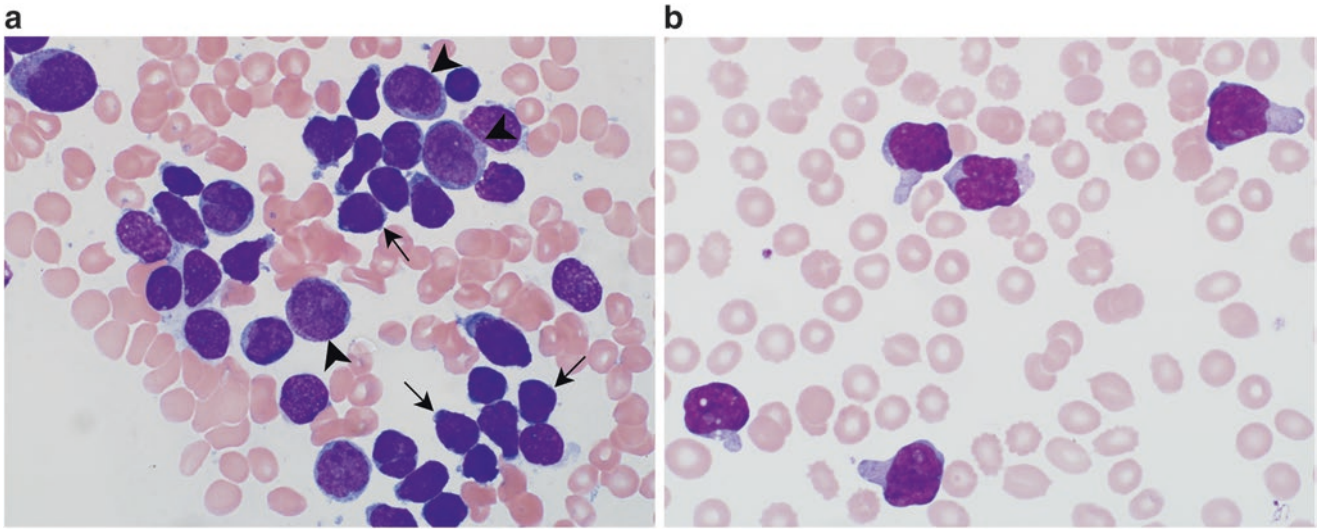

Fig. 13.5 Morphologic features of mixed phenotype acute leukemia, T/myeloid, not otherwise specified (MPAL, T/myeloid, NOS). The morphologic findings in MPAL, T/myeloid, NOS may be quite variable. (**a**) In this first example from a Wright-Giemsa-stained bone marrow aspirate, there is a dimorphic appearance, with one blast population smaller in size, resembling lymphoblasts (arrows), and a second blast population larger in size, resembling myeloblasts (arrowheads). (**b**) In contrast, in this second example, the morphologic features of the blasts are more uniform, characterized by small to intermediate size, nuclear contour indentations, high nuclear-to-cytoplasmic ratio, and asymmetric cytoplasmic extensions (hand-mirror morphology). This appearance morphologically resembles some cases of T-lymphoblastic leukemia (Wright-Giemsa, peripheral blood)

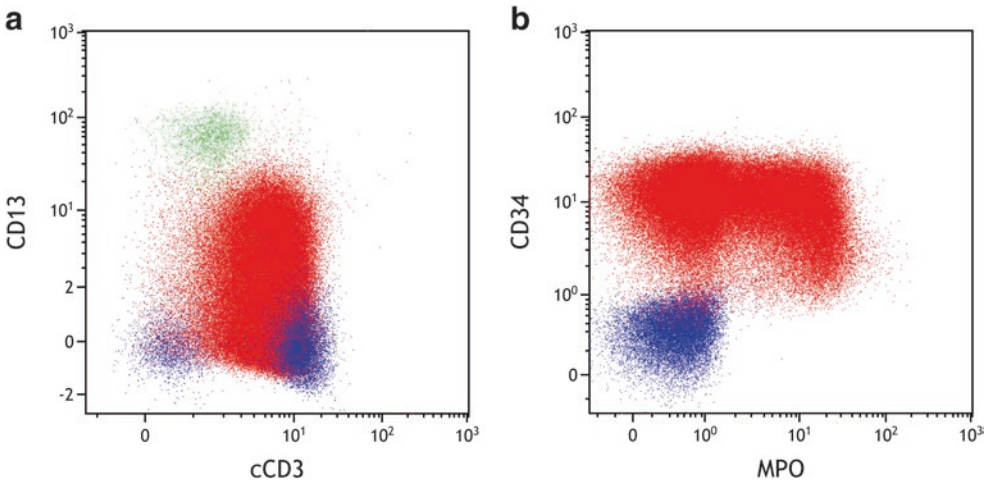

Fig. 13.6 Flow cytometric findings in MPAL, T/myeloid, NOS. As for acute undifferentiated leukemia, comprehensive flow cytometric immunophenotyping is essential for diagnosing a case of mixed phenotype acute leukemia, T/myeloid type. (**a**) By using antibody to the CD3ε chain, the blasts (red) are positive for cCD3, confirming T-lineage derivation. This cCD3 positivity is demonstrated by a portion of the blasts expressing at least equal intensity of cCD3 expression to that of normal control T cells (blue, lower right). Importantly, the residual granulocytes/monocytes (green) serve as negative internal controls for cCD3. (**b**) The blasts (red) also express MPO, which, in conjunction with the cCD3 positivity, establishes the diagnosis of MPAL, T/myeloid type. The blasts also show positivity for CD13 (dim) (**a**) and CD34 (**b**)

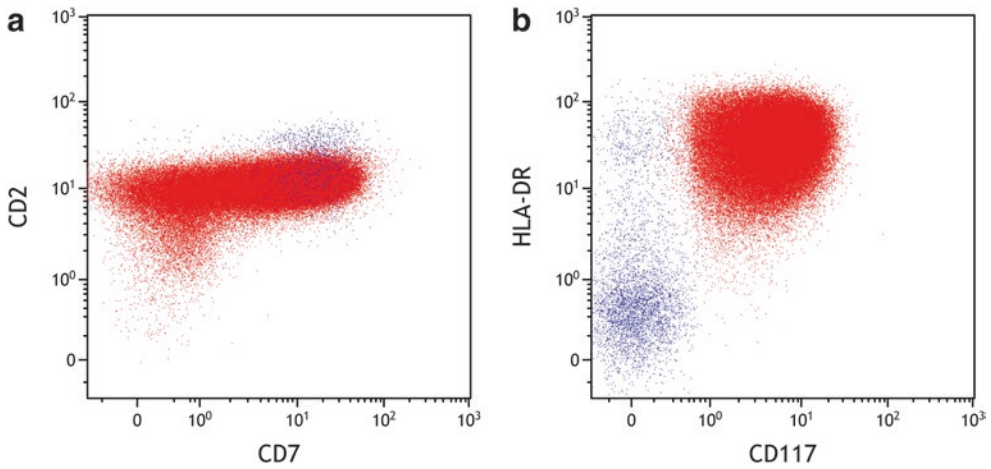

Fig. 13.7 Flow cytometric findings in MPAL, T/myeloid, NOS. In addition to the requisite cCD3 expression, the blasts in MPAL, T/myeloid, commonly express other T-lineage-associated markers such CD2, CD5, and/or CD7, but usually do not express surface CD3 (sCD3). (**a**) Blasts (red) are revealed that are uniformly positive for CD2 with variable expression of CD7, compared with normal T cells (blue). In addition to MPO, the blasts in MPAL, T/myeloid frequently express one or more myeloid-associated markers, such as CD13 (see Fig. 13.6a), CD33 (not shown), or CD117 (*b*, blasts depicted in red). (**b**) Although T-lymphoblastic leukemia is normally negative for HLA-DR, T/myeloid leukemia may demonstrate HLA-DR expression

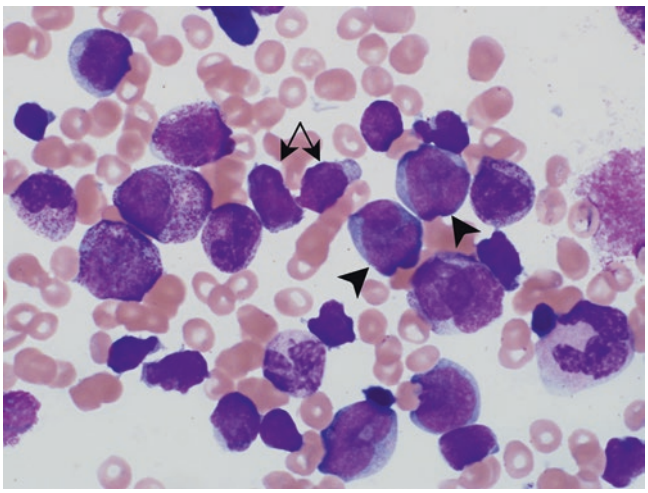

Fig. 13.8 Morphologic features of mixed phenotype acute leukemia, B/myeloid, not otherwise specified (MPAL, B/myeloid, NOS). MPAL, B/myeloid, NOS (similar to MPAL, T/myeloid, NOS) may comprise either single, uniform-appearing blasts or a dimorphic blast population, as seen in this figure. Some blasts are small, with less open chromatin and scant cytoplasm resembling lymphoblasts (arrows); others are larger, with finer chromatin and more abundant cytoplasm, resembling myeloblasts (arrowheads)

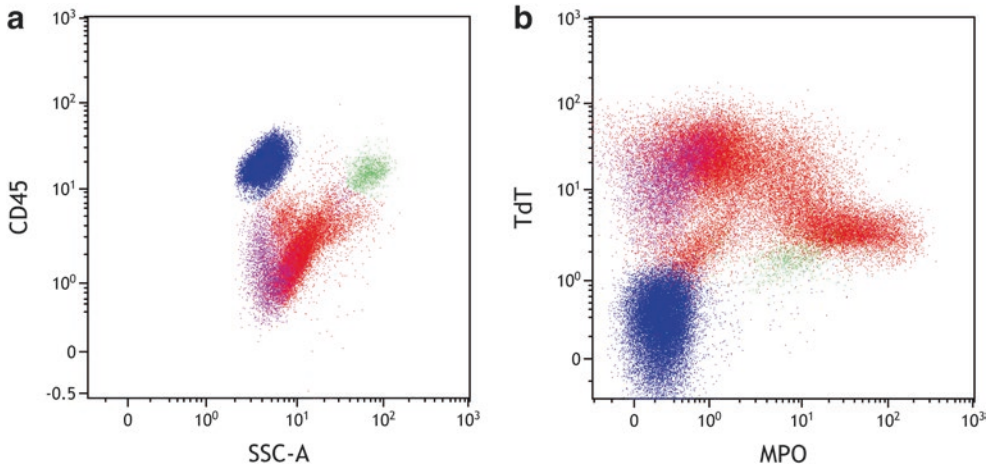

Fig. 13.9 Flow cytometric findings in MPAL, B/myeloid, NOS. The two morphologically distinctive populations demonstrated in Fig. 13.8 are also reflected in the accompanying flow cytometric immunophenotyping. (**a**) Two distinct blast populations (one depicted in red and the other in pink) are seen on the CD45 versus side scatter histogram, in which background granulocytes are depicted in green and mature lymphoid cells in blue. (**b**) Both blast populations are positive for TdT, confirming immaturity, but only one population is positive for MPO (partial, red), consistent with myeloid lineage; the other blast population is negative for MPO (pink). The presence of MPO positivity meets WHO criteria for myeloid lineage

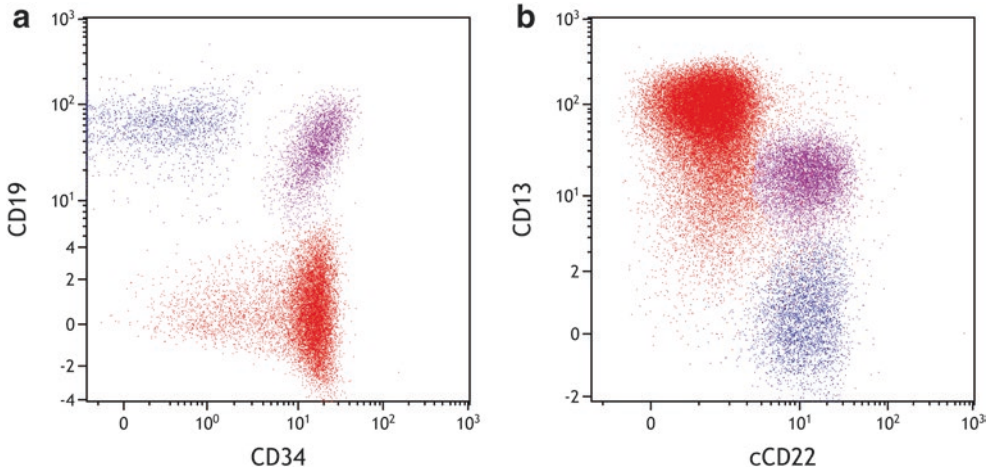

Fig. 13.10 Flow cytometry in MPAL, B/myeloid, NOS. The blasts in MPAL, B/myeloid, NOS (either one or both populations) must meet WHO criteria for B lineage and myeloid expression (Table 13.2). (**a**) In this example, the blasts in pink are strongly positive for CD19, suggesting but not confirming B lineage (compare with background mature B cells depicted in blue). According to the WHO classification, no single marker is sufficient to indicate B lineage, in contrast to myeloid and T lineage. Based on the CD19 expression level, expression of additional B-cell-associated markers (CD10, cCD22, and CD79a) is required for B-lineage assignment. (**b**) In this case, strong CD19 expression coupled with strong cCD22 confirms the B lineage (blasts depicted in pink). In addition to MPO, the second blast population also expressed the myeloid-associated marker CD13 (red blast population)

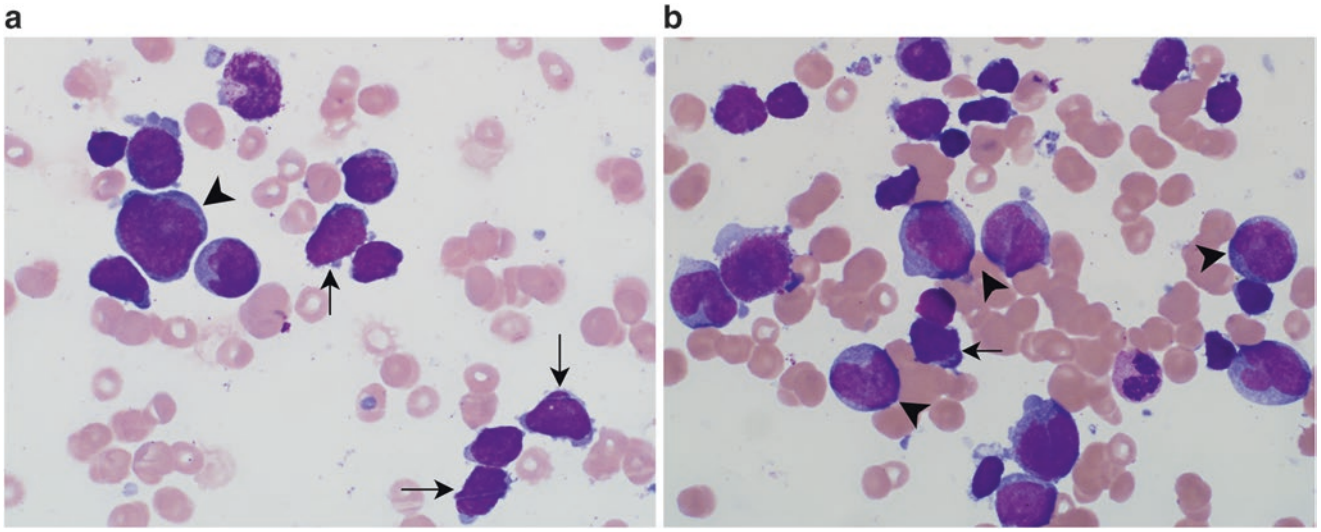

Fig. 13.11 Morphologic features of mixed phenotype acute leukemia (MPAL) with t(9;22)(q34.1;q11.2); *BCR-ABL1*. This is a rare type of acute leukemia that not only meets the criteria for MPAL, B/myeloid, but also harbors the recurring cytogenetic abnormality t(9;22)(q34;q11.2); *BCR-ABL1*. Similar to other types of MPAL, there are no diagnostic morphologic clues to the diagnosis, and many cases show dimorphic blast populations. (**a**) In this example, a dimorphic appearance is evident, with some areas of the bone marrow aspirate revealing small blasts with features typical of lymphoblasts (arrows). (**b**) Other areas exhibit larger blasts with more abundant cytoplasm and monocytic appearance (arrowheads). In this circumstance, it is important to distinguish a truly separate myeloid and lymphoblast population and not misinterpret the myeloid-appearing component as a morphologic variation within a pure B-lymphoblastic leukemia

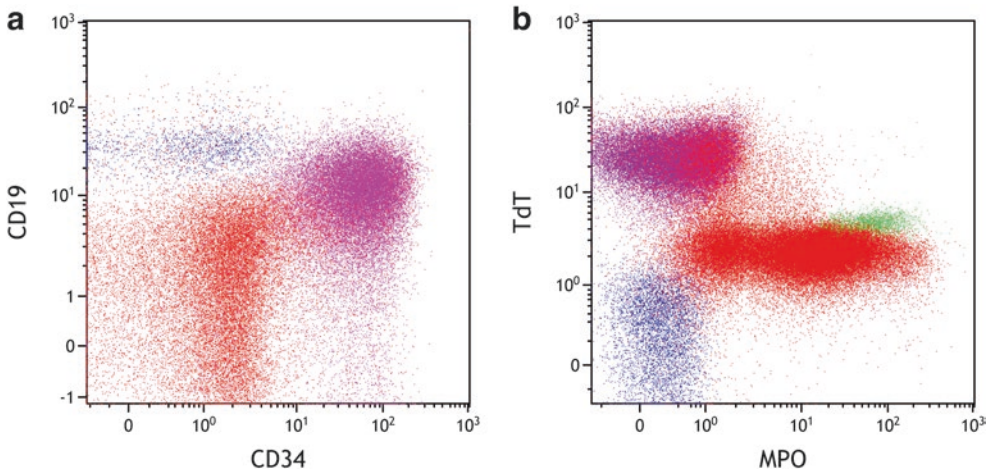

Fig. 13.12 Flow cytometric findings in MPAL with t(9;22)(q34.1;q11.2); *BCR-ABL1*. Flow cytometric immunophenotyping clearly shows two distinct blast populations (one depicted in pink and one in red). (**a**) The blasts depicted in pink are positive for CD19 (strong), CD34, and TdT and are negative for MPO (mature B cells in blue; maturing granulocytes in green). (**b**) In contrast, the blasts depicted in red are positive for MPO and TdT (small subset) and negative for CD19 and CD34 (*a*). The strong CD19 expression is suggestive of B-lineage blasts (depicted in pink), and the MPO expression confirms myeloid lineage of blasts (red) in this acute leukemia

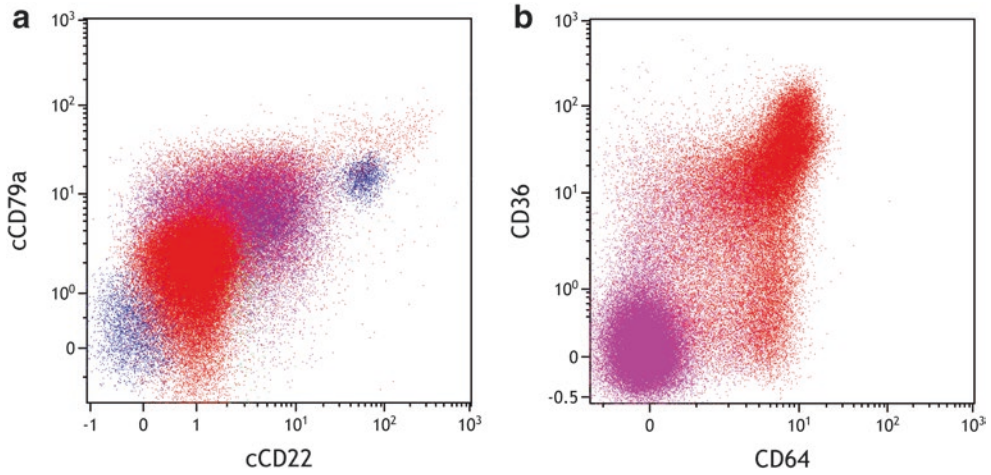

Fig. 13.13 Flow cytometric findings in MPAL with t(9;22)(q34.1;q11.2); *BCR-ABL1*. (**a**) In conjunction with the images in Fig. 13.12, the blasts depicted in pink strongly express CD79a (in addition to strong CD19), confirming their B-lineage commitment. (**b**) The co-expression of bright CD36/CD64 on the separate blast population (red) confirms monocytic differentiation, as was observed in the bone marrow aspirate in Fig. 13.11b

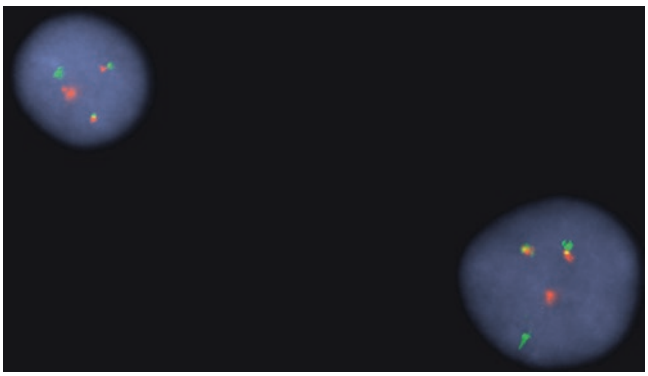

Fig. 13.14 Fluorescence in situ hybridization (FISH) in mixed phenotype acute leukemia with t(9;22)(q34.1;q11.2); *BCR-ABL1*. FISH, using a dual-color, dual-fusion probe set for *BCR* and *ABL1*, is performed on interphase cells from a patient with mixed phenotype acute leukemia. The *BCR* probe is labeled with SpectrumGreen and the *ABL1* probe, with SpectrumOrange. The two interphase cells reveal the typical abnormal pattern characteristic of a reciprocal translocation involving *BCR* and *ABL1* (i.e., one green signal (intact *BCR*), one orange signal (intact *ABL1*), and two yellow (green/orange) fusion signals (the fusion of *BCR* and *ABL1* on both chromosomes 9 and 22). According to the WHO classification, the diagnosis of mixed phenotype acute leukemia with t(9;22)(q34.1;q11.2); *BCR-ABL1* should not be rendered in patients with a history of chronic myeloid leukemia, *BCR-ABL1* positive. One other recurring genetic abnormality that may be seen in MPAL is t(v;11q23.3); *KMT2A (*previously called *MLL)* rearranged (not shown)

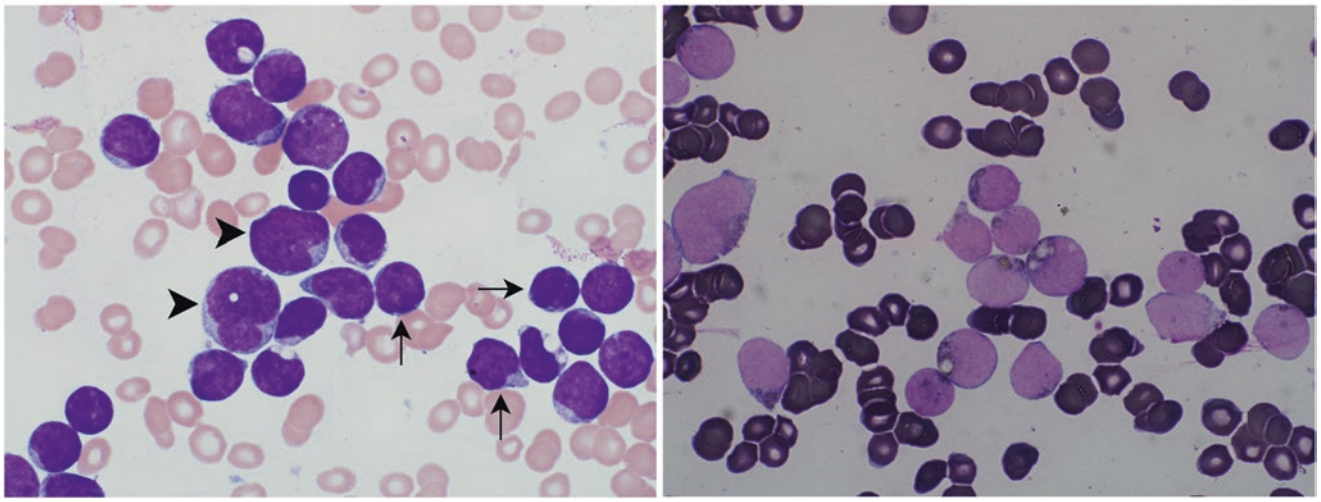

Fig. 13.15 Morphologic and cytochemical features in acute myeloid leukemia with dimorphic populations. MPALs may have dimorphic blast populations, but the presence of a dimorphic population does not necessarily indicate MPAL. (**a**) A dimorphic blast population is present in this example, which shows lymphoblast-like cells (arrows) and myeloblast-like cells (arrowheads). (**b**) All of the blasts are essentially positive for MPO, indicating uniform myeloid lineage commitment (cytochemical MPO, bone marrow aspirate; cytoplasmic brown stain connotes positivity). Flow cytometric immunophenotyping also confirms a single blast population, which expresses MPO, CD117 (bright), and CD33 (bright) and is negative for cCD3, CD19, CD79a, or cCD22 (not shown). For cases with a dimorphic population, it is important to perform an extensive immunophenotypic workup to avoid an overdiagnosis of MPAL

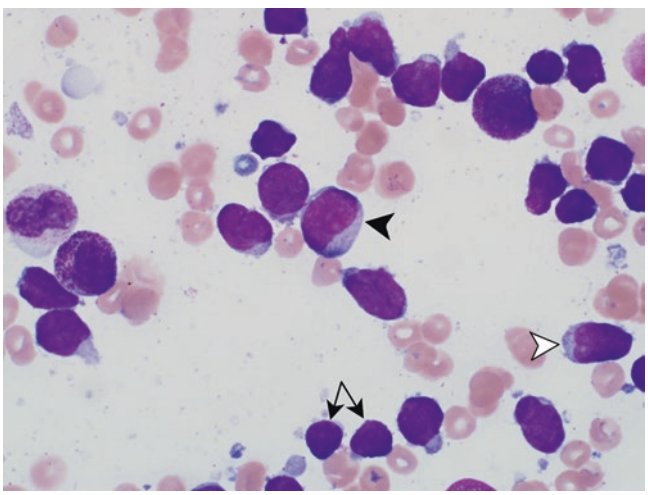

Fig. 13.16 Spectrum of morphologic features in pure lymphoblastic leukemia. The presence of a spectrum of blast morphologies or dimorphic appearance is not uncommon in both B- and T-lymphoblastic leukemia. In this example of B-lymphoblastic leukemia, the blasts range from small with scant cytoplasm, condensed chromatin, and inconspicuous nucleoli (arrows) to intermediate ones with more cytoplasm and open chromatin (open arrowhead) and to large blasts with abundant amounts of light blue cytoplasm and dispersed chromatin (arrowhead). Immunophenotypic studies are essential to make an accurate diagnosis

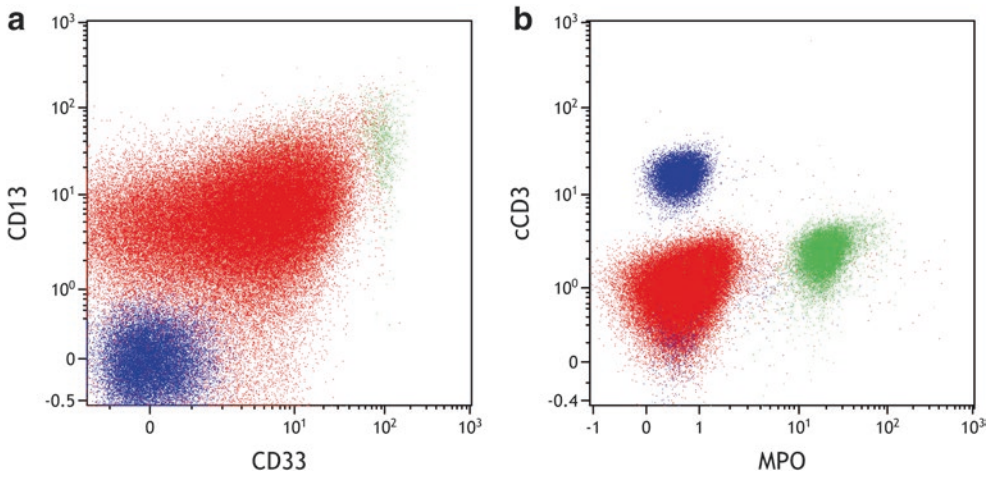

Fig. 13.17 Aberrant myeloid antigen expression in lymphoblastic leukemia. Both B- and T-lymphoblastic leukemias may express one or more myeloid-associated markers, including CD13, CD33, and/or CD117 (see Table 13.3). However, it is important to not overinterpret the expression of these markers as MPAL (either B/myeloid or T/myeloid). For MPAL, the expression of MPO or monocytic differentiation is required for myeloid lineage (see Table 13.2). (**a**) This B-lymphoblastic leukemia shows aberrant CD13 and CD33 expression (blasts depicted in red; T cells in blue; granulocytes in green) (bright CD19, bright cCD22, and bright CD79a expression on the blasts, not shown). (**b**) Importantly, this leukemia does not express MPO (blasts, red; T cells, blue; granulocytes, green) or monocytic differentiation (not shown); therefore, the diagnosis is B-lymphoblastic leukemia with aberrant myeloid antigen expression and not mixed phenotype acute leukemia, B/myeloid type

References

1. Arber DA, Orazi A, Hasserjian R, Thiele J, Borowitz MJ, Le Beau MM, et al. The 2016 revision to the World Health Organization classification of myeloid neoplasms and acute leukemia. Blood. 2016;127:2391–405. https://doi.org/10.1182/blood-2016-03-643544.
2. Borowitz MJ, Béné MC, Harris NL, Porwit A, Matutes E, et al. Acute leukaemias of ambiguous lineage. In: Swerdlow SH, Campo E, Harris NL, Jaffe ES, Pileri SA, Stein H, et al., editors. WHO classification of tumours of haematopoietic and lymphoid tissues. Lyon: IARC; 2008. p. 150–5.
3. Béné MC, Castoldi G, Knapp W, Ludwig WD, Matutes E, Orfao A, et al. Proposals for the immunological classification of acute leukemias. European Group for the Immunological Characterization of Leukemias (EGIL). Leukemia. 1995;9:1783–6.
4. Porwit A, Béné MC. Acute leukemias of ambiguous origin. Am J Clin Pathol. 2015;144:361–76. https://doi.org/10.1309/AJCPSTU55DRQEGTE.
5. Heesch S, Neumann M, Schwartz S, Bartram I, Schlee C, Burmeister T, et al. Acute leukemias of ambiguous lineage in adults: molecular and clinical characterization. Ann Hematol. 2013;92:747–58. https://doi.org/10.1007/s00277-013-1694-4.
6. van den Ancker W, Westers TM, de Leeuw DC, van der Veeken YF, Loonen A, van Beckhoven E, et al. A threshold of 10% for myeloperoxidase by flow cytometry is valid to classify acute leukemia of ambiguous and myeloid origin. Cytometry B Clin Cytom. 2013;84:114–8. https://doi.org/10.1002/cyto.b.21072.
7. Steensma DP. Oddballs: acute leukemias of mixed phenotype and ambiguous origin. Hematol Oncol Clin North Am. 2011;25:1235–53. https://doi.org/10.1016/j.hoc.2011.09.014.
8. Yang W, Tran P, Khan Z, Rezk S, O'Brien S. MLL-rearranged mixed phenotype acute leukemia masquerading as B-cell ALL. Leuk Lymphoma. 2017;58:1498–501. https://doi.org/10.1080/10428194.2016.1246728.
9. Wolach O, Stone RM. How I treat mixed-phenotype acute leukemia. Blood. 2015;125:2477–85. https://doi.org/10.1182/blood-2014-10-551465.
10. Weinberg OK, Seetharam M, Ren L, Alizadeh A, Arber DA. Mixed phenotype acute leukemia: a study of 61 cases using World Health Organization and European group for the immunological classification of Leukaemias criteria. Am J Clin Pathol. 2014;142:803–8. https://doi.org/10.1309/AJCPPVUPOTUVOIB5.
11. Borowitz MJ. Mixed phenotype acute leukemia. Cytometry B Clin Cytom. 2014;86:152–3. https://doi.org/10.1002/cyto.b.21155.

Histiocytic Disorders

14

Payal Sojitra and Tracy I. George

The Histiocyte Society has revised the classification of histiocytoses and neoplasms of the macrophage and dendritic cell lineages (Table 14.1) [1]. Not all of these disorders involve the bone marrow, but the most common disorders that involve the bone marrow are shown in Figs. 14.1, 14.2, 14.3, 14.4, 14.5, 14.6, 14.7, 14.8, 14.9, 14.10, 14.11, and 14.12 and contrasted in Table 14.2.

Langerhans cell histiocytosis (LCH) remains the most characteristic histiocytosis involving the bone marrow; it is generally diagnosed in childhood [2]. The characteristic histologic appearance of LCH is shown in Figs. 14.1, 14.2 and 14.3. It should be noted that a definitive diagnosis requires CD1a and/or CD207 (langerin) staining in the appropriate cells (Fig. 14.2). Although the ultrastructural detection of Birbeck granules is characteristic of LCH, it is no longer required for the diagnosis. Somatic mutations of *BRAF* have been described in a large subset of patients with LCH [3], and immunohistochemical stain for *BRAF* V600E is now available [4].

Histiocytic sarcoma is a rare neoplasm of mature histiocytes, which may involve the bone marrow secondarily (Fig. 14.4). It is important to exclude other neoplasms such as acute monocytic leukemia, lymphomas, carcinomas, and sarcomas before making a diagnosis of histiocytic sarcoma.

Other histiocytic disorders that rarely involve the bone marrow include Rosai-Dorfman disease, with its typical S100 protein-positive histiocytes and emperipolesis [5]; Erdheim-Chester disease, with CD68-positive and S100 protein-/CD1a-negative foamy histiocytes and Touton-type giant cells [6]; follicular dendritic cell sarcoma with CD21-, CD35-, and CD23-positive markers of follicular dendritic cells (FDCs) as shown in Fig. 14.12 [7]; and interdigitating cell sarcoma, in which the tumor cells express S100 protein but lack FDC markers and CD1a [8].

In contrast to these histiocytic neoplasms and the histiocytoses described above, hemophagocytic lymphohistiocytosis (HLH) or hemophagocytic syndromes are a group of reactive histiocytic disorders in which the clinical and laboratory findings represent a common endpoint of activated histiocytes and immune dysregulation. HLH is classified into primary or familial HLH and secondary or acquired HLH. Secondary hemophagocytic syndromes include those associated with infection, malignancy, and autoimmune disease. The diagnostic criteria for HLH (Table 14.3) were developed for individuals with familial HLH, but these criteria are also used in adults who primarily have secondary HLH [9]. Recent studies have suggested that genetic testing for HLH should be performed in both pediatric and adult patients [10]. Figures 14.5, 14.6, 14.7, 14.8, 14.9, and 14.10 show morphologic evidence of hemophagocytosis for a variety of primary and secondary HLHs. Importantly, morphologic hemophagocytosis is only one criterion for the diagnosis of HLH; by itself, it has little specificity for this disease. Secondary HLH is also associated with autoimmune disease. This is confusing because the term *macrophage activation syndrome* is also used to describe the final pathway of activated histiocytes and immune dysregulation complicating systemic inflammatory disorders, most commonly juvenile idiopathic arthritis and adult-onset Still's disease. Criteria have been published for macrophage activation syndrome complicating systemic juvenile idiopathic arthritis (Table 14.4) [11]; these criteria differ from HLH criteria in that the cytopenias are less severe, ferritin levels are lower, and increased soluble CD25 and decreased/absent NK-cell activity are less commonly observed. Finally, sarcoidosis may rarely involve the bone marrow (Fig. 14.11) [12].

P. Sojitra • T.I. George (✉)
Department of Pathology, University of New Mexico School of Medicine, Albuquerque, NM, USA
e-mail: tracygeorge@salud.unm.edu

T.I. George, D.A. Arber (eds.), *Atlas of Bone Marrow Pathology*, Atlas of Anatomic Pathology,
https://doi.org/10.1007/978-1-4939-7469-6_14

Table 14.1 Revised classification of histiocytosis and neoplasms of the macrophage-dendritic cell lineage

Group	Entities
L	Langerhans cell histiocytosis (LCH)
	Indeterminate cell histiocytosis
	Erdheim-Chester disease (ECD)
	Mixed ECD and LCH
C	Cutaneous non-LCH histiocytosis
	Cutaneous non-LCH histiocytosis with major systemic component
M	Primary malignant histiocytosis
	Secondary malignant histiocytosis
R	Familial Rosai-Dorfman disease (RDD)
	Classic RDD
	Extranodal RDD
	Neoplasia-associated RDD
	Immune disease-associated RDD
	Other non-C, non-L, non-M, and non-H histiocytoses
H	Primary hemophagocytic lymphohistiocytosis (HLH)
	Secondary HLH
	HLH of unknown/uncertain origin

Adapted from Emile et al. [1]

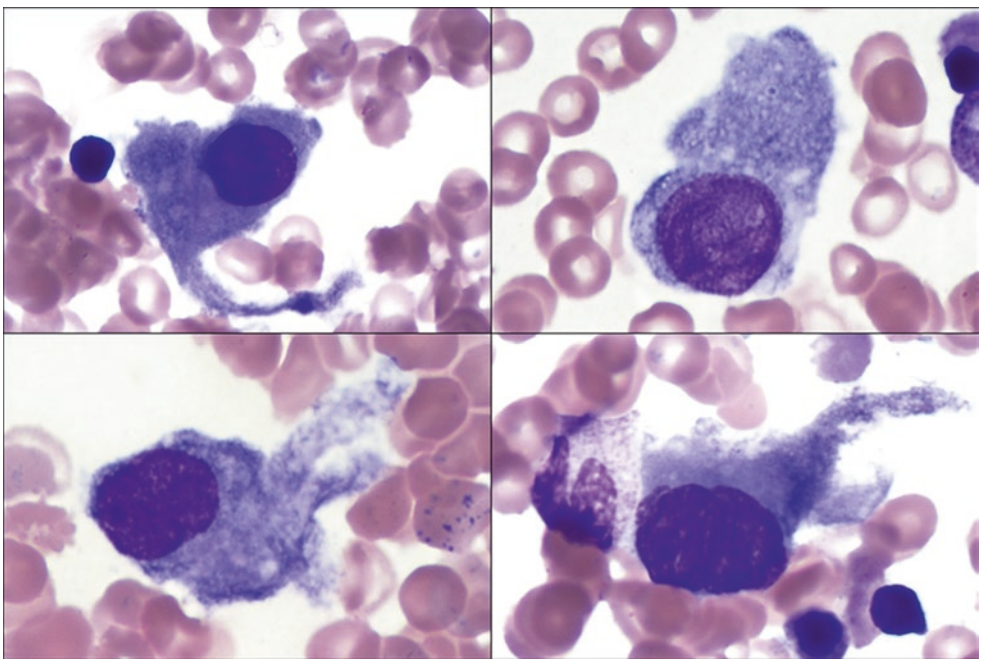

Fig. 14.1 Langerhans cell histiocytosis. This 1-year-old girl presented with anemia of 8.5 g/dL, thrombocytopenia of 42×10^9/L, hepatosplenomegaly, and disseminated intravascular coagulation. A Wright-Giemsa-stained bone marrow aspirate smear revealed scattered histiocytic cells that are large in size, with deeply basophilic cytoplasm showing prominent cytoplasmic processes. The nuclei are round to oval shaped with reticulated chromatin and grooved nuclei. Occasional nucleoli are noted

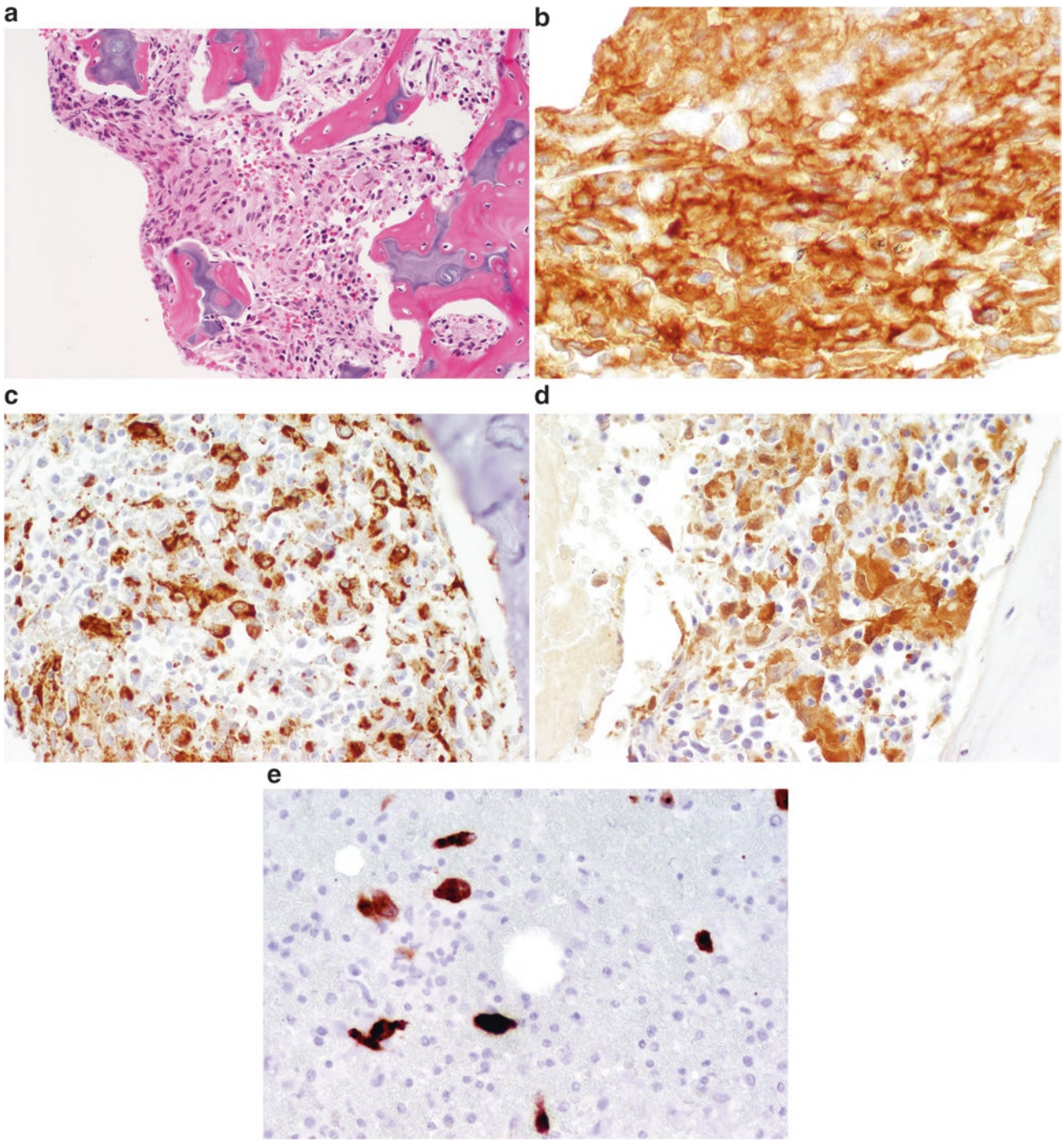

Fig. 14.2 Langerhans cell histiocytosis. (**a**) A hematoxylin and eosin (H&E)-stained bone marrow trephine section reveals an extensive infiltrate of large, clustered cells with abundant eosinophilic cytoplasm and monocytoid nuclei. The bony trabeculae show bony remodeling, as appropriate for a child of this age with incomplete ossification of bone. (**b**) The neoplastic cells show strong and uniform membranous expression with an immunohistochemical stain for CD1a. (**c**) The neoplastic infiltrate demonstrates cytoplasmic and membranous expression of CD68, confirming the histiocytic nature of these cells. (**d**) S100 protein immunostain highlights the neoplastic cells with nuclear and cytoplasmic staining. The elongated cytoplasmic processes can be seen. (**e**) On this bone marrow section, scattered neoplastic cells are also highlighted by an immunohistochemical stain for langerin. The langerin stain shows deep cytoplasmic staining of these cells

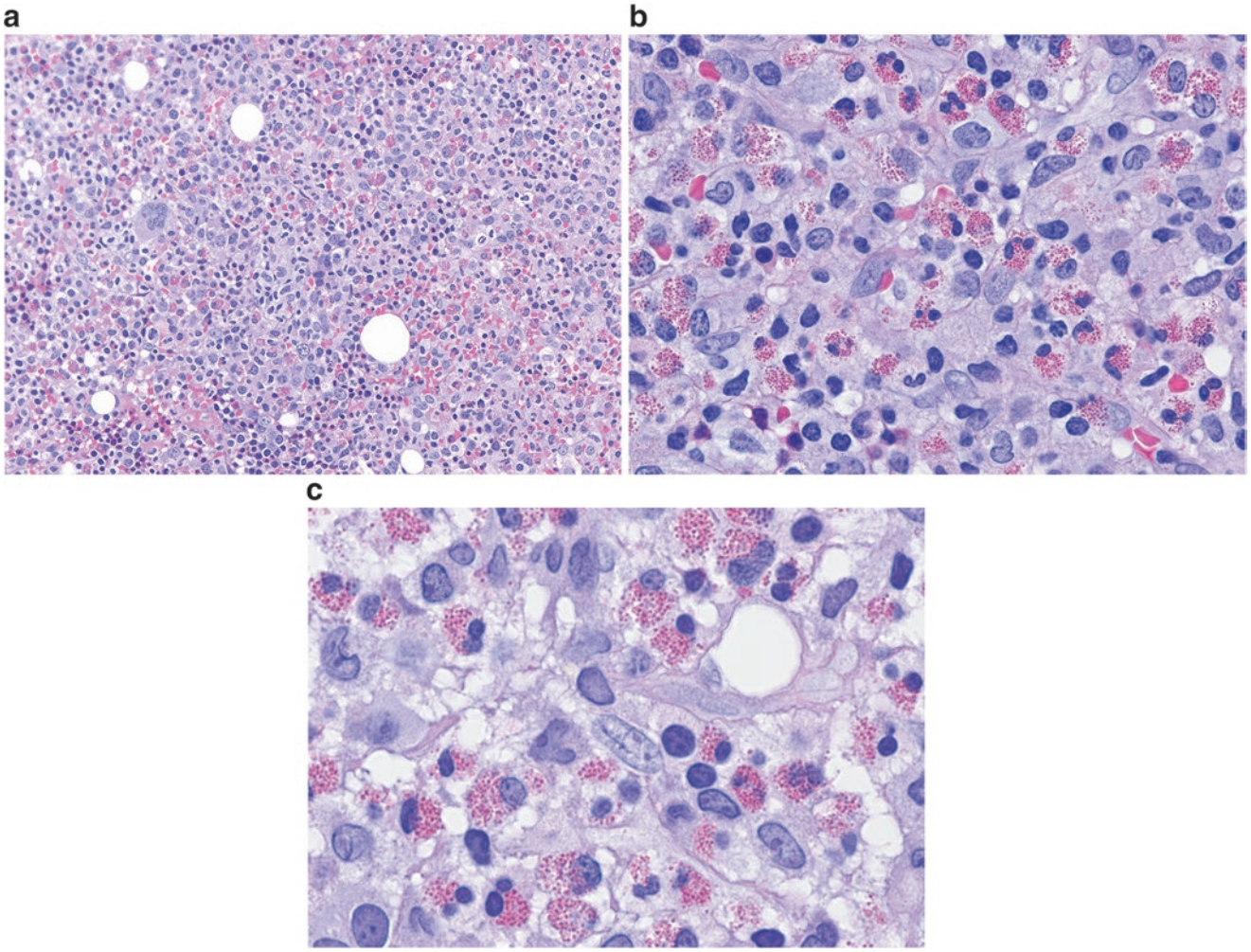

Fig. 14.3 Langerhans cell histiocytosis. (**a**) In this hypercellular bone marrow, a prominent histiocytic infiltrate and eosinophilia are noted. (**b** and **c**) Higher-power views reveal that some histiocytes show characteristic elongated coffee bean-like nuclei with grooved or folded nuclei (*Courtesy of* Luke Shier, MD)

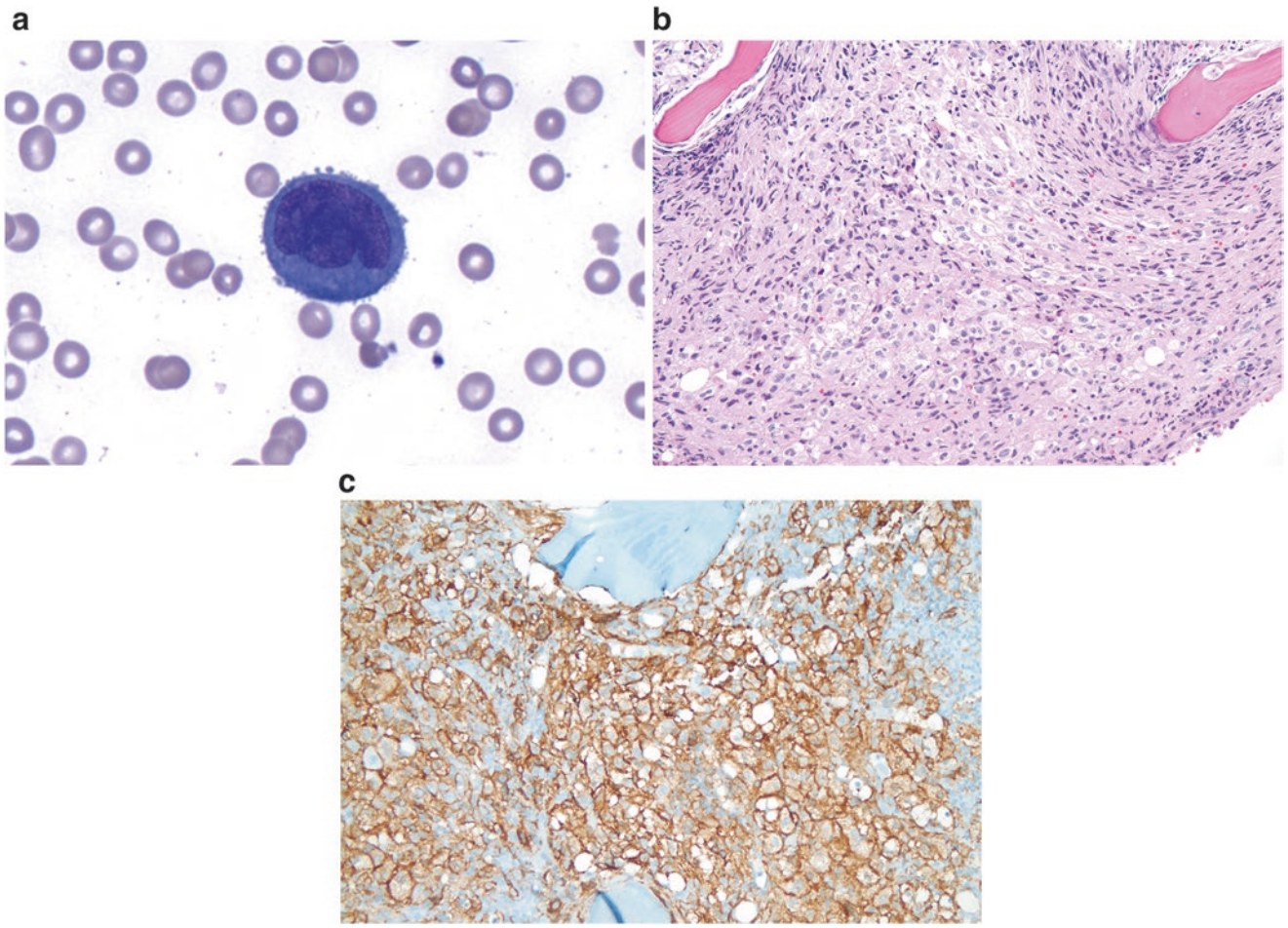

Fig. 14.4 Histiocytic sarcoma. (**a**) This hemodilute aspirate smear contains a large histiocytic cell with abundant basophilic cytoplasm and an enlarged and convoluted nucleus. (**b**) The bone marrow biopsy is effaced by an infiltrate of large cells with abundant eosinophilic cytoplasm and enlarged convoluted nuclei. A few bony trabeculae are present in the background; they are thinned with bony remodeling. (**c**) An immunohistochemical stain for CD163 highlights the neoplastic infiltrate with prominent membranous staining of the large cells, while sparing hematopoiesis in the upper right hand portion of the image

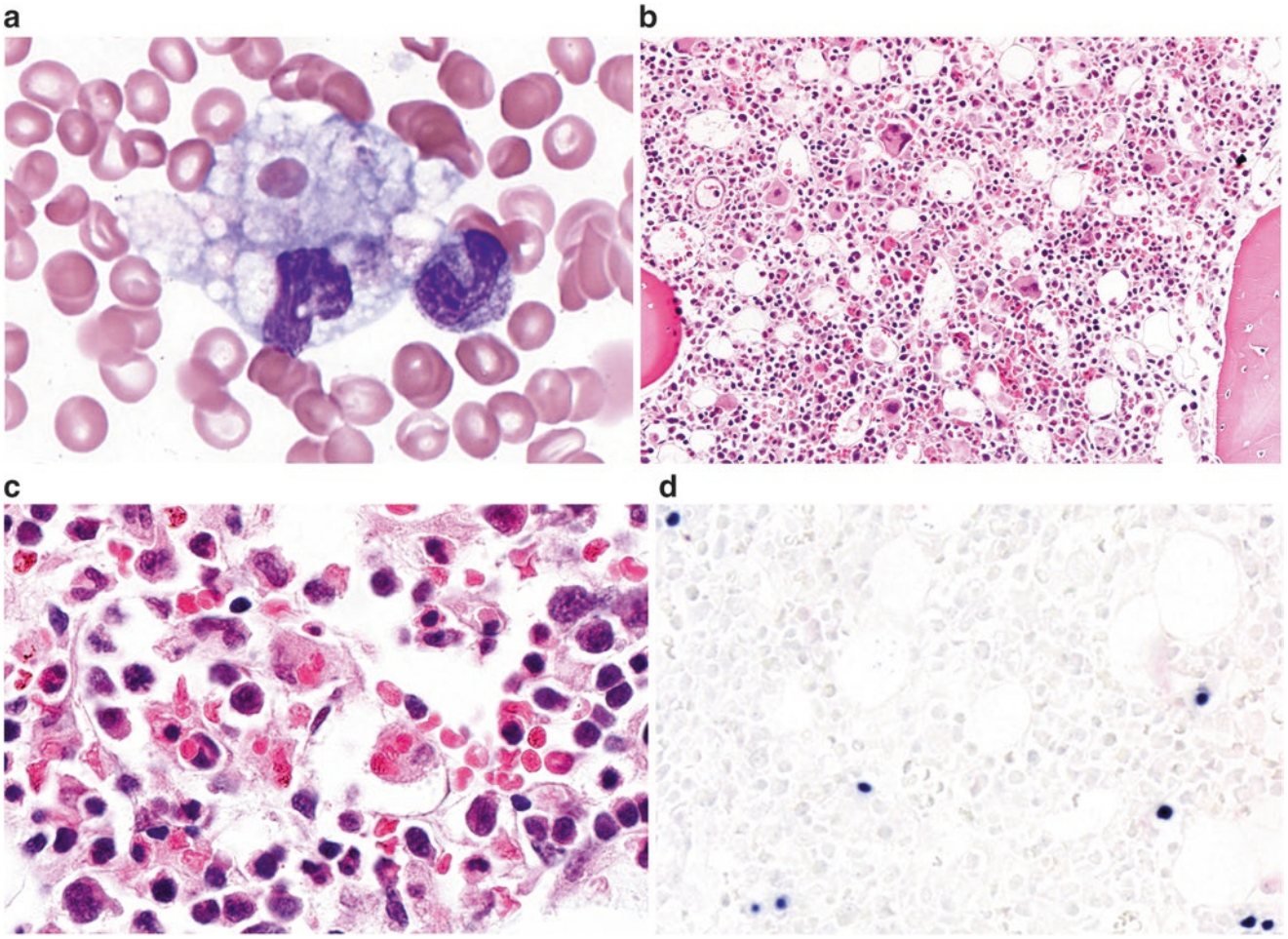

Fig. 14.5 Epstein-Barr virus (EBV)-associated hemophagocytic syndrome. This 14-month-old Hispanic boy presented with pancytopenia, elevated liver function tests, coagulopathy, hepatosplenomegaly, and a 2-week history of fever and a vasculitic rash. Ferritin was 8100 ng/L, LDH was 3168 U/L, soluble CD25 was elevated, and the EBV DNA load was 3723 copies/mL. Studies for cytomegalovirus (CMV), herpes simplex virus (HSV), parvovirus B19, respiratory viruses, and blood/urine/CSF cultures were all negative. No mutations were identified in *PRF1* or *MUNC13-4*, and there was no support for immune deficiency. (**a**) On a bone marrow aspirate smear, an activated histiocyte is present, engulfing an erythrocyte adjacent to a toxic band neutrophil. Hemophagocytosis was easy to find in the aspirate smear, and bare histiocytes were also present. (**b**) The bone marrow core biopsy at low power is mildly hypocellular for age, at 80% cellularity. A slight increase in megakaryocytes is present. Sinuses are dilated, and there are increased histiocytes showing erythrophagocytosis. (**c**) A higher-power image of the core biopsy demonstrates increased numbers of histiocytes within dilated sinuses, with prominent erythrophagocytosis. (**d**) In situ hybridization study for EBV-encoded small RNAs (EBERs) on the bone marrow biopsy highlights scattered lymphoid cells. The patient received antivirals and followed the HLH protocol for therapy. The complete blood cell count normalized, and subsequent bone marrows were normal. Of acquired hemophagocytic syndromes, approximately one third are due to infection. Viral infections outnumber other infections associated with acquired HLH, but virtually all infections have been associated. EBV is the most common virus among virus-induced hemophagocytic syndromes, and its prognosis is worse than for other viruses and acquired HLH

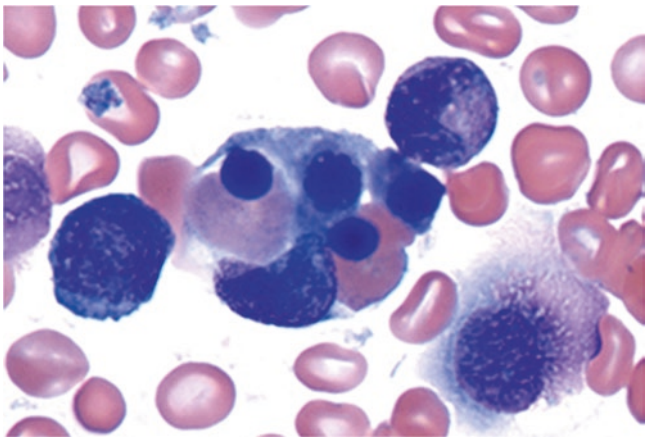

Fig. 14.6 Familial hemophagocytic lymphohistiocytosis. This 5-month-old presented with pancytopenia. A homozygous *RAB27A* mutation was found, and a diagnosis of Griscelli syndrome, an autosomal recessive syndrome, was made. The *RAB27A* gene is important in melanosome transport and proper function of cytotoxic T cells. Mutations in *RAB27A* result in hypopigmented skin and gray hair in infancy, typical of Griscelli syndrome, as well as recurrent infections and HLH. The bone marrow aspirate smear showed overt hemophagocytosis. Illustrated is a histiocyte with ingested erythroid precursors. An adjacent smudge cell is also present. Increased smudge cells are not uncommon when increased histiocytes are present. Familial or primary HLH is commonly due to inborn defects in lymphocytes that normally mediate control of infection and inflammatory conditions. These include a number of genetic disorders

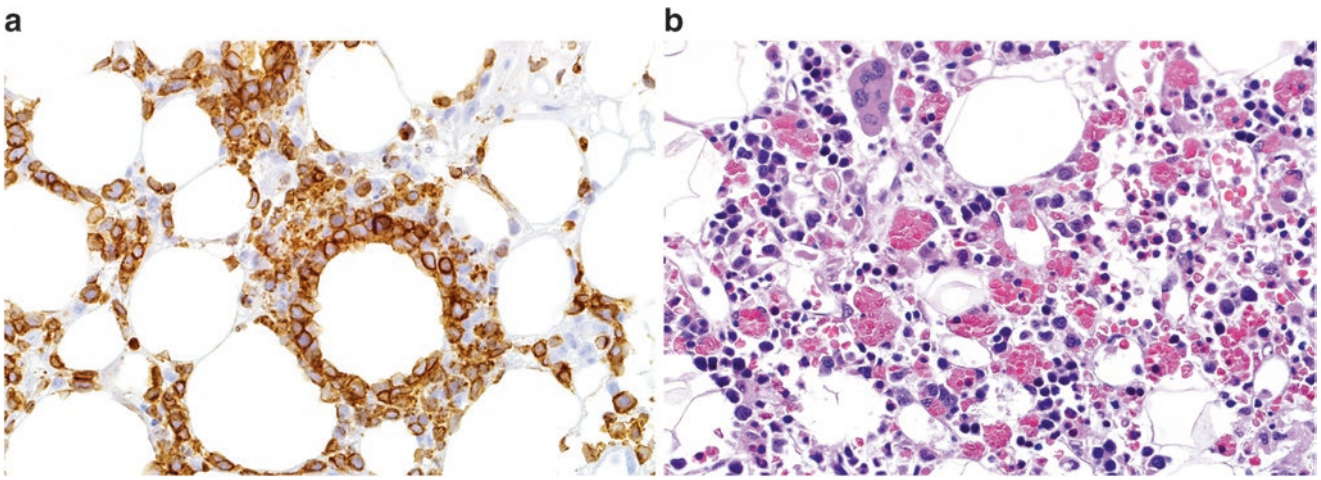

Fig. 14.7 Malignancy-associated hemophagocytic syndrome. Subcutaneous panniculitis-like T-cell lymphoma was diagnosed from a skin biopsy from the right upper arm of this 28-year-old woman. (**a**) High-power image of the subcutis highlights rimming of fat lobules by CD3-positive lymphoma cells. (**b**) There was no evidence of lymphoma in the bone marrow, but the patient met criteria for hemophagocytic syndrome. The bone marrow biopsy highlights numerous histiocytes stuffed with erythrocytes, showing a "bean bag" appearance on H&E-stained section

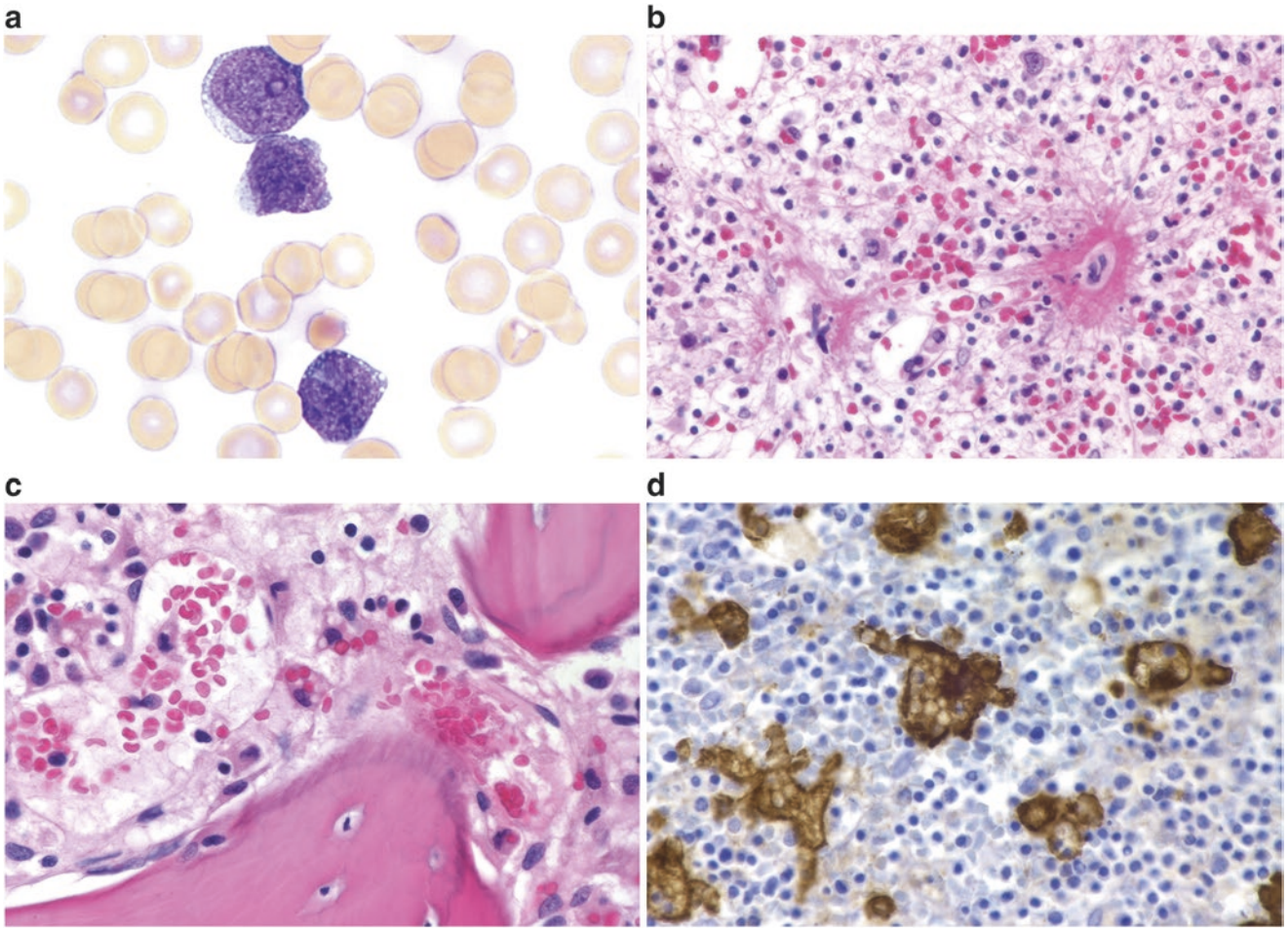

Fig. 14.8 Malignancy-associated hemophagocytic syndrome. This patient with acute lymphoblastic leukemia was found to have hemophagocytic syndrome at autopsy, with erythrophagocytosis found in the bone marrow, spleen, liver, and mesenteric lymph nodes. (**a**) Typical lymphoblasts are identified in the blood smear, with a high nuclear-to-cytoplasmic ratio, smooth chromatin, and a small amount of basophilic cytoplasm. (**b**) The bone marrow was hypocellular for the patient's age, with a prominence of stroma where the hematopoiesis has dropped out. A vessel at the right appears necrotic. (**c**) On higher power, the biopsy demonstrates dilated marrow sinuses containing bare histiocytes and histiocytes engulfing erythrocytes in the center of the image. (**d**) Immunohistochemical stain for CD163 can be quite useful to highlight histiocytes. Cell outlines can be seen within the cytoplasm of the CD163-positive histiocytes, helping to illustrate the phagocytosis of cells

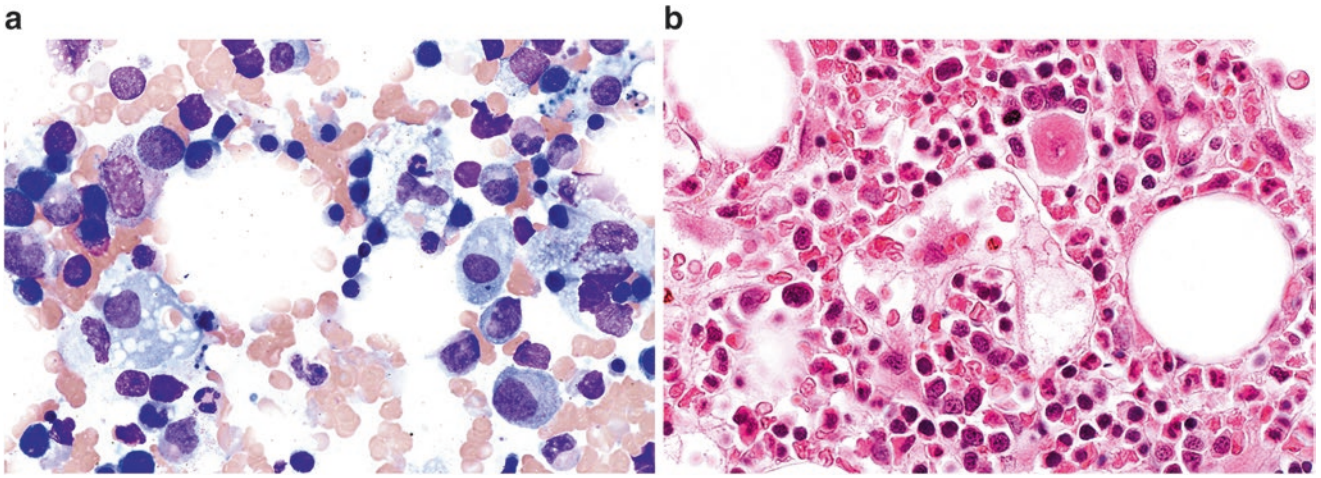

Fig. 14.9 Malignancy-associated hemophagocytic syndrome. Diffuse large B-cell lymphoma presenting as a retroperitoneal mass was diagnosed in this 76-year-old man. A staging bone marrow found no evidence of lymphoma, but the patient did have hemophagocytic syndrome. (**a**) Bone marrow aspirate demonstrates histiocytes containing erythrocytes and nucleated cells. (**b**) The trephine biopsy shows a dilated sinusoid in the middle of the image, with erythrophagocytosis

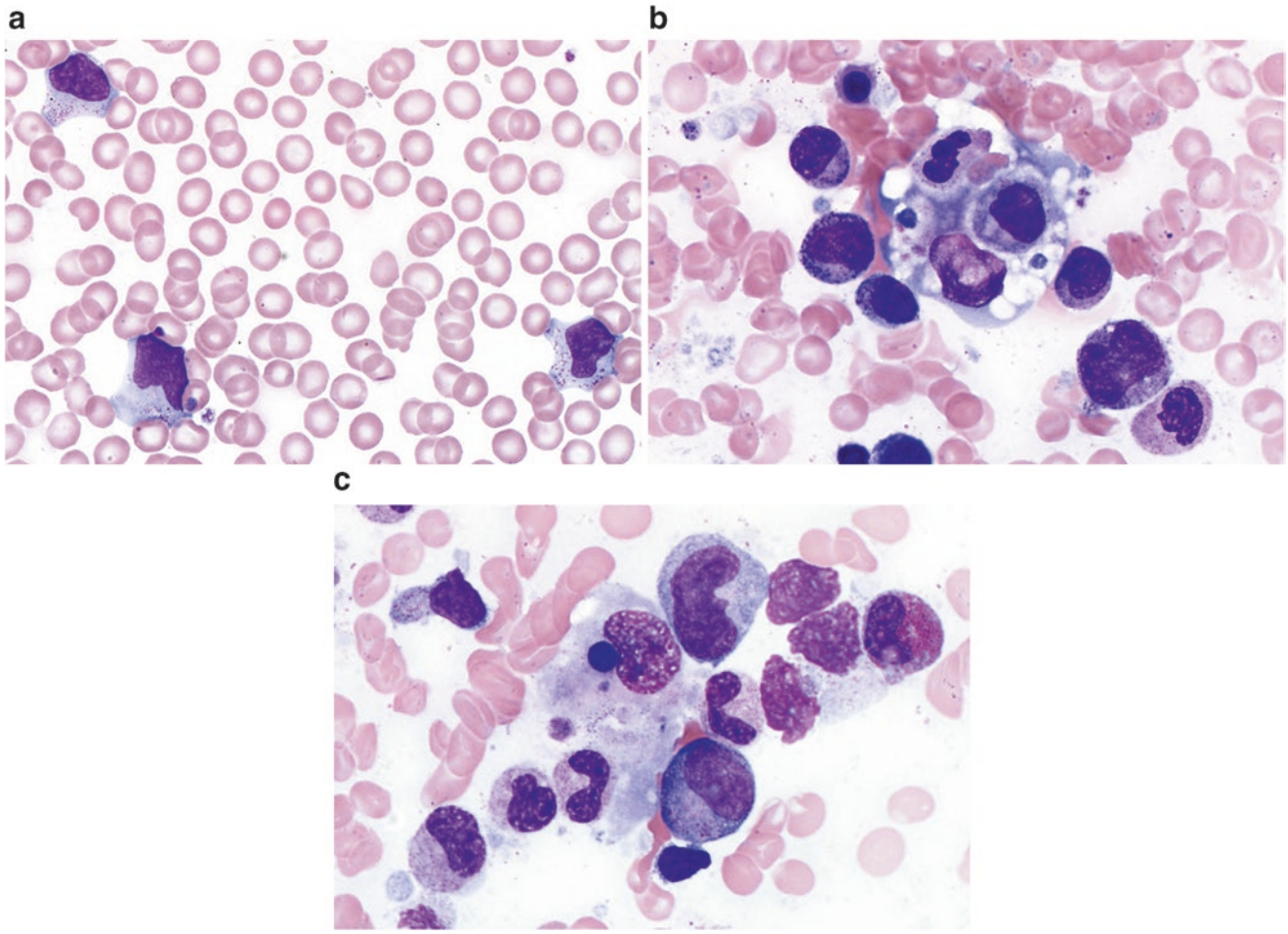

Fig. 14.10 Malignancy-associated hemophagocytic syndrome. This 12-year-old Native American girl presented with aggressive NK-cell leukemia and hemophagocytic syndrome. NK-cell and T-cell malignancies have a high association with hemophagocytic syndrome, but hemophagocytic syndrome has been reported with virtually all of the hematologic malignancies. (**a**) Here, the peripheral blood shows the "angry"-appearing large granular lymphocyte-like cells of aggressive NK-cell leukemia with abundant lightly basophilic cytoplasm containing large azurophilic granules. The nuclei are irregular with prominent nucleoli and partially condensed chromatin. (**b**) The bone marrow aspirate smear demonstrates phagocytosis of nucleated cells, including a leukemic cell at 2 o'clock. (**c**) In this image, a large neoplastic cell is adjacent to the histiocyte at 1 o'clock

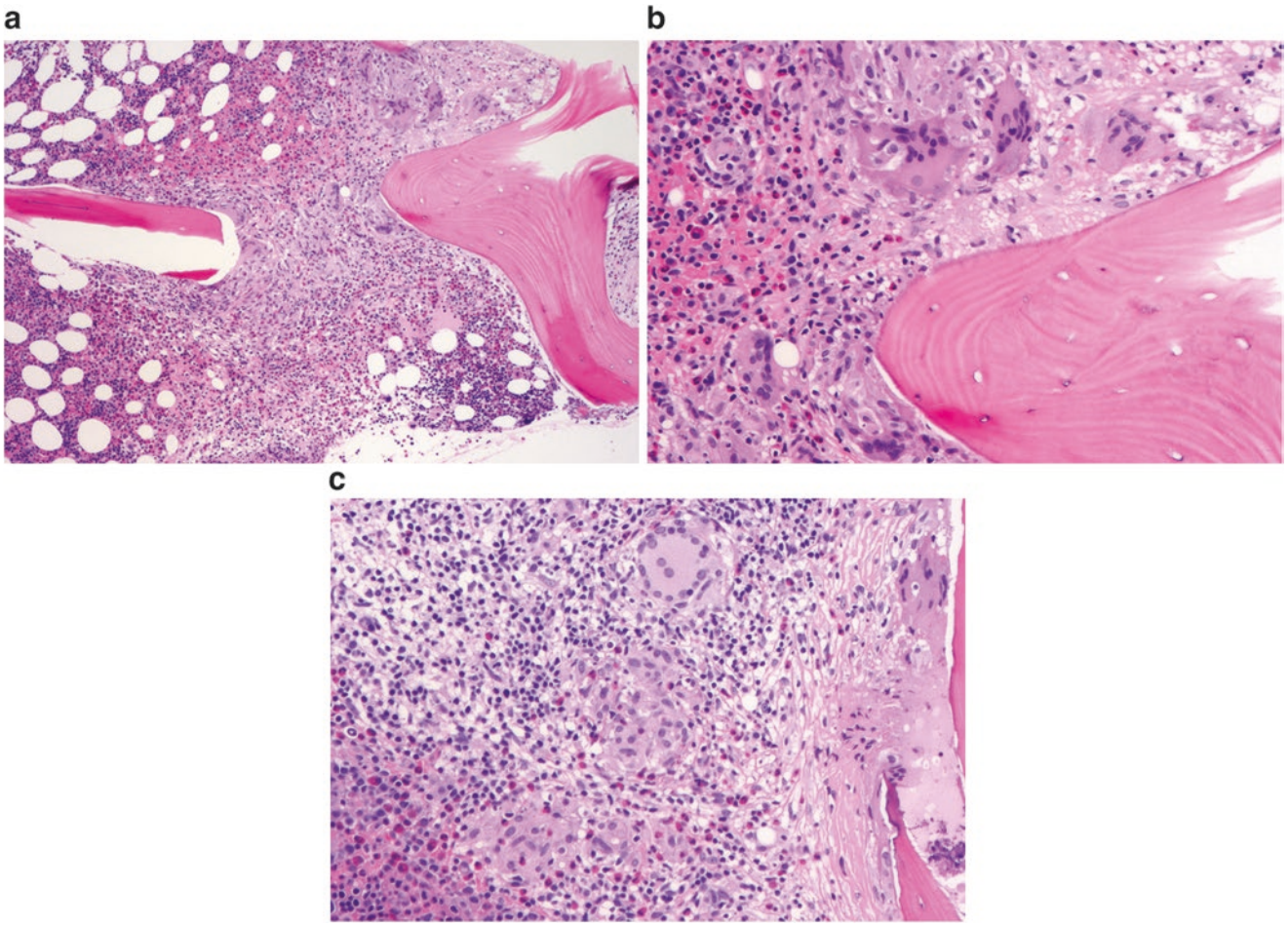

Fig. 14.11 Sarcoidosis. This 44-year-old woman presented with myalgias, arthralgias, anemia, and hypercalcemia. Imaging PET study showed a diffuse increased uptake within the bone marrow. A diagnosis of sarcoidosis was made after an infectious workup was negative; special stains for fungi and acid-fast bacilli were negative (*not shown*). (**a**) This bone marrow biopsy shows multifocal involvement by noncaseating granulomata with multiple multinucleated giant cells and eosinophilia surrounding the bone. Immunohistochemistry confirmed that the histiocytic cells were highlited by CD68 but were negative for S100 protein, langerin, and *BRAF*V600E (*not shown*). Interestingly, focal CD1a expression was noted. (**b**) On a higher-power view of the bone marrow biopsy, the bony trabeculae are rimmed by multinucleated giant cells. Bone marrow involvement in sarcoidosis is unusual, but it has been described in about 10% of cases [11]. These patients often present with cytopenias, hypercalcemia, and increased bony activity on PET scans. (**c**) In this image, the histiocytic infiltrate surrounding bone comprises histiocytes, lymphocytes, eosinophils, and multinucleated giant cells. At the top of the image, a Langhans giant cell is noted with nuclei arranged in a horseshoe-shaped pattern in the periphery of the cell; these multinucleated giant cells are formed by fusion of macrophages. Necrosis is absent. The differential diagnosis in this patient also included Langerhans cell histiocytosis, infection, and other immune disorders

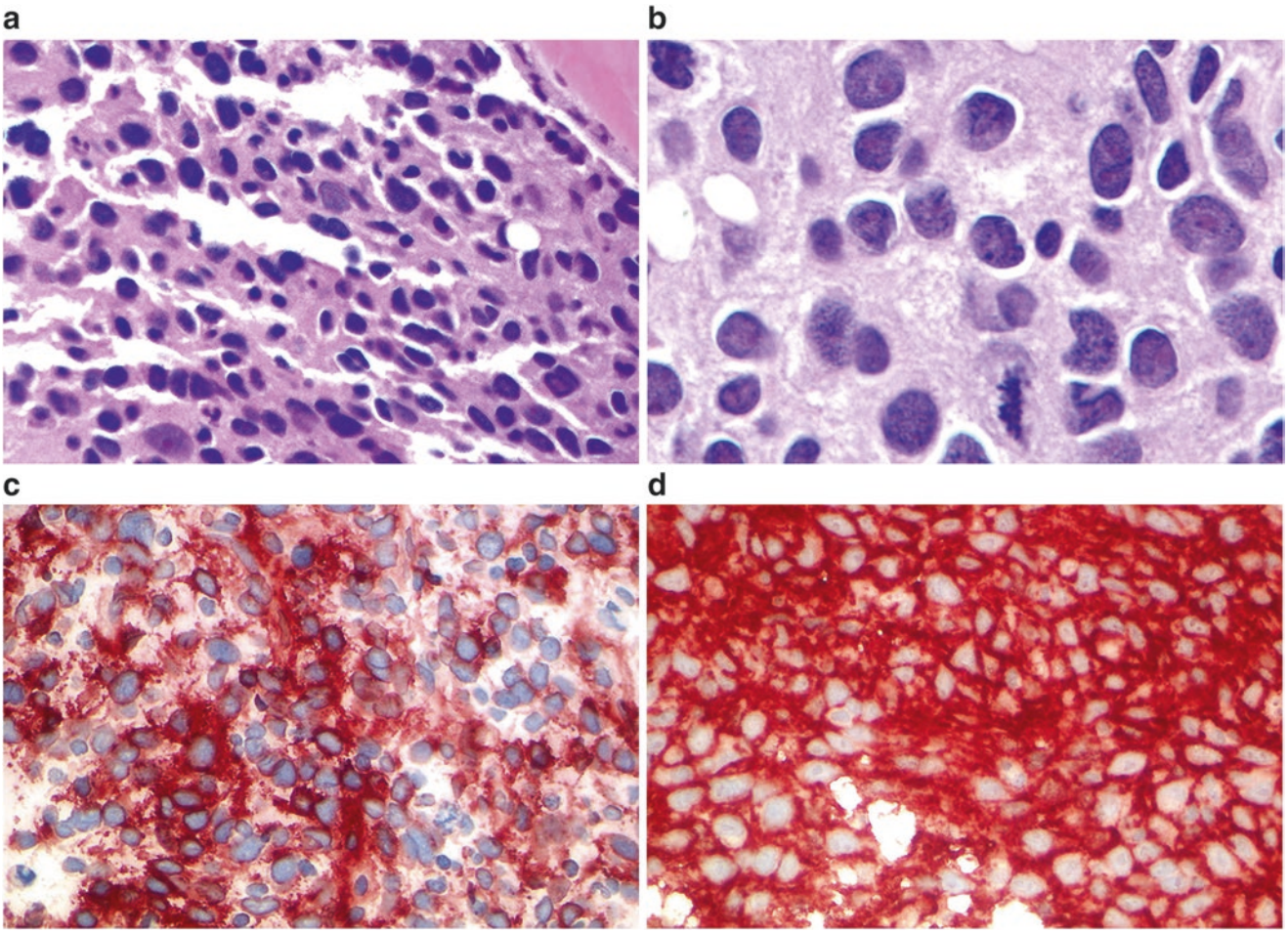

Fig. 14.12 Follicular dendritic cell sarcoma involving the bone marrow. (**a**) The H&E-stained bone marrow trephine section shows that the neoplastic cells extensively replace the normal bone marrow elements with ovoid tumor cells having indistinct cytoplasmic outlines. (**b**) Higher power shows large neoplastic cells with fine granular chromatin, distinct eosinophilic nucleoli, and a mitotic figure. (**c**) The neoplastic cells show membranous expression with an immunohistochemical stain for CD21, as well as strong and uniform membranous expression for CD23 (**d**) (*Courtesy of* Carlos Bueso-Ramos, MD)

Table 14.2 Comparison of histiocytic and dendritic neoplasms involving the bone marrow

	LCH	RDD	Histiocytic sarcoma	Reactive histiocytosis[a]
Hematologic findings	Leukocytosis	Leukocytosis	Cytopenias	May be abnormal depending on associated condition
	Elevated ESR	Elevated ESR		
		Polyclonal HG		
		Low albumin		
Distribution of histiocytes	Scattered and clusters	Sinusoidal	Clusters and sheets	Sinusoidal
Eosinophils	+	–	–	+/–
Emperipolesis	–	+	–	–
CD1a	+	–	–	–
S100	+	+	–	–
CD68	+	+	+	+
CD163	+/–	+	+/–	+
Langerin	+	–	–	–
BRAF V600E	+ (50%)	–	–	–

ESR erythrocyte sedimentation rate, *HG* hypergammaglobulinemia, *LCH* Langerhans cell histiocytosis, *RDD* Rosai-Dorfman disease
[a]Reactive histiocytosis includes hemophagocytic lymphohistiocytosis, sarcoidosis, and histiocytes associated with infection, inflammation, or accompanying malignancy

Table 14.3 Diagnostic criteria for hemophagocytic lymphohistiocytosis (HLH)[a]

Molecular diagnosis consistent with HLH[d]
Or any five of the following eight criteria
1. Fever
2. Splenomegaly
3. Cytopenia affecting at least two lineages
Hemoglobin[b] <9 g/dL
Platelet count <100 × 10^9/L
Absolute neutrophil count <1 × 10^9/L
4. Hypertriglyceridemia (>3 mmol/L) and/or hypofibrinogenemia (<1.5 g/L)
5. Hemophagocytosis (bone marrow, spleen, lymph node)
6. Low to absent NK-cell activity
7. Elevated ferritin[c] (≥500 ng/mL)
8. Elevated soluble CD25 (≥2400 U/mL)

[a]Diagnostic criteria for hemophagocytic lymphohistiocytosis used in the HLH-2004 trial [9]
[b]In infants <4 weeks old, hemoglobin <10 g/dL is used
[c]Though extremely high ferritin levels (≥10,000 μg/L) correlate with HLH, this is not specific; high ferritin levels are reported with malignancy and iron overload [13]
[d]Mutations in a number of different genes have been described with HLH. These include but are not limited to *AP3B1*, *BLOC1S6*, *CD27*, *ITK, LYST*, *MAGT1*, *PRF1*, *RAB27A*, *SH2D1A*, *SLC7A7*, *STX11*, *STXBP1*, *UNC13D(MUNC13-4*), and *XIAP(BIRC4)*

Table 14.4 Classification criteria for macrophage activation syndrome complicating systemic juvenile idiopathic arthritis[a]

Febrile patient with known/suspected systemic juvenile idiopathic arthritis and ferritin >684 ng/mL
And any two of the following
1. Platelet count ≤181 × 10^9/L
2. Aspartate aminotransferase >48 U/L
3. Triglycerides >156 mg/dL
4. Fibrinogen ≤360 mg/dL

Adapted from Ravelli et al. [11]
[a]Laboratory abnormalities should not be due to other comorbid conditions

References

1. Emile JF, Abla O, Fraitag S, Horne A, Haroche J, Donadieu J, et al. Histiocyte Society. Revised classification of histiocytoses and neoplasms of the macrophage-dendritic cell lineages. Blood. 2016;127:2672–81.
2. Haupt R, Minkov M, Astigarraga I, Schafer E, Nanduri V, Jubran R, et al. Langerhans cell histiocytosis: guidelines for diagnosis, clinical work-up, and treatment of patients till the age of 18 years. Pediatr Blood Cancer. 2013;60:175–84.
3. Badalian-Very G, Vergilio JA, Degar BA, MacConaill LE, Brandner B, Calicchio ML, et al. Recurrent *BRAF* mutations in Langerhans cell histiocytosis. Blood. 2010;116:1919–23.
4. Ihle MA, Fassunke J, Konig K, Grunewald I, Schlaak M, Kreuzberg N, et al. Comparison of high resolution melting analysis, pyrosequencing, next generation sequencing and immunohistochemistry to conventional Sanger sequencing for the detection of p.V600E and non-p.V600E *BRAF* mutations. BMC Cancer. 2014; 14:13.
5. Huang Q, Chang KL, Weiss LM. Extranodal Rosai-Dorfman disease involving the bone marrow: a case report. Am J Surg Pathol. 2006;30:1189–92.
6. Kim NR, Ko YH, Choe YH, Lee HG, Huh B, Ahn GH. Erdheim-Chester disease with extensive marrow necrosis: a case report and literature review. Int J Surg Pathol. 2001;9:73–9.
7. Jiang L, Admirand JH, Moran C, Ford RJ, Bueso-Ramos CE. Mediastinal follicular dendritic cell sarcoma involving bone marrow: a case report and review of the literature. Ann Diagn Pathol. 2006;10:357–62.
8. Grogg KL, Lae ME, Kurtin PJ, Macon WR. Clusterin expression distinguishes follicular dendritic cell tumors from other dendritic cell neoplasms: report of a novel follicular dendritic cell marker and clinicopathologic data on 12 additional follicular dendritic cell tumors and 6 additional interdigitating cell tumors. Am J Surg Pathol. 2004;28:988–98.
9. Henter JI, Horne A, Aricó M, Egeler RM, Filipovich AH, Imashuku S, et al. HLH-2004: diagnostic and therapeutic guidelines for hemophagocytic lymphohistiocytosis. Pediatr. Blood Cancer. 2007;48:124–31.
10. Campo M, Berliner N. Hemophagocytic lymphohistiocytosis in adults. Hematol Oncol N Am. 2015;19:915–25.
11. Ravelli A, Minoia F, Davì S, Horne A, Bovis F, Pistorio A, et al. Paediatric Rheumatology International Trials Organisation; Childhood Arthritis and Rheumatology Research Alliance; Pediatric Rheumatology Collaborative Study Group; Histiocyte Society. 2016 classification criteria for macrophage activation syndrome complicating systemic juvenile idiopathic arthritis: a European League Against Rheumatism/American College of Rheumatology/ Paediatric Rheumatology International Trials Organisation collaborative initiative. Ann Rheum Dis. 2016;75:481–9.
12. Yachoui R, Parkber BJ, Nguyen TT. Bone and bone marrow involvement in sarcoidosis. Rheumatol Int. 2015;35:1917–24.
13. Moore C, Ormseth M, Fuchs H. Causes and significance of markedly elevated serum ferritin levels in an academic medical center. J Clin Rheumatol. 2013;19:324–8.

Myeloproliferative Neoplasms and Mastocytosis

15

Luke R. Shier and Tracy I. George

This chapter covers the myeloproliferative neoplasms (MPNs) (Table 15.1) and mastocytosis (Table 15.2). Figures 15.1–15.38 illustrate the bone marrow pathology of the MPNs, including relevant clinical, laboratory, cytogenetic, and molecular genetic findings necessary for the classification of these neoplasms.

The MPNs are clonal neoplasms characterized by increased bone marrow cellularity, organomegaly, and increased effective cellular maturation resulting in elevated blood levels of one or more cell lines (erythrocytosis, leukocytosis, thrombocytosis). Though dysplasia is typically absent, the MPNs can evolve into acute leukemia or an end-stage myelofibrosis. The disease course is typically long, developing over many years. A common theme of tyrosine kinase activation unites the MPNs (Table 15.3). As can be seen in Table 15.3, there is considerable overlap of clinical, laboratory, and pathologic features of these neoplasms; over time, one type of MPN may develop features of another. The category of MPN, unclassifiable, represents those MPNs that are not classifiable using current criteria (Tables 15.4 – 15.12).

Table 15.1 Classification of myeloproliferative neoplasms

Chronic myeloid leukemia, *BCR-ABL1* positive
Polycythemia vera
Primary myelofibrosis
Essential thrombocythemia
Chronic neutrophilic leukemia
Chronic eosinophilic leukemia, not otherwise specified[a]
Myeloproliferative neoplasm, unclassifiable

[a]Chronic eosinophilic leukemia, not otherwise specified, remains in the classification of myeloproliferative neoplasms, but myeloid and lymphoid neoplasms associated with eosinophilia and specific genetic mutations including platelet-derived growth factor receptor alpha (*PDGFRA*), platelet-derived growth factor receptor beta (*PDGFRB*), fibroblast growth factor receptor 1 (*FGFR1*), and *PCM1-JAK2* are considered separate diseases and are covered in Chap. 16

L.R. Shier
Department of Pathology and Laboratory Medicine, University of Ottawa, Ottawa, ON, Canada

T.I. George (✉)
Department of Pathology, University of New Mexico School of Medicine, Albuquerque, NM, USA
e-mail: tracygeorge@salud.unm.edu

T.I. George, D.A. Arber (eds.), *Atlas of Bone Marrow Pathology*, Atlas of Anatomic Pathology,
https://doi.org/10.1007/978-1-4939-7469-6_15

Table 15.2 Classification of mastocytosis

Cutaneous mastocytosis
Systemic mastocytosis[a]
Indolent systemic mastocytosis[b]
Smoldering systemic mastocytosis[c]
Systemic mastocytosis with an associated hematological neoplasm[d]
Aggressive systemic mastocytosis[e]
Mast cell leukemia[f]
Mast cell sarcoma

Major criterion: Multifocal dense aggregates of mast cells in bone marrow and/or other extracutaneous organs
Minor criteria:
More than 25% of total mast cells are spindle shaped or have atypical morphology in either sections or smears
Activating point mutation at codon 816 in *KIT*
Expression of CD25 with or without CD2 in mast cells
Serum total tryptase >20 ng/mL, unless an associated clonal hematological non-mast cell lineage disease is present
B findings:
Serum tryptase level >200 ng/mL and bone marrow biopsy with >30% mast cells
Signs of dysplasia or myeloproliferation insufficient to diagnose a hematologic neoplasm, with normal or slightly abnormal blood cell counts
Hepatomegaly without liver function impairment, palpable splenomegaly without hypersplenism, and/or lymphadenopathy
C findings:
Cytopenias (absolute neutrophil count [ANC] <1.0 × 10^9/L; hemoglobin <10 g/dL; platelets <100 × 10^9/L)
Palpable hepatomegaly with impairment of liver function, ascites, and/or portal hypertension
Large osteolytic lesions and/or pathologic fractures
Palpable splenomegaly with hypersplenism (e.g. symptomatic splenomegaly)
Malabsorption with weight loss due to gastrointestinal involvement by mastocytosis
(*Adapted from* Arber et al. [1] and Horny et al. [2])
[a]Diagnosis of systemic mastocytosis is made when one major criterion and one minor criterion or three minor criteria are present
[b]Indolent systemic mastocytosis does not have B or C findings, as described below
[c]Smoldering systemic mastocytosis is defined as having at least two B findings, but no C findings
[d]Systemic mastocytosis with an associated hematological neoplasm has been previously described as systemic mastocytosis with an associated clonal hematological non-mast cell lineage disease. The associated hematological neoplasm should meet WHO criteria for that particular neoplasm, and criteria for systemic mastocytosis should be met, as defined above
[e]Aggressive systemic mastocytosis meets above criteria for systemic mastocytosis with one or more "C" findings, but no evidence of mast cell leukemia
[f]Mast cell leukemia is diagnosed when 20% or more mast cells are present on bone marrow aspirate smears

Table 15.3 Myeloproliferative neoplasms: clinical, morphologic, and genetic findings

MPN	Genetics[a]	Blood smear	Bone marrow	Fibrosis	Splenomegaly
Chronic myeloid leukemia	*BCR-ABL1*	Leukocytosis with immature granulocytes, basophilia	Hypercellular, marked myeloid hyperplasia, small megs	Variable	++
Polycythemia vera	*JAK2*	Polycythemia may be evident or masked by iron deficiency with a microcytic hypochromic anemia, +/− mild neutrophilia, mild basophilia, or thrombocytosis	Hypercellular, panmyelosis +/− erythroid hyperplasia, atypical meg hyperplasia	Increased in fibrotic phase	++
Primary myelofibrosis	*JAK2, MPL, CALR*	Leukoerythroblastic smear with dacrocytes, giant and bizarre platelets	Hypercellular, myeloid hyperplasia, atypical meg hyperplasia, bizarre/pleomorphic megs	Increased in fibrotic phase	+++
Essential thrombocythemia	*JAK2, MPL, CALR*	Thrombocytosis, can have meg nuclei	Normocellular, normal myeloid/erythroid (M/E) ratio, atypical meg hyperplasia with mature large forms	Minimal	−/+
Chronic neutrophilic leukemia	*CSF3R*	Leukocytosis, toxic neutrophilia, minimal left shift	Hypercellular, myeloid hyperplasia	Variable	++
Chronic eosinophilic leukemia, not otherwise specified	None described[b]	Persistent eosinophilia >1.5 × 10^9/L	Abnormal bone marrow morphology resembling MDS, MPN, or MDS/MPN	Variable	+/−

CEL, NOS, chronic eosinophilic leukemia, not otherwise specified; MDS, myelodysplastic syndromes; meg, megakaryocyte; MPNs, myeloproliferative neoplasms
[a]Dysregulated protein tyrosine kinases underlie the genetic basis of the myeloproliferative neoplasms, with specific genes involved as indicated
[b]With the separate classification of myeloid and lymphoid neoplasms with eosinophilia and mutations in *PDGFRA*, *PDGFRB*, *FGFR1,* and *PCM1-JAK2*, the category of CEL, NOS is exceedingly narrow and is defined by an increase in myeloblasts in the blood or bone marrow and/or the presence of nonspecific cytogenetic abnormalities

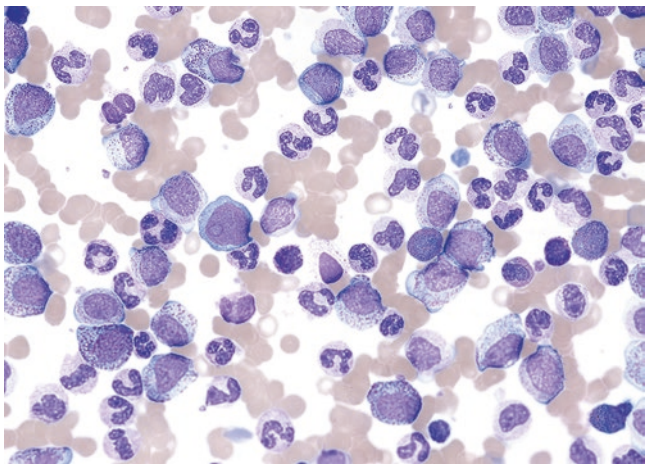

Fig. 15.1 Chronic myeloid leukemia, chronic phase. The Wright-Giemsa-stained peripheral blood smear shows a striking leukocytosis with a prominence of segmented neutrophils and immature granulocytes. The majority of immature granulocytes are myelocytes, with smaller numbers of metamyelocytes, promyelocytes, and rare blasts

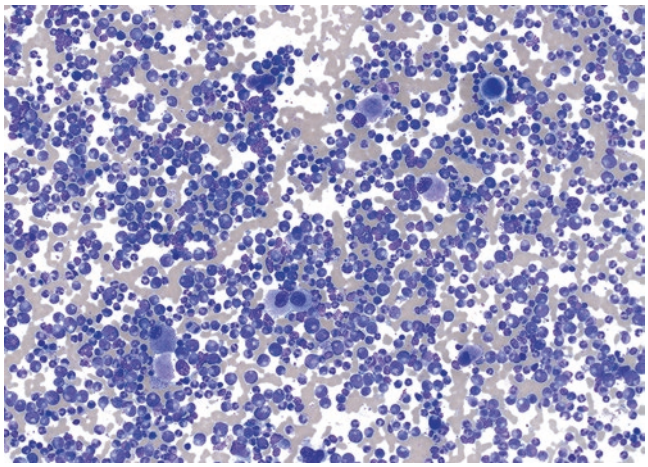

Fig. 15.2 Chronic myeloid leukemia, chronic phase. A low power of this Wright-Giemsa-stained bone marrow aspirate smear is remarkable for the striking hypercellularity due to a granulocytic hyperplasia. Increased numbers of small, hypolobated megakaryocytes (dwarf megakaryocytes) and micromegakaryocytes can also be seen

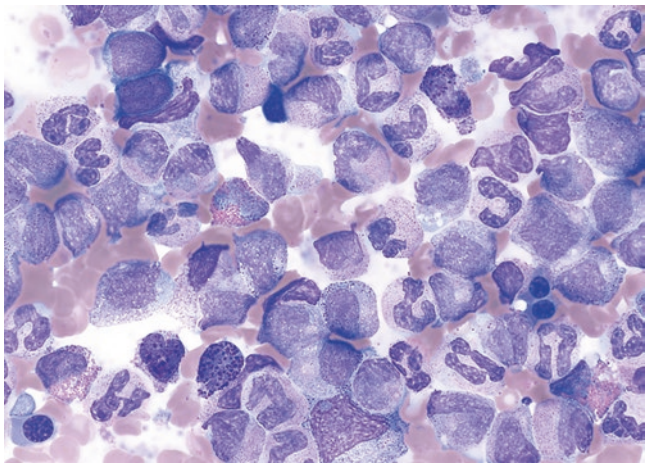

Fig. 15.3 Chronic myeloid leukemia, chronic phase. The Wright-Giemsa-stained bone marrow aspirate smear confirms the granulocytic hyperplasia with intact maturation to segmented neutrophils. A prominence of myelocytes and segmented neutrophils is shown, with increased eosinophils and basophils. Erythropoiesis is minimal, and myeloblasts are not increased in number

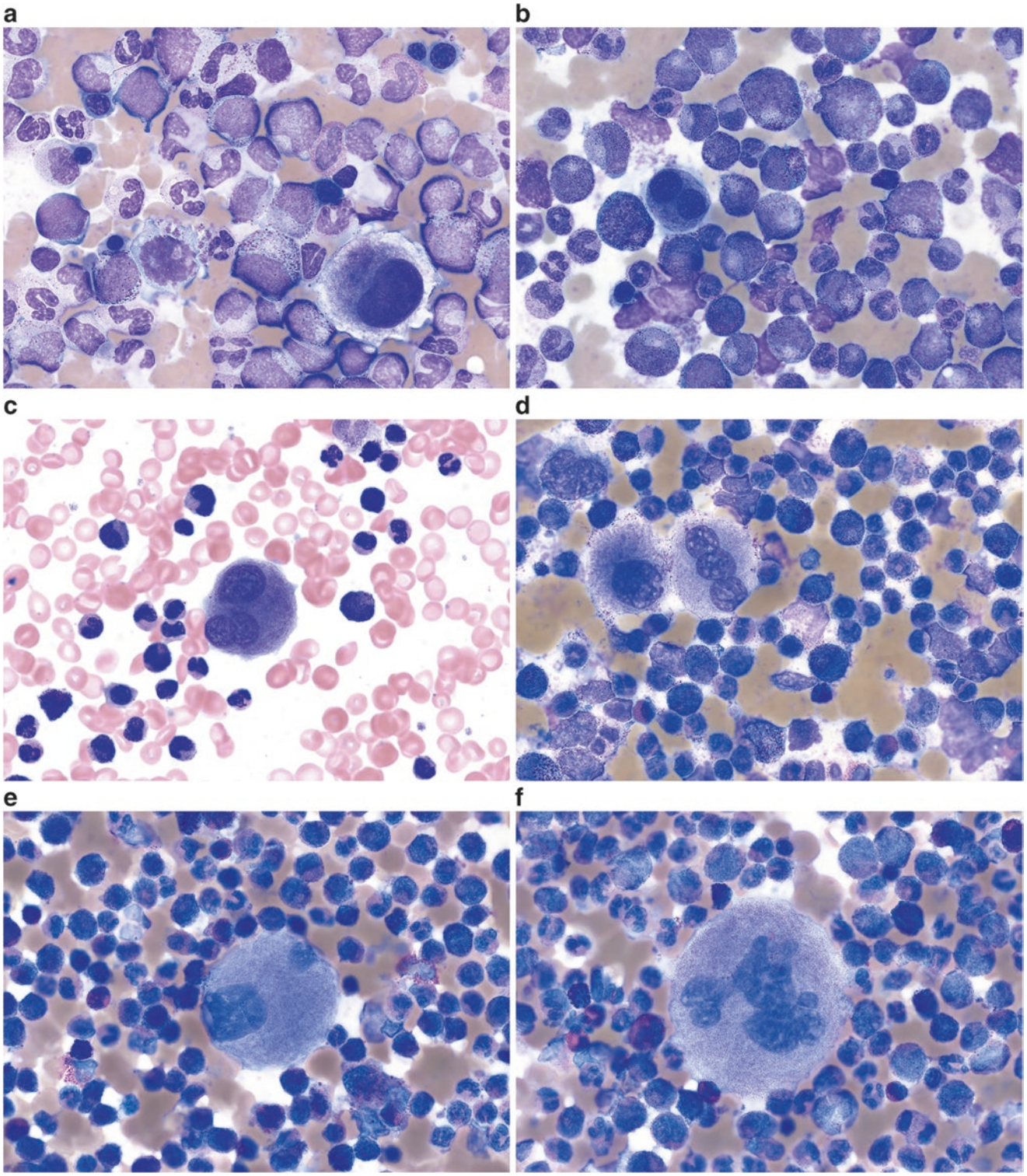

Fig. 15.4 Chronic myeloid leukemia, chronic phase. A variety of megakaryocytes is shown within Wright-Giemsa-stained aspirate smears. (**a**) A small, hypolobated megakaryocyte or "dwarf megakaryocyte" is shown on the aspirate smear in a granulocytic-rich background. Only rare erythroid precursors are present. (**b**) A binucleate micromegakaryocyte can be seen in the center left of the image. The background shows a proliferation of immature granulocytes, including many myelocytes, metamyelocytes, and promyelocytes, without an increase in blasts. (**c**) An atypical megakaryocyte is shown with separated nuclear lobes. (**d**) Additional atypical megakaryocytes are shown in a background rich in neutrophils and precursors. (**e**) A large megakaryocyte with widely separated nuclear lobes is shown in a background rich in neutrophils and basophils. (**f**) An enlarged, mature megakaryocyte with lobulated nuclei is present in a background rich in neutrophils, eosinophils, and basophils

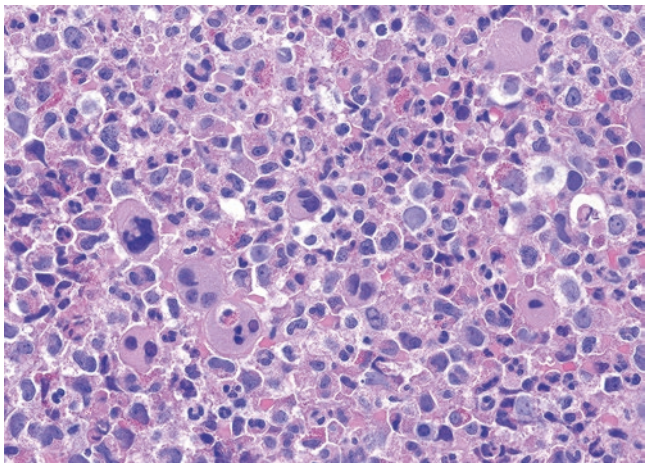

Fig. 15.5 Chronic myeloid leukemia, chronic phase. On this H&E-stained trephine biopsy specimen, a proliferation of small, atypical megakaryocytes can be seen amidst numerous segmented neutrophils and eosinophils in this hypercellular marrow

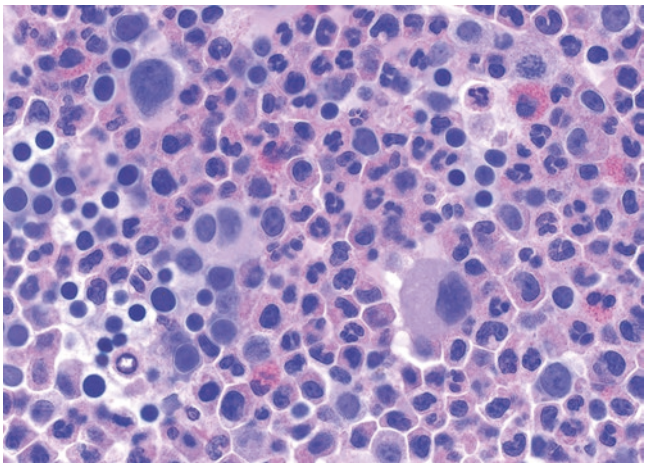

Fig. 15.6 Chronic myeloid leukemia, chronic phase. This H&E-stained trephine biopsy highlights a few scattered atypical, small megakaryocytes and many segmented neutrophils and eosinophils

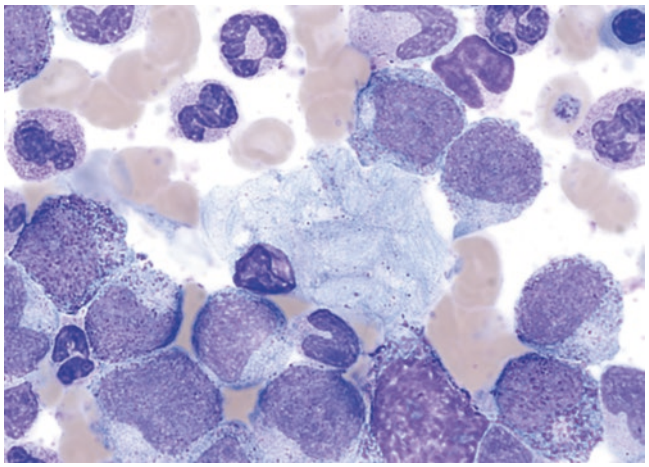

Fig. 15.7 Chronic myeloid leukemia (CML), chronic phase. On this Wright-Giemsa-stained aspirate smear, a macrophage or pseudo-Gaucher cell can be seen in the center. Increased numbers of macrophages are typically seen in CML, reflecting increased turnover

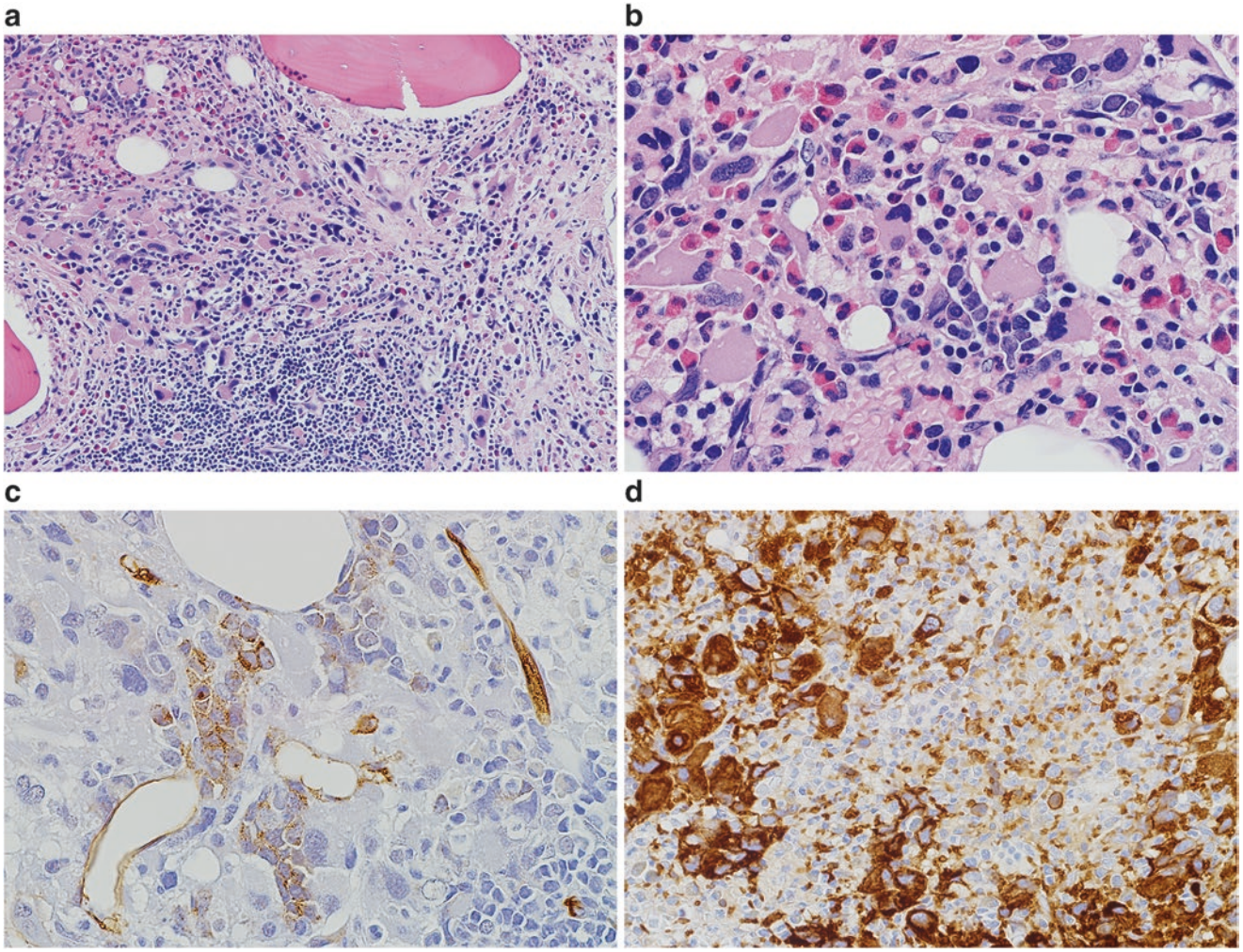

Fig. 15.8 Chronic myeloid leukemia, accelerated phase. This 55-year-old woman presented with a persistent microcytic anemia. A peripheral blood smear showed a leukoerythroblastic smear with 26% basophils, and bone marrow aspirate enumerated 13% myeloblasts (*not shown*). (**a**) The corresponding H&E-stained bone marrow biopsy specimen is hypercellular, with extensive fibrosis and scattered reactive lymphoid aggregates; the edge of a lymphoid aggregate is noted at the bottom of the image. There is a significant proliferation of clustered, small, hypolobated megakaryocytes. Large clusters of small, abnormal megakaryocytes associated with marked reticulin or collagen fibrosis is one criterion for accelerated disease in CML; this is typically associated with at least one additional criterion for accelerated disease described in Table 15.4. (**b**) A higher-power image from the bone marrow biopsy highlights increased immature mononuclear cells consistent with blasts distributed interstitially, as well as within bone marrow sinuses. A prominent eosinophilia is present, as well as small, hypolobated megakaryocytes. Granulocytic maturation is intact, and erythropoiesis also appears intact. (**c**) Immunohistochemical stain directed at CD34 performed on the bone marrow biopsy highlights focal aggregates of CD34-positive blasts, estimated at approximately 15% of total nucleated cells. (**d**) Immunohistochemical stain directed against CD42b performed on the bone marrow biopsy highlights the large numbers of micromegakaryocytes and dwarf megakaryocytes, as well as a population of more immature cells, which are favored to be megakaryoblasts

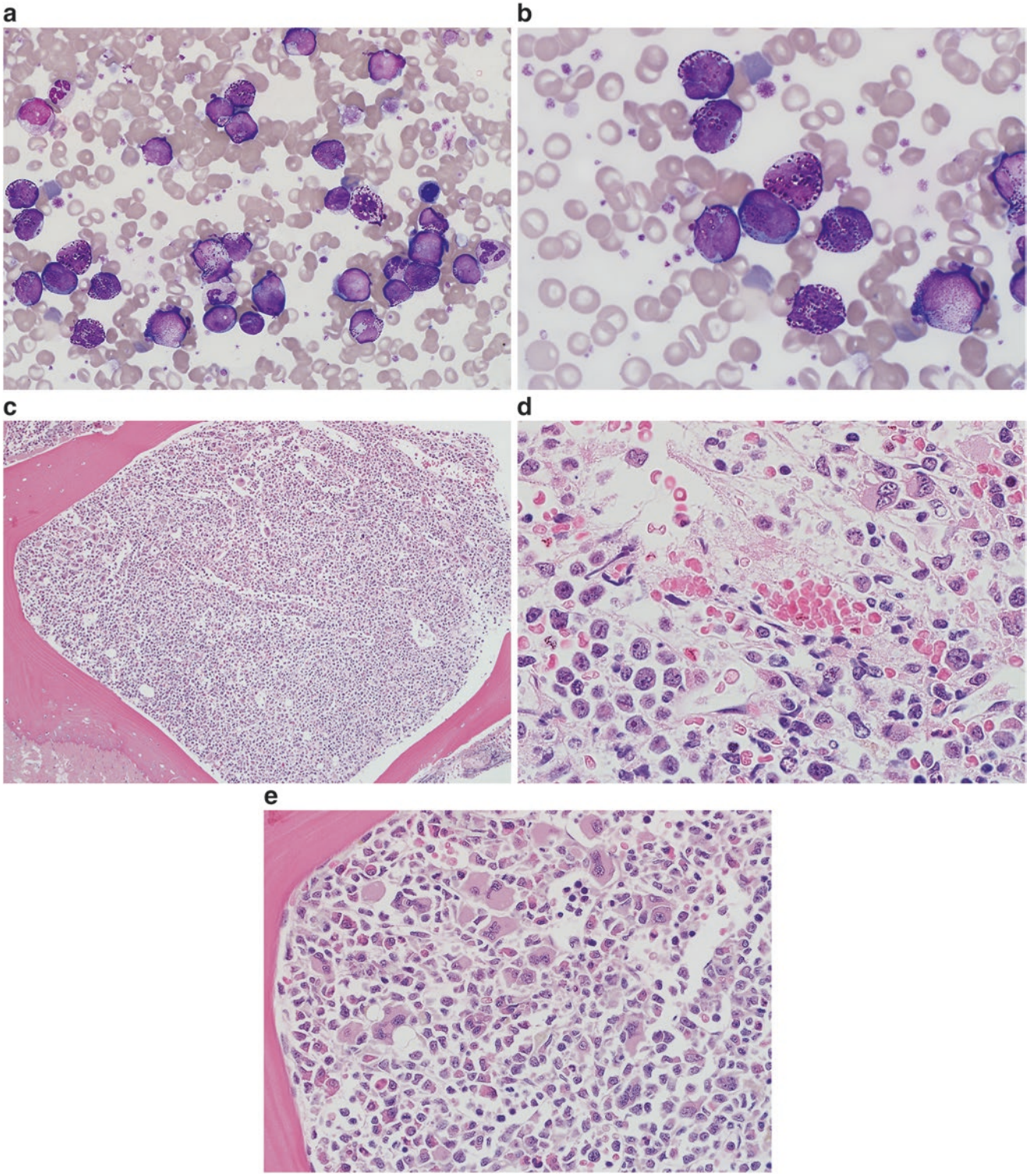

Fig. 15.9 Chronic myeloid leukemia, blast phase. This 62-year-old woman presented with a leukocytosis of 39×10^9/L, splenomegaly, and breast masses. A peripheral blood smear showed a striking basophilia of 60%, with many basophils showing immature features, and 5% myeloblasts (*not shown*). (**a**) The Wright-Giemsa-stained bone marrow aspirate smear shown here highlights numerous blasts, many of which show prominent basophilic differentiation, as well as mature basophils. (**b**) A higher-power image of the blasts with basophilic features (*top of image*) is shown, with mature basophils toward the bottom of the field. (**c**) The corresponding trephine biopsy is 100% cellular. At this low power, dilated bone marrow sinuses are prominent. (**d**) At high power, numerous blasts are present, running through the bone marrow sinuses. The basophilic granulation is difficult to appreciate in the biopsy sections because basophilic granules are water-soluble. In the upper right, a few atypical megakaryocytes are also present. (**e**) Another area of the biopsy shows the typical proliferation of small, hypolobated megakaryocytes in a background enriched in blasts. By flow cytometry, a prominent population of CD117-positive blasts was identified, with only a minor subset expressing CD34 and CD33. Cytogenetic karyotyping revealed the t(9;22)(q34.q;q11.2). Breast biopsy revealed a well-differentiated, infiltrating ductal carcinoma

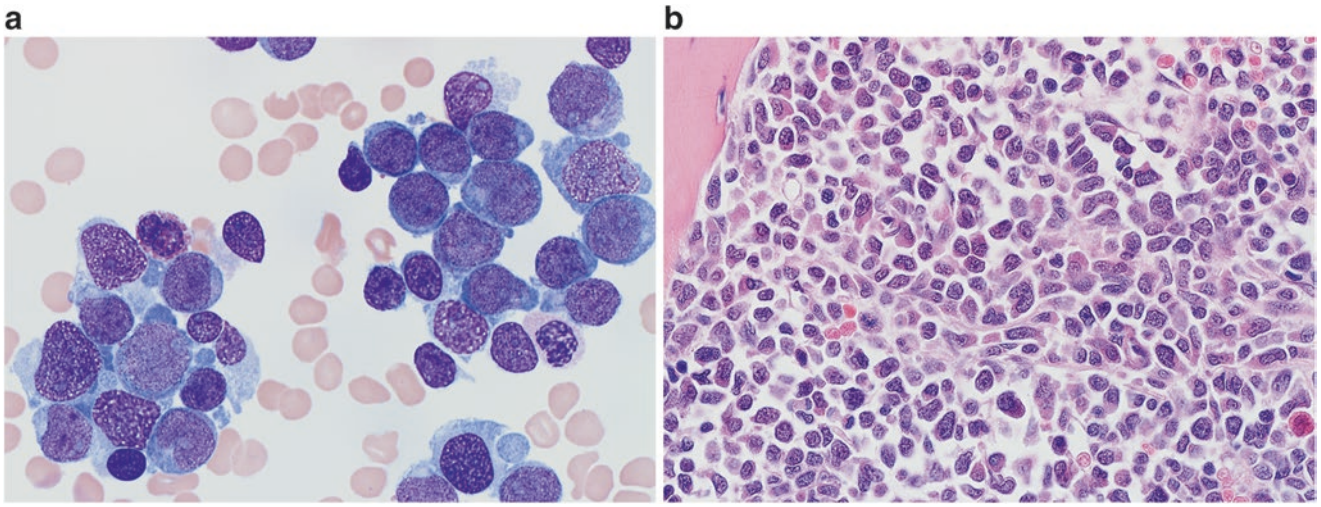

Fig. 15.10 Chronic myeloid leukemia, blast phase (mixed phenotype, B/myeloid). This 53-year-old man presented with a white blood cell count of 255×10^9/L, hemoglobin 8 g/dL, platelet count 30×10^9/L, and 36% circulating blasts. (**a**) The bone marrow aspirate smear reveals two populations of blasts: a larger population of myeloblasts with larger size, abundant lightly basophilic cytoplasm, smooth chromatin, and prominent nucleoli and a smaller population of B lymphoblasts characterized by smaller size, scant basophilic cytoplasm, round nuclear contours, and partially-condensed chromatin. (**b**) The corresponding bone marrow biopsy is hypercellular and replaced by myeloblasts and B lymphoblasts. Quantitative polymerase chain reaction (PCR) was positive for *BCR-ABL1* transcripts, with a *BCR-ABL1/ABL1* ratio of 1.2. The translocation (9;22) was present in all 20 metaphases by cytogenetic analysis. In the blast phase of CML, blasts are typically myeloid, but they may be lymphoid in up to one third of cases. Rarely, as in this case, a mixed phenotype of blasts may be seen

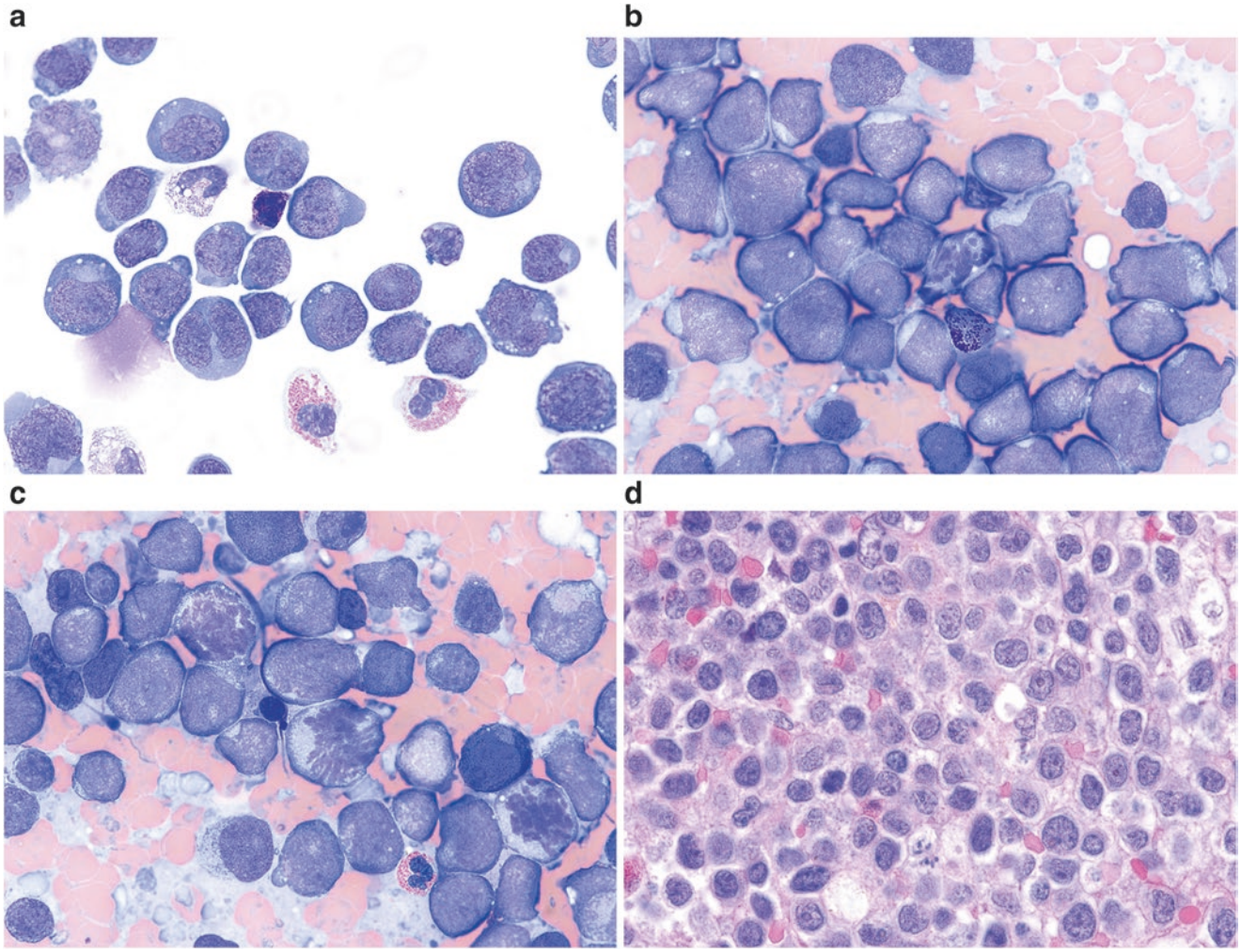

Fig. 15.11 Chronic myeloid leukemia, blast phase. (**a**) The Wright-Giemsa-stained aspirate smear contains numerous large blasts, with abundant darkly basophilic cytoplasm, round to indented nuclei, smooth chromatin, and prominent nucleoli in a background containing eosinophils, basophils, and neutrophils. (**b**) Another view of the aspirate shows numerous myeloblasts with moderate, lightly basophilic cytoplasm and smooth chromatin, with a basophil near the center of the image. (**c**) Numerous mitotic figures are present amidst the myeloblasts in this image, with an occasional eosinophil. (**d**) The corresponding H&E-stained trephine biopsy shows sheets of immature mononuclear cells consistent with blasts

Table 15.4 Natural history of chronic myeloid leukemia[a]

Chronic phase: <10% blasts
Accelerated phase (10–19% blasts), also defined by:
Increasing or persistent white blood cell count (>10 x 10^9/L), despite therapy
Increasing or persistent splenomegaly, despite therapy
Persistent thrombocytopenia (PLT <100 × 10^9/L), unrelated to therapy
Persistent thrombocytosis (PLT >1000 × 10^9/L), despite therapy
Peripheral blood basophilia ≥20%
Additional clonal chromosomal abnormalities at diagnosis (including a second Ph+, +8, isochromosome 17q, +19, a complex karyotype, or abnormalities of 3q26.2)
Clonal evolution during therapy
Large clusters of small, abnormal megakaryocytes associated with marked reticulin or collagen fibrosis, typically associated with one or more of the above criteria
"Provisional" criteria regarding resistance to tyrosine kinase inhibitor (TKI) therapy:
Hematologic resistance to the first TKI or failure to achieve a complete hematologic response to first TKI
Any hematologic, cytogenetic, or molecular indications of resistance to two sequential TKIs
Occurrence of two or more mutations in *BCR-ABL1* during TKI therapy
Blast phase (≥20% blasts)[b]
Also defined by extramedullary proliferation of blasts

(*Criteria for accelerated phase adapted from* Arber et al. [1])

[a]The blast percentage in the blood and bone marrow defines which phase of CML a patient may have, but additional clinical and laboratory findings are also important

[b]The presence of lymphoblasts in blood or marrow should prompt evaluation for lymphoblastic transformation of CML

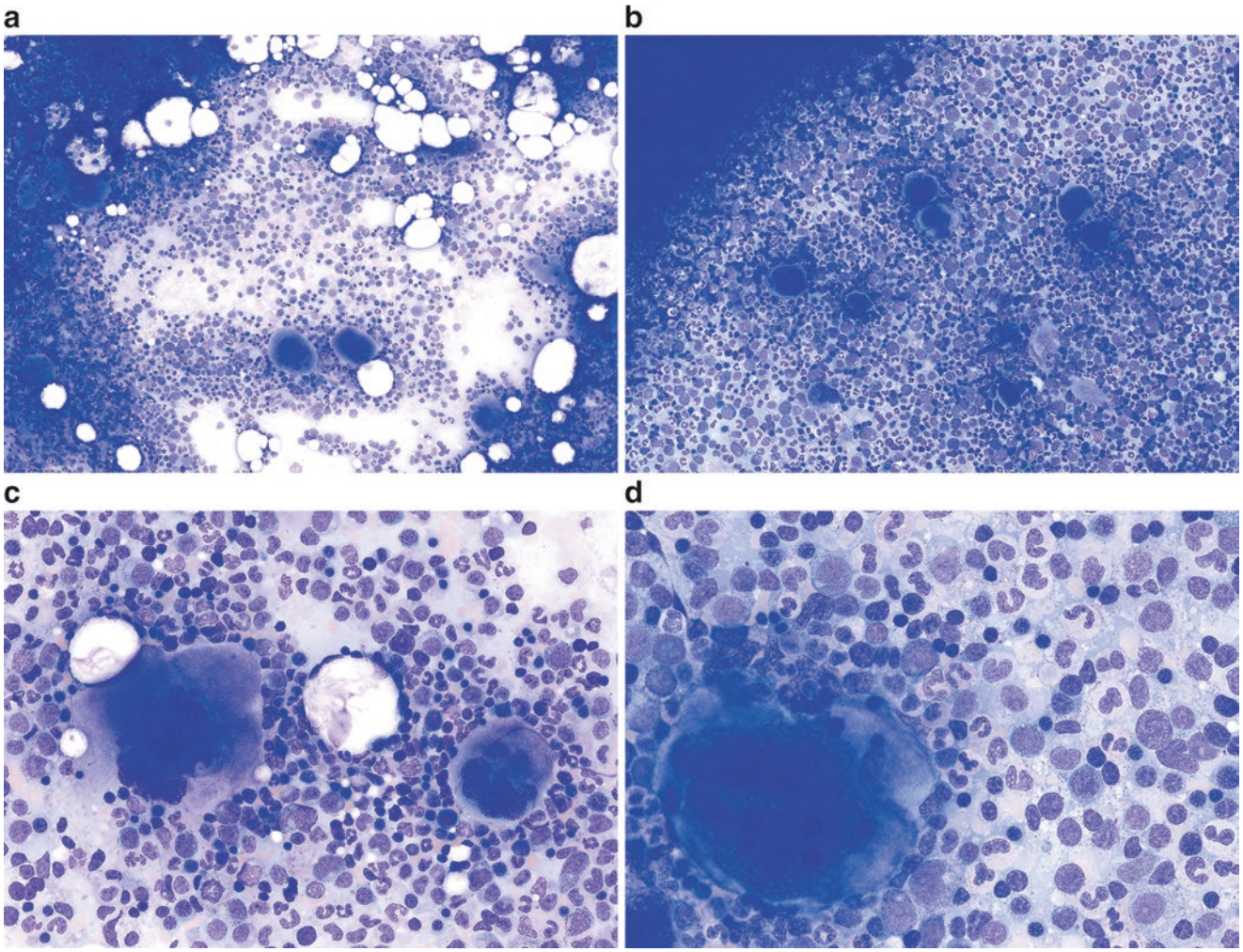

Fig. 15.12 Polycythemia vera (PV). (**a** and **b**) On these Wright-Giemsa-stained aspirate smears, an increased number of pleomorphic megakaryocytes can be seen, with abundant granulopoiesis and erythropoiesis present in the background. (**c**) Two mature megakaryocytes are present. The megakaryocyte at left is enlarged in size and hyperlobulated; the megakaryocyte at right is of normal size but is atypically lobulated. (**d**) A markedly enlarged and atypical megakaryocyte is present amidst granulopoiesis and erythropoiesis. PV is a clonal proliferation resulting in increased erythrocytes and an expansion of red cell mass independent of erythropoietin regulation. Almost all patients carry a mutation in *the Janus 2 kinase* (*JAK2*) gene. Criteria for the diagnosis are presented in Table 15.5

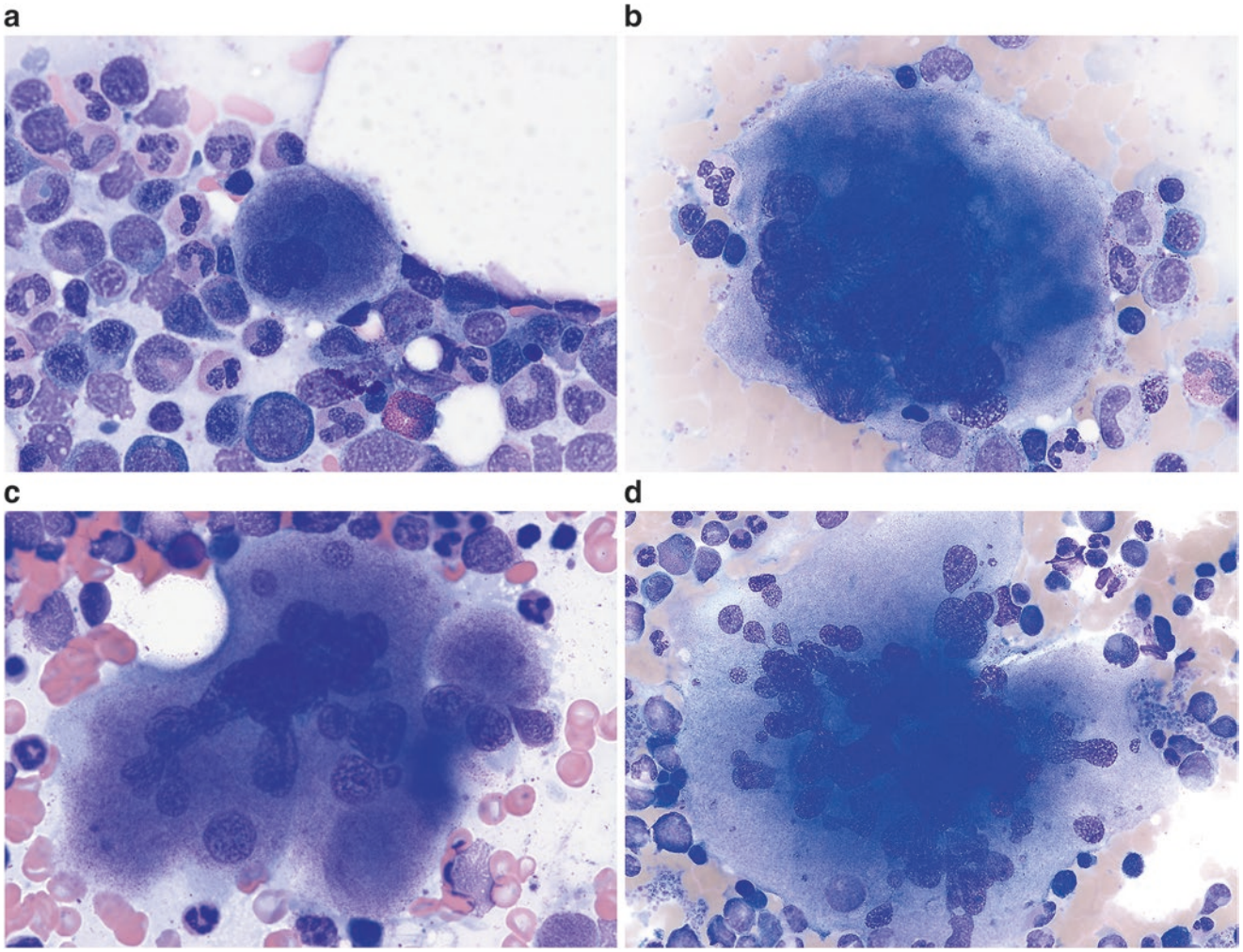

Fig. 15.13 Polycythemia vera. A series of megakaryocytes are shown from Wright-Giemsa-stained aspirate smears, ranging from normal size (**a**) to markedly enlarged and hyperlobulated (**b**) to enlarged megakaryocyte with separated nuclear lobes and hyperlobulation (**c** and **d**). The pleomorphism of megakaryocyte morphology is typical of PV and primary myelofibrosis

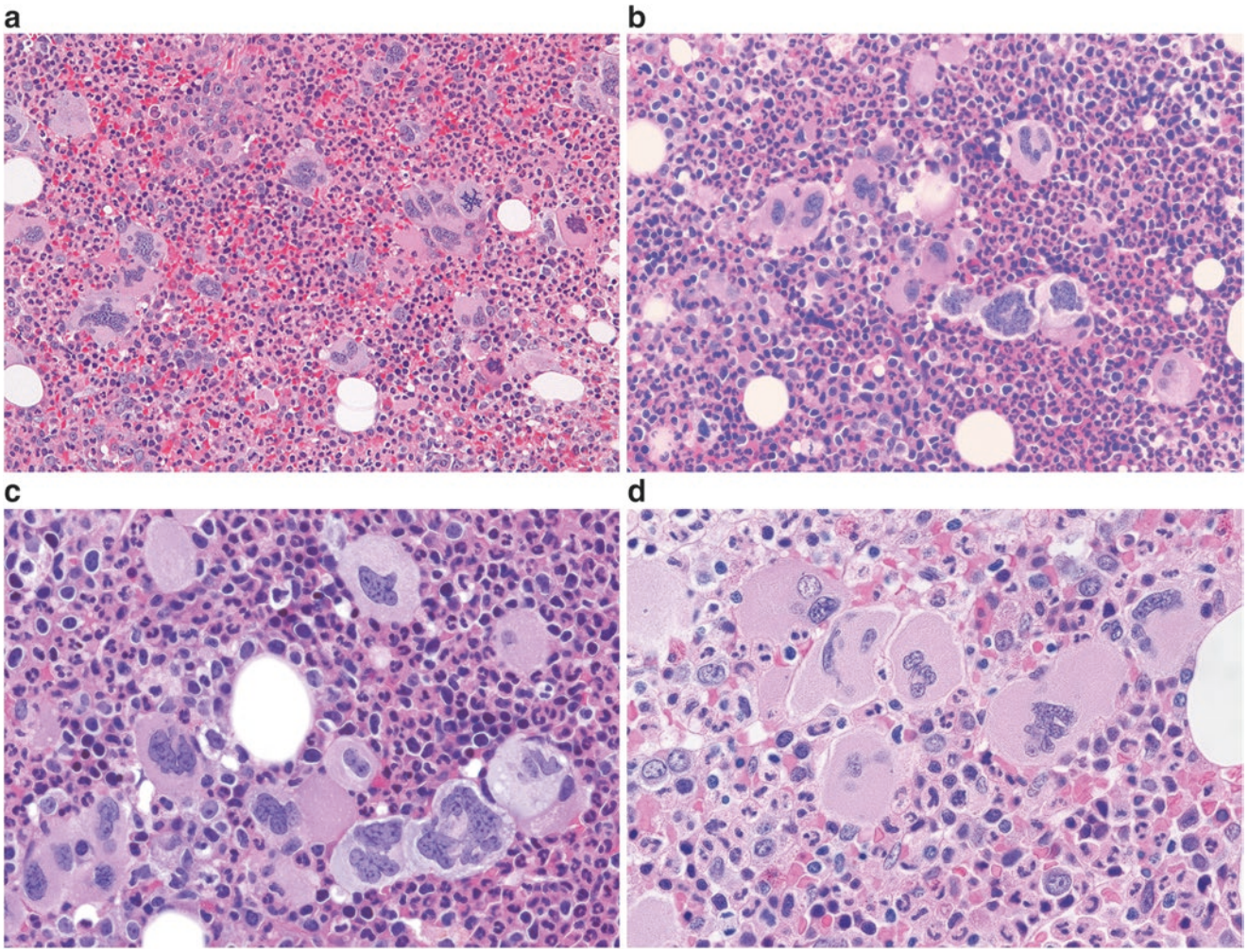

Fig. 15.14 Polycythemia vera. The trephine biopsy is hypercellular for the patient's age, with panmyelosis. (**a**) The atypical megakaryocytes are prominent, with pleomorphic forms shown, including occasional tight clusters. (**b**) At higher power, a cluster of megakaryocytes is shown ranging in size from small to large, with a background showing increased granulopoiesis. (**c**) Additional clusters of megakaryocytes show atypical, pleomorphic megakaryocytes with bulbous nuclei. (**d**) This cluster of large, pleomorphic megakaryocytes shows atypical nuclear features

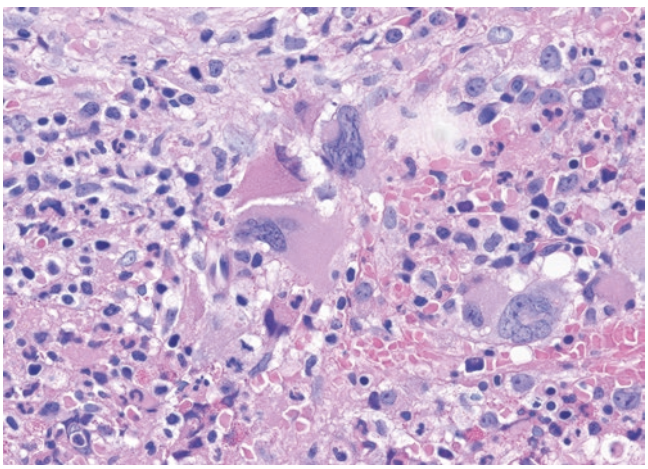

Fig. 15.15 Post-polycythemic myelofibrosis. This trephine biopsy shows a cluster of highly atypical and pleomorphic megakaryocytes at center, amidst a background rich in fibrosis, with granulopoiesis and erythropoiesis visible in the background. The megakaryocytes are hyperchromatic, with cloudlike nuclei. In the "spent" phase of the disease, the bone marrow is involved by marked fibrosis with morphologic changes in blood and bone marrow that are similar to those seen in primary myelofibrosis, including leukoerythroblastosis with teardrops, marrow fibrosis, and atypical megakaryocytic hyperplasia

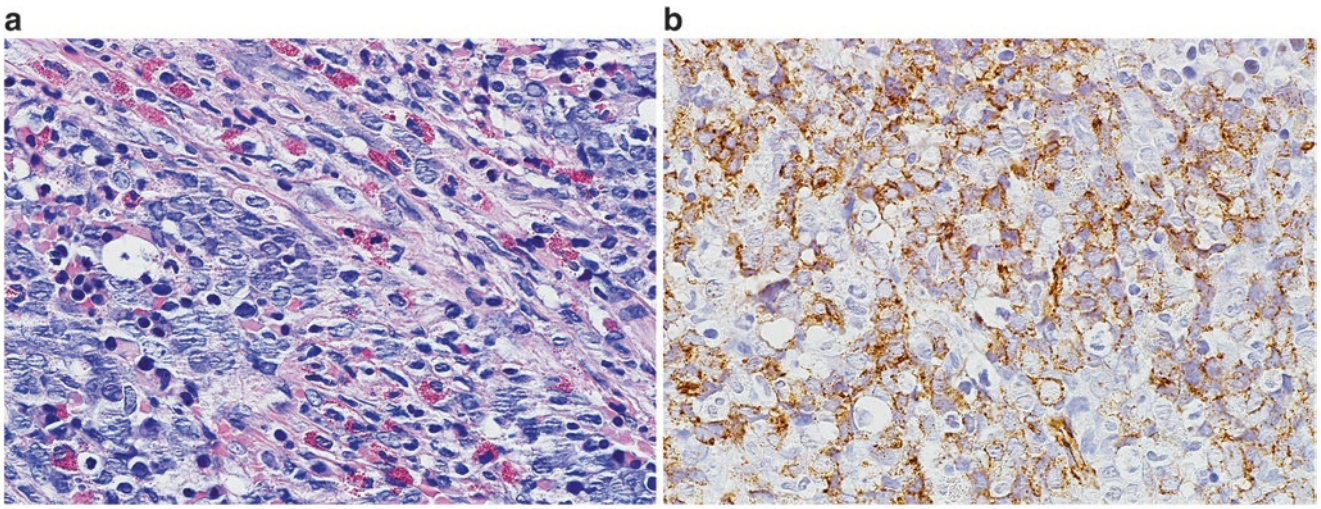

Fig. 15.16 Acute myeloid leukemia arising from polycythemia vera. This 44-year-old man had a history of PV and was found to have a microcytosis and thrombocytopenia on complete blood count, with 22% circulating blasts. (**a**) The trephine biopsy highlights sheets of immature cells consistent with blasts, along with a prominent eosinophilia and intact erythropoiesis. Cellular streaming is also present, indicative of fibrosis. (**b**) Immunohistochemical stain directed against CD34 was performed on the biopsy and highlights sheets of CD34-positive blasts, comprising approximately 25% of total nucleated cells. It is estimated that over 20 years, up to one half of patients will develop acute leukemia

Table 15.5 WHO criteria for the diagnosis of polycythemia vera[a]

Major criteria
Hemoglobin >16.5 g/dL in men, >16.0 g/dL in women; hematocrit >49% in men, >48% in women; or increased red blood cell (RBC) mass (>25% above mean normal predicted value)
Hypercellular bone marrow biopsy with panmyelosis (increase in the erythroid, granulocytic, and megakaryocytic lineages; in polycythemia vera, the megakaryocytes are mature and pleomorphic)
JAK2 V617F or exon 12 mutation
Minor criterion
Low serum erythropoietin level

Adapted from Arber et al. [1]

[a]Diagnosis requires all major criteria or the first two major criteria and the minor criterion. The bone marrow biopsy criterion may not be required in patients with a sustained erythrocytosis, with hemoglobin >18.5 g/dL in men (hematocrit, 55.5%) or >16.5 g/dL in women (hematocrit, 49.5%) and a *JAK2* mutation, and a subnormal erythropoietin level

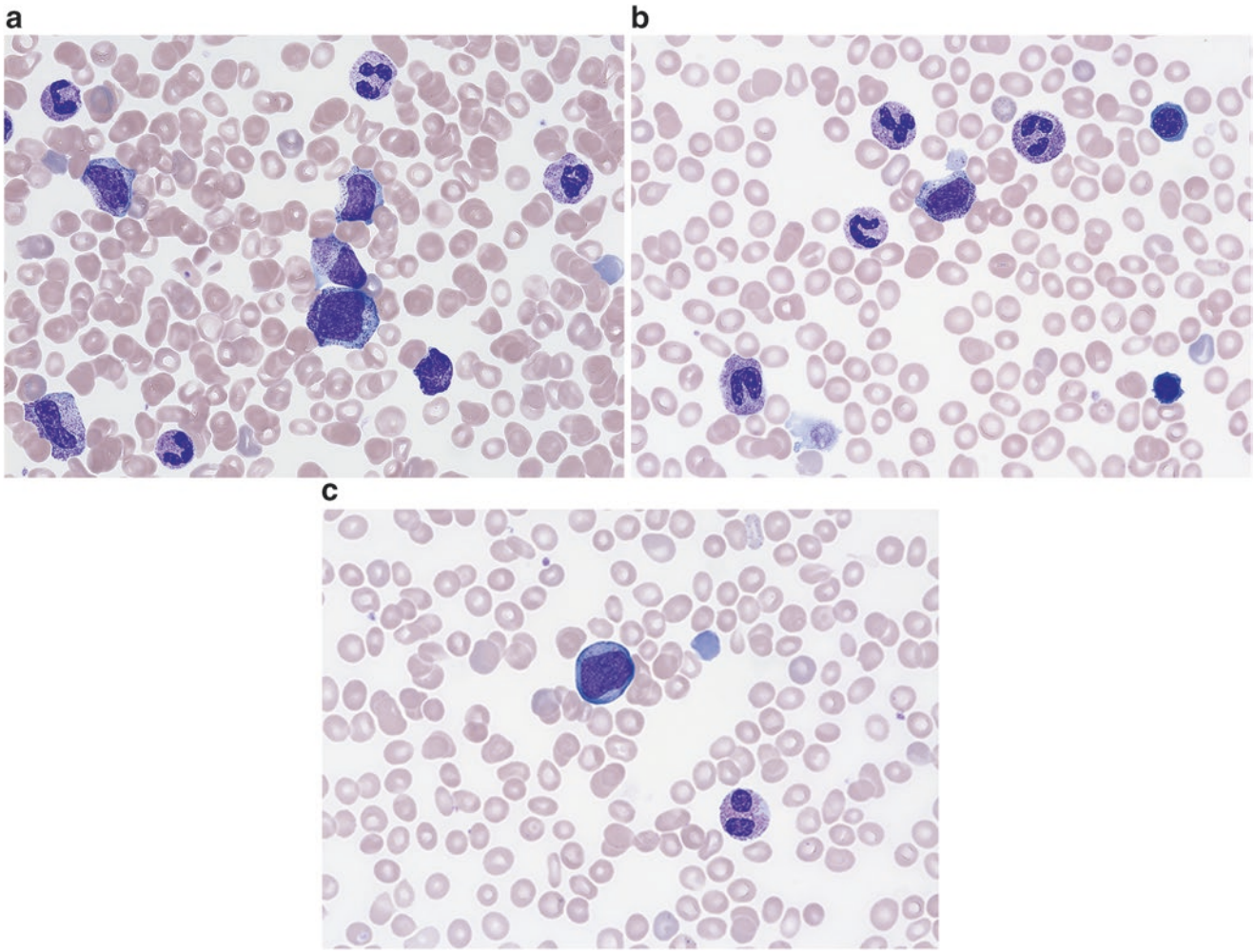

Fig. 15.17 Primary myelofibrosis, prefibrotic phase. The peripheral blood smear shows leukocytosis with neutrophilia and immature granulocytes (**a**); nucleated red cells, rare dacrocytes, and a giant and bizarre hypogranular platelet (**b**); and rare circulating blasts (**c**)

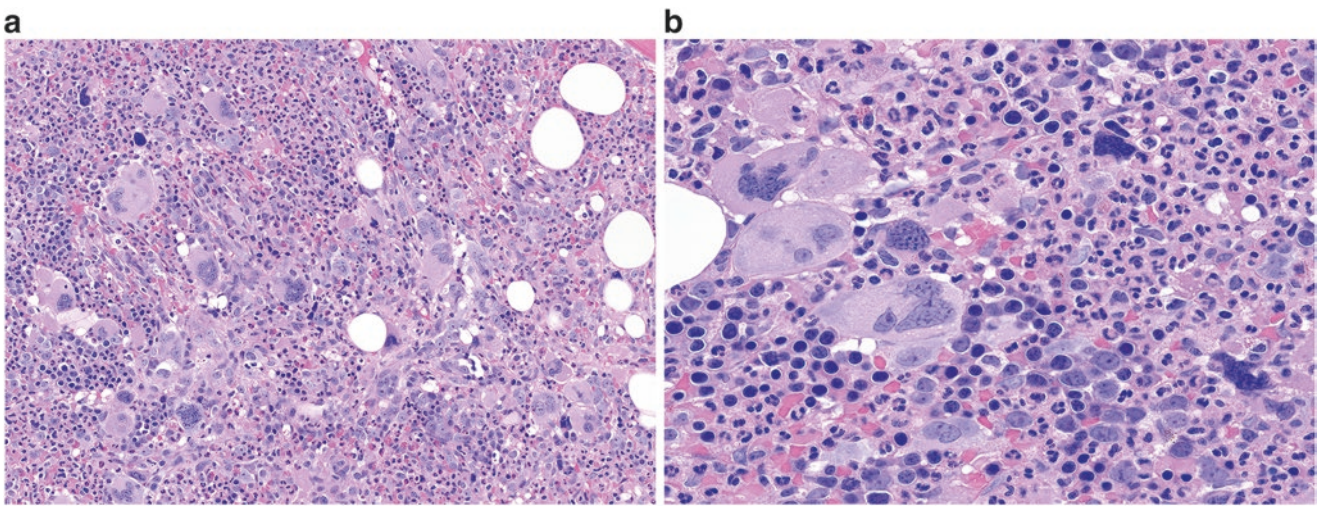

Fig. 15.18 Primary myelofibrosis, prefibrotic phase. (**a**) The trephine biopsy shows a hypercellular marrow with a striking, atypical megakaryocytic hyperplasia. Megakaryocytes are pleomorphic and include hyperchromatic forms and those with bulbous and cloudlike nuclei. The background is notable for a granulocytic hyperplasia. (**b**) On higher power, a panmyelosis appears present, with erythropoiesis and granulopoiesis seen in the background. A cluster of enlarged and pleomorphic megakaryocytes is shown, with irregular nuclear lobation and hyperchromatic nuclei

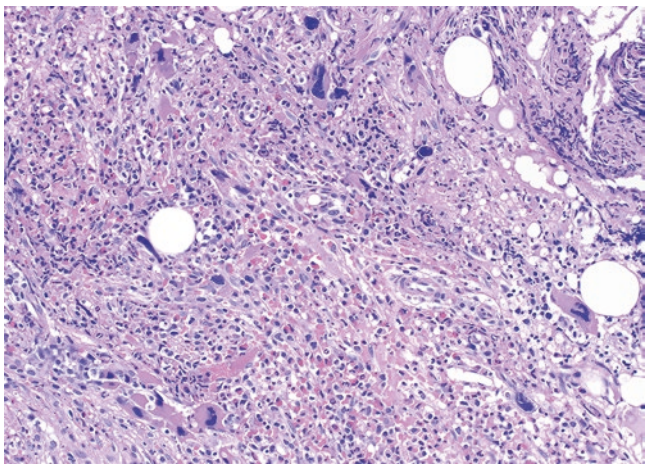

Fig. 15.19 Primary myelofibrosis. A transition from the prefibrotic phase to an overt fibrotic phase can be seen in this bone marrow biopsy, in which the presence of cellular streaming indicates fibrosis. Primary myelofibrosis is a clonal disorder characterized by a proliferation of megakaryocytes and granulocytic precursors accompanied by reactive marrow fibrosis. The replacement of the bone marrow by fibrosis leads to extramedullary hematopoiesis, with subsequent hepatosplenomegaly and compression of adjacent normal structures. Up to 40% of patients are asymptomatic at diagnosis, with physical examination and abnormal blood tests suggesting the diagnosis

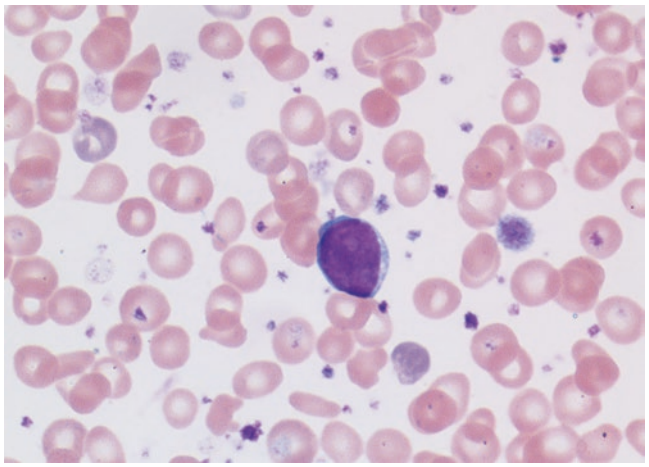

Fig. 15.20 Primary myelofibrosis, leukoerythroblastosis. This peripheral blood smear from a patient with the overt fibrotic phase of primary myelofibrosis shows a blast in the center of the smear, with frequent dacrocytes (teardrop-shaped red blood cells) in the background and many platelets, including large, hypogranular forms. The typical nucleated red blood cell is not shown

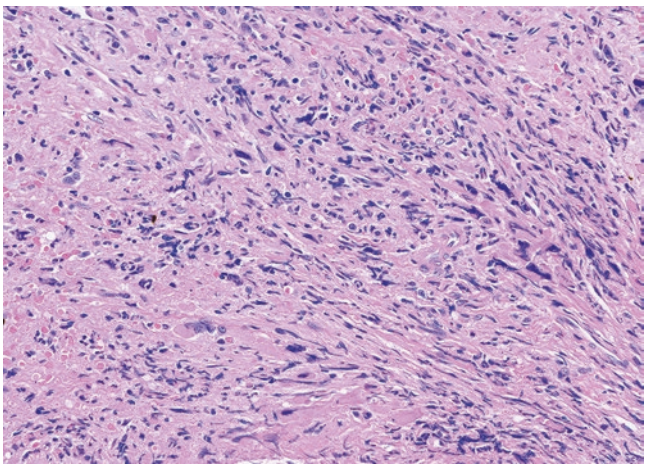

Fig. 15.21 Primary myelofibrosis, overt fibrotic phase. This trephine biopsy specimen is markedly fibrotic, with cellular streaming and decreased trilineage hematopoiesis. Scattered atypical, pleomorphic megakaryocytes can be seen

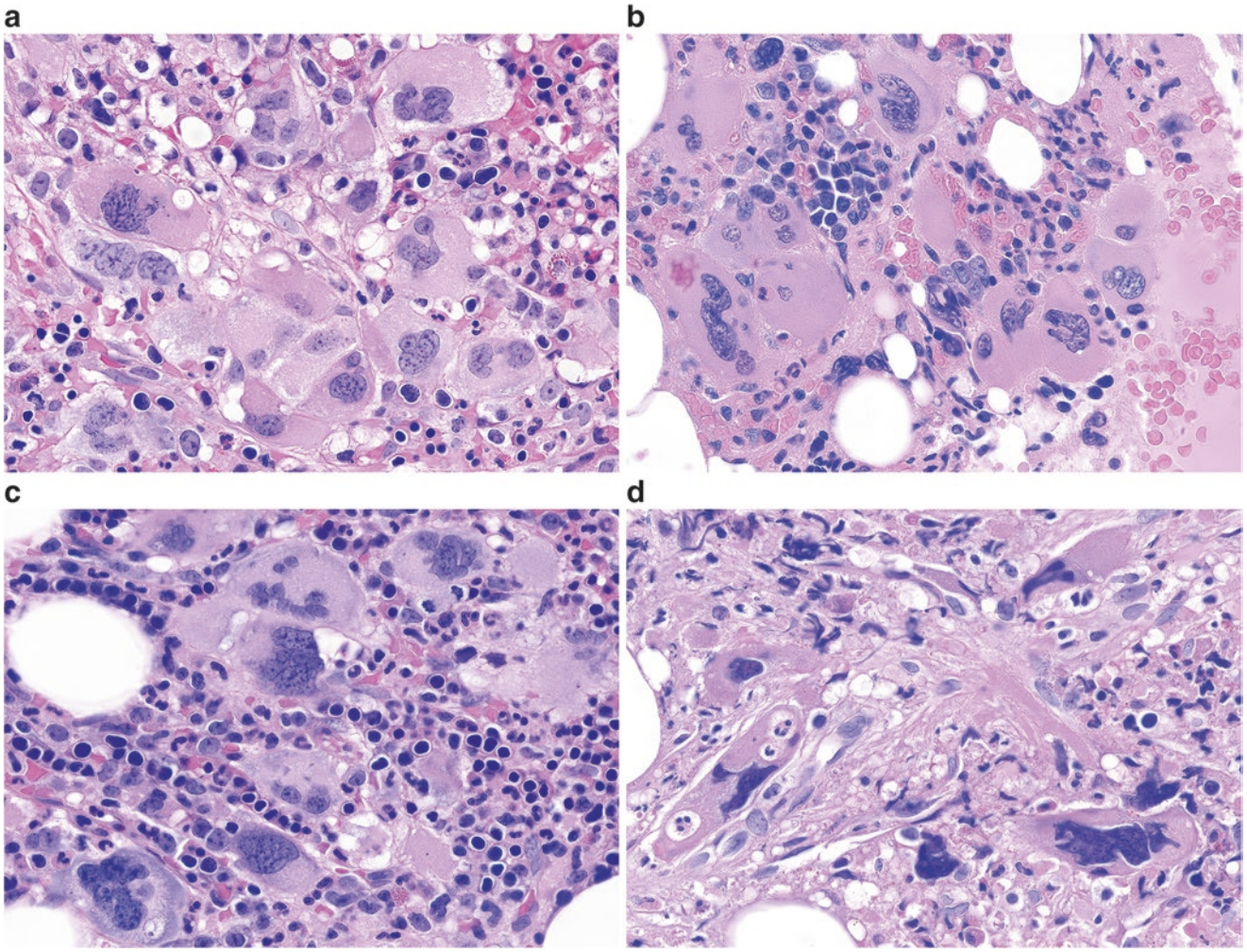

Fig. 15.22 Primary myelofibrosis, megakaryocytes. (**a**–**d**) Increased numbers of pleomorphic atypical megakaryocytes are shown in tight clusters in these H&E-stained trephine biopsy sections

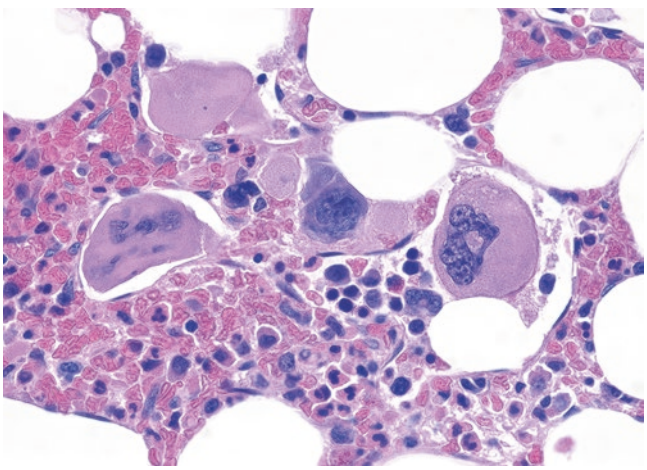

Fig. 15.23 Primary myelofibrosis, overt fibrotic phase. Intrasinusoidal hematopoiesis is shown in this trephine biopsy. The presence of intrasinusoidal hematopoiesis is not specific for primary myelofibrosis; it may be seen in other myeloproliferative neoplasms

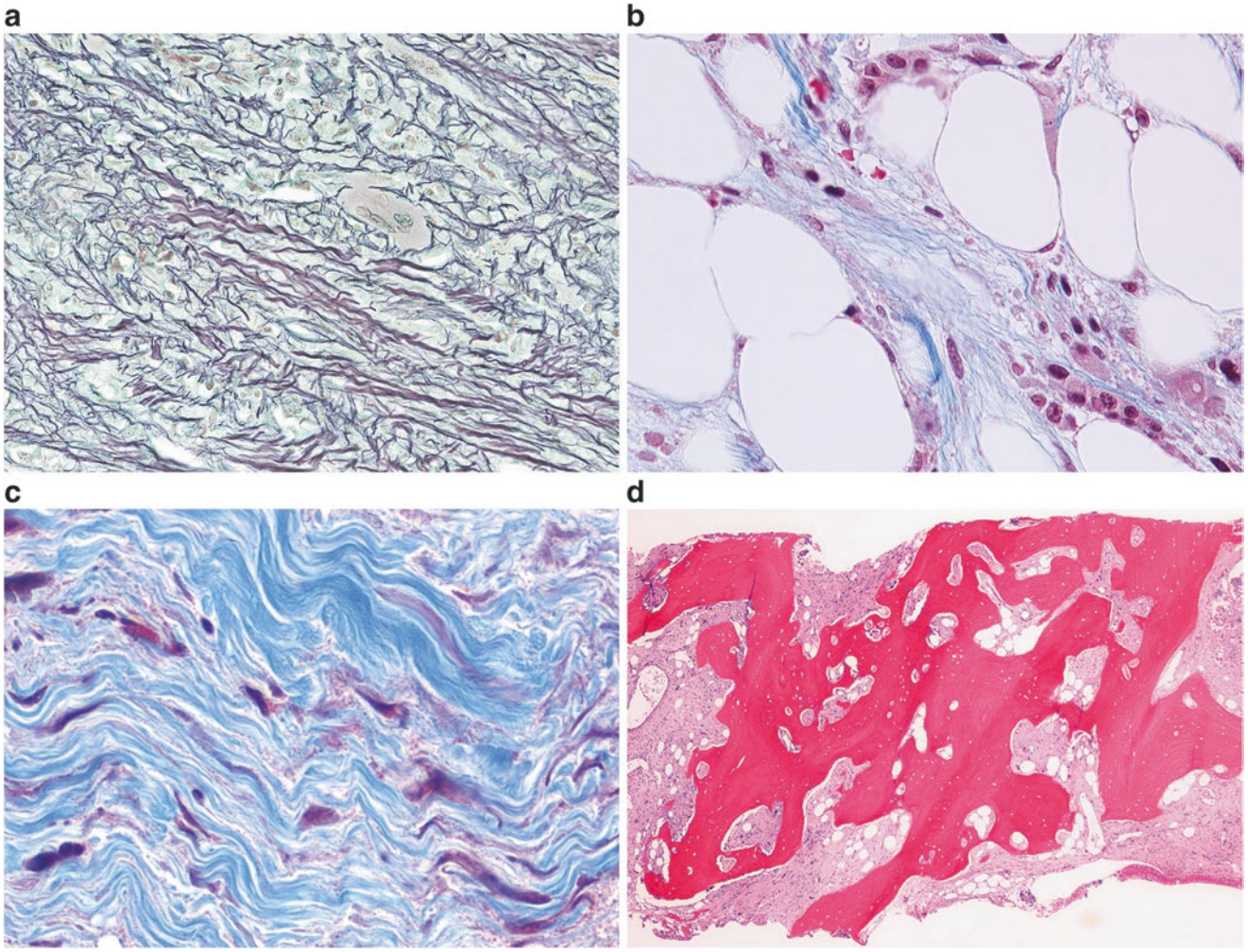

Fig. 15.24 Primary myelofibrosis, overt fibrotic phase. Markedly increased reticulin fibrosis with numerous intersections is shown in this trephine biopsy (**a**). A Masson's trichrome stain shows mild collagen fibrosis (**b**) and marked collagen fibrosis (**c**). Grading for fibrosis is described in Tables 15.7 and 15.8. Grade 3 osteosclerosis is shown in this trephine biopsy, with markedly sclerotic bony trabeculae (**d**). Dilated sinuses are present between trabeculae

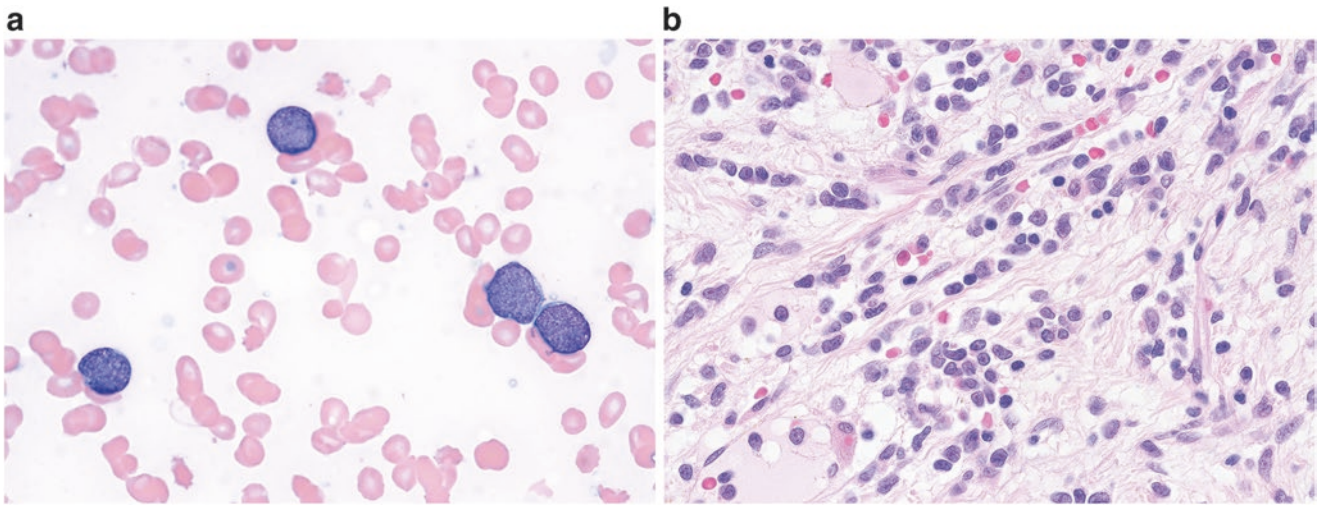

Fig. 15.25 Acute myeloid leukemia arising from primary myelofibrosis. (**a**) Increased blasts are present with large size, scant wispy cytoplasm, and smooth chromatin. Patients in the overt fibrotic phase of disease may progress to myelodysplasia and/or acute leukemia. (**b**) This bone marrow biopsy specimen highlights increased blasts present in small and large aggregates, as well as within marrow sinuses

Table 15.6 Natural history of primary myelofibrosis

	Prefibrotic phase	Overt fibrotic phase
Diagnosis	–	Most patients diagnosed
Median survival	18 y	7 y
CBC and differential	Anemia, variable PLT, mild leukocytosis	More frequent in this phase
		Anemia
		Variable PLT with thrombocytopenia
		Variable WBC with leukopenia
Peripheral blood smear morphology	+/– nucleated red blood cells	Leukoerythroblastic smear with many dacrocytes
	+/– immature granulocytes	
	+/– large platelets	Giant and bizarre platelets
	+/– rare dacrocytes	Megakaryocyte nuclei
	Occasional blasts present in a minority of patients	Micromegakaryocytes
		Higher blast counts
Bone marrow	Hypercellular	Variable cellularity
	Increased M/E ratio	Marked fibrosis
		Osteosclerosis
		Intrasinusoidal hematopoiesis
	Left-shifted granulocytic hyperplasia	Decreased granulopoiesis and erythropoiesis
	Increased megakaryocytes with clustering, pleomorphism, coarse lobulations	Preserved atypical megakaryocytic hyperplasia
		Reactive lymphoid aggregates
	Reactive lymphoid aggregates	
Cytogenetics	–	Abnormal cytogenetics and unfavorable karyotype more frequent in this phase
JAK2, *CALR*, *MPL* mutations	Present	Present
Additional mutations	High-risk mutations such as *SRSF2* and *IDH1/2* found at similar frequencies	High-risk mutations such as *SRSF2* and *IDH1/2* found at similar frequencies
		ASXL1, *EZH2* more frequently present
		Two or more mutated genes more frequently reported

CBC, complete blood cell count; M/E, myeloid/erythroid; PLT, platelet count; PMF, primary myelofibrosis; WBC, white blood cell count
Adapted from Guglielmelli et al. [3]

Table 15.7 Grading of bone marrow fibrosis[a]

Grade	Description
MF-0	Normal bone marrow
MF-1	Loose network of reticulin with many intersections
MF-2	Diffuse and dense increase in reticulin fibrosis with extensive intersections Occasional focal bundles of collagen and/or focal osteosclerosis
MF-3	Diffuse and dense increase in reticulin fibrosis with coarse bundles of collagen, often with osteosclerosis

Adapted from Thiele et al. [4] *and* Kvasnicka et al. [5]
[a]Grading system applies to both reticulin and collagen fibrosis. Thus, both a reticulin stain and a Masson's trichrome stain must be used together. Reticulin and collagen fibers should be assessed only in hematopoietic areas of the bone marrow. The final score is determined by the highest grade present in at least 30% of the marrow area

Table 15.8 Grading of collagen fibrosis in bone marrow[a]

Grade	Description
0	Normal (perivascular collagen deposition)
1	Focal collagen deposition in paratrabecular or central locations
2	Paratrabecular and/or central deposition of collagen with focal connecting meshwork *or* generalized apposition of collagen in paratrabecular areas
3	Diffuse deposition of collagen

Adapted from Kvasnicka et al. [6]
[a]The final score is determined by the highest grade present in at least 30% of the marrow area

Table 15.9 Grading of osteosclerosis in bone marrow[a]

Grade	Description
0	Normal bone trabeculae
1	Focal budding or new bone in paratrabecular locations
2	Diffuse new bone formation with thickening of trabeculae
3	Extensive new bone formation with interconnecting meshwork and effacement of the bone marrow spaces

Adapted from Kvasnicka et al. [6]
[a]The final score is determined by the highest grade present in at least 30% of the marrow area

Table 15.10 Criteria for the diagnosis of prefibrotic primary myelofibrosis[a]

Major criteria
Bone marrow histology: atypical megakaryocytic hyperplasia without grade 2 or 3 fibrosis, a hypercellular marrow with granulocytic hyperplasia, and often an erythroid hypoplasia
Exclusion of other MPN, MDS, or myeloid neoplasms[b]
Mutation of *JAK2*, *MPL*, or *CALR*[c]
Minor criteria
Anemia
WBC $\geq 11 \times 10^9$/L
Increased LDH[d]
Palpable splenomegaly

LDH lactate dehydrogenase, *MDS* myelodysplastic syndromes, *MPN* myeloproliferative neoplasm, *PMF* primary myelofibrosis, *WBC* white blood cell count

Adapted from Arber et al. [1]

[a]Diagnosis requires all three major criteria and at least one minor criterion. The minor criteria must be confirmed in two consecutive measurements

[b]The differential diagnosis of PMF is quite extensive and includes MPNs other than PMF, MDS, acute panmyelosis with myelofibrosis, acute myeloid leukemia, mastocytosis, malignant histiocytosis, vitamin D deficiency, connective tissue disease, autoimmune myelofibrosis, lymphoma, hairy cell leukemia, plasma cell myeloma, metastatic cancer, renal osteodystrophy, infections, and gray platelet syndrome

[c]In the absence of a *JAK2*, *MPL*, or *CALR* mutation, there must be the presence of another clonal marker (*e.g.*, mutation in *ASXL1*, *EZH2*, *TET2*, *IDH1*, *IDH2*, *SRSF2*, *SF3B1*) or absence of minor reactive reticulin fibrosis (grade 1)

[d]Above the upper limit of normal

Table 15.11 Criteria for the diagnosis of fibrotic primary myelofibrosis[a]

Major criteria
Atypical megakaryocytic proliferation with grade 2 or 3 fibrosis[b]
Exclusion of other MPNs, MDS, or other myeloid neoplasms[c]
JAK2, *CALR*, or *MPL* mutation[d]
Minor criteria
Anemia
WBC $\geq 11 \times 10^9$/L
Increased LDH[e]
Palpable splenomegaly
Leukoerythroblastic smear[f]

LDH lactate dehydrogenase, *MDS* myelodysplastic syndromes, *MPN* myeloproliferative neoplasm, *WBC* white blood cell count

Adapted from Arber et al. [1]

[a]Diagnosis requires all major criteria and at least one minor criterion

[b]See Table 15.7 for grading of bone marrow fibrosis

[c]The other MPNs, including chronic myeloid leukemia, essential polycythemia, and polycythemia vera, must be excluded, along with MDS and other myeloid neoplasms

[d]In the absence of a *JAK2*, *MPL*, or *CALR* mutation, there must be the presence of another clonal marker (*e.g.*, mutation in *ASXL1*, *EZH2*, *TET2*, *IDH1*, *IDH2*, *SRSF2*, *SF3B1*) or absence of reactive fibrosis

[e]Above the upper limit of normal

[f]The presence of immature granulocytes and nucleated red blood cells. Dacrocytes (teardrop-shaped red blood cells) are typically also present in this phase

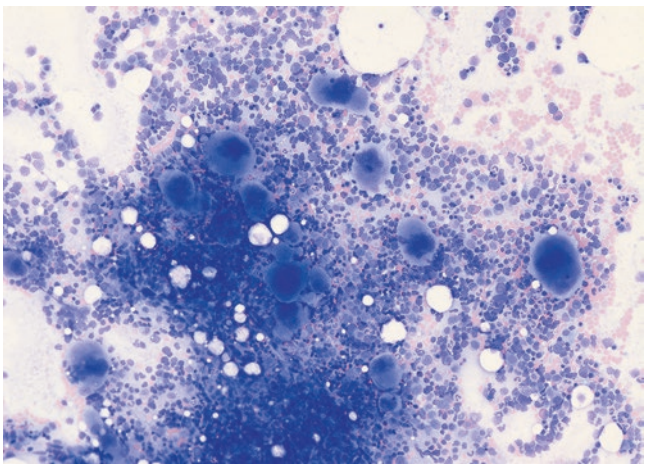

Fig. 15.26 Essential thrombocythemia. This Wright-Giemsa-stained bone marrow aspirate smear shows a proliferation of mature large and enlarged megakaryocytes in a background of intact hematopoiesis

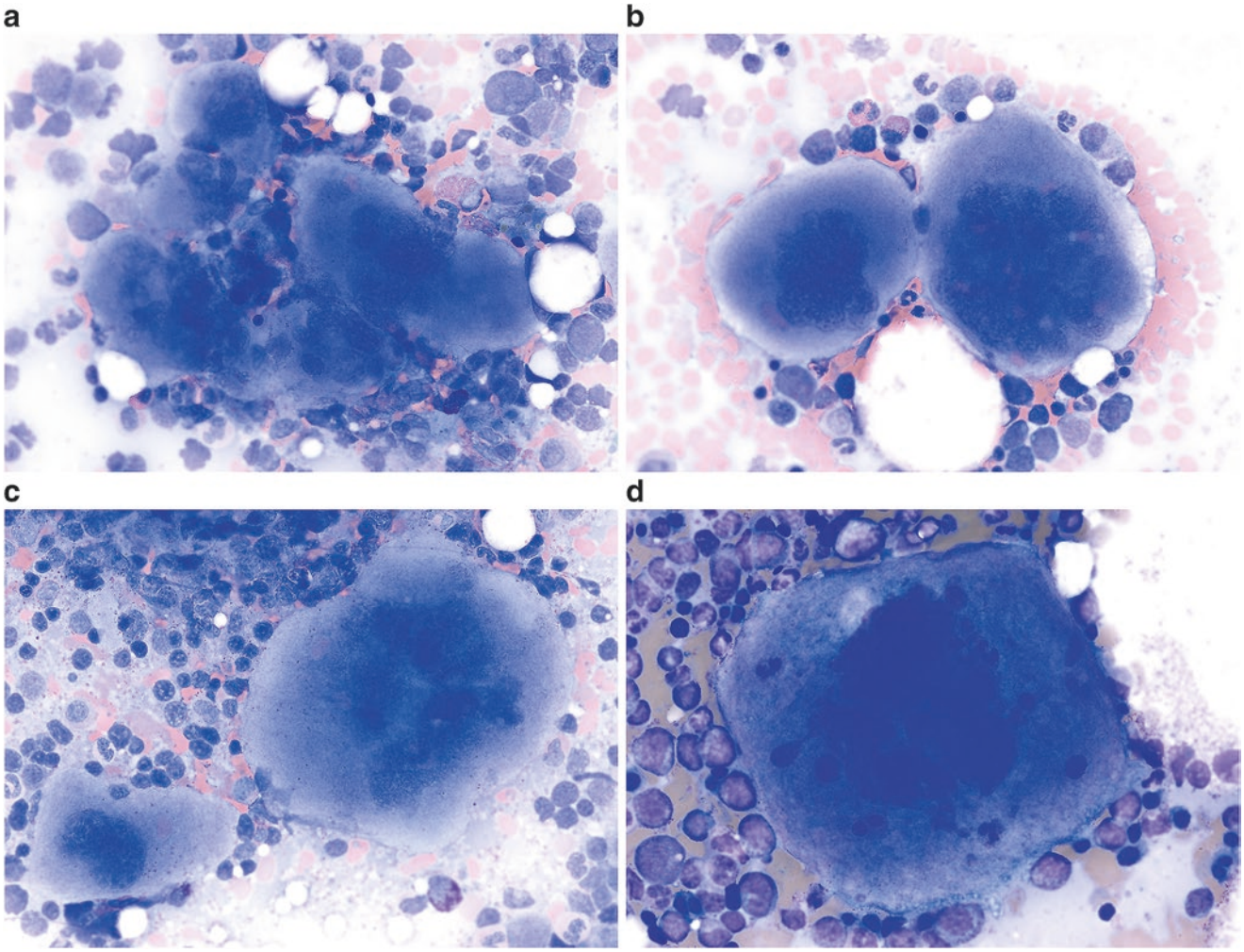

Fig. 15.27 Essential thrombocythemia, megakaryocytes. (**a**–**d**) Clusters of enlarged and giant mature megakaryocytes are shown with hyperlobulated nuclei. Essential thrombocythemia is characterized by a clonal population of mature megakaryocytes in the bone marrow, producing excess platelets often exceeding 1000×10^9/L. Most patients are asymptomatic, with routine blood tests leading to the diagnosis

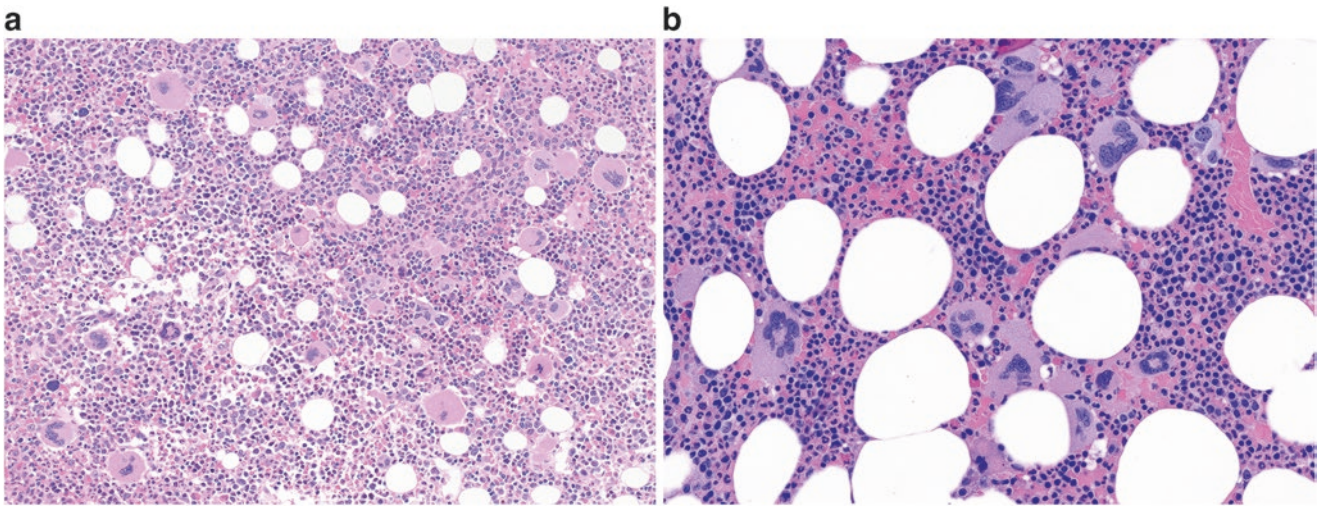

Fig. 15.28 Essential thrombocythemia. (**a**) The bone marrow is typically normocellular, with a normal myeloid/erythroid (M/E) ratio and increased numbers of megakaryocytes, which are loosely clustered or distributed singly throughout the bone marrow, as shown in this H&E-stained trephine biopsy. (**b**) At higher power, the loose clustering of mature megakaryocytes is seen, with many being enlarged. Criteria for the diagnosis of essential thrombocythemia are presented in Table 15.12

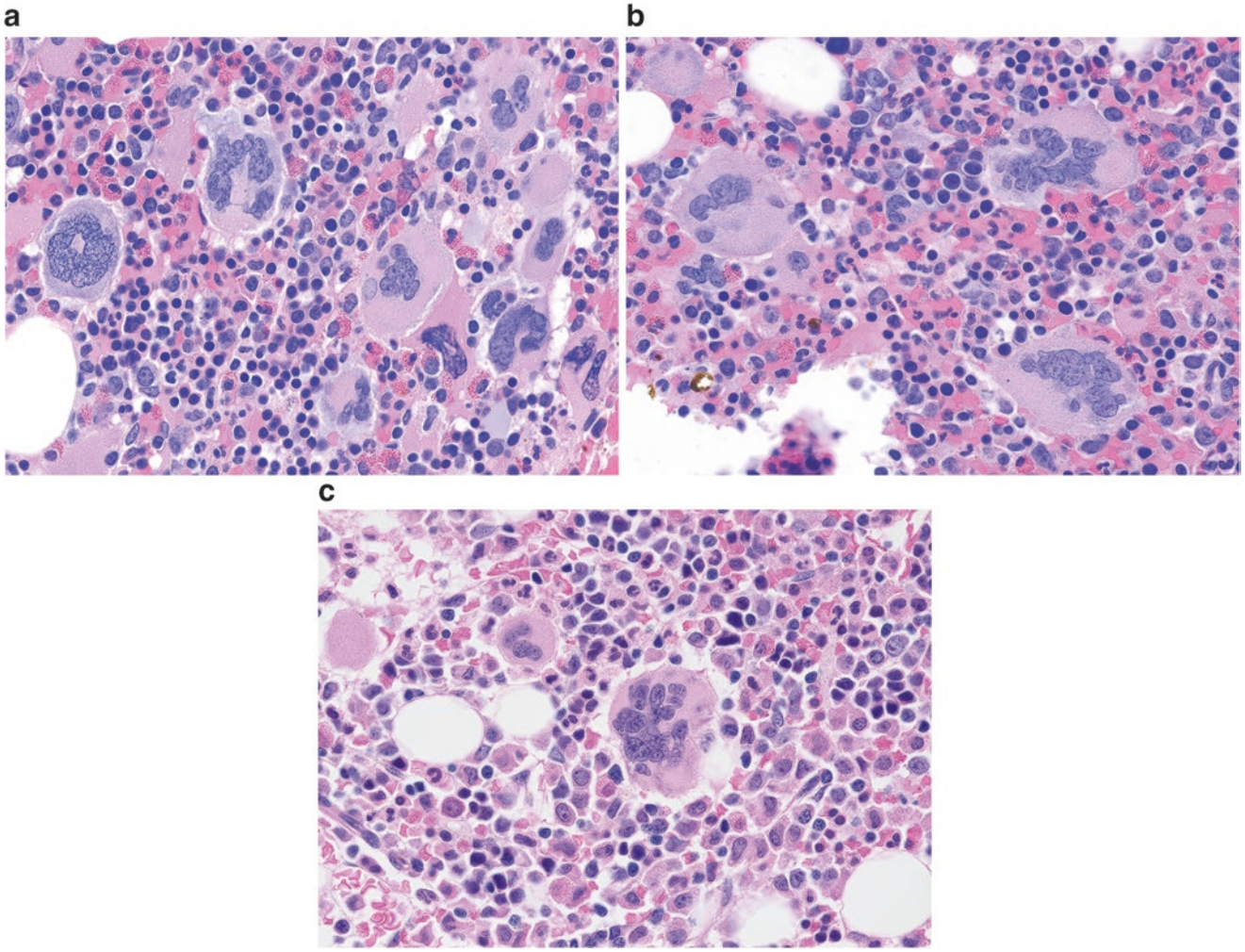

Fig. 15.29 Essential thrombocythemia. (**a**–**c**) These H&E-stained trephine biopsies show predominantly loosely clustered, enlarged megakaryocytes, which are hyperlobulated

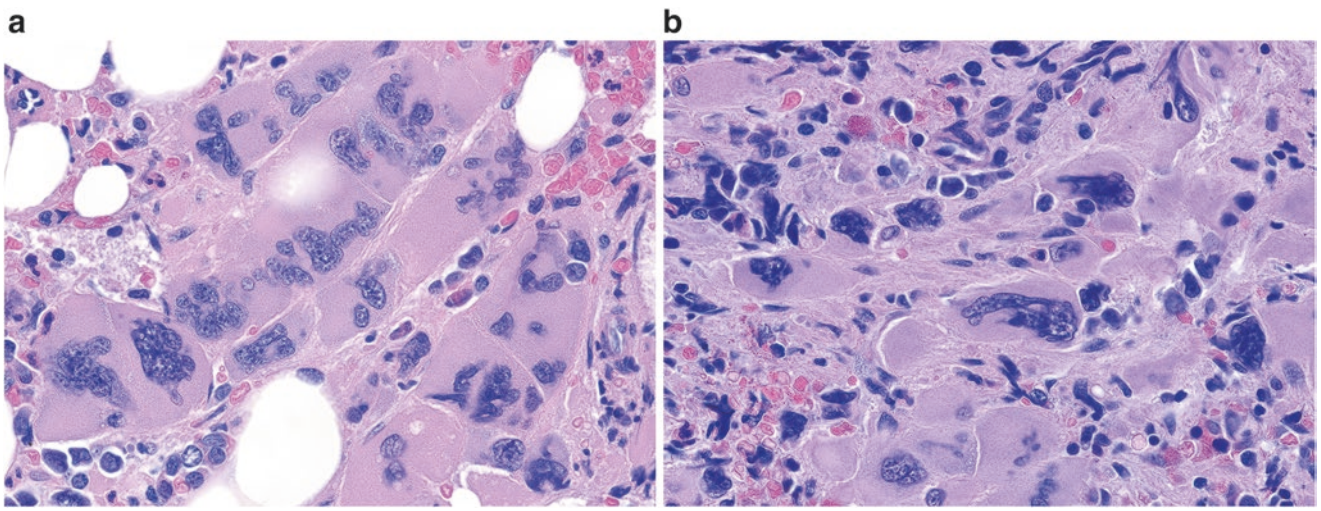

Fig. 15.30 Post-essential thrombocythemia (post-ET) myelofibrosis. This trephine biopsy shows clusters of markedly atypical megakaryocytes. (**a**) Some megakaryocytes are enlarged and hyperlobulated, but form a tight cluster which is atypical for ET. (**b**) Other megakaryocytes have more hyperchromatic nuclei, and they are seen against a background of fibrosis. Rarely, transformation to acute leukemia or post-ET myelofibrosis may be seen in patients. A well-documented history of ET is necessary before this diagnosis can be made, and a review of the original diagnostic material should be performed. In particular, separating ET from prefibrotic primary myelofibrosis can be challenging; ET should be normocellular, with normal granulopoiesis and erythropoiesis, a normal M/E ratio, and an increase in enlarged, mature megakaryocytes. A hypercellular marrow with an increased M/E ratio and pleomorphic megakaryocytes would favor primary myelofibrosis

Table 15.12 Criteria for the diagnosis of essential thrombocythemia[a]

Major criteria
Persistent platelet count ≥450 × 10^9/L
Bone marrow biopsy with atypical megakaryocytic hyperplasia with enlarged mature megakaryocytes[b]
Not meeting criteria for other MPNs, MDS, or other myeloid neoplasms
JAK2, *MPL*, or *CALR* mutation
Minor criterion
Clonal marker or absence of support for reactive thrombocytosis[c]

Adapted from Arber et al. [1]

[a]Diagnosis requires that all four criteria be met or the first three major criteria and the minor criterion

[b]The bone marrow biopsy should not show a significant increase or left shift in neutrophilic granulopoiesis or erythropoiesis. Typically, there is no fibrosis or rarely grade 1 fibrosis

[c]Reactive causes of thrombocytosis include iron deficiency, hemolytic anemia, postsplenectomy, cancer, infection, inflammatory states, drug effects, acute blood loss, acute infection/inflammation, exercise, or rebound from thrombocytopenia

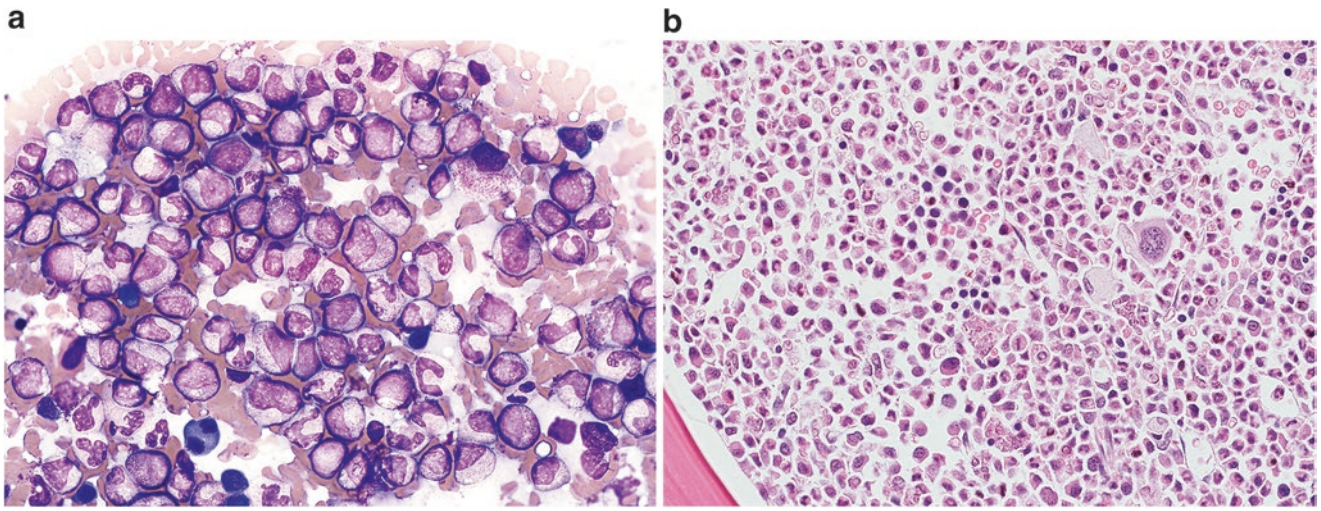

Fig. 15.31 Chronic neutrophilic leukemia. This 47-year-old man presented with a marked neutrophilia of approximately 50 × 10^9/L for 6 months with normal hemoglobin and platelet count. A peripheral smear (*not shown*) showed toxic changes and a minimal granulocytic left shift. Clinically, the patient had fever, purpura, and myalgias; he had an extensive evaluation that was negative for an infectious or neoplastic etiology. (**a**) The bone marrow aspirate is remarkable for a granulocytic hyperplasia with complete maturation without dysplasia or increased blasts. The M/E ratio was 48:1. (**b**) The corresponding bone marrow biopsy is 100% cellular, with a striking granulocytic hyperplasia. Cytogenetic analysis revealed a normal male karyotype. Molecular analysis revealed a *CSF3R* T618I mutation. The diagnosis of CNL requires the exclusion of other myeloproliferative neoplasms, myelodysplastic syndromes, and other myeloid neoplasms, with no alternative explanation for the neutrophilia, such as an infection or tumor. In the era before the discovery of *CSF3R* mutations, up to 20% of patients had an underlying neoplasm, usually plasma cell myeloma

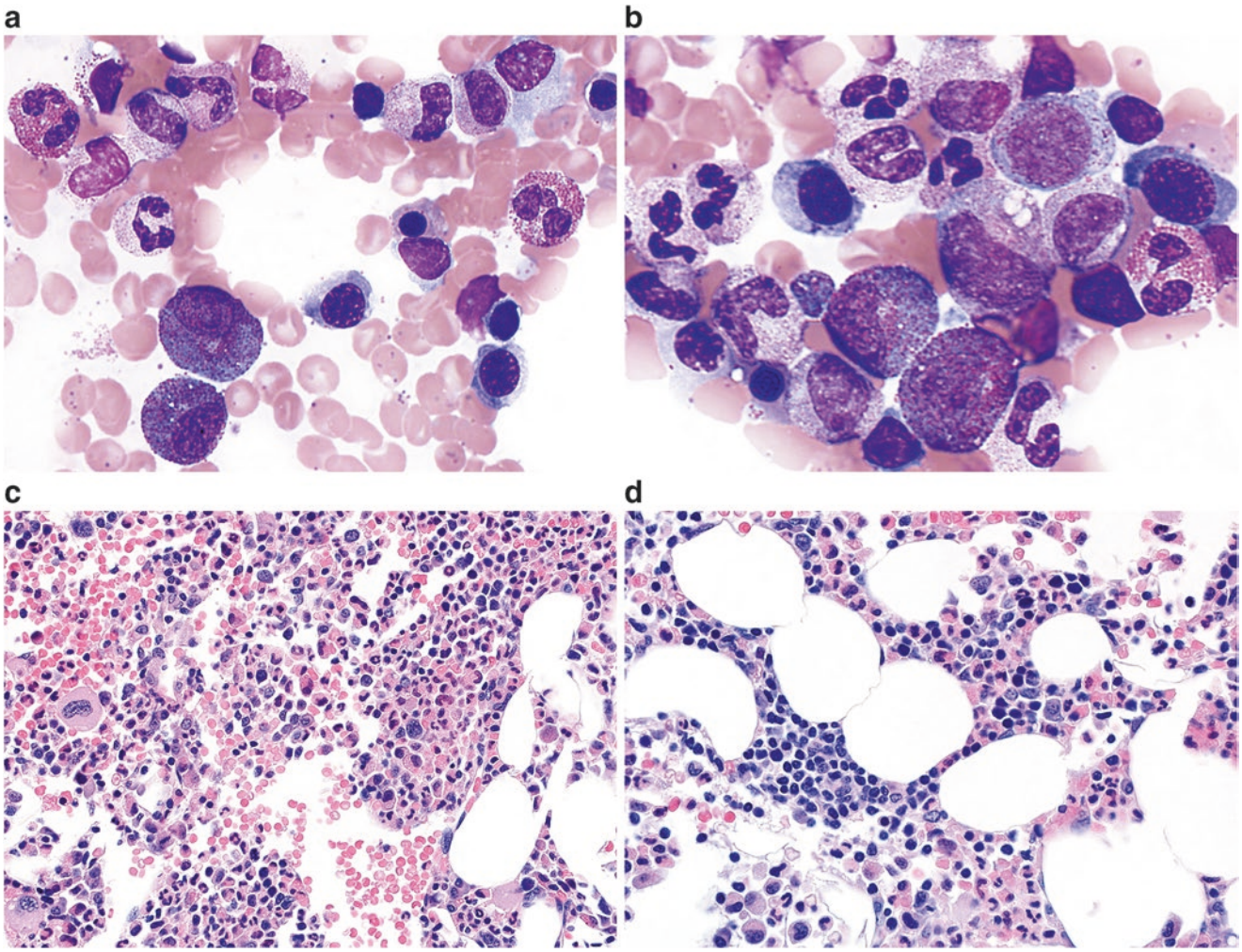

Fig. 15.32 Chronic eosinophilic leukemia, not otherwise specified. This 64-year-old woman presented with a leukocyte count of 19.2×10^9/L, with 57% eosinophils and a platelet count of 109×10^9/L, without anemia. The diagnosis of chronic eosinophilic leukemia, not otherwise specified, was met with the finding of del(16)(q23q24) by cytogenetics and the absence of any of the following: the Philadelphia chromosome, abnormalities of *PDGFRA*, *PDGFRB*, *FGFR1*, *PCM1-JAK2*, or rearrangement of *CBFB*. Flow cytometry was unremarkable with no evidence of an abnormal T-cell population, and there was no evidence of a plasma cell neoplasm or systemic mastocytosis. (**a** and **b**) Wright-Giemsa-stained bone marrow aspirate smear highlights the marked marrow eosinophilia without an increase in blasts or significant dysplasia in erythroid and granulocytic precursors. The M/E ratio was increased at 6:1. (**c** and **d**) Results of the trephine biopsy were normocellular for age and generally reflected the aspirate smear, with additional findings of a subset of small, hypolobated megakaryocytes and a small, reactive lymphoid aggregate

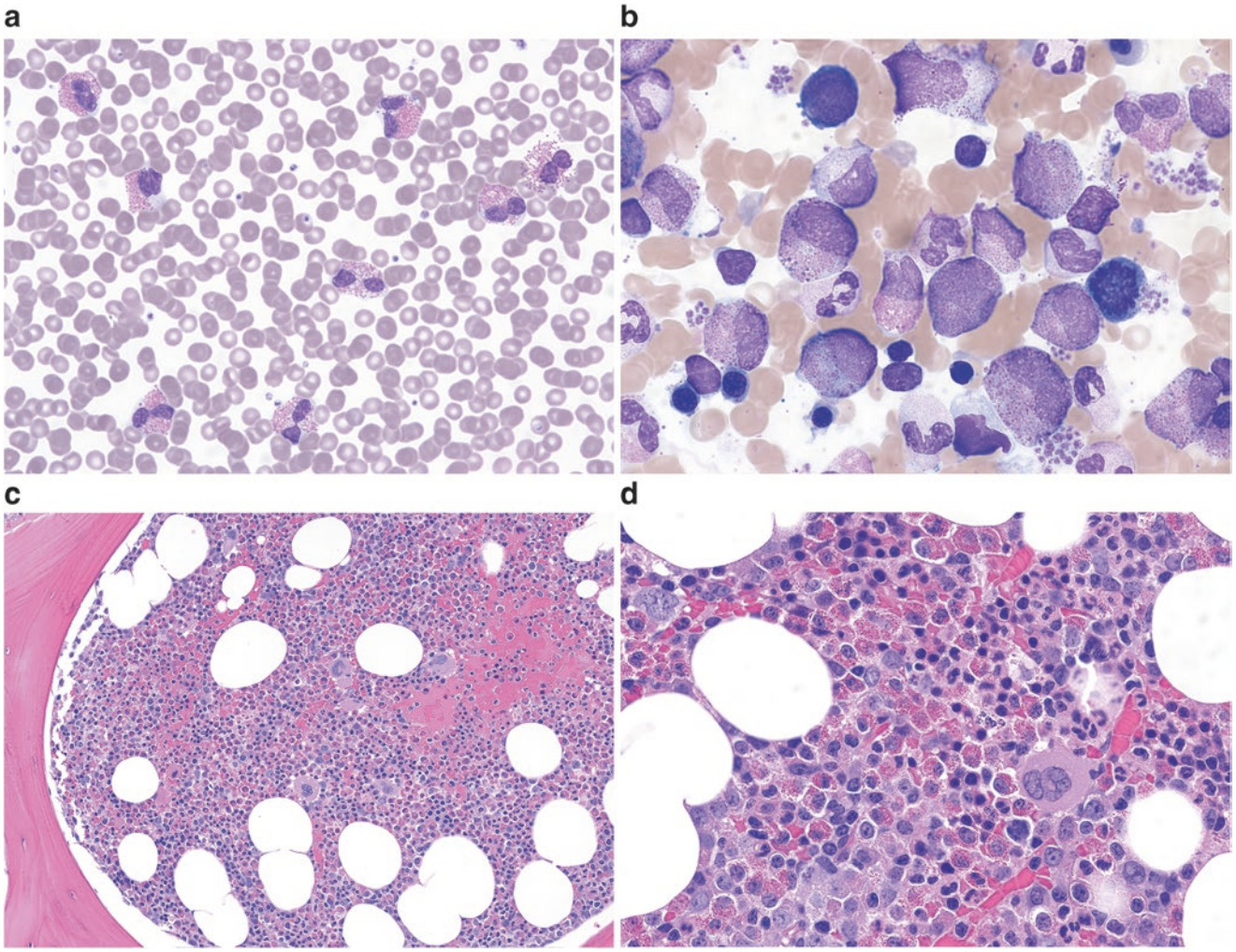

Fig. 15.33 Idiopathic hypereosinophilia. (**a**) An eosinophilia is present in the peripheral blood, where the eosinophils are mature and unremarkable. Occasional eosinophils may have granules that do not completely fill the cytoplasm, but this is a nonspecific feature. (**b**) In this Wright-Giemsa-stained aspirate smear, mature eosinophils and eosinophilic precursors are increased. It is normal to see occasional basophilic granules in early eosinophilic precursors. Dysplastic features are not observed. (**c**) In the H&E-stained trephine biopsy, the bone marrow is hypercellular due to an increase in marrow eosinophils. (**d**) A higher-power image shows the marrow eosinophilia in a background of adequate granulopoiesis, erythropoiesis, and megakaryocytes. The absence of either abnormal bone marrow features or abnormal cytogenetics differentiates idiopathic hypereosinophilia and idiopathic hypereosinophilic syndrome from chronic eosinophilic leukemia, not otherwise specified. A diagnosis of idiopathic hypereosinophilic syndrome is recommended for those patients without evidence of chronic eosinophilic leukemia, not otherwise specified, or secondary eosinophilia. Idiopathic hypereosinophilic syndrome is defined as eosinophilia greater than 1.5×10^9/L for 6 or more months without an identifiable cause and with evidence of organ damage from eosinophilia. Idiopathic hypereosinophilia is differentiated from hypereosinophilic syndrome by the absence of organ damage

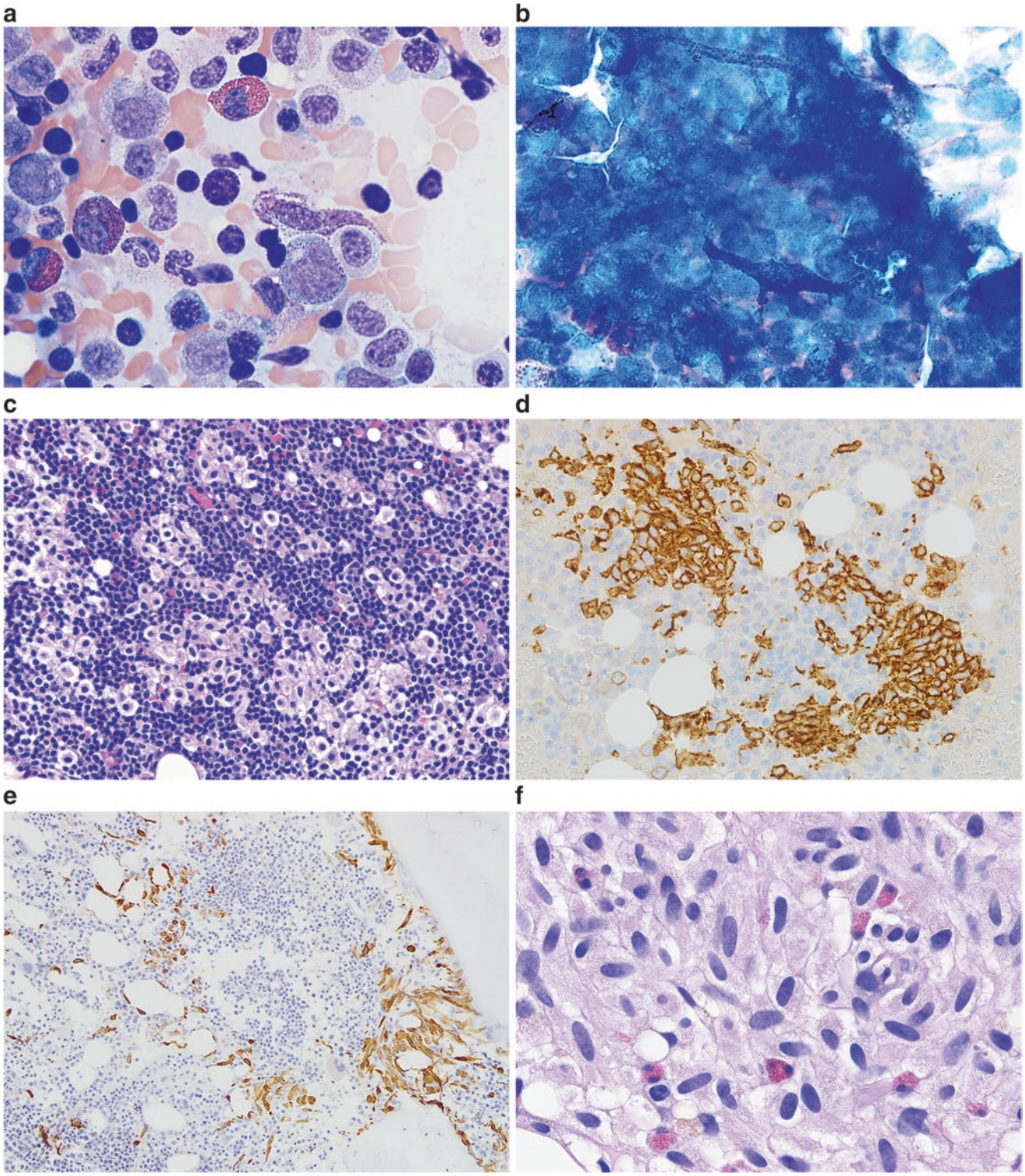

Fig. 15.34 Indolent systemic mastocytosis. This 53-year-old woman presented with a lytic lesion involving the right femur, which was found to be systemic mastocytosis. (**a**) The bone marrow aspirate smear showed rare spindle-shaped hypogranular mast cells with elongated cytoplasmic processes in a background of trilineage hematopoiesis. (**b**) It is often easier to see the mast cells within or near the bone marrow particles on aspirate smears, as in this image. (**c**) In this trephine biopsy, the clear mast cells have abundant, lightly eosinophilic cytoplasm and round to oval nuclei; they are admixed with reactive, small lymphocytes. (**d**) Immunohistochemical stain directed against KIT (CD117) highlights the mast cells surrounding small lymphocytes. (**e**) Tryptase is the most specific marker for mast cells; in this image, it marks numerous spindle-shaped mast cells present in aggregates surrounding a lymphoid aggregate, as well as interstitially within the bone marrow. (**f**) In this high-power image from another patient, individual mast cells can be seen with bland oval nuclei and abundant, lightly eosinophilic cytoplasm admixed with eosinophils. Mastocytosis is a heterogenous disease due to a clonal proliferation of mast cells, with most patients having an activating tyrosine kinase mutation in the *KIT* gene (typically D816V). This patient had a normal complete blood cell count and lacked "B" and "C" findings, so a diagnosis of indolent systemic mastocytosis was made. The classification of mastocytosis is listed in Table 15.2

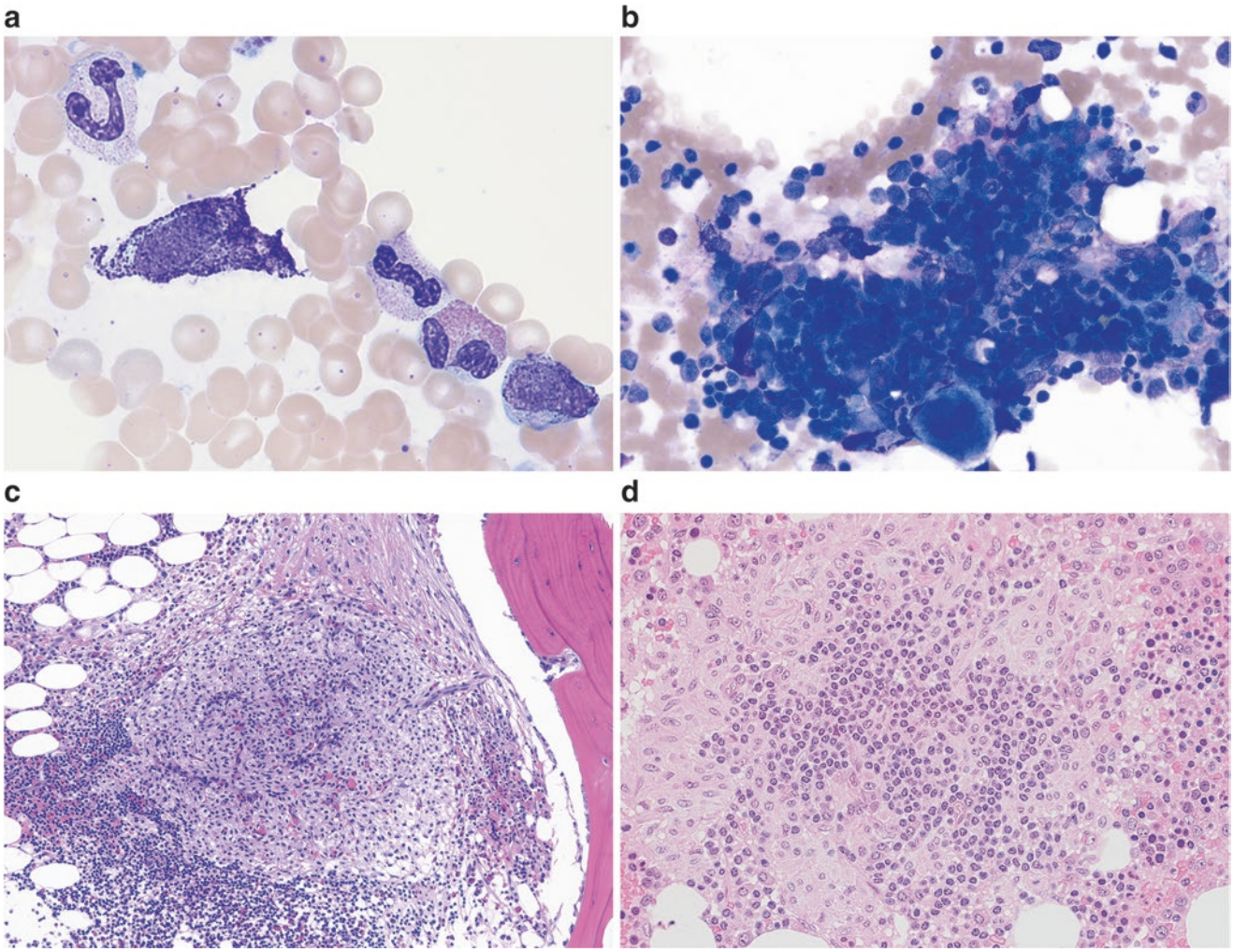

Fig. 15.35 Systemic mastocytosis. This 45-year-old man had a long history of cutaneous mastocytosis with elevated serum tryptase (80–100 μg/L) and a mast cell burden of 30%. The absence of C findings prevents a classification of aggressive systemic mastocytosis, but the high mast cell burden is not typical for indolent disease and is concerning for incipient smoldering systemic mastocytosis. (**a**) The Wright-Giemsa-stained aspirate smear shows a spindle-shaped mast cell (atypical type I mast cell) with oval nucleus without nucleoli. (**b**) Multiple spindle-shaped mast cells are noted in close association with a small bone marrow particle. (**c**) In the H&E-stained trephine biopsy, a paratrabecular aggregate of mast cells is present, surrounded by a cuff of small lymphocytes. The mast cells are clear, with abundant lightly eosinophilic cytoplasm. (**d**) In this image, the mast cells surround lymphocytes and plasma cells.

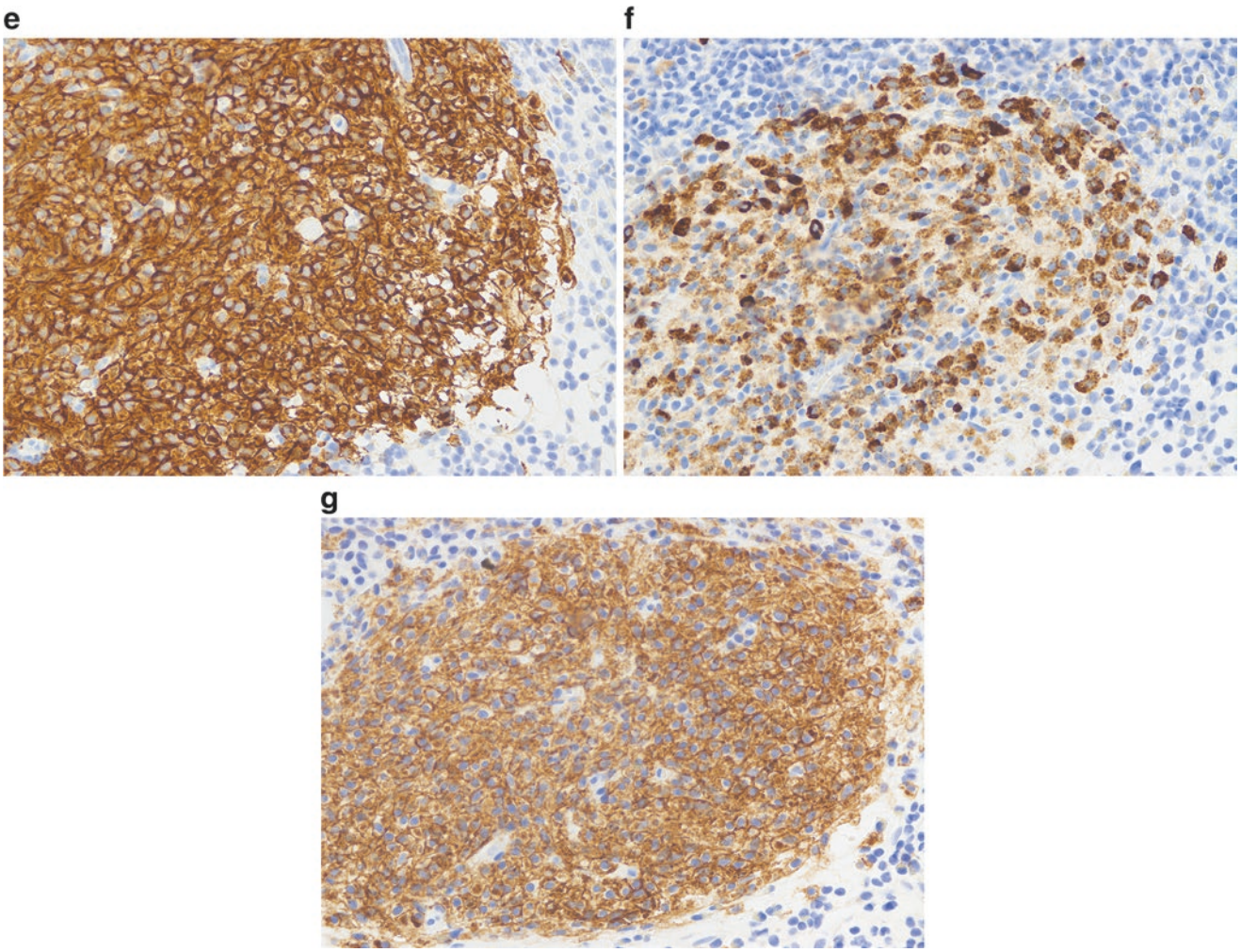

Fig. 15.35 (continued) (**e**) Immunohistochemical stain directed against KIT (CD117) nicely highlights this large mast cell aggregate. CD117 will stain mast cells with brighter staining, but will also mark myeloblasts, promyelocytes, and proerythroblasts, although with dimmer staining. (**f**) In this image, an immunohistochemical stain directed against tryptase shows variable staining of mast cells. While the most specific immunohistochemical marker for mast cells in the bone marrow is tryptase, be aware that tryptase can be only partially expressed by mast cells in the gastrointestinal tract and occasionally in advanced mastocytosis involving the bone marrow. (**g**) Immunohistochemical stain against the IL2 receptor (CD25) also marks the mast cell aggregate. CD25 is expressed by neoplastic mast cells and works robustly in both flow cytometry and immunohistochemistry. CD25 expression in mast cells is associated with the D816V *KIT* mutation. Given that loose proliferations of CD25-positive mast cells may be seen in other disorders, such as myeloid neoplasms with eosinophilia and mutations of *PDGFRA*, *PDGFRB*, and *FGFR-1*, cytogenetic karyotyping and FISH/PCR to specifically evaluate for the cytogenetically cryptic *PDGFRA* mutation is recommended. *KIT* mutation testing may be performed on peripheral blood, bone marrow aspirate, and formalin-fixed/EDTA-decalcified bone marrow biopsies; some laboratories perform flow sorting of mast cells or microdissection techniques, but whole bone marrow is fine if the techniques used are sufficiently sensitive

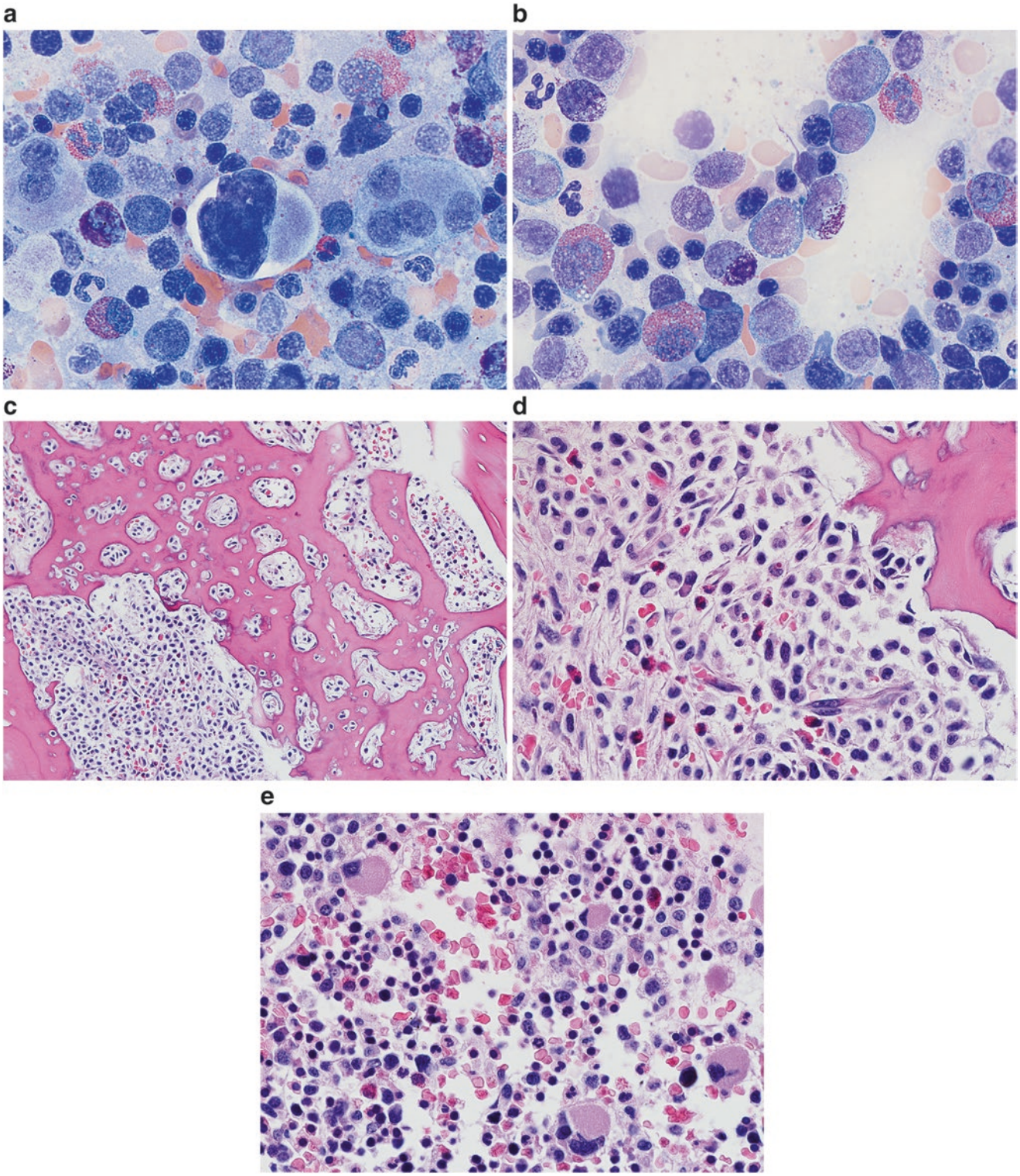

Fig. 15.36 Systemic mastocytosis with an associated hematological neoplasm. This 68-year-old woman presented with neutrophilia, monocytosis, anemia, and thrombocytopenia. The peripheral blood smear showed features typical of chronic myelomonocytic leukemia (*not shown*) without circulating mast cells. (**a**) The Wright-Giemsa-stained aspirate smear shows overtly dysplastic megakaryocytes at the center, with an adjacent promastocyte (atypical type II mast cell) at left showing an indented nucleus. Background eosinophilia is also present; overall, 13% mast cells were noted, with a majority of promastocytes. (**b**) This image shows examples of the atypical mast cells; all the mast cells are round in shape, but they are abnormally hypogranular when compared with a normal mast cell. It is more common to find promastocytes in advanced mastocytosis than in indolent disease. (**c**) On the H&E-stained trephine biopsy, prominent osteosclerosis is noted with a paratrabecular aggregate of mast cells. (**d**) On higher power, these aggregated mast cells have abundant clear cytoplasm, whereas individual mast cells are mostly round with indented nuclei or bilobed nuclei (promastocytes). There are also admixed fibroblasts and eosinophils. (**e**) Other areas of the trephine biopsy showed features of chronic myelomonocytic leukemia, with a hypercellular marrow with increased dysplastic megakaryocytes.

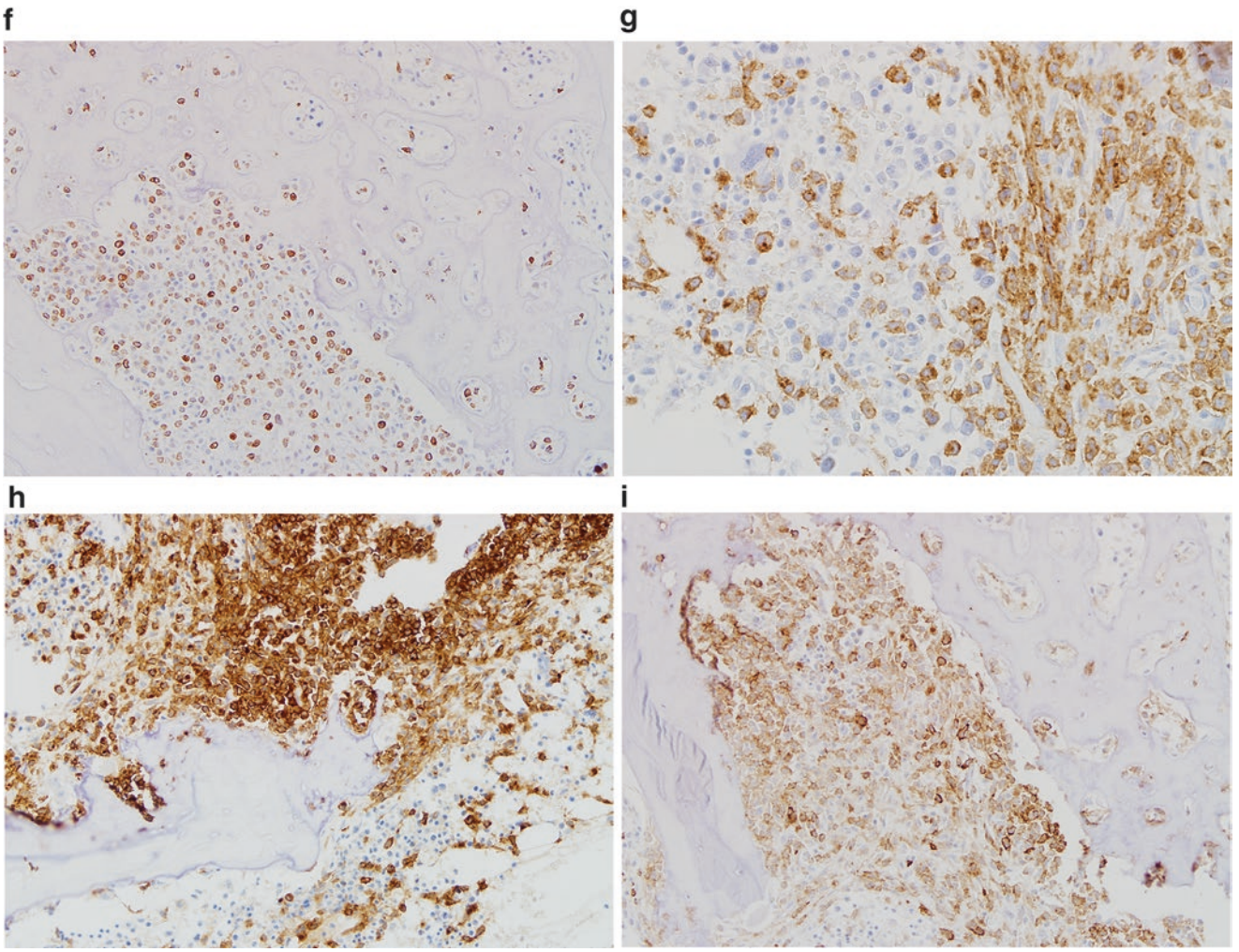

Fig. 15.36 (continued) (**f**–**h**) Immunohistochemistry performed on the biopsy highlights the mast cells with antibodies against tryptase, KIT (CD117), and CD25, respectively. (**i**) It is also important to note that neoplastic mast cells can express CD30, as shown here. An associated hematological neoplasm will accompany systemic mastocytosis in approximately 40% of patients. Typically, these are myeloid neoplasms such as chronic myelomonocytic leukemia; myelodysplastic syndrome; myelodysplastic/myeloproliferative neoplasm, unclassifiable; or acute myeloid leukemia. Sometimes, these other malignancies can obscure the mastocytosis present in the bone marrow, which is revealed only after therapy

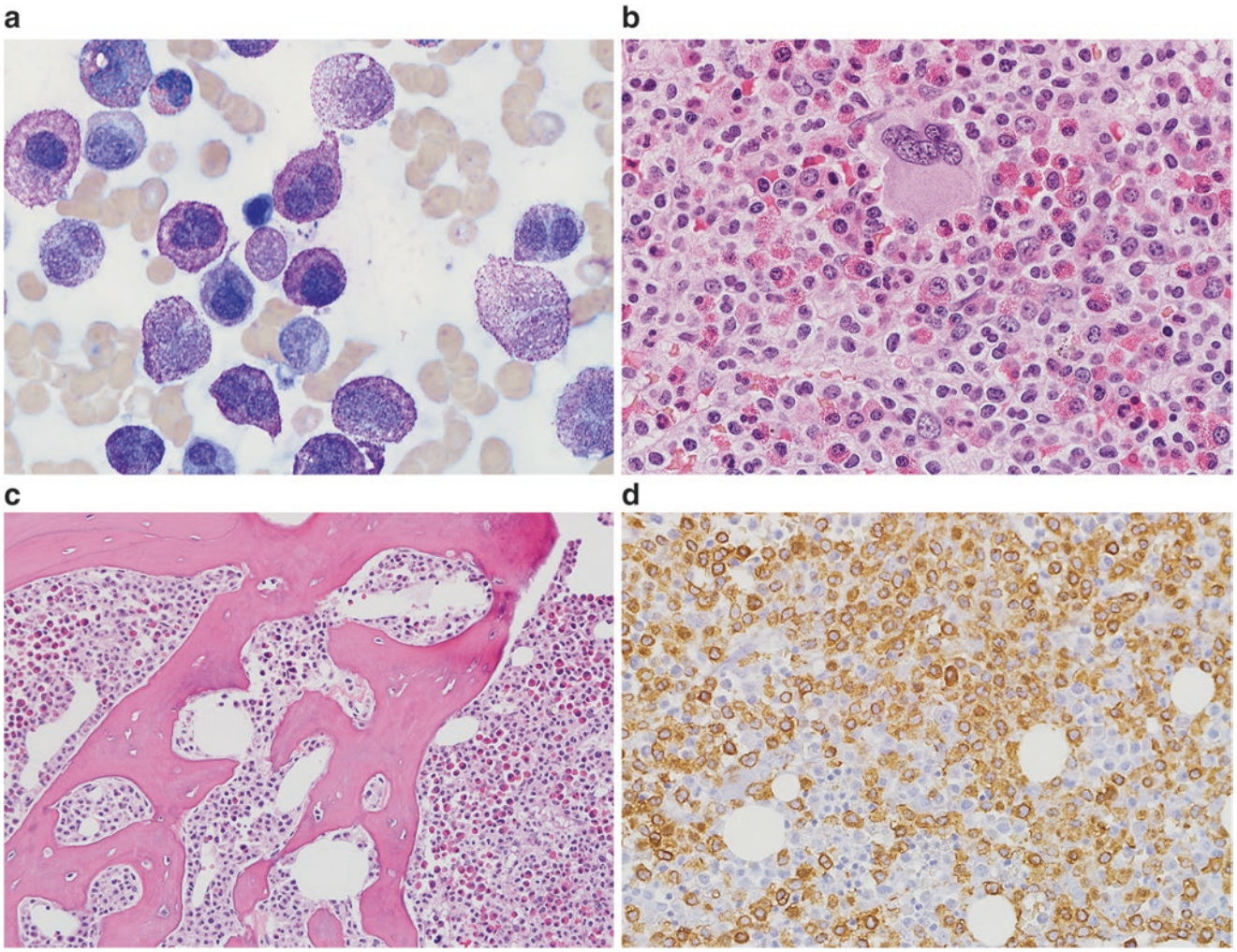

Fig. 15.37 Mast cell leukemia. This 50-year-old man presented with splenomegaly and weight loss, with a leukocytosis characterized by a marked eosinophilia, neutrophilia, and monocytosis and a normocytic anemia with hemoglobin of 8 g/dL, with a normal platelet count. (**a**) Mast cells found in this Wright-Giemsa-stained bone marrow aspirate smear were similar to rare circulating mast cells seen in the peripheral blood (*not shown*). Mast cells comprised 26% of nucleated cells on the aspirate smears; they are large in size and hypogranular, with notched and bilobed nuclei (promastocytes). (**b**) A marrow eosinophilia is also present, as shown in the H&E-stained trephine biopsy. The mast cells are the clear cells with abundant, lightly eosinophilic cytoplasm; many show bilobed nuclei. (**c**) A lower-power image of the bone marrow biopsy highlights the marked trabecular thickening (osteosclerosis). (**d**) An immunohistochemical stain for tryptase performed on the bone marrow biopsy nicely highlights the numerous round mast cells present. The mast cells expressed bright CD117 and CD25 and lacked expression of CD34. Mast cell leukemia is extremely rare; by definition, more than 20% mast cells must be found on aspirate smears. Most patients will present with the aleukemic variant of mast cell leukemia, with less than 10% circulating mast cells; an accompanying eosinophilia can also be present. Most mast cells are immature or atypical in shape (promastocytes, spindle-shaped mast cells), and the bone marrow biopsy is typically effaced by an infiltrative pattern of neoplastic mast cells

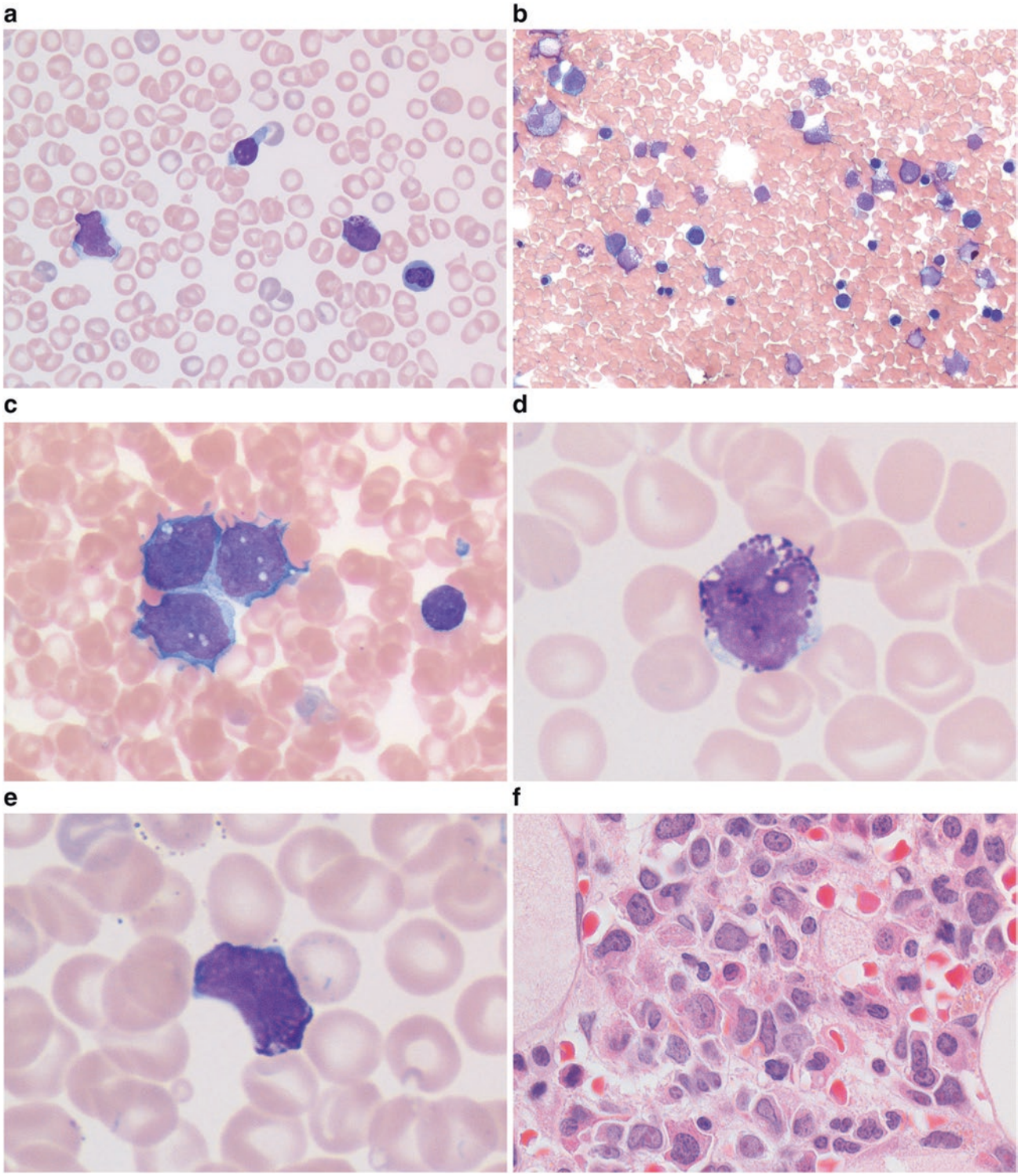

Fig. 15.38 Myelomastocytic leukemia, peripheral blood smear. This 35-year-old woman presented with persistent pancytopenia. Peripheral blood smear (not shown) contained circulating myeloblasts and metachromatic blasts (immature mast cells). Bone marrow aspirate smears (**a**) and touch preparations (**b**) were hemodilute and showed populations of myeloblasts (**c**) and metachromatic blasts (**d, e**), where the latter cells contain blast-like nuclei with large metachromatic granules in the cytoplasm. There was also dysplasia in erythroid and granulocytic precursors. (**f**) The H&E-stained trephine biopsy is filled with immature mononuclear cells containing immature chromatin consistent with blasts. Some granulocytic maturation can also be seen, as well as cells with more abundant cytoplasm and oval nuclei containing immature chromatin. (**g**) An immunohistochemical stain for tryptase stain highlights the mast cell population in the biopsy, showing an interstitial pattern without the dense aggregates seen in systemic mastocytosis. (**h**) An immunohistochemical stain directed at KIT (CD117) highlights two cell populations on the bone marrow biopsy: a bright population corresponding to mast cells and a dim population representing myeloblasts.

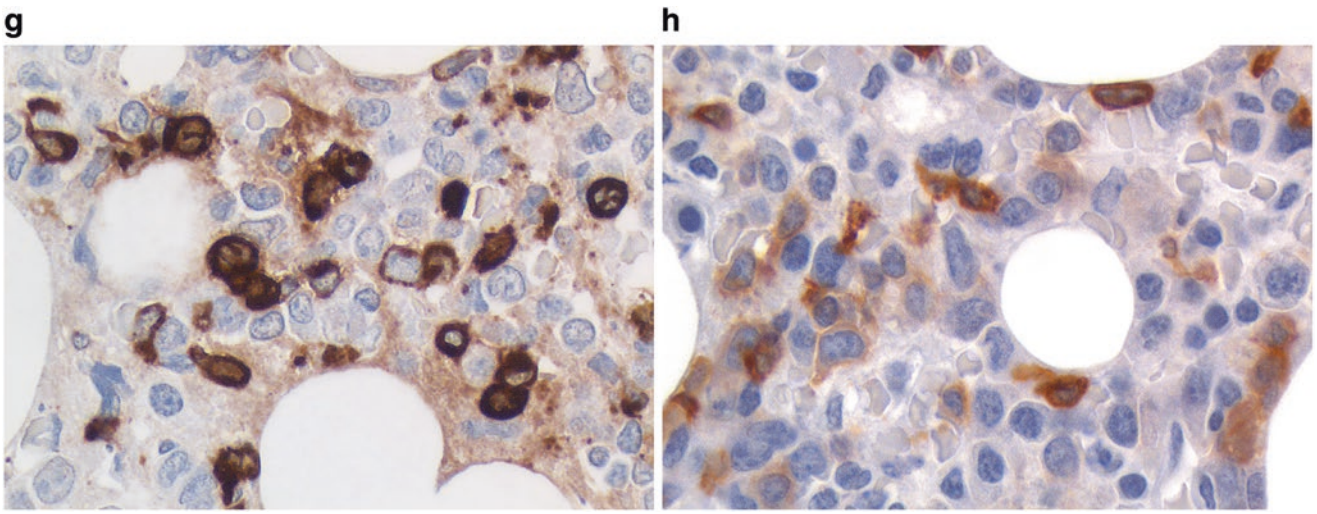

Fig. 15.38 (continued) Flow cytometry confirmed the two discrete cell populations representing mast cells and myeloblasts. There was no evidence of the D816V *KIT* mutation, and criteria were not met for systemic mastocytosis or mast cell leukemia. Distinguishing mast cell leukemia (as in Fig. 15.37) from systemic mastocytosis with acute myeloid leukemia from myelomastocytic leukemia (shown here) can be challenging, requiring a multipronged approach with morphology, flow cytometry, immunohistochemistry, cytogenetics, and molecular genetic testing, informing a robust clinical history and physical examination. To diagnose myelomastocytic leukemia, there should be >5% myeloblasts and >10% mast cells present in either peripheral blood or bone marrow, without meeting criteria for systemic mastocytosis. As shown in these images, the mast cells are typically immature (metachromatic blasts) (*Case originally reported by* Arredondo et al. [6])

References

1. Arber DA, Orazi A, Hasserjian R, Thiele J, Borowitz MJ, Le Beau MM, et al. The 2016 revision to the World Health Organization classification of myeloid neoplasms and acute leukemia. Blood. 2016;127:2391–405.
2. Horny H-P, Metcalfe DD, Bennett JM, Bain BJ, Akin C, Escribano L, Valent P. Mastocytosis. In: Swerdlow SH, Campo E, Harris NL, Jaffe ES, Pileri SA, Stein H, et al., editors. WHO classification of tumours of haematopoietic and lymphoid tissues. Lyon: International Agency for Research on Cancer; 2008. p. 54–63.
3. Guglielmelli P, Pacilli A, Rotunno G, Rumi E, Rosti V, Delaini F, et al. Presentation and outcome of patients with 2016 WHO diagnosis of prefibrotic and overt primary myelofibrosis. Blood. 2017. [Epub ahead of print]. https://doi.org/10.1182/blood-2017-01-761999.
4. Thiele J, Kvasnicka HM, Facchetti F, Franco V, van der Walt J, Orazi A. European consensus on grading bone marrow fibrosis and assessment of cellularity. Haematologica. 2005;90:1128–32.
5. Kvasnicka HM, Beham-Schmid C, Bob R, Dirnhofer S, Hussein K, Kreipe H, et al. Problems and pitfalls in grading of bone marrow fibrosis, collagen deposition and osteosclerosis – a consensus-based study. Histopathology. 2016;68:905–15.
6. Arredondo AR, Gotlib J, Shier L, Medeiros B, Wong K, Cherry A, et al. Myelomastocytic leukemia versus mast cell leukemia versus systemic mastocytosis associated with acute myeloid leukemia: a diagnostic challenge. Am J Hematol. 2010;85:600–6.

Suggested Reading

Chabot-Richards D, Shier LR, George TI. Pathology of the myeloproliferative neoplasms. In: Greer JP, Appelbaum F, Arber DA, Dispenzieri A, Fehniger T, Glader B, et al., editors. Wintrobe's clinical hematology. 14th ed. (in press) ed. Philadelphia: Lippincott Williams and Wilkins; 2017.

George TI, Sotlar K, Valent P, Horny H-P. Mastocytosis. In: Jaffe ES, Arber DA, Harris NL, Quintanilla-Martinez L, editors. Hematopathology. 2nd ed. Philadelphia: Elsevier; 2017. p. 911–30.

Gotlib J, Maxson JE, George TI, Tyner JW. The new genetics of chronic neutrophilic leukemia and atypical CML: implications for diagnosis and treatment. Blood. 2013;122:1707–11.

Reiter A, Gotlib J. Myeloid neoplasms with eosinophilia. Blood. 2017;129:704–14.

Wang SA, Tam W, Tsai A, Arber DA, Hasserjian RP, Geyer JT, et al. Targeted next-generation sequencing identifies a subset of idiopathic hypereosinophilic syndrome with features similar to chronic eosinophilic leukemia, not otherwise specified. Mod Pathol. 2016;29:854–64.

Wang SA, Hasserjian RP, Tam W, Tsai AG, Geyer JT, George TI, et al. Bone marrow morphology is a strong discriminator between chronic eosinophilic leukemia, not otherwise specified from reactive idiopathic hypereosinophilic syndrome. Haematologica. 2017. [Epub ahead of print]. https://doi.org/10.3324/haematol.2017.165340.

Myeloid and Lymphoid Neoplasms with Eosinophilia

16

Joanna M. Chaffin and Natasha Marie Savage

Myeloid and lymphoid neoplasms with eosinophilia and abnormalities of *PDGFRA*, *PDGFRB*, or *FGFR1* were first formally accepted as a set of entities in the 2008 edition of the World Health Organization's *Classification of Tumours of Haematopoietic and Lymphoid Tissues*. In the 2016 edition, myeloid and lymphoid neoplasms with eosinophilia and t(8;9)(p22;p24.1);*PCM1-JAK2* are now recognized as a provisional entity. Collectively, these represent a heterogeneous group of neoplasms in which eosinophilia is typical but not required. Most commonly, patients are men in their 40s or 50s, although they may present across a broad age range. Abnormalities of *PDGFRA* usually resemble chronic eosinophilic leukemia (CEL). Rarely, patients may display characteristics of acute myeloid leukemia (AML) or T lymphoblastic leukemia/lymphoma (T-ALL), although eosinophilia remains a consistent feature. Additionally, mast cells with abnormal immunophenotype may be increased in bone marrow biopsies, mimicking systemic mastocytosis (SM). Most abnormalities of *PDGFRA* are the result of a cryptic 4q12 (*CHIC2*) deletion, necessitating fluorescence in situ hybridization (FISH) analysis or polymerase chain reaction (PCR) for identification (Figs. 16.1, 16.2, 16.3, 16.4, 16.5, 16.6, 16.7, 16.8, 16.9, and 16.10, Table 16.1). Patients with abnormalities of *PDGFRB* often present with features of chronic myelomonocytic leukemia (CMML) with eosinophilia, but atypical chronic myeloid leukemia (aCML), CEL, and juvenile myelomonocytic leukemia (JMML) phenotypes are also reported (Figs. 16.11, 16.12, 16.13, 16.14, 16.15, and 16.16, Table 16.2). The presentation of abnormalities of *FGFR1* is highly variable and partly dependent on the specific gene rearrangement (Figs. 16.17, 16.18, 16.19, and 16.20, Table 16.3). In t(8;13)(p11;q12), lymphadenopathy is common, and a "bilineal lymphoma" phenotype is often seen. In t(8;9)(p11;q33), monocytosis and tonsillar involvement are characteristic. The t(6;8)(q27;p11–12) presents in an older age group with more prominent eosinophilia and erythrocytosis. Unlike abnormalities of *PDGFRA*, conventional karyotyping can detect most abnormalities associated with *PDGFRB* and *FGFR1*. The recognition of these neoplasms is vital, as patients with abnormalities of *PDGFRA* and *PDGFRB* are exquisitely sensitive to imatinib. Unfortunately, definitive, effective targeted monotherapy has not yet been discovered for patients with abnormalities of *FGFR1*, resulting in a poor prognosis. The use of ponatinib in combination with chemotherapy and possible allogeneic transplantation may improve the prognosis, however.

J.M. Chaffin • N.M. Savage (✉)
Department of Pathology, Medical College of Georgia at Augusta University, Augusta, GA, USA
e-mail: jomchaffin@gmail.com; nsavage@augusta.edu

T.I. George, D.A. Arber (eds.), *Atlas of Bone Marrow Pathology*, Atlas of Anatomic Pathology,
https://doi.org/10.1007/978-1-4939-7469-6_16

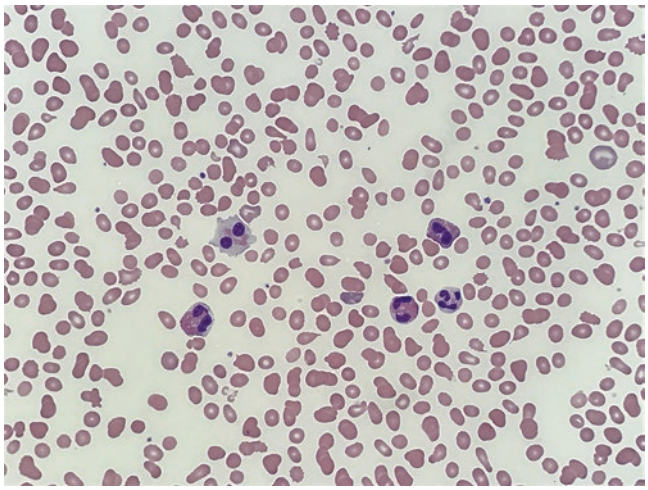

Fig. 16.1 Previously, most patients with eosinophilia and abnormalities of *PDGFRA* fell into the wastebasket category of hypereosinophilic syndrome (HES) [1]. However, we now know that between 10% and 25% of patients with "HES" have abnormalities of *PDGFRA* [2]. Peripheral blood samples typically show features of chronic eosinophilic leukemia (CEL), although occasional patients present with acute myeloid leukemia (AML), T lymphoblastic leukemia/lymphoma (T-ALL), or rarely myeloid sarcoma [3–5]. Even with phenotypic presentations other than CEL, peripheral eosinophilia usually remains a consistent feature. "Normal" eosinophils are round to oval, 10 to 15 μm in diameter, and have a nuclear-cytoplasmic ratio of 1:3. They are identified via their characteristic refractile coarse, orange-red granules, which are typically uniform in size and generally evenly fill the cytoplasm. In the most mature eosinophil form, the nucleus segments into two or more lobes connected by a thin filament; about 80% of segmented eosinophils will have a two-lobed appearance, with lobes of equal size and ovoid shape, with dense chromatin. The remainder of segmented eosinophils will have three lobes, and occasionally an eosinophil will exhibit four or five lobes. In patients with abnormalities of *PDGFRA*, eosinophilic atypia may be present, but it is variable and not required [3]. Moreover, eosinophils are typically mature, with only rare eosinophilic precursors. Anemia and thrombocytopenia are common, whereas monocytosis and basophilia are infrequent [6]. In this peripheral blood smear example, eosinophilic morphology is variable

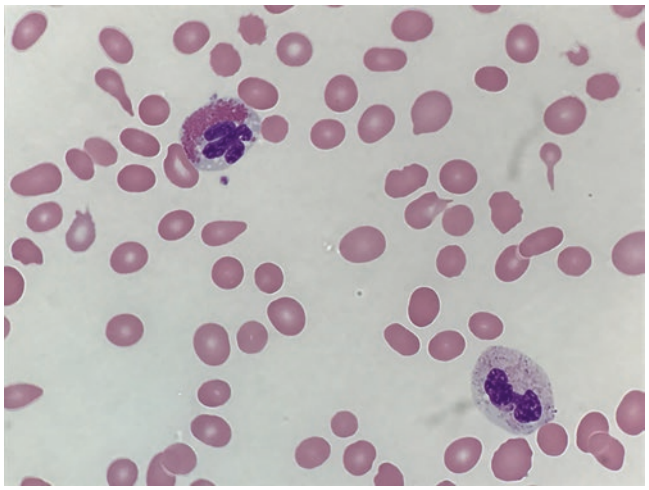

Fig. 16.2 In this smear obtained from a patient with *PDGFRA* abnormality, granules puddle to one side, unevenly filling the cytoplasm. In addition, the nuclear segmentation is atypical, with a "cross-like" appearance. In the lower right corner, a dysplastic granulocyte is seen with hypogranular cytoplasm

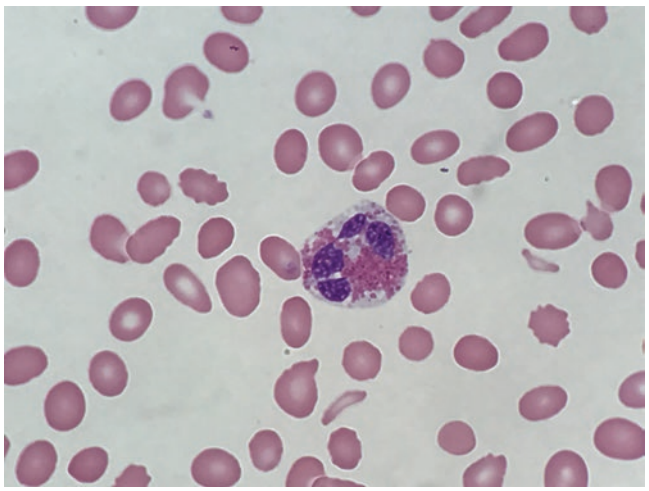

Fig. 16.3 Review of the smear from the same patient as in Fig. 16.2 also revealed occasional mature eosinophils with increased nuclear lobes (four in this example). Although most "normal" eosinophils have only two nuclear lobes, having three or more lobes does not necessarily mean a malignant diagnosis, as these can be seen in patients with benign, secondary eosinophilia, which may be due to skin rash, allergies, asthma, certain infections, and other lymphoproliferative processes. Nevertheless, eosinophilic morphologic atypia may help direct the workup

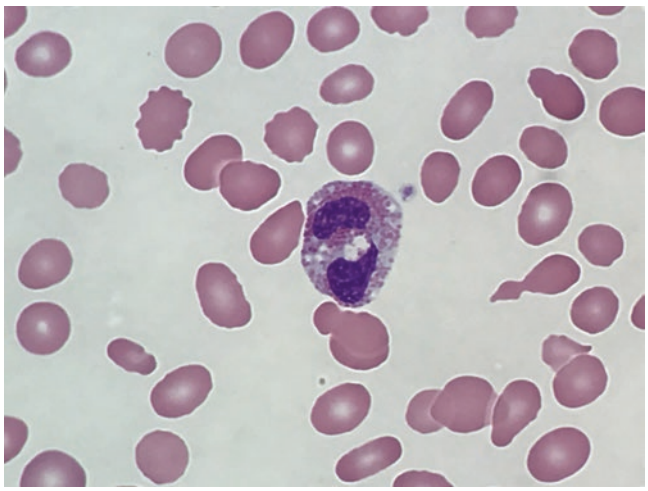

Fig. 16.4 In this eosinophil, the only abnormality is a few cytoplasmic vacuoles; the morphology is otherwise typical, with a bilobed nuclear appearance and a thin filament connecting the two "potato-shaped" nuclear lobes. In the background, red blood cells and platelets are slightly decreased; occasional dacrocytes and several echinocytes are noted

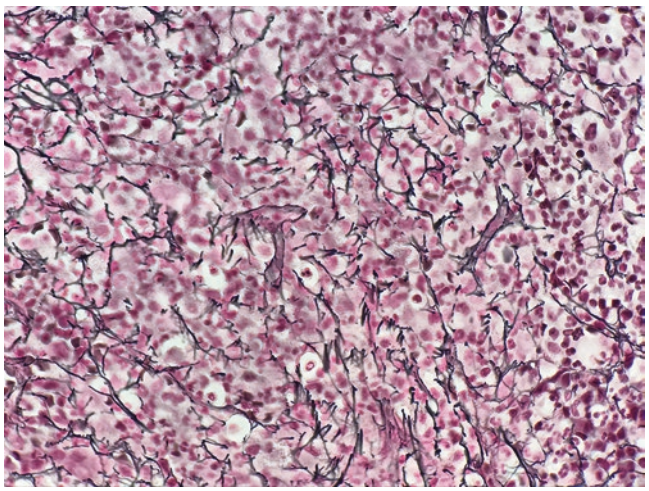

Fig. 16.6 Fibrosis may also be increased, as seen in this example via reticulin histochemical stain. This fibrosis accounts for the dacrocytes noted in the peripheral blood smear

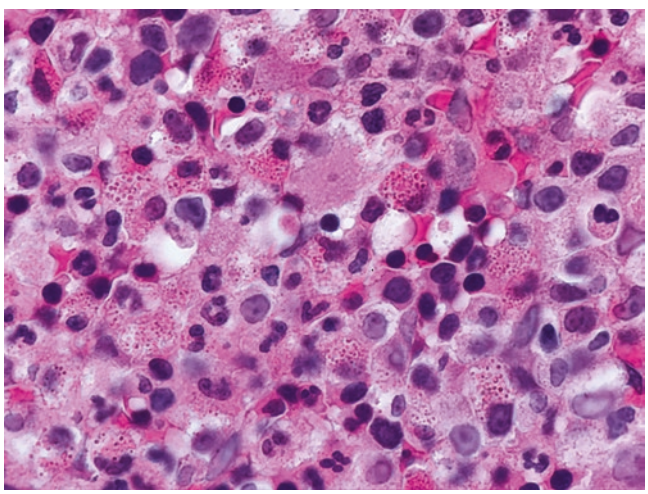

Fig. 16.5 In patients with abnormalities of *PDGFRA*, bone marrow trephine biopsies are typically hypercellular with increased eosinophils and their precursors [3]. These eosinophils may show evidence of activation by immunophenotyping, with CD23, CD25, and/or CD69 positivity. In this example, the bone marrow biopsy is hypercellular owing to a granulocyte hyperplasia, including numerous eosinophilic precursors

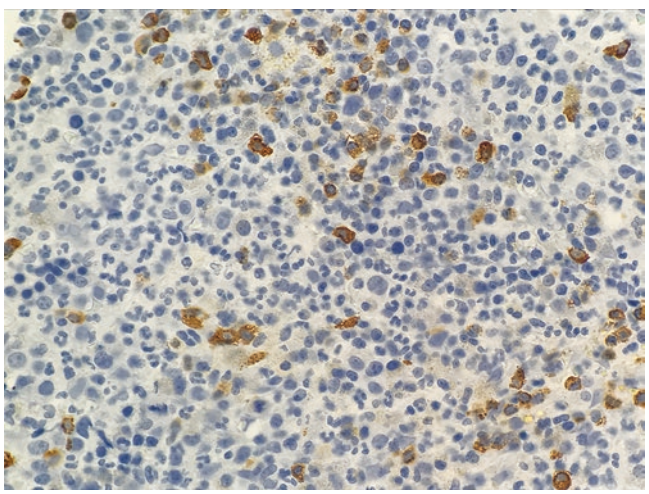

Fig. 16.7 Mast cells are often increased as well, in a loose fashion or sometimes in cohesive clusters [3]. Because of atypical features such as spindled morphology and/or aberrant immunophenotype, patients with abnormalities of *PDGFRA* may be confused with those having systemic mastocytosis (SM). Although aberrant mast cell immunophenotype and atypical morphology may be noted, *KIT* D816V mutation is not present, and serum tryptase levels are usually less than 20 ng/mL, so the diagnostic criteria for SM are not typically met. In this example, mast cells are prominently increased but without dense clustering as is typical for SM; moreover, spindled forms are rarely seen (mast cell tryptase immunohistochemical stained bone marrow biopsy)

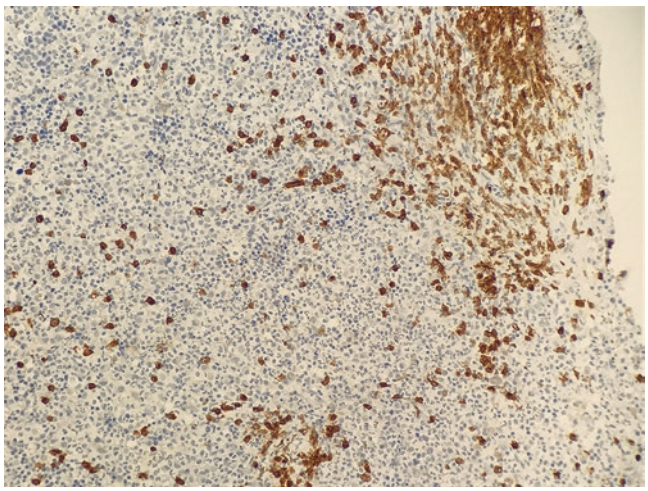

Fig. 16.8 In this patient with *PDGFRA* abnormality, one dense cluster of mast cells is noted via CD117 stain (upper right). In addition, mast cells are also increased in an interstitial, noncohesive fashion. In the background, a hypercellular marrow is appreciated, with myeloid hyperplasia

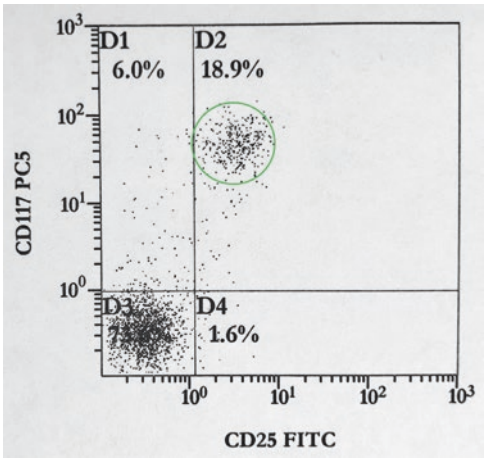

Fig. 16.9 The mast cell immunophenotype may be atypical in patients with abnormalities of *PDGFRA*, with most cases being CD25 positive and CD2 negative, but even CD2/CD25 positive cases have been described [3]. In our lab, a custom tube is performed to detect CD117-bright events, as mast cells generally express brighter levels of CD117 than other cells in the marrow. These CD117-bright events (i.e., mast cells) usually fall within the monocyte-to-granulocyte gate. In this patient with a *PDGFRA* abnormality, a CD25 versus CD117 flow cytometry histogram shows a dense cluster of CD117-bright mast cells with aberrant CD25 (green circle)

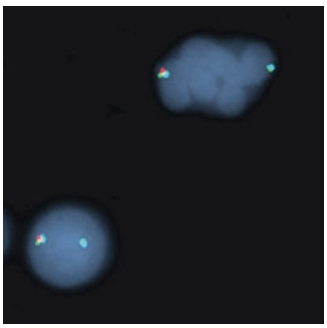

Fig. 16.10 Although a number of fusion partners for *PDGFRA* have been identified (Table 16.1), the most common by far is *FIP1L1* [3]. The *FIP1L1-PDGFRA* fusion gene is created by an interstitial deletion on chromosome 4q12 [1]; this deletion includes cysteine-rich hydrophobic domain 2 (*CHIC2*) [7]. The deletion is most often cryptic, requiring florescence in situ hybridization (FISH) or polymerase chain reaction (PCR) for identification, but rarely it may be caused by chromosomal rearrangement [3, 8, 9]. In this image, *FIP1L1* is denoted by a green probe, *CHIC2* by a red probe, and *PDGFRA* by an aqua probe. Nuclei are seen with one intact *FIP1L1*/*CHIC2*/*PDGFRA* signal and one signal with *FIP1L1*/*PDGFRA* indicating *CHIC2* deletion. Karyotype was normal, stressing the importance of FISH and/or PCR analysis in these patients to detect this cryptic abnormality. Detecting this abnormality is especially important, as an initial dose of 100 mg per day of imatinib leads to complete hematologic response in the majority of patients [10]. More than 90% of patients will achieve a complete molecular response while on maintenance therapy [10, 11] (*PDGFRA* FISH) (Photo courtesy of Dr. Robert Jenkins of the Mayo Clinic)

Table 16.1 Myeloid and lymphoid neoplasms with eosinophilia and abnormalities of *PDGFRA*: reported fusion partners

Fusion partner gene name	Fusion partner gene location
FIP1L1	4q12
BCR	22q11
ETV6	12p13
STRN	2p22
CDK5RAP2	9q33
KIF5B	10p11
FOXP1	3p13

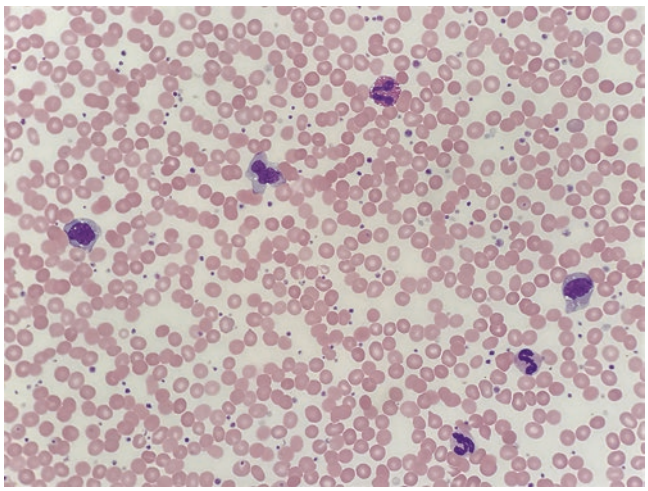

Fig. 16.11 In 1994, Golub et al. first described a *PDGFRB* gene fusion in a patient presenting with a chronic myelomonocytic leukemia (CMML)-like picture [12]. Since that time, over 30 fusion partners have been described [13], far more than in patients with abnormalities of *PDGFRA* (Table 16.2). In patients with abnormalities of *PDGFRB,* peripheral blood and bone marrow are almost always involved; leukocytosis is typical, with possible anemia and thrombocytopenia. Monocytosis and eosinophilia are usually seen. Rarely, basophilia is also prominent. Overall, the phenotypic features are usually in keeping with CMML with eosinophilia, but some patients present with features more suggestive of atypical chronic myeloid leukemia (aCML) or CEL. Rarely, they present with phenotypic features of acute lymphoblastic leukemia (ALL), AML, or juvenile myelomonocytic leukemia (JMML). In this example from a peripheral blood smear, monocytosis is prominent

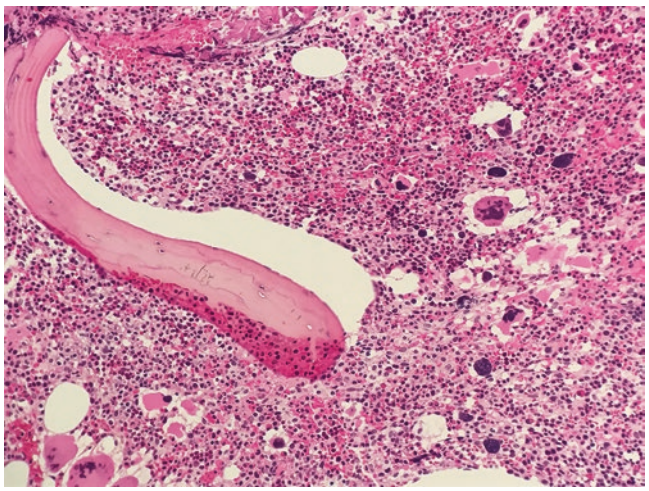

Fig. 16.13 The bone marrow is typically hypercellular with accompanying fibrosis. As in cases with *PDGFRA* abnormalities, mast cell aggregates (not meeting criteria for SM) can be seen. In this example, the hypercellular bone marrow shows granulocytic and megakaryocytic hyperplasia

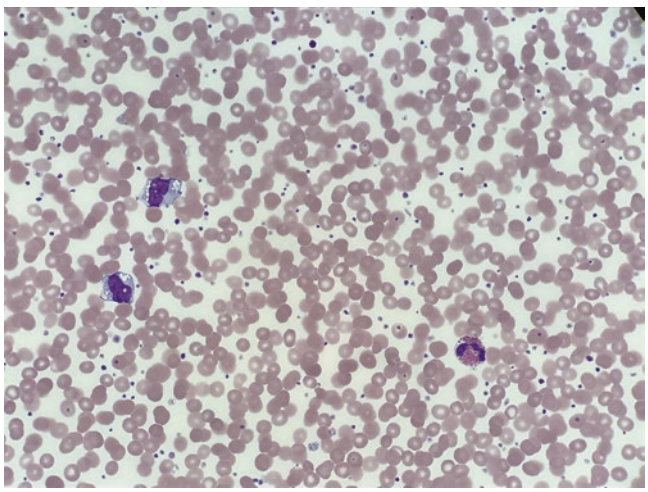

Fig. 16.12 Although eosinophilia may be seen in an otherwise conventional case of CMML, the presence of eosinophilia should alert the pathologist to the possibility of an abnormality of *PDGFRB*. Again, this is especially true given that most patients with abnormalities of *PDGFRB* are now known to have excellent morphologic and molecular response to imatinib, with a recent study citing a 10-year overall survival of 90% [14]. In this patient's peripheral blood smear, monocytosis is seen, along with eosinophilia

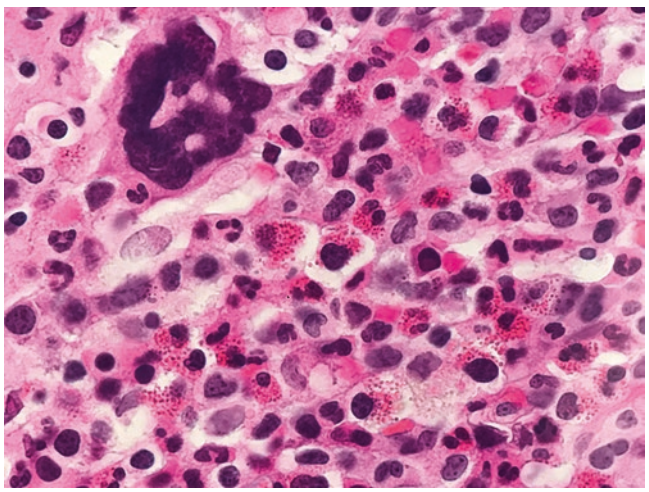

Fig. 16.14 Higher-power examination of the same biopsy as in Fig. 16.13 reveals associated eosinophilia. Note the dysplastic, enlarged megakaryocyte in the upper left corner (hematoxylin and eosin-stained bone marrow biopsy, original magnification ×1000)

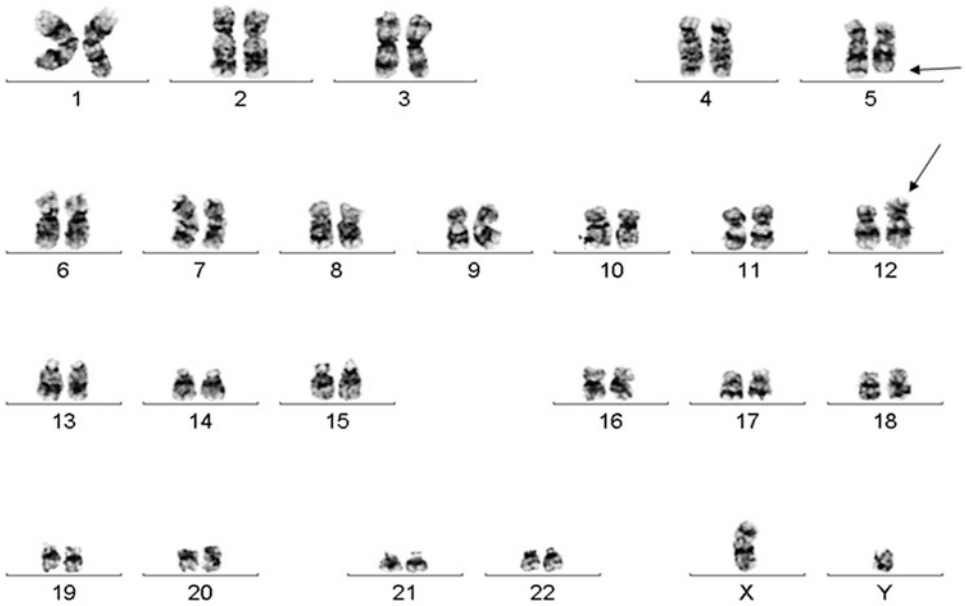

Fig. 16.15 Of the tyrosine kinase receptors described here, *PDGFRB* is the most promiscuous regarding fusion partners (as already stated), but by far the most common fusion is *ETV6-PDGFRB*. Unlike the *FIP1L1-PDGFRA* fusion gene, conventional cytogenetics typically readily identifies 5q33 rearrangements and is therefore useful at the time of initial presentation. In this example, karyotype readily identifies the translocation t(5;12)(q33.1;p13.2), resulting in the formation of the *PDGFRB-ETV6* fusion gene. This G-banded karyotype demonstrates 46,XY,t(5;12)(q33.1;p13.2)

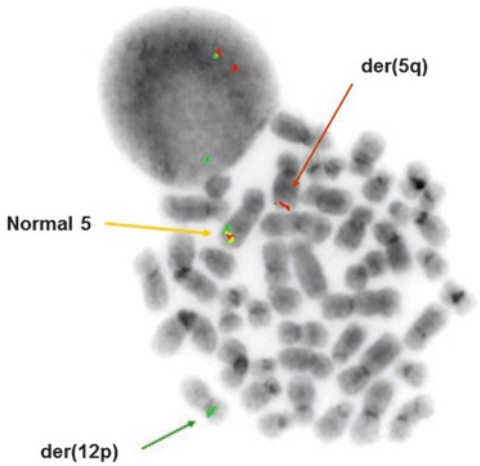

Fig. 16.16 Multicolor FISH has also been useful in recognizing *PDGFRB* rearrangements or confirming suspected fusions detected on karyotype, by using probes that closely flank both ends of the gene [15]. Other probes can be added once a suspected fusion partner is identified. In this example, metaphase FISH with a *PDGFRB* break-apart probe demonstrates one normal signal for chromosome 5 as well as abnormal signals, confirming *PDGFRB* rearrangement

Table 16.2 Myeloid and lymphoid neoplasms with eosinophilia and abnormalities of *PDGFRB*: reported fusion partners and various associations

Fusion partner gene name	Fusion partner gene location	Association
ETV6	12p12	Chronic myelomonocytic leukemia with eosinophilia, chronic eosinophilic leukemia
CCDC88C	14q32	Chronic myelomonocytic leukemia with eosinophilia
CCDC6	10q21	Atypical chronic myeloid leukemia with eosinophilia, myeloproliferative neoplasm with eosinophilia
TRIP11	14q32	Only reported in patients of Asian ancestry
TPM3	1q21	Chronic eosinophilic leukemia
CAPRIN1	1p11	Chronic eosinophilic leukemia
GIT2	12q24	Chronic eosinophilic leukemia
RABEP1	17p13	Chronic myelomonocytic leukemia, T lymphoblastic leukemia
CEP85L	6q22	Myeloproliferative neoplasm with eosinophilia, T lymphoblastic leukemia
PRKG2	4q21	Chronic basophilic leukemia
COL1A1	17q21	
NDE1	16p13	Chronic myelomonocytic leukemia
SPTBN1	2p21	
PDE4DIP	1q21	Myelodysplastic/myeloproliferative neoplasm with eosinophilia
TP53BP1	15q15-q21	Atypical chronic myeloid leukemia with eosinophilia
SPECC1	17p11	Juvenile myelomonocytic leukemia
GOLGA4	3p22	Atypical chronic myeloid leukemia with eosinophilia, myeloproliferative neoplasm with eosinophilia
HIP1	7q11	Chronic myelomonocytic leukemia with eosinophilia
BIN2	12q13	
MYO18A	17q11	
NIN	14q22	Atypical chronic myeloid leukemia with eosinophilia
SART3	12q23	
ERC1	12p13	
WDR48	3p21	Chronic eosinophilic leukemia
DTD1	20p11	
KANK1	9p24	Essential thrombocythemia

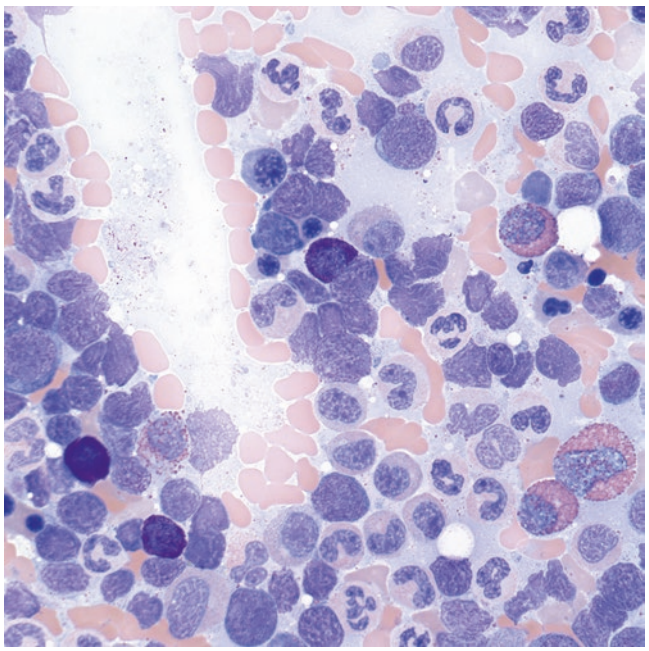

Fig. 16.17 Cases with *FGFR1* abnormalities are much more heterogeneous in presentation than those with abnormalities of *PDGFRA* (typically presenting as CEL) and *PDGFRB* (typically presenting as CMML with eosinophilia) (Table 16.3). In the peripheral blood, leukocytosis is typical, with neutrophilia and a left shift [16]. Eosinophilia is also common (85% of cases), but not as common as in cases *PDGFRA* rearrangements [17]. Other features are often associated with certain fusion partners. Specifically, monocytosis and tonsillar involvement are particularly common in patients with t(8;9)(p11;q33–34) [18]. Basophilia may be seen in patients with t(8;22)(p11;q11), resulting in a diagnostic challenge with the more common and treatable CML [19]. Erythrocytosis may be present, mimicking polycythemia vera (PV), in cases with t(6;8)(q27;p11–12) [20, 21]. The bone marrow is usually hypercellular because of granulocyte hyperplasia and blast counts are variable, but a subset of cases will present in frank acute leukemia: AML, mixed-phenotype acute leukemia, and ALL have been described. In this patient with *FGFR1* translocation, the morphologic features favor a myeloid neoplasm not meeting criteria for acute leukemia. Interestingly, eosinophilia was not noted in the peripheral blood, but could be seen in the bone marrow aspirate smears. In addition, mast cells were increased but without atypia (Photo courtesy of Dr. Robert Ohgami of Stanford University)

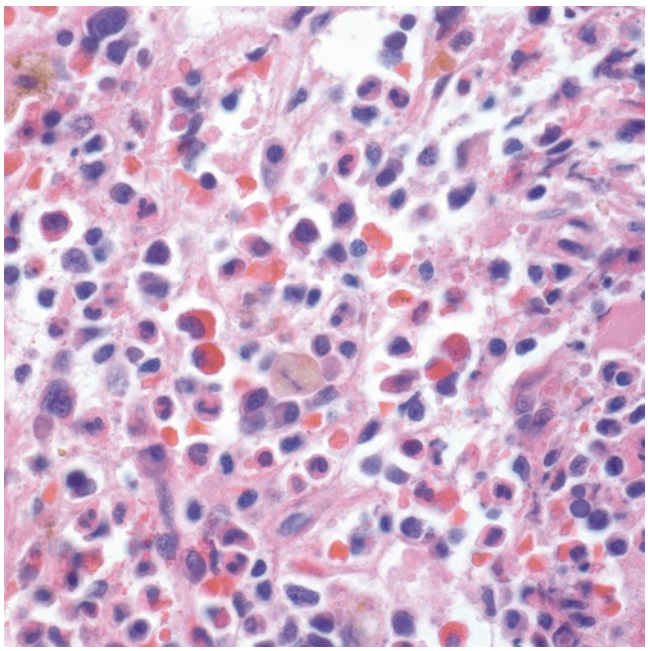

Fig. 16.18 In this biopsy obtained from a patient with t(8;22)(p11;q11), the marrow is hypercellular, with granulocytic hyperplasia and eosinophilia. Similar to cases with *PDGFRB*, most cases will be detected via conventional karyotyping, but unlike *PDGFRA* and *PDGFRB*, definitive targeted monotherapy is not currently available, resulting in a poor prognosis. However, ponatinib in combination with chemotherapy and possible allogeneic transplantation may improve the prognosis [22] (Photo courtesy of Dr. Robert Ohgami of Stanford University)

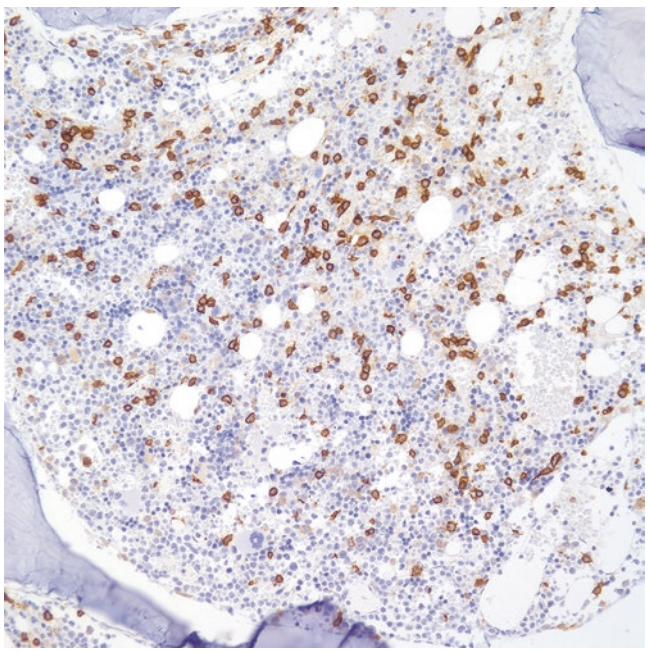

Fig. 16.19 Although not as common as in cases with *PDGFRA* and *PDGFRB* rearrangements, atypical mast cell aggregates with aberrant immunophenotype have been identified in patients with *FGFR1* abnormalities [18]. Mast cells are increased and dispersed singly throughout this biopsy in a patient with abnormality of *FGFR1* (Photo courtesy of Dr. Robert Ohgami of Stanford University)

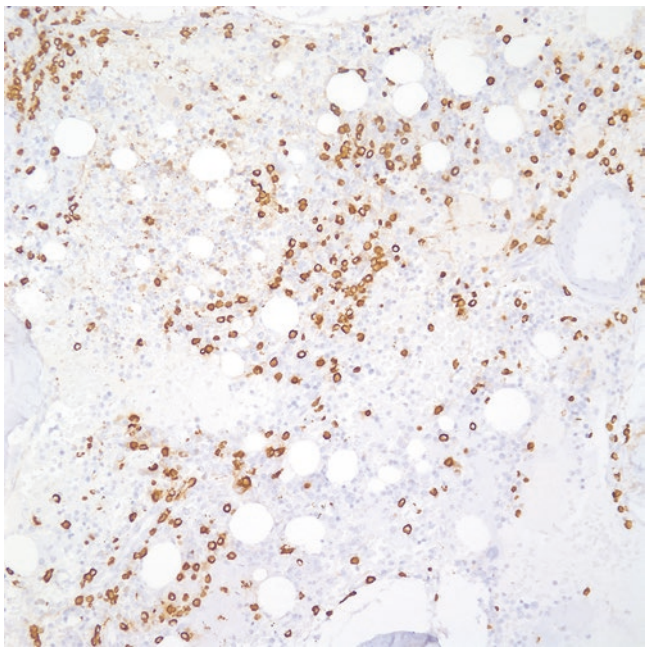

Fig. 16.20 In this patient with abnormality of *FGFR1*, a loose mast cell cluster is seen in the upper left corner. These mast cells did not express CD25 (mast cell tryptase immunohistochemical stained bone marrow biopsy) (Photo courtesy of Dr. Robert Ohgami of Stanford University)

Table 16.3 Myeloid and lymphoid neoplasms with eosinophilia and abnormalities of *FGFR1*: reported fusion partners and various associations

Fusion partner gene name	Fusion partner gene location	Association
ZMYM2 (ZNF198)	13q12	A subset with lymphadenopathy and "bilineal lymphoma"
CNTRL	9q33–34	Monocytosis, tonsillar involvement
FGFR1OP	6q27	Older age, more prominent eosinophilia, erythrocytosis
BCR	8q11	Older age, leukocytosis with neutrophilia and basophilia
Not stated	1q25	Peripheral monocytosis and myeloproliferative neoplasm-like findings in the bone marrow
CUX1	7q22	T lymphoblastic leukemia
NUP98	11p15	Acute myeloid leukemia
ERVK (HERVK)	19q13.3	Acute myeloid leukemia secondary to myelodysplastic/ myeloproliferative neoplasm
FGFR1OP2	12p11	T lymphoblastic lymphoma with eosinophilia
TRIM24 (TIF1)	7q34	
LRRFIP1	2q37	Myelodysplastic syndrome
MYO18A	17q23	Myelodysplastic/ myeloproliferative neoplasm with eosinophilia and basophilia

References

1. Cools J, DeAngelo DJ, Gotlib J, Stover EH, Legare RD, Cortes J, et al. A tyrosine kinase created by fusion of the *PDGFRA* and *FIP1L1* genes as a therapeutic target of imatinib in idiopathic hypereosinophilic syndrome. N Engl J Med. 2003;348:1201–14.
2. Gotlib J. World Health Organization-defined eosinophilic disorders: 2015 update on diagnosis, risk stratification, and management. Am J Hematol. 2015;90:1078–89.
3. Bain BJ, Gilliland DG, Horny HP, Vardiman JW. Myeloid and lymphoid neoplasms with eosinophilia and abnormalities of *PDGFRA*, *PDGFRB* or *FGFR1*. Pathology and genetics of tumours of haematopoietic and lymphoid tissues. In: Swerdlow SH, Campo E, Harris NL, Jaffe ES, Pileri SA, Stein H, et al., editors. World Health Organization classification of tumours. Lyon: IARC Press; 2008. p. 68–73.
4. Metzgeroth G, Walz C, Score J, Siebert R, Schnittger S, Haferlach C, et al. Recurrent finding of the *FIP1L1-PDGFRA* fusion gene in eosinophilia-associated acute myeloid leukemia and lymphoblastic T-cell lymphoma. Leukemia. 2007;21:1183–8.
5. Chen D, Bachanova V, Ketterling RP, Begna KH, Hanson CA, Viswanatha DS. A case of nonleukemia myeloid sarcoma with FIP1L1-PDGFRA rearrangement: an unusual presentation of a rare disease. Am J Surg Pathol. 2013;37:147–51.
6. Savage NM, George TI, Gotlib J. Myeloid neoplasms associated with eosinophilia and rearrangement of *PDGFRA*, *PDGFRB*, and *FGFR1*: a review. Int J Lab Hematol. 2013;35:491–500.
7. Pardanani A, Ketterling RP, Brockman SR, Flynn HC, Paternoster SF, Shearer BM, et al. CHIC2 deletion, a surrogate for *FIP1L1-PDGFRA* fusion, occurs in systemic mastocytosis associated with eosinophilia and predicts response to imatinib mesylate therapy. Blood. 2003;102:3093–6.
8. Baxter EJ, Hochhaus A, Bolufer P, Reiter A, Fernandez JM, Senent L, et al. The t(4;22)(9q12;q11) in atypical chronic myeloid leukaemia fuses BCR to PDGFRA. Hum Mol Genet. 2002;11:1391–7.
9. Tashiro H, Shirasaki R, Noguchi M, Gotoh M, Kawasugi K, Shirafuji N. Molecular analysis of chronic eosinophilic leukemia with t(4;10) showing good response to imatinib mesylate. Int J Hematol. 2006;83:433–8.
10. Legrand F, Renneville A, Macintyre E, Mastrilli S, Ackermann F, Cayuela JM, et al. The spectrum of *FIP1L1-PDGFRA*-associated chronic eosinophilic leukemia: new insights based on a survey of 44 cases. Medicine (Baltimore). 2013;92:e1–9.
11. Pardanani A, D'Souza A, Knudson RA, Hanson CA, Ketterling RP, Tefferi A. Long-term follow-up of *FIP1L1-PDGFRA*-mutated patients with eosinophilia: survival and clinical outcome. Leukemia. 2012;26:2439–41.
12. Golub TR, Barker GF, Lovett M, Gilliland DG. Fusion of *PDGF* receptor-beta to a novel Ets-like gene, *Tel*, in chronic myelomonocytic leukemia with t(512) chromosomal translocation. Cell. 1994;77:307–16.
13. Vega F, Medeiros LJ, Bueso-Ramos CE, Arboleda P, Miranda RN. Hematolymphoid neoplasms associated with rearrangements of *PDGFRA*, *PDGFRB*, and *FGFR1*. Am J Clin Pathol. 2015;144:377–92.
14. Cheah CY, Burbury K, Apperley JF, Huguet F, Pitini V, Gardembas M, et al. Patients with myeloid malignancies bearing *PDGFRB* fusion genes achieve durable long-term remissions with imatinib. Blood. 2014;123:3574–7.
15. Baxter EJ, Kulkarni S, Vizmanos JL, Jaju R, Martinelli G, Testoni N, et al. Novel translocations that disrupt the platelet-derived growth factor receptor beta (*PDGFRB*) gene in *BCR-ABL*-negative chronic myeloproliferative disorders. Br J Haematol. 2003;120:251–6.
16. Jackson CC, Medeiros LJ, Miranda RN. 8p11 myeloproliferative syndrome: a review. Hum. Pathol. 2010;41:461–76.
17. Patnaik MM, Gangat N, Knudson RA, Keefe JG, Hanson CA, Pardanani A, et al. Chromosome 8p11.2 translocations: prevalence, FISH analysis for *FGFR1* and *MYST3*, and clinicopathologic correlates in a consecutive cohort of 13 cases from a single institution. Am J Hematol. 2010;85:238–42.
18. Savage NM, Johnson RC, Gotlib J, George TI. Myeloid and lymphoid neoplasms with *FGFR1* abnormalities: diagnostic and therapeutic challenges. Am J Hematol. 2013;88:427–30.
19. Demiroglu A, Steer EJ, Heath C, Taylor K, Bentley M, Allen SL, et al. The t(8;22) in chronic myeloid leukemia fuses *BCR* to *FGFR1*: transforming activity and specific inhibition of *FGFR1* fusion proteins. Blood. 2001;98:3778–83.
20. Popovici C, Zhang B, Grégoire MJ, Jonveaux P, Lafage-Pochitaloff M, Birnbaum D, et al. The t(6;8)(q27;p11) translocation in a stem cell myeloproliferative disorder fuses a novel gene, *FOP*, to fibroblast growth factor receptor 1. Blood. 1999;93:1381–9.
21. Vizmanos JL, Hernández R, Vidal MJ, Larráyoz MJ, Odero MD, Marín J, et al. Clinical variability of patients with the t(6;8)(q27;p12) and *FGFR1OP-FGFR1* fusion: two further cases. Hematol J. 2004;5:534–7.
22. Khodadoust MS, Luo B, Medeiros BC, Johnson RC, Ewalt MD, Schalkwyk AS, et al. Clinical activity of ponatinib in a patient with *FGFR1*-rearranged mixed-phenotype acute leukemia. Leukemia. 2016;30:947–50.

Myelodysplastic/Myeloproliferative Neoplasms (MDS/MPN)

17

Aaron Paul Rupp and Devon Chabot-Richards

Myelodysplastic/myeloproliferative neoplasms (MDS/MPN) are a group of entities comprised of clonal myeloid neoplasms with shared myeloproliferative and myelodysplastic features:

- Chronic myelomonocytic leukemia (CMML) (Figs. 17.1, 17.2, 17.3, 17.4, 17.5, 17.6, 17.7, 17.8, 17.9, and 17.10)
- Atypical chronic myeloid leukemia (aCML) (Figs. 17.11, 17.12, 17.13, 17.14, 17.15, and 17.16)
- Juvenile myelomonocytic leukemia (JMML) (Figs. 17.17, 17.18, 17.19, 17.20, 17.21, and 17.22)
- Myelodysplastic/myeloproliferative neoplasm, unclassifiable (MDS/MPN, U) (Figs. 17.23, 17.24, 17.25, and 17.26)
- Myelodysplastic/myeloproliferative neoplasm with ring sideroblasts and thrombocytosis (MDS/MPN-RS-T) (Figs. 17.27, 17.28, 17.29, 17.30, and 17.31)

Shared features typically include cytopenia(s), unilineage or multilineage dysplasia, hypercellular bone marrow with certain increased circulating cell types, and less than 20% blasts. Recent updates with the World Health Organization classification of myeloid neoplasms and acute leukemia focus on the expanding role of cytogenetic and molecular studies in accurately classifying MDS/MPN, in addition to clinical, laboratory, and morphologic criteria.

A.P. Rupp (✉) • D. Chabot-Richards
Department of Pathology, University of New Mexico,
Albuquerque, NM, USA
e-mail: arupp@salud.unm.edu; dchabot-richards@salud.unm.edu

T.I. George, D.A. Arber (eds.), *Atlas of Bone Marrow Pathology*, Atlas of Anatomic Pathology,
https://doi.org/10.1007/978-1-4939-7469-6_17

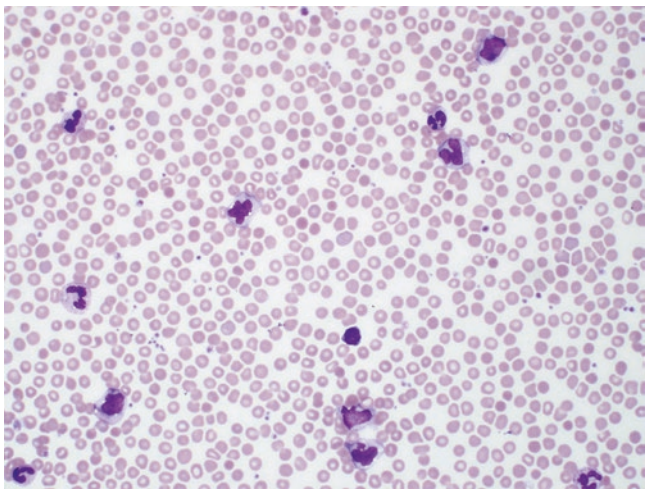

Fig. 17.1 Chronic myelomonocytic leukemia (CMML). This peripheral blood smear demonstrates monocytosis with a predominance of mature forms as well as dimorphic erythrocytes with mild anisocytosis and poikilocytosis. The diagnosis of CMML includes the criterion of persistent peripheral blood monocytosis greater than 1×10^9/L and greater than 10% monocytes on differential

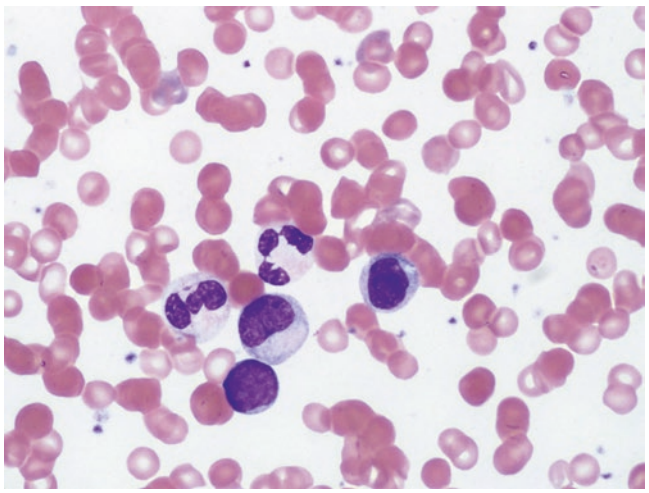

Fig. 17.3 Chronic myelomonocytic leukemia (CMML). Higher magnification of a peripheral blood smear reveals a left shift including blasts with a spectrum of maturation of the monocyte precursors with associated dysplastic hypogranular neutrophils. Dysplasia in one or more myeloid lineages is included in the diagnostic criteria for CMML. If dysplasia is absent or minimal, a diagnosis of CMML can still be made if a cytogenetic or molecular abnormality is present (excluding *BCR-ABL1* fusion, *PDGFRA* rearrangement, *PDGFRB* rearrangement, *FGFR1* rearrangement, or *PCM1-JAK2* fusion) and other causes of monocytosis have been excluded. The most common genetic findings are +8, −7/del(7q), and 12p abnormalities

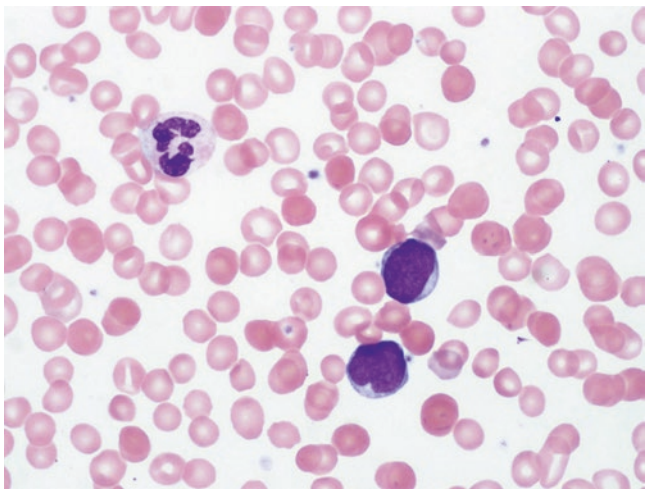

Fig. 17.2 Chronic myelomonocytic leukemia (CMML). Higher magnification of a peripheral blood smear reveals a blast and a promonocyte; promonocytes are blast equivalents for this diagnosis. For a diagnosis of CMML, the blasts (myeloblasts and monoblasts) and blast equivalents (promonocytes) must comprise less than 20% of cells in the blood or bone marrow

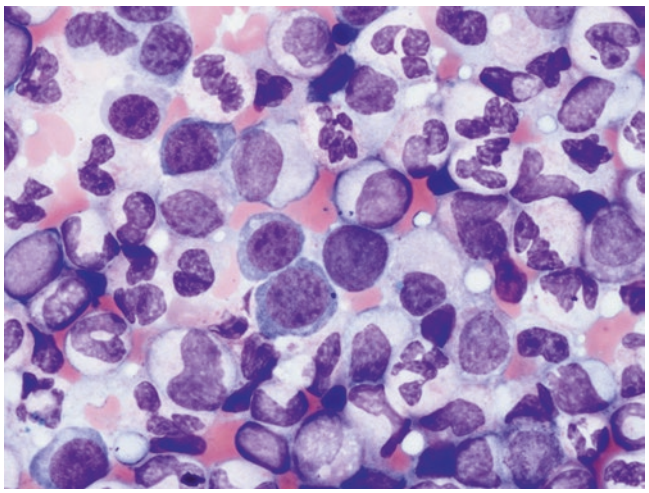

Fig. 17.4 Chronic myelomonocytic leukemia (CMML). This bone marrow aspirate demonstrates complete and sequential maturation with increased monocytic precursors and monocytes. An accurate differential count of immature monocytes is critical. Monoblasts show fine, open chromatin and may have prominent nucleoli. The nuclear contours are smooth with only minimal irregularity. Dysgranulopoiesis is present, with hypogranular neutrophils and rare pelgeroid forms observed

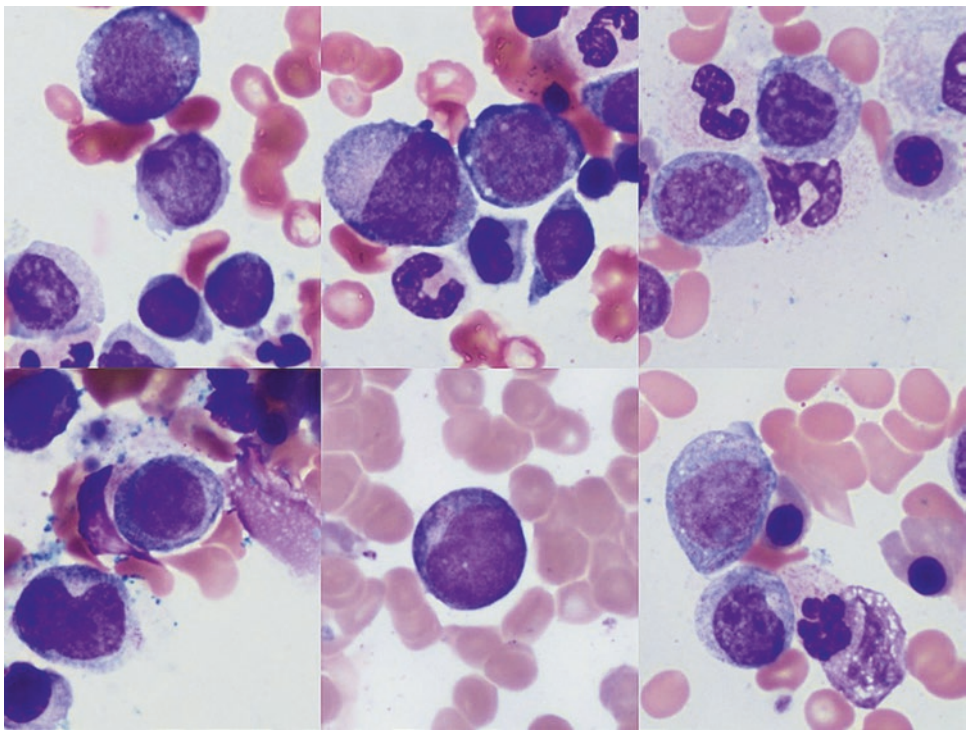

Fig. 17.5 Chronic myelomonocytic leukemia (CMML). Promonocytes, an intermediate form between monoblasts and mature monocytes, are included in the blast count when evaluating for CMML and may present a challenge when counting cells from the peripheral blood or bone marrow, as precise morphologic evaluation is essential for diagnosis. These cells have more mature nuclear chromatin, light nuclear folds or creases, and nucleoli. The cytoplasm is light blue to gray, and a few lilac-colored granules and vacuoles may be seen

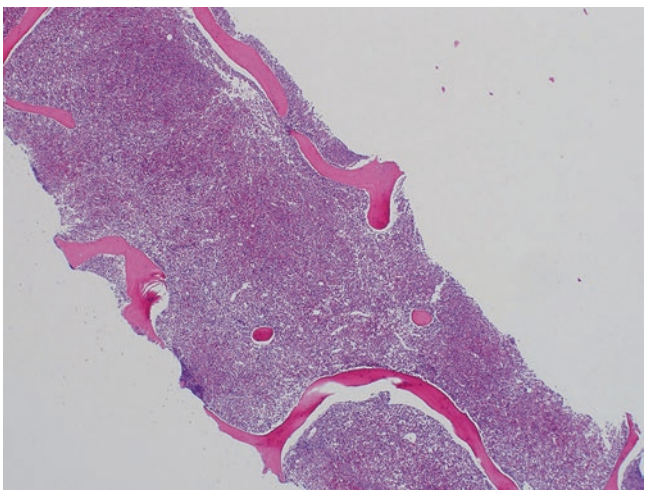

Fig. 17.6 Chronic myelomonocytic leukemia (CMML). CMML is a clonal malignancy with features of both myeloproliferation and myelodysplasia. The hypercellular bone marrow demonstrates the myeloproliferative component of CMML with a cellularity of 100%. A hypercellular bone marrow with a proliferation of myeloid and monocytic lineages is common in CMML, but normocellular or hypocellular marrows may occur

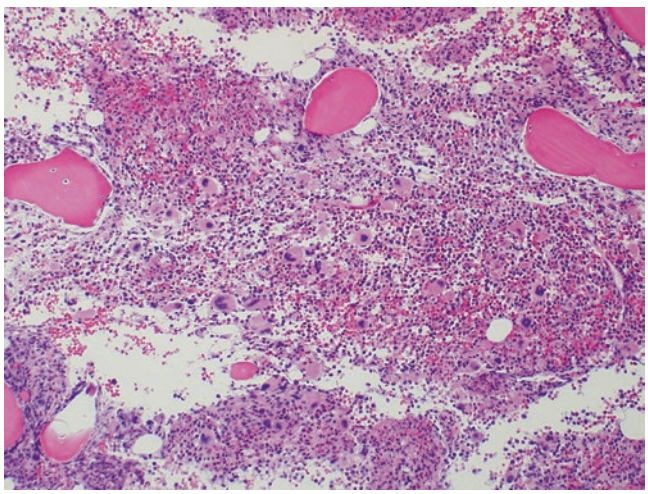

Fig. 17.7 Chronic myelomonocytic leukemia (CMML). In this higher-power view of the bone marrow, megakaryocytic dysplasia is apparent, with small, clustered, and hypolobated forms present

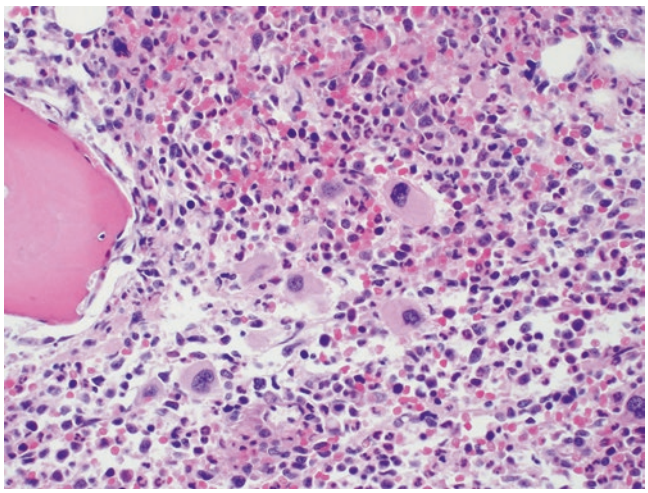

Fig. 17.8 Chronic myelomonocytic leukemia (CMML). Small and hypolobated megakaryocytes are apparent in this bone marrow biopsy specimen. Dysplasia in megakaryocytes is common in CMML. Dysmegakaryocytopoiesis includes micromegakaryocytes, nuclear hypolobation, and multinucleation

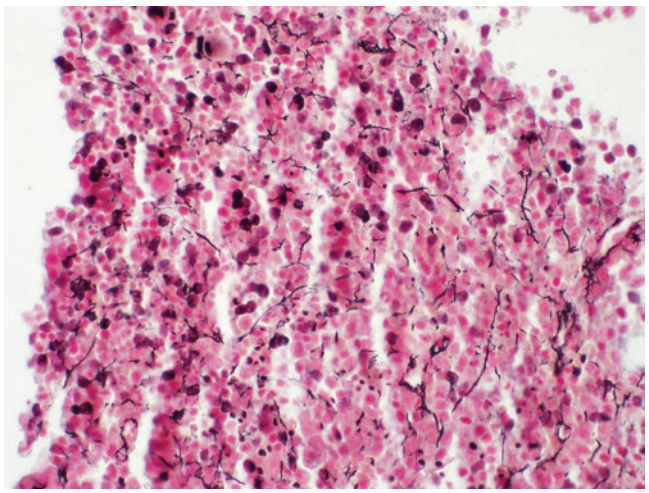

Fig. 17.10 Chronic myelomonocytic leukemia (CMML). Reticulin fibers are highlighted by a reticulin stain on the bone marrow biopsy specimen. A mild to moderate increase in reticulin fibers may be present in CMML

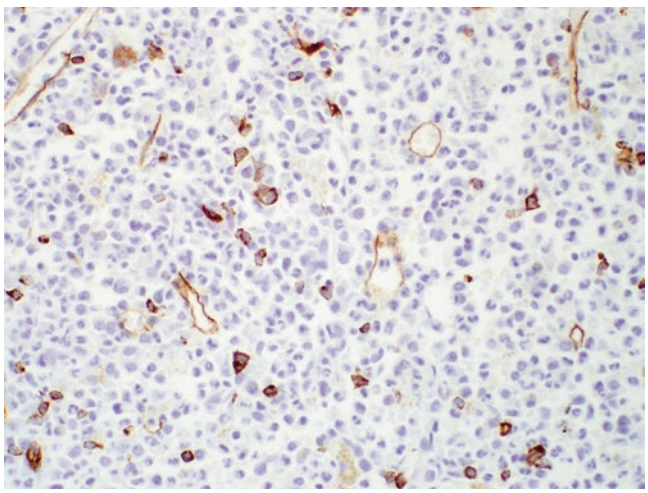

Fig. 17.9 Chronic myelomonocytic leukemia (CMML). Myeloblasts are highlighted by immunohistochemistry for CD34 on the bone marrow biopsy. True monoblasts are typically CD34 negative, but myeloblasts may also be increased in CMML. For a diagnosis of CMML, the blasts (myeloblasts and monoblasts) and blast equivalents (promonocytes) must comprise less than 20% of cells in the blood or bone marrow. The blast count separates CMML-0 (less than 2% blasts in peripheral blood and less than 5% in bone marrow) from CMML-1 (2–4% blasts in peripheral blood and 5–9% blasts in bone marrow) and CMML-2 (5–19% blasts in peripheral blood, 10–19% in the bone marrow, or the presence of Auer rods), which carries prognostic importance

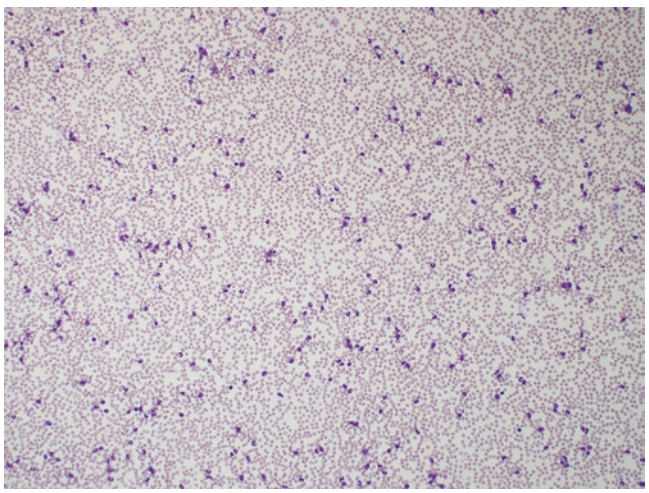

Fig. 17.11 Atypical chronic myeloid leukemia (aCML). This peripheral blood smear demonstrates leukocytosis. The diagnosis of aCML requires leukocytosis (WBC $\geq 13 \times 10^9$/L). Further workup is required. *BCR-ABL1* fusion, *PDGFRA* rearrangement, and *PDGFRB* rearrangements must be excluded. Separating aCML from chronic neutrophilic leukemia (CNL) may include workup for *CSF3R* mutations (more common in CNL), *SETBP1* mutations (more common in aCML), and/or *ETNK1* mutations (more common in aCML)

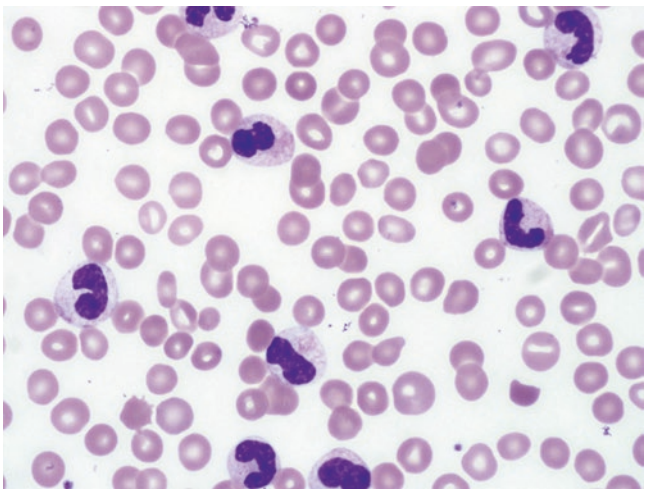

Fig. 17.12 Atypical chronic myeloid leukemia (aCML). A peripheral blood smear demonstrates dysgranulopoiesis with pelgeroid neutrophils showing decreased granulation. Dysplasia in neutrophils may include size aberration, hypolobation, irregular hypersegmentation, decreased granularity, abnormal granules, and/or Auer rods. A diagnosis of aCML includes the diagnostic criterion of prominent dysgranulopoiesis. Blast count of the peripheral blood (or bone marrow) should not exceed 20%

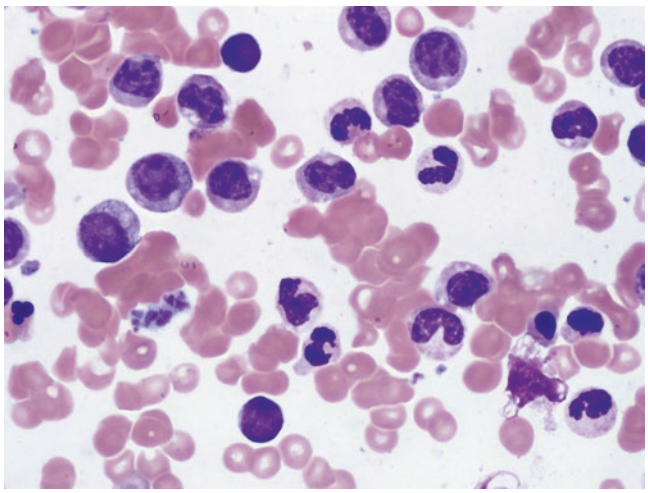

Fig. 17.14 Atypical chronic myeloid leukemia (aCML). In aCML, neutrophil precursors must comprise at least 10% of leukocytes, and there must be only minimal basophilia or monocytosis. Prominent dysgranulopoiesis is required in aCML; however, dysplasia may be seen in erythroid (pictured) and megakaryocytic lineages. Dyserythropoiesis includes nuclear budding, nuclear bridging, karyorrhexis, multinucleation, hyperlobation, and megaloblastoid change, as well as cytoplasmic morphologic abnormalities including ring sideroblasts, vacuolization, and periodic acid-Schiff positivity

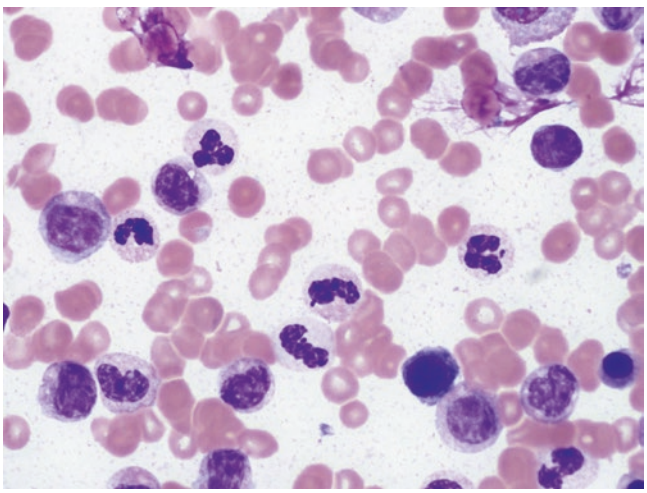

Fig. 17.13 Atypical chronic myeloid leukemia (aCML). This bone marrow aspirate demonstrates morphology similar to that of the peripheral blood smear. Dysplastic, hypogranulated neutrophils with exaggerated chromatin clumping are present. Myeloid precursors are increased, with numerous myelocytes

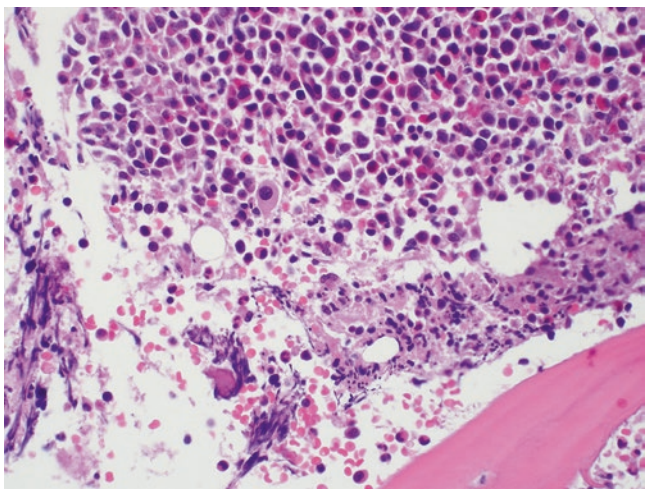

Fig. 17.15 Atypical chronic myeloid leukemia (aCML). aCML is a clonal malignancy with features of both myeloproliferation and myelodysplasia. This hypercellular bone marrow biopsy specimen demonstrates the myeloproliferative component of aCML, with hypercellularity due to a maturing granulocytic proliferation with left shift. Erythroid precursors are decreased. For aCML, the blast count of the bone marrow should not exceed 20%

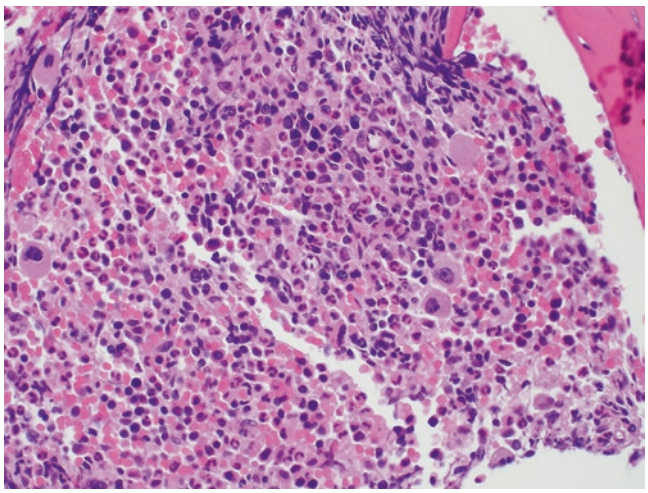

Fig. 17.16 Atypical chronic myeloid leukemia (aCML). Prominent dysgranulopoiesis is required in aCML, but dysplasia also may be seen in erythroid and megakaryocytic (pictured) lineages. Dysmegakaryocytopoiesis includes micromegakaryocytes, nuclear hypolobation, and multinucleation. The bone marrow biopsy reveals small, dysplastic, hypolobated megakaryocytes within the hypercellular granulocytic proliferation

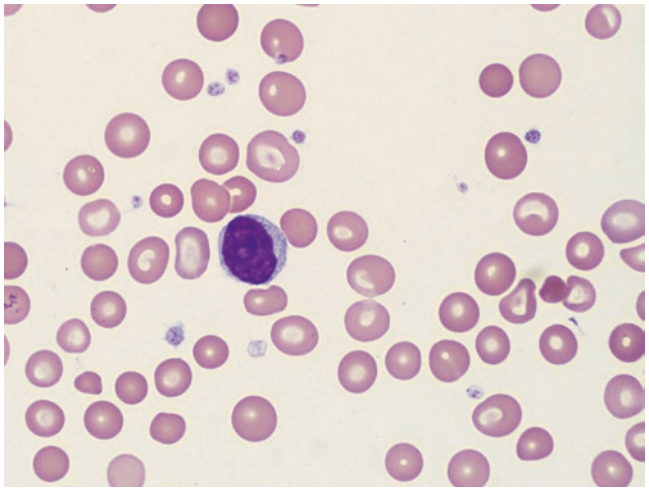

Fig. 17.18 Juvenile myelomonocytic leukemia (JMML). A peripheral blood smear demonstrates a prototypic promonocyte with abundant light gray-to-blue cytoplasm, fine chromatin, and nuclear folding. Prominent nucleoli or lilac-colored granules may or may not be present. In JMML, blasts and equivalents (promonocytes) must be less than 20% in the peripheral blood or bone marrow

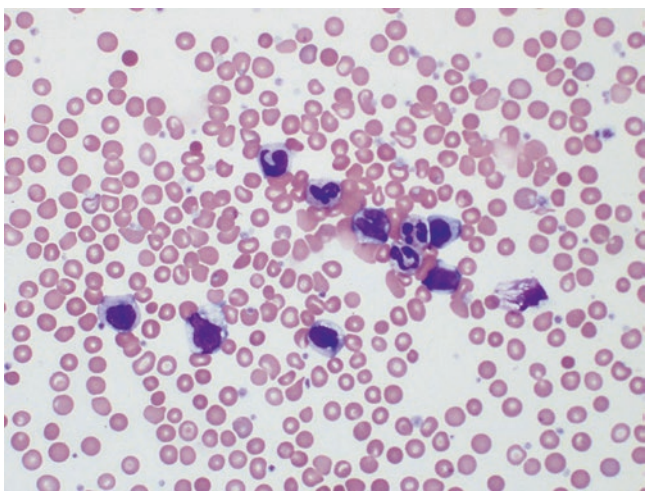

Fig. 17.17 Juvenile myelomonocytic leukemia (JMML). This blood smear in JMML shows anemia, neutropenia, and monocytosis. Diagnostic criteria for JMML are complex and were recently updated. Four criteria must be initially met: monocytosis, blasts and equivalents (promonocytes) less than 20%, splenomegaly, and absence of a *BCR-ABL1* rearrangement. JMML may then be diagnosed if a genetic abnormality involving *PTPN11*, *KRAS*, *NRAS*, *CBL*, or *NF1* is present. If not, then monosomy 7 (or any other chromosomal abnormality) plus two of the following is required for diagnosis: increased hemoglobin F, immature granulocytes or nucleated red blood cells on the peripheral blood smear, GM-CSF hypersensitivity in vitro, or STAT5 hyperphosphorylation

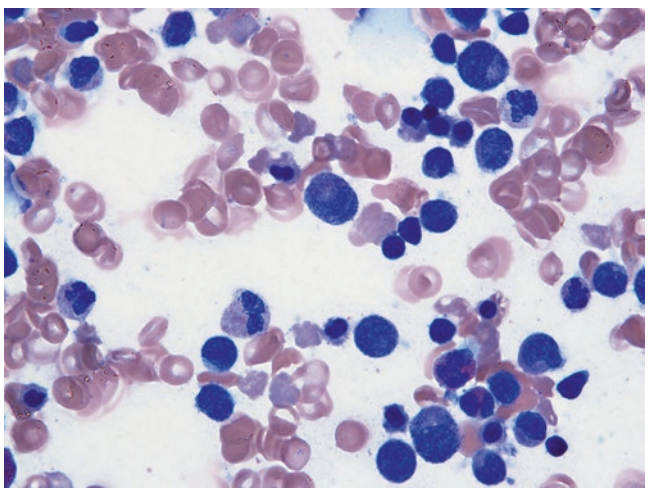

Fig. 17.19 Juvenile myelomonocytic leukemia (JMML). Erythroid and megakaryocytic abnormalities are common in JMML, but these findings are nonspecific. This bone marrow aspirate demonstrates erythroid dysplasia with nuclear budding. Megaloblastoid changes are often present. Note that there is not an increase in blasts, as blasts and equivalents (promonocytes) must be less than 20% in the peripheral blood or bone marrow in JMML

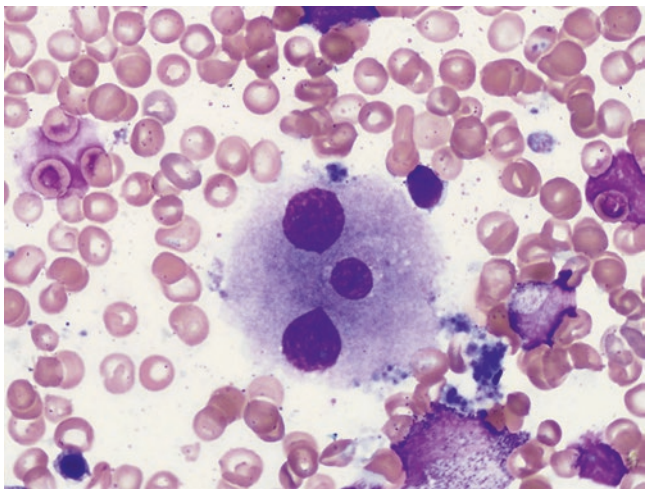

Fig. 17.20 Juvenile myelomonocytic leukemia (JMML). Erythroid and megakaryocytic abnormalities are common in JMML. This bone marrow aspirate demonstrates dysmegakaryopoiesis with prominent, separated nuclei ("pawn ball" morphology)

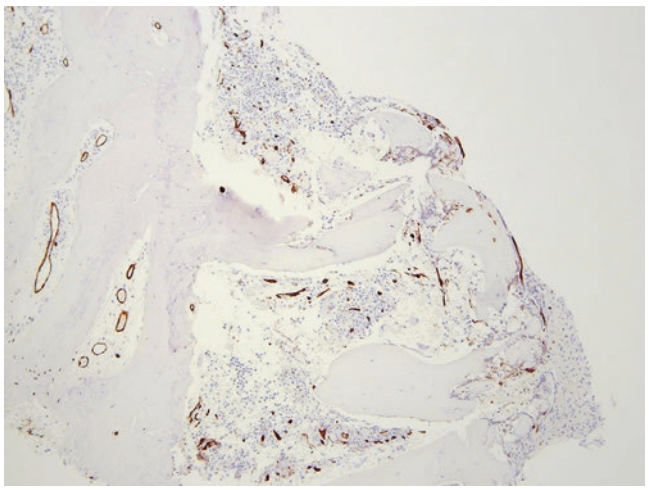

Fig. 17.22 Juvenile myelomonocytic leukemia (JMML). CD34 immunohistochemistry on the bone marrow biopsy does not reveal increased blasts. In JMML, blasts and equivalents (promonocytes) must be less than 20% in the peripheral blood or bone marrow and are typically less than 5% of the cellular marrow

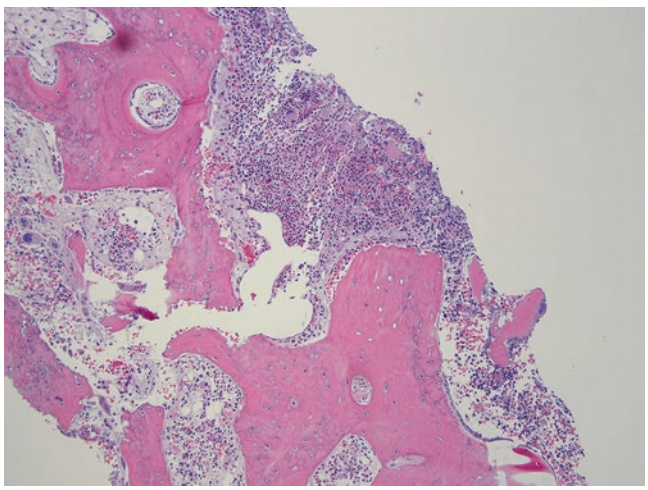

Fig. 17.21 Juvenile myelomonocytic leukemia (JMML). The bone marrow findings in JMML are variable. This bone marrow biopsy is hypercellular for age, with increased granulocytes. There is left shift of the granulocytic and erythroid lineages. A reticulin stain may show a mild increase in fibrosis

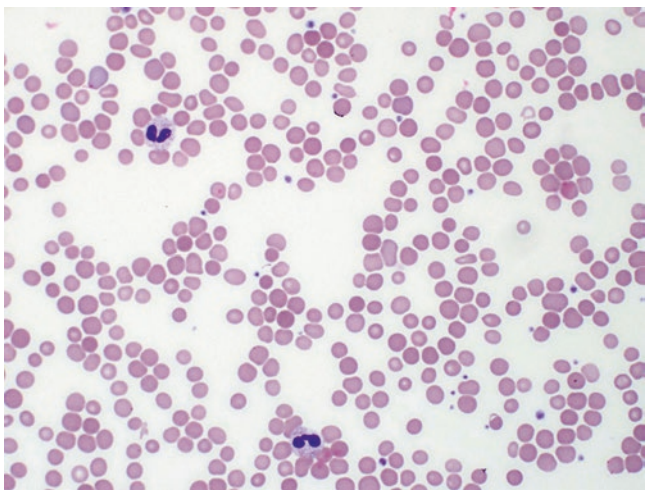

Fig. 17.23 Myelodysplastic/myeloproliferative neoplasm, unclassifiable (MDS/MPN, U). A peripheral blood smear reveals anemia, dysplastic pelgeroid neutrophils, and thrombocytopenia. A diagnosis of MDS/MPN, U requires at least one cytopenia and one increased lineage in the peripheral blood, with less than 20% blasts in the blood and bone marrow

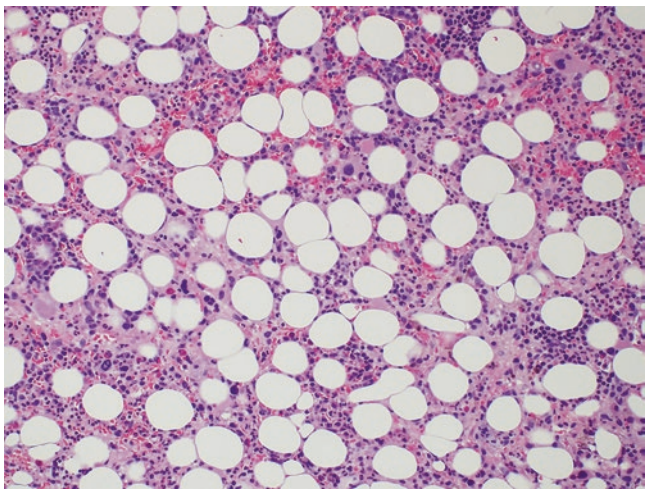

Fig. 17.24 Myelodysplastic/myeloproliferative neoplasm, unclassifiable (MDS/MPN, U). The bone marrow biopsy in this pancytopenic patient reveals a dysplastic, hypercellular marrow with less than 20% blasts. Prominent myeloproliferative features are a diagnostic criterion of MDS/MPN, U. In addition to the criteria of dysplastic and proliferative features, patients with MDS/MPN, U must have de novo disease that cannot be assigned to any other category and must lack a prior MPN or MDS history, confounding pharmacotherapies, or designated genetic abnormalities, including *BCL-ABL1*, *PDGFRA*, *PDGFRB*, *FGFR1*, isolated del(5), t(3;3)(q21;q26), or inv(3)(q21q26)

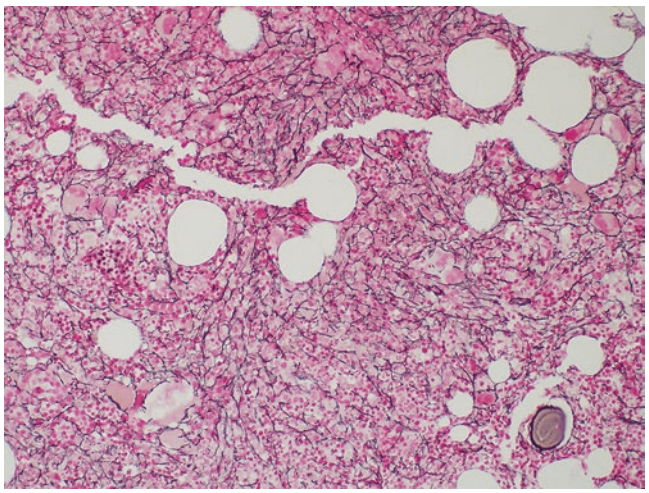

Fig. 17.26 Myelodysplastic/myeloproliferative neoplasm, unclassifiable (MDS/MPN, U). A reticulin stain highlights increased reticulin fibers. Fibrosis may be mildly to moderately increased in MDS/MPN, U. Cases with prominent fibrosis are seen rarely, leading to diagnostic overlap with primary myelofibrosis

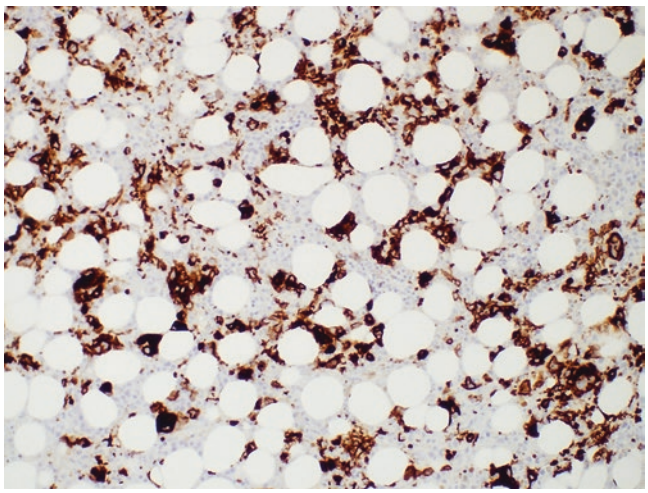

Fig. 17.25 Myelodysplastic/myeloproliferative neoplasm, unclassifiable (MDS/MPN, U). Immunohistochemistry for CD42b on this bone marrow biopsy highlights dysplastic, clustered megakaryocytes in a hypercellular marrow. This stain can be useful to identify small megakaryocytes. Megakaryocytes are most often small with nuclear hypolobation, but they can show enlarged, hyperlobated, and pleomorphic forms

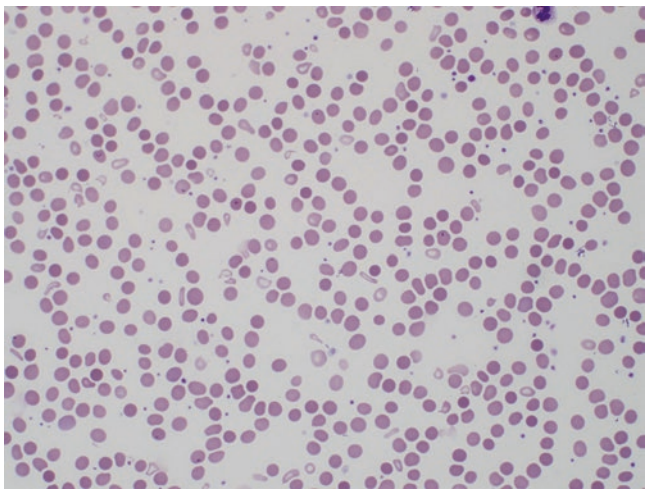

Fig. 17.27 Myelodysplastic/myeloproliferative neoplasm with ring sideroblasts and thrombocytosis (MDS/MPN-RS-T). A peripheral blood smear demonstrates macrocytic anemia with marked anisocytosis, poikilocytosis, and thrombocytosis. Refractory anemia and thrombocytosis are required for diagnosis. This once-provisional entity used to be termed *refractory anemia with ring sideroblasts associated with marked thrombocytosis* (RARS-T), but it is now called MDS/MPN-RS-T

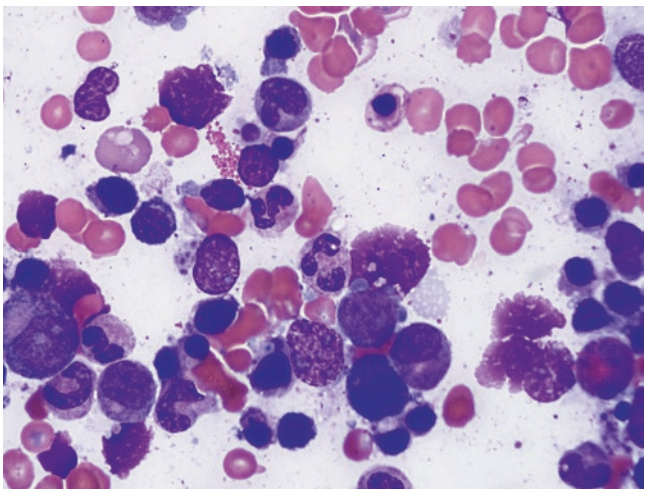

Fig. 17.28 Myelodysplastic/myeloproliferative neoplasm with ring sideroblasts and thrombocytosis (MDS/MPN-RS-T). This bone marrow aspirate demonstrates mild dyserythropoiesis with subtle nuclear blebbing. Dyserythropoiesis in the bone marrow with 15% or more ring sideroblasts is required for a diagnosis of MDS/MPN-RS-T. This percentage requirement is unaltered by the presence or absence of a *SF3B1* mutation (in contrast to MDS with ring sideroblasts)

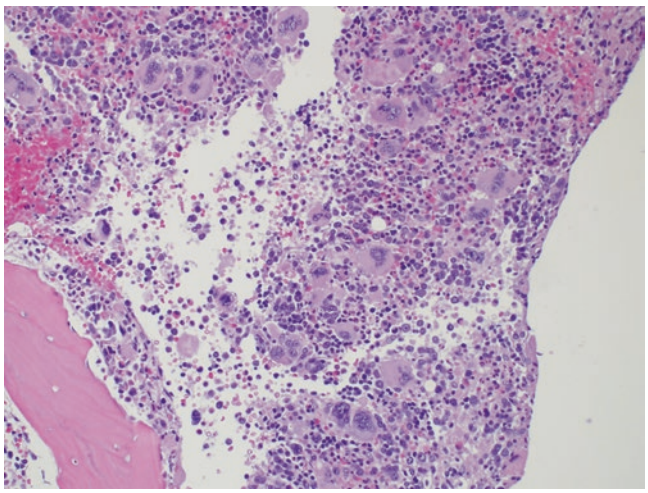

Fig. 17.30 Myelodysplastic/myeloproliferative neoplasm with ring sideroblasts and thrombocytosis (MDS/MPN-RS-T) . This bone marrow biopsy contains megakaryocytes displaying anisocytosis, hyposegmentation, irregular lobulation, hyperchromatic nuclei, and bulbous nuclei ("cloud-like" nuclei) with clustering. Megakaryocytes with features similar to those seen in primary myelofibrosis (PMF) or essential thrombocythemia (ET) are a diagnostic requirement for MDS/MPN-RS-T. PMF and ET do not typically have anemia or ring sideroblasts

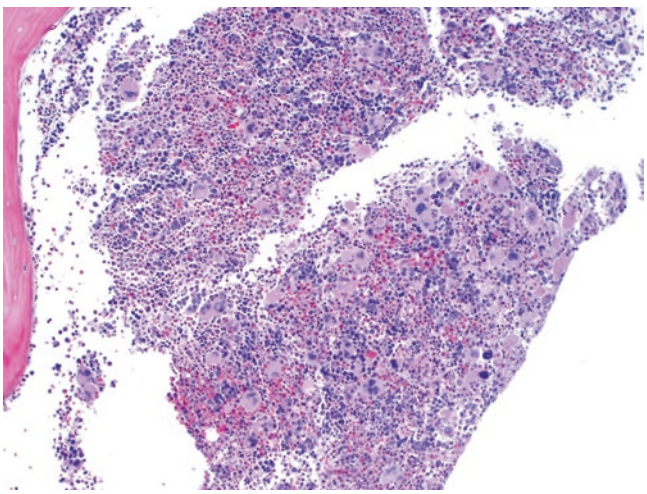

Fig. 17.29 Myelodysplastic/myeloproliferative neoplasm with ring sideroblasts and thrombocytosis (MDS/MPN-RS-T). This bone marrow biopsy reveals a hypercellular marrow. Increased megakaryocytes are present. MDS/MPN-RS-T is associated with *SF3B1* mutations. Co-mutations with *JAK2* V617F, *CALR*, and *MPL* are also described

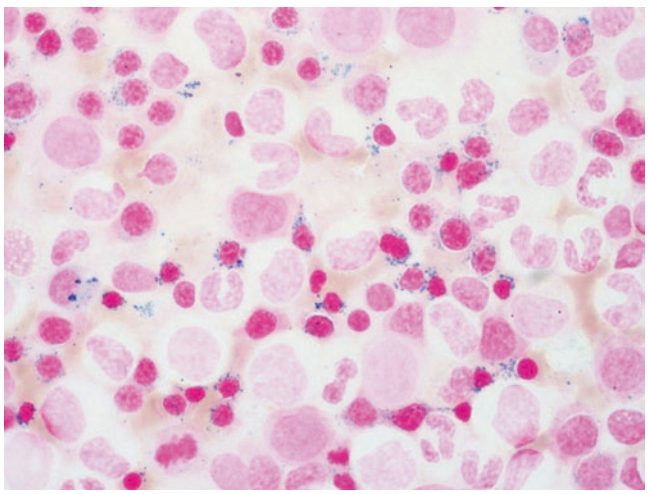

Fig. 17.31 Myelodysplastic/myeloproliferative neoplasm with ring sideroblasts and thrombocytosis (MDS/MPN-RS-T). Iron stain on this bone marrow aspirate reveals ring sideroblasts with coarse iron granules ringing the nuclei. Dyserythropoiesis in the bone marrow and 15% ring sideroblasts or more are required for a diagnosis of MDS/MPN-RS-T

Suggested Reading

1. Arber DA, Orazi A, Hasserjian R, Thiele J, Borowitz MJ, Le Beau MM, et al. The 2016 revision to the World Health Organization classification of myeloid neoplasms and acute leukemia. Blood. 2016;127:2391–405.
2. Elliott MA, Tefferi A. Chronic neutrophilic leukemia 2016: update on diagnosis, molecular genetics, prognosis, and management. Am J Hematol. 2016;91:341–9.
3. Foucar K. Myelodysplastic/myeloproliferative neoplasms. Am J Clin Pathol. 2009;132:281–9.
4. Geyer JT, Orazi A. Myeloproliferative neoplasms (BCR-ABL1 negative) and myelodysplastic/myeloproliferative neoplasms: current diagnostic principles and upcoming updates. Int J Lab Hematol. 2016;38:12–9.
5. Karow A, Baumann I, Niemeyer CM. Morphologic differential diagnosis of juvenile myelomonocytic leukemia—pitfalls apart from viral infection. J Pediatr Hematol Oncol. 2009;31:380.
6. Mughal TI, Cross NC, Padron E, Tiu RV, Savona M, Malcovati L, et al. An International MDS/MPN Working Group's perspective and recommendations on molecular pathogenesis, diagnosis and clinical characterization of myelodysplastic/myeloproliferative neoplasms. Haematologica. 2015;100:1117–30.
7. Orazi A, Bennett JM, Germing U, Brunning RD, Bain BJ, Thiele J, et al. Myelodysplastic/myeloproliferative neoplasms. In: Swerdlow SH, Campo E, Harris NL, Jaffe ES, Pileri SA, Stein H, et al., editors. WHO classification of tumours of haematopoietic and lymphoid tissues. 4th ed. IARC, Lyon; 2008. p. 75–86.
8. Patnaik MM, Parikh SA, Hanson CA, Tefferi A. Chronic myelomonocytic leukaemia: a concise clinical and pathophysiological review. Br J Haematol. 2014;165:273–86.
9. Savona MR, Malcovati L, Komrokji R, Tiu RV, Mughal TI, Orazi A, et al. An international consortium proposal of uniform response criteria for myelodysplastic/myeloproliferative neoplasms (MDS/MPN) in adults. Blood. 2015;125:1857–65.
10. Stieglitz E, Taylor-Weiner AN, Chang TY, Gelston LC, Wang YD, Mazor T, et al. The genomic landscape of juvenile myelomonocytic leukemia. Nat Genet. 2015;47:1326–33.
11. Wang SA, Hasserjian RP, Fox PS, Rogers HJ, Geyer JT, Chabot-Richards D, et al. Atypical chronic myeloid leukemia is clinically distinct from unclassifiable myelodysplastic/myeloproliferative neoplasms. Blood. 2014;123:2645–51.

Metastatic Tumors in the Bone Marrow

18

Mohammad Vasef

The vast majority of the non-hematolymphoid neoplasms in the bone marrow are metastatic in nature (Figs. 18.1, 18.2, 18.3, 18.4, 18.5, 18.6, 18.7, 18.8, 18.9, 18.10, 18.11, 18.12, 18.13, 18.14, 18.15, 18.16, 18.17, 18.18, 18.19, 18.20, 18.21, 18.22, 18.23, 18.24, 18.25, 18.26, 18.27, 18.28, 18.29, 18.30, 18.31, 18.32, 18.33, 18.34, 18.35, 18.36, 18.37, and 18.38). Accurate diagnosis and subtyping require careful histomorphologic examination with integration of immunohistochemical results and, in certain cases, cytogenetics and molecular genetic findings.

The incidence of bone marrow metastasis varies significantly among different tumors. Tumors with the highest frequency of bone marrow metastasis include carcinomas of the breast (Figs. 18.1, 18.2, 18.3, 18.4, 18.5, 18.6, and 18.7), prostate (Figs. 18.18, 18.19, 18.20, and 18.21), gastrointestinal tract (Figs. 18.16, 18.17), and lung (Figs. 18.8, 18.9, 18.10, and 18.11) in adults and neuroblastoma (Figs. 18.24, 18.25, 18.26, 18.27, 18.28, and 18.29) in the pediatric age group. The published incidence of bone marrow metastasis for a given tumor differs significantly because of variability in techniques used to assess the bone marrow, as well as differences in patient selection. Studies using only bone marrow aspirate most likely have underestimated the true incidence of metastatic disease in bone marrow. Highly sensitive detection methods for circulating tumor cells can detect very low levels of disseminated tumor cells in patients with breast cancer and other types of cancer—much lower than can be identified by routine microscopic examination. The clinical significance of this very low-level involvement has been debated, however.

Carcinoma of the breast is the most common metastatic disease detected in the bone marrow in women. Prostate and lung carcinomas are the most common metastatic diseases among men. Among all the histologic subtypes of lung cancer, small cell carcinoma has the highest incidence of bone marrow involvement. Other, less common tumors with bone marrow metastasis in adults include colon and gastric adenocarcinoma. Neuroblastoma has the highest incidence of bone marrow metastasis in children. Other tumors with a high incidence of marrow involvement in children include rhabdomyosarcoma (Figs. 18.36, 18.37, and 18.38), primitive neuroectodermal tumor (PNET)/Ewing sarcoma (Figs. 18.30, 18.31, 18.32, and 18.33), retinoblastoma (Figs. 18.34, 18.35), and medulloblastoma.

Circulating tumor cells are rarely detected in peripheral blood smears, particularly at the feather edge of the smear. Typically, these are seen in small clusters or are singly distributed and may mimic lymphoma cells.

Histomorphologic assessment of bone marrow is important in the staging of a newly diagnosed solid tumor or in monitoring of disease and therapeutic response. Trephine biopsy is crucial in assessing metastatic tumors because associated fibrosis renders most metastatic solid tumors unaspirable. In addition, bilateral trephine biopsies may improve the diagnostic yield because of the patchy distribution of some metastatic tumors. Common metastatic tumors in children, including neuroblastoma, rhabdomyosarcoma, and Ewing sarcoma, are often present in both aspirate smears and trephine biopsy; however, in rare occasions only aspirate smears are diagnostic.

In rare circumstances, a bone marrow core biopsy or an image-guided bone biopsy may be performed to obtain tumor tissue for molecular genetic studies. In these circumstances, it is crucial to preserve the integrity of the DNA by avoiding strong, acid-based decalcification solution. A useful alternative would be EDTA-based solutions. Limited mutation-specific antibodies such as *BRAF* V600E or *EGFR* mutation-specific antibodies are available, which would work on tissues previously decalcified in strong, acid-based solutions.

M. Vasef (✉)
Department of Pathology, University of New Mexico Health Sciences Center, Albuquerque, NM, USA
e-mail: mvasef@salud.unm.edu

T.I. George, D.A. Arber (eds.), *Atlas of Bone Marrow Pathology*, Atlas of Anatomic Pathology,
https://doi.org/10.1007/978-1-4939-7469-6_18

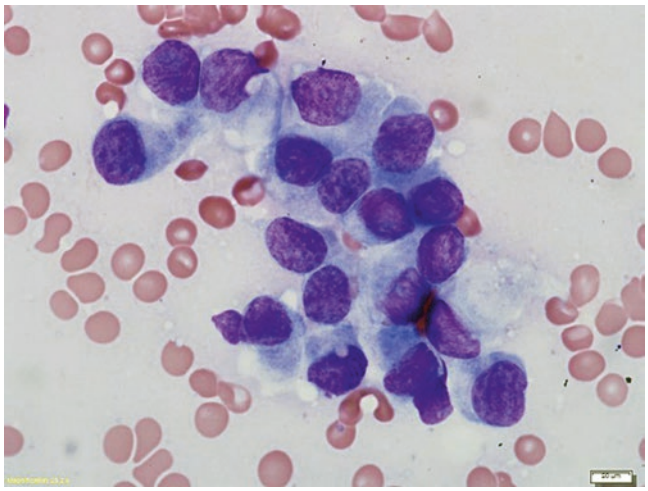

Fig. 18.1 Wright-stained touch imprint of a bone marrow trephine biopsy from a patient with a remote history of breast carcinoma shows a cluster of loosely cohesive metastatic carcinoma cells with large, oval nuclei and moderate amounts of wispy cytoplasm

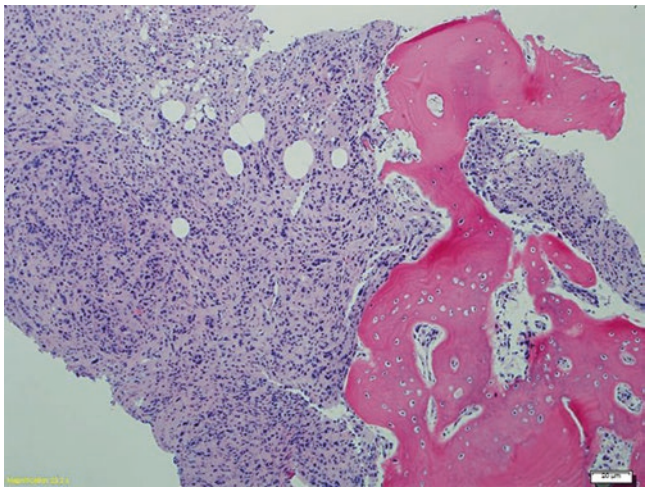

Fig. 18.3 Low-power view of an H&E-stained bone marrow trephine biopsy specimen demonstrates extensive involvement by metastatic lobular carcinoma of the breast. The patient had been diagnosed with stage II lobular carcinoma of the breast 10 years ago and had been treated with mastectomy and adjuvant chemotherapy. She now presents with anemia and leukopenia. Metastatic classic lobular carcinoma often tends to be distributed singly within the marrow space and may mimic a hematopoietic neoplasm

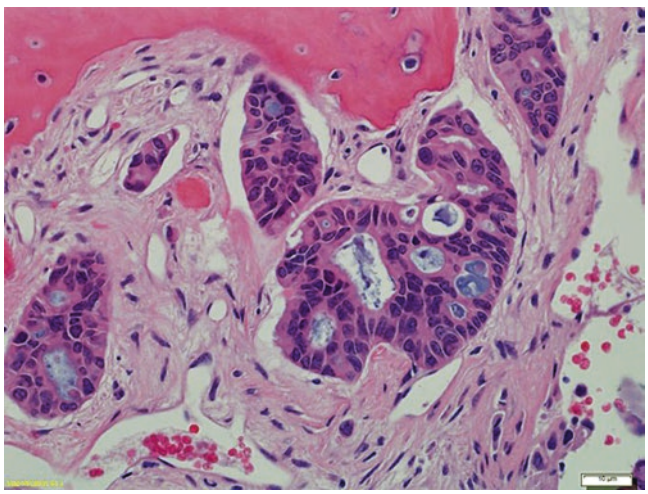

Fig. 18.2 Concurrent bone marrow trephine biopsy shows metastatic ductal carcinoma of breast primary with cribriform architecture similar to the histologic appearance of the tumor in the original breast site. Notice a component of intrasinusoidal tumor distribution, as well as a significant desmoplastic stromal response

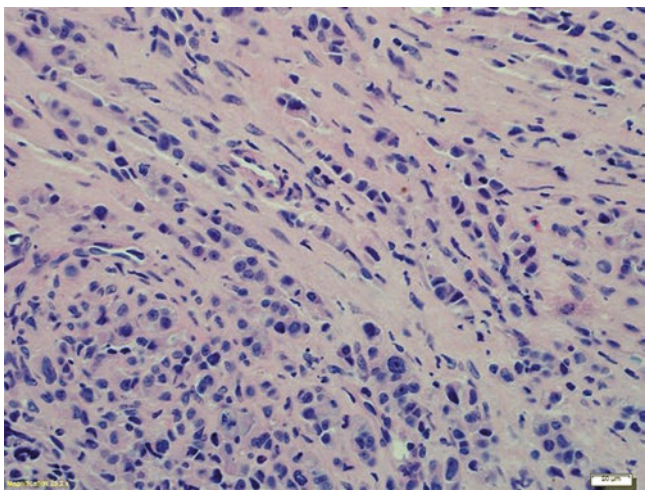

Fig. 18.4 High-power view of the bone marrow shows extensive bone marrow replacement by metastatic epithelial cells with intermediate-sized nuclei and scant to moderate amounts of cytoplasm. Notice the frequent single-file distribution typical of lobular breast carcinoma. Metastatic classic lobular carcinoma is often distributed singly within the bone marrow space, without a significant desmoplastic response, and can mimic a hematopoietic neoplasm

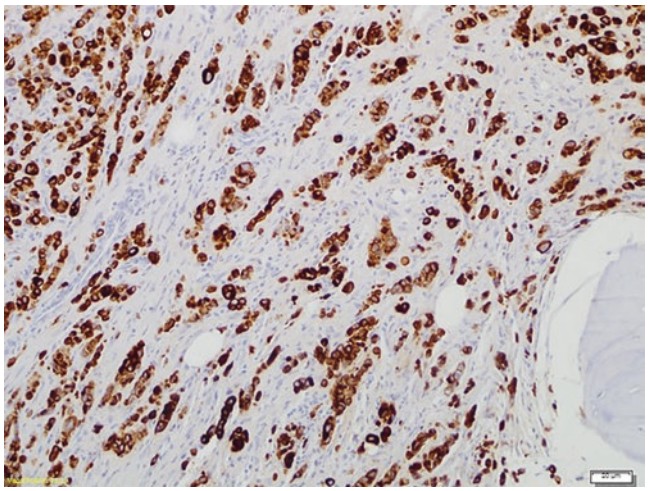

Fig. 18.5 Paraffin immunohistochemical stain using pankeratin antibody highlights the frequent single-file distribution, as well as individually distributed metastatic lobular carcinoma, in this bone marrow core biopsy specimen

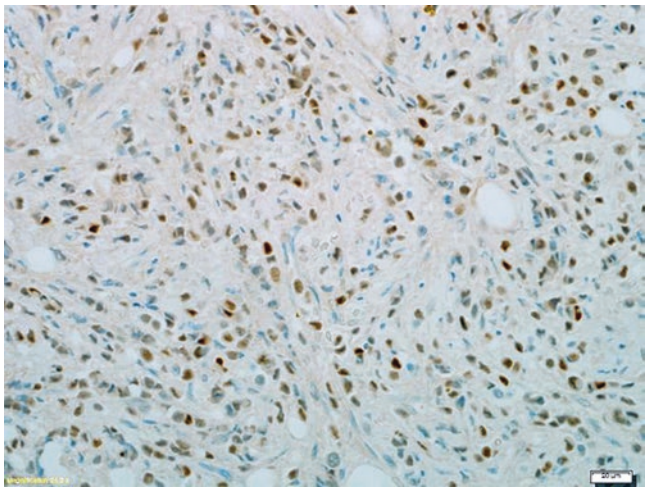

Fig. 18.7 Paraffin immunohistochemical stain using anti-estrogen receptor (anti-ER) antibody highlights metastatic carcinoma cells distributed singly within the bone marrow space in this example of metastatic classic lobular breast carcinoma

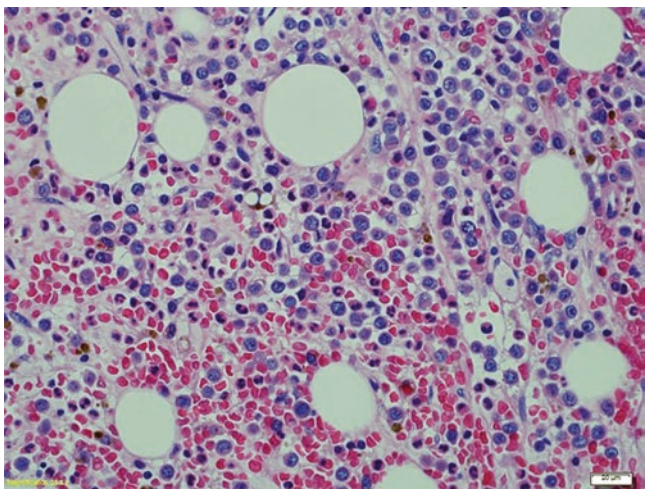

Fig. 18.6 High-power view of a bone marrow core biopsy involved by metastatic classic lobular breast carcinoma shows small neoplastic cells with regular nuclei distributed singly and interspersed among significantly decreased residual hematopoietic cells. In the absence of a prior clinical history of breast cancer and without ancillary studies, the classic lobular carcinoma can be erroneously interpreted as a hematopoietic malignancy

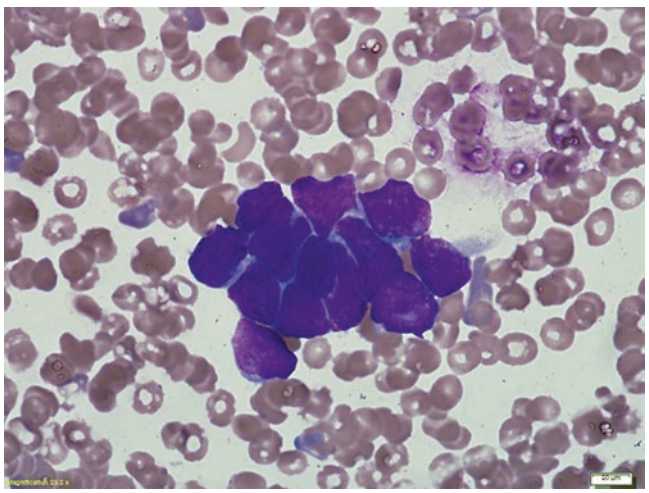

Fig. 18.8 Wright-stained bone marrow aspirate shows a cluster of cohesive tumor cells with a high nuclear-cytoplasmic (N:C) ratio, hyperchromatic nuclei, and nuclear molding from a patient with metastatic high-grade neuroendocrine small cell carcinoma of lung origin

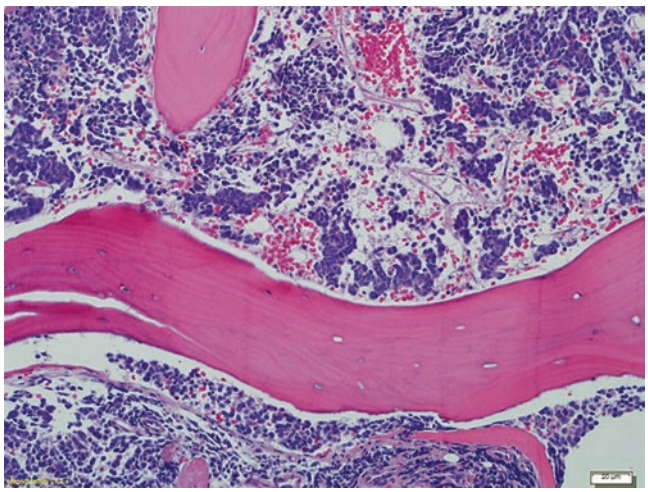

Fig. 18.9 H&E-stained bone marrow trephine biopsy shows extensive marrow involvement by metastatic small cell carcinoma of the lung

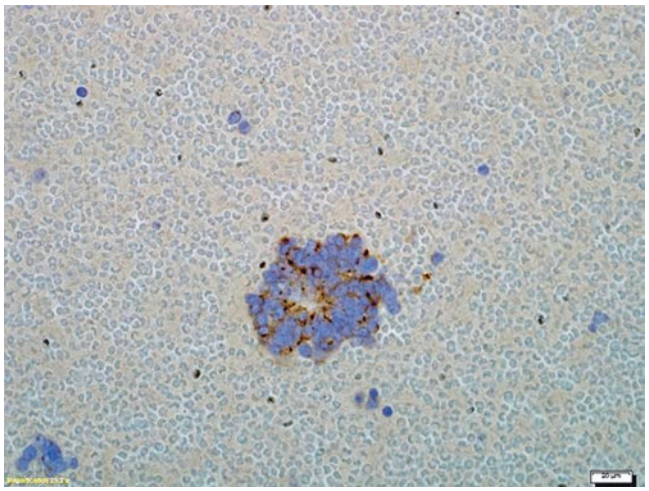

Fig. 18.11 Immunohistochemical stain using anti-chromogranin antibody performed on the marrow clot section highlights clusters of metastatic small cell carcinoma of the lung with a paranuclear, dotlike pattern of chromogranin expression

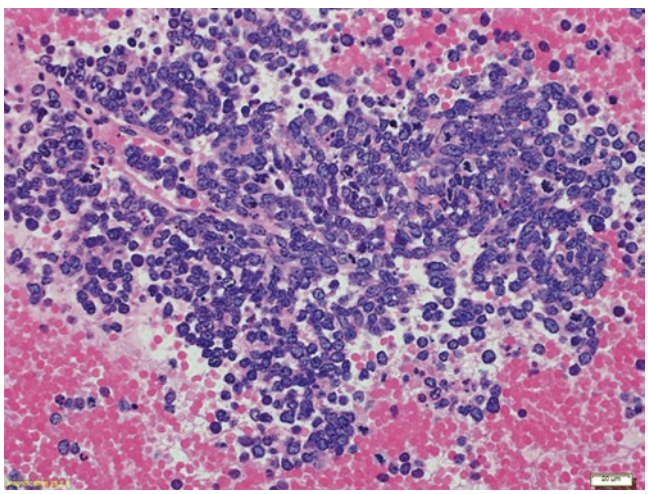

Fig. 18.10 H&E-stained histologic section of bone marrow clot section shows a large aggregate of metastatic small cell carcinoma of lung primary. The neoplastic cells show a so-called salt-and-pepper chromatin pattern with a high mitotic rate without a significant stromal response, which raises the differential diagnosis of a hematopoietic tumor or a sarcoma such as Ewing sarcoma

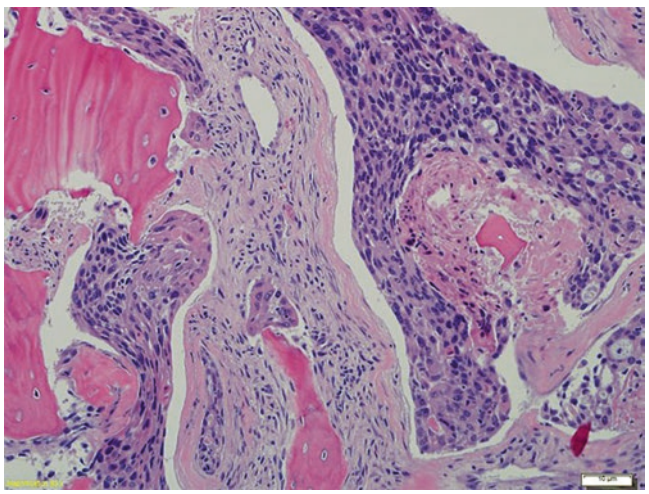

Fig. 18.12 This H&E-stained bone marrow trephine biopsy specimen from a 38-year-old woman with squamous cell carcinoma of the uterine cervix shows extensive intrasinusoidal involvement by metastatic deposits of poorly differentiated carcinoma. Extensive desmoplastic stromal reaction and prominent stromal fibrosis with focal bone resorption are also present

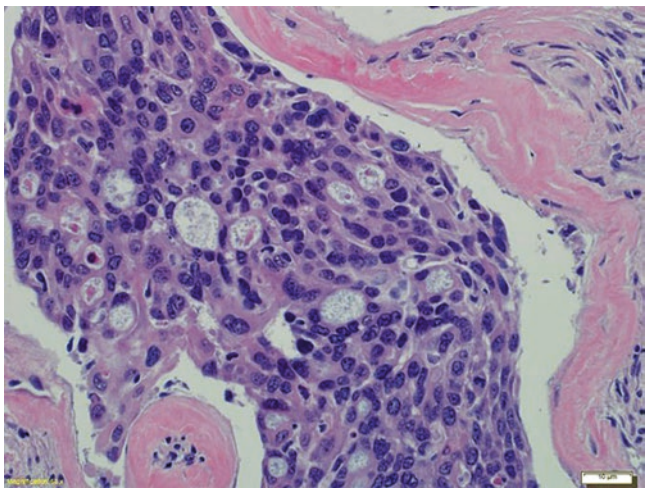

Fig. 18.13 The poorly differentiated metastatic carcinoma from the same patient as in Fig. 18.12, with metastatic squamous cell carcinoma of the uterine cervix, shows glandular differentiation and mucin production in this microscopic field

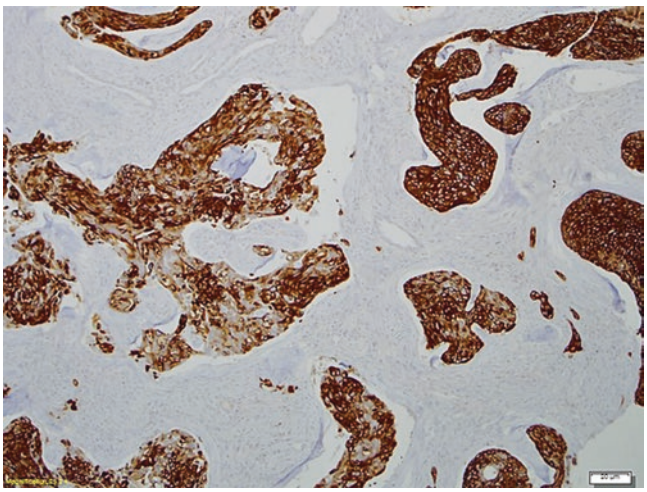

Fig. 18.15 Immunohistochemical stain performed on the bone marrow trephine biopsy reveals strong expression of keratin 5/6, supportive of metastatic squamous cell carcinoma in this poorly differentiated tumor

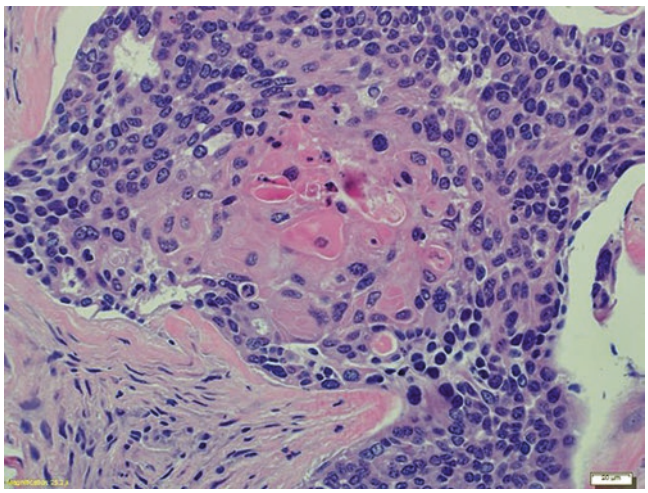

Fig. 18.14 The H&E-stained section of marrow core biopsy of the patient with metastatic squamous cell carcinoma shows focal keratinization in this field. Review of the histologic sections from the primary site similarly demonstrated foci of glandular differentiation and keratinization

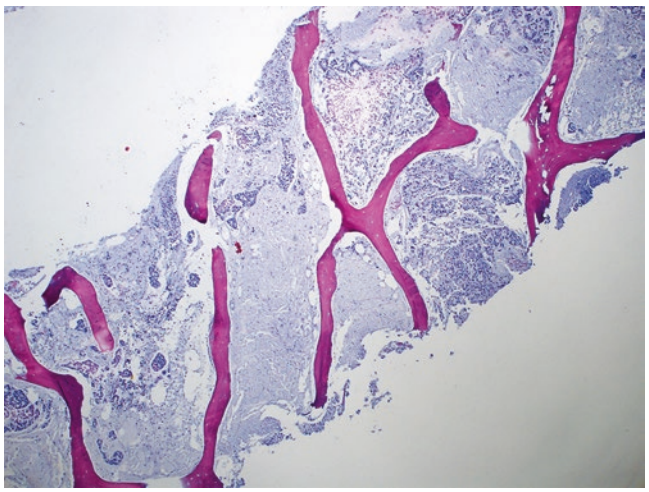

Fig. 18.16 H&E-stained section of bone marrow trephine biopsy from a 45-year-old patient with a history of metastatic mucinous adenocarcinoma of the colon reveals extensive acellular, mucinous material replacing the marrow space, with scattered clusters and aggregates of malignant cells within the mucinous pool

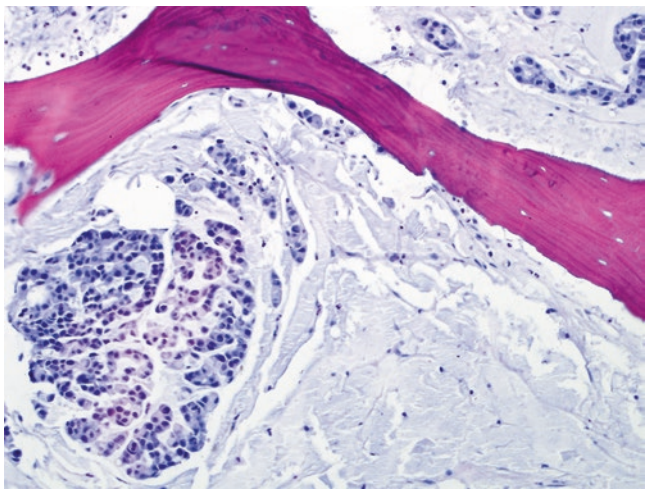

Fig. 18.17 H&E-stained high-power view of metastatic mucinous adenocarcinoma involving this bone marrow shows clusters of tumor cells with acinar and cribriform patterns floating free in pools of mucin

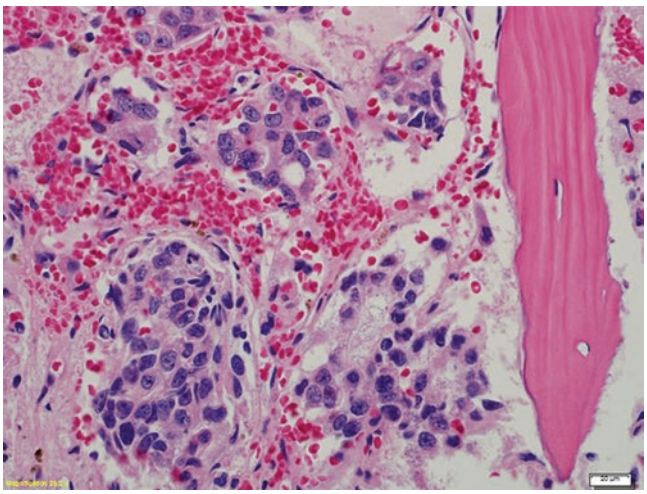

Fig. 18.19 Concurrent H&E-stained bone marrow trephine biopsy from the same patient as in Fig. 18.18 shows extensive marrow involvement by metastatic, well-differentiated prostatic adenocarcinoma with an intrasinusoidal distribution pattern

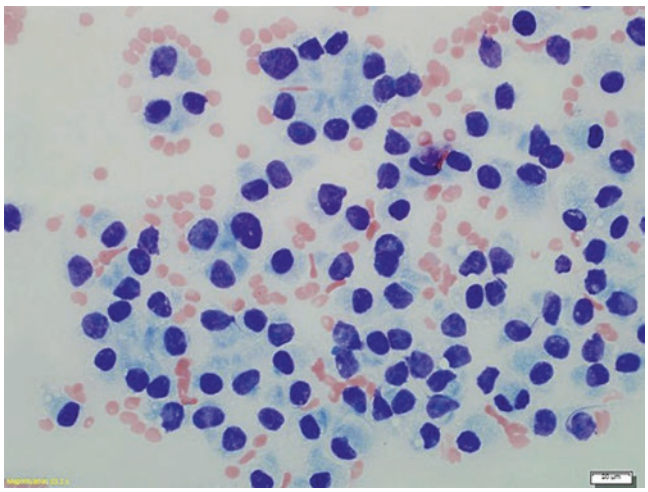

Fig. 18.18 Wright-stained bone marrow touch imprint from a patient with a history of prostatic carcinoma reveals a well-differentiated adenocarcinoma with acinar formation, consistent with marrow involvement by metastatic prostatic adenocarcinoma

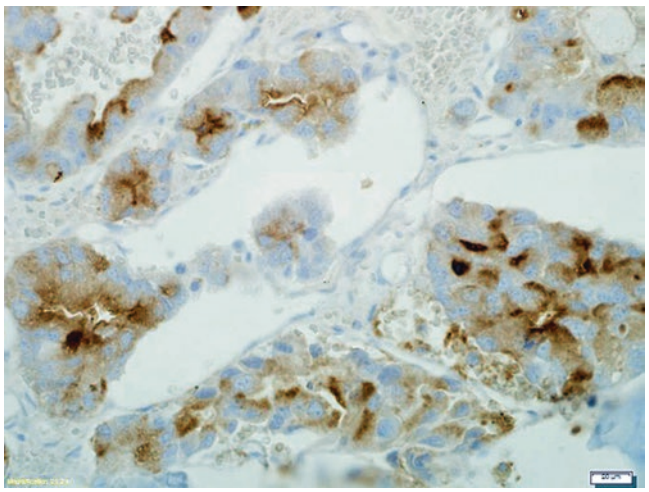

Fig. 18.20 Paraffin immunohistochemical stain using prostate-specific antigen (PSA) antibody marks neoplastic cells in this bone marrow biopsy involved by a moderately differentiated adenocarcinoma of prostatic origin

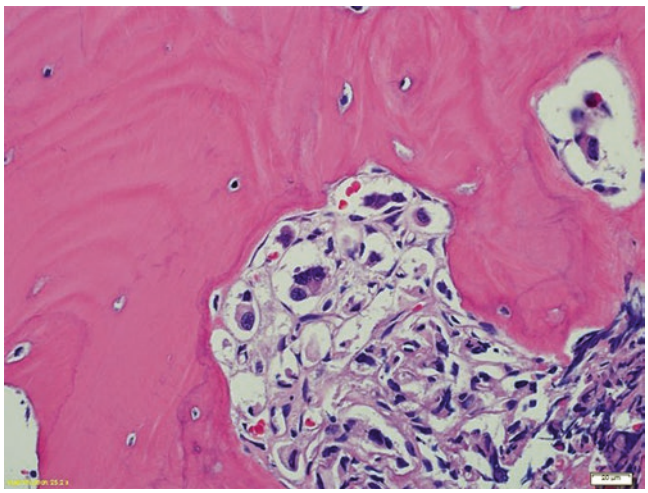

Fig. 18.21 H&E-stained bone marrow trephine biopsy with extensive involvement by a poorly differentiated prostatic adenocarcinoma with prominent bone sclerosis. Bone metastasis is common in prostate cancer and is typically associated with a sclerotic reaction

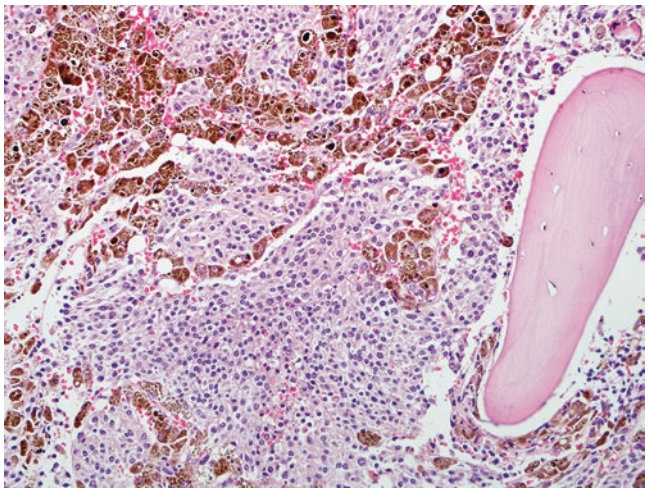

Fig. 18.23 High-power view of the bone marrow trephine biopsy shows extensive metastatic malignant melanoma replacing the marrow space. Abundant pigment-laden macrophages are also present, consistent with melanophages

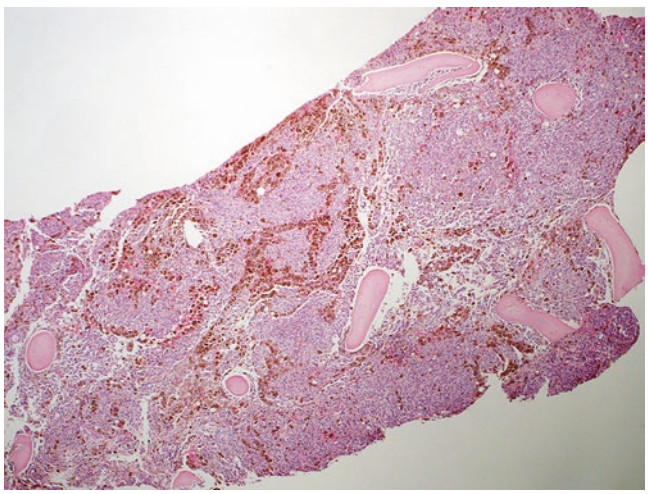

Fig. 18.22 Low-power view of a bone marrow core biopsy shows extensive involvement by metastatic malignant melanoma. Notice prominent pigment deposition

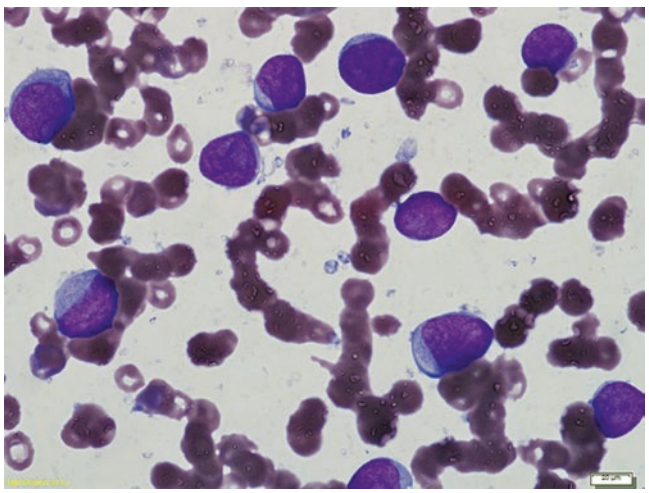

Fig. 18.24 Wright-stained bone marrow aspirate smear from an 11-year-old boy with a recent diagnosis of retroperitoneal neuroblastoma reveals singly distributed metastatic neuroblastoma cells with small, regular nuclei, occasional distinct nucleoli, and scant amounts of cytoplasm resembling lymphoblasts

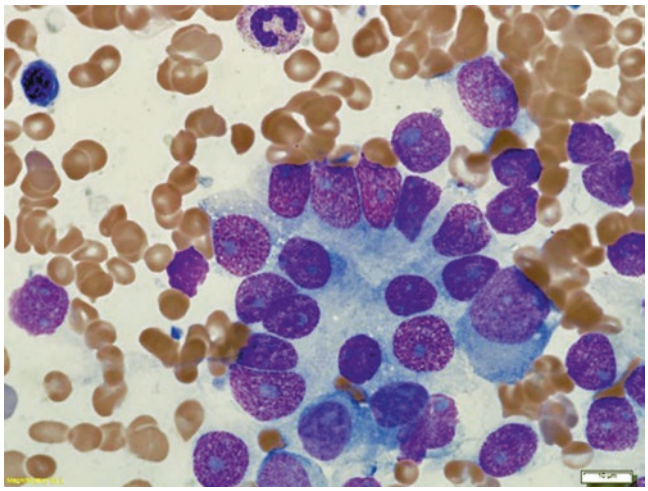

Fig. 18.25 This Wright-stained bone marrow aspirate smear from a child with metastatic neuroblastoma reveals tumor cells with partially degenerated, regular nuclei with prominent nucleoli and indistinct cytoplasmic borders surrounding fibrillary material consistent with a Homer Wright rosette formation

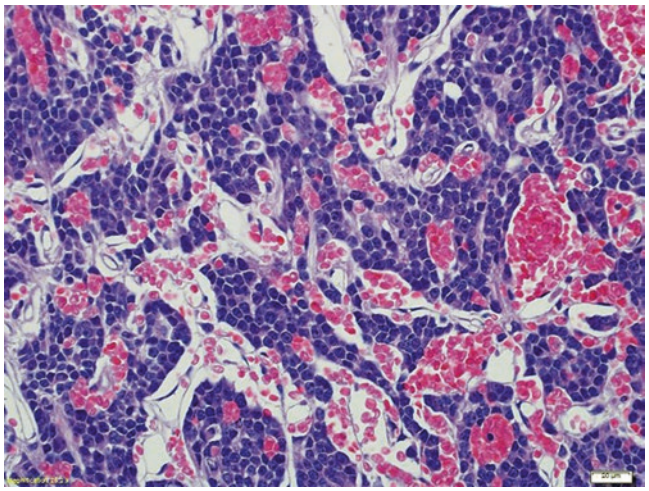

Fig. 18.27 High-power view of bone marrow trephine biopsy with extensive metastatic neuroblastoma reveals irregularly shaped, large aggregates of tumor cells surrounding dilated sinuses. There is markedly decreased trilineage hematopoiesis. Analysis using fluorescence in situ hybridization (FISH) revealed amplification of the *MYCN* gene, suggestive of a poor prognosis

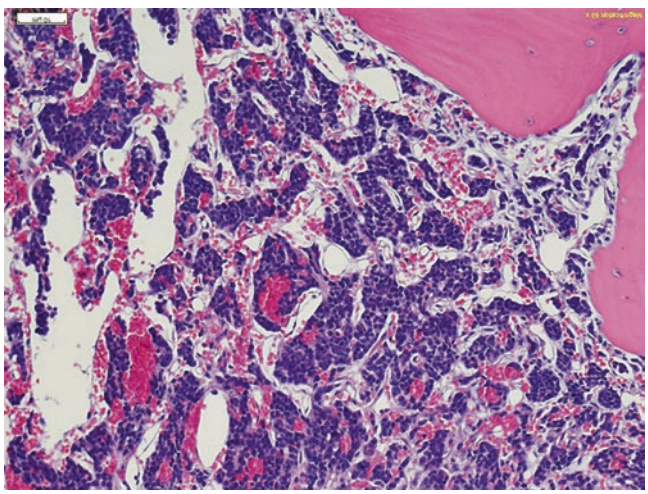

Fig. 18.26 H&E-stained staging bone marrow trephine biopsy from a child with a history of neuroblastoma reveals extensive marrow involvement by metastatic neuroblastoma distributed in compact aggregates of uniform and monotonous tumor cells

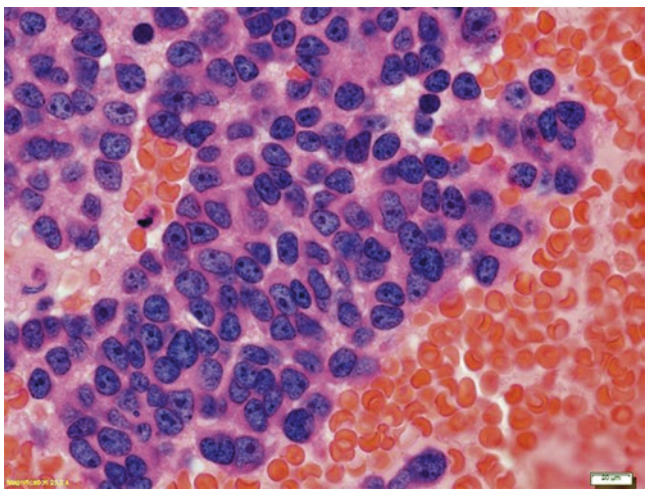

Fig. 18.28 H&E-stained bone marrow clot section from a child with stage IV neuroblastoma reveals aggregates of metastatic tumor cells with indistinct cytoplasmic borders in a background of fibrillary material, with occasional rosette formations

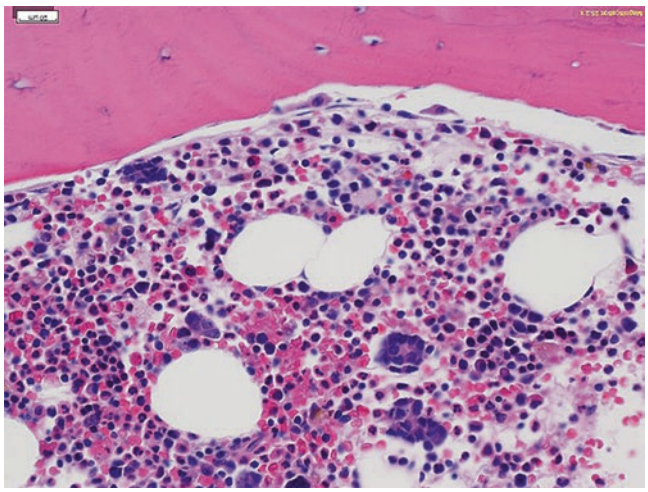

Fig. 18.29 This H&E-stained bone marrow trephine biopsy from a child with a history of stem cell transplantation and chimeric antibody therapy for high-stage neuroblastoma reveals a normocellular marrow with active hematopoiesis and minute foci of metastatic tumor cells, consistent with relapsed neuroblastoma

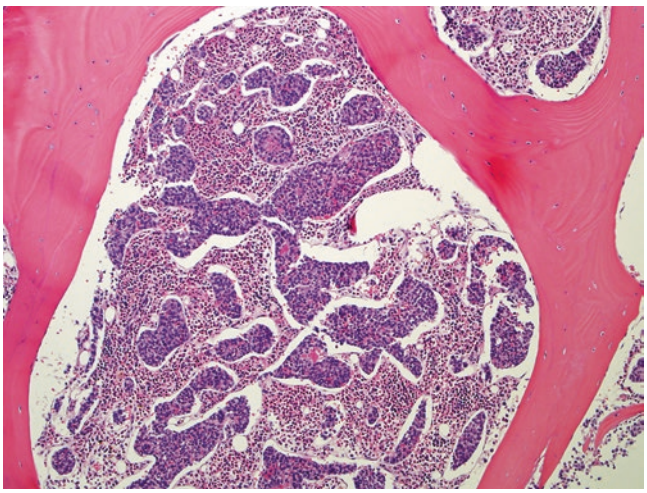

Fig. 18.31 H&E-stained low-power view of this bone marrow core biopsy shows extensive bone marrow involvement by Ewing sarcoma/PNET

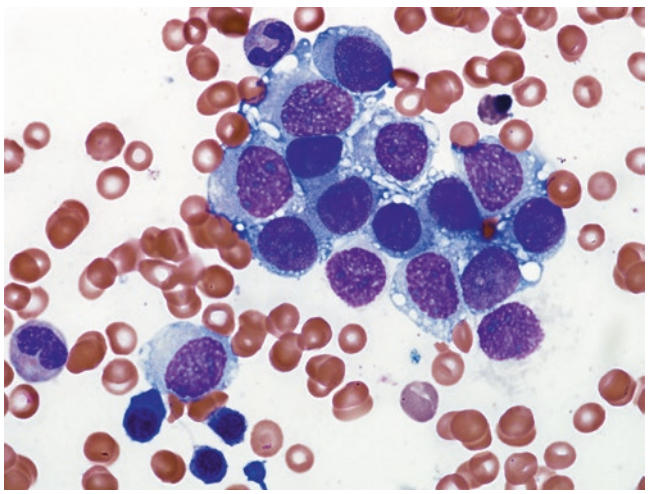

Fig. 18.30 Wright-stained bone marrow aspirate smear reveals a loose aggregate of small cells with round nuclei, finely dispersed chromatin, one or more small nucleoli, and scant cytoplasm. The tumor cells expressed FLI1 and CD99 by immunohistochemistry, and FISH analysis detected the *FLI1-EWS* fusion gene, supporting a diagnosis of Ewing sarcoma/primitive neuroectodermal tumor (PNET)

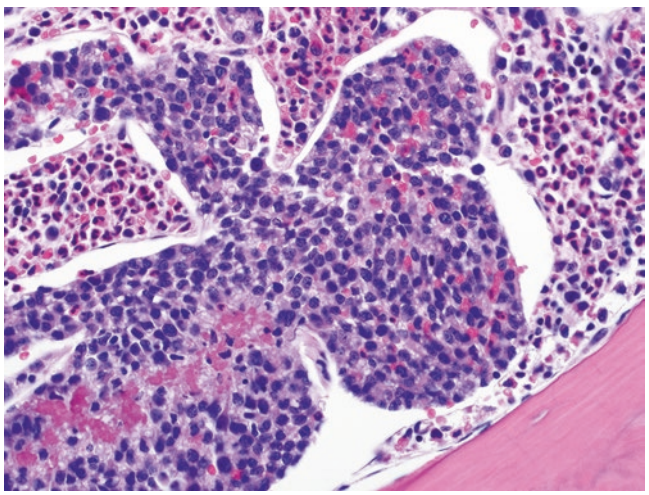

Fig. 18.32 High-power view of bone marrow core biopsy shows large aggregates of Ewing sarcoma associated with tumor necrosis in the center portion of the tumor aggregate. Ewing sarcoma frequently undergoes necrosis

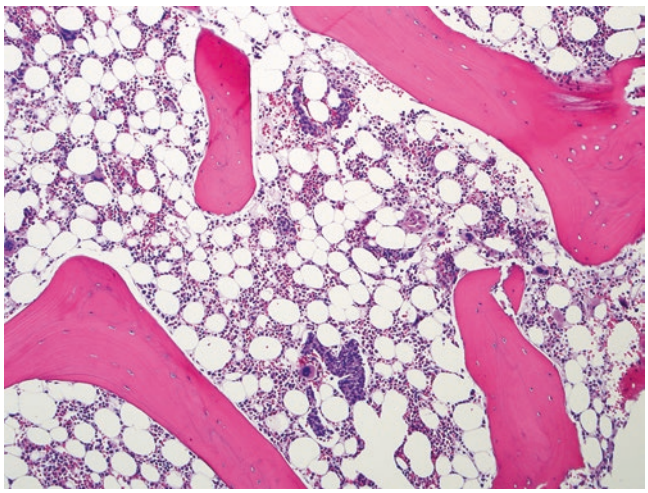

Fig. 18.33 This H&E-stained bone marrow core biopsy shows residual foci of Ewing sarcoma in a child who received intensification chemotherapy. Therapy-related myeloid malignancy has occurred in a subset of patients with refractory Ewing sarcoma treated with intensified chemotherapy

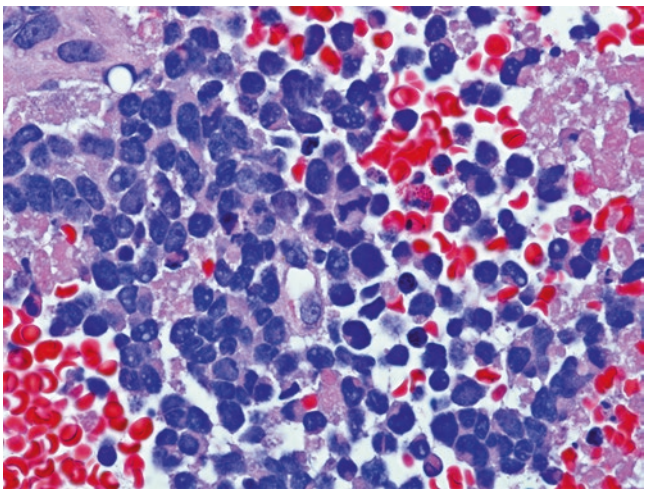

Fig. 18.35 High-power view of the bone marrow clot section involved by poorly differentiated metastatic retinoblastoma. The neoplastic cells are composed of singly distributed tumor cells with high N:C ratio, increased mitoses, and tumor necrosis

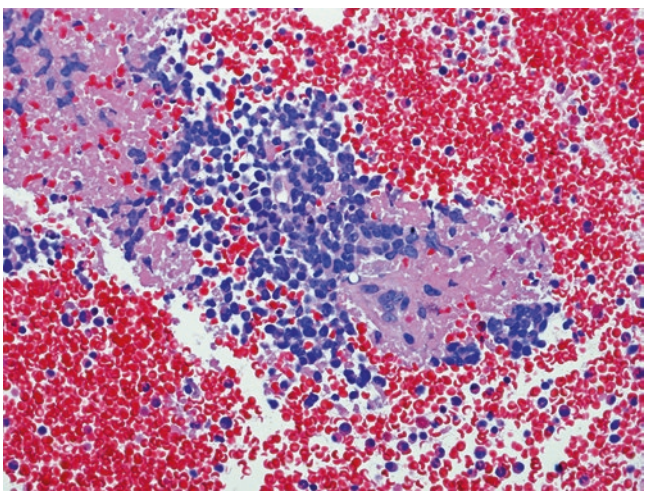

Fig. 18.34 H&E-stained bone marrow clot section from a 3-year-old child with poorly differentiated retinoblastoma of the right eye shows marrow involvement by a small blue-cell tumor, with extensive necrosis consistent with metastatic retinoblastoma. The neoplastic cells expressed neuron-specific enolase and synaptophysin by immunohistochemistry

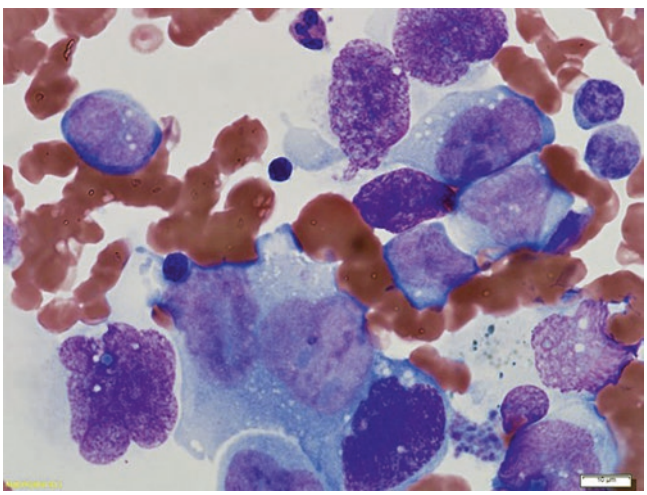

Fig. 18.36 Wright-stained staging bone marrow aspirate smear from a 19-year-old patient with recent diagnosis of testicular alveolar rhabdomyosarcoma shows scattered neoplastic cells, including a bilobed malignant cell with features of a rhabdomyoblast

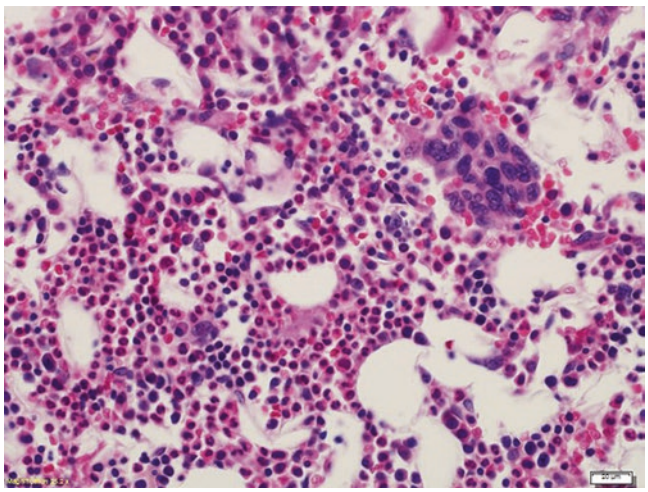

Fig. 18.37 Bone marrow core biopsy reveals a small focus of metastatic rhabdomyosarcoma. The uninvolved bone marrow shows active trilineage hematopoiesis

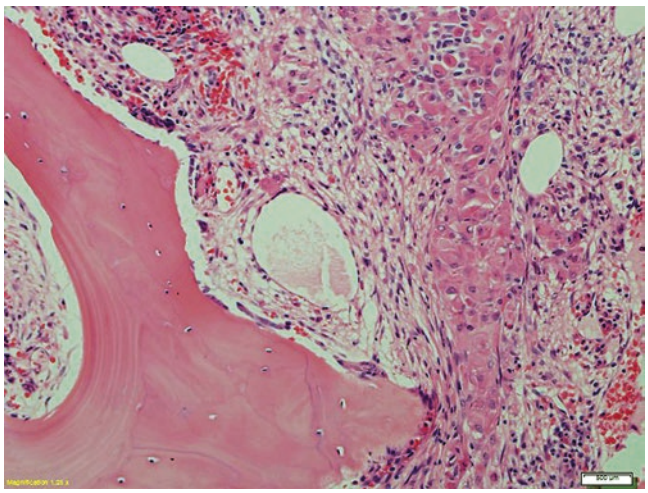

Fig. 18.38 Posttherapy bone marrow trephine biopsy of a patient with extensive marrow involvement by rhabdomyosarcoma reveals patchy foci of residual tumor cells, which have undergone maturation due to tumor response to chemotherapy

Suggested Reading

1. Chabot-Richards D, Buehler K, Vasef MA. Detection of EGFR exon 19 E746-A750 deletion and EGFR exon21 point mutations in lung adenocarcinoma by Immunohistochemistry: a comparative study to EGFR exons 19 and 21 mutations analysis using PCR followed by high-resolution melting and pyrosequencing. J Histotechnology. 2015;38:56–62.
2. Cotta CV, Konoplev S, Medeiros LJ, Bueso-Ramos CE. Metastatic tumors in bone marrow: histopathology and advances in the biology of the tumor cells and bone marrow environment. Ann Diagn Pathol. 2006;10:169–92.
3. Grzywacs B. Metastatic tumors involving bone marrow. In: Foucar K, McKenna RW, Peterson LC, Kroft SH, editors. Tumors of the bone marrow. AFIP Atlas of Tumor Pathology Series, vol. 4. Washington, DC: American Registry of Pathology; 2016. p. 787–805.
4. Russell HV, Golding LA, Suell MN, Nuchtern JG, Strother DR. The role of bone marrow evaluation in the staging of the patients with otherwise localized, low-risk neuroblastoma. Pediatr Blood Cancer. 2005;45:916–9.

Index

T.I. George, D.A. Arber (eds.), *Atlas of Bone Marrow Pathology*, Atlas of Anatomic Pathology,
https://doi.org/10.1007/978-1-4939-7469-6